Development of an *in vitro* 3D model of the proximal tubule interstitial interface as a high throughput renal fibrosis assay platform.

Elena Tasinato

Doctor of Philosophy

Bioscience Institute, Faculty of Medical Sciences

Industrial supervisor: Dr Colin D. A. Brown

Academic supervisor: Prof. Lyle Armstrong

April 2023

“Superficially, it might be said that the function of the kidneys is to make urine; but in a more considered view one can say that the kidneys make the stuff of philosophy itself.”

Homer W. Smith,

From Fish to Philosopher

“Nothing is so painful to the human mind as a great and sudden change.”

Mary Shelley,

Frankenstein

Table of Contents

Table of Figures

Chapter 1. Introduction

Chapter 2. Materials & Methods

Chapter 3. Establishment of isolation protocols and characterization of cellular components of the proximal tubule interstitial interface.

Chapter 4. Characterisation of 3D *in vitro* proximal tubule model.

Chapter 6. Discussion and conclusive remarks.

Abstract

Chronic kidney disease (CKD) is a progressive, irreversible disease with a worldwide prevalence of 10-13 %. Hypertension and diabetes are the main causes of CKD, and they seem to be determined by epigenetic factors as well as socioeconomical conditions. This condition is asymptomatic until generic symptoms arise in patients with CKD, such as fatigue and itchiness, therefore the disease can be assessed only via specific functional and laboratory tests, the most indicative being the measurement of glomerular filtration rate (GFR). When such parameter falls beneath 60 mL/min per 1·73 m^2 for longer than 3 months, the patient is considered to have developed chronic kidney disease that will eventually lead to end stage renal disease (ESRD) (Moll et al., 2013). Regardless of its aetiology, the underlying pathophysiological mechanism of CKD is renal fibrosis which is characterised by progressive scarring of the renal parenchyma which, in turn, leads to loss of basic kidney functions such as reabsorption, secretion, and excretion of solutes. Current pharmacological treatments for CKD are limited to blood pressure management via angiotensin-converting enzyme (ACE) inhibitors and angiotensin II receptor blockers (ARBs), or management of glycemia in diabetes. Therefore, such therapies do not treat the underlying causes of CKD but components of the metabolic syndrome associated with it. There is urgent need for development of compounds that may target directly known mechanisms associated with the condition such as fibrosis and oxidisation (Turner et al., 2012). The call for the development of novel treatments combined with a global shift of interest towards replacing, refining, and reusing *in vivo* animal models of disease has led to an evolution and expansion within the *in vitro* disease modelling field. Therefore, we developed a 3D *in vitro* renal fibrosis model that recapitulates the key cellular events underlying tubule-interstitial fibrosis in the proximal tubule interstitial interface. The model is generated via treatment of primary human proximal tubule cells (hPTC) and renal fibroblasts (HRF) in co-culture from autologous donor kidney with key endogenous pro-fibrotic cytokines and hormones, and it is used as an assay platform to generate dose-response assays where the magnitude of maladaptive molecular mechanisms such as cell dedifferentiation and trans-differentiation, and cell cycle dysregulation are measured via high content imaging and high throughput flow cytometry and are put in relationship with the dose of pro-fibrotic compound used. The model is suitable for the high throughput screening of the *in vitro* efficacy of anti-fibrotic compounds and for the investigation of unknown molecular mechanisms of fibrosis.

COVID-19 Impact Statement

The Covid-19 pandemic and subsequent restrictions have impacted the research work carried out throughout this PhD project, especially during my first year of work, between March 2020 and September 2020. The plan for the first year of the project was to optimise and validate protocols for the isolation of primary cells from the human kidney cortex, using imaging and flow cytometry to phenotype each cell type. Restricted access to core University facilities such as the Bioimaging Unit and the Flow Cytometry Core Facility, which were completely inaccessible until July 2020 and reopened after the summer, meant that the experimental work had to be carried out elsewhere. The industrial partner which funded this research project via the Intensive Industrial Innovation Programme (IIIP) of the European Regional Development Fund (ERDF), Newcells Biotech Ltd, granted me unrestricted access to their widefield fluorescence microscope and flow cytometer for this period of time which has been essential for the success of the experimental work presented in Chapter 3. The possibility to have had contact and collaboration with the technical staff at the Flow Cytometry Core Facility would have been beneficial towards the development of my knowledgebase and skillset as a young researcher, and would have ensured assay robustness and appropriate antibody panels design since the beginning of the project. Furthermore, the original plan around this project was to rely on both the University laboratory facilities and the ones at Newcells Biotech Ltd. The latter is a spinout startup of Newcastle University led by my academic and industrial supervisors, Prof. Lyle Armstrong and Dr Colin DA Brown. Up until March 2020, the startup was based within the NU Medical School, and as soon as the pandemic started, its laboratories had to move to a non-University facility for the research work to continue. The laboratory move and the initial lack of tissue culture facilities such as incubators and biological safety cabinets meant that I could only continue with primary cell culture work at the new non-University facility, while I had been able to work on cell lines as well as primary cells up until March 2020. If cell line work could have been possible, it would have strengthened the data displayed within the thesis in terms of *in vitro* model development and assay validation. Because of the Covid-19 pandemic, I obtained a 3 months fees-free extension to conclude the lab work needed to finish this project and write up the thesis.

Chapter 1. Introduction

1.6 The Kidney

The kidneys are recognized as the organs that excrete endogenous and exogenous solutes from the human body, such as metabolic waste and xenobiotics. A complex series of physiological processes lead to the formation and excretion of urine. The existence of the kidneys allows for the maintenance of a constant internal environment within the human body which is achieved by modulating water and solutes concentration, extracellular fluid volume, acid-base balance, erythrocyte production, vascular resistance, and bone integrity.

1.1.1 Gross Anatomy & Microanatomy

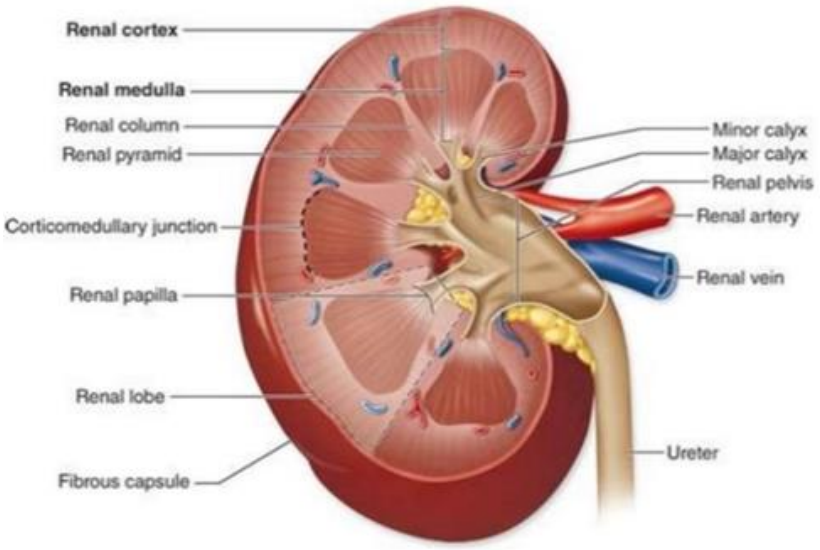

Figure 1.1. Gross kidney anatomy. The kidney is divided into distinct anatomical sections, where each renal lobe can be divided into renal cortex and renal medulla. Adapted from "The Urinary System." In Junqueira's Basic Histology: Text and Atlas, 15e. by Mescher, A. L. (2018) New York, NY: McGraw-Hill Education.

Figure 1.1 shows the gross anatomy of the kidney, which has identifiable major internal divisions and associated blood vessels. For instance, the renal artery can be located at the hilum of each kidney where it enters and splits into two major segmental arteries. The renal pyramids are encompassed by arcuate arteries which in turn bifurcate into interlobar arteries. These arteries emerge from arcuate arteries, lengthening into the renal cortex to form the renal microvasculature. The afferent arteriole emerges from the interlobular artery, entering the nephron branching into the glomerulus, a cluster of capillaries part of the renal corpuscle. A unique feature of the renal microvasculature is denoted by such capillaries draining into the efferent arteriole rather than draining into a venule. In the renal cortex, the efferent arteriole offshoots into peritubular capillaries whereas in the medulla it continues into vasa recta, thus constructing an ulterior capillary network that accompanies the loop of Henle progressing

into the medulla. Structurally, a bisected kidney can be divided into cortex and medulla. The nephron is mostly found in the former and it is the functional unit of the kidney. It is responsible for all three renal physiological processes that result in the creation of urine: filtration, reabsorption, and secretion of solutes. On average, the number of nephrons in each human kidney spans from 1 to 4 million. The segments composing the nephron can be further categorised into five structures, according to histological characterisation: the renal corpuscle, comprising the glomerulus and the Bowman's capsule, the proximal tubule, the loop of Henle, the distal tubule, and the collecting duct (as shown in **Figure 2.2)**.

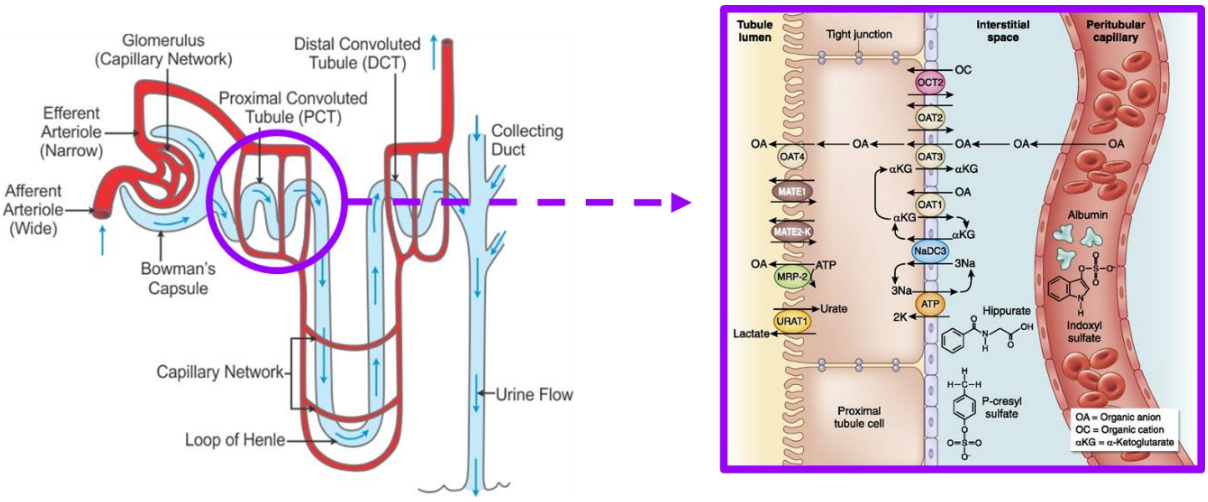

Figure 1.2. Diagram of a nephron with focus on the main histological and functional features of the proximal tubule segment. Adapted from Wang et al., "Proximal Tubular Secretory Clearance: A Neglected Partner of Kidney Function", CJASN 2018.

The nephron commences with the renal corpuscle, consisting of a cluster of capillaries known as the glomerulus. The Bowman's capsule, a structure consisting of parietal epithelial cells, encompasses the glomerulus. Specialised epithelial cells known as podocytes envelope the endothelium of fenestrated capillaries composing the glomerulus, which possess interdigitating processes that form filtration slits. These slits comprise the filtration membrane alongside the capillaries' fenestrated endothelium and their basement membrane (glomerular basal membrane, GBM). The parietal layer of the Bowman's capsule forms the external surface of the capsule and surrounds the glomerulus and its podocyte lining, creating the capsular space. Furthermore, mesangial cells are also found in the renal corpuscle. They play a role in maintaining the integrity of the glomerulus by providing physical support to the capillaries and modulating blood flow through contraction and relaxation. The Bowman's capsule continues into a tubular epithelial structure, which is divided into segments depending on their function and morphology. The first segment is the proximal tubule, which will be discussed in more detail later in this chapter. It is followed by the descending thin limb of the loop of Henle that descends deep down the renal medulla. At its deepest descent point, the loop of Henle abruptly turns in a hairpin turn becoming the ascending loop of Henle. By ascending towards the cortex, its epithelium thickens becoming the ascending thick limb of the loop of Henle. Next, the tubule passes next to the Bowman's capsule and the afferent and efferent arterioles forming the macula densa, becoming then the distal convoluted tubule. Finally, several tubules from different nephrons merge into a collecting duct which descends

from the cortex to the medulla. In turn, several collecting ducts merge into papillary collecting ducts that empty the fluid contained into the tubules, now called urine, into the renal calyx which continues into the ureter (Eaton & Pooler, 2018) (Ogobuiro & Tuma, 2024).

1.1.2 Physiology

Kidneys, ureters, and the urethra form the renal system which on average filter 200 litres of blood a day. The nephron is the anatomical-functional unit to which the kidney as a whole organ can be reduced. Its physiological function is to excrete from the human body metabolites, excess ions, and xenobiotics while keeping in the blood useful solutes. The nephron is able to regulate the blood electrochemical composition, its osmolarity, and its acid-base balance (Ogobuiro & Tuma, 2024). Urine is produced via three processes which take place among all the nephron's segments: filtration, reabsorption, and secretion. Some epithelial segments of the nephron can carry out two of these functions concomitantly, whereas others can only perform one. These processes are tightly regulated by proteins, hormones, and peptides released by other organs and by the kidney itself; the ultimate objective being the maintenance of the homeostasis of the human body's internal environment. The endogenous compounds that act on the kidney primarily change the renal blood flow in order to upkeep ion composition, volume, and tonicity of the extracellular fluid (Barrett et al., 2017).

Glomerular filtration is the first step towards urine formation. Glomerular endothelial cells, podocytes and the glomerular basement membrane form the filtration membrane which filters the blood coming from the systemic blood stream into the afferent arteriole. This filtration membrane retains plasma proteins in the blood stream because of its special composition: both glomerular endothelial cells and podocytes contribute to the formation of the glomerular basement membrane which is composed mainly of laminin and fibronectin (Mescher, 2018). Once the blood has passed the filtration membrane it is known as the ultrafiltrate, and the amount of ultrafiltrate produced at each minute determines the glomerular filtration rate (GFR) which is a widely used clinical parameter determined in patients to assess their renal function. This value is estimated by administering to the patient or animal a compound inert to renal metabolism which is then sampled in blood and urine. In brief, GFR is regulated by the blood flow within the afferent arteriole and the glomerular capillaries, which is in turn under the influence of factors that regulate the capillary bed size. Mesangial cells contract in response to several hormones such as vasopressin and angiotensin II, and by contracting they reduce blood flow, thus reducing the GFR. The hydrostatic pressure gradient between the lumen of the glomerular capillaries and the Bowman's capsule allows compounds to flow from the blood stream to the ultrafiltrate. The nephron can autoregulate its own filtration pressure via the juxtaglomerular apparatus, a specialized structure formed by the afferent arteriole and the distal convoluted tubule. Juxtaglomerular cells secrete renin when the pressure within the afferent arteriole drops, acting upon the renin – angiotensin – aldosterone system (Barrett et al., 2018).

Compounds are absorbed and secreted in multiple segments of the nephron, and these two processes can be summarized as the net amount of compound transferred by the tubules. Compounds which are absorbed by the tubules move from the tubular lumen to the

interstitium, and subsequently, to the capillary lumen, whereas compounds which are secreted move in the opposite direction, from the blood to the tubular lumen, and subsequently they will be excreted into urine. Transport takes place as passive diffusion of compounds in the interstitium, facilitated diffusion driven by electrochemical gradient, and primary active transport against such gradient. The capability to measure this last form of transport *in vitro* is extremely important in the characterisation of any tubular model. A mechanism called tubule-glomerular feedback affects the filtration rate at the glomerular level based on the ionic composition of the ultrafiltrate. The macula densa within the juxtaglomerular apparatus acts as a sensor for the osmotically active ions Na^+ and Cl^- which determine the amount of water within the tubules and in the interstitium. Another important feature of the tubules is the transport of water, which takes place via specialised water channels called aquaporins. Aquaporin 1 is expressed in the apical and basolateral side of the proximal tubule and in the descending limb of the loop of Henle, making these segments of the nephron permeable to water, whereas the absence of the water channels in the ascending limb makes it impermeable to water. The distal tubule is also impermeable to water, whereas the collecting ducts express aquaporin 2. The specific distribution of water channels along the nephron segments leads to the osmolality gradient increasing when moving from the cortex to the inner medulla, which is the fundamental mechanism by which the kidney is able to concentrate solutes in the urine (Barrett et al., 2018).

1.7 The Proximal Tubule

Within the nephron, the outer parietal layer forming the epithelial surface of the Bowman's capsule progresses into proximal convoluted tubule (PCT). This structure is located within the renal cortex, and it is described as the initial tubular part of the nephron comprised by simple cuboidal epithelial cells resting on a basement membrane. The fundamental physiological roles of these highly differentiated epithelial cells are the reabsorption and secretion of solutes, from the peritubular capillaries to the tubules' lumen. The histological features of this epithelium include its brush border on the apical surface of the cell is covered in long microvilli, a characteristic that allows for wider and simpler uptake of ions and compounds from the proximal tubule lumen to the cell, and the tight junctions that link the cells, a leak-tight barrier that strictly controls the movements of water and solutes (Eaton & Pooler, 2018). Specifically, the differentiation of proximal tubule cells into polarized cells which can selectively transport solutes happens during organ development and it is tightly regulated by the presence or absence of the proteins that constitute the tight junction that renders the tubular epithelium leak tight. These proteins are part of the claudin and occludin families, one of the most studied being ZO-1 (zonula occludens 1). All polarized cells have an apical and a basolateral membrane, as cells with the same phenotype and function interact via the lateral tight junction. With regards to proximal tubule cells, the presence of ZO-1 correlates to loss of proliferative phenotype, as the transcription factor ZONAB interacts with the DNA to modulate proliferation during development. Therefore, ZO-1 can be viewed as a "STOP" sign for proliferating epithelial cells, and the disruption of the cell signalling pathway that leads to translocation of ZO-1 to the tight junction is involved in maladaptive molecular events that are involved in tight junction dissolution and epithelial barrier function dysregulation (Pozzi & Zent, 2010). Polarized proximal tubule cells contain one primary cilium per cell, which protrudes towards the lumen of the proximal tubule. It is considered non-motile and its function is to act as a sensor for urine flow, as based on the flow rate the size of the tubular bed is regulated (Eymael et al., 2022). The proximal tubule is usually divided into three segments, S1, S2 and S3, based mainly on their ultrastructure, visible via electron microscopy, and function. S1 and S2 correspond to the proximal convoluted tube (pars convoluta), which is found right after the glomerulus and S3 to the straight part (pars recta) leading into the descending thin limb of the loop of Henle. Segments S1 and S2 contain a highly functioning endocytosis-lysosomal apparatus, while S3 is the most metabolically active segment. Because of these differences in their ultrastructure, each segment's drug-induced nephrotoxic response diverges from the other (Cristofori et al., 2007)

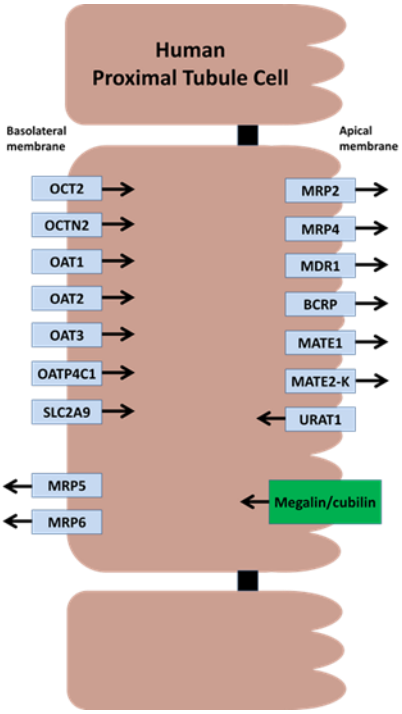

Figure 1.3. Diagram representing the proximal tubule cell with the main basolateral and apical transporters involved in the nephrotoxic response and drug-transporter interactions, namely organic cation transporter-2 (OCT2), organic cation/carnitine transporter-2 (OCTN2), organic anion transporter-1 (OAT1), organic anion transporter-2 (OAT2), organic anion transporter-3 (OAT3), Solute Carrier Organic Anion Transporter Family Member 4C1 (OATP4C1), solute carrier family 2 member 9 (SLC2A9), multidrug resistance protein-5 (MRP5), multidrug resistance protein-6 (MRP6), multidrug resistance protein-2 (MRP2), multidrug resistance protein-4 (MRP4), multidrug resistance-1 (MDR1), breast cancer resistance protein (BCRP), multidrug and toxin exclusion 1 (MATE1), multidrug and toxin exclusion 2 (MATE2-K), urate transporter 1 (URAT1), Megalin/Cubilin (Original image).

The first site to be reached by whole blood in the kidney is the glomerulus, where filtration takes place. The filtration rate of the glomerulus can be up to 180 L of fluids a day; hence the human body needs an efficient way of retaining useful molecules and discard wasteful ones. Therefore, the main physiological functions of the proximal tubule epithelial cells are to reabsorb the essential substances into the blood stream, such as water, glucose, vitamins and electrolytes, and to secrete waste compounds into the ultrafiltrate passing through the tubular lumen, such as xenobiotics and products of metabolism (Eaton & Pooler, 2018). Reabsorption and secretion in the proximal tubule are made possible by the presence of several transporters located alternatively on the basolateral side (facing the basement membrane, leading to reabsorption into the blood stream) and the apical side (facing the tubular lumen, leading to secretion into the urine). The two main super families to which these transporters belong to are the ATP-binding cassette (ABC) and solute carrier (SLC). ABC transporters use active transport to move solutes against their electrochemical gradient by utilizing the energy produced by ATP hydrolyzation, while SLC transporters use a form of either facilitated transport or co-transport to move organic cations and anions along or against their electrochemical gradient. Among the most well studied renal transporters there are the basolateral uptake organic anion transporter-1 and -3 (SLC22A6 or OAT1, SLC22A8 or

OAT3) and organic cation transporter-2 (SLC22A2 or OCT2), while on the apical side of the epithelium are located efflux transporters such as multidrug and toxin extrusion proteins (SLC47A1 or MATE1 and SLC47A2 or MATE2/2-K), P-glycoprotein (P-gp or MDR1 or ABCB1), and breast cancer resistance protein (ABCG2 or BCRP) (Miners et al., 2017). A summary of these transporters and their localization is shown in **Figure 1.3**. Furthermore, proximal tubule cells are a relevant metabolic site: compounds which are "transiting" through the epithelium to be reabsorbed into the peritubular capillaries or secreted into the ultrafiltrate are metabolized by several enzymes, including proteins belonging to the CYP450 family, uridine-diphosphate-glucuronosyltransferases (UGTs), glutathione-S-transferases, esterases, and sulfotransferases. These enzymes carry out detoxification reactions, reiterating the role the proximal tubule plays in renal drug elimination (Bajaj et al., 2018).

1.7.1 The proximal tubule interstitial interface: epithelial cells, endothelial cells, and fibroblasts

Although all the functions carried out by the kidney can be reduced to the physiology of its anatomical-functional unit, the nephron, the renal interstitium actively participates in the cross-talk between the tubular epithelium and the vasculature, whereby epithelial cells influence the biological behaviour of the cellular components of the tubule interstitium such as mesenchymal cells through an array of signalling pathways (Prunotto et al., 2012). Furthermore, the renal interstitium plays a fundamental role in maladaptive processes that occur in the pathogenesis of most renal diseases (Zeisberg & Kalluri, 2015). During organ development, it guides epithelial segmentation and specialization. The composition of the renal interstitium comprises interstitial fluid, proteoglycans, extracellular matrix, and cells that reside in the interstitium. Fibroblasts are found in this zone; their cellular bodies extend in branches and processes formed by microfibrillary bundles.

Macrophages are also commonly found in the interstitium, although more commonly in the medulla than in the cortex, and they seem to be found spatially close to the fibroblasts in the same zone. Immune cells in the kidney are involved in the progression and pathogenesis of several disorders of interest, such as CKD, acute kidney injury, and diabetic nephropathy. According to Park, JG et al. 2020, the main immune cell resident within the renal parenchyma seems to be the macrophage, despite this notion being based on murine studies, while more recent studies seem to suggest a high proportion of T cells in the human parenchyma (Park et al., 2020). The renal parenchyma is formed by 18 cell types which are phenotypically different and that are organised in structures that allows them to carry out specific tasks. This zonation of the kidney results in these cell types responding to injury and disease in different ways, which is in part due to immune cells being distributed in the interstitium and being involved in the maintenance of the homeostasis of the organ's milieu. The immune "arsenal" of the kidney comprises resident dendritic cells, macrophages, and migrating lymphocytes and neutrophils. Upon activation of injured renal cells, the released chemokines attract infiltrating immune cells such as lymphocytes, monocytes, and natural killer cells that may undergo proliferation within the inflamed renal interstitium. Depending on the course of the disease, immune cells may follow the adaptive route, whereby these cells can switch phenotype from inflammatory to healing, by secreting anti-inflammatory and pro-regenerative cytokines for

the injured epithelium, or the maladaptive one, where they end up perpetuate the damage they were initially tasked to halt. This maladaptive response can in fact lead to chronic inflammation, and in turn, fibrosis, deeming the renal immune system as a key actor within the progression of renal disease (Winfree et al., 2022). Most studies on resident immune cells in the kidney have focused on macrophages in mouse, which are known to express the murine specific marker F4/80. Though, this marker does not translate to human renal macrophages, therefore recent advances in the capabilities of single-cell RNA sequencing combined with fluorescence-activated cell sorting have helped identifying a set of cross-species genetic and protein markers, namely CD74, and CD81 (Zimmerman et al., 2019). In the context of investigating the renal immune system, single-cell RNA sequencing has been employed to map the spatiotemporal state of immune cells in the renal parenchyma. One study by Stewart BJ et al. in particular revealed how immune cells localisation and crosstalk between such cells and epithelial cells follows specific anatomical patterns within the organ in adult and during development. These more recent in depth studies regarding the renal immune system and response to injury can facilitate the investigation of progressive immune-mediated renal diseases such as CKD and the identification of novel targets for drug development (Stewart et al., 2019).

Dendritic cells are found in the interstitium as one of the immune-mediating components of this milieu, whereas contractile perivascular cells or pericytes are found in the transitional area between cortical afferent arterioles and the peritubular capillaries in the cortex, and in close contact with the vasa recta in the medulla. The space, which is not filled by the tubules, the vasculature, and all the above-mentioned cellular components is made from a complex extracellular matrix which could be compared to an artificial hydrogel. The extracellular matrix (ECM) is composed of a reticulum of microfibers: Collagens I, III, and VI are the most common types of collagen found in the interstitium, assembled in bundles that wrap the tubules, whereas collagen IV and V are mostly abundant in the basement membranes. Glycosaminoglycan (GAG) and interstitial fluid fill the extracellular space, while fibronectin and laminin constitute the tubular basement membrane as their function is to connect the cellular components of the nephron and the vasculature to the surrounding fibrillous matrix. Renal fibroblasts are responsible for the production and deposition of the extracellular matrix, in fact these cells are highly capable to synthesize proteins which is indicated by the presence of a strikingly developed rough endoplasmic reticulum. Therefore, the tubular interstitium not only functions as a support structure for the tubules and vessels, but it also allows ions and compounds to be exchanged between the tubular lumen and the capillary lumen via diffusion (Lemley & Kriz, 1991). Renal fibroblasts are mesenchymal cells found in the interstitial space of the kidney. They are responsible for the growth and maintenance of the connective tissue that forms the renal parenchyma. They synthesize and deposit the extracellular matrix in the kidney, and they are involved in scar tissue formation phenomena which occur under both healthy and maladaptive circumstances during tissue repair. They can transdifferentiate into myofibroblasts, which have contractile properties and can be identified histologically by the presence of α smooth muscle actin (αSMA). Renal fibroblasts are deemed to be one of the major drivers of the pathological processes underlying fibrosis because of their role in scar tissue formation. Fibrosis can be defined as tubular-interstitial scarring resulting from renal

injury, the most striking histological feature being accumulation of surplus extracellular matrix thus replacing functional parenchyma which leads to impaired organ function. Thus, renal fibroblasts are activated to myofibroblasts by pro-fibrotic and inflammatory stimuli that ultimately involve TGFβ and related signalling pathways. Activated myofibroblasts deposit an increased amount of extracellular matrix and have a higher rate of proliferation (Strutz & Zeisberg, 2006). Because of the fundamental role of renal fibroblasts in the development of renal fibrosis and the importance of the cross-talk between tubular epithelial cells and fibroblasts in the maintenance of a healthy milieu *in vivo*, and its dysregulation in the aetiology of fibrosis (Tan et al., 2016), this cell type has recently become the focus of much research surrounding renal pathologies.

The renal vasculature is a key anatomical and functional component of the kidney and, consequently, of the nephron. Although the discourse around kidney research tends to focus on the epithelial component of this organ, the tubular epithelium could not exert its physiological functions without the presence of its endothelial counterpart. The renal vascular network can be subdivided in arterial, venous, lymphatic vessels, and capillaries, which form the microvasculature that accompanies the epithelial tubules towards the collecting ducts. Two types of microvasculature are found in the kidney cortex, namely the glomerular capillaries and the peritubular capillaries. These are constituted by fundamentally different patterned vasculature: although both are composed of fenestrated endothelium, glomerular endothelial cells lack diaphragmatic fenestrae (Stolz & Sims-Lucas, 2015). Fenestrae are windows or round openings which mediate the exchange of solutes and water between the blood and the ultrafiltrate streaming respectively in capillaries and tubular lumens. The lack of diaphragms in the glomerular fenestrated endothelium allows for fluid filtration into the tubular lumen but impedes the passage of erythrocytes into the ultrafiltrate (Stan et al., 2004). The vascular endothelial growth factor (VEGF) pathway seems to be playing a central role in the development and maintenance of the renal vascular pattern which are fundamental for appropriate filtration and reabsorption of solutes. Of the four VEGF ligands (A, B, C, D), VEGF-A is the most effective one as its presence is cardinal to the ureteric bud and metanephric mesenchyme development. Its receptors, VEGFR1 and VEGFR2 are expressed virtually everywhere in the nephron (Stolz & Sims-Lucas, 2015). Peritubular endothelial cells play an active role in solute exchange, like their epithelial counterparts, the proximal tubule cells. It has been demonstrated that the presence of both cell types in culture leads to maintenance of appropriate phenotype for both cells type and prolongs survival of these cells in culture, which is likely to be associated with cross talk between epithelial and endothelial cells (Tasnim & Zink, 2012). Renal peritubular endothelial cells are therefore involved in the physiopathology of diseases that involve the proximal tubule and, in general, the renal parenchyma. For instance, capillary rarefaction of the peritubular capillaries is fundamental in the aetiology of chronic kidney disease. Peritubular rarefaction is correlated to the extremity of renal fibrosis in patients with CKD and it is a predictor of end stage renal disease (ESRD). In animal models, capillary rarefaction and loss of endothelial fenestrae seem to take place quickly after pro-fibrotic insult (Kida, 2020). Renal peritubular endothelial cells are notoriously difficult to isolate from the human kidney cortex because of their low proliferation potential and maintenance of phenotype, which identify endothelial cells which

express adhesion molecules CD31 and VE-cadherin, vascular endothelial growth factor receptor 2 (VEGFR2), and plasmalemma vesicle associated protein 1 (PV-1) (Ligresti et al., 2016), (Stan et al., 2004).

1.8 Disorders of the proximal tubule

Renal disorders can be segregated either by aetiology or based on the site of lesion. In terms of site of lesion, the two macro-areas defined as glomerular disorders or disorders of the tubule-interstitium, the latter being the main focus of this thesis. In brief, glomerular disorders can present as nephrotic, thus involving deposition of immune complexes at the podocyte level without a direct involvement of the immune cells, or nephritic, where the immune complex deposition occurs at the filtration membrane level and it involves a local immune reaction performed by circulating and resident immune cells (Perlman et al., 2013).

1.3.1 Congenital disorders: disturbance of transport processes, polycystic kidney disease (PKD), nephropathic cystinosis, and congenital nephrotic syndrome.

The kidney can be affected by several inherited disorders that can cause progressive loss of organ function. Fanconi syndrome is a disorder of the proximal tubule which can be caused by acquired factors such as nephrotoxicity but it is more commonly induced by genetic mutations to genes NaPi-II, EHHADH, and HNF4A. It affects the reabsorption of solutes such as amino acids, glucose, uric acid, phosphate, and bicarbonate, resulting in excessive excretion of the solutes in the urine which, in turn, causes polyuria, dehydration, electrolyte loss, and metabolic acidosis (Kashoor & Batlle, 2019). Polycystic kidney disease is an inherited condition which leads to formation of multiple fluid-filled cysts in the kidneys which appear enlarged as compared to non-pathological organs, which progressively leads to renal damage and end-stage renal disease. Current available treatments focus on reducing renal volume by slowing the decline of the renal function (Finnigan & Leslie, 2022). Nephropathic cystinosis is a genetic condition caused by autosomal recessive mutations to the CTNS gene, which results in the accumulation of cystine crystals in all biological tissues due to impaired clearance of cystine from lysosomes, which in turn leads to corneal crystal deposition and proximal tubule Fanconi syndrome. If left untreated, the condition leads to end stage renal disease (ESRD) both for infantile and juvenile nephropathic cystinosis (Bäumner & Weber, 2018). Congenital nephrotic syndrome is a rare renal condition present since birth characterised by proteinuria, low blood protein concentration and oedema. The condition is largely caused by genetic defects affecting the components of the glomerular filtration barrier such as podocin and nephrin, the only effective therapy being organ transplantation. Before transplant, the disease is managed by intravenous albumin administration to prevent life-threatening oedema (Jalanko, 2009).

1.3.2 Metabolic disorders and diabetic nephropathy

The global increase in prevalence of metabolic disorders associated with obesity is reflected by a rise in prevalence of type 2 diabetes, which in turn leads to diabetic nephropathy. Other factors relative to the metabolic syndrome contribute to the progressive decline of renal function independently to the presence of type 2 diabetes, such as hypertension and high fat and sugar diets, although the molecular mechanisms underlying the relationship between these disorders and the impact on renal disease are yet to be understood. Diabetic nephropathy is initiated by a rise in glomerular filtration rate (GFR), glomerular hypertrophy and microalbuminuria; in case glycemia and systolic blood pressure are not pharmacologically

controlled they can contribute to further increase in GFR and renal injury (Maric & Hall, 2011). The changes in composition of the ultrafiltrate found in diabetic kidneys affect the proximal tubule, which in diabetic nephropathy is exposed to high concentrations of glucose and albumin. As a compensation mechanism, glucose is hyper-reabsorbed in the proximal tubule by upregulating transporter SGLT2. The rise in intracellular glucose concentration in proximal tubule cells leads to cellular functional damage mediated by hypoxia, inflammation, and oxidative stress, which in turn lead to scarring and tubule-interstitial fibrosis (Vallon, 2011).

1.3.3 Chronic kidney disease: pathogenesis, clinical manifestations, and available treatments.

Chronic kidney disease (CKD) is an irreversible, progressive disease that has a prevalence of 10 -13 % among the population. Patients remain asymptomatic until complications linked to renal disfunction arise, and it is characterized by loss of function of the renal parenchyma, that is, disintegration of the nephrons. Chronic kidney disease is diagnosed by evaluation of the glomerular filtration rate (GFR) when it has fallen below 60 mL / min / 1.73 m^2 of body surface area, proteinuria below 30 mg/day, histological anomalies at the biopsy level, and perturbations of the acid-base homeostasis (Obrador Vera, 2017). Until very recently, the only available treatments were aimed at preserving the remaining renal function or at replacing it via dialysis and transplant (Ferenbach & Bonventre, 2016). In April 2021, for the first time after 20 years, the Food and Drugs Administration (FDA) has approved a new compound for the treatment of CKD: the SGLT2 inhibitor dapagliflozin. Patients with advanced CKD are left asymptomatic because the kidney can compensate its own functional loss via compensatory hyperfiltration, which means that each nephron is subject individually to a state of hypertension to cope with the diminished hydrostatic pressure gradient between the glomerular capillary bed and the Bowman's capsule. This hypertensive state leads to further sclerosis and epithelial cell damage along the segments of the nephron, which in turn leads to excretory failure. Osmotically active ions such as Na^+ cease to be excreted hence leading to excessive water retention, which leads to systemic hypertension, heart failure, and pulmonary oedema. Metabolic acidosis and hyperkalaemia are also associated to CKD because of failure to regulate the homeostasis of the human body's internal environment. Hyperkalaemia leads to an increase in aldosterone-mediated K^+ transport in the distal tubule to enhance solute excretion, although deficient renin production due to damaged renal parenchyma can halt the triggering of the renin-angiotensin-aldosterone system, causing a potentially fatal rise in levels of K^+ in the blood. Metabolic acidosis is another risk in patients with CKD resulting from insufficient excretion of acids from the human body, which in turn can lead to a sudden decrease in blood pH. Furthermore, CKD can cause normocytic, normochromic anaemia due to decreased production in erythropoietin, and CKD-Mineral Bone Disorder which is an osteodystrophy caused by a decrease in renal production of 1, 25 – dihydroxycholecalciferol, a hormone which regulates Ca^{2+} reabsorption in the digestive tract and parathyroid hormone release, resulting in enhanced Ca^{2+} bone depletion (Perlman & Heung, 2019).

1.3.4 Acute kidney injury: pathogenesis, clinical manifestations, and available treatments.

While drug metabolism can take place in many organs such as liver, lung, gastrointestinal tract and kidney, the main route of excretion of xenobiotics and metabolites is the renal based.

Renal clearance is defined as the process of drug elimination from the body performed by the kidney, shown quantitatively as the volume of plasma cleared of drug by the kidney per unit of time (Hon, 2016). Because of the prominent role of the kidney in drug elimination, potential nephrotoxic compounds are filtered by the glomerulus into the tubular lumen where the apical side of the proximal tubule is exposed to high concentrations of xenobiotics, as compared to other segments of the nephron, while the basolateral side of the epithelium is exposed to the nephrotoxic drug still present in the plasma contained in the peritubular capillaries. Furthermore, once xenobiotics and metabolites reach the apical tubular side, they are transported inside the proximal tubule cell (Perazella, 2019). Drug uptake in the apical compartment takes place via endocytosis carried out by the glycoproteins megalin and cubilin. Megalin is a low-density lipoprotein (LDL) receptor, and it has many ligand binding domains, while cubilin is a large multiligand, peripheral membrane protein. These two proteins perform the endocytic uptake of several endogenous ligands such as vitamin-binding proteins, lipoproteins, and hormones (Christensen & Birn, 2002). Some of the drugs taken up via megalin/cubilin endocytosis are cationic aminoglycosides and heavy metals. The pharmacology behind aminoglycosides-induced nephrotoxicity has been described in detail: once they are taken up by megalin/cubilin, they accumulate into the lysosomal compartment and form myeloid bodies (fragments of damaged organelles), causing cell damage and death. The clinical presentations of this injury cascade are proximal tubulopathy and acute kidney injury (AKI) (Perazella, 2018). AKI occurs in 20 to 30% of patients in intensive care units, 6% of this cohort eventually requiring renal dialysis (Pannu & Nadim, 2008). Acute kidney injury is defined as a sudden and severe impairment of kidney function reflected by a drastic decrease in glomerular filtration rate which clinical presentation frequently involves mixed aetiology including nephrotoxicity, sepsis and adverse cardiovascular events. In the clinical setting, AKI is classified in the three categories of pre-renal AKI, when changes in the perfusion of the renal vasculature lead to GFR decrease, post-renal AKI, which is related to urinary tract obstruction which, in turn, leads to inflammation of the renal parenchyma and impaired blood flow, and intrinsic AKI, which is classified based on the site of injury rather than on the type of insult, such as tubular, glomerular, interstitial, and vascular (Makris & Spanou, 2016). Patients in critical care are often treated with multiple medications: this is necessary because of the complexity of critical illnesses, but it can lead to drug-drug interactions that, in turn, cause nephrotoxicity. In fact, concurrent use of multiple nephrotoxic antimicrobial agents, such as neomycin, gentamycin, tobramycin and amphotericin B, is unavoidable in intensive care units (Pannu & Nadim, 2008). Another pathway of drug-induced proximal tubule injury takes place via basolateral uptake of solutes from the peritubular vascular compartment: this is enabled by members of the organic anion transporters (OATs) and organic cation transporters (OCTs) families. Drugs compete with endogenous metabolites to be taken up by these transporters from the plasma contained in the peritubular capillaries, and once inside the proximal tubule cell they exit via apical transporters. In the presence of loss-of-function mutations to genes encoding for the apical efflux transporters, nephrotoxic drugs accumulate inside the proximal tubule cell, instead of being secreted in the urine, causing tubular necrosis. Examples of drugs that follow the basolateral pathway are the cancer chemotherapeutic cisplatin, transported by OCT-2, and tenofovir, transported by OAT-1 (Perazella, 2018). Increased drug concentration in the proximal tubule cell leads to the formation of reactive oxygen species

(ROS), reactive nitrogen species, and oxidative stress which, in turn, trigger inflammation and apoptosis, disrupts protein and DNA synthesis, and cellular repair (Perazella, 2019). The cytokine TNF-α and its proinflammatory pathway have shown to be involved in the nephrotoxic response to intracellular drug accumulation, especially in studies regarding cisplatin-induced AKI where cisplatin seems to be inducing upregulation of TNF-α expression (Ramesh & Reeves, 2004). Another mechanism of drug-induced tubular injury is crystalline-induced tubular injury, which takes place when drugs cleared via renal clearance are insoluble in the urine. This occurs more frequently in patients with reduced urinary flow rates, altered urine pH and in overdose cases. Drugs that follow this nephrotoxicity pathway are methotrexate, acyclovir, ciprofloxacin, and indinavir (Perazella, 2019).

1.3.5 Transition from AKI to CKD

Acute kidney injury (AKI) can have long term consequences on the renal parenchyma, as growing clinical evidence demonstrates the existence of a correlation between AKI and chronic kidney disease (CKD). AKI seems to be a risk factor for CKD, but despite the large number of studies carried out on patient databases, the pathophysiology and the molecular mechanisms underlying the transition from AKI to CKD are still under investigation. Both conditions share several "actors" and processes that seem to be at the centre of what eventually will lead to renal fibrosis: damage to the tubular epithelial cells with subsequent scarring, fibroblast recruitment and activation to myofibroblast, macrophage and other immune cells infiltrating in the interstitium, and capillary rarefaction. Specifically, capillary rarefaction in the glomerulus and the peritubular capillaries could be acting as trigger for the cascade of events that lead to progressive renal fibrosis, which is defined as scarring of the renal parenchyma leading to loss of organ function, as it leads to hypoxia and generation of reactive oxygen species (ROS). The reason why fibrosis arises after acute kidney injury could be because it benefits the rapid healing process that the renal parenchyma undergoes right after the nephrotoxic insult: histological studies on patients' biopsies show that scarring occurs in a self-limiting fashion where tubules have failed to repair themselves, which suggests that other inputs are needed for the renal fibrosis process to become self-perpetuating. Most recent experimental studies point at the tubular epithelial cell as the main driver of the transition from AKI to CKD. After injury, these cells can acquire both pro-fibrotic and pro-inflammatory phenotype since they can secrete a plethora of cytokines (e.g. TGFβ, TNFα, and IL-6) thus modifying immune cells' behaviour. Injured tubular epithelial cells can dedifferentiate into their mesenchymal predecessors thus expressing mesenchymal markers such as vimentin, becoming able to proliferate, and then lose the mesenchymal marker by re-differentiating into functional epithelial cells to overcome injury. This process is known as partial epithelial to mesenchymal transition (pEMT) will be discussed in detail in the next section (1.3.6), the focus being the *de novo* proliferative capacity acquired after injury by the tubular epithelial cell. At this stage, cell cycle events could influence the progression of a singular event of tubular injury to self-sustained fibrosis, thus creating a pro-inflammatory milieu that promotes fibrosis which underlies CKD (Guzzi et al., 2019).

1.3.6 Renal fibrosis in the proximal tubule: the role of proximal tubule cells and renal fibroblasts in fibrosis, partial epithelial-to-mesenchymal transition, dedifferentiation, and cell cycle dysregulation.

Renal fibrosis is a complex phenomenon that involves the proximal tubule interstitial interface, its milieu, and the cell types it comprises. Histologically, it is described as an increased deposition of extra-cellular matrix (ECM) in the tubule-interstitium which, in turn, leads to a loss of renal function. The primary causes underlying renal fibrosis can be nephrotoxic, mechanical, metabolic, and immunological injuries. One of the main culprits of this degenerative process in the kidney is the renal fibroblast, a mesenchymal cell which is the main producer of ECM and that can be activated into a contractile cell called myofibroblast. Furthermore, myofibroblasts can produce much more ECM than their inactivated peers. These cells arise not only from fibroblast activation but also from epithelial cells, endothelial cells and pericytes. All these cells end up participating in the excessive deposition of ECM which replaces functional tissue and vasculature which in turn leads to hypoxia. TGFβ1 is considered to be the most potent pro-fibrotic endogenous compound known (Hewitson, 2012). Concomitantly, during the pathogenesis process, proximal tubule epithelial cells are subject to epithelial-to-mesenchymal transition, whereby these cells are thought to acquire contractile properties and lose their specialized solute transporter and barrier function. Disintegration of proteins that make up the tight junctions such as ZO-1 and E-Cadherin, upregulation of mesenchymal markers such as vimentin, and increased motility are key events in this process. Whether proximal tubule cells can transition completely to the mesenchymal phenotype *in vivo* is still up for debate, as the most recent studies point towards the 'partial epithelial-to-mesenchymal transition' theory which entails tubular epithelial cells partially dedifferentiating and co-expressing epithelial and mesenchymal markers while remaining attached to the basement membrane. As explored in **1.3.5**, there is an epidemiological correlation between acute kidney injury (AKI) and chronic kidney disease (CKD), which has been confirmed by *in vivo* studies (Belayev & Palevsky, 2014).

According to Allison S. (Allison, 2015) epithelial-to-mesenchymal transition (EMT) can be classed as a cellular event found in renal fibrosis, despite the relevance of such mechanism to the development of the disease and the overall contribution to the myofibroblast population not having yet being clearly elucidated. The two studies considered in this research highlight review piece demonstrate that partial EMT is crucial in the aetiology of renal fibrosis. Grande MT, *et al*. reveals that Snail1 reactivation in renal epithelial cells is crucial for fibrosis development, inducing partial epithelial-to-mesenchymal transition (EMT) (Grande, Sánchez-Laorden, López-Blau, De Frutos, et al., 2015). Furthermore, the research demonstrates that Snail1-induced fibrosis can be reversed in vivo, offering potential avenues for novel anti-fibrotic therapies in the treatment of obstructive nephropathy. The second study by Lovisa S., *et al.* also focuses on two transcriptional regulators of EMT, namely Twist1 and Snai1, which were knocked out in experimental mice, demonstrating that the renal tubular cells in these mice were protected against several renal insults and renal fibrosis was attenuated. Furthermore, previous studies from the same group highlighted a potential link between cell cycle arrest of tubular epithelial cells and chronic kidney disease: the Twist1 and Snai1 knockout mice were used to demonstrate that EMT contributes to the lack of cell cycle

progression found in renal fibrosis. In fact, this study draws the conclusion that the activation of the EMT program leads to tubular epithelial cells losing key transporters and partial inability to proliferate (Lovisa et al., 2015). In the seminal work published by LeBleu *et al.* multiple murine experimental models were used to investigate the origin and function of myofibroblasts in the context of renal fibrosis, using models that allowed for visualization of α smooth muscle actin (αSMA), which is a key marker of contractility in myofibroblasts, and fate mapping techniques. After unilateral urinary obstruction (UUO) was performed on the experimental animals, it was demonstrated that a high number of myofibroblasts could be found in the renal interstitium, whereas this phenomenon was rarely seen in healthy mice. The study considered the finding of many different research groups in regard to the origin of myofibroblasts in kidney fibrosis, as several theories involving EMT, EndoMT, and the conversion of pericytes into myofibroblasts were cited. The authors demonstrate and conclude that, after pro-fibrotic damage has occurred, myofibroblasts arise from two main sources: about 50% arise from proliferation of resident renal fibroblasts, whereas 35% derive from bone marrow-derived mesenchymal stem cells under TGFβ1 stimulus. Fate mapping experiments show that 5% of these myofibroblasts derive from tubular epithelial cells that have undergone full EMT, and 10% derive from endothelial cells that have been subjected to EndoMT, despite many epithelial cells showing de novo acquisition of αSMA without having fully transdifferentiated to myofibroblasts (LeBleu et al., 2013). With this premise, a number of studies considered and cited in a review article regarding the role of partial epithelial-to-mesenchymal transition by Sheng and Zhuang (Sheng & Zhuang, 2020a) have pointed towards the idea that, despite epithelial cells still acquiring some of the mesenchymal features presented by fibroblasts and myofibroblasts, it seems more likely that tubular epithelial cells in the kidney only partially transition to this state rather than fully differentiating into mesenchymal cells. The activation of pEMT pathways, which involve TGFβ1, lead to G2/M cell cycle arrest, which in turn leads to improper tubular cell proliferation after injury, whether chronic or acute. Interestingly, the induction of a "partially activated" phenotype in tubular epithelial cells could be sufficient to induce such cells to produce a pro-fibrotic secretome which is initially useful in response to injury but contributes to the maintenance of an inflammatory and, subsequently, fibrotic milieu in the renal interstitium. The response to injury from epithelial cells in the kidney has been investigated in depth, as they are known to lose polarity, key transporter function, change their morphology and acquire migratory type, whilst displaying a pro-inflammatory phenotype. Alongside these notions, injured epithelial cells are also expected to exert a phenotype typical of the embryonic mesenchyme, as during nephrogenesis they express αSMA while transitioning into mature epithelium. According to Humphreys BD, *et al.* the framework used to describe epithelial-to-mesenchymal transition in response to injury could be misleading as it assimilates the phenotype that injured tubular epithelial cells have acquired to survive within a hostile environment to the one of epithelial cells during nephrogenesis, without taking mentioning the pathological secretome that these cells exert after injury. The authors are very clear about the fact that despite renal epithelial cells *in vitro* have proven to up-regulate mesenchymal and fibroblast genes and to deposit collagen fibrils after pro-fibrotic treatment or nephrotoxic insult, there is little evidence that such process might be happening *in vivo* (Humphreys et al., 2010). The controversy around EMT and its involvement in the progression of fibrosis has interested other organs such as

lungs and liver. In a very comprehensive review article, Kriz W, *et al*. put in perspective the hypothesis that renal tubular epithelial cells can downregulate epithelial markers and upregulate mesenchymal ones in response to injury, which gives them the ability to transmigrate through the tubular basement membrane and settle into the renal interstitium as ECM-producing myofibroblasts. The authors suggest that the *de novo* expression of markers such as vimentin, αSMA, and the loss of tight junction markers by epithelial cells are not unequivocally associated with EMT, although the experimental studies supporting EMT seem to usually acknowledge such concept as a fact without disputing its centrality and validity in the context of the progression of renal fibrosis. This article also supports the view that most recent pro-EMT studies are carried out *in vitro*, whereas there does not seem to be a wide enough body of evidence *in vivo* to support this hypothesis as one of the larger sources of myofibroblasts in the kidney (Kriz et al., 2011). Having considered the different views present in the relevant literature around EMT, my personal opinion based on the studies carried out *in vitro* in renal epithelial cells and fibroblasts undergoing pro-fibrotic stimuli, supports the one around the triggering of partial epithelial-to-mesenchymal transition after injury, marked by a loss of epithelial barrier function but retention of some epithelial features such as tight junction markers in a dysregulated manner.

Cell proliferation is recognised as a repair mechanism which is at the basis of the wound healing cascade, and it is affected differently in tubular epithelial cells and renal fibroblasts. In a non-fibrotic state, the renal cell pool undergoes very little turnover as most cells in the tubule-interstitium are considered to be in G_0 phase of the cell cycle (quiescent). Depending on the degree and type of injury, different renal cell types can re-enter the cell cycle or enter cell cycle arrest (Y. S. Wu et al., 2021). After injury akin to AKI, renal epithelial cells are thought to proliferate and differentiate to cover any gaps on the basement membrane; whereas after sustained and repeated cytokine-mediated stimuli *in vivo*, like in CKD, tubular epithelial cells seem to undergo G2/M cell cycle arrest (L. Yang et al., 2010). Conversely, renal fibroblasts which are normally found in quiescent state in the interstitium, over-proliferate and transition to myofibroblasts when stimulated with pro-fibrotic cytokines thus being found in the S phase of the cell cycle (Y. S. Wu et al., 2021). Upon the initiation of EMT/pEMT in proximal tubule cells, epithelial barrier function dysregulation, loss of cell-cell tight junctions, and *de novo* acquisition of mesenchymal markers take place (Lamouille et al., 2014). Therefore, tight junction markers ZO-1 (zonula occludens 1), E-cadherin and vimentin could be considered as suitable biomarkers of EMT/pEMT in histological investigations. With regard to renal fibroblasts, when undergoing fibrotic stimuli, they are activated into myofibroblasts which produce an excess of ECM. This phenotypical change could be detected by measuring acquisition of α smooth muscle actin (α-SMA) by renal fibroblasts as well as detecting an increase in collagen I and fibronectin production.

TGFβ1 is regarded as the driver of renal fibrosis, with large bodies of evidence supporting the theory proposing that this pleiotropic cytokine can promote epithelial-to-mesenchymal transition in renal epithelial cells and fibroblast-to-myofibroblast activation in renal fibroblasts, both *in vivo* and *in vitro.* The effects of TGFβ1 are mediated by TGFβ type 2 receptor (TβRII) which phosphorylates the TGFβ type 1 receptor leading to activation of intracellular signalling pathways, in particular Smad signalling. TGFβ1 has very different

effects on tubular epithelial cells as compared to renal fibroblasts: it has been shown to induce apoptosis, reduced proliferation, and dedifferentiation in the former, whereas it enhances proliferation, myofibroblast transdifferentiation and ECM deposition in the latter by stimulating the transcription of genes encoding for collagen I and fibronectin. Moreover, TGFβ1 promotes dedifferentiation in hPTC, which acquire a migratory phenotype and *de novo* expression of α smooth muscle actin (α-SMA), and become capable of depositing collagen I, collagen IV, and fibronectin in the tubule-interstitium (Gewin & Zent, 2012). The second pro-fibrotic compound in order of importance as found in the current literature seems to be TNFα, a pleiotropic proinflammatory cytokine which is generally upregulated in chronic inflammatory states. In the kidney, it is produced and secreted mainly by immune cells, but also endothelial and epithelial cells contribute to its release. TNFα is secreted as a plasma-membrane protein by the metalloproteinase TNFα converting enzyme (TACE), and it binds to two receptors, TNFR1 and TNFR2, to exert its effects on target cells (Ramseyer & Garvin, 2013). Alongside its pro-apoptotic properties, TNFα has shown to induce epithelial-to-mesenchymal transition (EMT) on renal epithelial cells *in vitro* (Wan et al., 2013). Importantly, TNFα increases the response of the proximal tubule to angiotensin II (Ramseyer & Garvin, 2013). Another compound that seems to be at the focus of much research in the field is angiotensin II: this peptide hormone is an effector of the renin-angiotensin-aldosterone system (RAAS) which controls blood pressure. At the proximal tubule level, this compound influences Na^+ and H_2O reabsorption thus being associated with hypertension. Evidence suggests that intermittent activation of RAAS contributes to tubule-interstitial fibrosis progression. Angiotensin II binds to receptors AT1 and AT2 which are expressed by proximal tubule cells; specifically, AT1 mediates to an increase in production of reactive oxygen species (ROX) which, in turn, leads to EMT. In summary, angiotensin II contributes directly to renal fibrosis by upregulation of pro-fibrotic growth factors, promotion of EMT, and ECM deposition (Chen et al., 2012). As the correlation between AKI and CKD has been taken into consideration as a risk factor in the progression of renal fibrosis in the tubule-interstitium, the nephrotoxic compound polymyxin B can be introduced as case-study for this transition *in vivo* and *in vitro*. Polymyxin B is an antibiotic against Gram-negative bacteria which use was discontinued due to nephrotoxic events in patients. The proximal tubule is known to be the site of cellular injury, resulting in acute kidney injury that can lead to renal failure if left untreated. Polymyxin B accumulates and interferes at the mitochondrial level of the tubular epithelium, resulting in the generation of reactive oxygen species, cellular injury and apoptosis (de Fátima Fernandes Vattimo et al., 2016).

When considering measurements regarding renal injury, it is now necessary to involve in the discourse release of stress biomarkers specific for the kidney. The classical methods of assessing kidney injury in the clinic revolved around measurements of serum creatinine and blood urea nitrogen. At the cellular level, the proximal tubule is considered to be the main site of nephrotoxic injury as its anatomical location, right after the glomerulus, exposes it to high concentrations of xenobiotics, it expresses several drug transporters that exchange solutes between the blood stream and the lumen, and it is highly metabolically active. For these reasons, investigations have focused on unravelling pathways that lead to tubular toxicity and the hallmarks associated with these phenomena, such as the FDA-approved triad

of proteins kidney injury molecule-1 (KIM-1), clusterin, and neutrophil gelatinase-associated lipocalin (NGAL) (Griffin et al., 2019). The search for suitable soluble biomarkers predictive of kidney injury has intensified in the recent years due to the ubiquitous global prevalence of both acute kidney injury (AKI) and chronic kidney disease (Tummalapalli et al., 2016). Although some renal injury biomarkers, such as kidney injury molecule 1, were first discovered due their increase in secretion in patients' urine after AKI (Bonventre, 2008), there is now an interest in investigating the correlation between CKD and KIM-1 excretion. KIM-1 is made up of a cytoplasmic and an extracellular portion and its identified as a type I membrane protein. It is shed in urine after renal injury (Song et al., 2019). The literature on the relationship between KIM-1 and CKD is conflicting, with some clinical studies reporting a correlation between renal function decline and rise in KIM-1 excretion, and others not having found a significant correlation between the two phenomena (Tummalapalli et al., 2016). Clusterin is a glycoprotein which is found in several tissues and fluids in the human body, but it is infamously known for being upregulated in *in vivo* models of kidney injury. Its role in renal tissues is unclear, although some investigations point towards a potential protective and anti-inflammatory role after injury (Guo et al., 2016). Neutrophil gelatinase-associated lipocalin (NGAL) is a protein expressed by various epithelial cells that interacts with solute transporters. It is deemed to be an early biomarker of acute kidney injury (AKI) and it is associated with the response to tubular epithelial damage (Soni et al., 2010). The soluble measurable endpoints discussed so far concern the epithelial component of the proximal tubule interstitial interface, hence a different class of biomarkers shall be considered to assess response to pro-fibrotic stimuli by other components of the fibrotic *milieu*, such as human renal fibroblasts. Chemokines are chemotactic cytokines: their main feature is the ability to recruit leukocytes during the inflammatory response. These cytokines are divided in four families; different cellular components of the immune system respond to different families as they express specific chemokine-associated receptors. In the kidney, chemokines can be secreted by interstitial fibroblasts, epithelial tubular cells, podocytes, ad endothelial cells upon inflammatory stimulation. Among the chemokine families, presence the CXCL family in the renal tissue is associated with AKI whereas presence of CCL chemokines seems to be associated with chronic inflammation and chronic kidney disease, in particular MCP-1 and IL-8 are associated with progressive renal disorder (Chung & Lan, 2011).

1.4 In vitro models of the proximal tubule

1.4.1 2D human *in vitro* models of the proximal tubule

Among the segments of the nephron, the proximal tubule is considered an important area with regards to drug handling and subsequent nephrotoxicity. To gain understanding of how each apical and basolateral transporter interacts with potentially toxic compounds, extensive efforts have been put in the *in vitro* modelling of the proximal tubule. Several studies have shown that proximal tubule cells can be cultured on permeable membranes, so called "2D-models", while retaining segment-specific markers, functional expression of transporters, and injury-related biomarker release after nephrotoxic insult. Brown *et al*. describe the isolation of human proximal tubule epithelial cells (HPTECs or hPTC) from fresh human kidney which are subsequently cultured on membranes forming a monolayer. In this pivotal study, hPTC show to retain their epithelial phenotype and expression of several transporters such as NaPi-IIa, SGLT1, SGLT2, OCT2, OCTN2, OAT1, OAT3, OAT4, MDR1, MRP2, and BCRP both at mRNA and protein level. OAT1 and OAT3 transporter function is validated via para-aminohippuric acid (PAH) uptake assay, while OCT-2 and MDR-1 functionality is proven via creatinine uptake assay (Brown, Sayer, Windass, Haslam, de Broe, et al., 2008). Because of low availability of fresh human tissue, other 2D proximal tubule models have been developed with the use of conditionally immortalized proximal tubule cells (ciPTEC). These cells are derived from healthy donors and they endogenously retain metabolic enzyme and some transporter function, but over culture time expression of OAT1 and OAT3 is lost (Vriend et al., 2021). To overcome this issue, stable OATs expression is induced via transduction (Nieskens et al., 2016). Furthermore, induced expression of transporters involved in drug handling in ciPTEC had been validated also for BCRP, MRP-4 and P-gp (Caetano-Pinto et al., 2016). However, the use of ciPTEC has several limitations, and also, the possibility of only being able to induce expression of a restricted number of transporters without losing epithelial phenotype after few passages. Recent advances in stem cell technologies, have led many research groups to produce induced pluripotent stem cells (iPSCs)-derived kidney tissue for nephrotoxicity and drug discovery scopes. This technology allows the reversal of adult somatic cells to a pluripotent state similar to their transient embryonic state and "coax" their differentiation towards one specific cell type. To direct the differentiation of iPSCs towards nephrons, protocols try to recapitulate embryonic renal development. The kidney arises from the embryonic mesoderm: specifically, the collecting ducts from the ureteric bud and the nephrons from the metanephric mesenchyme. Using a combination of growth factors involved in signalling pathways relevant during in vivo nephrogenesis, it has been possible to generate iPSCs-derived nephrogenic progenitors that lead to the formation of self-organizing organoids and segment-specific monolayers (Little, 2016). It has been demonstrated that iPSCs can be differentiated into proximal tubule cells (Kandasamy et al., 2015) and into podocytes monolayers (Rauch et al., 2018). So far, two protocols have been published which report the establishment and characterisation of proximal tubule cells showing appropriate tubular epithelial marker expression and functional transporter activity (Kandasamy et al., 2015), (Chandrasekaran et al., 2021). With such progress in development of renal epithelium from stem cell, would allow the generation of expandable patient-specific nephrotoxicity platforms soon.

1.4.2 3D human *in vitro* models of the proximal tubule: existing models, use in research, limitations

The described 2D proximal tubule models are invaluable tools for nephrotoxicity testing but they have several limitations. Despite being relatively simple to culture and their low cost, 2D culture hPTC dedifferentiate quite quickly and only grow on one plane, which does not replicate *in vivo* tubular structure. Furthermore, *in vivo* proximal tubule cells are surrounded by other cell types that form a physiological microenvironment which is hard to replicate in 2D culture. Conversely, 3D proximal tubule models have shown to be more suitable for the *in vitro* to *in vivo* translation of data collected in nephrotoxicology studies: these models have demonstrated to be more sensitive to toxic compounds as compared to 2D models using the same cell type (Sánchez-Romero et al., 2016). One of the first breakthroughs in 3D proximal tubule modelling was achieved by Humes et al. in 1999 when developing a system to improve renal substitution therapy that could also have metabolic and transport activity, which was lacking in haemodialysis. hPTC were seeded around high-flux hollow-fibre cartridges coated in synthetic extracellular matrix (ECM) that were used as tubular scaffolds. A bioreactor was used to promote cell growth and expansion (Humes et al., 1999). Another study that aimed at the production of a bioartificial kidney to enhance clearance of metabolic toxins in haemodialyzed patients from Jansen et al., described the use of hollow fibres to enable the formation of a 3D ciPTEC monolayer paired with a flow system: the study demonstrated toxin secretion into the urine and transporter activity in ciPTEC (Jansen et al., 2016). One of the advantages of 3D cultures is the possibility of including extracellular matrix in the model. *In vivo*, renal cells are embedded and supported by the ECM which is composed by collagen IV, laminin, fibronectin and proteoglycans. The composition of this “endogenous gel” changes under pathological conditions and it plays a key role both as trophic support and in tissue regeneration. Astashkina *et al*. have developed a 3D model using primary hPTC where cells are embedded in hyaluronic acid-derived gel: cell-matrix interactions have shown to positively affect epithelial phenotype in culture, providing a more physiologically relevant response to exposure to nephrotoxic compounds (Astashkina et al., 2012). Moreover, the advent of microfluidics in the 3D modelling field has led to interesting developments. *In vivo*, tubular epithelial cells are exposed to continuous fluid flow: replicating these physiological conditions has become possible thanks to the development of kidney microchips. These microfluidic devices use microchip technology which is a cell culture system on micrometric scale that integrates fundamental aspects of native kidneys such as morphological features, co-culture, flow shear stress and mechanical strain. Ferrel et al. have developed a microfluidic renal epithelial cell culture system that incorporates electrodes for the measurement of transepithelial electrical resistance (TEER), to monitor cell growth and confluency, composed of apical and basolateral microfluidic chambers. Flow conditions in the model are meant to replicate the physiological state of the kidney (Ferrell et al., 2010). Recently, Vriend *et al*. have illustrated the culture of ciPTEC on the microfluidic plate OrganoPlate® to develop high-throughput screening assays to investigate drug-transporter interactions. Besides the limitations arising from the use of an immortalize cell line, this 3D platform has demonstrated to be suitable for several endpoint read-outs, such as transporter functionality studies, transporter expression studies, confocal imaging, and quantitative imaging assays (Vriend et

al., 2018). As previously mentioned, *in vivo* proximal tubule cells, on their basolateral side, are resting on the basement membrane and embedded in the ECM, which contains resident renal fibroblasts, which in turn is in contact with the peritubular capillaries. Lin *et al*. have developed a 3D vascularized proximal tubule model called 3D VasPT where two adjacent tubules are covered in confluent epithelial and endothelial monolayers, embedded in a permeable ECM. The two tubular structures are bio-printed and then perfused to investigate renal reabsorption and secretion. This model allows further investigation of epithelial-endothelial crosstalk which can be suitable for modelling of renal diseases which pathophysiology involves both cell types (Lin et al., 2019a). Another study uses a 3D bioprinting platform to develop a kidney-on-a-chip comprising endothelial cells (HUVEC, Human Umbilical Vein Endothelial Cells), renal fibroblasts and proximal tubule cells. The model shows extensive microvascular formation and ECM deposition, that prove to have a trophic effect on hPTC polarization (King et al., 2017)

1.5 Models of renal tubule-interstitial fibrosis

1.5.1 Animal models of CKD: the unilateral ureteral obstruction model (UUO).

Over the past few decades, the approach in regard to the use of animal models of disease in the UK and globally has shifted towards the principle of the 3Rs. These involve the replacement, reduction, and refinement of the techniques and technologies used to house and treat animals in laboratories. The first principle, which is the most relevant to this thesis, invites scientists to avoid altogether the use of animals to address scientific questions, which prompts us to focus on the development of robust *in vitro* assay platform that can predict in vivo outcomes. Even though enormous progress has been made in the recent past to advance the *in vitro* technology, animal models are still useful for example to study disorders that affect several organs or system within the same biological being. The principle of reduction prompts researchers to design and analyse experiments involving the use of animals in a reproducible and robust fashion, in order to reduce the number of animals used to answer a research question. Lastly, the principle of refinement requires scientists to focus on the welfare and wellbeing of the research animals used in experiments, employing the most advanced technologies to ensure minimal suffering and harm to the animals used. National public institutes such as the National Centre for the 3Rs in the UK provide funding and guidance for researchers that work in the field of disease modelling, with a push towards the development of *in vitro* models as close as possible to the tissue of interest. Specifically, this PhD project was carried out entirely with human primary tissue and human cell lines following the first principle of the 3Rs.

In vivo animal models of disease are currently the gold standard of disease modelling to investigate the mechanisms that lead to the pathological state, to identify new drug targets and to screen for safety and efficacy of novel compounds. Experimental animals are very different from humans in terms of gene and protein expression, *in vivo* experiments can be long and expensive, and they pose serious ethical questions to researchers handling them. Thanks to new enlightened policies from the European regulatory bodies, with regard to animal experimentation there has been a push towards the ethical principle of the 3Rs,

replace, refine, reduce, which promoted the development of tissue engineered human disease platforms (DesRochers et al., 2014).

Several *in vivo* models of CKD have been developed over the last few decades, mostly in rodents such as mouse and rat. These models provide insight in the systemic effects of the disorders and offer a source of clinically accepted measurements of disease progression such as glomerular filtration rate (GFR), blood urea nitrogen (BUN), and albuminuria.

Glomerular and tubule-interstitial fibrosis can develop spontaneously on rodents with certain genetic backgrounds. MRL/lpr and NZB/W mice can develop lupus nephritis that resembles the human syndrome at the histological level, Sprague-Dawley rats face a progressive decline in GFR and increase in albuminuria with ageing, the self-explanatory spontaneously hypertensive rats (SHR) develop primary hypertension that ultimately leads to CKD, while the Buffalo/mna rat is useful to study glomerular fibrosis as they incur in spontaneous podocyte effacement and proteinuria. Other *in vivo* models of disease have been genetically engineered to study the specific involvement of certain genes or mutations in podocytopathies or genetic disorders such the Alport syndrome. More interestingly, acquired models of CKD include the immune-induced models Thy-1 nephritis and anti-GBM, where an immune response against parts of the glomerulus itself is triggered by administering an antibody against antigens expressed in the nephron. Non-immune CKD models allow for more progressive renal fibrosis to develop; for example, the 5/6 nephrectomy, or sub-total nephrectomy, resembles the loss of functional renal mass which occurs in humans after acute renal failure. The compensatory hypertension leads the rodent's kidney to glomerular sclerosis and tubule-interstitial scarring. Radiation nephropathy is induced by administering a local dose of radiations to the rodent's kidneys: capillary rarefaction and hypoxia are the first signs of renal fibrosis, followed by injury carried out by complex cross-talk between endothelial, tubular cells and the interstitium. Furthermore, nephrotoxic compounds can be administered to the rodent to induce glomerular damage; these include administration of adriamycin and puromycin, folic acid, cyclosporin A, and deoxycorticosterone acetate (DOCA) (H.-C. Yang et al., 2010).

Finally, one of the most relevant models to investigate tubule-interstitial fibrosis is the unilateral ureteral obstruction (UUO) model. This model is very palatable for high throughput studies as it is highly reproducible, efficient in terms of disease progression, and the non-diseased kidney can be used as control for histological investigations. Human chronic obstructive nephropathy is mimicked in murine models by the unilateral ureteral obstruction (UUO) model whereby regular urine flow is obstructed. This condition eventually leads to renal fibrosis via previously described molecular mechanisms and cell signalling pathways. Once the obstruction is removed, the recovery from the progressive damage can be helped by treatments that halt the progression of fibrosis. The animal *in vivo* model provides an accelerated version of the human condition, making it suitable for pharmacological treatment testing (Martínez-Klimova et al., 2019a). Unilateral ureteral obstruction is achieved by surgical ligation of one of the two ureters with a fabric thread. The operation is performed on anesthetised rodents on a warm plate. The first physiopathological events to occur after ureter ligation are a decrease in GFR, activation of the renin-angiotensin-aldosterone system (RAAS), and vasoconstriction that leads to initial apoptosis of tubular and endothelial cells.

Oxidative stress takes place as a consequence of RAAS activation, thus leading to the start of the immune-mediated inflammatory process which involves the production by the tissue itself of pro-inflammatory cytokines such as TGFβ1 (transforming growth factor 1), TNFα (tumour necrosis factor α), and NF-κβ (nuclear factor κβ) which attract leukocytes. Furthermore, the pro-inflammatory cell signalling pathways TGF-β/Smad and Wnt/β-catenin are activated, the latter pathway having as one of its protein targets the transcription factor Snail1 (Martínez-Klimova et al., 2019b), which seems to be at the centre of the epithelial-to-mesenchymal transition "dedifferentiation programme" since it leads epithelial cells to acquire migratory/proliferative phenotype, loss of E-Cadherin, and de novo deposition of fibronectin circumscribed to the tubules without the involvement of myofibroblasts (Grande, Sánchez-Laorden, López-Blau, de Frutos, et al., 2015). As previously mentioned, immune-mediated inflammation progresses because epithelial, endothelial, and interstitial cells release cytokines and chemokines that lead to the recruitment of macrophages and monocytes to the tubule-interstitium: due to a positive feedback mechanism, these immune cells start secreting their own TGF-β and TNFα, thus contributing even further to the creation of a pro-inflammatory milieu. TGF-β also triggers the transition of resident renal fibroblasts to contractile myofibroblasts, which under these conditions increase their deposition of extracellular matrix (ECM) in the interstitium. All these cellular events to lead to what is known as fibrosis, which is a somewhat histological term to describe the scarring or sclerosis that is visible in *ex vivo* sections once the disease has progressed in the animal (Martínez-Klimova et al., 2019b). Although the non-ligated kidney had been used as negative control for many years, this did not take into consideration the systemic effects that the progressive renal disorder would have on the whole biological system, thus leading the non-ligated kidney to compensatory hyperfiltration which skews any potential readout obtained from the control kidney (Atkinson et al., 2021).

1.5.2 Human *in vitro* models of renal fibrosis

Having acquired a large amount of knowledge about the progression of renal fibrosis in animal models, there is a push to translate these findings in models that can resemble closely the cellular and molecular events which have been described so far in the human being. As such, the closest model attainable to a human being is to use cells which once belonged to a human kidney, whether these cells have been immortalized, reprogrammed, or transfected will determine how close the disease is to the clinical presentation, at the histological and molecular level. The high prevalence of CKD and the call for more complex, high throughput *in vivo*-like tissue engineered kidney models has led to development of some kidney fibrosis *in vitro* models. In 2007, Kopp's research group proposed two TGFβ1 fibrosis-induced 2D *in vitro* models using HK-2 cells and fibroblasts from different origin. After pro-fibrotic stimulation both mesenchymal and epithelial cells formed nodules and increased extracellular matrix production. Inhibitors of the TGFβ1 pathway were added after injury had taken place to highlight the potential use of the nodule formation assay and ECM accumulation assay as high throughput platforms for discovery of anti-fibrosis compounds (Q. Xu et al., 2007). In a study from Wang et al., NRK49F rat renal fibroblasts were treated with TGFβ1 to mimic the renal fibrotic milieu. Automated microscopy was used to screen a library of 340 potentially anti-fibrotic compounds from the Traditional Chinese Medicine and select

those which could decrease ECM accumulation and revert αSMA+ phenotype (X. Wang et al., 2018). In a study from 2013, Zhou et al. have established a renal fibrosis model on a microfluidic platform using HK-2 cells that shows it is possible to induce and quantify epithelial to mesenchymal transition (EMT) via immunofluorescence staining for αSMA, FSP-1 and loss of E-Cadherin, which are three different key markers of epithelial-to-mesenchymal transition. E-Cadherin and other tight-junction markers such as Zonula Occludens-1 (ZO-1) are expressed by renal epithelial cells when they form a leak-tight monolayer in culture and epithelial barrier function is present, while mesenchymal markers such as αSMA and FSP-1 are acquired by said cells when the transition to mesenchymal phenotype takes place (M. Zhou et al., 2014). In an interesting study, Nugraha et al. have developed a hydrogel-based 3D model of the proximal tubule interstitial interface: they embedded HKC-8 cells and human renal fibroblasts into two separate layers of hydrogel which were put in contact to allow monitoring the cross-talk between proximal tubule cells and fibroblasts during nephrotoxic insults. The epithelial layer was treated with known nephrotoxicants such as cyclosporin A and gentamicin and the degree of epithelial injury and the effect on fibroblasts was assessed via immunofluorescence staining, biomarker release and gene expression analysis (Nugraha et al., 2017).

Although the *in vivo* and *in vitro* models of progressive renal fibrosis presented thus far offer an invaluable tool to investigate the pathophysiology of chronic kidney disease, they present some significant limitations which propel the field of kidney disease models to develop novel models that will counteract such shortcomings. *In vivo* animal models either face ethical challenges or do not adhere to the 3Rs (reduce, replace, refine), while the available *in vitro* models mainly lack the structural complexity required to mimic molecular interactions between cellular components which are at the basis of the cellular events underlying the progression of renal fibrosis. Furthermore, often the "starting material" used to build such *in vitro* models do not recapitulate *in vivo* kidney function due to the limitations in using non-primary cells such as iPSC-derived or transfected cell lines which only partially retain key tubular functions such as reabsorption and secretion of solutes. Therefore, development of a new, more structurally complex *in vitro* 3D model of the proximal tubule interstitial interface comprising tubular epithelial, mesenchymal, and endothelial cells is necessary to further advance research concerning the understanding and treatment of progressive renal fibrosis leading to chronic kidney disease (CKD). To overcome the lack of physiological relevance of the tubular epithelial cell lines used in other studies, primary cellular material isolated from the human kidney cortex obtained from deceased patients shall be used, as primary tissue is itself the gold standard of renal physiological relevance. The "building blocks" of the model shall be thoroughly characterised via phenotyping and the selected isolation methods should allow to retrieve simultaneously large amounts of different cell types from the kidney cortex in order to construct an autologous *in vitro* model on the most high throughput platform available. The model should demonstrate ability to secrete and absorb solutes, aside from appropriate genotypical and phenotypical characteristics. Furthermore, the developed *in vitro* model of renal fibrosis should be designed to multiplex assays using cutting-edge high throughput techniques such as high content imaging.

High Content Imaging (HCI) or High Content Screening (HCS) is a technique based on automated microscopy. It enables researchers to measure biological changes (e.g.

immunofluorescence stained proteins, RNA, morphological changes) in single cells which are treated with libraries of compounds. Several features that make up a specific phenotype are measured to give a snapshot of a single cell at a specific timepoint and under specific conditions. The cells studied with HCI are cultured onto multi-well plates. Hence, via this technique one can acquire an enormous amount of information about every cell present on the plate and can screen entire libraries of compounds on a single plate. Such large amount of data requires appropriate software and computing power to be analysed and displayed into mean fluorescence intensity (FI) or mean grey value graphs. Although this technique was initially developed on histology microscope slides, it can be applied to 3D microtissues that retain in vivo physiological features which increases the predictive power of compound screening (Buchser et al., 2004). High Content Imaging (HCI) has been used to select promising lead anti-fibrotic compounds or to investigate their mechanism on several in vitro models. Palano et al. have established a cardiac fibrosis assay platform by culturing primary human cardiac fibroblasts on a micro-well format. The cells were treated with known anti-fibrotic compounds and the phenotypical changes were detected via HCI. The platform was able to successfully detect anti-fibrotic activity (Palano et al., 2020). Since COVID-19 patients present severe lung scarring, Marwick et al. have developed an HCI screening assay for anti-fibrotic therapeutic development by culturing human primary lung fibroblasts on a 384-well plate. The assay measures TGFβ-induced extra cellular matrix (ECM) deposition and it was used to screen between 2734 potential anti-fibrotic lead compounds (Marwick et al., 2021). Another study focusing on lung fibrosis by Sieber et al. aims to detect compounds able to revert fibroblasts activation into myofibroblasts through HCI. In this instance, the technique is used to distinguish between αSMA+ and αSMA- phenotypes (Sieber et al., 2018). High content imaging is an extremely powerful novel technique that combines advances in the fields of cellular biology, microscopy, robotics, and bioinformatics and it could lead to break-through improvements in the treatment of complex conditions such as kidney fibrosis.

1.6 Research Aims & Objectives

Chronic kidney disease (CKD) is a condition with limited pharmacological treatment that leaves patients in dialysis or in need of a transplant, which costs billions to healthcare systems worldwide. Renal fibrosis is the pathophysiological mechanism underlying CKD. Of our knowledge, the *in vitro* models of renal fibrosis available in the field are not complex enough to recapitulate the tubular-interstitial *milieu* where the disease progresses.

Following the first principle of the 3Rs (replacing completely the use of animals in research), the overall aim of this project is to develop a fully human renal fibrosis *in vitro* assay platform that mimics the underlying cellular events that lead to the progression of chronic kidney disease specifically at the proximal tubule interstitial interface. The platform should be able to predict in vivo outcomes of lead compounds developed to halt the disease. If used to test libraries of compounds, this model could be used to select the most promising compounds which then could be used on animal models of disease. The hypothesis of the thesis is two-fold, as the first research question answers whether primary proximal tubule cells in co-culture with other cellular components of the proximal tubule interstitial interface mimic more closely the in vivo physiology of such segment of the nephron, while the second question answers whether the treatment of such model with pro-fibrotic compounds can mimic progressive renal fibrosis at a histological and cellular level.

To select for the most *in vivo*-like 3D model, different combinations of the cell types that make up the proximal tubule interstitial interface will be co-cultured with human primary proximal tubule epithelial cells from donors. Drug handling, expression of genes encoding for drug transporters, stress biomarker release, response to nephrotoxic insults, and monolayer integrity will be compared between the 3D models to determine which one is the most physiologically relevant. Once the "best" model is selected, it will be used to establish a renal fibrosis high content imaging (HCI) assay platform to screen for potential anti-chronic kidney disease (CKD) compounds. The isolation method to obtain relatively large numbers of human primary proximal tubule cells (hPTC) from the human kidney cortex via Percoll® density gradient centrifugation had been previously optimized in our research group. The first aim of this project is to isolate from the renal cortex and characterise the two building blocks of the interstitial interface: human renal peritubular endothelial cells (HRPECs) and human renal fibroblasts (HRF). The two cell types are isolated via three different isolation methods: Percoll® density gradient centrifugation, Magnetic Activated Cell Sorting (MACS), and a combination of both methods. The isolation methods are compared via immunofluorescence staining and flow cytometry. The most efficient isolation method for each cell type is selected and culture conditions are optimized.

Proximal tubule cells, human renal fibroblasts and endothelial cells are co-cultured on 24-well translucent Transwell® plates or 24-well transparent ThinCert™ plates (depending on the assay requirements) in all possible different combinations - this means all different cell types are grown both in contact co-culture and in separate compartments, referred to as non-contact co-culture. The constructed 3D models are compared to proximal tubule cells in monoculture, which represents the currently available previously characterised model (Brown, Sayer, Windass, Haslam, de Broe, et al., 2008), via a number of techniques deemed

suitable for the assessment of appropriate proximal tubule interstitial interface functionality. As compared to the monoculture epithelial model, the selected 3D model of the proximal tubule interstitial interface should demonstrate better epithelial barrier formation, resulting in higher transepithelial/transendothelial electric resistance (TEER) measurements and lower paracellular permeability to fluorescence compound Lucifer Yellow, successful cell polarisation investigated by immunofluorescence staining of proteins involved in tight junction complex formation and apical cilium presence, higher expression of key solute transporters at the mRNA level quantified via Real Time Quantitative Polymerase Chain Reaction (RT-qPCR), better *in vitro* handling of radiolabelled compounds creatinine and para-aminohippurate (PAH) due to upregulated expression of key transporters measured by radiolabelled flux assay, higher epithelial cell viability measured by quantifying intracellular ATP (adenosine triphosphate), and lower stress biomarker release, namely KIM-1, NGAL, clusterin, measured by chemiluminescent assay.

One of the 3D models will be taken forward to establish an *in vitro* model of renal fibrosis for high content imaging. To our knowledge, studies regarding multicellular 3D models of the proximal tubule interstitial interface suitable for these scopes have not been published yet. Primary proximal tubule cells will be cultured onto the apical membrane of the 96-Transwell® inserts while renal fibroblasts will be cultured on the bottom of the well, not in direct contact with the epithelial cells. First, conditions of culture for the model will be optimized and healthy phenotype will be defined via immunofluorescence staining and stress biomarkers release. The co-culture model will be treated with a cocktail of known pro-fibrotic cytokines, namely TGFβ1, TNFα, and Angiotensin II, and fibrotic phenotype will be characterised. Three fibrosis biomarkers will be considered for each cell type. Upon initiation of pro-fibrotic activated cellular and molecular events, epithelial cells loose protein complexes that form cell-cell tight junctions which are essential in the maintenance of epithelial barrier function. Therefore, upon treatment of proximal tubule cells with pro-fibrotic cytokines we expect epithelial cells to show changes in expression of the tight junction markers zonula occludens 1 (ZO-1) and E-Cadherin. Furthermore, we expect epithelial cells to acquire some mesenchymal phenotypical features marked by *de novo* expression of vimentin, which would correlate with pEMT. Fibroblasts undergoing fibrotic stimuli are activated into myofibroblasts which produce an excess of extra-cellular matrix (ECM). This phenotypical change will be detected by measuring acquisition of α smooth muscle actin (αSMA) by renal fibroblasts as well as detecting an increase in collagen I and fibronectin production. Primary monoclonal or polyclonal antibodies raised in three different animal species will bind to the biomarkers and secondary antibodies conjugated to three distinct fluorophores will in turn bind to the primary antibodies. Cell cycle dysregulation events will be assayed via high throughput flow cytometry. The assay will be validated by measuring the amount of stress biomarkers released by proximal tubule cells after pro-fibrotic treatment via MSD assay. Automated microscope for high content imaging ImageXpress Pico will be able to focus and acquire images from both bottom of wells (HRFs) and apical membrane (hPTC). Images will be analysed via stitching and segmentation performed with CellReporterXpress.

Chapter 2. Materials & Methods

2.1 Human samples and ethics

Human kidneys initially meant for transplant were provided by tissue banks, which have obtained the relevant ethical approval for use in research. Upon reception of the organ, each kidney was examined via visual observation and, during cortex dissection, visibly fibrotic, necrotic, and cystic tissue sections were carefully avoided for subsequent normal cell isolation. **Table 2.1** describes ethical numbers and donor patients characteristics.

Internal kidney code	Donor code	Year of Birth	Gender	Cause of death	Medical history	Drug history	Patient diagnosis
K1	44710-99YC	1943	M	Unknown	Unknown	Unknown	Rejected kidney transplant donor
K2	44716-13SE	1960	M	Unknown	Unknown	Unknown	Rejected kidney transplant donor
K3	44735-54JT	1994	M	Unknown	Unknown	Unknown	Rejected kidney transplant donor
K4	44743-15EX	1957	M	Unknown	Unknown	Unknown	Rejected kidney transplant donor
K5	44762-03BR	1959	M	Intracranial haemorrhage	Unknown	Unknown	Rejected kidney transplant donor
K6	1-263-258	1946	M	Intracranial haemorrhage	Hypertension, Arthritis, Depression, Alcohol dependence	Heavy drinker 7-9 units/day; Smoker, 10 cigarettes/day	Rejected kidney transplant donor
K7	1-262-216	1957	F	Intracranial haemorrhage	Hypertension, skin cancer	Light drinker- 1-2 units/day	Rejected kidney transplant donor
K8	ODT154277	1944	F	Intracranial haemorrhage	Diabetes	Non-drinker, non-smoker	Rejected kidney transplant donor
K9	1-263-189	1953	M	Intracranial haemorrhage	Hypertension, Bowel cancer	Occasional drinker, < 1 unit/day	Rejected kidney transplant donor
K10	1-263-185	1945	M	Hypoxic brain damage	No known conditions	Occasional drinker, < 1 unit/day	Rejected kidney transplant donor
K11	1-262-211	1945	F	Intracranial – type unclassified	No known conditions	Occasional drinker, < 1 unit/day	Rejected kidney transplant donor

K12	1-262-224	1955	M	Intracranial haemorrhage	Hypertension, cardiac disease	Very heavy drinker, <9 units/day	Rejected kidney transplant donor
K13	1-262-564	1995	M	Hypoxic brain damage	Type I diabetes mellitus	Occasional drinker, < 1 unit/day, Smoker, 5 cigarettes/day, history of drug abuse	Rejected kidney transplant donor

Table 2.1. Table describing kidney internal and tissue bank donor codes, patients' year of birth, gender, cause of death, medical history, drug history, and patient diagnosis.

2.2 Isolation of proximal tubule interstitial interface components from the human kidney cortex

2.2.1 Isolation of human proximal tubule cells (hPTC)

The described methodology is followed to isolate human proximal tubule cells (hPTC) from the renal cortex and it was optimised in our research group before the start of this project, as described by Brown *et. al*, (Brown et al., 2008). Macroscopically normal tissue is decapsulated under sterile conditions. The kidney is sliced through latitudinally so that a thin cortical slice is produced. This procedure is repeated until the medulla can be seen. The cortical tissue obtained is minced to ensure the pieces are about 1 mm^3. About 8 g of minced cortical tissue are suspended in isolation buffer (Roswell Park Memorial Institute (RPMI) 1640 Medium (Lonza, Switzerland), 5% v/v Foetal Calf Serum, 2% v/v Penicillin/Streptomycin) and they are digested in a collagenase solution (Worthington Biochemical, USA). The tissue-collagenase solution is incubated with agitation overnight at 4˚C and then at 37˚C for 1 hour prior to hPTC isolation procedure. The digested cell mixture is passed through a 40 µm nylon cell strainer. The cells are then centrifuged at 1200 rpm for 10 minutes at 4˚C. The supernatant is removed, and the pellet is resuspended in 50 mL of fresh isolation medium. The cells are centrifuged again at 1200 rpm for 7 minutes at 4˚C and resuspended in 50 mL isolation medium. The resulting cell suspension is loaded on a discontinuous Percoll® density gradient media (Cytiva, USA) made up in RMPI 1640 medium 11 with densities of 1.04 and 1.07 g/ml. The Percoll® gradients are centrifuged at 3000 rpm for 25 minutes at 4˚C.

The proximal tubule cell layer is localized as follows:

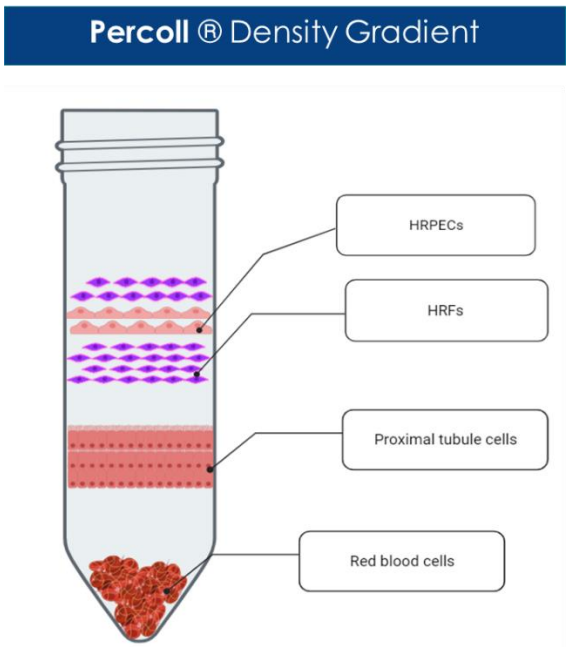

Figure 2.1. Schematic representation of cellular layers former in a 50 mL Falcon tube after Percoll® density gradient centrifugation is performed on a single cell suspension obtained from the digestion of the human kidney cortex.

The proximal tubule cells are centrifuged at 1200 rpm for 7 minutes at 4˚C. The supernatant is discarded, and the pellet is resuspended in 50 mL of fresh isolation media. This step is repeated once more. The pellet is finally resuspended in fresh culture medium REGM™ Renal Epithelial SingleQuot Kit (Lonza, Switzerland) with growth factors: Insulin, Hydrocortisone, GA-1000, Adrenaline, T3, Transferrin, Foetal Calf Serum, Epithelial growth factor. All growth factors are added to 500 mL of basal medium at the concentrations and volumes provided by the manufacturer. The obtained hPTC are counted and seeded at the cell seeding density of 375.000 cells/mL onto culture flasks and plates for experiments.

2.2.2 Isolation of human renal fibroblasts (HRF)

Human renal fibroblasts are isolated from the human kidney cortex via expansion and subsequent selection via Magnetic Activated Cell Sorting (MACS) of cells expressing FSP-1 marker. Human kidneys are dissected and digested as described in **2.2.1**, and cells undergo the same procedure above described that leads to the formation of the Percoll® density gradient layers depicted in **Figure 2.1.** The top layers obtained from Percoll® density gradient suspensions are centrifuged at 1200 rpm for 7 minutes at 4˚C. The supernatant is discarded, and the pellet is resuspended in fresh isolation media. This step is repeated once more. Each tube of Percoll® yields to a pellet which is resuspended in FGM™-2 Fibroblast Growth Medium (Lonza, Switzerland) supplemented with 3 mM of L-Ascorbic Acid (Sigma-Aldrich, USA) and seeded onto a T-25 cell culture flask (Thermo Fisher Scientific, UK). Magnetic activated cell sorting (MACS) is an isolation technique in which different cell types are sorted depending on their surface markers (antigens). Magnetic beads conjugated to an antibody against a specific surface marker are used to capture the cells in a column that undergoes a magnetic field. MACS is used to isolate fibroblasts from the renal cortex and outer medulla. Fibroblasts are

selected based on their positivity to FSP-1 (fibroblast specific protein 1). This step is performed once the cells cultured in T-25 flasks have reached confluency (usually 1 to 2 days). Cell culture media is discarded and flasks are washed with 5 mL PBS. 3 mL of TrypLE™ Express Enzyme (Thermo Fisher Scientific, UK) per flask are added and cells are incubated in the incubator for 10 minutes at 37°C. After the incubation, 7 mL of serum-containing medium are added to each flask to inactivate the TrypLE™. 10 mL of cell suspension solution per flask are transferred to 10 mL Falcon tubes and these are centrifuged at 300 g for 5 minutes. The obtained cell pellet is resuspended in 50 mL of ice-cold MACS buffer (PBS pH 7.2, 0.5% Bovine Serum Albumin, 2 mM EDTA). Cell number is determined via Cell Counter (check brand). This is referred as "Total cell number" and it is used to determine what volume of MicroBeads and number of columns are needed for the isolation. Cells (in volumes of buffer) are portioned to obtain a maximum of 10^8 cells per tube. They are centrifuged at 300 g for 5 minutes; the supernatant is discarded, and they are resuspended in 800 µl buffer. Cells are incubated with 200 µl per tube of Anti Fibroblasts MicroBeads, human (Miltenyi Biotec, Germany) in the dark on ice for 30 minutes. Cells are washed with 3 mL of MACS buffer, centrifuged at 300 g for 5 minutes; the supernatant is discarded. The cell pellet is resuspended in 1 mL of MACS buffer. The magnetic separation is carried out using LS MACS™ columns (Miltenyi Biotec, Germany) and a MIDI MACS™ separator (Miltenyi Biotec, Germany), according to the initial number of cells and the expected number of isolated cells to be obtained from the separation. The column is placed in the magnetic field of the separator, and it is prepared by rinsing it with 3 mL of MACS buffer. Subsequently, 1 mL single cell suspension is applied onto the column. The flow through is discarded. The column is washed three times with 3 mL of MACS buffer, each time discarding the flow through. The column is then removed from the separator, and 5 mL of MACS buffer is added to it. The magnetic labelled cells, which have been retained inside the column until now, are flushed out by firmly pushing a plunger into the column. The collected magnetic labelled cells are centrifuged at 300 g for 10 minutes. The supernatant is discarded, and the cells are resuspended in FGM-2™ Fibroblast Growth Medium (Lonza, Switzerland) supplemented with 3 mM of L-Ascorbic Acid. The obtained cells are seeded at the cell seeding density of 500.000 cells/mL onto culture flasks and plates for experiments.

If the human renal fibroblasts are going to be used for high content imaging experiments that investigate extra-cellular matrix deposition and fibroblast-to-myofibroblast transition, it will be necessary to coat the tissue culture plates with appropriate hydrogels to reduce plastic stiffness and subsequent fibroblast-to-myofibroblast trans-differentiation and acquisition of contractile properties (Schwager et al., 2019a). Corning® Transwell® 96-well bottoms and CELLSTAR® 96-well black walled clear bottom plates (Greiner Bio-One, Austria) are coated with synthetic extracellular matrix 0.001 % v/v BiogelX™ Peptide INK solution in dH_2O. The plates coated with the pre-gel solution are incubated in the incubator overnight. After overnight incubation, 150 µL of FGM™-2 medium supplemented with 3mM L-ascorbate per well are added. The plates are subsequently incubated in the incubator for at least 2 hours; when ready to use, leftover medium (non-gelified) is aspirated from all wells and cells are seeded at seeding density 500,000 cells/mL.

2.2.3 Isolation of human renal peritubular endothelial cells (HRPEC)

Human renal peritubular endothelial cells (HRPEC) are isolated from the human kidney cortex via expansion and subsequent selection via Magnetic Activated Cell Sorting (MACS) of cells expressing CD31 marker. Human kidneys are dissected and digested as described in 2.2.1, and cells undergo the same procedure above described that leads to the formation of the Percoll® density gradient layers depicted in **Figure 2.1.** The top layers obtained from Percoll® density gradient suspensions are centrifuged at 1200 rpm for 7 minutes at 4˚C. The supernatant is discarded, and the pellet is resuspended in fresh isolation media. This step is repeated once more. Each tube of Percoll® yields to a pellet which is resuspended in EGM™-2 Endothelial Cell Growth Medium (Lonza, Switzerland) supplemented with 40 ng/mL of VEGF-A (PeproTech, USA) and seeded onto a T-25 cell culture flask. Magnetic activated cell sorting (MACS) is used to purify endothelial cell population from the cells obtained via Percoll® density gradient isolation. HRPEC are selected based on their positivity to CD31 (cluster of differentiation 31). This step is performed once the cells cultured in T-25 flasks have reached confluency (usually 1 to 2 days). Cell culture media is discarded and flasks are washed with 5 mL PBS. 3 mL of TrypLE™ Express Enzyme (Thermo Fisher Scientific, UK) per flask are added and cells are incubated in the incubator for 10 minutes at 37°C. After the incubation, 7 mL of serum-containing medium are added to each flask to inactivate the TrypLE™. 10 mL of cell suspension solution per flask are transferred to 10 mL Falcon tubes and these are centrifuged at 300 g for 5 minutes. The obtained cell pellet is resuspended in 50 mL of ice-cold MACS buffer (PBS pH 7.2, 0.5% Bovine Serum Albumin, 2 mM EDTA). Cell number is determined via Cell Counter (check brand). This is referred as “Total cell number” and it is used to determine what volume of MicroBeads and number of columns are needed for the isolation. Cells (in volumes of buffer) are portioned to obtain a maximum of 10^7 cells per tube. They are centrifuged at 300 g for 5 minutes; the supernatant is discarded, and they are resuspended in 60 µL MACS buffer. CD31 MicroBead Kit (Miltenyi Biotec, Germany) is used for the purification step. Cells are incubated with 20 µL FcR blocking reagent for 10 minutes at room temperature, then 20 µl per tube of Anti CD31 MicroBeads are added and cells are incubated in the dark on ice for 15 minutes. Cells are washed with 3 mL of MACS buffer, centrifuged at 300 g for 5 minutes; the supernatant is discarded. The cell pellet is resuspended in 1 mL of MACS buffer. The magnetic separation is carried out using LS MACS™ columns (Miltenyi Biotec, Germany) and a MIDI MACS™ separator (Miltenyi Biotec, Germany), according to the initial number of cells and the expected number of isolated cells to be obtained from the separation. The column is placed in the magnetic field of the separator, and it is prepared by rinsing it with 3 mL of MACS buffer. Subsequently, 1 mL single cell suspension is applied onto the column. The flow through is discarded. The column is washed three times with 3 mL of MACS buffer, each time discarding the flow through. The column is then removed from the separator, and 5 mL of MACS buffer is added to it. The magnetic labelled cells, which have been retained inside the column until now, are flushed out by firmly pushing a plunger into the column. The collected magnetic labelled cells are centrifuged at 300 g for 10 minutes. The supernatant is discarded, and the cells are resuspended in EGM-2™ Endothelial Cell Growth Medium supplemented with 40 ng/mL VEGF-A. The obtained cells are seeded at the cell seeding density of 500.000 cells/mL onto culture flasks and plates for experiments.

2.3 Characterisation of cell phenotypes

2.3.1 RNA isolation, Reverse Transcription, RT-qPCR

Real Time quantitative polymerase chain reaction (RT-qPCR) is used in this project to assess gene expression at the mRNA level of key solute transporters in hPTC in monoculture and in co-culture with other cell types that compose the proximal tubule interstitial interface, so it is used both to validate tubular epithelial phenotype and to compare expression of such genes between *in vitro* models.

RNA is isolated from cell cultures using the RNeasy® Plus Mini kit (Qiagen, Germany) for downstream quantitative applications such as RT-qPCR. Adherent cells grown in a monolayer on a vessel are washed with ice-cold PBS, which is then discarded. 0.25% v/v Trypsin-EDTA solution (Sigma Aldrich, USA) in PBS is added to the culture, and the cells are incubated for 3 to 5 minutes at 37°C in the incubator until visible cell colony detachment. To stop trypsinization, medium containing foetal calf serum (FCS) (Thermo Fisher Scientific, UK) is added. The cells are centrifuged at 300 g for 5 minutes, the supernatant is discarded, and cells are resuspended in lysis buffer (Buffer RLT Plus). The obtained lysate is homogenized by passing it 5 times through a 20-gauge needle fitted to an RNase-free syringe. The homogenized lysate is transferred onto a gDNA Eliminator spin column that allows removal of genomic DNA, and it is centrifuged for 1 minute at 8000 g. One volume of 70% ethanol is added to the flow through, the mixture is added to a RNeasy spin column, where the RNA binds to the column membrane, and it is centrifuged for 15 seconds at 8000 g. Buffer RW1 is added to the RNeasy spin column which is centrifuged for 15 seconds at 8000 g to wash the column membrane. Buffer RPE is added to the RNeasy spin column which is centrifuged for 15 seconds at 8000 g; this step is repeated twice to eliminate any possible carryover of Buffer RPE. The RNeasy spin column is placed on a new collection tube. RNase-free water is added directly to the membrane of the spin column, and it is centrifuged for 1 minute at 8000 g to elute the RNA. Final RNA concentration and purity are assessed with the micro-volume measurement spectrophotometer BioDrop µLITE+ (Montreal Biotech, Canada).

To synthesize the relevant cDNA via reverse transcription, RNA samples are mixed with random hexamers, which are used to prime the synthesis of DNA from RNA samples, and RNase-free water. They are incubated at 65˚C for 5 minutes and cooled immediately on ice.

The reverse transcription master mix that is added to the samples contains:

• M-MLV Reverse transcriptase 5X Reaction Buffer: Moloney Murine Leukemia Virus Reverse Transcriptase is a recombinant DNA polymerase that synthesizes a complementary DNA strand from single-stranded RNA. The enzyme also has RNase activity, and an inhibitor needs to be added to prevent the degradation of the RNA templates.

• Deoxyribonucleotide triphosphate (dNTPs) mix

• RNasin Ribonuclease Inhibitor: Human Placenta Ribonuclease Inhibitor (HPRI), it is a ribonuclease inhibitor isolated from human placenta. Because M-MLV RT also has RNase activity, an inhibitor needs to be added to prevent degradation of the RNA samples.

The reverse transcription mix is incubated at 42˚C for 2 hours, then at 95˚C for 3 minutes, before lowering the temperature to 4˚C. The obtained cDNA product is diluted in water and stored at -20˚C for further use or immediately used for subsequent RT-qPCR.

qPCR Quantitative Polymerase Chain Reaction (q-PCR) monitors in real time the amplification of a DNA molecule. PCR Primers are designed on Primer-BLAST (National Centre for Biotechnology Information, NCBI) to specifically anneal to known sequences of the DNA template. They are purchased in 100 µM stocks (Integrated DNA Technologies, USA) and are made of HPLC purified oligonucleotides. Prior the reaction initiation, primers are diluted to the working concentration of 10 µM and a mixture of forward and reverse primers is prepared. The reaction mix is purchased as SYBR Green® Master Mix (Thermo Fisher Scientific, UK). The primers used for the characterisation of the components of the proximal tubule interstitial interface and the 3D model generated were designed and the efficiency of the reaction was assessed via the generation of standard curves by Git Chung prior the beginning of this project. It contains reaction buffer, deoxyribonucleotide triphosphate molecules (dNTPs), thermosensitive DNA polymerase, and SYBR Green® dye. All reagents are kept on ice during preparation of each reaction mix. Each well of a 384-well PCR plate contains the following reagent composition: SYBR Green® Master Mix, forward and reverse primers mixture, dH_2O, and cDNA sample. The samples are loaded in triplicates to account for pipetting errors. The plate is sealed with an optically clear film. The plate is spun down at 2500 rpm for 2 minutes to eliminate bubbles and ensure mixing of samples with the master mix. The PCR plate is loaded into the QuantStudio™ 6 Flex Real-Time PCR System (Thermo Fisher Scientific, UK). To amplify the cDNA samples, PCR steps of denaturation, annealing, and extension are repeated (cycled) as follows: the plate is incubated for one cycle at 95˚C for 10 minutes, then for 45 cycles at 95˚C for 15 seconds, at 58˚C for 30 seconds, at 72˚C for 1 second, then for 1 cycle at 95˚C for 1 second, at 55˚C for 30 seconds and continuously for 95˚C, in the final cycle the temperature is lowered at 40˚C for 10 seconds.

To analyse the data obtained from the RT-qPCR, the $2^{-\Delta\Delta Ct}$ (delta-delta Ct method) is used, whereby Ct is the cycle threshold number obtained as result for each loaded sample. The mean between the Ct of each technical repeat is calculated, and the mean Ct obtained from the reference housekeeping gene GAPDH is subtracted from this number (ΔCt). Subsequently, the ΔCt of the control condition – in this case being hPTC in monoculture – is subtracted to the ΔCt of the test condition. The fold gene expression of each gene is then obtained by elevating 2 to the power of – ΔΔCt. Therefore, the fold gene expression of the control condition will always be equals to 1; whereas for the test conditions, values above 1 will indicate upregulation of gene expression as compared to the control, and values below 1 will indicate downregulation of gene expression as compared to the control condition.

The sequences of the primers used for experiments performed in this thesis are found in the table below:

Target	NCBI Reference Sequence	Forward Primer	Reverse Primer	Amplicon Length
GAPDH: Homo sapiens glyceraldehyde-3-phosphate dehydrogenase isoform 1	NP_001276675.1	AAAAGGGCCCTGACAACTCT	TGGTGGTCCAGGGGTCTTAC	90 bp
Cubilin: Homo sapiens cubilin (intrinsic factor-cobalamin receptor) (CUBN)	NM_001081.3	TGAAGGTGTGGGCAGGAAC	GAGACTGGAAGACGGCAGTG	120 bp
MATE1: Homo sapiens solute carrier family 47 (multidrug and toxin extrusion), member 1 (SLC47A1)	NM_018242.2	ATCGGGATCGCGCTGATGTT	TGTACCTGAGCCTGCTGACA	149 bp
OAT1: Homo sapiens solute carrier family 22 (organic anion transporter), member 6 (SLC22A6), transcript variant 1	NM_004790.4	ACCAGTCCATTGTCCGAACC	TGTCTGCCGGATCATTGTGG	116 bp
OCT2: Homo sapiens solute carrier family 22 (organic cation transporter), member 2 (SLC22A2)	NM_003058.3	ACCTGGTGATCTACAATGGCT	TGAGGAACAGATGTGGACGC	145 bp
Megalin: Homo sapiens LDL receptor related protein 2 (LRP2)	NM_004525.2	ATTGATGGCACAGGAAGAGA	GCTAGCCTCATGACACTGAT	134 bp
NaPi2a: Homo sapiens solute carrier family 34 (type II sodium/phosphate cotransporter), member 1 (SLC34A1), transcript variant 1	NM_003052.4	ATGGTCTCCTCTGGCTTGCT	TTGGTGACAGAGGTGCCGAT	80 bp
SLGT2: Homo sapiens solute carrier family 5 member 2 (SLC5A1), transcript 1	NM_003041.3	ACCTCTACTTCGCCATTGTGCT	CCTGGGGCTCATTCATCTCCAT	225 bp
SMCT1: SLC5A8 solute carrier family 5 (iodide transporter), member 8	NM_145913	ACATTAAGCACAGTGTCCTCC	TACACCACACTCATTCCTTGG	131 bp
SMCT2: Solute carrier family 5 (sodium/glucose	NM_178498.3	TGGAACTCTGAGCACCGTGG	AGCTTGTCGGAGAGA TGAGG	99 bp

cotransporter), member 12 (SLC5A12)				
SLC2A9: Homo sapiens solute carrier family 2 (facilitated glucose transporter), member 9 (SLC2A9), transcript variant 1	NM_020041.2	TCACAGATGAC ACCAGCCAC	ACAGGTTGTA GCCGTAGAGG	176 bp
URAT1: Homo sapiens solute carrier family 22 (organic anion/urate transporter), member 12 (SLC22A12), transcript variant 1	NM_144585.3	GTGTACTGCCT GTTCCGCT	CGTCCACTCCA TCAGGAGA	84 bp
OAT3: Homo sapiens solute carrier family 22 member 8 (SLC22A8), transcript variant 2	NM_00118473 2.2	TGGCTACATGC AGGAACTGG	ACCTGTGCTCG CATATCCAC	127 bp
MDR1: Homo sapiens ATP binding cassette subfamily B member 1 (ABCB1), transcript variant 3	NM_000927.5	TTCACTTCAGT TACCCATCTCG	GTCTGCCCACT CTGCACCTTC	138 bp
MRP1: Homo sapiens ATP binding cassette subfamily C member 1 (ABCC1), transcript variant 1	NM_004996. 4	TGGCATCACCT TCTCCATCC	GAGAGCAGGG ACGACTTTCCG	161 bp
MRP2		CACCATCATGG ACAGTGACAA GG	CCGCACTCTAT AATCTTCCCG	96 bp

Table 2.2. Table containing all information regarding primers used during this project in the context of RT-qPCR.

2.3.2 Flow cytometry

Flow cytometry is a laser-based technique used for examining the expression of specific proteins on cell surface and intracellular markers, phenotyping different cell types in a heterogeneous cell population, and analysing cell size and granularity. A single-cell suspension is needed to perform the experiment. Each flow cytometry sample acquired and displayed in this thesis contained $25*10^3$ cells. Cells are washed with ice-cold PBS, detached from the cell culture vessel via incubation with TrypLE™ Express Enzyme, centrifuged and pelleted. The pellet is kept on ice to make sure the cell surface marker of interest does not go inside the cell. The supernatant is aspirated, and the cells are resuspended in residual supernatant. Chilled FACS buffer (PBS pH 7.2, 0.5% Bovine Serum Albumin, 2 mM EDTA) is added to the cell suspension. Cells are passed through a 40 µm nylon mesh to disaggregate cell clumps. Cells are washed with PBS, centrifuged for 5 minutes at 300 g, and the cell viability dye Zombie Aqua™ Fixable Viability Kit (BioLegend, USA) is added. The cells are incubated for 15 minutes on ice in the dark. They are then washed with FACS buffer. Mouse serum (Sigma

Aldrich, USA) is added to block any non-specific antibody binding, and the cells are incubated 10 minutes on ice in the dark. Cells are permeabilized and fixed using the kit Cyto-Fast™ Fix/Perm Buffer Set (BioLegend, USA) following manufacturer's instructions. Finally, primary conjugated antibodies are added to the cells which are incubated for 1 hour on ice in the dark. Cells are washed with FACS buffer and centrifuged for 10 minutes at 300 g. The cell pellets are resuspended in FACS buffer, transferred to FACS tubes and run onto the Attune NxT Flow Cytometer (Thermo Fisher Scientific, UK).

Multicolour antibody panels are created and optimised with the help of the cytometer's Flow Cytometry Panel Builder Tool (Thermo Fisher Scientific, UK) and all antibodies are purchased by BioLegend. To correct for fluorescence spill-over between primary antibodies conjugated to different fluorophores, the compensation method is used including an unstained control, whereby single-stained samples containing a known percentage of cells positive for a certain marker are run to set appropriate voltage intensity for each laser. The instrument then calculates the compensation matrix, which estimates the spill-over of each channel into the others, which is applied to each subsequent experiment using a specific multicolour antibody panel. To analyse the data collected via this technique, "fluorescence minus one" samples (FMOs) are used to set quadrant or histogram gates which indicate the threshold between cell populations negative and positive to specific markers.

The multicolour antibody panels optimised for experiments performed throughout this project are shown below:

Human Proximal Tubule Cells (hPTC) phenotyping multicolour panel

Species	**Primary Antibody**	**Conjugated Fluorophore**	**Dilution (Antibody / Block solution)**
Mouse	Anti AQP-1	APC-Cy7	1/50 µL
Mouse	Anti AQP-2	R-PE	1/50 µL
Mouse	Anti UMOD	FITC	1/50 µL

Human Renal Fibroblasts (HRF) phenotyping multicolour panel

Species	**Primary Antibody**	**Conjugated Fluorophore**	**Dilution (Antibody / Block solution)**
Mouse	Anti CD44	Alexa Fluor™ 647	1/50 µL
Mouse	Anti CD90	APC – Cy7	1/50 µL
Mouse	Anti CD105	PerCP – Cy5.5	1/50 µL
Mouse	Anti FSP-1	R-PE	1/50 µL

Human Renal Peritubular Endothelial Cells (HRPEC) phenotyping multicolour panel

Species	**Primary Antibody**	**Conjugated Fluorophore**	**Dilution (Antibody / Block solution)**
Mouse	Anti CD31	Blue Violet™ 421	1/50 µL
Mouse	Anti VE-Cadherin	APC	1/50 µL

Mouse	VEGFR2	R-PE	1/50 µL

Table 2.3. Tables containing all information regarding primary conjugated antibodies used during this project in the context of flow cytometry.

2.3.3 Immunofluorescence staining on cells fixed on ThinCert™ membranes and glass coverslips

Immunofluorescence staining is a technique that allows marking and localization of proteins on and inside the cell by tagging each protein with a primary antibody, that in turn is tagged by a secondary antibody, against the species in which the primary one was raised, conjugated with a fluorophore.

Sample preparation: fixation, embedding and snap-freezing.

Cells are cultured on different *vessels* depending on experimental purposes, so they are going to be prepared for immunofluorescence staining (IF) accordingly. Corning® Transwell® inserts in 24-well plates (Corning, USA) are kept intact prior to fixation, while cells cultured on flasks are passaged (as described in 2.4) on 25 mm glass coverslips on the bottom of a 6-well plate prior fixation.

The medium is aspired from the wells, the fixative (4% v/v paraformaldehyde in PBS) is added, and the cells are incubated for 15 minutes at room temperature in the dark. The wells are then washed twice with PBS. If the Corning® Transwell® inserts are going to be cryo-sectioned with a cryostat, they are incubated with 30% w/w sucrose in PBS overnight. The inserts are then removed from the wells, and the filters are cut out of the inserts by using a scalpel. A mould is placed into dry ice and a thin layer of OCT embedding matrix (Thermo Fisher Scientific, UK) is applied to the bottom of the mould. One filter per mould is then placed in the freezing embedding medium until it is completely covered by it. The frozen embedding medium blocks are mounted on the cryostat, and cross-sectional 20 µm slices of filters are cut.

Immunofluorescence staining procedure

Cryo-preserved samples mounted on microscope coverslips are defrosted in PBS. A hydrophobic circle is drawn around the cell sample using a liquid blocker PAP pen (Sigma Aldrich, USA), to prevent the antibodies to leak from the designated space. If the primary antibody target is located in the cytoplasm or nucleus of the cell, samples are incubated in PBS with permeabilizer 0.3% v/v Triton-X 100 for 10 minutes to allow permeabilization of the cell membrane. Permeabilized samples are incubated in block solution (PBS 0.3% (v/v) Triton X-100, 1% (w/v) Bovine Serum Albumin, and 10% (v/v) Bovine Serum) in a humidified chamber for 1 hour at room temperature. Primary antibody solutions are prepared by diluting the appropriate amount of antibody in block solution. Primary antibody solutions are added to the samples, or block solution without the primary antibody to negative control samples. The samples are left to incubate in a humidified chamber overnight at 4°C. On the following day, the samples are washed 3 times for 5 minutes in PBS with 0.3% Triton-X 100 to remove the primary antibody which did not bind to the cells. The secondary antibody solutions are

prepared by diluting the appropriate amount of antibody in block. Samples are incubated with secondary antibody solutions in a humidified chamber for 1 hour at room temperature, then they are washed 3 times for 5 minutes in PBS with 0.3% Triton-X 100 to remove the secondary antibody which did not bind. To visualize the nucleus, they are incubated in 10 µg/ml Hoechst 33342 stain (Thermo Fisher Scientific, UK), then washed again 3 times for 5 minutes in PBS. The samples are mounted on microscope slides using SlowFade™ Gold Antifade Mountant (Thermo Fisher Scientific, UK) and imaged.

If the immunofluorescence staining procedure is performed directly on intact Corning® Transwell® inserts which have not been sectioned after fixation, the protocol illustrated above is adapted to the cell culture vessel by performing all steps, namely permeabilization, blocking, primary and secondary antibody incubations, and nucleus staining, in the inserts' well. The volumes used for all passages of the immunofluorescence staining procedure are 200 µL for the apical compartment (insert chamber) and 600 µL for the basolateral compartment (well chamber). The inserts' permeable filters are then cut out of the inserts with a scalpel and are mounted with SlowFade™ Gold Antifade Mountant onto glass microscope slides, sandwiched between the glass slide and a glass coverslip.

Cells are imaged using the widefield fluorescence microscope Zeiss Axio Imager with Apotome (Zeiss, Germany), confocal fluorescence inverted microscope Zeiss LSM800 AiryScan, high content imaging microscope Zeiss CellDiscoverer7, and high content imaging microscope ImageXpress Pico (Molecular Devices, USA) depending on the application.

All primary and secondary antibodies used for this project are listed below:

Species	**Primary Antibody**	**Cell type / Locum marked**	**Dilution (Antibody / Blocking buffer)**
Mouse	Anti-acetylated tubulin	hPTC / Primary cilium	1 / 1500
Rabbit	Anti pericentrin	hPTC / Primary cilium	1 / 500
Rabbit	Anti-GLUT-9	hPTC / basolateral membrane	1 / 200
Rabbit	Anti URAT-1	hPTC / apical membrane	1 / 100
Mouse	Anti AQP-1	hPTC / cytoplasm, plasma membrane	1 / 500
Rabbit	Anti FSP-1	HRF / cytoplasm, plasma membrane	1 / 1000
/	Lotus Tetragonolobus Lectin (LTL)	hPTC	1 / 1000
Mouse	Anti ICAM-1	HRPEC / cytoplasm, plasma membrane	1 / 1000
Mouse	Anti PV-1	HRPEC / diaphragmatic fenestration	1 / 500

Rabbit	Anti ZO-1	hPTC / tight junction	1 / 50
Rabbit	Anti OAT1	hPTC / basolateral membrane	1 / 500
Rabbit	Anti OAT3	hPTC / basolateral membrane	1 / 400
Rabbit	Anti Megalin	hPTC / apical membrane	1 / 1000

Species	**Secondary Antibody**	**Dilution (Antibody / Blocking buffer)**
Goat	Anti-Mouse Alexa Fluor 488™	1 / 300
Goat	Anti-Rabbit Alexa Fluor 647™	1 / 300

Table 2.4. Tables containing all information regarding primary and secondary antibodies used during this project in the context of immunofluorescence staining.

2.3.4 Endothelial Tube Formation Assay (ETFA) with HRPEC

The endothelial tube formation assay (ETFA) is performed with human renal peritubular endothelial cells (HRPEC) isolated via Percoll® density gradient centrifugation and via Percoll® density gradient centrifugation followed by MACS CD31+ to assess their ability to form microvasculature *in vitro.*

To allow for tube formation in vitro, a synthetic extracellular matrix is needed, therefore CELLSTAR® 96-well black walled clear bottom plates are coated with 65 µL per well of 10 mg/mL Corning® Matrigel® Growth Factor Reduced Basement Matrix (Corning, USA). Endothelial cells are detached from their cell culture vessel as described in 2.4 and suspended in a single-cell suspension. Cells isolated via Percoll® density gradient centrifugation are seeded onto the matrix at the seeding density of 20.000 cells/well, while the purified population is seeded at 40.000 cells/well. Cells are mixed with EGM™-2 medium containing appropriate vasculogenesis inhibitory and promoting compounds. Cells are incubated for 18 hours in the incubator. At the 18 hours timepoint, supernatant is carefully aspirated from all well taking care not to damage any tube that may have formed, and wells are washed twice with Hank's Balanced Salt Solution (Gibco™ HBSS, Thermo Fisher Scientific, UK). Wells are incubated with 8 µg/mL of Calcein AM dye (BioLegend, USA) for 40 minutes in the incubator. Calcein AM is nonfluorescent, and it is converted to a green, fluorescent dye when it permeates into live cells by intracellular esterases. After incubation, wells are washed twice with HBSS, and the plate is immediately imaged. Imaging of fluorescent tubular structures formed is carried out with ImageXpress Pico Automated Cell Imaging System (Molecular Devices, USA), and total tubule length, mean tubule length, total tubule area, mean tubule area, percentage area tubule covered, average tubule thickness, segments, branch points, nodes, total node area, mean node area, percentage area node covered, connected sets, and length per set are quantified by a custom algorithm designed by image analysis software CellReporterXpress (CRX, Molecular Devices, USA).

2.4 Tissue culture

2.4.1 Culture of monolayers

All the tissue culture procedures are carried out in Class II biosafety cabinets. Work surfaces are sterilized using 10% Chemgene™ HLD4L (StarLab, UK) and 70% v/v ethanol / 30% v/v deionised water sprays. Depending on the aim of the experiments, primary cells isolated from fresh tissue are seeded onto different vessels such as T25 flasks, T75 flasks, Corning® Transwell® inserts in 24-well and 96-well plates, ThinCert® inserts in 24-well plates (Greiner Bio-One, Austria), and CELLSTAR® 96-well black walled clear bottom plates (Greiner Bio-One, Austria).

Primary cells are incubated at 37°C, 5% CO_2 and monitored daily. The growth medium is changed every 48 hours. If cells need to be passaged onto coverslips or other vessels for further experiments, the growth medium is discarded and the flask containing the cells to be passaged is washed with DPBS (Dulbecco's Phosphate-Buffered Saline). 3 mL of TrypLE™ Express Enzyme are added to the cell culture to detach the adherent cells from the flask. Cells are incubated at 37°C, 5% CO_2 for 3-5 minutes for detachment to occur. To stop the proteolytic reaction, 7 mL of medium containing Foetal Calf Serum (FCS) are added to the culture, and the cells are centrifuged at 1500 rpm for 5 minutes. The supernatant is aspired, and the pellet is resuspended in 1 ml of medium. The cells are counted and seeded onto coverslips (or other type of support).

2.5 Culture of 3D *in vitro* models

2.5.1 Establishment of contact co-culture models with hPTC, HRF and HRPEC

Several protocols are trialled to establish appropriate co-culture conditions for 3D *in vitro* models of the proximal tubule interstitial interface. The first trialled approach involves isolating cells from kidneys donated by different patients (non-autologous), and cells are co-cultured directly in physical contact with each other or they are spatially separated by a permeable membrane. Corning® Transwell® inserts in 24-well and 96-well plates, and ThinCert® inserts in 24-well plates are used to co-culture the 3D models.

The contact co-culture 3D *in vitro* models are generated by first isolating human renal fibroblasts (HRF) and human peritubular renal epithelial cells (HRPEC) from one donor kidney as described in 2.2.2 and 2.2.3. The cells are seeded onto the apical side of the plates' inserts at the cell seeding density of 500.000 cells/mL. Referring to the diagrams depicted in **Figure 2.2** below, 3D constructs containing only HRPEC (**Figure 2.2, [B]**) are initially fed with 200 µL EGM™-2 medium (supplemented with 40 ng/mL VEGF-A – as described in 2.2.3) on the apical chamber and 600 µL of the same medium on the basolateral chamber, while constructs containing only HRF (**Figure 2.2, [C]**) are fed with with 200 µL FGM™-2 (supplemented with 3 mM L-ascorbate – as described in 2.2.2) medium on the apical chamber and 600 µL of the same medium on the basolateral chamber. Constructs containing both HRPEC and HRF (**Figure 2.2, [C]**) are fed with a 1:1 mixture of EGM™-2 and FGM™-2 media in the same volumes. Medium is changed every 48 hours until cell confluency is reached. When a further kidney is donated to our research group, human proximal tubule cells are isolated as described in 2.2.1 and they are seeded onto the apical side of the plates' inserts at the cell seeding density of 375.000 cells/mL onto HRPEC and HRF. In the presence of hPTC, media is

changed to 200 µL REGM™ for the apical chamber, while for the basolateral chamber 600 µL of EGM™-2 or FGM™-2 or the 1:1 mix are used according to cell type. Constructs are cultured for 7-8 days from the day of hPTC seeding, to allow for epithelial barrier formation, and they are used for characterisation experiments.

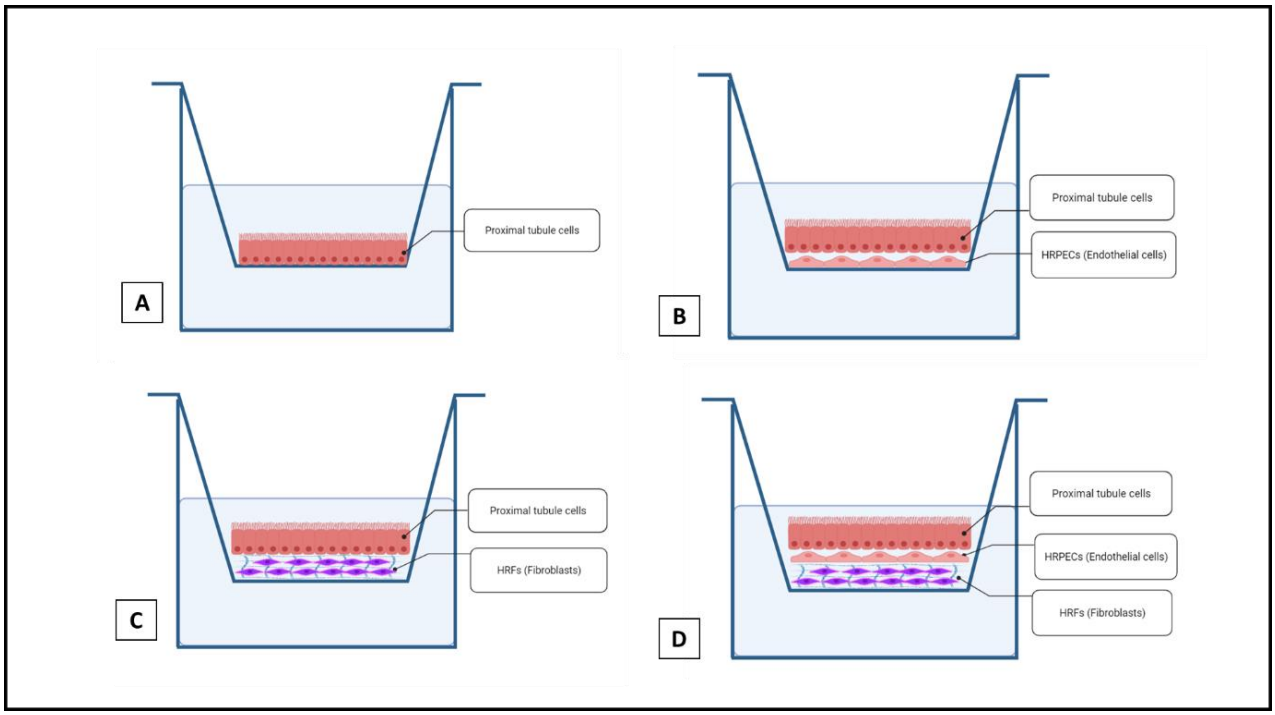

Figure 2.2. Graphical representation of 3D models cultured on Transwell inserts (A) hPTC seeded on the apical side of the insert (Control) (B) HRPEC and hPTC in contact co-culture on the apical side of the insert (C) HRF and hPTC in contact coculture on the apical side of the insert (D) HRF, HRPEC, hPTC in contact co-culture on the apical side of the insert.

Another trialled protocol to establish the 3D co-culture models involves culturing components of the proximal tubule epithelial interface on the two sides of the plates' inserts' permeable membrane (apical side and underside), so to physically separate the different cell types allowing epithelial cells to form an epithelial barrier without it being disrupted by the presence of other cell types but for the epithelial cells to still benefit from the trophic support of the interstitial components. Also in this case, the cellular components making up the constructs are isolated from two different donor kidneys (non-autologous). 3D models are established by first isolating human renal fibroblasts (HRF) and human peritubular renal epithelial cells (HRPEC) from one donor kidney as described in 2.2.2 and 2.2.3. The cells are seeded onto the apical side of the plates' inserts' membranes at the cell seeding density of 500.000 cells/mL. Referring to the diagrams depicted in **Figure 3** below, HRPEC only (**Figure 3 [B]**), HRF only (**Figure 3 [C]**), and HRPEC + HRF (**Figure 3 [C]**) are seeded onto the apical side of the inserts' membranes and fed every 48 hours with appropriate media combinations. When a new kidney is received by our research group, human proximal tubule cells (hPTC) are isolated and seeded onto the underside of the inserts' membrane. Media is aspirated from all compartments; inserts are removed from the original plate and they are flipped upside down onto the lid of a new empty plate. 50 µL of a single-cell suspension of hPTC is applied at the seeding density of 2.000.000 cells/mL onto the underside of the inserts'

membrane. The flipped inserts are transferred into the incubator and cells are left to attach to the membrane for 4 hours. After the incubation, inserts are flipped back into the upright position into the plates' wells, and the basolateral compartment is filled with 600 µL REGM™ while the apical compartments are filled with 200 µL of appropriate media, according to the cell type presence in culture.

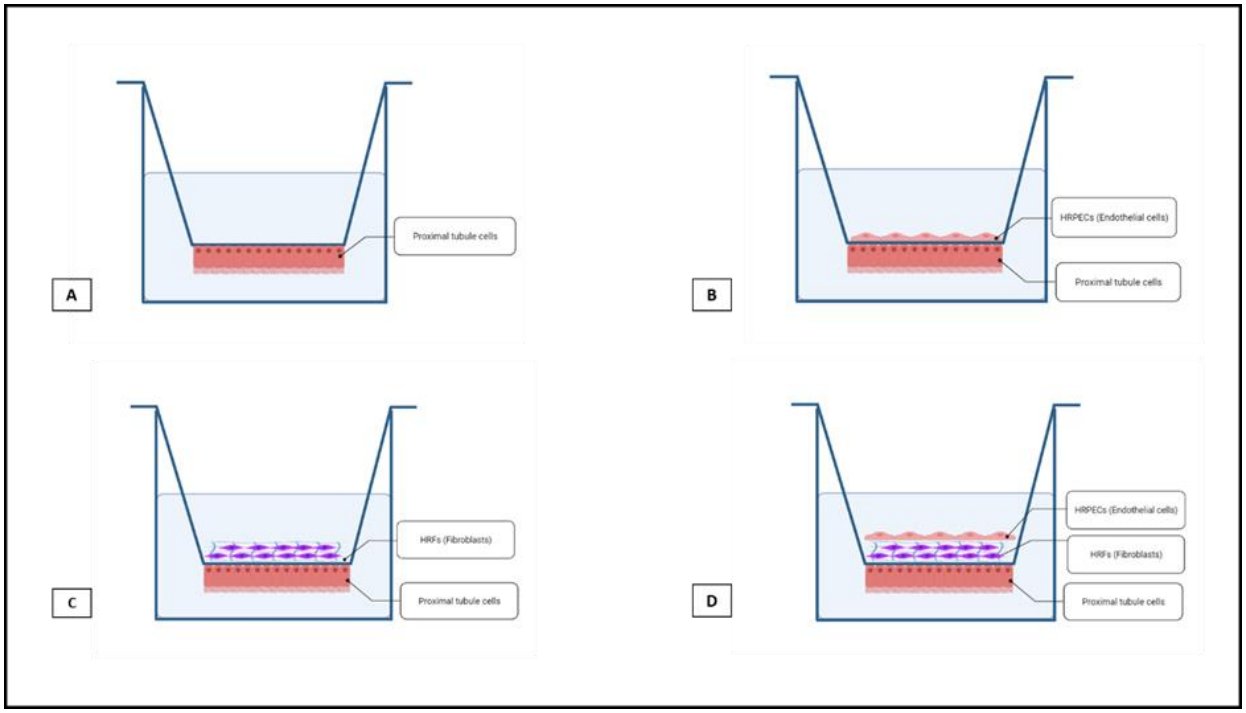

Figure 2.3. Graphical representation of 3D models cultured on Transwell® inserts [A] hPTCs seeded on the underside of the insert [Control] [B] HRPEC on the apical side, hPTC on the underside of the insert [C] HRF on the apical side, hPTC on the underside of the insert [D] HRPEC and HRF co-cultured on the apical side, hPTC on the underside of the insert.

2.5.2 Halting fibroblasts migration into the epithelial monolayer: γ-irradiation, mitomycin C treatment, and gel embedment.

Further efforts to establish a 3D co-culture model of the proximal tubule interstitial interface are focused on retaining epithelial barrier function exerted by the tubular epithelial monolayer while exploiting the trophic properties of the human renal fibroblasts' presence in co-culture. To halt fibroblast migration into the epithelial monolayer in the contact co-culture models, three protocols are trialled, namely irradiation of fibroblast feeder layer, mitomycin C treatment of fibroblasts, and embedment of fibroblasts in a synthetic extracellular matrix. Feeder cells are cellular populations which have been growth-arrested by an external stimulus and they are employed to promote cell proliferation and attachment of the target cell population by releasing growth factors in the cell culture medium and by producing extracellular matrix. Hence, feeder cells are unable to proliferate but continue to be metabolically active throughout their lifespan in co-culture. The most common methods employed to arrest proliferation of the fibroblast feeder layer are γ-irradiation and mitomycin C treatment. γ-irradiation arrests the cell cycle by causing breakage at the DNA double-strand level, whereas the chemotherapeutic agent mitomycin C is able to cross-link opposite strands

of DNA forming a covalent bond, thus halting separation between DNA strands during replication (Llames et al., 2015).

γ-irradiation

To halt human renal fibroblast growth via γ-irradiation, HRF are isolated from a donor kidney as described in 2.2.2 and cultured onto a T-75 flask to confluency. Confluent cells are γ-irradiated following the protocol optimised in Prof. Armstrong's research group using Faxitron CP-160 radiation machine. Following irradiation, the growth medium is discarded and the flask containing the cells to be passaged is washed with DPBS (Dulbecco's Phosphate-Buffered Saline). 3 mL of TrypLE™ Express Enzyme are added to the cell culture to detach the adherent cells from the flask. Cells are incubated at 37°C, 5% CO_2 for 3-5 minutes for detachment to occur. To stop the proteolytic reaction, 7 mL of medium containing Foetal Calf Serum (FCS) are added to the culture, and the cells are centrifuged at 1500 rpm for 5 minutes. The supernatant is aspired, and the pellet is resuspended in 1 ml of medium. The cells are counted and seeded at a seeding density of 500.000 cells/mL onto the apical side of the plates' inserts, as depicted in **Figure 2.4, [B];** apical and basolateral chambers of the well are filled respectively with 200 µL and 600 µL of FGM™-2 supplemented with 3 mM L-ascorbate. When a second kidney is received from a donor, hPTC are isolated as described in 2.2.1 and are seeded onto the irradiated fibroblasts. The 3D constructs are fed with 200 µL REGM™ on the apical compartment of the well, and 600 µL FGM™-2 on the basolateral compartment. Media is changed every 48 hours until the epithelial barrier is formed.

Mitomycin C treatment

Human renal fibroblasts are treated with mitomycin C to stop their proliferation and maintain their metabolic activity. HRF are isolated from a donor kidney as described in 2.2.2 and cultured onto a T-75 flask to confluency. Confluent cells are treated with an 8 µg/mL mitomycin C solution (Bio-Techne, USA) which is pipetted directly into the cell culture media in the flask. The flask is incubated overnight in the incubator. The following day, the media is aspirated from the flask and treated cells are detached from the cell culture vessel as previously described. HRF are seeded at a cell seeding density of 500.000 cells/mL onto the apical side of the plates' inserts; the apical and basolateral chambers of the well are filled respectively with 200 µL and 600 µL of FGM™-2 supplemented with 3 mM L-ascorbate. When a further kidney is donated to our research group, hPTC are isolated as described in 2.2.1 and are seeded onto the mitomycin C-treated fibroblasts, as depicted in **Figure 2.4, [C]**. The 3D constructs are fed with 200 µL REGM™ on the apical compartment of the well, and 600 µL FGM™-2 on the basolateral compartment. Media is changed every 48 hours until the epithelial barrier is formed.

Hydrogel embedment

To halt fibroblast migration into the epithelial cell monolayer while keeping fibroblasts viable and metabolically active, cells were embedded in an array of synthetic hydrogels (Manchester Biogel, UK) that would mimic the extracellular matrix found in the renal tubule-interstitium.

Among the gels trialled to establish the 3D contact co-culture model, the hydrogel Alpha RGD PeptiGel® was taken forward. Inserts' membranes are pre-wetted with PBS for 1 hour to allow for better gel coating, while Alpha RGD PeptiGel® is centrifuged at 1600 g for 1 minute to avoid bubble formation. 1 mL of gel Is transferred to a new tube. HRF are isolated from a donor kidney as described in 2.2.2 and cultured onto a T-75 flask to confluency. Cells are detached from cell culture vessel and counted as previously described and the single-cell suspension is resuspended in 200 µL of FGM™-2 supplemented with 3 mM L-ascorbate. The cell suspension is transferred to the tube containing 1 mL of gel, and it is carefully mixed with a positive displacement pipette in order to obtain a homogenous gel-cells mix. 100 µL of the mixture are pipetted onto the apical side of each insert, while 1 mL of FGM™-2 medium is pipetted into the basolateral chamber of the well. The plate is incubated for 5 minutes in the incubator, and 250 µL of FGM™-2 are added to the apical chamber after incubation. To allow for homogenous gelification, the media is changed for both compartments three times within the first hour of incubation. Embedded cells are incubated overnight in the incubator, and media is changed once more. When a second kidney is donated to our research group, hPTC are isolated as described in 2.2.1 and are seeded onto the fibroblasts embedded in Alpha 2 RGD PeptiGel®, as depicted in **Figure 2.4, [D]**. The 3D constructs are fed with 200 µL REGM™ on the apical compartment of the well, and 600 µL FGM™-2 on the basolateral compartment. Media is changed every 48 hours until the epithelial barrier is formed.

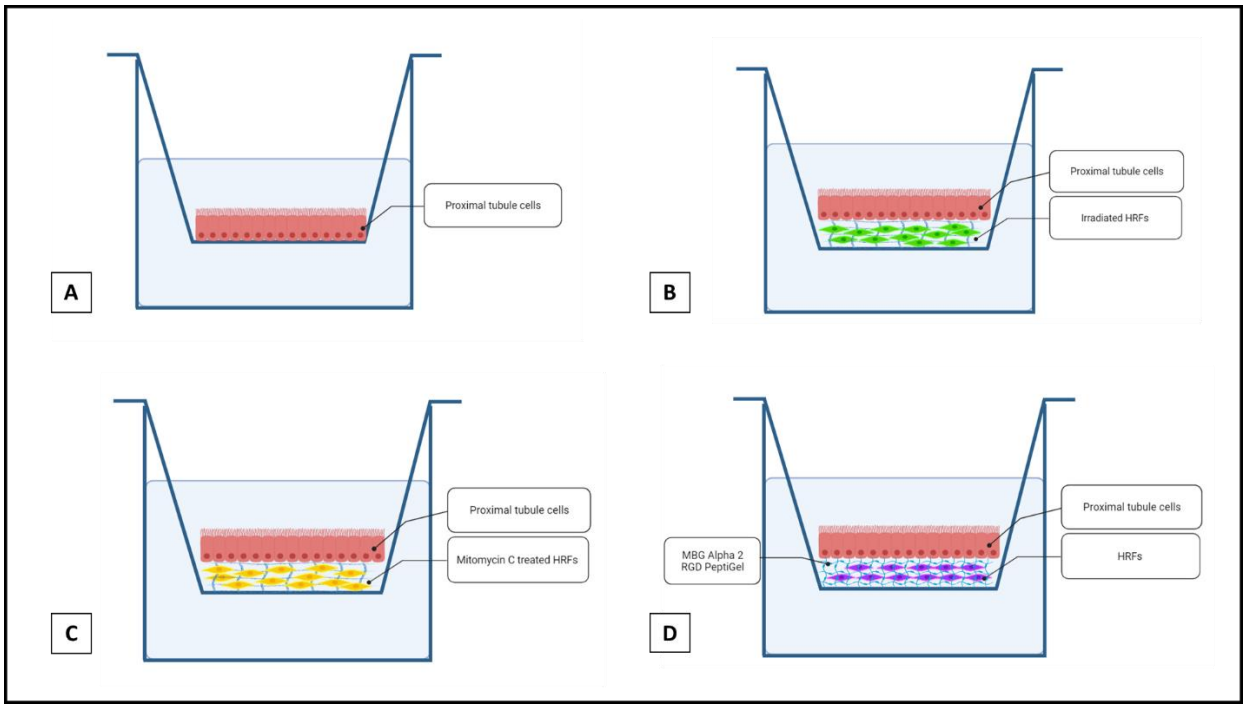

Figure 2.4. Graphical representation of 3D models cultured on Transwell® inserts [A] hPTCs seeded on the apical side of the insert [Control] [B] Irradiated HRF feeder layer and hPTC in contact co-culture on the inserts' apical side [C] HRF treated with mitomycin C and hPTC in contact co-culture on the inserts' apical side [D] HRF embedded in Alpha 2 RGD PeptiGel® and hPTC in contact co-culture on the inserts' apical side.

2.5.3 Non-contact co-culture models with hPTC, HRF and HRPEC

All the co-culture methods described so far entailed isolating the different components of the proximal tubule interstitial interface from two separate kidneys, increasing the biological variability within the 3D *in vitro* models which would then be reflected in the assays used to characterise the models. Therefore, the models depicted in **Figure 2.5** were generated by isolating human renal fibroblasts (2.2.2), human renal peritubular endothelial cells (2.2.3) and human proximal tubule cells (2.2.1) from the same human kidney cortex. HRPEC (**Figure 2.5, [B]**) and HRF (**Figure 2.5, [C]**) are first expanded via Percoll® density gradient isolation, cultured to confluency onto T-75 flasks in EGM™-2 medium supplemented with 40 ng/mL VEGF-A and FGM™-2 medium supplemented with 3 mM L-ascorbate, respectively, which are then purified via MACS based on positivity to CD31 and FSP-1. HRPEC are seeded at 500.000 cells/mL on the bottom of the well of a 96-Transwell® plate with no coating, whereas HRF are seeded at the same seeding density onto well bottoms coated with Biogel-X hydrogel with appropriate media. Simultaneously, proximal tubule cells are isolated from the same human kidney cortex via Percoll® density gradient isolation and seeded directly onto the inserts of a 96-Transwell® plate in REGM™ medium. HRPEC, HRF and hPTC are cultured to near-confluency for 3 to 4 days, and they are assembled in co-culture as represented in **Figure 2.5** until the epithelial barrier is formed. Media is changed every 48 hours to 100 µL REGM™ for the apical chamber, while for the basolateral chamber 200 µL of EGM™-2 or FGM™-2 are used according to cell type.

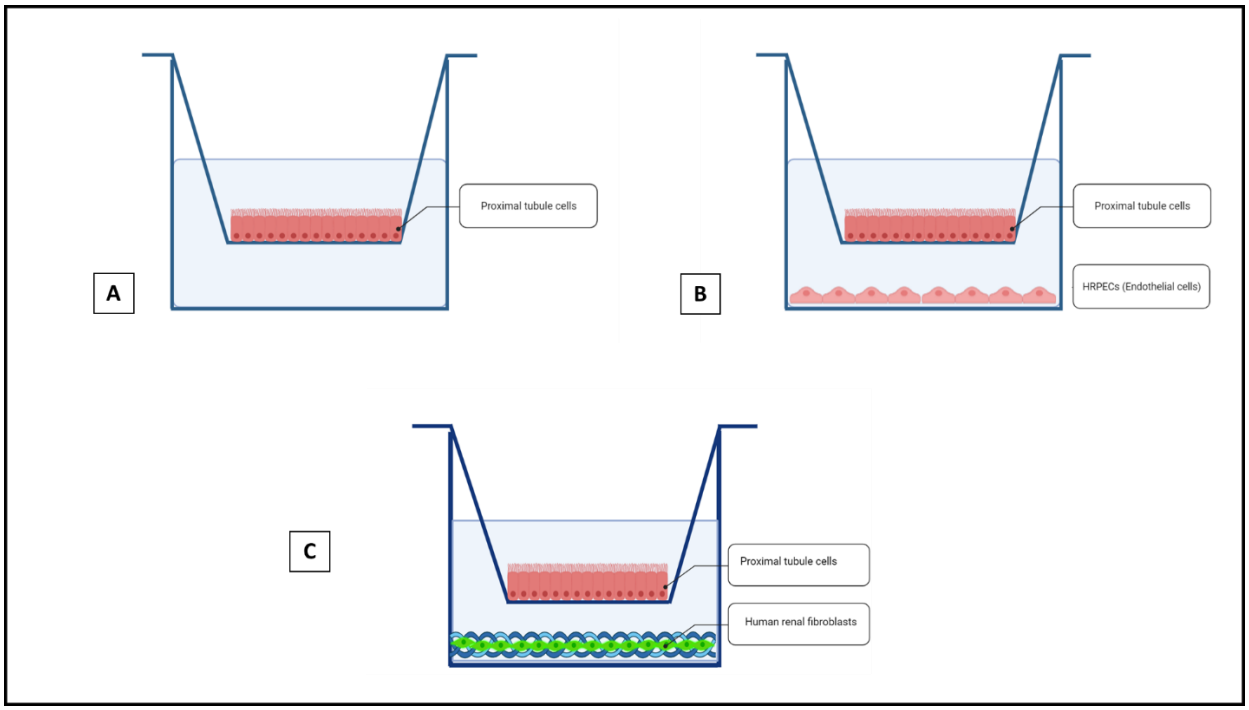

Figure 2.5. Graphical representation of 3D models cultured on Transwell® inserts [A] hPTCs seeded on the apical side of the insert [Control] [B] hPTC on the apical side of the insert, HRPEC on the bottom of the well [C] hPTC on the apical side of the insert, HRF on the bottom of the well.

2.6 Characterisation of 3D *in vitro* models

2.6.1 Transepithelial Electrical Resistance (TEER)

Transepithelial / transendothelial electrical resistance (TEER) is a quantitative assay that measures the integrity of tight junctions in endothelial and epithelial monolayers and co-culture models, which gives an indication of whether the epithelial barrier has formed *in vitro,* rendering the proximal tubule interstitial interface models apt for further functional measurements. To perform this assay on Corning® Transwell® inserts in 24-well and 96-well plates, the EVOM™ Epithelial Volt / Ohm (TEER) Meter (World Precision Instruments, UK) is used. The cells are cultured on a semipermeable membrane which divides the well into apical and basolateral compartments. Two "chopsticks"/electrodes are placed in the two compartments. The ohmic resistance is measured and calculated first by measuring the resistance of the semipermeable membrane only (blank), then by measuring the resistance across the cell monolayer or co-culture model. The data obtained are reported as $\Omega*cm^2$ to take into account the surface area on which the cells are cultured. TEER values are recorded daily from day 3-4 of culture of primary epithelial cells, and optimal TEER value ("TEER threshold") is considered reached when it is equal or above 60 $\Omega*cm^2$.

2.6.2 Lucifer Yellow leakage across 3D models

Lucifer Yellow (LY) is a fluorescent dye used to determine apparent paracellular permeability of confluent epithelial cells cultured on permeable membranes. This assay assumes that tight junctions formed between epithelial cells will allow only a relatively small amount of this compound to permeate from the apical to the basolateral compartment. Since Lucifer Yellow is fluorescent, it is possible to add it to one of the two compartments and measure its "leakage" to the other compartment at specific timepoints by sampling a volume of liquid from the compartment of interest and measuring the fluorescence intensity.

Lucifer Yellow (LY) powder is dissolved in Krebs buffer at 37°C, pH 7.4 to give a 10 µM solution. This solution is added to the apical compartment of Transwell® inserts while Krebs buffer (NaCl (140 mM), KCl (5.4 mM), MgSO4 (1.2 mM), KH2PO4 (0.3 mM), NaH2PO4 (0.3 mM), CaCl2 (2mM), glucose (5 mM), and HEPES or MES (10 mM)) is added to the basolateral compartment. The cells are incubated for the desired time on a thermostat-controlled heated platform that ensures the temperature is kept at 37°C for the whole duration of the assay. At the desired sampling timepoint, 50 µL are sampled from the basolateral compartment and transferred to a black-walled 96-well assay plate with clear bottom. In the meantime, a six point standard curve is derived through serial dilution of the 10 µM Lucifer Yellow solution. Fluorescence intensity (FI) is immediately measured with CLARIOstar™ Plate Reader (BMG Labtech, UK) and interpolated with the standard curve.

2.6.3 Radiolabelled creatinine and para-amino hippuric acid (PAH) flux and uptake across 3D models

Measurement of creatinine flux and para-amino hippuric acid (PAH) flux is performed as previously published by the Brown et al., 2008 to assess transporter function of proteins OCT2, MATE1, OAT1, and OAT3 in hPTC in monoculture as compared to the 3D co-culture

models. Prior to the start of this assay, cell confluency on translucent Transwell® multiwell plates is assessed via transepithelial electrical resistance (TEER) and can be determined by using the WPI EVOM™ voltohmeter equipped with chopstick electrodes. This instrument works under the basis that most of the electrical current that is applied to an epithelium flows between the cells, thus providing a measure of how tight cell-cell junctions are. According to previous publications from our research group (Brown, Sayer, Windass, Haslam, de Broe, et al., 2008), the TEER of a confluent human proximal tubule cell monolayer is around 60 $\Omega*cm^2$, which is considered our "threshold" value to perform experiments. Since in this project various cell types are used, some of which do not reach 60 $\Omega*cm^2$ at confluency, experiments were performed when proximal tubule cells in monoculture (control condition) reached the said value. Confluent monolayers or 3D models cultured onto translucent Transwell® permeable filter support are washed by dipping each insert into three beakers of Krebs buffer at 37°C pH 7.4 (NaCl (140 mM), KCl (5.4 mM), MgSO4 (1.2 mM), KH2PO4 (0.3 mM), NaH2PO4 (0.3 mM), CaCl2 (2mM), glucose (5 mM), and HEPES or MES (10 mM)). Cells are then equilibrated with differential pH across apical and basolateral compartments (respectively pH 6.8 and 7.4) and the temperature of the plates is kept at 37°C throughout the whole assay by a thermostat-controlled heated platform. Prior the beginning of the flux measurement, half of the inserts are incubated for 30 minutes with compounds that inhibit creatinine and PAH transport, namely 100 µM dolutegravir (DTG) for creatinine flux and 200 µM probenecid for PAH flux. The flux assay begins when Krebs buffer present in the apical or basolateral compartments is aspirated and replaced with solutions containing the radiolabelled compounds creatinine (14C isotope activity of 0.5 µCi/mL) and PAH (3H isotope activity of 1 µCi/mL) both at concentration of 10 µM. These solutions also contain 10 µM radiolabelled mannitol which enables the measurement of paracellular flux. After 60 minutes of flux of the radiolabelled compounds across apical and basolateral compartments, 50 µL from the contralateral chamber are sampled. The sample is ejected into a scintillation vial. The experiment is terminated by dipping the inserts into three beakers of Krebs buffer at 4°C. The permeable membranes are excised from the inserts with a scalpel and placed into scintillation vials. These samples provide a measure of the amount of radiolabelled compound that accumulated inside the cells over 60 minutes of flux, which is indicative of substrate uptake from either apical or basolateral compartment. Radioactivity in all samples was determined by liquid scintillation spectrophotometry after 2 mL of Optiphase Hisafe 2 scintillation solvent (Perkin Elmer, UK) was added. Radioactivity in terms of disintegration per minute was detected using TriCarb 2910 liquid scintillation counter (Perkin Elmer, UK).

2.6.4 FITC-albumin uptake

The FITC-Albumin uptake assay is used to compare transporter function capabilities between hPTC monolayers and 3D *in vitro* co-culture models cultured on permeable inserts as it characterises the membrane binding sites of large molecules and their subsequent uptake into proximal tubule cells. FITC is a fluorophore coupled to albumin through the ε-amino group of lysines of albumin. The FITC molecule fluoresces upon excitation at 495 nm, emitting light at 530 nm which is measured by CLARIOstar™ Plate Reader. Quantification of FITC-Albumin is calculated using an eight-points standard curve to determine the amount of FITC-Albumin uptaken per µl of cell lysate. FITC-Albumin is dissolved in Krebs buffer to a working

concentration of 50 µg/mL. Cells and 3D constructs are washed with warm Krebs buffer, and FITC-Albumin is added at increasing concentration for every condition of culture. Cells are incubated on a hot plate at 37°C for 3 hours to allow for protein uptake. To stop the uptake reaction, cells are washed in ice-cold Krebs. The cells are then incubated with lysis buffer for 1 hour in 0.25 mL per insert of 0.1% SDS. The cellular lysates are aliquoted into an empty 96-well plate and the fluorescence emitted by each well is measured by the plate reader. The collected data is interpolated with the standard curve to quantify the amount of fluorescently labelled albumin incorporated by the cells. The data is represented as a dose-response graph for each culture condition whereby the increasing concentration of FITC-Albumin which the cells are exposed to [1, 10, 100 µg/mL] is depicted on the X axis (dose) whereas the amount of FITC-Albumin uptaken by the cells is expressed on the Y axis (response).

2.6.5 CellTiter-Glo® Luminescent Cell Viability Assay

This assay determines the number of viable cells present in culture by measuring the intracellular ATP present in culture. The assay is performed directly onto the cells cultured in medium by applying the CellTiter-Glo® Reagent (Promega, USA) which lysates the cells present in culture. The lysate is transferred to a clear bottom white walled 96-well plate and the ATP is measured by luminescence with CLARIOstar™ Plate Reader. The experiment is performed on 3D models and monolayer following manufacturer's instructions.

2.6.7 Click-iT™ EdU Cell Proliferation Assay

EdU (5-ethynyl-2´-deoxyuridine) is a thymidine analog which is incorporated into DNA during active DNA synthesis. Detection is based on click chemistry: a copper catalysed covalent reaction between an azide and an alkyne. In this application, the alkyne is found in the ethynyl moiety of EdU, while the azide is coupled to Alexa Fluor® 647 dye. Standard flow cytometry methods are used for determining the percentage of S-phase cells in the population. The experiment is performed on 3D models and monolayers following manufacturer's instructions.

2.6.8 Annexin V-FITC / PI Apoptosis / Necrosis Assay (Immunofluorescence staining)

The aim of this assay is to detect apoptotic and necrotic cells in hPTC monolayers and 3D co-culture models via fluorescence microscopy. Shortly after the initiation of the apoptosis process, the membrane molecules phosphatidylserine are translocated outside the cell membrane, on the cell surface. The presence of these molecules on the cell surface is detected by staining with the protein Annexin V conjugated to the fluorophore FITC, while the addition of the intercalating agent propidium iodide (PI) highlights necrotic cells. This kit is used on live cells according to manufacturer's instructions with the addition of 10 µg/ml Hoechst 3342 staining dye solution as nuclear counterstain after fixation.

2.6.9 MSD U-Plex Assay for stress biomarkers release (KIM-1, NGAL, Clusterin)

The aim of this assay is to determine whether hPTC in co-culture with other cellular components of the interstitial interface release in the cell culture medium a significantly lower amount of stress biomarkers as compared to the monoculture condition. A custom MSD U-Plex Assay for stress biomarker release from proximal tubule cells had been designed and

optimized in our research group prior the start of this project as described in Bajaj et al., 2018. A panel of three relevant biomarkers were selected based on the literature, namely KIM-1 (Kidney Injury Model 1), NGAL (Neutrophil gelatinase-associated lipocalin), and clusterin.

50 µL of cell culture medium are sampled from hPTC monolayers and for each 3D *in vitro* model taken into account for this experiment, and they are transferred to an empty 96-well plate for stress biomarker release analysis. Biotinylated capture antibodies are coated on U-PLEX plates using U-PLEX linkers. These linkers self-assemble onto unique spots on the U-PLEX plate. Analytes in the sample bind to the capture reagents, detection antibodies conjugated with electro-chemiluminescent labels (SULFO-TAG) bind to the analytes to complete the immunoassay sandwich. Once the assay is complete, the U-PLEX plate is loaded into the MSD instrument (QuickPlex SQ120, ACROBiosystems, USA) where a voltage is applied to the plate electrodes causing the captured labels to emit light. The instrument measures the intensity of emitted light, which is proportional to the amount of analyte present in the sample, to provide a quantitative measure of each analyte in the sample. The experiments are performed following manufacturer's instructions.

2.7 Characterisation of high throughput 3D *in vitro* model of renal fibrosis

2.7.1 Establishment of fibrotic phenotype via pro-fibrotic endogenous and exogenous compound treatment

The aim of this protocol is to treat hPTC and HRF in monoculture on CELLSTAR® 96-well black walled clear bottom plates and in co-culture on Corning® Transwell® inserts in 96-well plates with pro-fibrotic endo- and exogenous compound combinations to establish dose / response curves that will correlate the increasing dose of treatment used to the biological endpoints measured via TEER measurement, high content imaging, high throughput flow cytometry, cell viability assay, stress biomarker release assay, and human chemokine microarray to establish a 3D *in vitro* renal fibrosis assay platform.

Cells are isolated and cultured to confluency as described in 2.2.1 and 2.2.2. When confluency is reached (for monocultures) or TEER threshold value (for co-cultures), plates are treated with increasing concentrations of TGFβ1 [1, 10, 100 ng/mL], TNFα [1, 10, 100 ng/mL], Angiotensin II [10, 100, 1000 nM], Polymyxin B [1, 10, 100 µM], and IGF-1 [1, 10, 100 ng/mL] (PeproTech, USA) in RPMI-1640 (Roswell Memorial Park Medium) supplemented with 0.1 % FCS (Foetal Calf Serum). To investigate interactions between the endogenous compounds listed above, a matrix plate treatment plan is used, as depicted in the plate layout below. Two technical repeats per condition are included in the treatment plan to account for well-to-well variability and pipetting errors. For cells in monoculture, the treatment solutions are applied directly onto the wells, whereas for cells in co-culture the treatment solution is applied onto the insert chamber (apical compartment), while the basolateral compartment is filled with vehicle medium RPMI-1640 0.1 % FCS. Control wells (depicted in the plate layout as "0") are filled with vehicle medium, too. Plates are incubated for 24 hours, which is the selected timepoint of treatment. After 24 hours, plates are used for subsequent experiments.

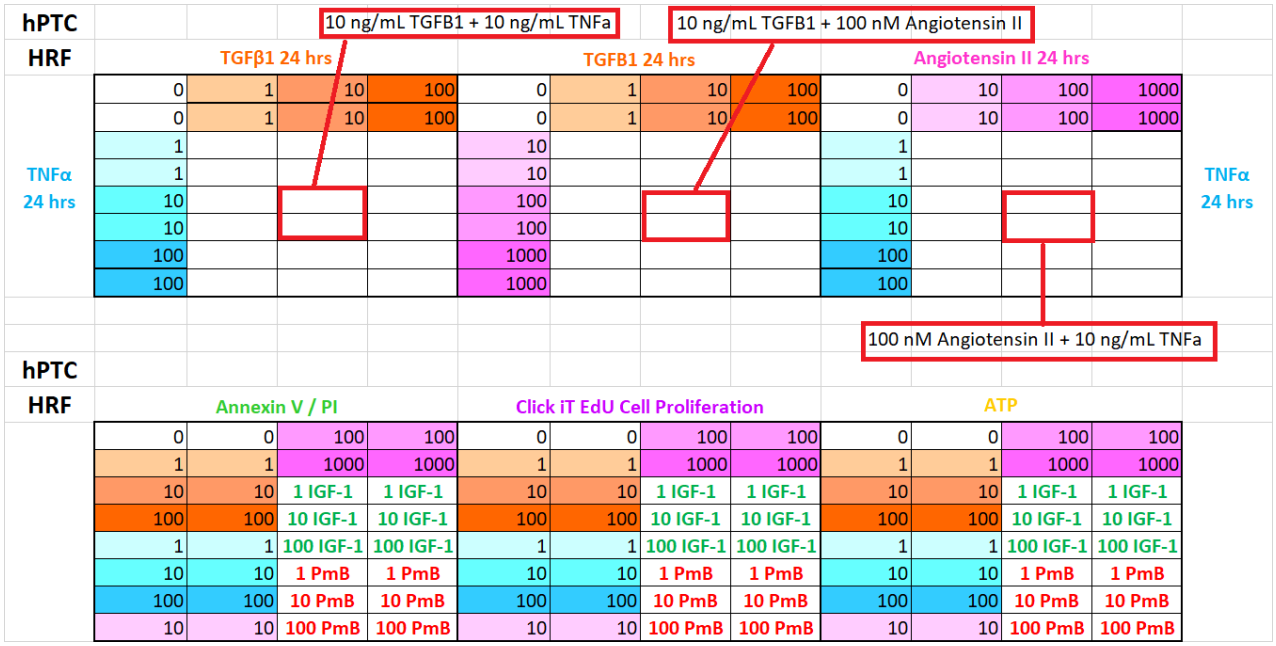

Figure 2.6. Plate layout depicting the treatment scheme used to induce renal fibrosis in hPTC and HRF in monoculture and co-culture.

2.7.2 TEER

To monitor epithelial barrier disruption caused by pro-fibrotic treatment of hPTC, trans-epithelial electrical resistance (TEER) is measured in cells in co-culture cultured onto Transwell® inserts in 96-well plates from day 3-4 of hPTC culture as described in 2.6.1. The measurements collected after 24 hours of treatment with pro-fibrotic compounds are plotted as dose-response graphs where the increasing dose of treatment is depicted on the X axis (dose) while TEER in $\Omega*cm^2$ is shown on the Y axis (response).

2.7.3 Immunofluorescence staining for high content imaging on 96-Transwell™ platform

Treated hPTC and HRF in monoculture and co-culture undergo immunofluorescence staining to tag with fluorophores proteins which are known to be relevant in the molecular processes that underly the progression of renal fibrosis *in vivo*, such as epithelial-to-mesenchymal transition (EMT / pEMT), *de novo* expression of mesenchymal markers, acquisition of contractile properties for renal fibroblasts and fully dedifferentiated epithelial cells, and extracellular matrix deposition.

Fixation and immunofluorescence staining procedures described in 2.3.3 are adapted to suit the 96-well and 96- Transwell™ plate format. In brief, after 24 hours of treatment all media is aspirated from all wells and compartments, and cells are fixed with 4% PFA in PBS for 15 minutes at room temperature in the dark. After PBS rinsing, cells undergo the described steps of permeabilization, blocking incubation to reduce unspecific signal, overnight incubation with primary antibodies (or with blocking buffer for “secondary antibody only” wells), incubation with secondary antibodies, and nucleus staining with Hoechst 33342 stain.

All information regarding primary and secondary antibodies (Abcam, UK) used for these experiments can be found in the table below:

hPTC

Species	Primary Antibody	Locum marked	Dilution (Antibody / Blocking buffer)
Rabbit	Anti ZO-1	Tight junction	1 / 50
Mouse	Anti E-Cadherin	Tight junction	1 / 100
Goat	Anti-Vimentin	Cytoplasm / cytoskeleton	1 / 1000

Species	Secondary Antibody	Protein tagged	Dilution (Antibody / Blocking buffer)
Goat	Anti-Rabbit Alexa Fluor 647™	ZO-1	1 / 300
Goat	Anti-Mouse Alexa Fluor 488™	E-Cadherin	1 / 300
Donkey	Anti-Goat Alexa Fluor 549™	Vimentin	1 / 300

HRF

Species	Primary Antibody	Locum marked	Dilution (Antibody / Blocking buffer)
Mouse	Anti αSMA	Cytoplasm / cytoskeleton	1 / 500
Rabbit	Anti Collagen I	Extracellular matrix (ECM)	1 / 500
Chicken	Anti Fibronectin	Extracellular matrix (ECM)	1 / 100

Species	Secondary Antibody	Protein tagged	Dilution (Antibody / Blocking buffer)
Goat	Anti Mouse Alexa Fluor 488™	αSMA	1 / 300
Goat	Anti Rabbit Alexa Fluor 647™	Collagen I	1 / 300
Goat	Anti Chicken Alexa Fluor 549™	Fibronectin	1 / 300

Table 2.4. Tables containing all information regarding primary and secondary antibodies used to establish the renal fibrosis in vitro assay platform.

All primary antibodies are incubated simultaneously in blocking buffer since they are all raised in different hosts. Regarding the secondary antibodies used to mark proteins expressed by hPTC, incubations must be staggered to avoid secondary antibodies raised in goat to cross-react with the Donkey Anti Goat Alexa Fluor 549™ secondary antibody. Therefore, after overnight incubation of hPTC with the three primary antibodies listed above, cells are

incubated first with Donkey Anti Goat Alexa Fluor 549™ secondary antibody to mark Goat Anti Vimentin, then they are washed with PBS 3 times for 5 minutes and subsequently they are incubated with blocking buffer solution containing the two remaining secondary antibodies, namely Goat Anti Rabbit Alexa Fluor 647™ and Goat Anti Mouse Alexa Fluor 488™. This issue does not arise for HRF staining as selected primary and secondary antibodies do not incur in the risk of cross-reaction.

2.7.4 High throughput flow cytometry assays: Click-iT™ EdU Cell Proliferation Assay and Annexin V-FITC / PI Apoptosis / Necrosis Assay

Cell cycle and cell health assays are used in the context of the establishment of the renal fibrosis *in vitro assay* platform to monitor changes in percentage of proliferating, apoptotic, and necrotic cells among hPTC and HRF cell populations in monoculture and co-culture as dysregulation of such cellular events are known to be involved in the progression of renal fibrosis *in vivo*. Therefore, high throughput flow cytometry is used to establish dose-response curves where percentage of proliferating, apoptotic, and necrotic cells (Y axis) is plotted in relationship to the increasing dose of pro-fibrotic treatment (X axis).

These protocols have been adapted from the procedures described in 2.6.7 and 2.6.8 to suit the 96-well plate format. For technical reasons, Annexin V-FITC / PI Apoptosis / Necrosis Detection assay (Abcam, UK) is performed first on one section of the treated plate (according to plate layout depicted in **Figure 2.6**). Wells are washed with 100 µL of PBS per well 3 times for 5 minutes. Cells are incubated with 50 µL TrypLE™ Express Enzyme per well for 10 minutes in the incubator until complete cell detachment is observed. To inactivate the enzymatic reaction, 150 µL REGM™ or FGM™-2 medium (depending on the cell type in question) per well are added. The single-cell suspension contained in each well is transferred to a new empty 96-well plate. The plate is centrifuged for 5 minutes at 300 g to pellet cells, the supernatant is removed from all wells, and cells are resuspended in 200 µL per well of calcium containing Annexin V Binding Buffer (Abcam, UK). Cells are incubated for 5 minutes in the dark with 2 µL per well of apoptosis and necrosis markers Annexin V and PI. Cells are washed via centrifugation with Annexin V Binding Buffer for 5 minutes at 300 g. Cell pellets are resuspended in 200 µL per well of Annexin V Binding Buffer. Standard flow cytometry procedures are used to record the percentage of apoptotic and necrotic cells for each well via Attune™ NxT Flow Cytometer Autosampler (Thermo Fisher Scientific, UK).

To perform the Click-iT™ EdU Cell Proliferation Assay (Thermo Fisher Scientific, UK), cells are incubated with 10 µM EdU (5-ethynyl-2'-deoxyuridine) for 2 hours in the incubator to allow for the thymidine analog to be incorporated into the DNA of proliferating cells. After incubation, cells are detached into a single-cell suspension as described for the Annexin V-FITC / PI assay. Once cells are pelleted, they are resuspended in 100 µL per well of 1% w/w Bovine Serum Albumin in PBS. The plate is centrifuged at 300 g for 5 minutes to pellet the cells, and the supernatant is aspirated. 100 µL per well of fixative reagent are added, and the plate is incubated for 15 minutes at room temperature in the dark. All wells are washed with 200 µL per well of 1% w/w Bovine Serum Albumin in PBS, the plate is centrifuged at 300 g for 5 minutes, and the supernatant is discarded. Cells are resuspended in 100 µL permeabilization reagent per well. Cells are incubated with 250 µL per well of Click-iT™ reaction mix containing

buffer additive, PBS, $CuSO_4$, and Alexa Fluor 647™ azide for 30 minutes at room temperature in the dark. The plate is then washed with 100 µL permeabilization reagent per well and centrifuged at 300 g for 5 minutes. Supernatant is discarded and cells are resuspended in 100 µL permeabilization reagent per well. Standard flow cytometry procedures are used to record the percentage of proliferating cells for each well via Attune™ NxT Flow Cytometer Autosampler (Thermo Fisher Scientific, UK).

2.7.5 CellTiter-Glo® Luminescent Cell Viability Assay

This assay is used in the context of establishing a renal fibrosis *in vitro* assay platform to investigate the correlation between cell viability and increasing dose of pro-fibrotic treatment to which hPTC and HRF are exposed to. The assay measures intracellular ATP via the measurement of the generated luminescent signal, as described in 2.6.5. The data recorded by CLARIOstar™ Plate Reader is plotted as dose-response curve where luminescence is depicted on the Y axis (response) and increasing dose of pro-fibrotic treatment is shown on the X axis (dose).

2.7.6 MSD U-Plex Assay for stress biomarkers release (KIM-1, NGAL, Clusterin)

The stress biomarker release assay measures the production and release of KIM-1, NGAL, and clusterin by human proximal tubule cells in the cell culture medium. After 24 hours of treatment with pro-fibrotic compounds of hPTC in monoculture and co-culture, 50 µL of medium are sampled from each well and they are transferred to an empty 96-well plate. The collected samples are assayed as described in 2.6.9, according to manufacturer's instructions.

The data collected is plotted as actual amount of analyte per condition (in picograms), amount of analyte proportional to intracellular ATP (picograms of analyte / luminescence), and amount of analyte proportional to cell number (picograms of analyte / cell number) to account for variations in cell number induced by pro-fibrotic treatments over 24 hours in relationship to the increasing dose of pro-fibrotic compound (X axis).

2.7.7 Human Chemokine Antibody Array

The Human Chemokine Antibody Array – 38 targets (Abcam, UK) is used to screen among 38 chemokines that can be released by human renal fibroblasts under pro-fibrotic stimuli. Human renal fibroblasts in monoculture and co-culture with hPTC are treated with 100 ng/mL of TGFβ1 in RPMI-1640 0.1 % FCS for 24 hours, whereas control cells are incubated with vehicle medium. After 24 hours, the cell culture medium is sampled from treated and control cells. The assay works in a similar fashion to an ELISA, using a membrane as a substrate where capture antibodies are spotted to measure a different analyte per spot. One sample per condition is added to each membrane, which is then incubated with biotinylated antibodies followed by streptavidin HRP. The chemokine microarray membranes are then analysed measuring chemiluminescence (G:BOX Chemi XRQ gel doc system, Syngene, India), which is then quantified via densitometry using Fiji ImageJ. The experiments are carried out according to manufacturer's instructions.

The analysed protein targets in the cell culture medium are listed below:

BLC / CXCL13, CCL28, Ck beta 8-1 / CCL23, CTACK, CXCL16, ENA-78 / CXCL5, Eotaxin-1 / CCL11, Eotaxin-2 / CCL24, Eotaxin-3 / CCL26, Fractalkine / CX3CL1, GCP-2 / CXCL6, GRO / CXCL1+2+3, GRO alpha / CXCL1, HCC-4 / CCL16, I-309 / CCL1, I-TAC / CXCL11, IL-8 / CXCL8, IP-10 / CXCL10, Lymphotactin / XCL1, MCP-1 / CCL2, MCP-2 / CCL8, MCP-3 / CCL7, MCP-4 / CCL13, MDC / CCL22, MIG / CXCL9, MIP-1 alpha / CCL3, MIP-1 beta / CCL4, MIP-1 delta / CCL15, MIP-3 alpha / CCL20, MIP-3 beta / CCL19, MPIF-1 / CCL23, NAP-2 / CXCL7 / PPBP, PARC / CCL18, RANTES / CCL5, SDF-1 alpha / CXCL12alpha, SDF-1 beta / CXCL12beta, TARC / CCL17, TECK / CCL25.

2.7.8 High Content Imaging: ImageXpress Pico

hPTC and HRF cultured on CELLSTAR® 96-well black walled clear bottom plates in monoculture and in co-culture on Corning® Transwell® inserts in 96-well plates are imaged with high content imaging microscope ImageXpress Pico (Molecular Devices, USA). DAPI filter cube is used to excite cellular nuclei containing Hoechst 33342 dye, GFP filter cube is used to excite proteins tagged with fluorophore Alexa Fluor 488™, Texas Red filter cube excites proteins tagged with Alexa Fluor 594™, and Cy5 filter cube excites proteins tagged with Alexa Fluor 647™. Focus points and exposure times are determined when establishing the imaging protocol: focus is adjusted by focusing on four wells are the edges of the plate, while exposure time is automatically calculated by the microscope and kept constant for experiments carried out on the same type of plate.

2.7.9 Image Analysis: CellReporterXpress

Images collected by ImageXpress Pico are analysed with CellReporterXpress (Molecular Devices, USA) using the built-in cell scoring image analysis pipeline based on segmentation: the algorithm parameters such as cell dimensions and upper and lower thresholds of fluorescence intensity are established by training the algorithm on a number of images representative of the widest possible range of conditions. For proximal tubule cells (hPTC), two algorithms are established: one to measure the variations in protein expression among the cell borders (**Figure 2.7**), and one to measure the variations of protein expression within the borders of cellular nodules formed by migrating epithelial cells after pro-fibrotic treatment (**Figure 2.8**). For human renal fibroblasts, only one algorithm is established to measure changes in protein expression within the cellular borders (**Figure 2.9**).

The algorithms are able to quantify changes in all tagged proteins as the concentration of pro-fibrotic compound used to treat the cells increases. For hPTC, nuclear area, average nuclear intensity, E-Cadherin average cell intensity, vimentin average cell intensity, and ZO-1 average cell intensity are plotted as single-cell values in frequency of distribution curves and dose-response curves (Y axis – response). For HRF, nuclear area, average nuclear intensity, αSMA average cell intensity, fibronectin average cell intensity, and collagen I average cell intensity are plotted as single-cell values in frequency of distribution curves and dose-response curves (Y axis – response).

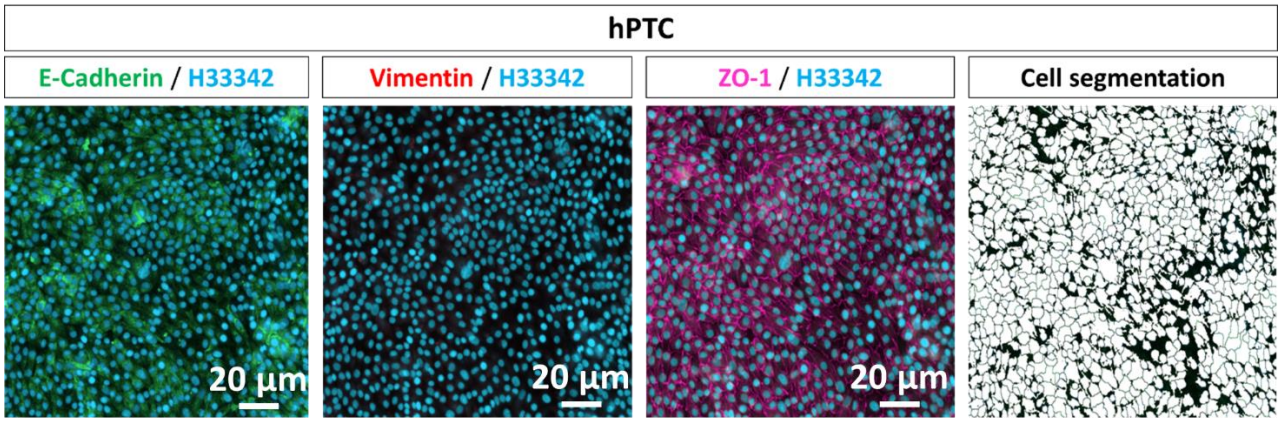

Figure 2.7. Representative images of hPTC immunofluorescence stained with anti E-Cadherin, anti vimentin, anti ZO-1 primary antibodies and appropriate secondaries used to establish algorithm parameters for cell segmentation used to obtain high content imaging measurements from the developed renal fibrosis in vitro model.

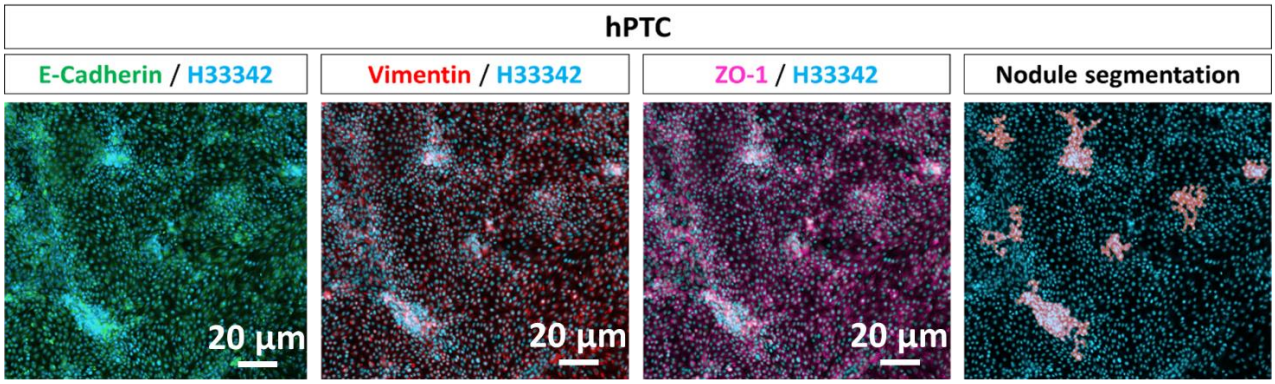

Figure 2.8. Representative images of hPTC immunofluorescence stained with anti E-Cadherin, anti vimentin, anti ZO-1 primary antibodies and appropriate secondaries used to establish algorithm parameters for epithelial nodule segmentation used to obtain high content imaging measurements from the developed renal fibrosis in vitro model.

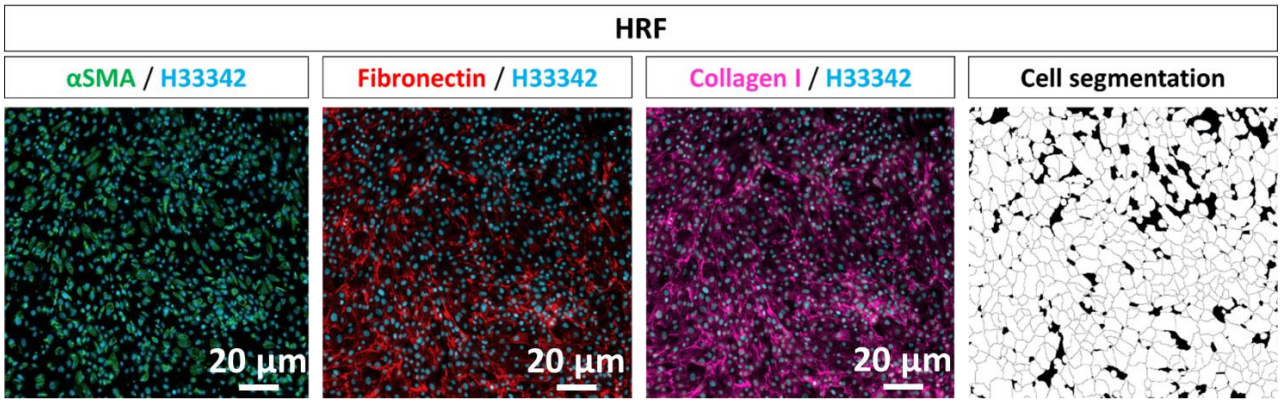

Figure 2.9. Representative images of HRF immunofluorescence stained with anti αSMA, anti fibronectin, anti collagen I primary antibodies and appropriate secondaries used to establish algorithm parameters for cell segmentation used to obtain high content imaging measurements from the developed renal fibrosis in vitro model.

2.7.10 Statistical analysis

Data collected from assays performed on the *in vitro* renal fibrosis platform are expressed as mean ± standard error of mean (SEM) of three biological replicates equivalent to three donor kidneys or mean ± standard deviation (SD) of two or more technical replicates if collected from only one biological replicate equivalent to one donor kidney. Data are analyzed with statistical analysis software GraphPad Prism 9 (GraphPad Software, USA). Firstly, the data undergoes normality tests of D'Agostino, Anderson-Darling, Shapiro-Wilk, and Kolmogorov-Smirnov, and based on the outcome of such tests the combined data is analysed to compare the difference in measurements elicited between the untreated condition [0 ng/mL] and the increasing doses of pro-fibrotic compounds used for the treatments using ordinary two-way ANOVA with main effects only, followed by a Dunnet's multiple comparison test, with a single pooled variance if the data is normally distributed or non-parametric Kruskal-Wallis test with Dunn's multiple comparisons test if the data does not pass the normality test.

Chapter 3. Establishment of isolation protocols and characterization of cellular components of the proximal tubule interstitial interface.

3.1 Introduction

The proximal tubule interstitial interface is composed by tubular epithelial cells, interstitial cells such as renal fibroblasts, and endothelial cells forming capillaries. Exogenous and endogenous compound excretion from the human body entails solute exchange between the tubular lumen, which at the proximal tubule level contains ultrafiltrate formed by the filtration of blood by the glomerulus, and the blood flowing through the peritubular capillaries. Therefore, cells which form the tubule-interstitium are highly differentiated to carry out the specialist task of transporting compounds across tubular and capillary lumina. The features of the three cell types taken into consideration for the development of a 3D *in vitro* model of the proximal tubule interstitial interface can be summarised by their phenotype, both in terms of relevant protein marker expression and functionality. **Chapter 2** focused on describing the isolation protocols utilised to obtain proximal tubule cells, human renal fibroblasts, and human renal peritubular endothelial cells from the kidney cortex, while the current chapter will firstly take the reader through the optimization steps that lead to the establishment of the isolation protocols afore described, to then demonstrate the validity of the protocols via genotyping and phenotyping.

Proximal tubule cells express several solute transporters which follow a specific polar distribution across the apical and basolateral membrane of the epithelial cell. Tight junction complexes play a key role in maintaining polarity, and, in turn, they are responsible for the formation of a leak-tight epithelium that only allows certain compounds to be moved across the tubule-interstitium. Another striking phenotypical feature of tubular epithelial cells is the cilium which protrudes from the apical membrane of the cell into the tubular lumen. Successful isolation and characterization of proximal tubule cells from the kidney cortex are demonstrated by Brown et al., 2008. The publication from our research group describes the established isolation protocol using Percoll® density gradient centrifugation to retrieve a mixture of proximal and distal tubule cells from the kidney cortex and focuses on the functional characterization of such population as compared to a purified distal tubule cell population. The experiments performed during the course of this project focused on comparing the mixed proximal / distal tubule cell population with a purified hPTC population in terms of protein and functional phenotype, and genotype regarding key transporters. Moreover, since the overall aim of this project is to develop a high throughput *in vitro* assay

platform suitable for imaging, phenotyping of the chosen tubular epithelial population is carried out via immunofluorescence staining of relevant markers.

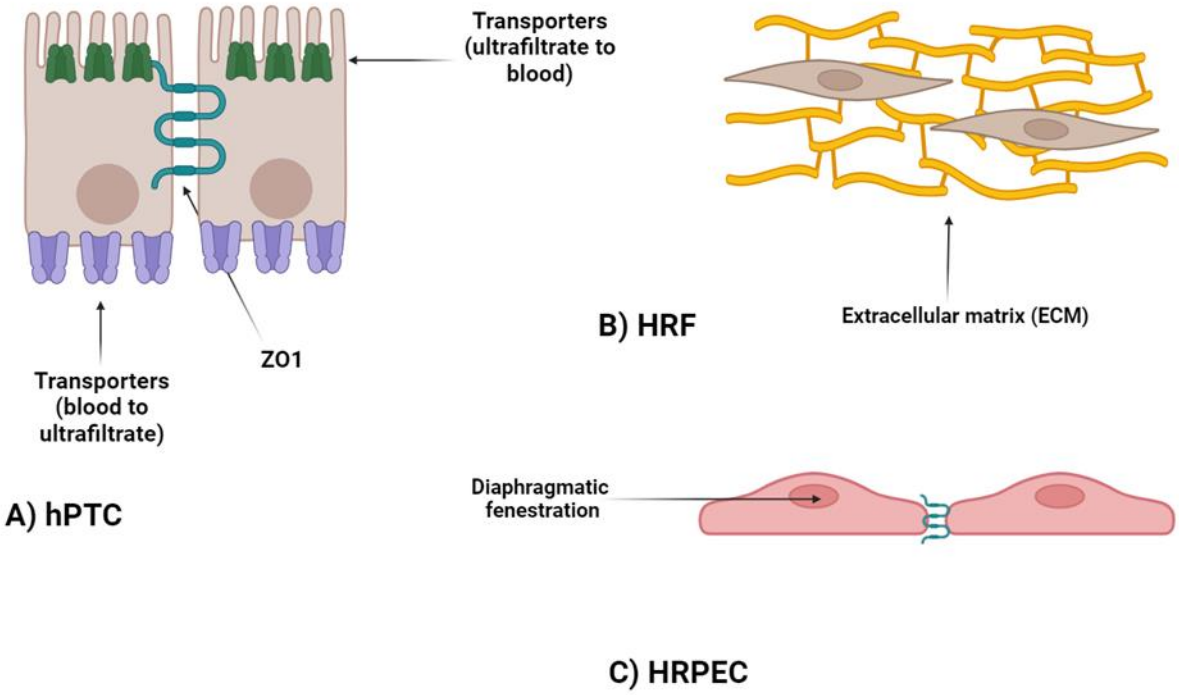

Figure 3.1. Diagram representing the three cellular components of the proximal tubule interstitial interface, proximal tubule cells (hPTC), human renal fibroblasts (HRF) embedded in extracellular matrix (ECM), and human peritubular endothelial cells (HRPEC) (Original image).

Human renal fibroblasts are essential components of the renal parenchyma which role is to provide structural and trophic support to other cell types present in the tubule-interstitium by depositing the extra cellular matrix and releasing growth factors such as fibroblast growth factors (FGFs) which have been found to be essential for appropriate tubular epithelial development and differentiation (Kurtzeborn et al., 2018). Epithelial-to-mesenchymal communication is a mechanism that underlies both maladaptive and repair processes in renal physiopathology via cross-talk between tubular epithelial cells and renal fibroblasts involving a plethora of endogenous soluble compounds including angiotensin II, TGFβ1, and sonic hedgehog and Wnt ligands (Tan et al., 2016). Therefore, the presence of human renal fibroblasts in the construction of an *in vitro* model of the proximal tubule interstitial interface has been deemed necessary, hence requiring the establishment of an isolation protocol which would allow to retrieve this cell type from the human kidney cortex alongside the human proximal tubule cells since this had not been developed before among our research group. Existing isolation protocols for the isolation and purification of renal fibroblasts from the human kidney cortex, even if concerning tissue from rodents, mainly focused on *ex vivo* propagation of mesenchymal cells (Grimwood & Masterson, 2009), (Nakai et al., 2021) and further cell sorting via positivity to mesenchymal markers. As described in **Chapter 2.2,** renal fibroblasts are isolated via Percoll® density gradient centrifugation followed by Magnetic Activated Cell Sorting (MACS) of cells positive for the marker FSP-1 (Fibroblast Specific Protein

1) (Nishitani et al., 2005a) which is expressed uniquely by fibroblasts in the tubule-interstitium therefore making it the ideal candidate as live isolation marker. One of the objectives of this project is to develop a patient-specific *in vitro* model of the proximal tubule interstitial interface, therefore finding appropriate isolation methods to obtain simultaneously human renal fibroblasts from fresh human kidneys alongside with proximal tubule cells has been one of the main challenges of the project.

Filtration, reabsorption, and secretion are renal functions which would not be feasible without the presence of neatly specialised endothelium in the renal parenchyma, as endothelial cells have adapted to specific *milieu* to support the tasks carried out by glomeruli, cortex, and medulla. Thus, renal endothelial cells are characterised by heterogeneous phenotypes, mirroring the functions of their epithelial counterparts. Maintenance of highly differentiated vascular architecture is fundamental for the kidney to carry out its physiological functions, hence transition to pathological phenotypes prompted by pro-fibrotic and pro-inflammatory stimuli in the context of the endothelium has devastating effects on the overall capability of the organ to maintain a balanced internal environment in the human body, as seen for endothelial-to-mesenchymal transition and capillary rarefaction, both maladaptive phenomena involved in progressive renal fibrosis, and ultimately, CKD. As this project revolves around the proximal tubule, our focus is on the endothelium surrounding the proximal tubule among the components of the renal vasculature: the cortical peritubular capillaries. These specialised structures are composed of renal peritubular endothelial cells which supply the epithelium and the interstitium with nutrients and oxygen while reabsorbing and secreting endogenous and exogenous compounds from the blood to the interstitium and vice versa. Apart from their capability of forming capillaries, the main feature of human renal peritubular endothelial cells (HRPEC) is the expression of plasmalemma vesicle-associated protein-1 (PV1) which covers the diaphragmed fenestrae found on the peritubular capillaries, present to ease the water and solute exchange between the ultrafiltrate and the blood. This protein and, consequently, the diaphragmatic fenestrae are not expressed by glomerular endothelial cells, thus allowing phenotypical characterisation of HRPEC *in vitro* (Dumas et al., 2021a). In this chapter, a novel method to isolate large quantities of human renal peritubular endothelial cells (HRPEC) from the human kidney cortex is described. The method has been inspired by the seminal work of Ligresti *et al.* (Ligresti et al., 2016), where the importance of epithelial cells depletion during the isolation process and presence of VEGF-A in culture was highlighted for the first time.

Aims

We hypothesise that it possible to successfully isolate and culture *in vitro* from the autologous human kidney cortex the singular cellular components of the proximal tubule interstitial interface and that they can retain the phenotype and functional characteristics found in vivo. The aims of this chapter are to take the reader through the development and optimisation of protocols to isolate such cell populations.

As anticipated in the previous paragraphs, this chapter will comprehend data obtained to validate the isolation methods used to retrieve hPTC, HRF, and HRPEC from the human kidney cortex. The aims of this chapter are:

- To compare tubular epithelial cell populations comprising pure hPTC and proximal / distal tubule cells via TEER measurement, flow cytometry, RT-qPCR, and radiolabelled creatinine flux assay.
- To assess epithelial barrier formation in the isolated hPTC population in relationship to transporters' gene expression and tight junction formation over culture time via TEER measurement, RT-qPCR, and immunofluorescence staining.
- To characterise polarised transporter expression and cilia presence at the protein level in hPTC monolayers via immunofluorescence staining and 3D imaging.
- To demonstrate appropriate phenotypical characterization of human renal fibroblasts isolated via newly established method via immunofluorescence staining and flow cytometry.
- To demonstrate isolation protocol optimisation for human renal peritubular endothelial cells achieved by phenotyping via immunofluorescence staining, flow cytometry and endothelial tube formation assay.

3.2 Purification of AQP1+ tubular epithelial cell population via MACS reduces distal tubule cell presence but reduces epithelial barrier function in hPTC monolayers.

In a previous publication from our research group, Brown *et al.* compared mixed hPTC / DTC populations to pure DTC, but not to pure hPTC, to demonstrate that the mixed cell population retrieved from the kidney cortex via Percoll® density gradient centrifugation is showing transporter expression and function typical of the proximal tubule. The hypothesis formulated prior to the design of the following experiments entails that a purer hPTC population could yield to higher transporter expression which will be mirrored by increased transporter function as compared to a mixed tubular epithelial population, thus conducing to a more *in vivo*-like proximal tubule model. These cells alongside cells isolated only via Percoll were cultured for seven days on ThinCert and Transwell inserts.

To obtain the mixed DTC / hPTC population, cells are isolated via Percoll® density gradient centrifugation are cultured on 24-well transparent Thincert™ inserts directly, whereas to purify hPTC after Percoll® density gradient centrifugation, proximal tubule cells are positively selected via MACS using a mouse antibody against aquaporin 1 (AQP1) (Maunsbach et al., 1997) coupled with micro beads against mouse IgG (Percoll® density gradient + MACS AQP1+).

Phenotyping and genotyping is carried out via phase contrast imaging, TEER measurement, RT-qPCR, flow cytometry, and transporter function assay. Results from these experiments show that phase-contrast images of renal epithelial cells isolated via the two different methods in **Figure 3.2 [A]** and **[B]** display different morphologies. Both images show cells with typical cobble-stone conformation, but in image **[A]** epithelial cells seem to be closer to each other and the tight junctions formed appear to be thicker as compared to the monolayer formed by the cells in image **[B]**. These results correlate with the TEER values shown in **Figure 3.2 [C]**, which shows that depleting DTC from the hPTC / DTC mixed population by selecting for AQP1+ cells yields to monolayers generating a lower TEER for the purer hPTC population. The phenotype exhibited by cell populations isolated with two different isolation methods is compared via flow cytometry, where density plots show that Percoll® density gradient centrifugation yields two distinct cell populations, while MACS AQP1+ purification effectively reduces it to one uniform population based upon size (FSC-A) and granularity (SSC-A) (**Figure 3.3**). A panel of three markers is selected, namely the proximal tubule cell marker AQP1 (Maunsbach et al., 1997), principal cells and collecting duct marker AQP2 (Takata et al., 2008), and distal tubule cell and thick ascending limb cell marker uromodulin (Tokonami et al., 2018). Moreover, both isolation methods seem to successfully isolate more than 80% AQP1 positive cells and almost no UMOD positive cells, but 30% of Percoll isolated cells are positive for AQP2 while only 10% of Percoll® density gradient + MACS AQP1+ isolated cells are positive for AQP2, confirming that MACS AQP1+ purification generates a purer population of proximal tubule cells from the renal cortex as compared to Percoll® density gradient centrifugation only. Complete gating strategy depicting single cell populations, doublets, live/dead cell populations, and fluorescence minus one controls are depicted in the same figure. Our research group used fluorescence minus one (FMO) controls instead of IgG isotype controls. This has to do with having to match each primary conjugated antibody to an IgG isotype control conjugated to the same fluorophore, which would prove to be expensive, despite IgG controls being essential to demonstrate specific binding of the primary antibody to the protein target to tag.

Gene expression of several transporters expressed mainly by proximal tubule cells are considered and compared for both isolation methods via RT-qPCR performed on RNA extracted from one biological repeat per isolation method (**Figure 3.4**). Although Percoll® density gradient followed by MACS AQP1+ yields to a purer proximal tubule cell population, thus hinting that expression of proximal tubule-specific genes should be higher, expression of not all transporters is found to be increased for this condition. Megalin, OCT2, MATE1, MRP2, SLC2A9, and NaPi2a expression is increased in the purified epithelial population as compared to cells isolated via Percoll® density gradient centrifugation only, in turn, relevant transporter expression such as OAT1, OAT3, MDR1, and URAT1 decreases in the purified population. Transporter OCT2 (organic cation transporter 2) is expressed on the basolateral membrane of polarized proximal tubule cells and it is responsible for the uptake of creatinine inside the cell, while experimental evidence suggests that apical transporters MATE1, MATE2K and MDR1 are responsible for the efflux of creatinine from the cell (Brown, Sayer, Windass, Haslam, De Broe, et al., 2008), (Mathialagan et al., 2017). Therefore, the secretory flux (J_{B-A}) of creatinine should be greater than the absorptive flux (J_{A-B}), resulting in net secretion (J_{net}) of the

compound from the basolateral to the apical compartment. When DTC / hPTC and pure hPTC monolayers are exposed to radiolabelled creatinine for one hour, both populations show active transport of creatinine from the basolateral membrane, as depicted in **Figure 3.5 [A]**, where J_{B-A} is greater than J_{A-B}, thus showing appropriate OCT2 functionality for both types of monolayers. Interestingly, Percoll® density gradient + MACS AQP1+ purified monolayers show greater net secretion (J_{net}) as compared to Percoll isolated monolayers, although the difference is not statistically significant. Moreover, effective inhibition of OCT2 via dolutegravir is displayed only by purified monolayers. These data taken together suggest that the presence of distal tubule cells in culture with proximal tubule cells could exert trophic support in the differentiation and polarization of the latter cell type; although pure hPTC do form tight junctions resulting in measurable TEER values, these measurements stay below the 60 $\Omega*cm^2$ threshold which is relative to the TEER value of a tubular epithelial barrier *in vivo*, indicating that expression of the tight junction protein complexes might be incomplete in pure hPTC after seven day of culture. Furthermore, this theory is strengthened by the genotyping data which shows incomplete gene expression of key drug transporters in pure hPTC as compared to DTC / hPTC mixed population. Furthermore, from a technical standpoint, Percoll® density gradient centrifugation has proven to be a relatively inexpensive and fast isolation method to obtain large quantities of tubular epithelial cells from the human kidney cortex without the employment of further time-consuming purification processes, deeming this isolation method ideal for the development of a high throughput *in vitro* model of the proximal tubule interstitial interface. This isolation method is employed for the culture of tubular epithelial cells for all the experiments carried out throughout the project.

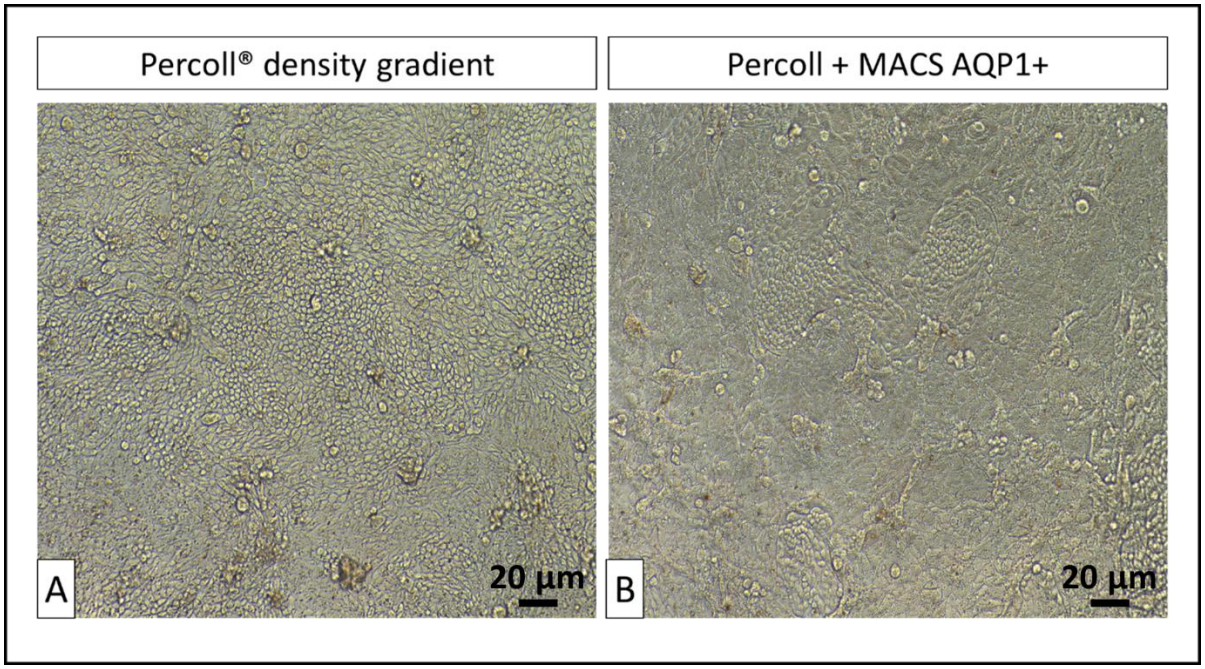

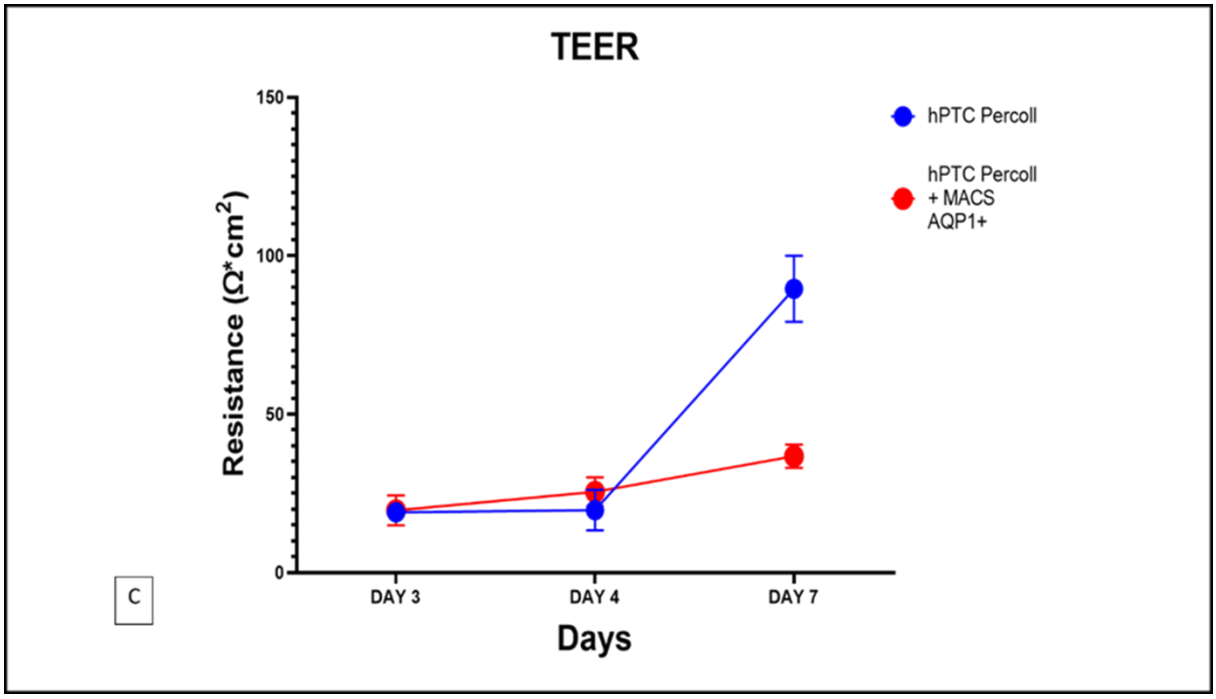

Figure 3.2. Phase-contrast images of epithelial cells isolated via [A] Percoll density gradient, showing typical cobblestone morphology and [B] Percoll + MACS AQP1+, showing enlarged morphology (scale bars=20 µm) [C] Trans Epithelial Electrical Resistance (TEER) measured over days of culture in hPTC isolated via the two different methods and cultured on 24-Transwell inserts shows a significant difference after 7 days in culture where purified hPTC exert lower TEER than the unsorted population. Data represent the mean between twelve technical replicates from one biological replicate while error bars represent SD (n=1).

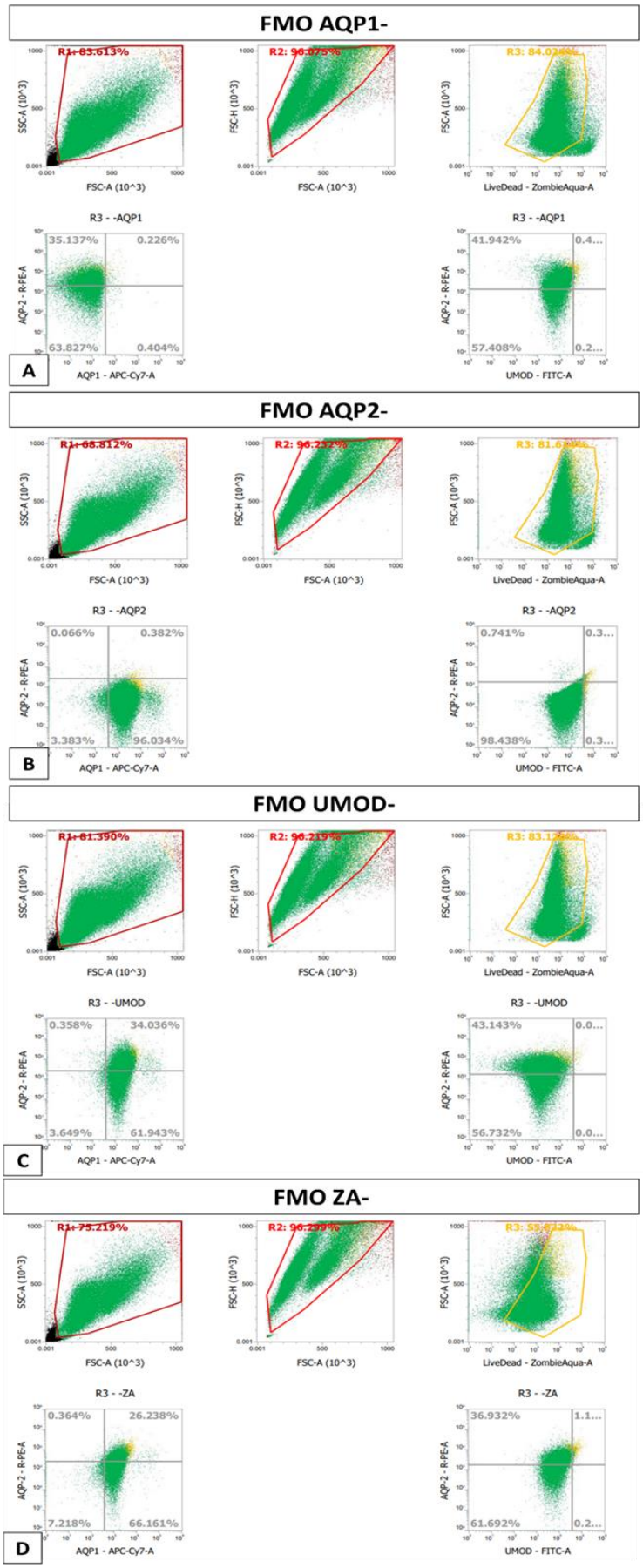
FMO AQP1-
R1: 83.613%
SSC-A (10^3)
FSC-A (10^3)
R2: 96.075%
FSC-H (10^3)
FSC-A (10^3)
R3: 84.026%
FSC-A (10^3)
LiveDead - ZombieAqua-A
R3 - -AQP1
35.137%
0.226%
63.827%
0.404%
AQP-2 - R-PE-A
AQP1 - APC-Cy7-A
R3 - -AQP1
41.942%
0.4...
57.408%
0.2...
AQP-2 - R-PE-A
UMOD - FITC-A
A
FMO AQP2-
R1: 68.812%
SSC-A (10^3)
FSC-A (10^3)
R2: 96.232%
FSC-H (10^3)
FSC-A (10^3)
R3: 81.6...
FSC-A (10^3)
LiveDead - ZombieAqua-A
R3 - -AQP2
0.066%
0.382%
3.383%
96.034%
AQP-2 - R-PE-A
AQP1 - APC-Cy7-A
R3 - -AQP2
0.741%
0.3...
98.438%
0.3...
AQP-2 - R-PE-A
UMOD - FITC-A
B
FMO UMOD-
R1: 81.390%
SSC-A (10^3)
FSC-A (10^3)
R2: 96.219%
FSC-H (10^3)
FSC-A (10^3)
R3: 83.1...
FSC-A (10^3)
LiveDead - ZombieAqua-A
R3 - -UMOD
0.358%
34.036%
3.649%
61.943%
AQP-2 - R-PE-A
AQP1 - APC-Cy7-A
R3 - -UMOD
43.143%
0.0...
56.732%
0.0...
AQP-2 - R-PE-A
UMOD - FITC-A
C
FMO ZA-
R1: 75.219%
SSC-A (10^3)
FSC-A (10^3)
R2: 96.299%
FSC-H (10^3)
FSC-A (10^3)
R3: 55.4...
FSC-A (10^3)
LiveDead - ZombieAqua-A
R3 - -ZA
0.364%
26.238%
7.218%
66.161%
AQP-2 - R-PE-A
AQP1 - APC-Cy7-A
R3 - -ZA
36.932%
1.1...
61.692%
0.2...
AQP-2 - R-PE-A
UMOD - FITC-A
D

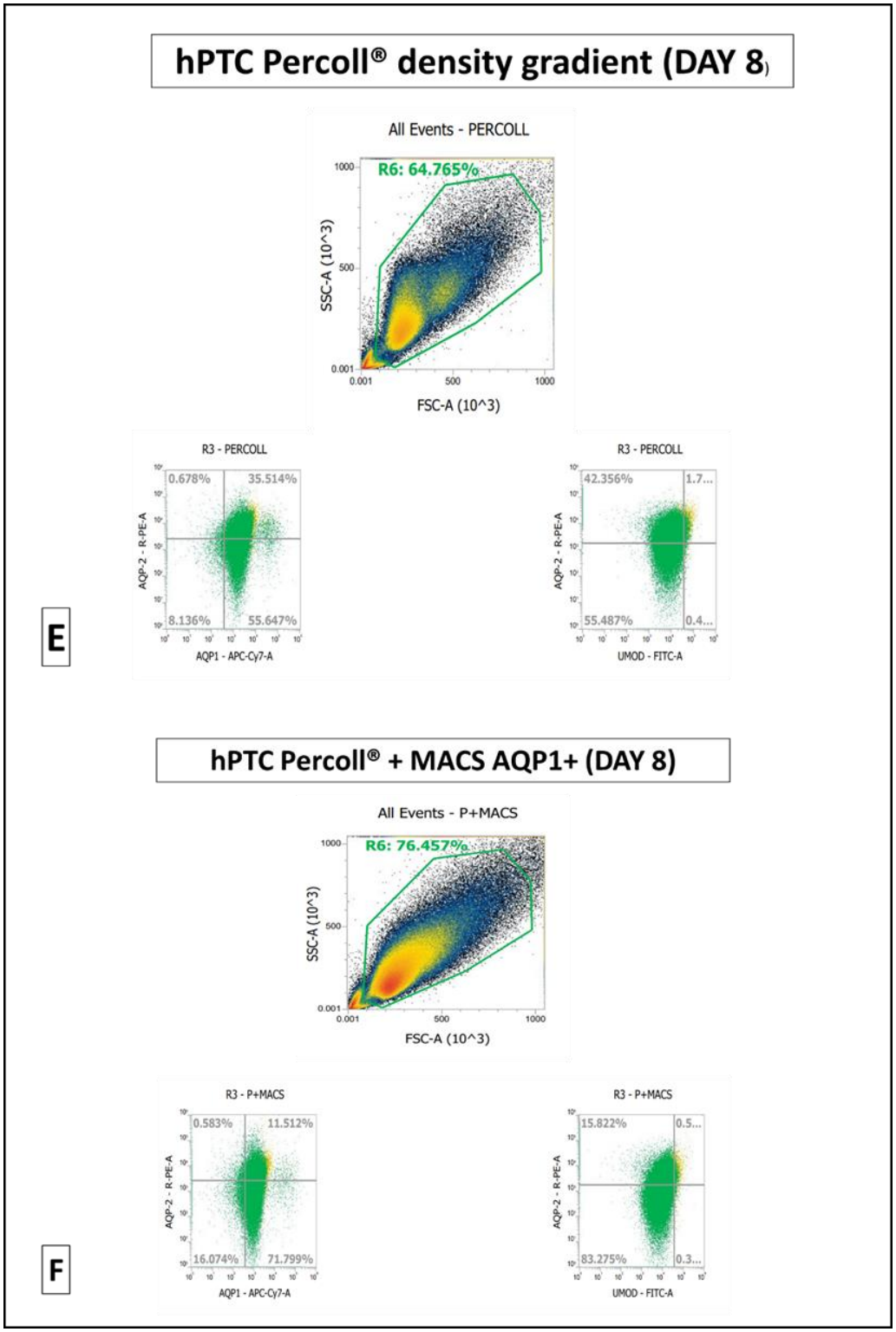

Figure 3.3. Flow cytometry dot plots depicting the percentage of live cells expressing tubular epithelial markers AQP-1, AQP-2, and UMOD (Uromodulin). Gating strategy based on fluorescence minus one (FMO) controls depicted in [A] AQP1-, [B] AQP2-, [C] UMOD-, [D] ZombieAqua-. Singlets depicted in FSC-A / SSC-A dot plots, doublets shown in FSC-A / FSC-H dot plots, live/dead cells shown in ZombieAqua / FSC-A dot plots. Fully stained samples obtained via [A] Percoll density gradient and [B] Percoll + MACS AQP1+ showing different

phenotype depending on isolation method used. Purified population in [F] shows lower AQP2+ percentage as compared to unsorted population in [E].

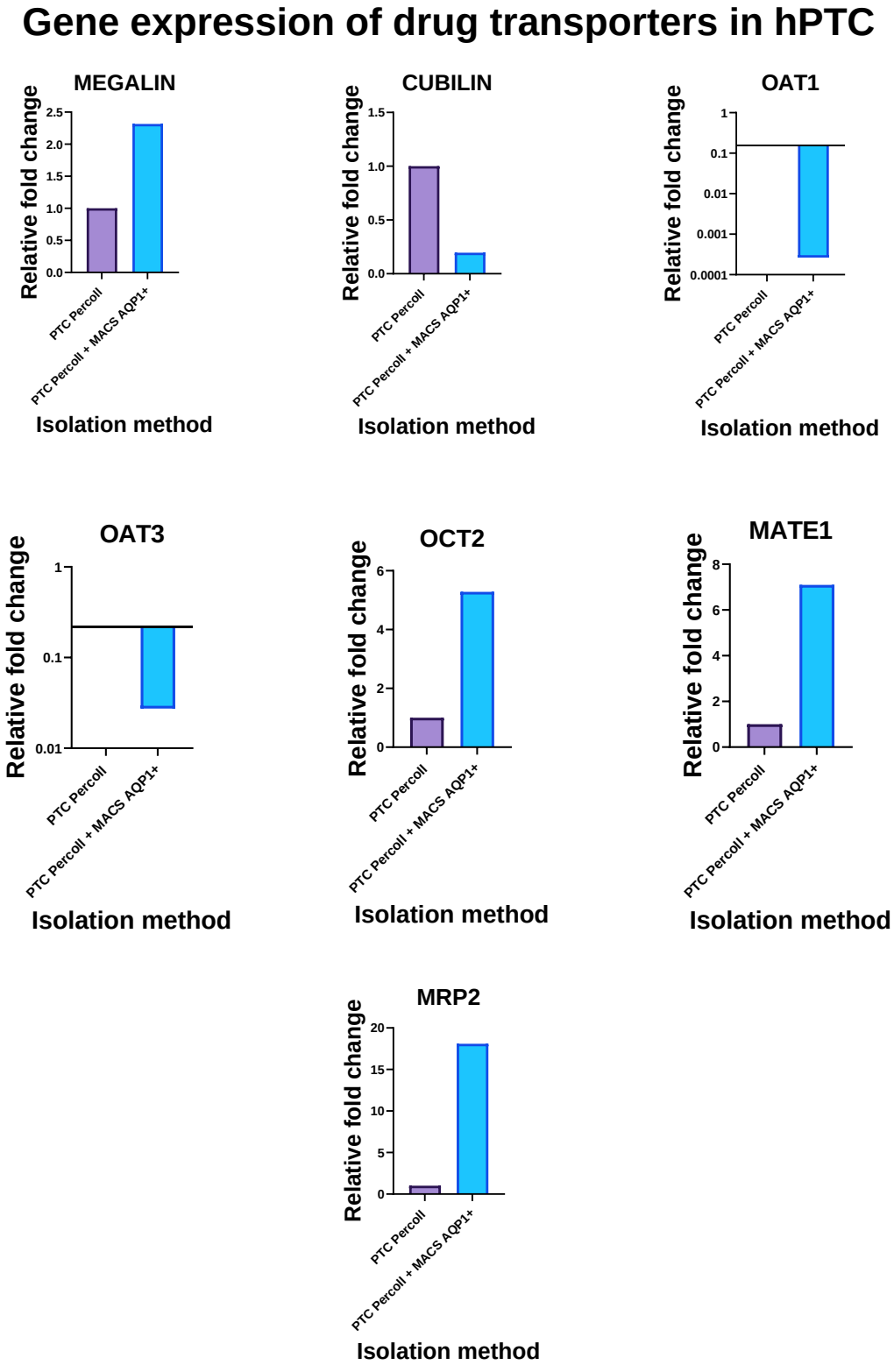

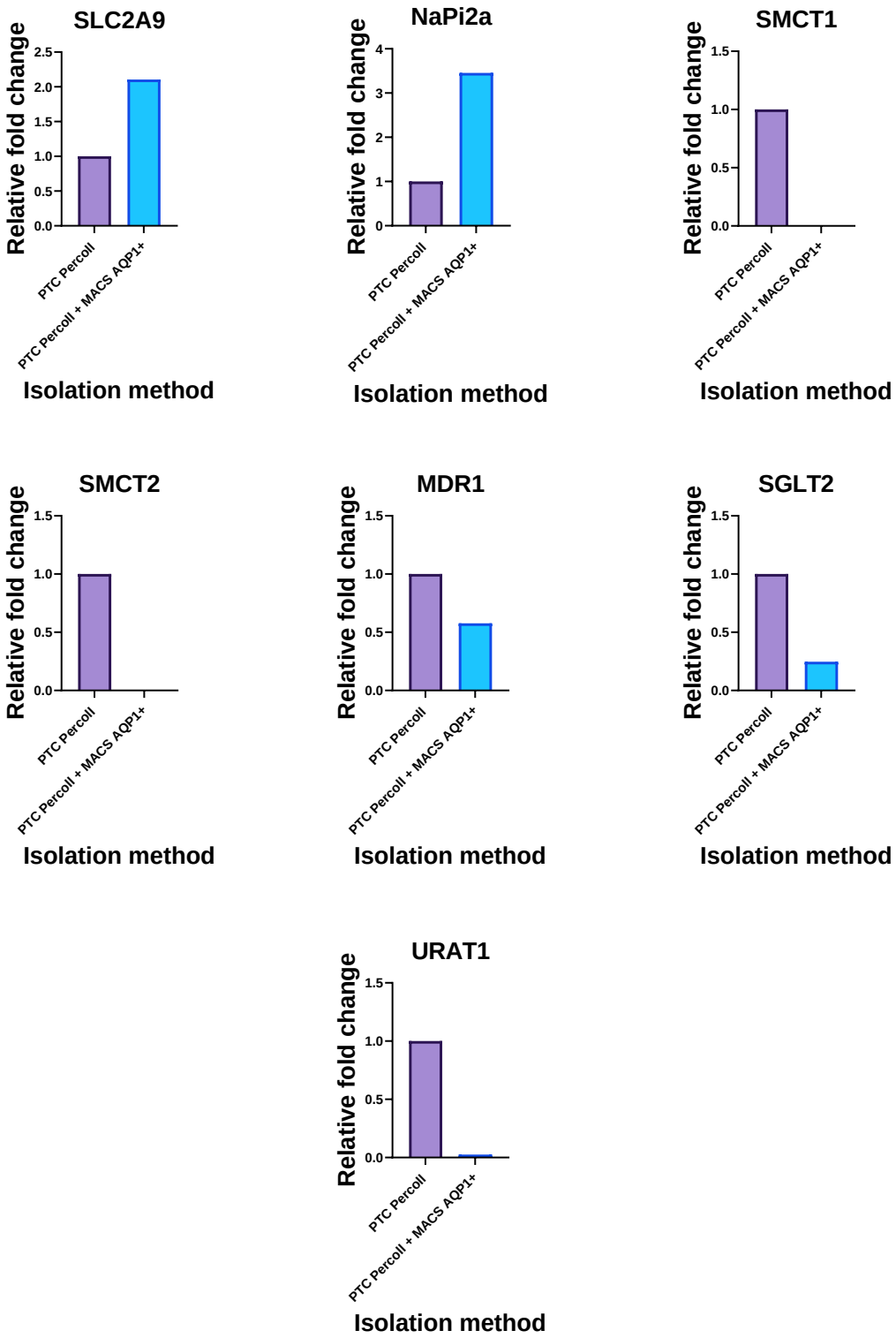

Figure 3.4. RT-qPCR data measuring hPTC relative fold change of the gene expression of drug transporters Megalin, Cubilin, OAT1, OAT3, OCT2, MATE1, MRP2, NaPi2a, SMCT2, MDR1, URAT1, SLC2A9 between two different isolation methods. Purified population 'PTC Percoll + MACS AQP1+' shows upregulation in genes encoding for key solute transporters Megalin, OCT2, MATE1, MRP2, SLC2A9, NaPi2a as compared to unsorted population 'PTC Percoll', and

downregulation of cubilin, OAT3, SMCT1, SMCT2, URAt1. Bars represent the mean between three technical replicates from one biological replicate (n=1) after 2^-(ΔΔCt) transformation

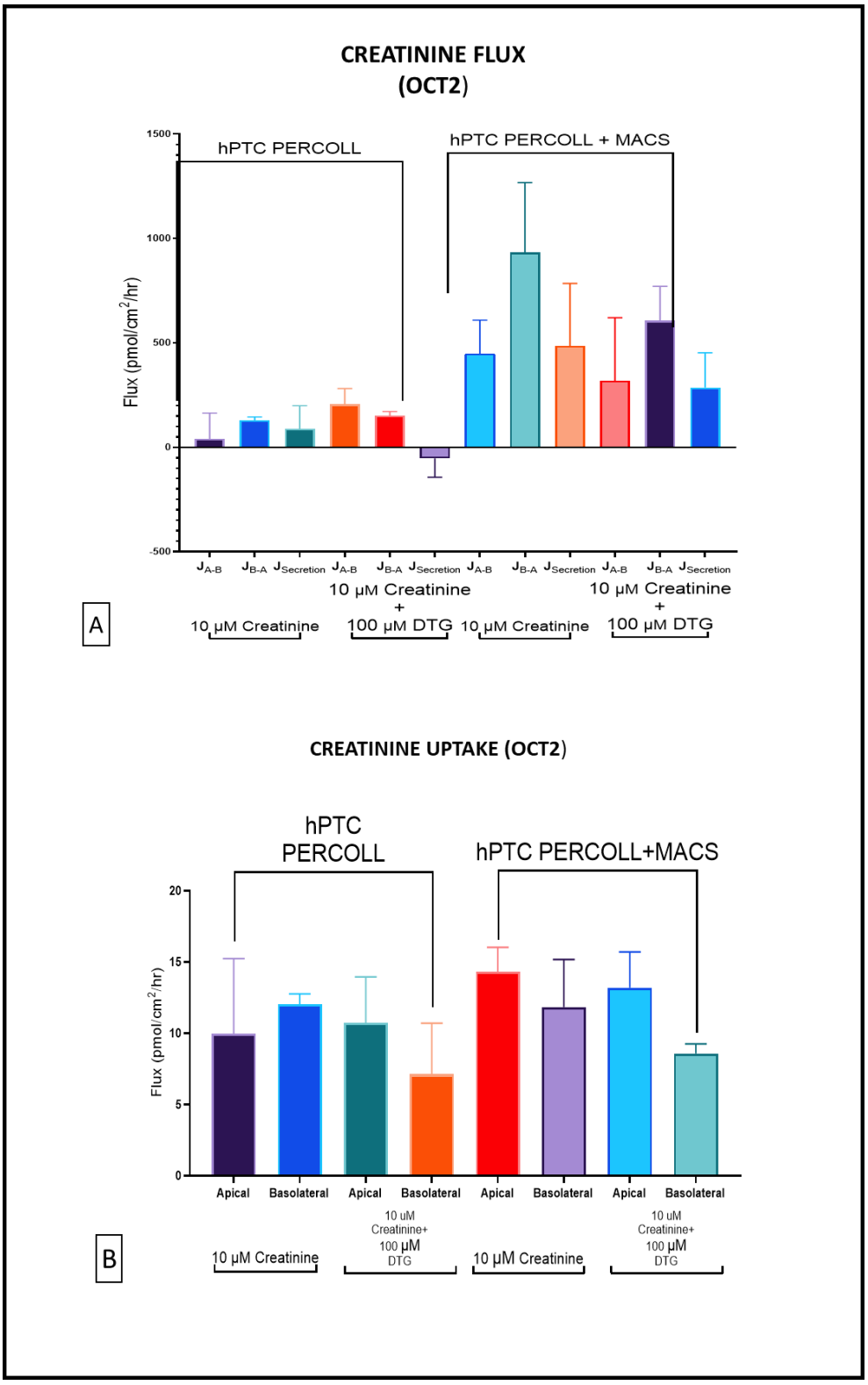

Figure 3.5. [A] Creatinine flux across the epithelial monolayers with and without OCT2 inhibitor (dolutegravir) after 60 minutes corrected for paracellular flux with mannitol. Purified hPTC population 'Percoll + MACS' shows higher creatinine net secretion as compared to the unsorted population 'Percoll' [B] Creatinine uptake from the epithelial monolayers with or

without OCT2 inhibitor after 60 minutes. Purified hPTC population 'Percoll + MACS' shows higher creatinine uptake as compared to the unsorted population 'Percoll' Data are presented as the mean ± SD between three technical replicates from one biological replicate (n=1).

3.3 hPTC cultured on permeable membranes form polarized monolayers which express drug transporters and exert epithelial barrier function *in vitro.*

Human proximal tubule epithelial cells (hPTC) are isolated from the human kidney cortex and cultured for 7 days on a flask. After 2 days in culture, they begin to form colonies that become confluent on day 5. hPTC typical epithelial morphology (Jun et al., 2018) can be seen in **Figure 3.6** below. Since the overall aim of this project is to develop an assay platform suitable for imaging, the characterization and phenotyping of hPTC is performed via immunofluorescence staining. Due to laboratory skills and microscopy equipment available at the beginning of this project, preliminary and antibody optimisation experiments are performed on epithelial cells cultured on gel-coated coverslips, to then transition to cryo-sectioned translucent 24-Transwell® inserts imaged with widefield fluorescence microscopes, to finally obtain high quality maximum intensity projection Z-stacks from planar transparent 24-well Transwell® or Thincert™ insert membranes mounted onto microscope slides.

hPTC seeded onto glass coverslips are stained with fluorescein labelled Lotus Tetragonolobus Lectin (LTL), a glycoprotein widely used as proximal tubule marker (H. Wu & Humphreys, 2020). The images in **Figure 3.7** show a confluent hPTC monolayer staining positively for LTL. The polarization of hPTC is key to their function to determine whether the hPTC monolayer cultured on Corning® Transwell® inserts is polarized, immunofluorescence staining for key polarization markers is performed on monolayers. Further characterisation shown in **Figure 3.8** displays abundant aquaporin-1 (AQP1) expression, and polarized expression of the sodium/phosphate co-transporter (NaPi2a) in the brush border of the hPTC membrane.

To investigate the presence of primary cilium at the apical pole of the proximal tubule, which underlines actual separation of the plasma membrane into two areas that differ by protein expression (Maggiorani et al., 2015), hPTC seeded onto translucent Transwell® insert membranes are cryo-sectioned and immunofluorescence stained with antibodies against alpha-acetylated tubulin (axoneme – green) and pericentrin (centrosome – red), where pericentrin is one of the components of the centrosome, the latter being a developmental precursor of the primary cilium. Essentially, in differentiated tubular epithelial cells the mature cilium substitutes the centrosome which reappears during mitosis (Mühlhans et al., 2011) (**Figure 3.9**). The white arrow in **Figure 3.9** highlights a cilium arising from one of the hPTC cultured onto the cryo-sectioned membrane. Due to the fragility of the microtissue grown onto the membrane, cryo-sectioning proved to be a technically challenging process, as it is noticeable by the cellular material pushed to the underside of the membrane by the sectioning process, thus shifting our efforts towards imaging such organelle onto a planar surface. Therefore, cilia are immunofluorescence stained with alpha-acetylated tubulin and pericentrin on 24-Transwell® insert membranes and imaged via widefield fluorescence microscopy, as portrayed in **Figure 3.10**, which show lack of unspecific binding of the secondary antibodies used against the above-mentioned primary antibodies, thus confirming the specificity towards the cilium highlighted in the presented images. Alternative ways o image primary cilia are CLEM (correlated light and electron microscope) imaging, which is a powerful method for studying primary cilia, and SEM. The first precisely reveals the distribution of tagged proteins along the ciliary membrane and axoneme. SEM provides 3D

measurements of ciliary length and orientation relative to nearby cellular structures. This chapter discusses different CLEM methods. One detailed approach involves processing samples for sequential fluorescence and SEM observation, ideal for robust antibody localization with minimal image manipulation. Another method first prepares samples for fluorescence imaging, followed by SEM processing, suitable for optimal fluorescence imaging, particularly in live cell studies (Macaluso FP et al., 2016).

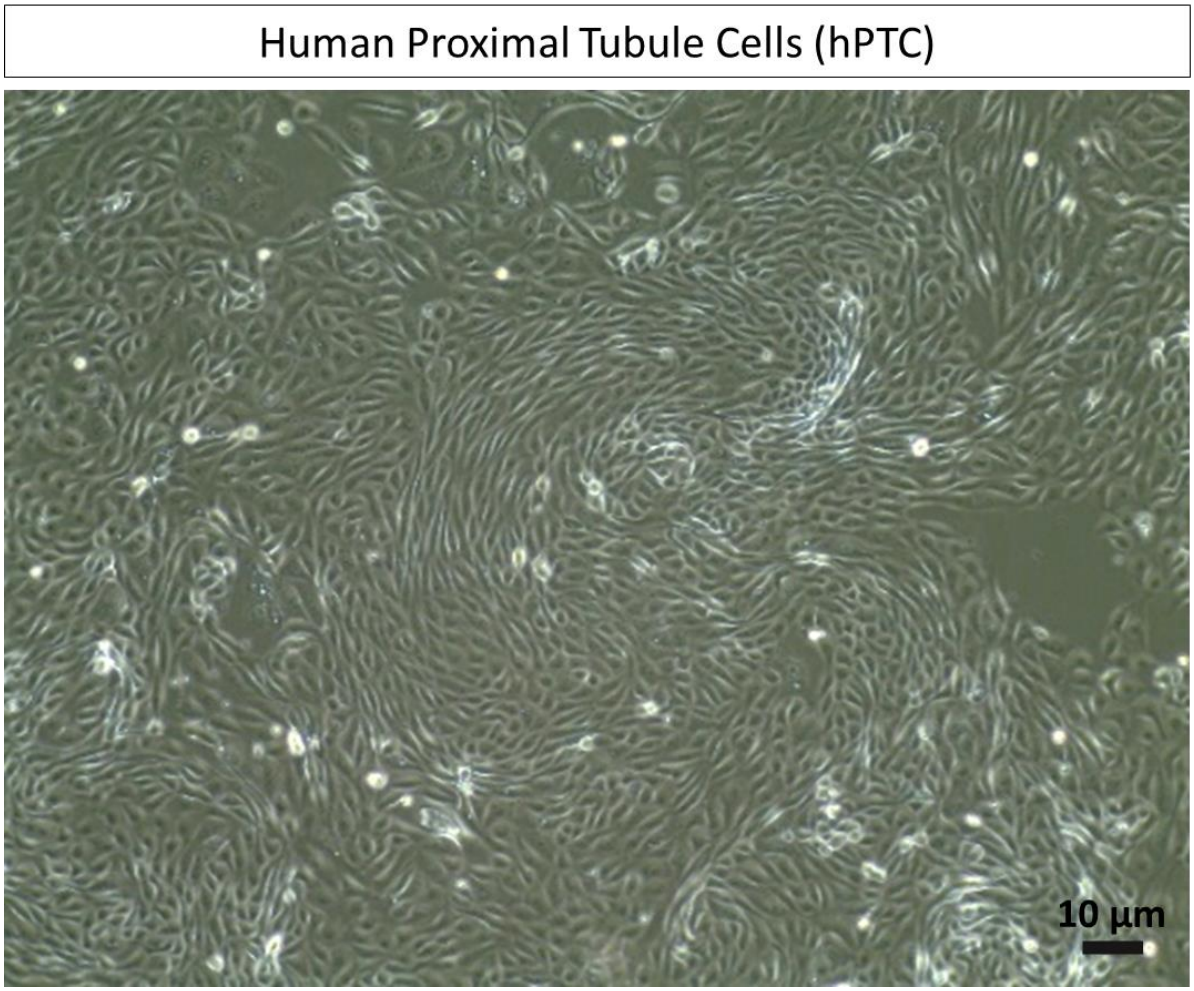

Figure 3.6. Phase-contrast image of the monolayer formed by hPTC seeded on a flask (DAY 7). Cell show typical cobblestone morphology and tight junction formation (scale bar=10µm).

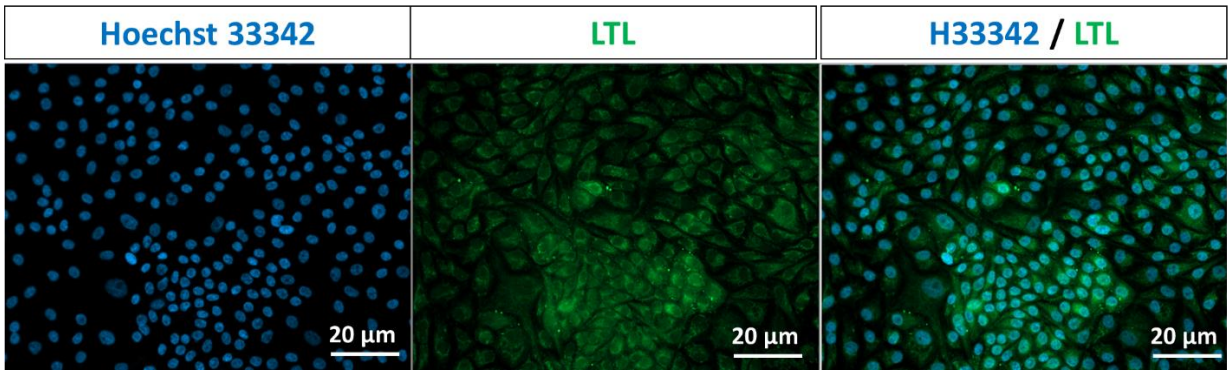

Figure 3.7. Fluorescence images of hPTC on glass coverslip positively stain for the proximal tubule-specific Fluorescein-conjugated Lotus Tetragonolobus Lectin (DAY 7) (scale bars=20µm).

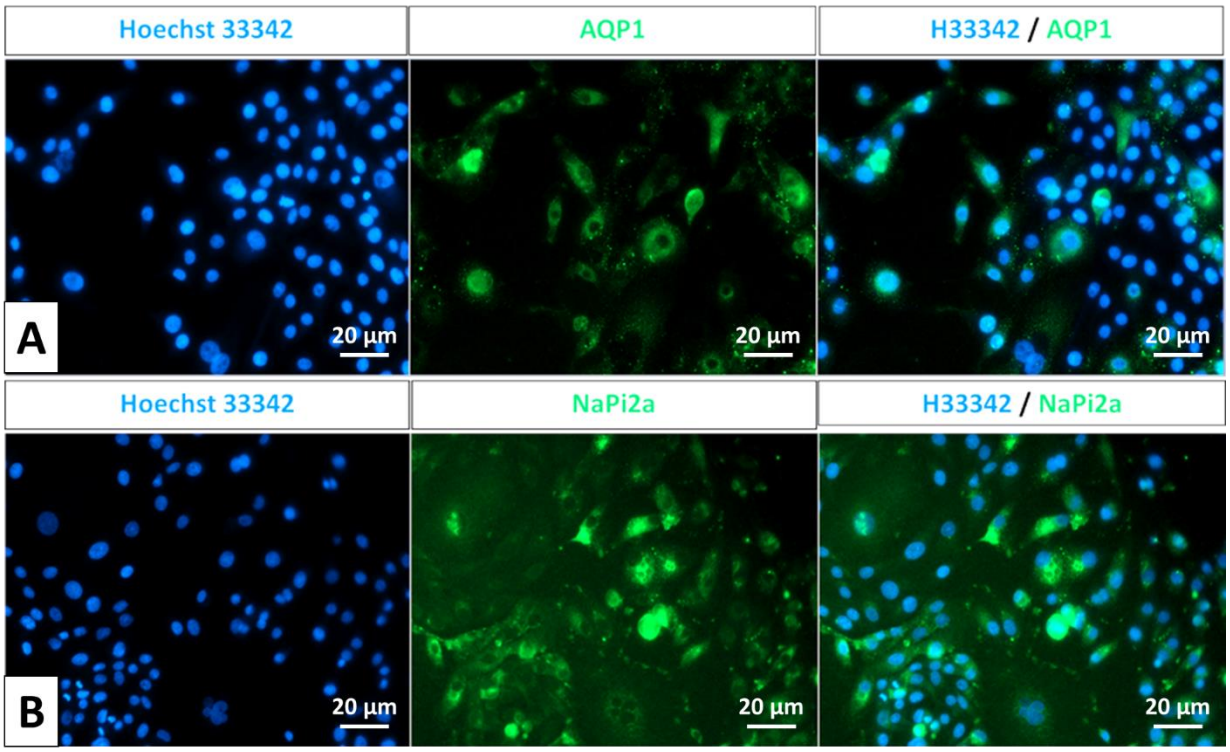

Figure 3.8. Fluorescence images of immunofluorescence stained primary human proximal tubule cells on glass coverslips stain positively for specific proximal tubule markers [A] aquaporin 1 (AQP1) and [B] transporter NaPi2a (in green), with Hoechst 3342 nuclear staining (in blue) (scale bars=20µm).

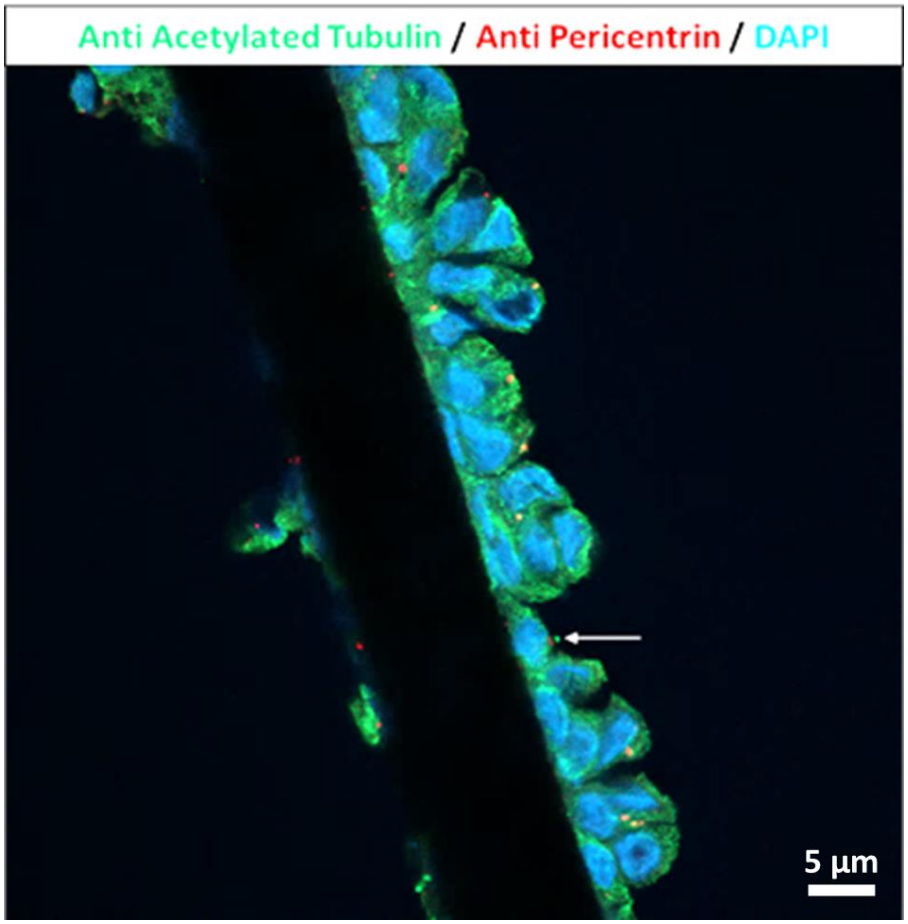

Figure 3.9. Cross-section of hPTC monolayer on Transwell® insert showing apical renal cilia growth (DAY 7) (scale bar=5µm).

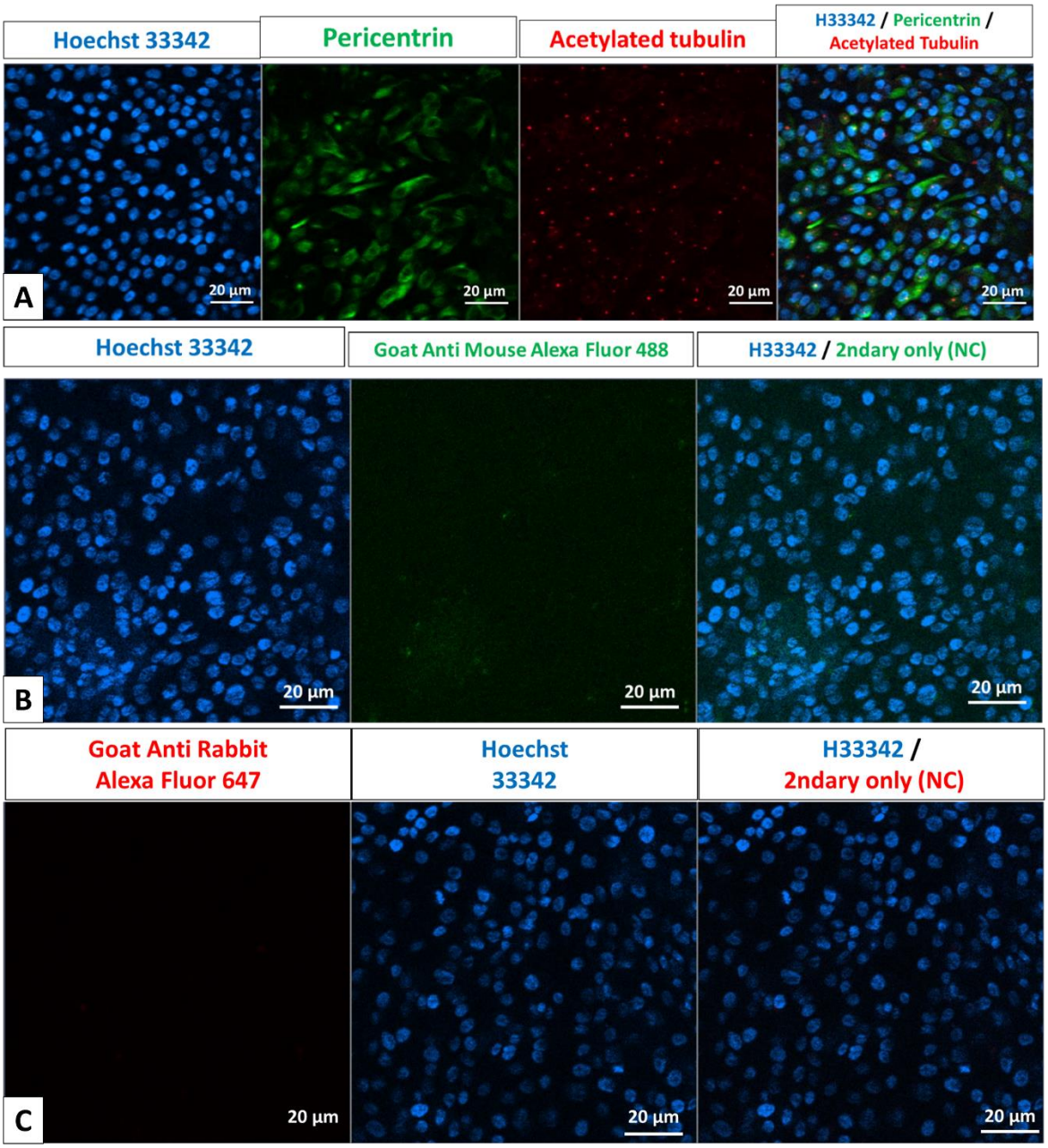

Figure 3.10. [A] Fluorescence images of hPTC on 24-Transwell inserts showing positive expression of pericentrin and acetylated tubulin, known markers apical renal cilia. (DAY 7) [B] "secondary antibody only" negative control for goat anti mouse Alexa Fluor 488™ [C] "secondary antibody only" negative control for goat anti mouse Alexa Fluor 647™) (scale bar=20µm).

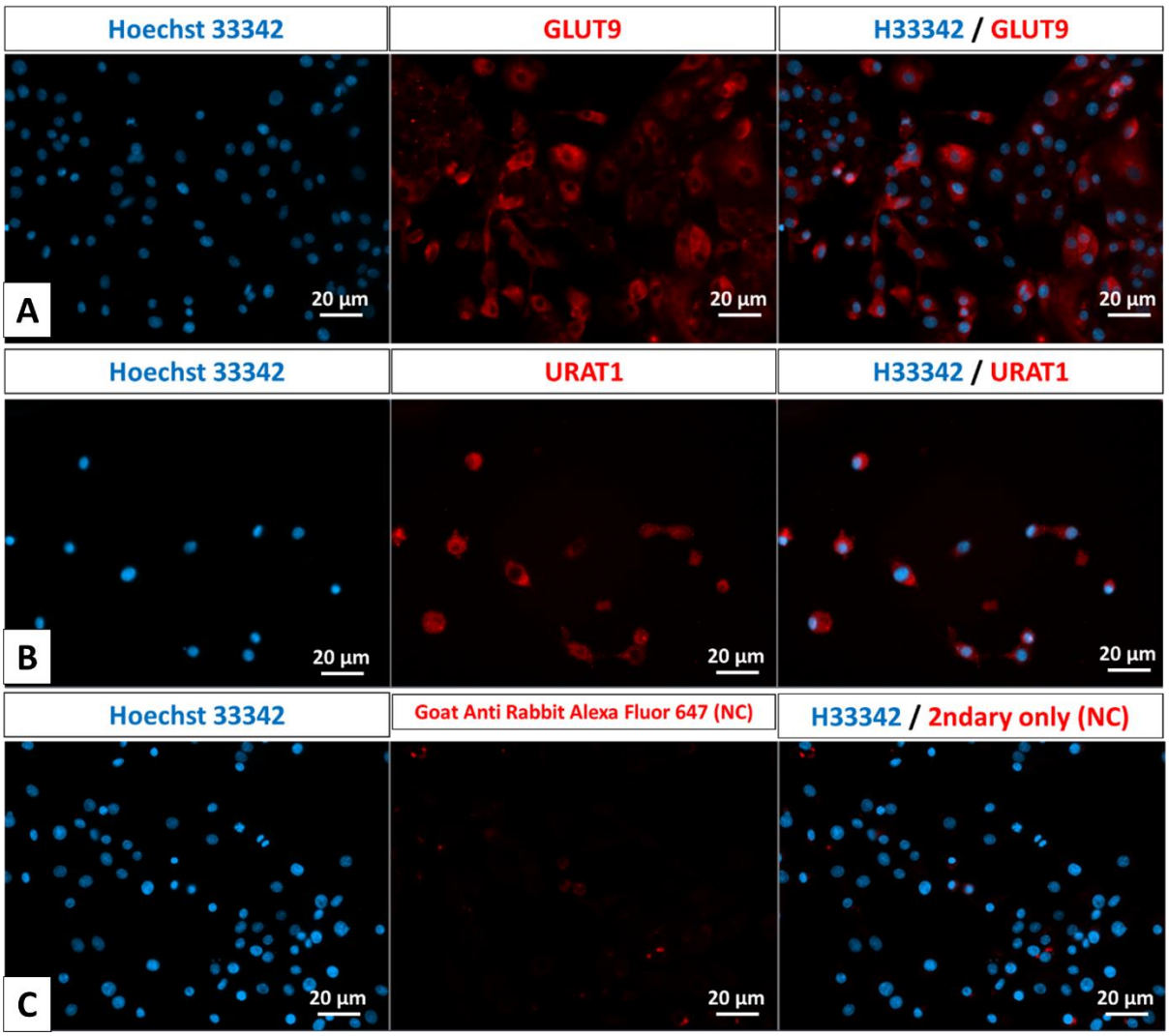

Figure 3.11. Fluorescence images of [A] GLUT-9 and [B] URAT-1 antibody optimization experiment performed on hPTC on glass coverslip, including [C] "secondary antibody only" control (scale bar=20µm).

Another way to characterise the polarization of hPTC monolayer is to identify proteins which are known to be expressed on the apical or basolateral side of the proximal tubule *in vivo*. The transporters glucose transporter 9 (GLUT9) and urate transporter 1 (URAT1) are the main urate transporters in the proximal tubule. Although it has been shown that GLUT9 has two isoforms (SLC2A9b and SLC2A9a) which can be detected on both sides of the epithelium, the transporter appears to be mainly located on the basolateral side, while URAT1 is expressed on the apical (luminal) side (Novikov et al., 2019). Firstly, to assess the feasibility of detecting GLUT9 and URAT1 in hPTC *in vitro,* primary antibodies against such proteins are trialled on cells cultured onto glass coverslips alongside with "secondary antibody only" negative control to confirm primary antibody specificity, as shown in **Figure 3.11.** hPTC monolayers cultured onto 24-Transwell® inserts are fixed with 4% PFA in PBS at day 7 of culture and immunofluorescence staining is performed with the same primary antibodies. Orthogonal maximum intensity projections of the intact monolayers are reconstructed on Zeiss ZEN Blue Lite® by acquiring z-stacks of the microtissues at multiple focal planes. To optimally reflect

transporter localization, digital sectioning of the microtissues is represented along the X- and Y-axis at the borders of the maximum intensity projection images of **Figures 3.12** and **3.13.** The images show definite polarised expression of both transporters on the appropriate side of the epithelium – characterised by the rows of co-planar nuclei **in blue** - thus confirming epithelial cell polarization.

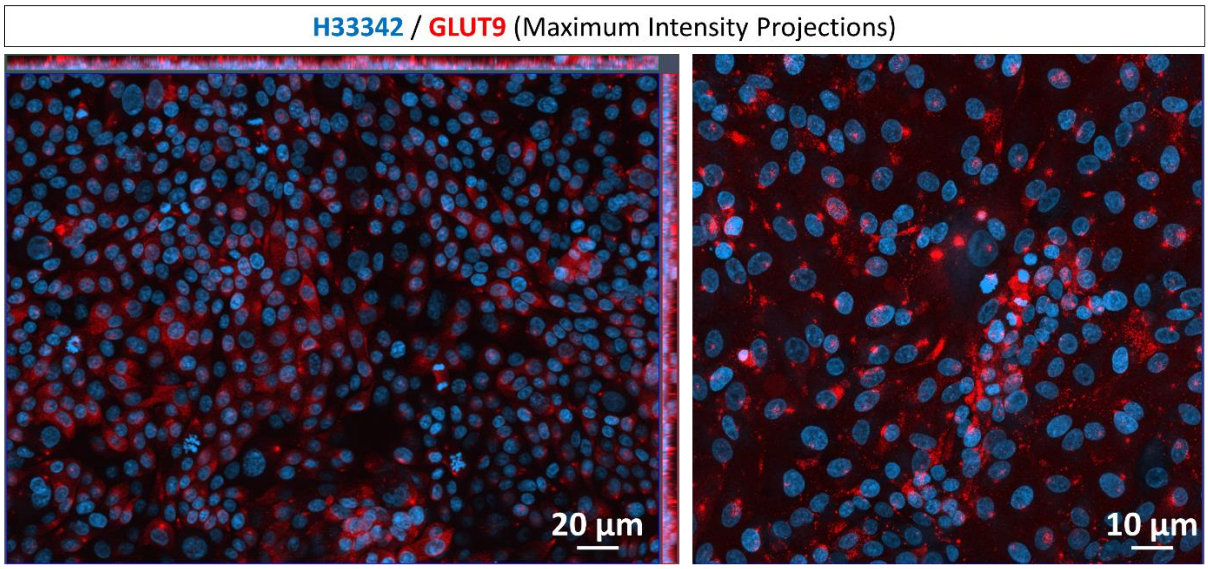

Figure 3.12. Maximum intensity projections of Z-stack of hPTC monolayer on Transwell® insert showing positive staining for the transporter GLUT-9 (red) and nuclear staining Hoechst 33342 (blue) (day 7) (scale bars=20µm, 10µm).

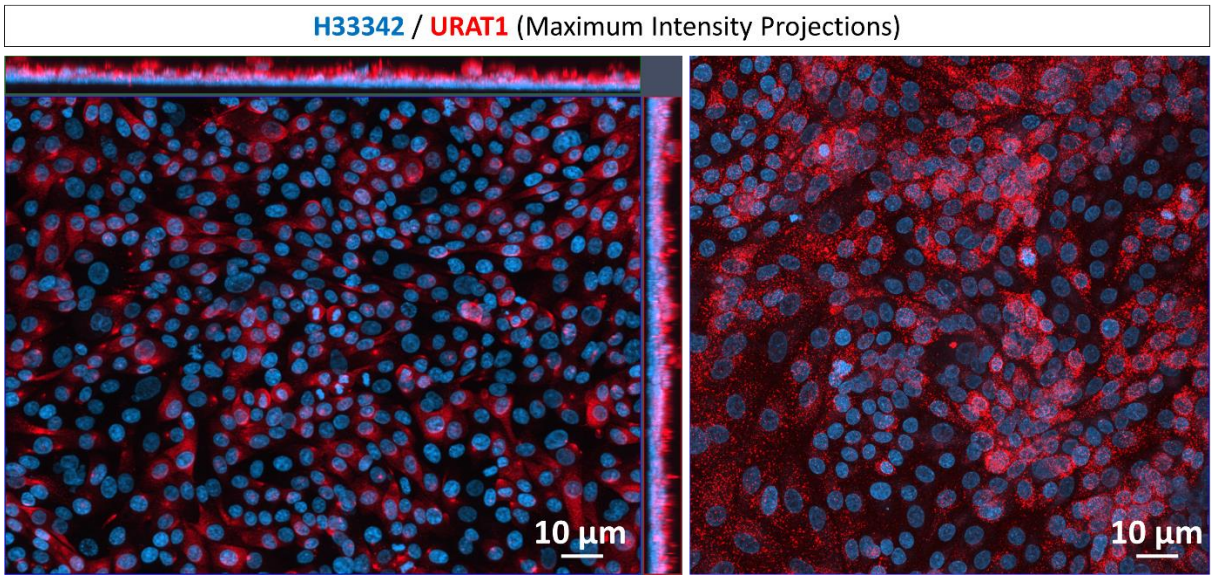

Figure 3.13. Maximum intensity projections of Z-stack of hPTC monolayer on Transwell® insert showing positive staining for the transporter URAT-1 (red) and nuclear staining Hoechst 33342 (blue) (day 7) (scale bar=10µm, 10µm).

3.4 hPTC monolayers show TEER increase and tight junction formation as drug transporters gene expression decreases over culture days.

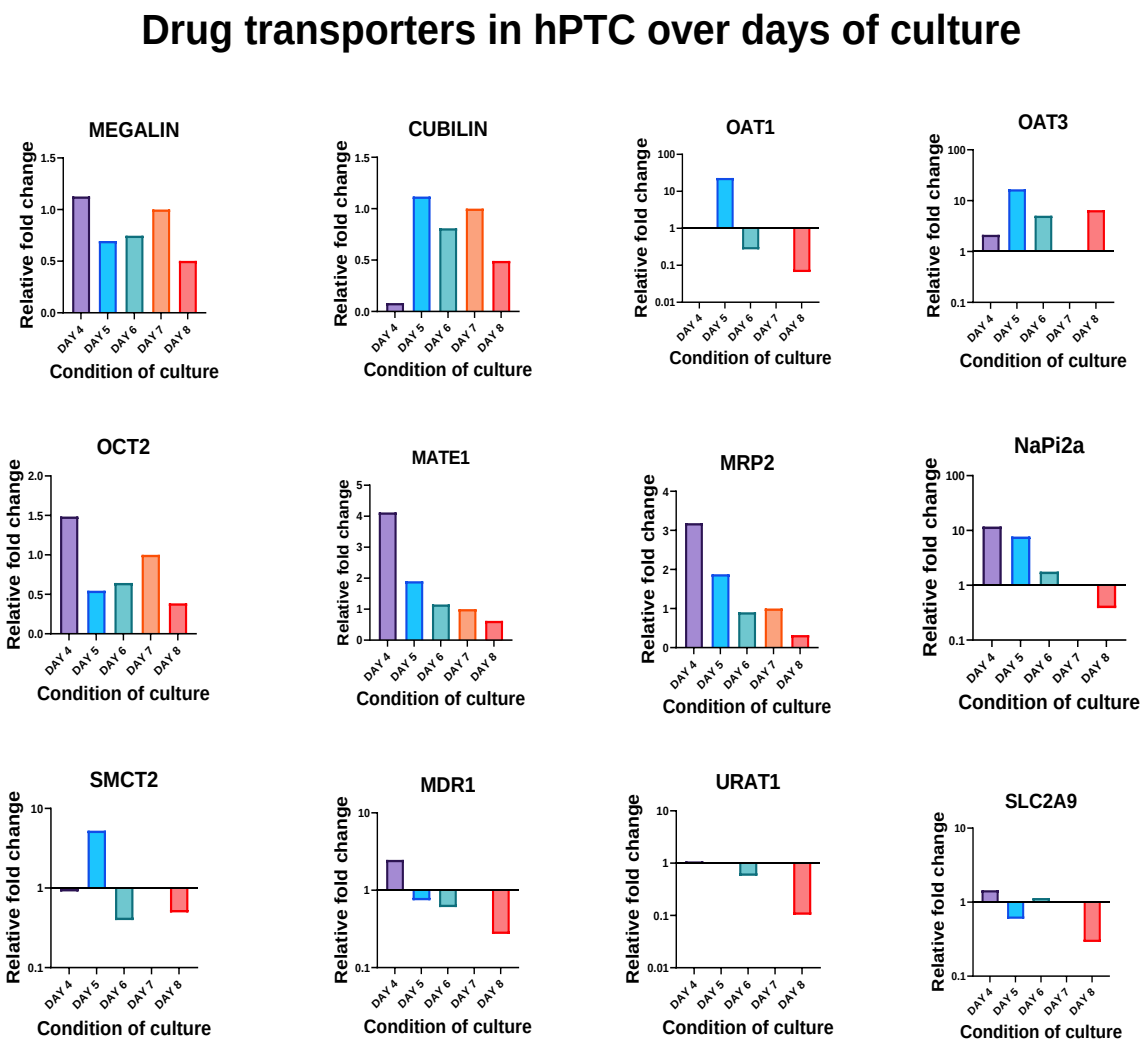

Figure 3.14. RT-qPCR data measuring hPTCs relative fold change of the gene expression of drug transporters Megalin, Cubilin, OAT1, OAT3, OCT2, MATE1, MRP2, NaPi2a, SMCT2, MDR1, URAT1, SLC2A9 over days of culture. As culture time progresses from day 4 to day 8, relative gene expression of key transporters decreases. Bars represent the mean between three technical replicates from one biological replicate (n=1) after 2^-(ΔΔCt) transformation.

As previously discussed, polarised solute transporters expression is a defining feature of differentiated proximal tubule cells which characterisation can be used to determine whether an *in vitro* model of the renal tubules mimics the movement of compounds *in vivo* from the tubule-interstitium to the lumen and vice versa. Therefore, to determine whether the isolated primary proximal tubule cells exert *in vivo*-like transporter expression and function, it is necessary to determine at which timepoint genotyping and radiolabelled compound flux experiments should be performed. Our research group had previously determined (Brown, Sayer, Windass, Haslam, De Broe, et al., 2008) that the TEER value in Ω·cm2 of a confluent polarized monolayer of primary human proximal tubule cells is 60 Ω·cm2 isolated via Percoll®

density gradient centrifugation. This value is used as threshold to determine whether hPTC are ready to be assayed. We hypothesise that transporters expression at the mRNA level will be higher closer to the day of isolation from the kidney cortex, but formation of leak-tight epithelium is essential for the measurement of functional solute transport and epithelial barrier disruption *in vitro.* Hence, the objective becomes to pinpoint the timepoint at which the tight junctions are effectively formed and measurable, and transporters are still expressed by the model. Therefore, with the following experiments we investigate expression of tight junction proteins such as ZO-1 and E-Cadherin over days of culture, and whether there is an inverted correlation between TEER value and mRNA expression of transporters. Furthermore, the chance of spontaneous epithelial-to-mesenchymal transition (EMT) of hPTC due to the transition from the *in vivo* milieu to the *in vitro* environment is ruled out by immunofluorescence staining with antibody against mesenchymal marker vimentin. For this scope, hPTC are cultured on 24-Transwell® inserts (transparent membrane), cells are fixed with 4% PFA, TEER values are measured and RNA samples are collected every day between day 4 and day 8 of culture. **Figure 3.15** shows that TEER values increase every day and that "threshold TEER value" is reached on day 7. As expected, the graphs displayed in **Figure 3.14** highlight that gene expression of all transporters decreases as time passes. Interestingly, expression of transporters megalin, cubilin, OCT2 and MRP2 is downregulated as time goes by but there seems to be a slight upregulation at day 7 of culture. Most transporters are upregulated on day 5 of culture but at this timepoint hPTC are not yet confluent nor polarized therefore monolayers cannot be used for flux assay just yet. Fluorescence images displayed in **Figure 3.16** show that hPTC have yet to reach confluency after four days in culture, which is underlined by the sporadic presence of ZO-1 (**in red**) around the cell membranes. Notably, at day 4 ZO-1 seem to be expressed in the cells cytoplasm without it been translocated to the tight junction. This feature is apparent at day 5 as well, where ZO-1 appears to be expressed both at the tight junction and in the cell's cytoplasm, suggesting incomplete epithelial barrier formation. Images ranging from day 6 to day 8 show closer cell nuclei (**in blue**) and ZO-1 forming a continuous reticulum around the cell membranes, indicating successful *in vitro* epithelial barrier formation. The initial expression of tight junction proteins in the cytoplasm and subsequent translocation to the tight junction over days of culture is ever so prominent when focusing on E-Cadherin expression (**Figure 3.17 – in green**), where the apparent increase in intensity of fluorescence – from a qualitative standpoint – as time progresses suggests upregulation of tight junction protein expression after six days of culture. **Figure 3.18** shows that although mesenchymal marker vimentin (**in orange**) is expressed in the nuclei and cytoplasm of hPTC, the protein is not translocated to the cytoskeleton where its expression would indicate effective EMT.

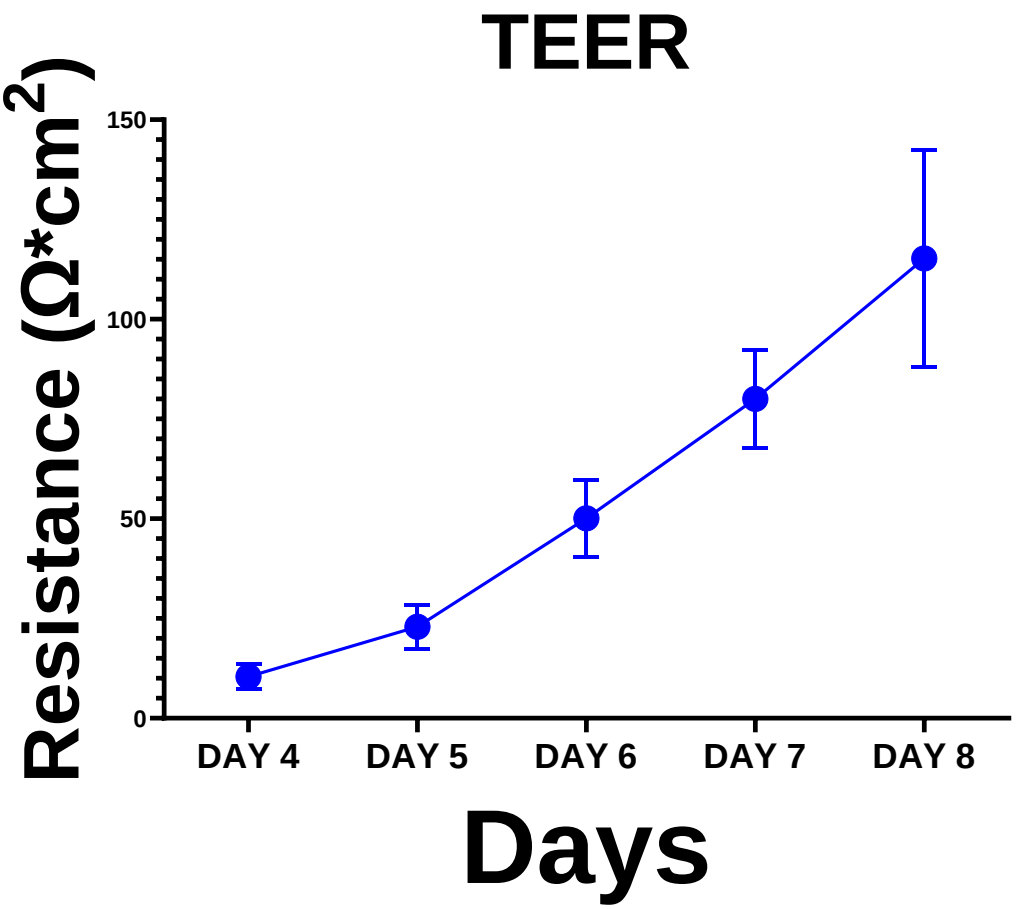

Figure 3.15. Trans Epithelial Electrical Resistance (TEER) measured over days of culture in hPTC cultured on 24-Transwell inserts. As culture time progresses from day 4 to day 8, TEER increases due to tight junction formation. Data represent the mean between twelve technical replicates from one biological replicate while error bars represent SD (n=1).

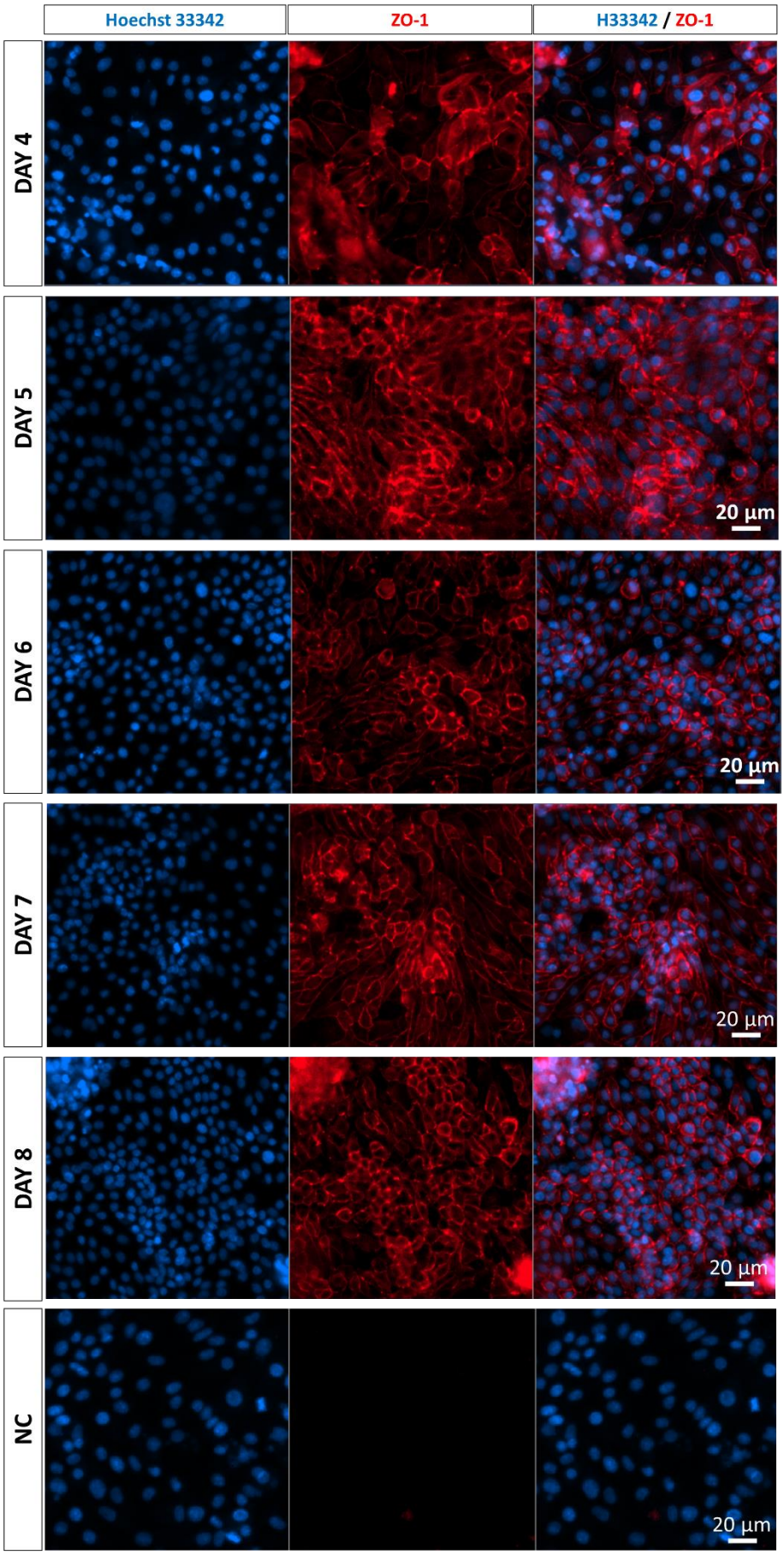
Hoechst 33342
ZO-1
H33342 / ZO-1
DAY 4
DAY 5
DAY 6
DAY 7
DAY 8
NC
20 µm
20 µm
20 µm
20 µm
20 µm

Figure 3.16. Fluorescence images representing positive ZO-1 expression (in red) over days of culture in hPTC monolayers cultured on black walled 96-well plates, denoting successful tight junction formation, including "secondary antibody only" negative control. ZO-1 expression becomes more consistent between day 5 and day 8. Nuclei are stained with Hoechst 33342 (in blue) (scale bars=20µm).

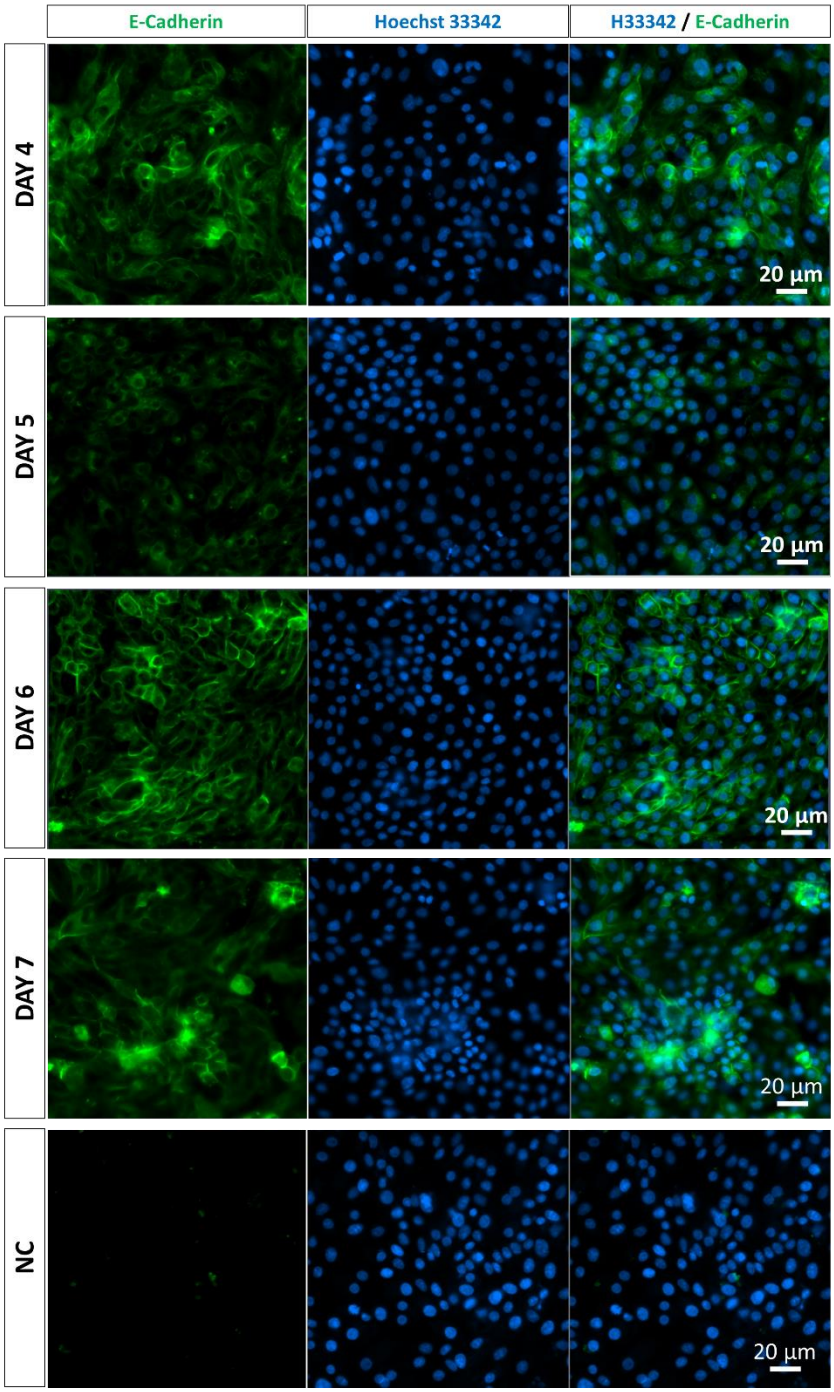

Figure 3.17. Fluorescence images representing positive E-Cadherin expression (in green) over days of culture in hPTC monolayers cultured on black walled 96-well plates, denoting successful tight junction formation including "secondary antibody only" negative control. E-Cadherin expression seems to increase over culture time, with the most consistent expression

at the tight junction at day 6. Nuclei are stained with Hoechst 33342 (in blue) (scale bars=20µm).

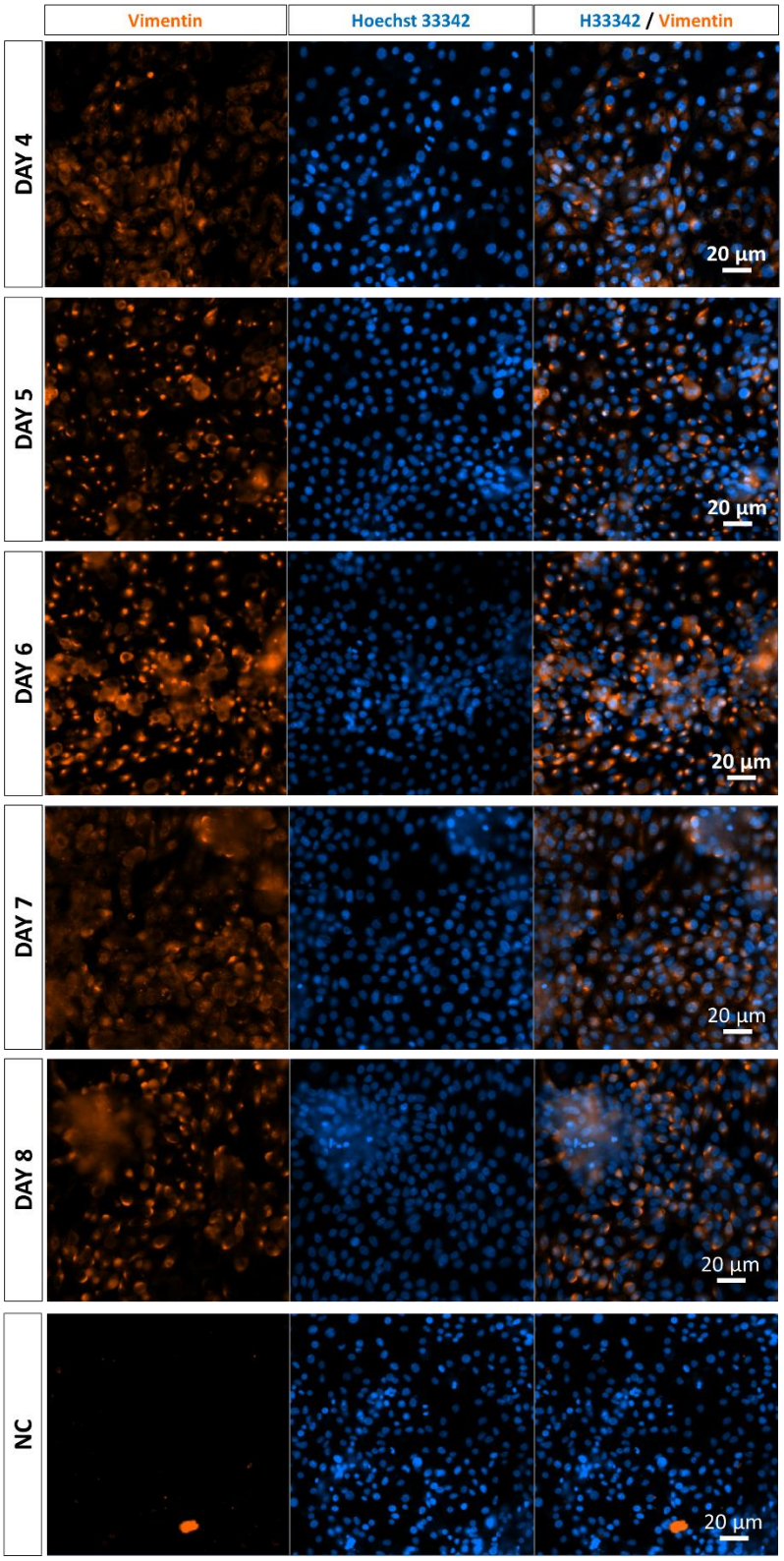

Figure 3.18. Fluorescence images representing vimentin expression (in orange) over days of culture in hPTC monolayers cultured on black walled 96-well plates, including "secondary antibody only" negative control. Vimentin is expressed in the nucleus over culture time and

not translocated to the cytoskeleton, indicating non-fibrotic phenotype. Nuclei are stained with Hoechst 33342 (in blue) (scale bars=20µm).

3.5 Purified human renal fibroblasts express renal fibroblast marker FSP1 and mesenchymal markers CD44, CD90, CD105.

Prior to the start of this project, preliminary co-culture experiments were performed by a member of our research group to investigate whether it would be feasible to obtain a viable 3D construct comprising of fibroblasts and endothelial cells. Cell lines NEO3 (NHDF-NEO, Neonatal human dermal foreskin fibroblasts) and HUVEC (Human umbilical vein endothelial cells) were used for this purpose. As Sorrell et al., 2007 demonstrate, endothelial cells seeded onto confluent fibroblast lawns can form a self-assembling 3D system if supplemented with high concentrations of ascorbate 2-phosphate in the growth medium. This co-factor stabilises the collagen I helix leading to increased extra-cellular matrix (ECM) deposition by fibroblasts. The presence of a complex ECM promotes HUVEC adhesion and vasculogenesis. **Figure 3.19** includes results gathered from the experiments performed on NEO3 fibroblasts, which were treated with 1.36 mM ascorbate 2-phosphate, as proposed in the aforementioned publication. **Figure 3.19 [A]** shows NEO3 positivity to fibroblast marker FSP-1, confirming cell line phenotype via immunofluorescence staining. TEER measurements shown in **Figure 3.19 [B]** suggest that 1.36 mM ascorbate 2-phosphate supplementation in the growth medium leads to an increase in the TEER generated by NEO3 monolayers cultured on Transwell® inserts; therefore, to assess whether the increase in TEER value in the presence of ascorbate is due to an increase in ECM production, expression of the genes encoding for Collagen I, namely COL1A1 and COL1A2, are examined. **Figure 3.19 [C]** shows relative fold change in mRNA expression of the two genes of interest in NEO3 when supplemented with ascorbate 2-phosphate, indicating an increase in expression of COL1A2 in the treated condition. The results obtained from these experiments informed the conditions of culture which were translated to primary fibroblasts in subsequent experiments, since primary human renal fibroblasts will be employed in the development of the renal fibrosis in vitro assay platform where the ability of fibroblasts to deposit ECM is deemed to be essential. Hence, the first step towards establishing a robust protocol for the isolation of human renal fibroblasts from the kidney cortex has been to identify whether such cell type can be found in one of the single-cell suspension layers obtained via Percoll® density gradient centrifugation and whether the cell morphology is visually comparable to the NEO3 cell line. For this purpose, the top layer obtained from a 50 mL Falcon™ tube containing kidney cortex digest that underwent Percoll® density gradient centrifugation is seeded onto a cell culture flask in FGM™-2 medium supplemented with 1.36 mM ascorbate 2-phosphate: the colonies formed by such cell suspension are represented in **Figure 3.20**, displaying spindle-like morphology comparable to cell line NEO3. Having identified that human renal fibroblasts can be found in the top layer of cell suspensions obtained by Percoll® density gradient centrifugation, a purification method is implemented to select specifically human renal fibroblasts. Thus, the fibroblast population isolated via Percoll® density gradient centrifugation is expanded to confluency in T-75 cell culture flasks and purified by Magnetic Activated Cell Sorting (MACS) using magnetic micro beads conjugated to the FSP-1 antibody (Fibroblast Specific Protein 1). After cell sorting,

fibroblasts are cultured and passaged up to three times to investigate mesenchymal phenotype retention after being passaged. **Figure 3.23** shows phase-contrast images of human renal fibroblasts at different passage numbers. Fibroblasts prior to passaging (passage 0) successfully grow to confluency**,** although hillocks of non-mesenchymal cells can be seen growing on top of the fibroblast lawn. After two passages, the fibroblast culture appears to be purer and more consistent, whereas after three passages cells appear to be sparser, thus suggesting a decrease in cell proliferative potential**.**

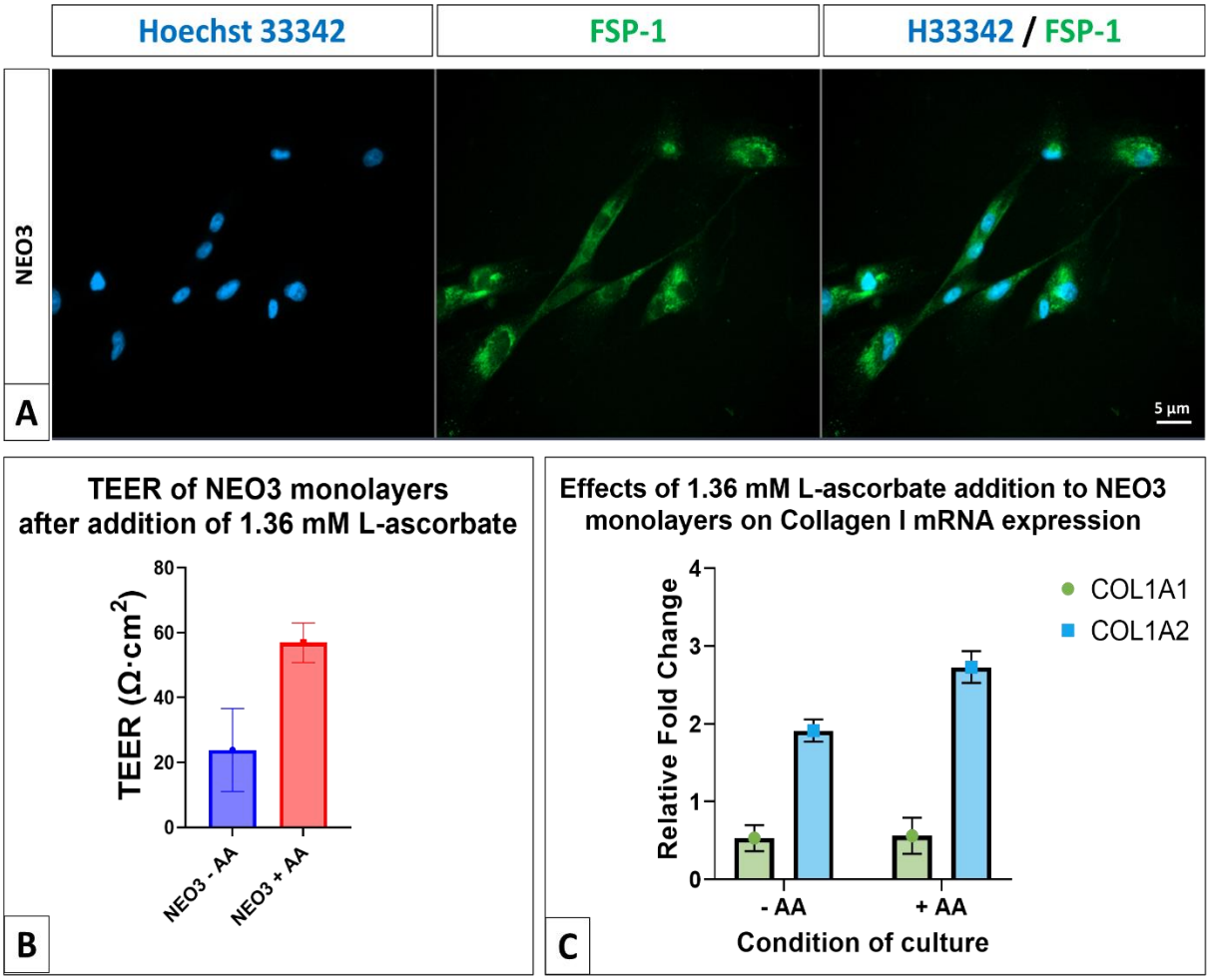

Figure 3.19. [A] Fluorescence images representing cell line NEO3 (neonatal foreskin fibroblasts) on glass coverslip showing positivity to FSP-1 marker specific for fibroblasts (scale bar=5µm) [B] TEER measurements of NEO3 cultured on 24-Transwell® inserts in absence (-AA) and presence (+AA) of 1.36 mM L-ascorbate in the culture media showing an increase in TEER in the presence of L-ascorbate [C] Effects of 1.36 mM L-ascorbate addition on expression of genes COL1A1 and COL1A2 encoding for collagen I in cell line NEO3. In the presence of L-ascorbate, expression of COL1A2 incresases. Data represent the mean between three technical replicates from one biological replicate while error bars represent SD (n=1).

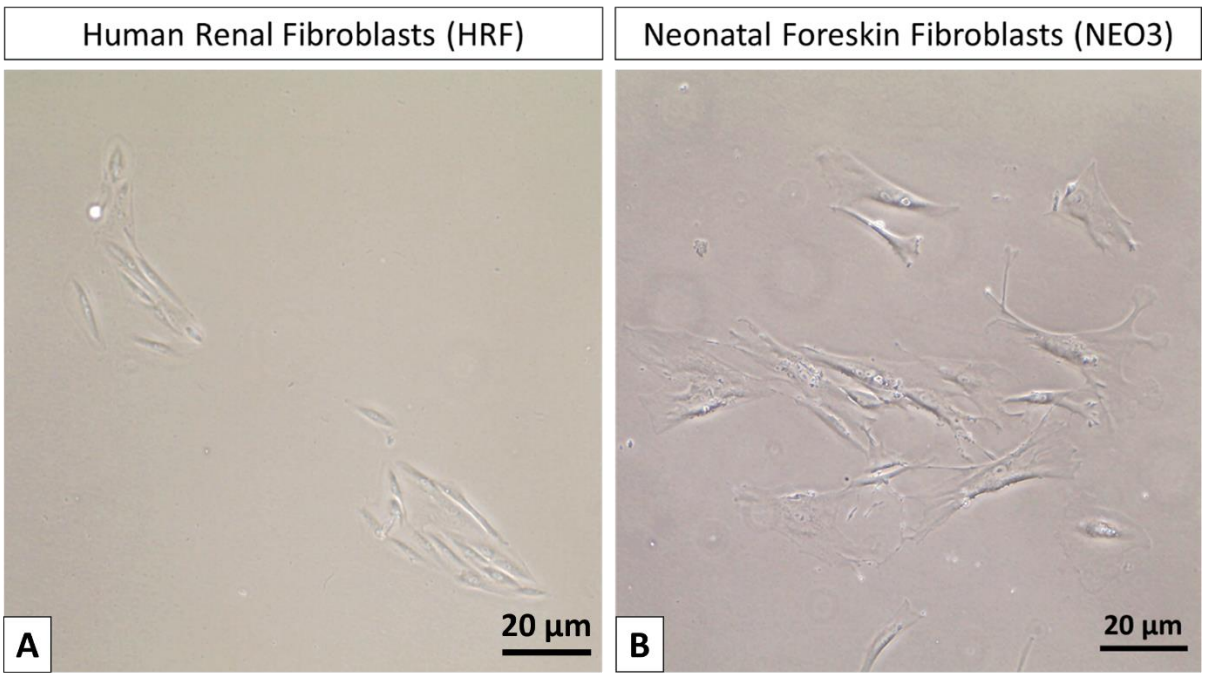

Figure 3.20. Phase-contrast images comparing mesenchymal spindle-like morphology of [A] human renal fibroblasts isolated from Percoll® density gradient centrifugation to [B] cell line NEO3 (scale bars=20µm).

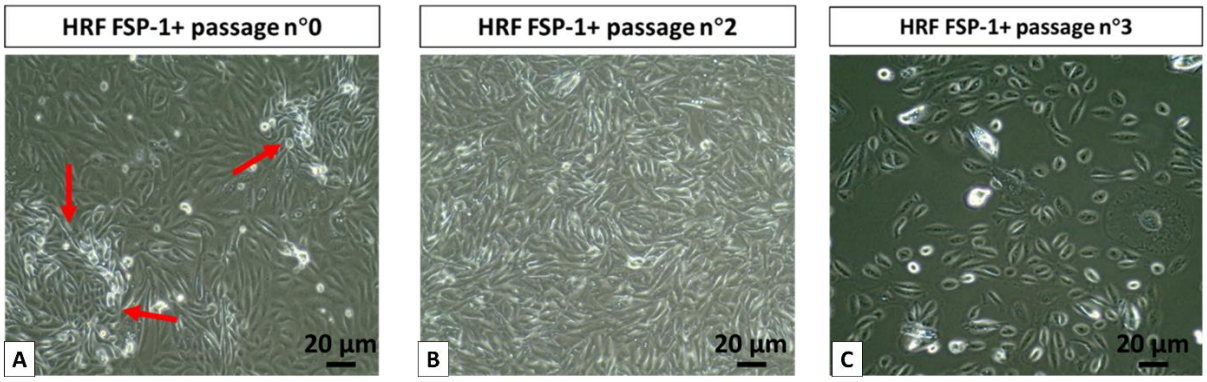

Figure 3.21. Phase-contrast images of MACS FSP1+ isolated human renal fibroblasts at different passage numbers [A] non-mesenchymal shaped cells (red arrows) spontaneously grow on top of confluent primary fibroblasts [B] after two passages, primary fibroblast culture appears more homogenous [C] after three passages, fibroblasts appear sparser (scale bars=20µm).

Isolated primary fibroblasts are further characterized via immunofluorescence staining for the marker FSP-1 (fibroblast specific protein 1), a calcium-binding protein that has been shown to be expressed specifically in the cytoplasm of resident parenchymal fibroblasts in various human organs (le Hir et al., 2005). **Figure 3.22** shows human renal fibroblasts stained positive for the selected marker. Besides FSP-1, no other protein has been recognized in the literature to be specific for fibroblasts. Human fibroblasts have shown to be phenotypically indistinguishable from mesenchymal stem cells (MSC) and to retain the ability of differentiating into adipocytes, chondrocytes and osteoblasts (Denu et al., 2016), (Maleki et al., 2014). Therefore, a panel of three mesenchymal antibodies has been selected to investigate whether the isolated human renal fibroblasts retain the mesenchymal properties after being passaged up to three times. **Figure 3.23** shows dot plots from a flow cytometry experiment performed at confluency (day 7 of culture) on human renal fibroblasts. A panel of primary antibodies against mesenchymal markers are selected to assess the phenotype of these cells, namely CD44, CD90, CD105, and FSP1 (fibroblast-specific protein 1). Among the total cell population analysed, 82% of human renal fibroblasts is double positive for CD44 and CD90, and 62% is double positive for CD44 and FSP1, demonstrating that most of the cells in culture exhibit mesenchymal phenotype.

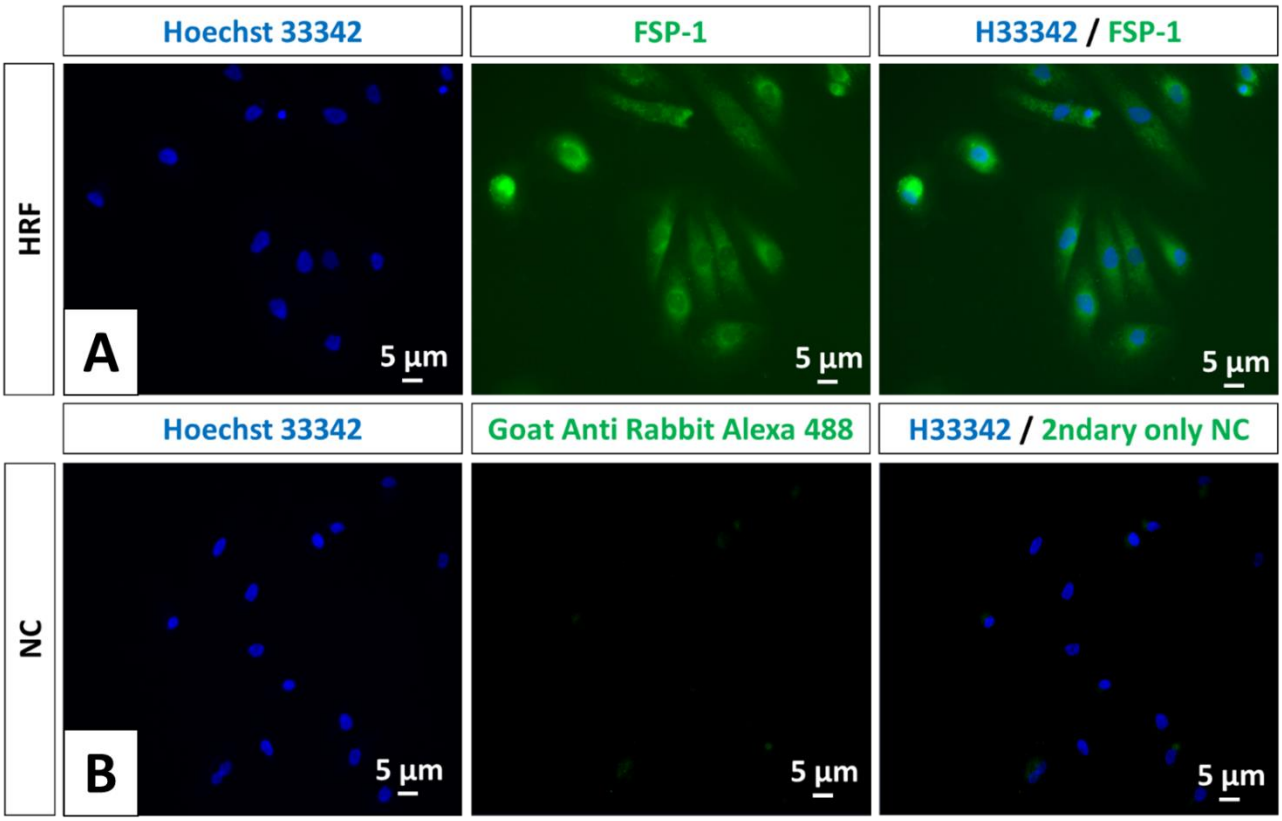

Figure 3.22. Fluorescent microscopy images of MACS-isolated human renal fibroblasts on glass coverslips showing [A] positivity for fibroblast-specific protein 1 (FSP-1), including [B] "secondary antibody only" negative control sparser (scale bars=5µm).

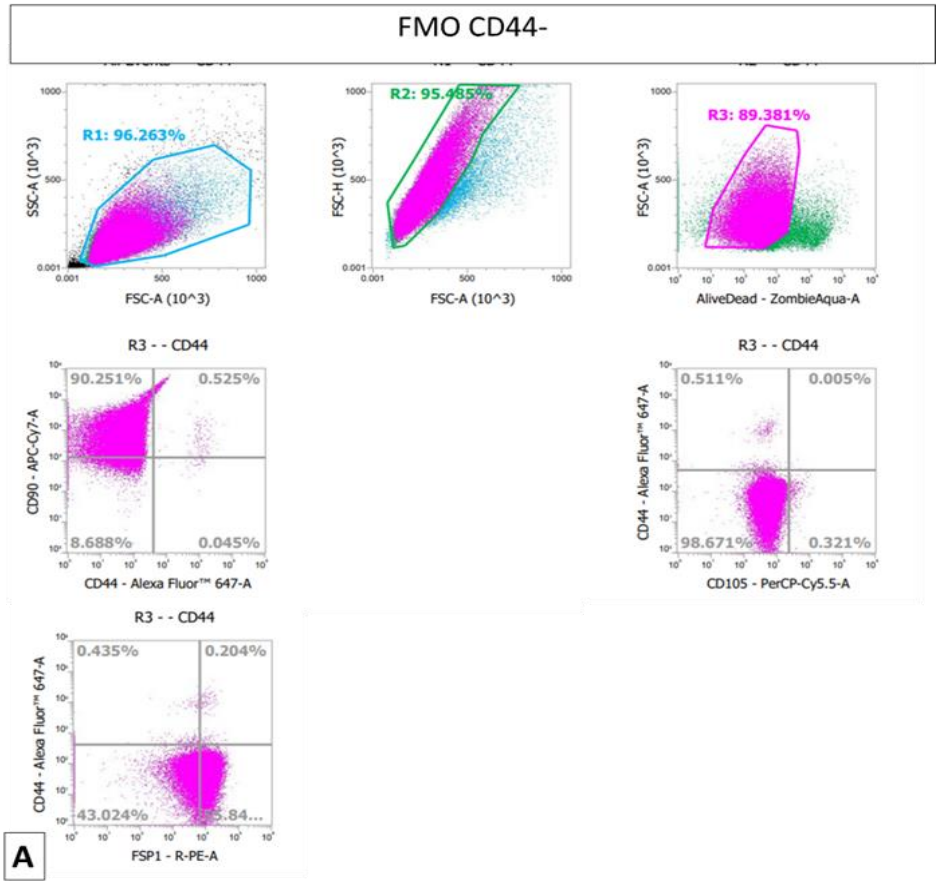
FMO CD44-
R1: 96.263%
SSC-A (10^3)
FSC-A (10^3)
R2: 95.485%
FSC-H (10^3)
FSC-A (10^3)
R3: 89.381%
FSC-A (10^3)
AliveDead - ZombieAqua-A
R3 - - CD44
90.251%
0.525%
8.688%
0.045%
CD90 - APC-Cy7-A
CD44 - Alexa Fluor™ 647-A
R3 - - CD44
0.511%
0.005%
98.671%
0.321%
CD44 - Alexa Fluor™ 647-A
CD105 - PerCP-Cy5.5-A
R3 - - CD44
0.435%
0.204%
43.024%
CD44 - Alexa Fluor™ 647-A
FSP1 - R-PE-A
A

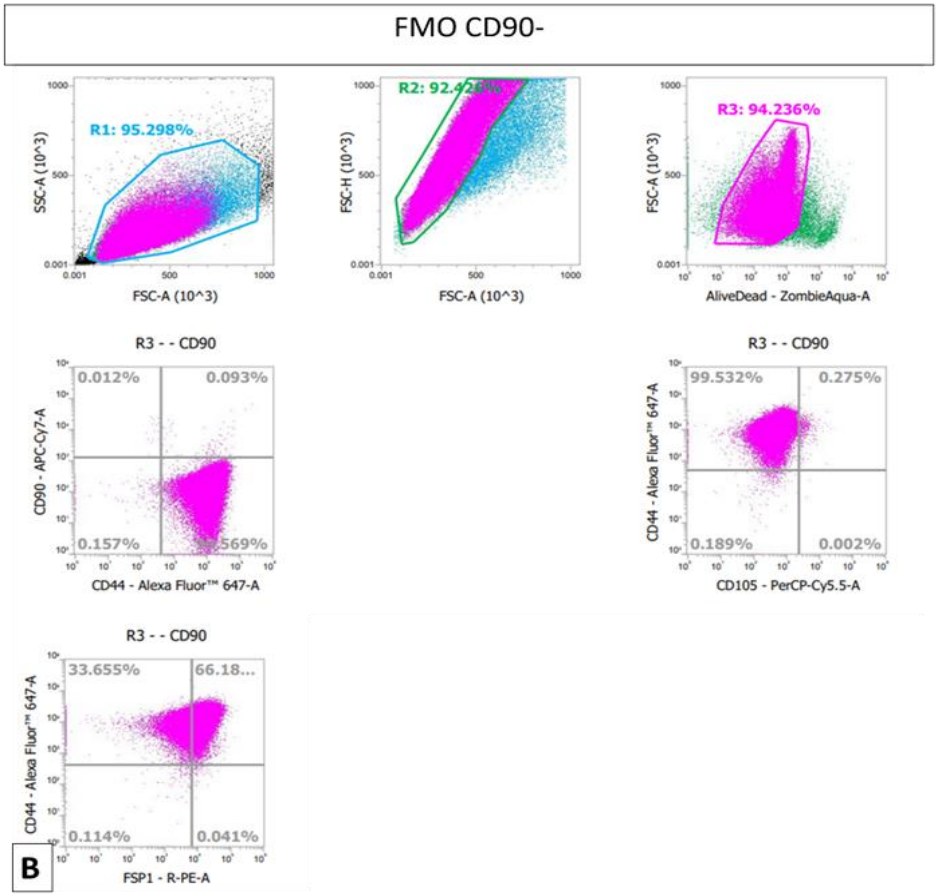
FMO CD90-
R1: 95.298%
SSC-A (10^3)
FSC-A (10^3)
R2: 92.426%
FSC-H (10^3)
FSC-A (10^3)
R3: 94.236%
FSC-A (10^3)
AliveDead - ZombieAqua-A
R3 - - CD90
0.012%
0.093%
0.157%
CD90 - APC-Cy7-A
CD44 - Alexa Fluor™ 647-A
R3 - - CD90
99.532%
0.275%
0.189%
0.002%
CD44 - Alexa Fluor™ 647-A
CD105 - PerCP-Cy5.5-A
R3 - - CD90
33.655%
0.114%
0.041%
CD44 - Alexa Fluor™ 647-A
FSP1 - R-PE-A
B

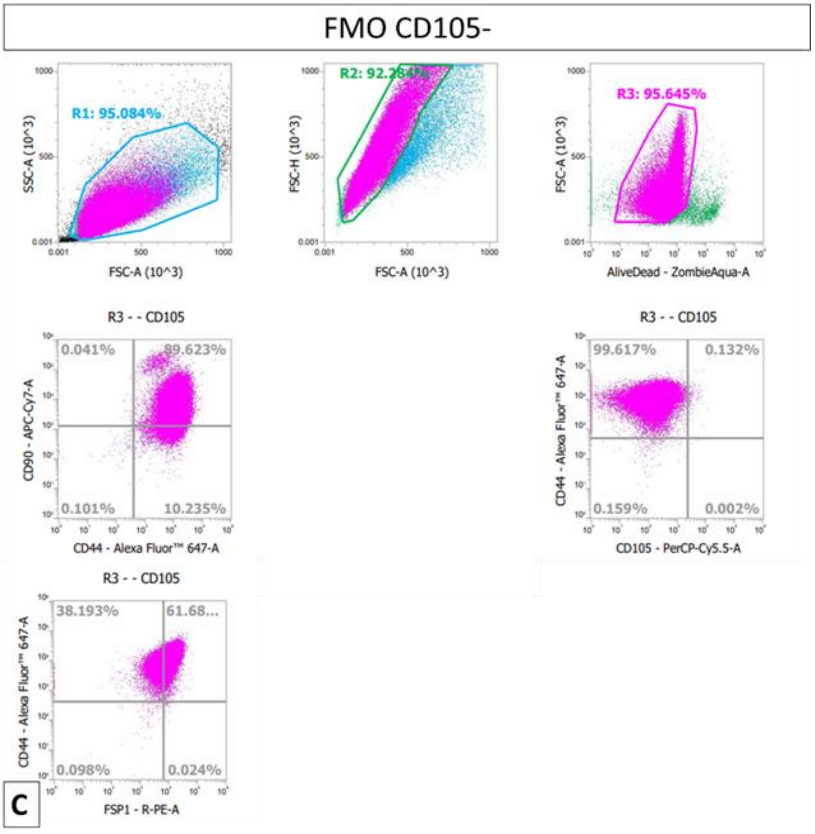
FMO CD105-
R1: 95.084%
SSC-A (10^3)
FSC-A (10^3)
R2: 92.284%
FSC-H (10^3)
FSC-A (10^3)
R3: 95.645%
FSC-A (10^3)
AliveDead - ZombieAqua-A
R3 - - CD105
0.041%
99.623%
0.101%
10.235%
CD90 - APC-Cy7-A
CD44 - Alexa Fluor™ 647-A
R3 - - CD105
99.617%
0.132%
0.159%
0.002%
CD44 - Alexa Fluor™ 647-A
CD105 - PerCP-Cy5.5-A
R3 - - CD105
38.193%
61.68...
0.098%
0.024%
CD44 - Alexa Fluor™ 647-A
FSP1 - R-PE-A
C

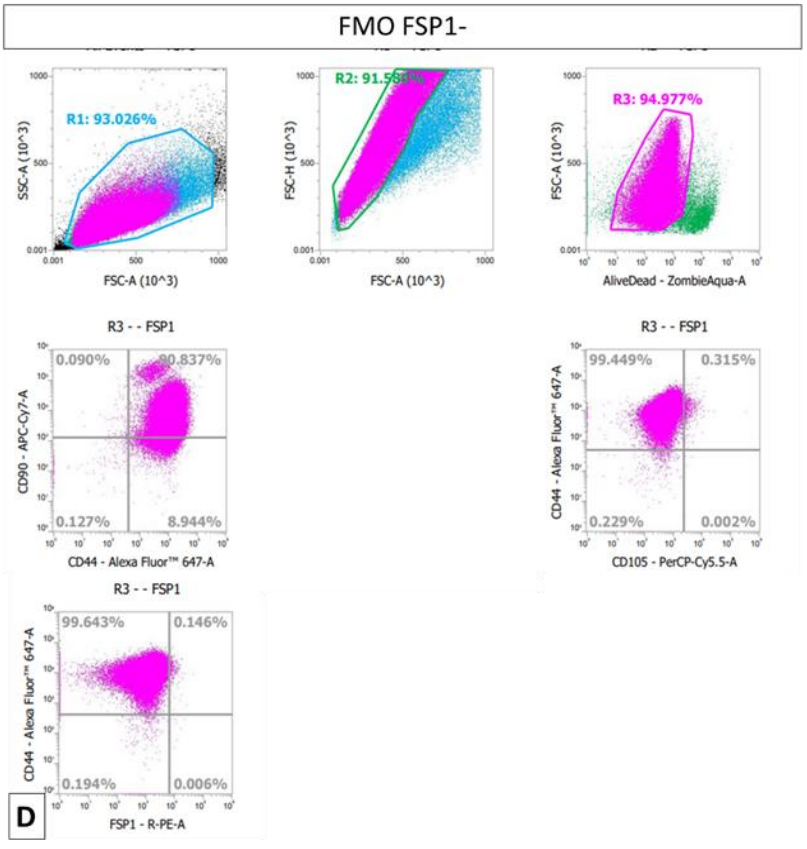
FMO FSP1-
R1: 93.026%
SSC-A (10^3)
FSC-A (10^3)
R2: 91.58...
FSC-H (10^3)
FSC-A (10^3)
R3: 94.977%
FSC-A (10^3)
AliveDead - ZombieAqua-A
R3 - - FSP1
0.090%
0.127%
8.944%
CD90 - APC-Cy7-A
CD44 - Alexa Fluor™ 647-A
R3 - - FSP1
99.449%
0.315%
0.229%
0.002%
CD44 - Alexa Fluor™ 647-A
CD105 - PerCP-Cy5.5-A
R3 - - FSP1
99.643%
0.146%
0.194%
0.006%
CD44 - Alexa Fluor™ 647-A
FSP1 - R-PE-A
D

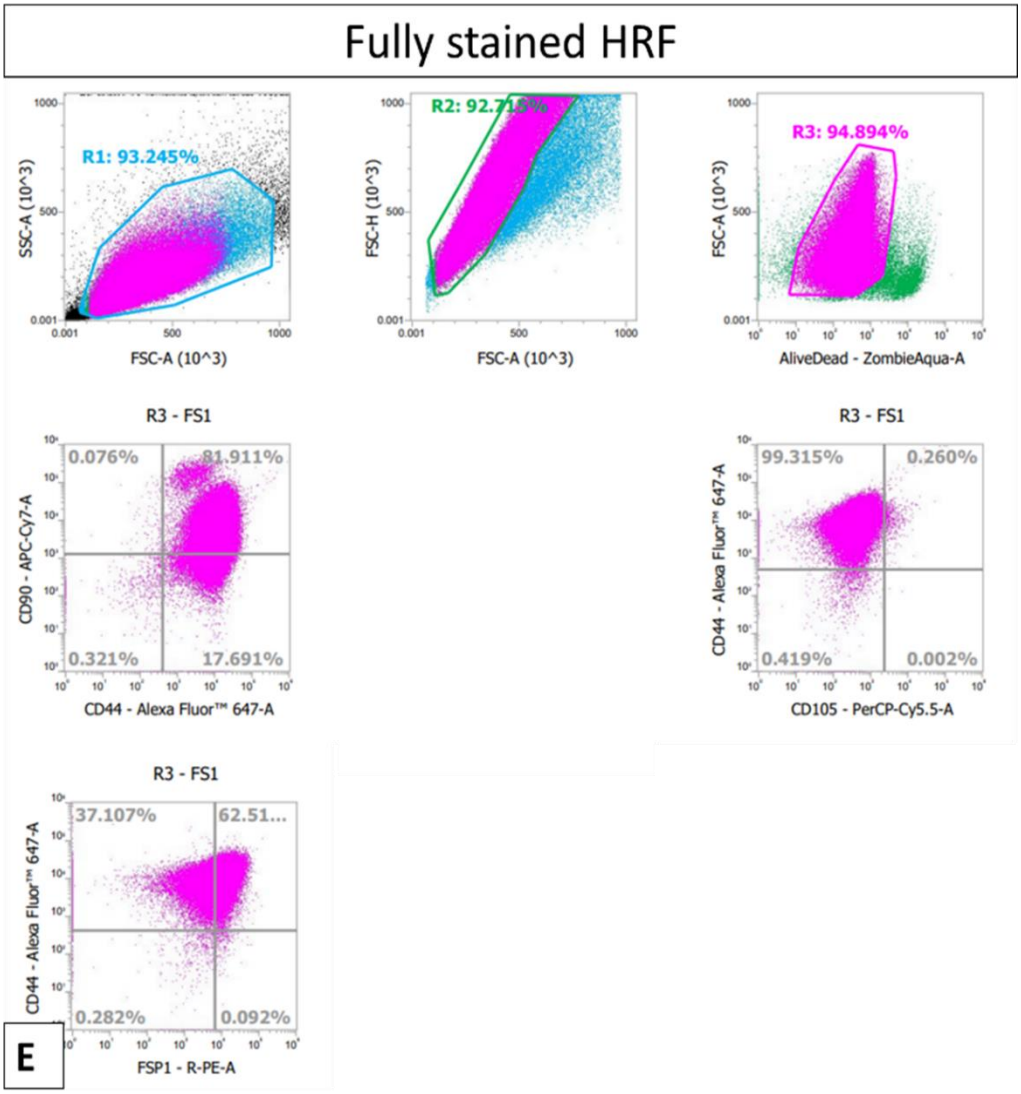

Figure 3.23. Flow cytometry dot plots representing the percentages of cells isolated via MACS FSP1+ showing positive staining for mesenchymal markers. Gating strategy based on fluorescence minus one (FMO) controls depicted in [A] CD44-, [B] CD90-, [C] CD105-, [D] FSP-1. Singlets depicted in FSC-A / SSC-A dot plots, doublets shown in FSC-A / FSC-H dot plots, live/dead cells shown in ZombieAqua / FSC-A dot plots. Cells at passage n 0 double positive: CD44+ CD90+ 81.911%; CD44+ CD105+ 0.260%; CD44+ FSP1+ 62.51%.

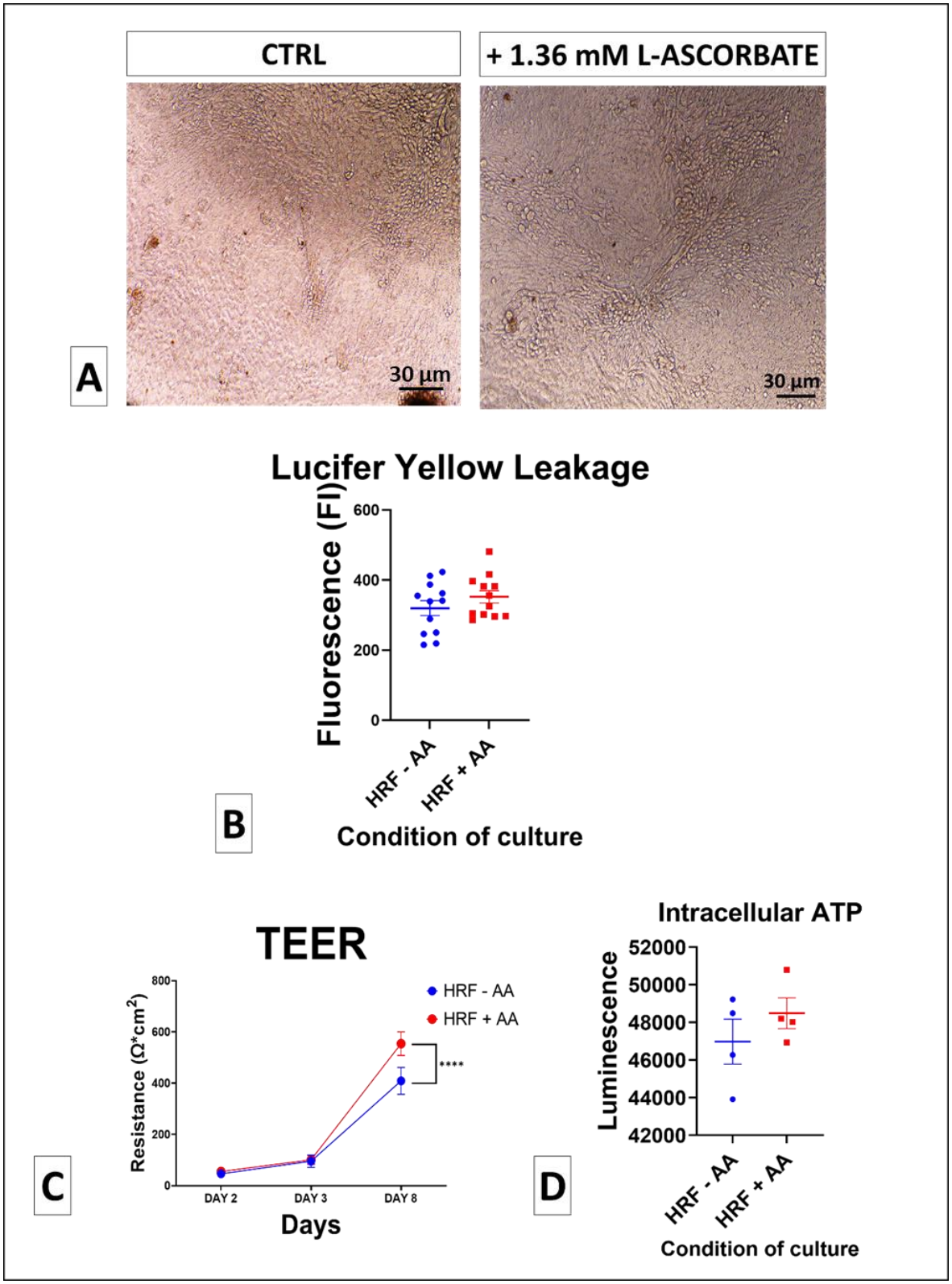

Figure 3.24. HRF are treated with 1.36 mM L-ascorbate (HRF + AA) and compared with untreated cells (HRF – AA). [A] Phase-contrast images show formation of visible fibrils in the presence of L-ascorbate (scale bars=30µm) [B] Lucifer Yellow leakage from apical to basolateral compartment shows a non-significant increase in paracellular leakage in cells treated with L-ascorbate [C] TEER measurement over culture days shows an increase in TEER in the presence of L-ascorbate [D] Cell viability assay measuring intracellular ATP shows

increased intracellular ATP in cells treated with HRF. Datapoints represent the mean between technical replicates from one biological replicate ([B], [C] 12, [D] 4). Error bars represent S.D. Statistical significance is depicted as '' ($p < 0.05$).*

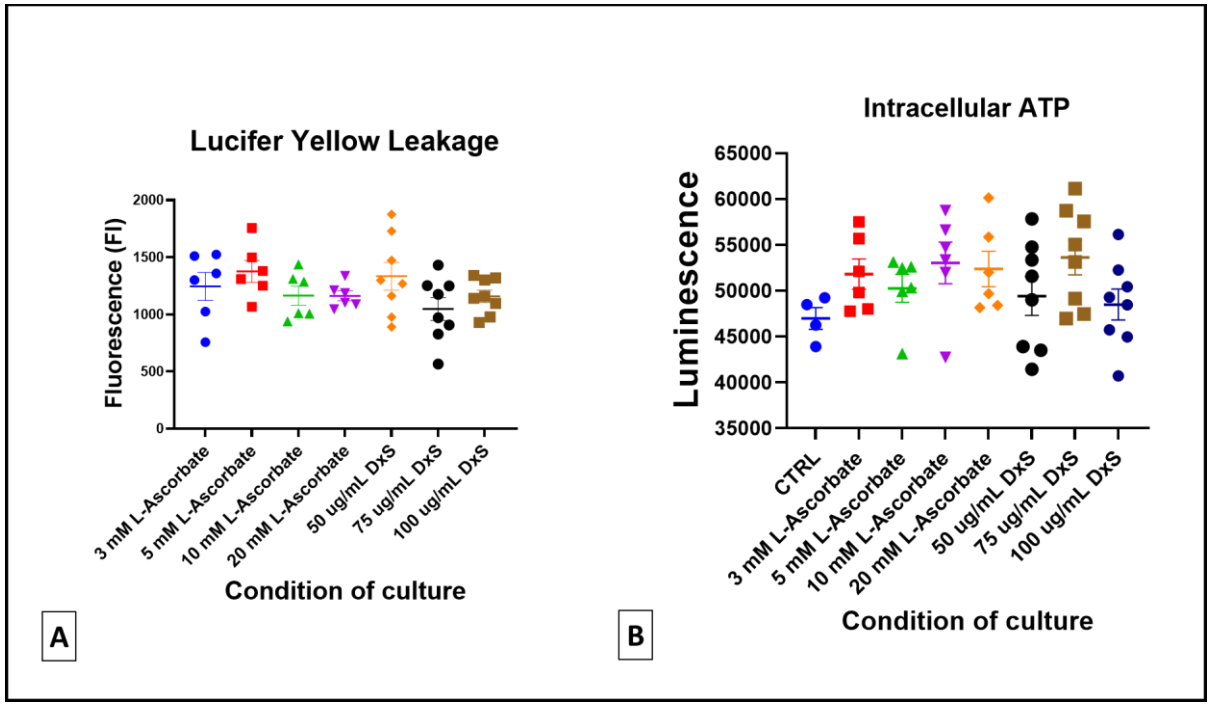

Figure 3.25. HRF are treated with a range of concentrations of L-ascorbate and dextran sulphate (DxS). [A] Lucifer Yellow leakage from apical to basolateral compartment of ThinCert™ inserts performed on 12 technical replicates and one biological replicate (n=1) shows no measurable differences in paracellular leakage after treatment [B] Cell viability assay measuring intracellular ATP performed on 12 technical replicates and one biological replicate (n=1) shows increased intracellular ATP after treatment with 3 mM L-ascorbate but not with other concentration of ascorbate and dextran sulphate. Error bars represent S.D. Statistical significance is depicted as '' ($p < 0.05$).*

Finally, to ensure culture conditions established for cell line NEO3 are suitable for primary human renal fibroblasts, experiments are performed to corroborate evidence indicating high cell viability and extra-cellular matrix (ECM) deposition under those conditions. Therefore, primary HRF are cultured on transparent ThinCert™ 24-well inserts and are supplemented with 1.36 mM L-ascorbate in FGM™-2 growth medium. Effects of L-ascorbate treatment on HRF cultures are characterized via phase-contrast images to highlight morphological changes in fibroblast lawn formation, Lucifer yellow leakage assay to investigate an expected increase in ECM deposition which would lead to a decrease in paracellular leak of such compound, trans epithelial electrical resistance (TEER) assay, and cell viability assay where treated cultures are compared to untreated ones (**Figure 3.24**). When L-ascorbate is present, phase-contrast images (**Figure 3.24, [A]**) show moderate 3D filament formation over the confluent monolayer of HRF. Although the difference in Lucifer Yellow leakage from the apical to the basolateral compartment of the insert is not a statistically significant (**Figure 3.24, [B]**), TEER measurements over 6 days of culture show that HRF treated with L-ascorbate form significantly tighter cell-cell connections (**Figure 3.24, [C]**). Cell viability assay (**Figure 3.24,**

[D]) shows an increase, although not significant, in intracellular ATP when HRF are treated. L-ascorbate seems to have an overall positive impact over fibroblast growth, therefore we decided to stimulate the cells with a range of concentrations of L-ascorbate to test whether a higher concentration could produce a significant increase in 3D filament production and cell viability.

Macromolecular crowding is a biological feature of microenvironments *in vivo*. This feature is not replicated *in vitro* where cells find themselves in immensely diluted spaces. It has been reported (Zeiger et al., 2012) that macromolecular crowding has an impact on the organization of proteins in the extracellular matrix and, if replicated *in vitro*, it results in changes of cell proliferation and adhesion. This is known to be especially important for ECM-producing cells like human renal fibroblasts. Therefore, primary HRF are treated with a range of concentrations of dextran sulphate, an inert macromolecule, to assess whether any changes in cell morphology and ECM deposition could be detected over time. HRF cultured on ThinCert™ inserts treated with a range of concentrations of L-ascorbate and dextran sulphate undergo cell viability assay and Lucifer Yellow leakage experiments to assess whether treatments can produce an effect on cell viability and leak tightness. Results are displayed in **Figure 3.25**. No significant differences in leak tightness are found between different treatments (**Figure 3.25, [A]**), while cells treated with all tested concentrations of L-ascorbate seemed to display, although not significantly, higher viability as compared to cells treated with dextran sulphate (**Figure 3.25, [B]**). In conclusion, supplementation of FGM-2 (fibroblast growth medium 2) with 3 mM L-ascorbate was deemed to be the optimal treatment to increase cell viability and ECM deposition in human renal fibroblasts.

3.6 Percoll® density gradient centrifugation followed by MACS CD31+ purification with VEGF-A supplementation leads to stable diaphragmatic fenestration expression in HRPEC *in vitro.*

The aim of this section is to take the reader through the different isolation methods that were used to successfully isolate human renal peritubular endothelial cells from the human kidney cortex. The optimized method conducted to the isolation of high yield of cells of the appropriate phenotype that could maintain these characteristics *in vitro.* Starting from the single cell suspension obtained from cortex digestion, the first implemented method involved direct selection of cells positive for endothelial marker CD31 via Magnetic Activated Cell Sorting (MACS). This method did not lead to a high enough yield to proceed to culture the cells. Since Percoll® density gradient centrifugation had been previously used to retrieve tubular epithelial cells from the kidney cortex, in this instance the method was used to *deplete* the digest from epithelial cells. Furthermore, the remaining cells isolated with this method were supplemented with VEGF-A (Vascular Endothelial Growth Factor A) which is known to be important in the formation and maintenance of fenestrated capillaries *in vivo* and *in vitro.* The addition of this compound to the cell culture medium was trialled also with the MACS CD31+ method. Ultimately, the method that lead to the successful isolation of HRPEC was a combination of Percoll® density gradient centrifugation method, expansion of cells with VEGF-A supplementation, MACS CD31+ cell selection, and polarisation via culture on Transwell™ or ThinCert® membranes.

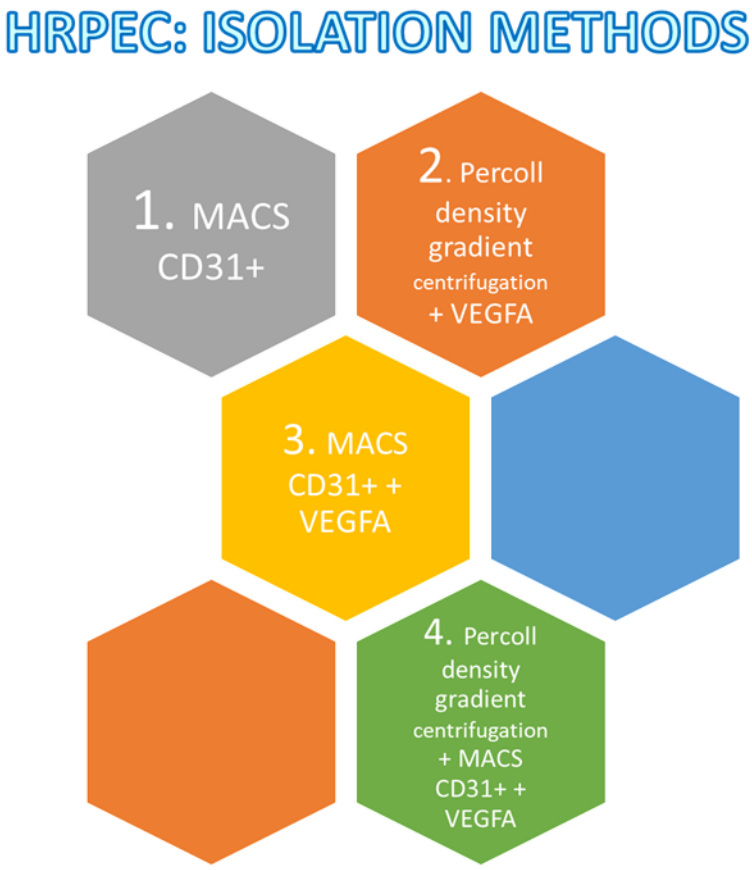

Figure 3.26. Diagram listing the isolation methods trialled to establish an efficient protocol for HRPEC isolation from the human kidney cortex.

3.6.1 Preliminary experiments

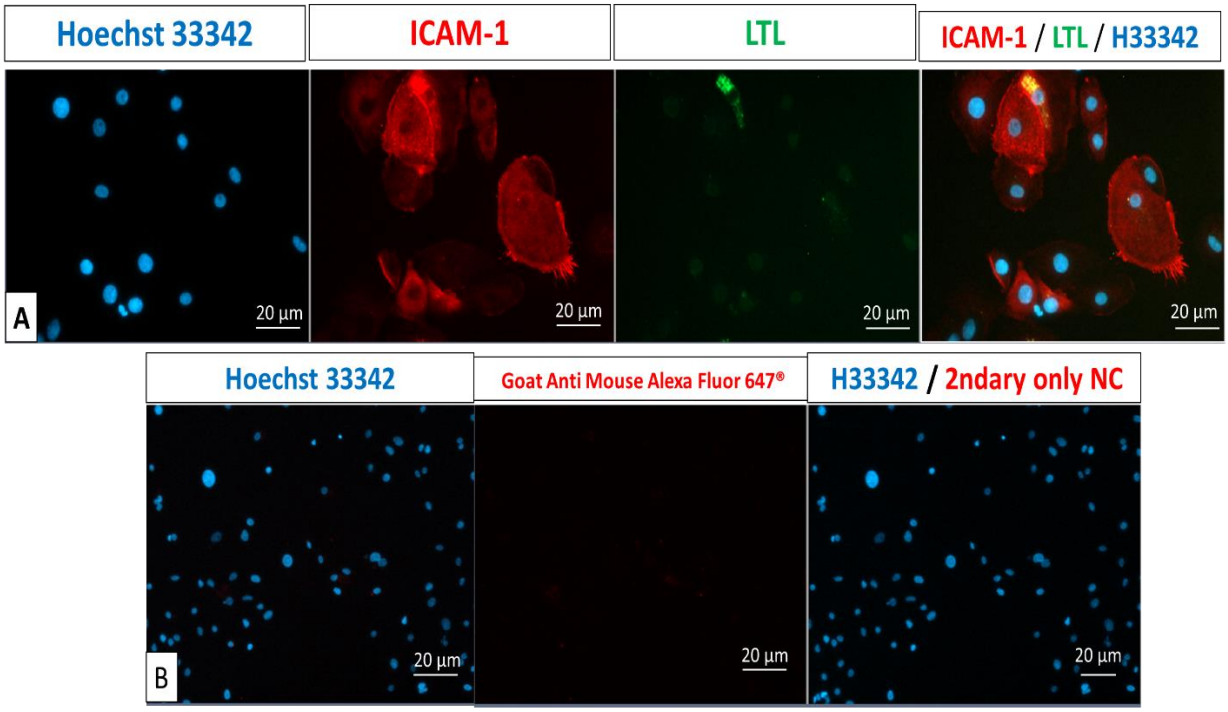

Figure 3.27. Fluorescence images of cells obtained from the top layer of a Percoll® density gradient centrifugation tube. Cells are cultured to confluency in T25 flasks and passaged onto glass coverslips to allow for imaging. [A] Cells show positivity to endothelial marker ICAM-1 and negativity to tubular epithelial marker Lotus Tetragonolobus Lectin (LTL), including [B] "secondary antibody only" negative control (scale bars=20µm).

Percoll® density gradient centrifugation of the kidney cortex is used to obtain tubular epithelial cells. Therefore, the remaining cells which cluster at the top layer of Percoll® tubes (**Figure 2.1**) are a mixture of other cellular components of the tubule-interstitium, namely renal fibroblasts and renal peritubular endothelial cells. The first experiments performed on this layer of cells and debris are aimed at investigating whether it would be possible to obtain any viable endothelial cells from the cluster. After Percoll® density gradient centrifugation, the top layer is cultured in T25 flasks in Endothelial Cell Growth Medium-2 (EGM™-2) to confluency. **Figure 3.27** shows fluorescent microscopy images of the immunofluorescent stained cells seeded onto glass coverslips. The cells are negative for the proximal tubule marker Fluorescein Lotus Tetragonolobus Lectin while they express ICAM-1 (Intercellular Adhesion Molecule 1), an endothelial marker widely expressed in the cortical vasculature (Watanabe, 2011). ICAM-1 is a cell surface protein that has been hereby used as an endothelial cell marker. As demonstrated in Bui TM et al., inflammation induces ICAM-1 expression in epithelial and immune cells, since it is a driver of inflammation response, therefore its use as an endothelial cell marker should be considered with caution and in combination with other markers in order to exclude potential confusion in phenotyping, especially around renal epithelial cells found in culture that could be subjected to injury (Bui et al., 2020).

3.6.2 HRPEC isolation via MACS CD31+ from digested kidney cortex

The first isolation method tested is magnetic-activated cell sorting (MACS) using CD31 MicroBead Kit, human. The cells cultured on cell culture-treated plastic flasks reached confluency after 14 days in culture. **Figure 3.28** shows data acquired from one donor, although the experiment was performed on three different donors which are not shown hereby. For all three donors, the percentage of double positive cells for CD31 / VEGFR2 and CD31 / VE-cadherin is very low, accounting for maximum 6% of the total live cell population for the third donor. More than two thirds of cell in culture do not exhibit endothelial phenotype, therefore we can confidently establish that MACS isolation on its own is not a suitable method for HRPEC isolation.

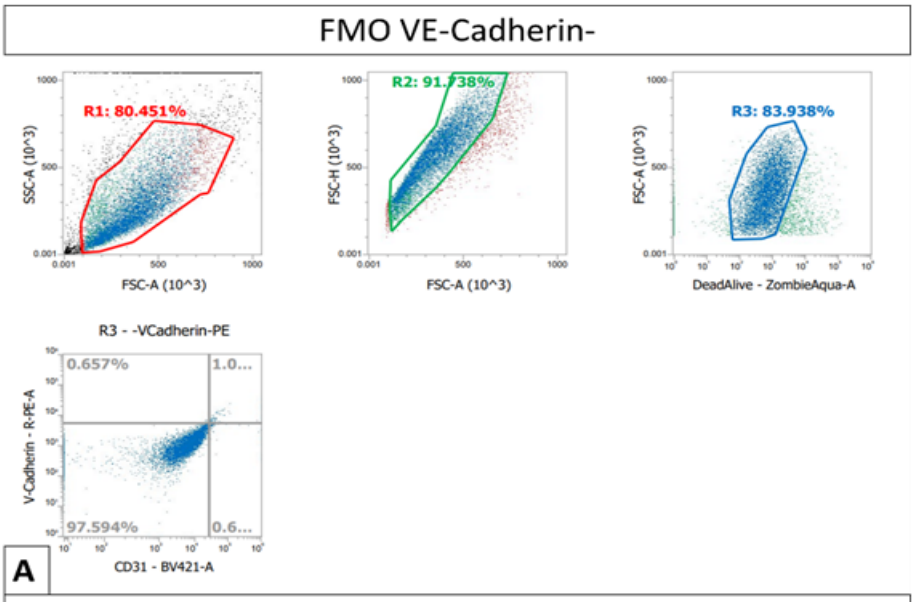
FMO VE-Cadherin-
R1: 80.451%
SSC-A (10^3)
FSC-A (10^3)
R2: 91.738%
FSC-H (10^3)
FSC-A (10^3)
R3: 83.938%
FSC-A (10^3)
DeadAlive - ZombieAqua-A
R3 - -VCadherin-PE
0.657%
1.0...
97.594%
0.6...
V-Cadherin - R-PE-A
CD31 - BV421-A
A

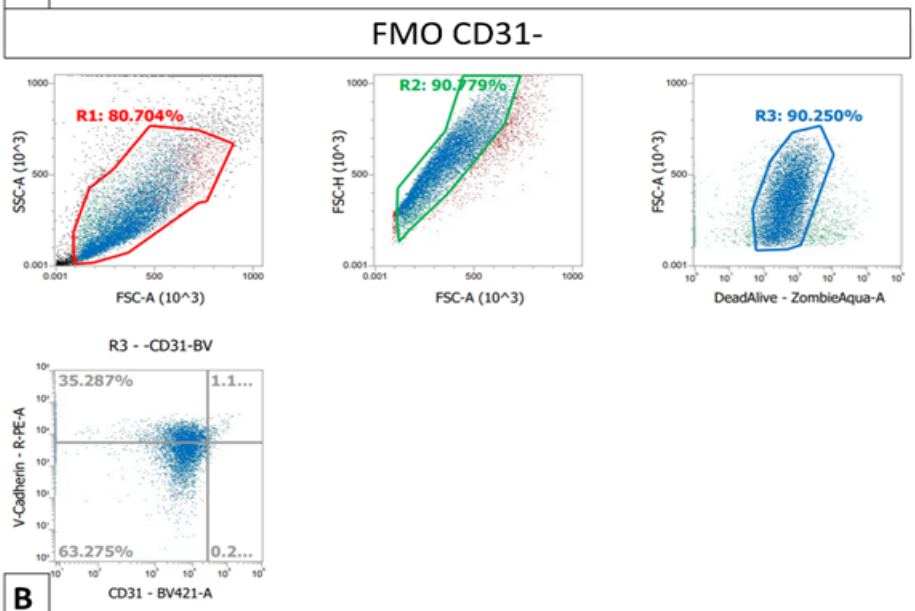
FMO CD31-
R1: 80.704%
SSC-A (10^3)
FSC-A (10^3)
R2: 90.779%
FSC-H (10^3)
FSC-A (10^3)
R3: 90.250%
FSC-A (10^3)
DeadAlive - ZombieAqua-A
R3 - -CD31-BV
35.287%
1.1...
63.275%
0.2...
V-Cadherin - R-PE-A
CD31 - BV421-A
B

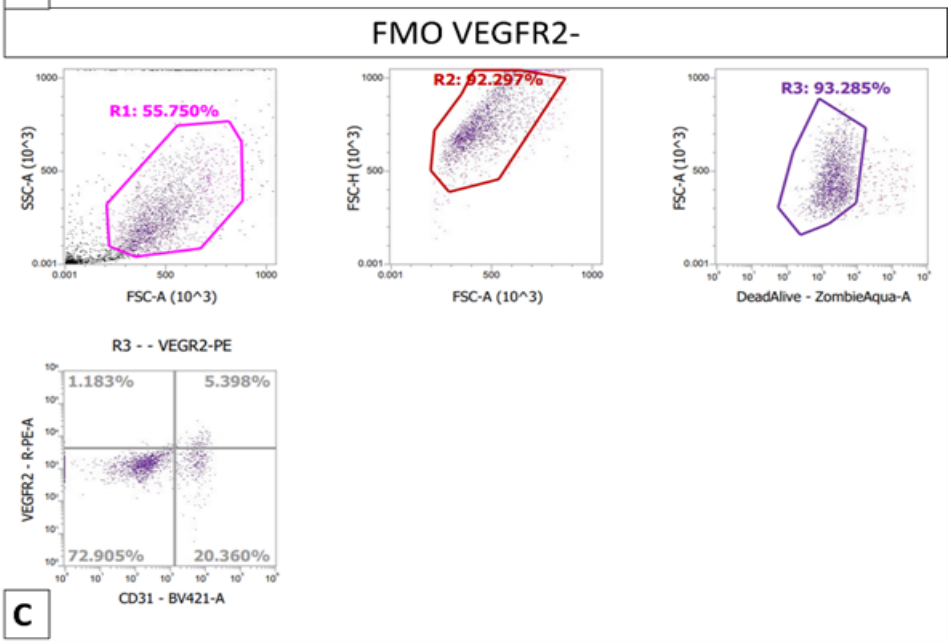
FMO VEGFR2-
R1: 55.750%
SSC-A (10^3)
FSC-A (10^3)
R2: 92.297%
FSC-H (10^3)
FSC-A (10^3)
R3: 93.285%
FSC-A (10^3)
DeadAlive - ZombieAqua-A
R3 - - VEGR2-PE
1.183%
5.398%
72.905%
20.360%
VEGFR2 - R-PE-A
CD31 - BV421-A
C

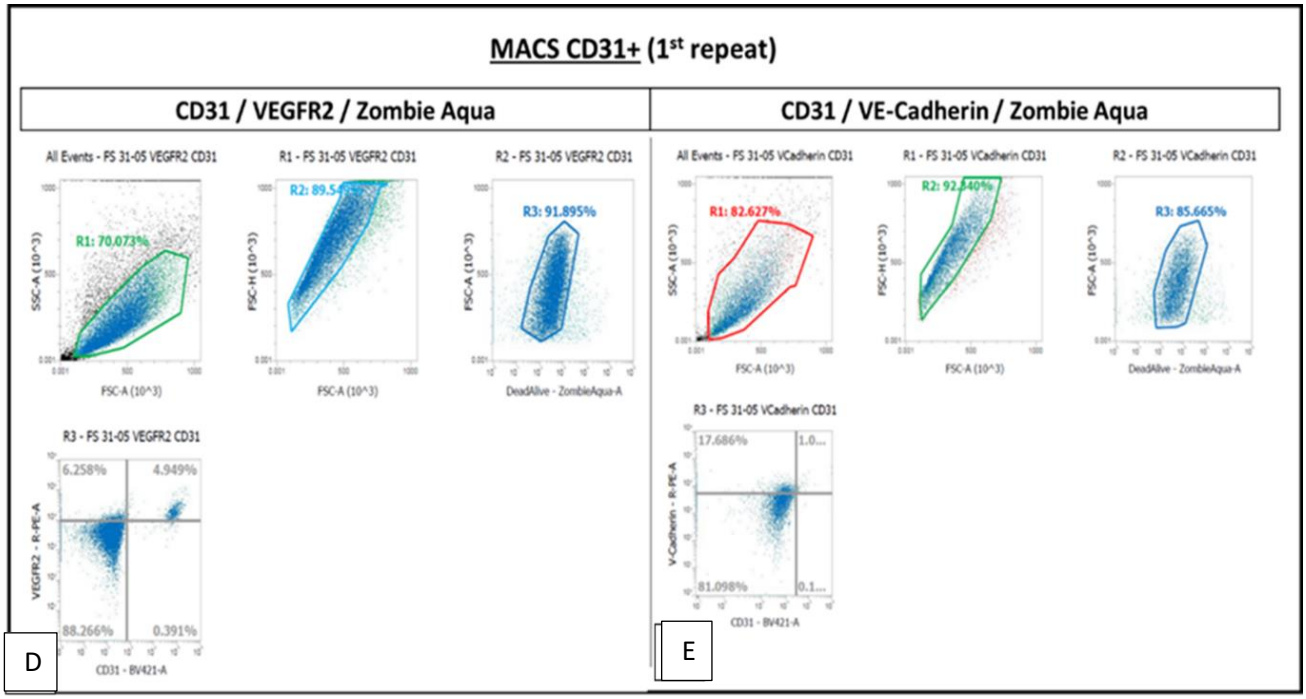

Figure 3.28. Flow cytometry dot plots representing the percentages of cells isolated via MACS CD31+ showing positive staining for endothelial markers. Gating strategy based on fluorescence minus one (FMO) controls depicted in [A] VE-Cadherin-, [B] CD31-, [C] VEGFR2-. Singlets depicted in FSC-A / SSC-A dot plots, doublets shown in FSC-A / FSC-H dot plots, live/dead cells shown in ZombieAqua / FSC-A dot plots. [C] CD31/VEGFR2 positive: Zombie Aqua- 91.895%, VEGFR2+ CD31+ 4.949%, VEGFR2+ CD31- 6.258%, VEGFR2- CD31+ 0.391%, VEGFR2- CD31- 88.266% [D]) CD31/VE-Cadherin positive: Zombie Aqua- 85.665%, VE-Cadherin+ CD31+ 3.160%, VE-Cadherin+ CD31- 18.618%, VE-Cadherin- CD31+ 1.195%, VE-Cadherin- CD31- 77.026%.

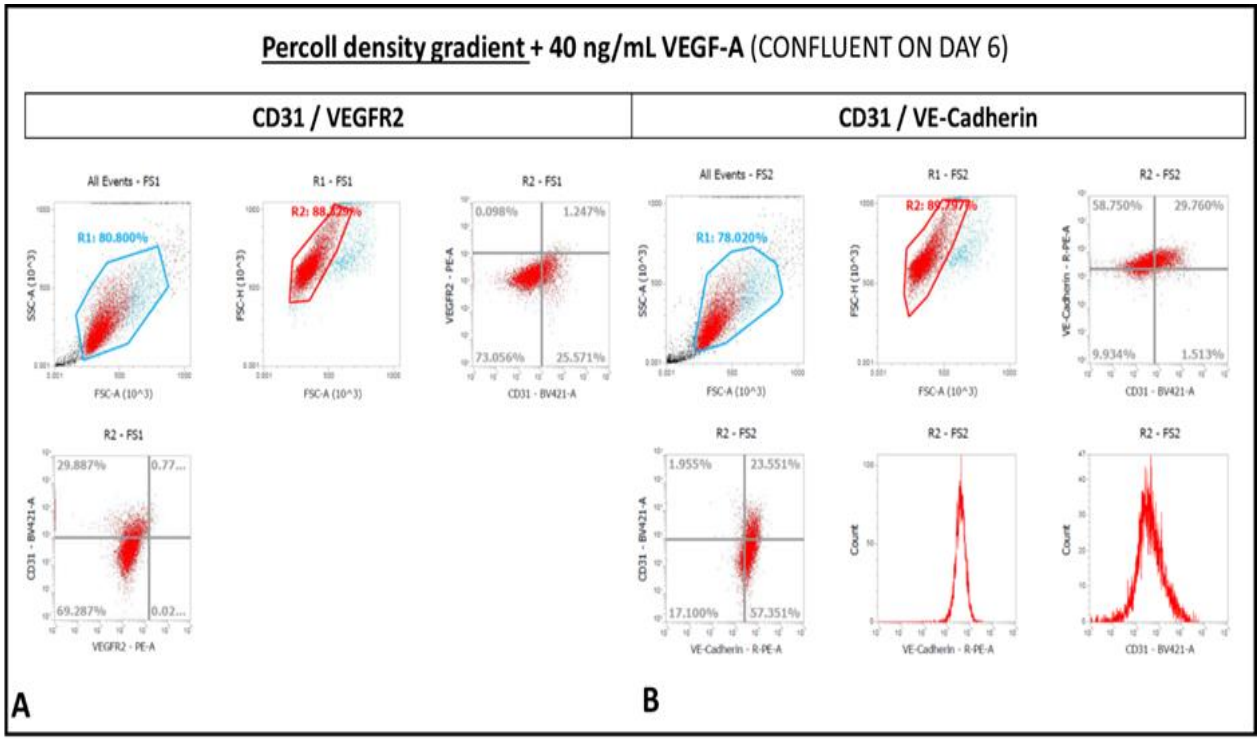

Figure 3.29. Flow cytometry dot plots and histograms representing the percentages of cells isolated via Percoll® density gradient centrifugation showing positive staining for endothelial markers. [A] CD31/VEGFR2 positive: Zombie Aqua- 88.329%, VEGFR2+ CD31+ 1.247%, VEGFR2+ CD31- +0.098%, VEGFR2- CD31+ 25.571%, VEGFR2- CD31- 73.056% [B] CD31/VE-Cadherin positive: Zombie Aqua- 89.797%, VE-Cadherin+ CD31+ 23.551%, VE-Cadherin+ CD31- 57.351%, VE-Cadherin- CD31+ 1.955%, VE-Cadherin- CD31- 17.10%.

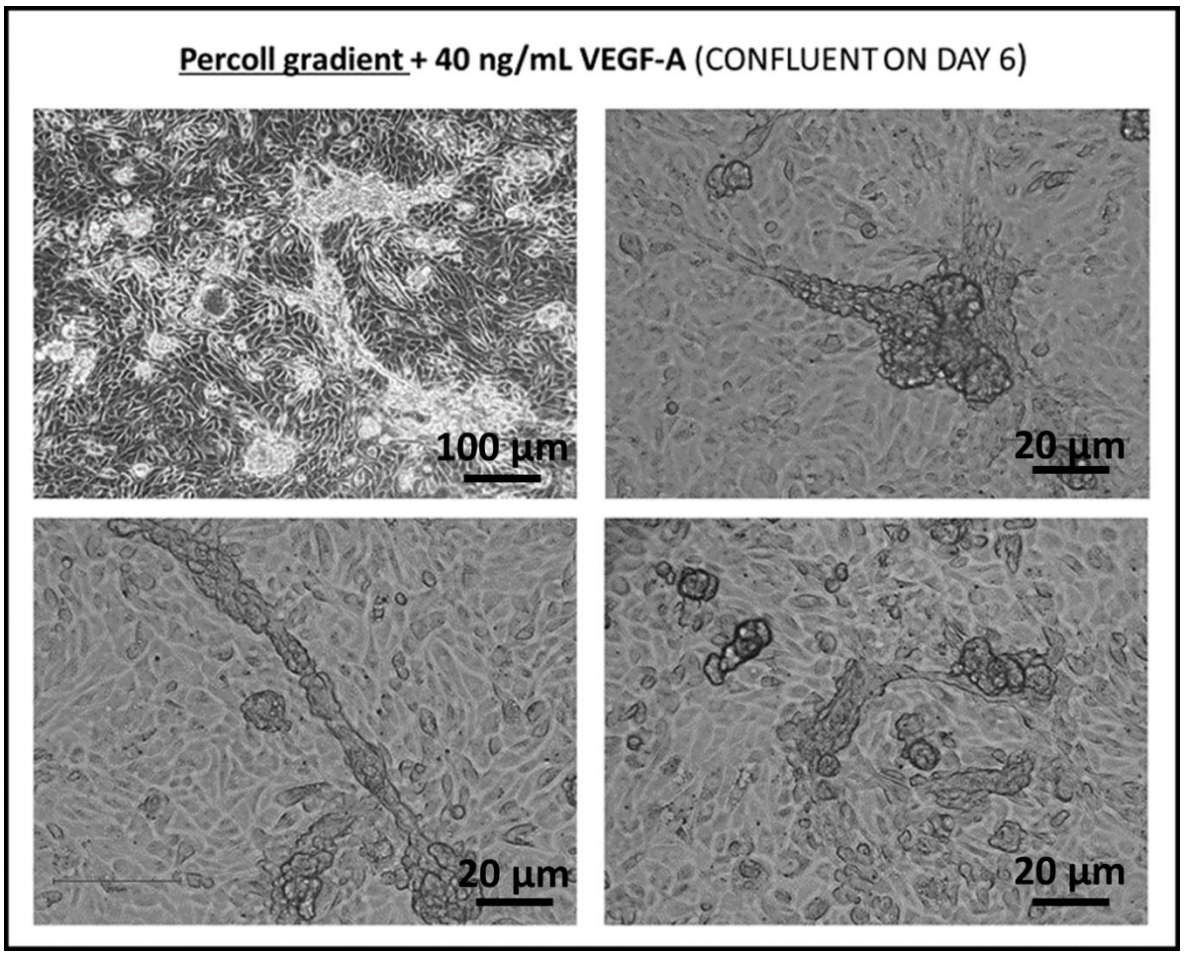

Figure 3.30. Phase-contrast images of overconfluent cells forming tubules arising from monolayers. Cells isolated via Percoll® density gradient centrifugation, cultured with EGM™-2 supplemented with 40 ng/mL VEGF-A on T75 flasks. Overconfluent cells are forming tubules arising from monolayers (scale bars=100µm, 20 µm).

The second isolation method tested is Percoll® density gradient centrifugation, which is regularly used in among our research group to successfully isolate high numbers of epithelial cells from the renal cortex, as above-stated. Flow cytometry FSC / SSC (forward scatter / side scatter) dot plots have previously shown that while epithelial cells cluster in the middle of the gradient obtained after Percoll® density gradient centrifugation, endothelial cells and fibroblasts cluster at the top of the gradient. The top layer of cells is seeded on plastic cell culture flasks and EGM™-2 medium is supplemented with 40 ng/mL of VEGF-A. Flow cytometry data in **Figure 3.29** show that although the percentage of CD31 / VEGFR2 double positive cells is still very low, the amount of CD31+ cells has increased to 29%, compared to less than 20% obtained via MACS CD31+ selection. Furthermore, CD31 / VE-Cadherin double positive cells dramatically increase to 23.551% as compared to 4.6% obtained via MACS. Interestingly, around 80% of cells seem to express VE-cadherin when isolated via Percoll® density gradient centrifugation method. Because of the improved yield that the application of this method leads to obtain, cells are further characterized via imaging. Cells successfully manage to form capillary-like structures (**Figure 3.30**) when overconfluent, and when passaged onto glass coverslips, they show positivity to diaphragmatic fenestration marker PV-

1 (**Figure 3.31**), thus indicating that a portion of the cells isolated via Percoll® density gradient centrifugation method retain the renal peritubular capillary phenotype *in vitro*.

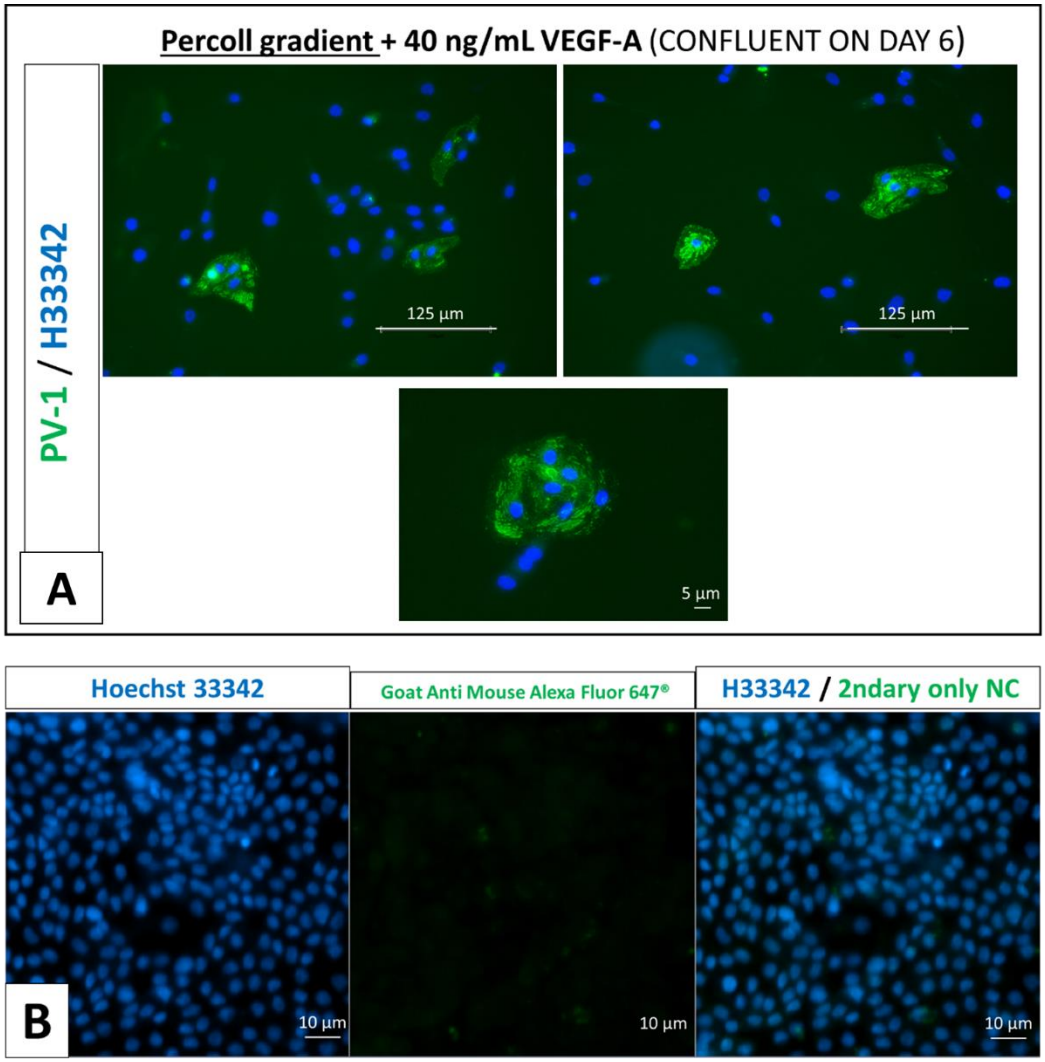

Figure 3.31. Fluorescence images of cells isolated via Percoll® density gradient centrifugation, EGM™-2 supplemented with 40 ng/mL VEGF-A, showing positivity for [A] PV-1 (plasmalemmal vesicle associated protein-1) indicative of diaphragmatic fenestration, including [B] "secondary antibody only" negative control (scale bars=125µm, 5 µm, 10 µm).

3.6.3 HRPEC isolation via MACS CD31+ from digested kidney cortex with VEGF-A supplementation

Since VEGF-A supplementation led to promising results, endothelial cells are selected once more via MACS CD31+, in this instance with addition of the growth factor in the medium. The data shown in **Figure 3.32** displays that percentage of CD31 / VEGFR2 double positive cells increases to 26.2% and CD31 / VE-Cadherin double positive cells amount to 22.204%.

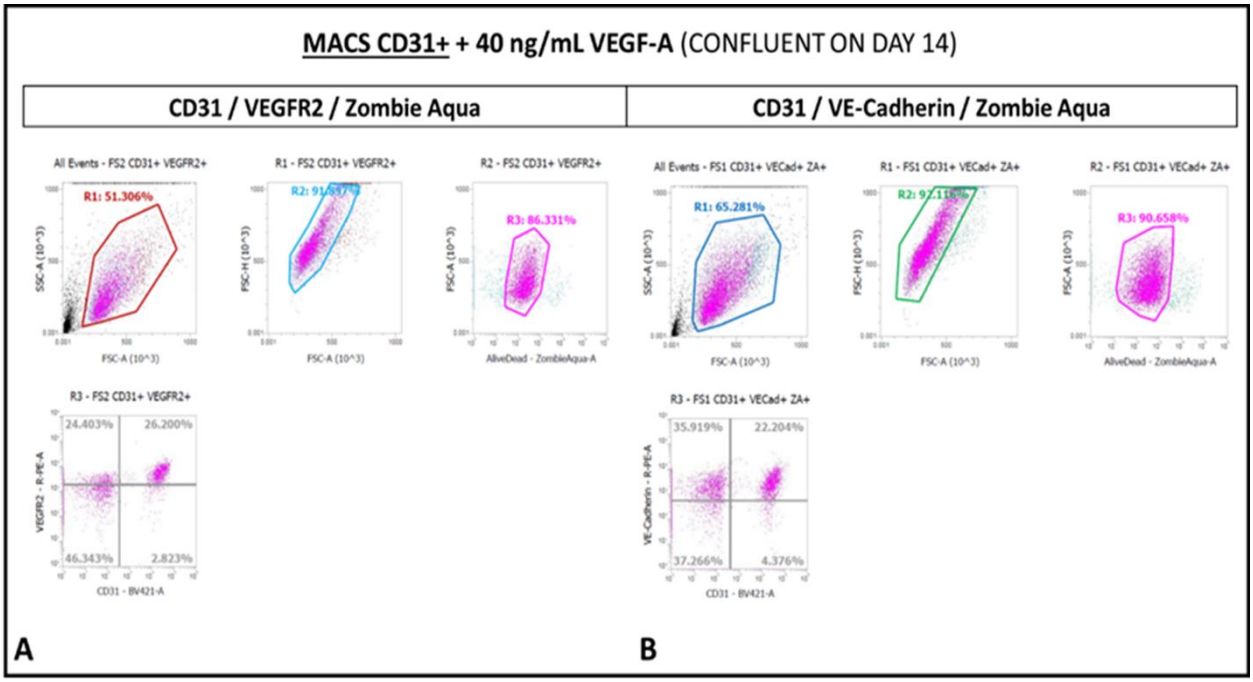

Figure 3.32. Flow cytometry dot plots representing the percentages of cells isolated via MACS showing positive staining for endothelial markers. [A] CD31/VEGFR2 positive: Zombie Aqua- 86.331%, VEGFR2+ CD31+ 26.2%, VEGFR2+ CD31- +24.403%, VEGFR2- CD31+ 2.823%, VEGFR2- CD31- 46.343% [B] CD31/VE-Cadherin positive: Zombie Aqua- 90.658%, VE-Cadherin+ CD31+ 22.204%, VE-Cadherin+ CD31- 35.919%, VE-Cadherin- CD31+ 4.376%, VE-Cadherin- CD31- 37.266%.

3.6.4 Comparison between isolation methods: Percoll® density gradient centrifugation and Percoll® density gradient centrifugation + MACS CD31+ with VEGF-A supplementation

The last isolation method trialled is a combination of Percoll® density gradient centrifugation to deplete epithelial cells and fibroblasts followed by expansion of cells in T-25 flasks, followed by positive selection of endothelial cells via MACS CD31+. The EGM™-2 culture medium is then supplemented with 40 ng/mL VEGF-A. The combined isolation method is compared to Percoll® density gradient centrifugation on its own via flow cytometry as shown in **Figure 3.33**. The simpler isolation method leads to 1.778 % VE-Cadherin+ cells [A], whereas the combined isolation method yields to 71.894 % of cells being VE-Cadherin+. Expression of VEGFR2 is comparable between the two methods, while CD31+ cells shift from 1 % to 10 % [B], [D]. Although cells are purified based on the presence of adhesion molecule CD31, and they have shown to express all other relevant endothelial markers, the expression of this protein is

lower than expected. As shown in **Figure 3.34 [B],** only 13% of purified HRPEC express CD31, whereas 73.42% of this cell population expresses PV-1 (**Figure 3.35**) which suggests that the latter might be a more appropriate marker to quantify the purity of HRPEC.

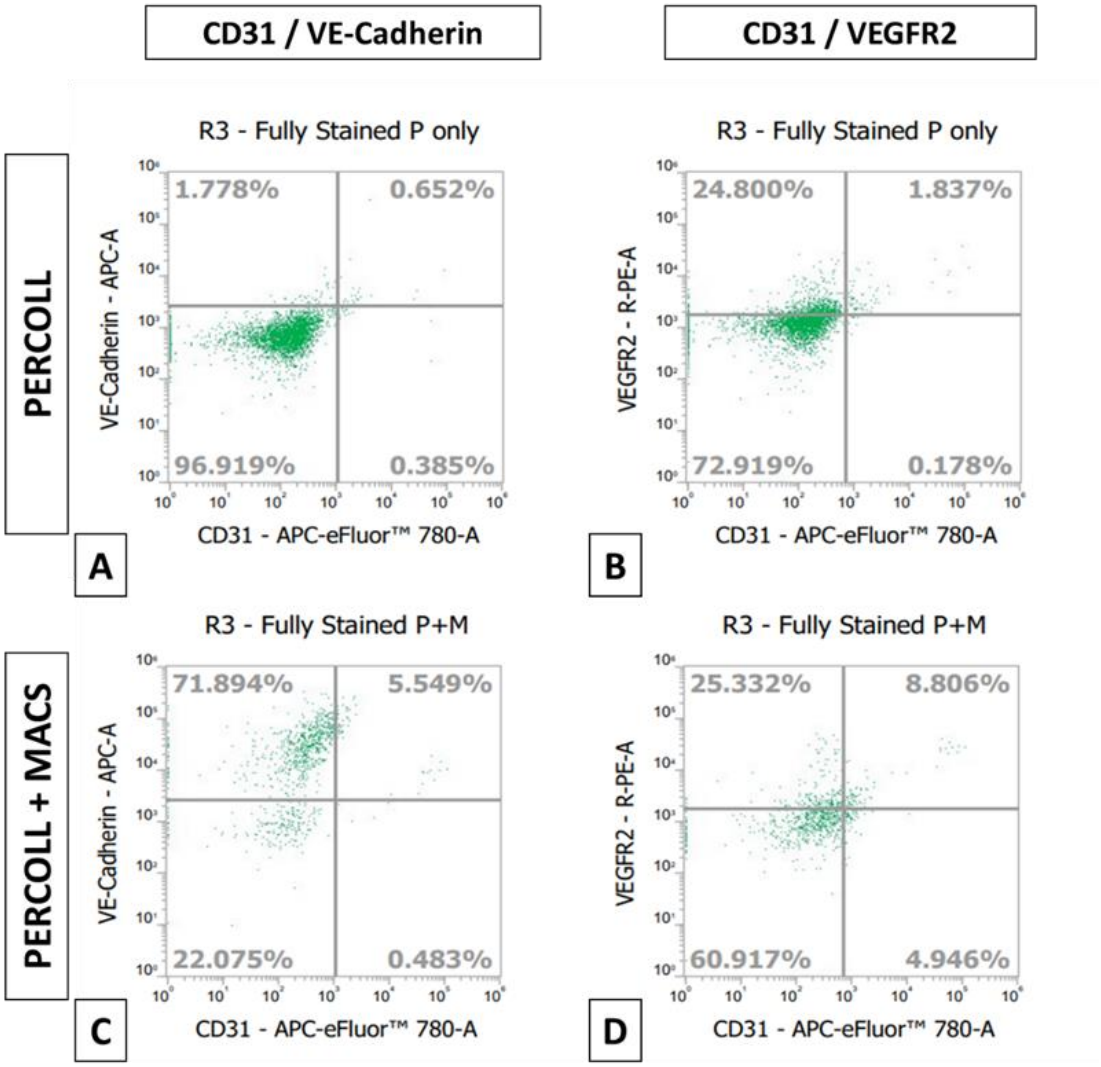

Figure 3.33. Flow cytometry dot plots comparing the percentages of cells isolated via Percoll® density gradient centrifugation and Percoll® density gradient centrifugation in combination with MACS CD31+ from one biological replicate (K15) showing positive staining for endothelial markers. [A] Percoll®: CD31/VE-Cadherin positive: VE-Cadherin+ CD31+ 0.652%, VE-Cadherin+ CD31- 1.778%, VE-Cadherin- CD31+ 0.385%, VE-Cadherin- CD31- 96.191% [B] Percoll®: VEGFR2+ CD31+ 1.837%, VEGFR2+ CD31- 24.800%, VEGFR2- CD31+ 0.178% , VEGFR2- CD31- 72.919%. [C] Percoll® + MACS: CD31/VE-Cadherin positive: VE-Cadherin+ CD31+ 5.549%, VE-Cadherin+ CD31- 71.894% , VE-Cadherin- CD31+ 0.483% , VE-Cadherin- CD31- 22.075% [D] Percoll® + MACS: VEGFR2+ CD31+ 8.806% , VEGFR2+ CD31- 25.332% , VEGFR2- CD31+ 4.946%, VEGFR2- CD31- 60.917% .

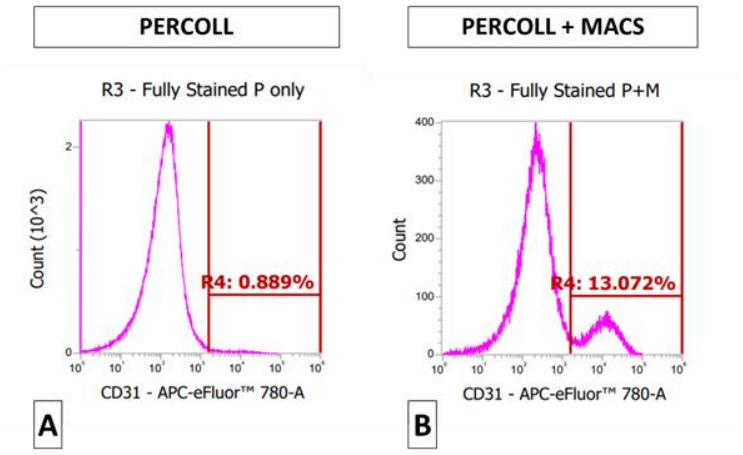

Figure 3.34. Flow cytometry histograms comparing the percentages of cells isolated via [A] Percoll® density gradient centrifugation and [B] Percoll® density gradient centrifugation in combination with MACS CD31+ from one biological replicate (K14) showing 13.072% positive staining for CD31.

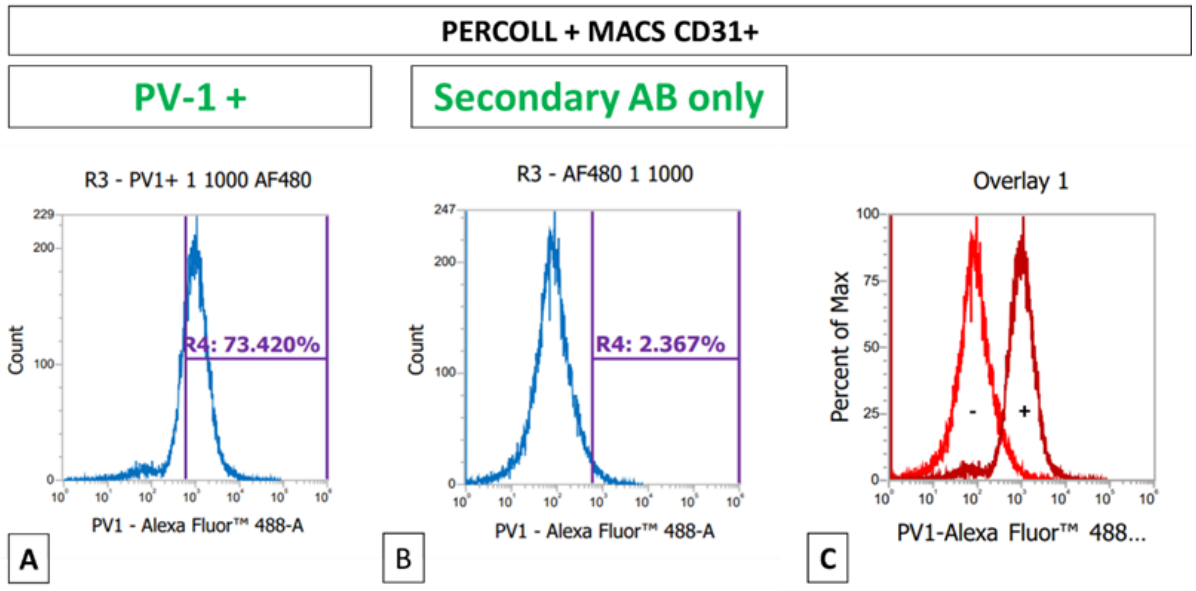

Figure 3.35. Flow cytometry histograms showing percentages of cells isolated via Percoll® density gradient centrifugation in combination with MACS CD31+ from one biological replicate (K15) [A] 73.22% cells staining positive for PV-1 + goat anti mouse Alexa Fluor 488 and [B] secondary antibody only (goat anti mouse Alexa Fluor 488), [C] overlay of histograms showing positive and negative cells.

Figure 3.36 displays further characterisation of HRPEC isolated via combined method. In particular, image **[B]** shows a 3D rendering of HRPEC capillaries formed at confluency on Transwell™ membranes: PV-1 (**in red**) is expressed along the capillary wall, thus suggesting that diaphragmatic fenestrations are maintained in our model and that they are localised where expected. Image **[C]** was obtained via transmission electron microscopy (TEM) of HRPEC confluent monolayers cultured on Transwell™ membranes: endothelial cells are forming tight junctions which are highlighted by black arrows. Transmission electron microscopy was fully outsourced to the Newcastle University electron microscopy research

facility, where endothelial samples cultured on Transwell were embedded in epoxy resin provided by the facility and subsequently delivered. Obtained images were returned to our group as depicted below.

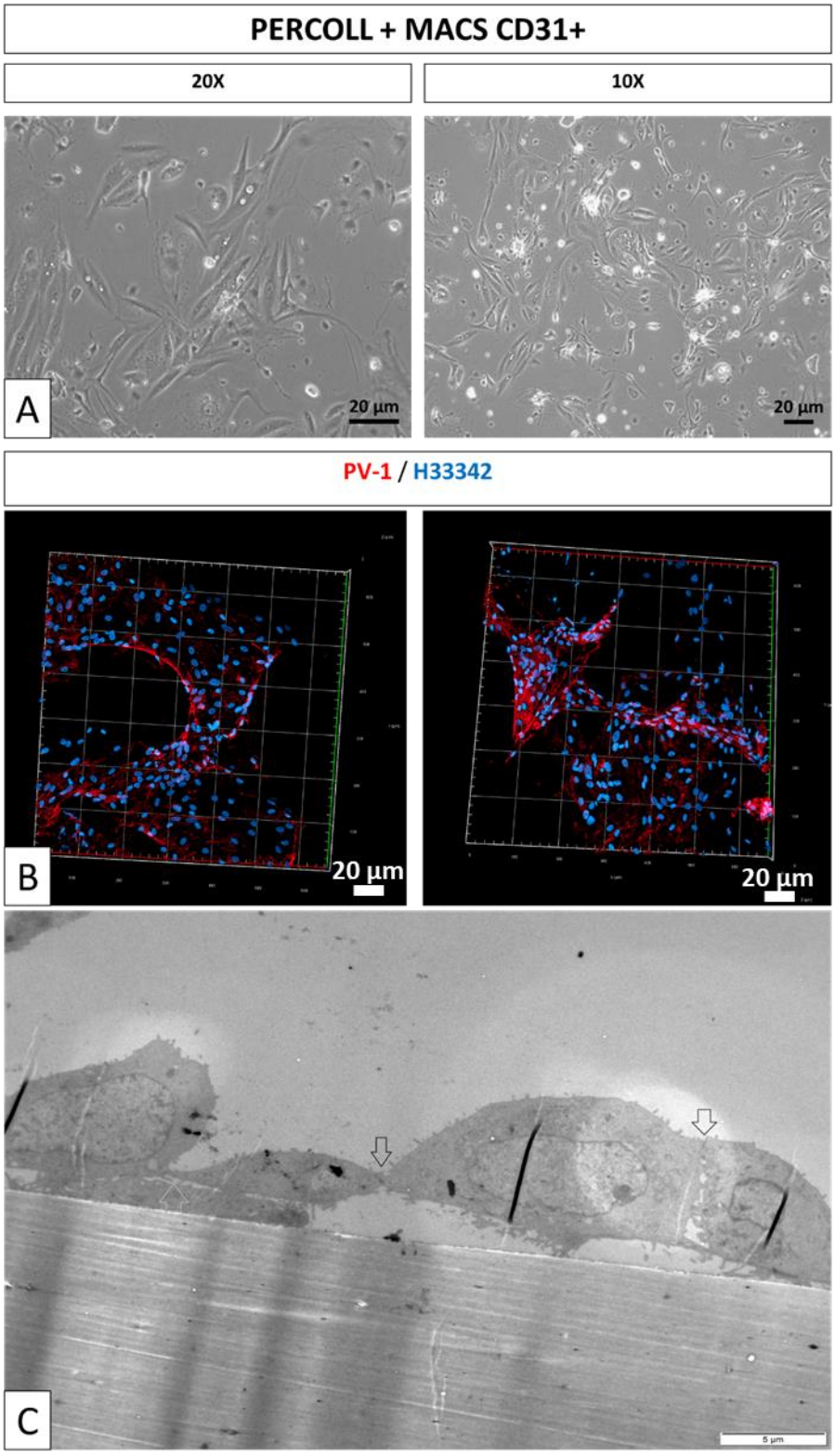

Figure 3.36. [A] Phase-contrast images of cells isolated via Percoll® density gradient centrifugation in combination with MACS CD31+ showing characteristic endothelial cell

morphology (scale bars=20µm) [B] fluorescence images showing capillary formation and polarised expression of PV-1 (scale bars=20µm) [C] transmission electron microscopy image of HRPEC monolayer forming tight junctions on Transwell membrane (black arrows) (scale bars=5µm).

3.7 HRPEC form capillaries in endothelial tube formation *in vitro* assay.

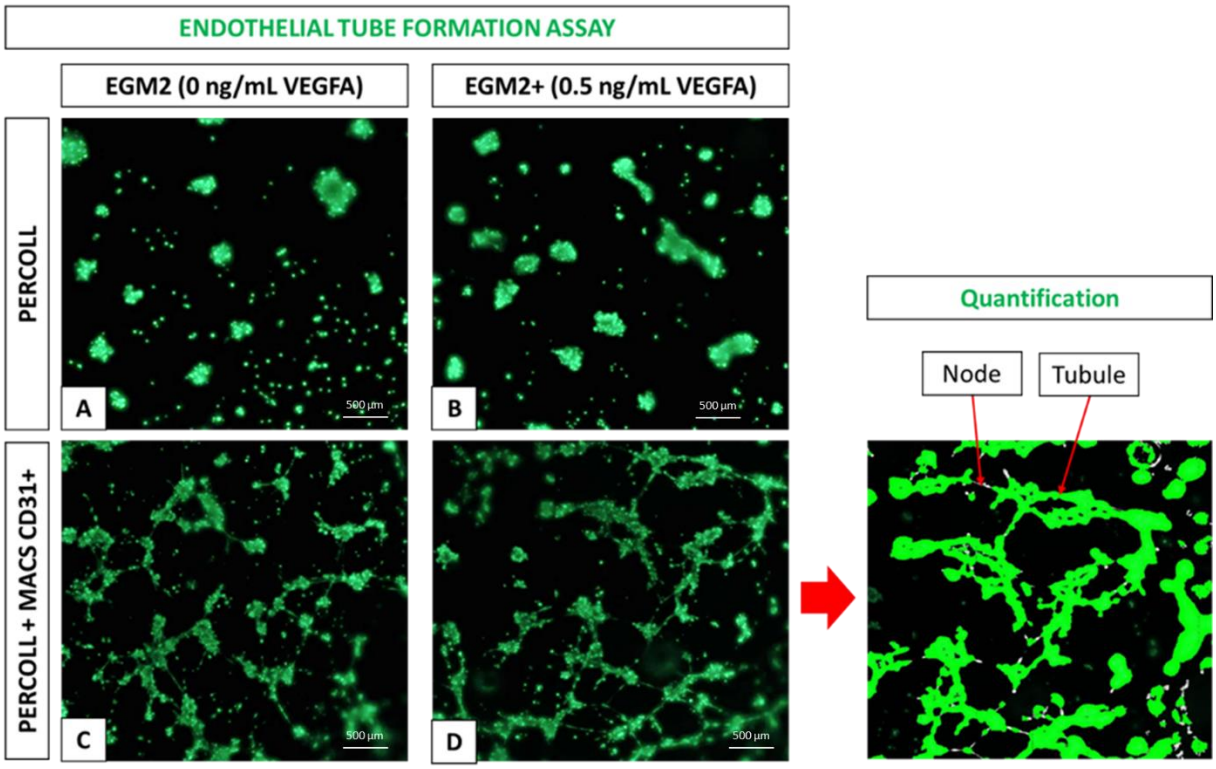

Figure 3.37. Examples of endothelial tube formation assay images and quantification performed [A], [C] without VEGF-A supplementation and [B], [D] with 0.5 ng/mL VEGF-A supplementation on [A], [B] Percoll® density gradient centrifugation and [C], [D] Percoll® density gradient centrifugation in combination with MACS CD31+. Purified populations represented in [C] and [D] successfully form capillaries in vitro, while unsorted populations in [A] and [B] do not (scale bars=500 µm).

Human renal peritubular endothelial cells can form microvasculature *in vitro* in specific conditions of culture. The endothelial tube formation assay measures whether a particular cell population can form capillaries when seeded onto a synthetic extracellular matrix. Cells isolated via Percoll® density gradient centrifugation and via Percoll® density gradient centrifugation followed by MACS CD31+ are cultured onto Matrigel® basement membrane in absence or presence of 0.5 ng/mL and 40 ng/mL VEGF-A. After 18 hours of culture, the microvascular structures are imaged via ImageXpress Pico 4X Objective and analysed via CellReporterXpress (**Figure 3.37**).

The experiment is performed on two biological replicates. The features of the microvasculature are considered in terms of tubules and nodes formed. These are quantified and plotted as comparison between the two isolation methods (**Figures 3.38 and 3.39**). The data suggests that both isolation methods lead to tubule formation that does not seem to be dependent on the presence and concentration of VEGF-A. Cells obtained via the combined isolation method (Percoll + MACS) lead to significantly increased total node area as compared to cells obtained by Percoll® density gradient centrifugation only (Percoll) [**Figure 3.38 D**], mean node area [**Figure 3.38 E**], and percentage area covered by nodes [**Figure 3.38 F**].

Therefore, features associated to tubules in terms of tube length, thickness, and area covered do not seem to be affected by isolation method nor concentration of VEGF-A in culture, whereas the purer population of cells isolated via Percoll + MACS seem to form a higher number of connections in between tubules, thus making this population better at forming microvasculature *in vitro*.

Endothelial Tube Formation Assay

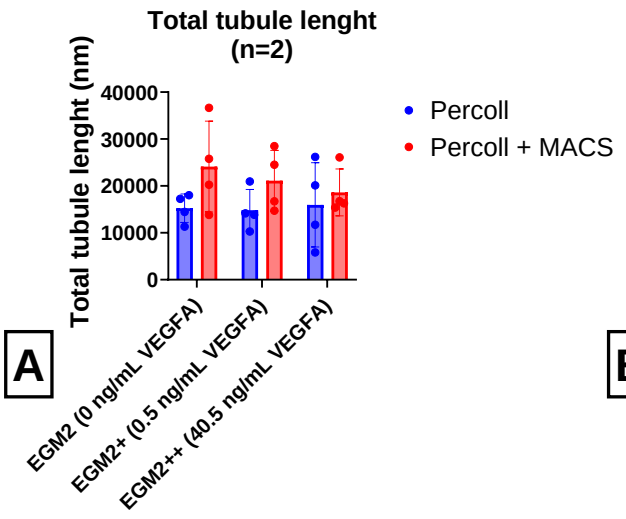

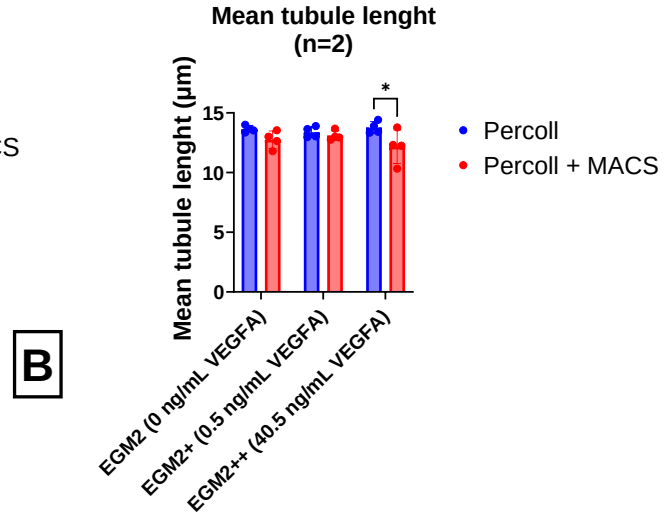

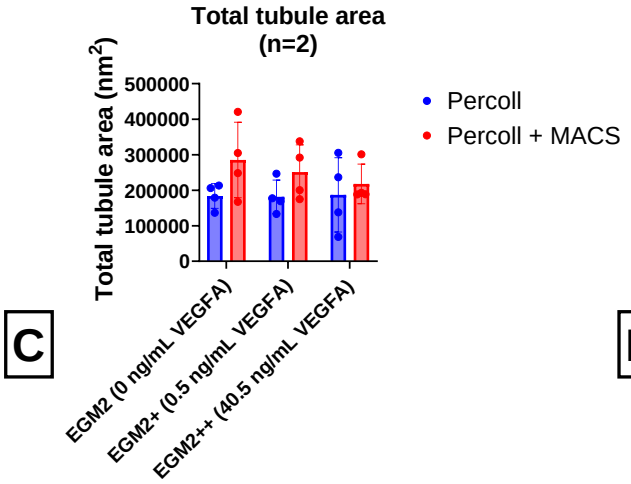

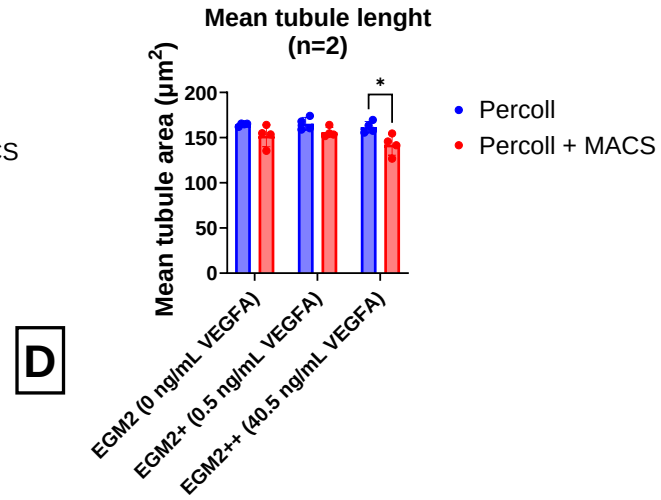

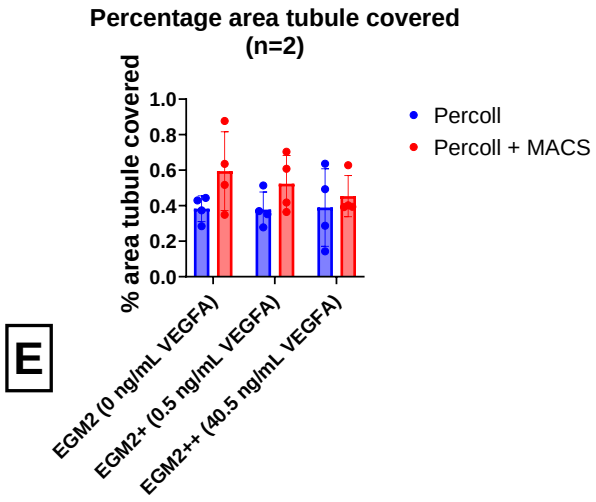

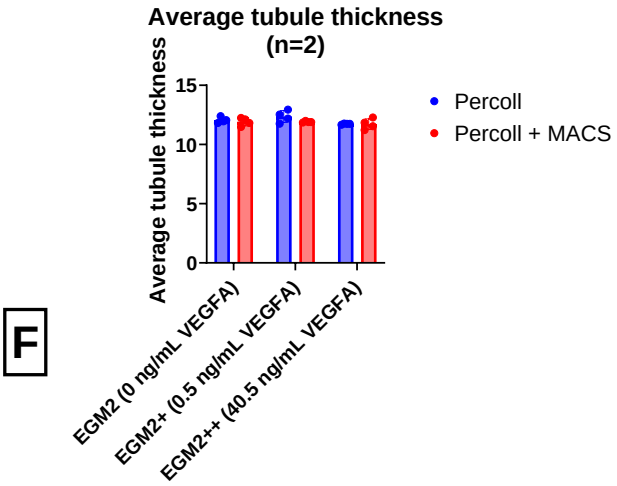

Figure 3.38. Endothelial tube formation assay performed after 18 hours of treatment with increasing concentrations of VEGF-A in HRPEC isolated via Percoll density gradient and Percoll density gradient [K9, K10] Percoll® density gradient centrifugation and Percoll® density gradient centrifugation in combination with MACS CD31+. [A] Total tubule length [C] Total tubule area [E] Percentage area tubule covered and [F] Average tubule thickness do not significantly vary across cell populations and media composition, while [B] Mean tubule length and [E] Mean tubule area are significantly different between purified and unsorted populations. Whole wells where imaged via ImageXpress Pico 4X Objective. Images were analysed via CXR. Datapoints represent the mean between two biological replicates and two technical replicates, while error bars represent SD. Statistical significance is depicted as '' ($p < 0.05$).*

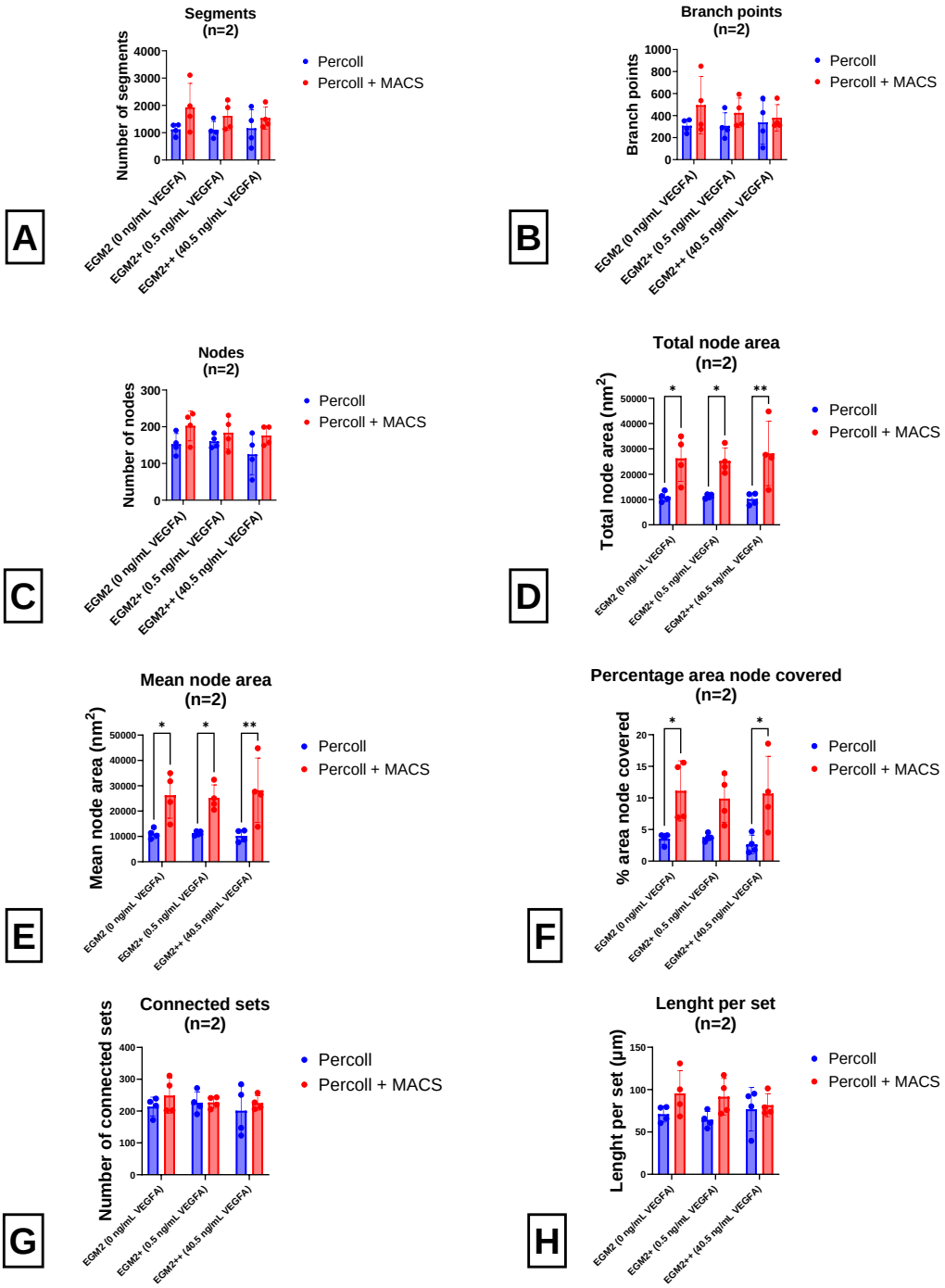

Figure 3.39. Endothelial tube formation assay performed after 18 hours of treatment with increasing concentrations of VEGF-A in HRPEC isolated via Percoll density gradient and Percoll density gradient [K9, K10] Percoll® density gradient centrifugation and Percoll® density gradient centrifugation in combination with MACS CD31+. [A] Segments [B] Branch points [C] Nodes [G] Connected sets [H] Length per set do not vary across cell populations and media compositions, while [D] Total node area [E] Mean node area [F] Percentage area node covered are significantly higher for purified cells as compared as in unsorted cells. Whole wells where

imaged via ImageXpress Pico 4X Objective. Images were analysed via CXR. Datapoints represent the mean between two biological replicates and two technical replicates, while error bars represent SD. Statistical significance is depicted as '' ($p < 0.05$).*

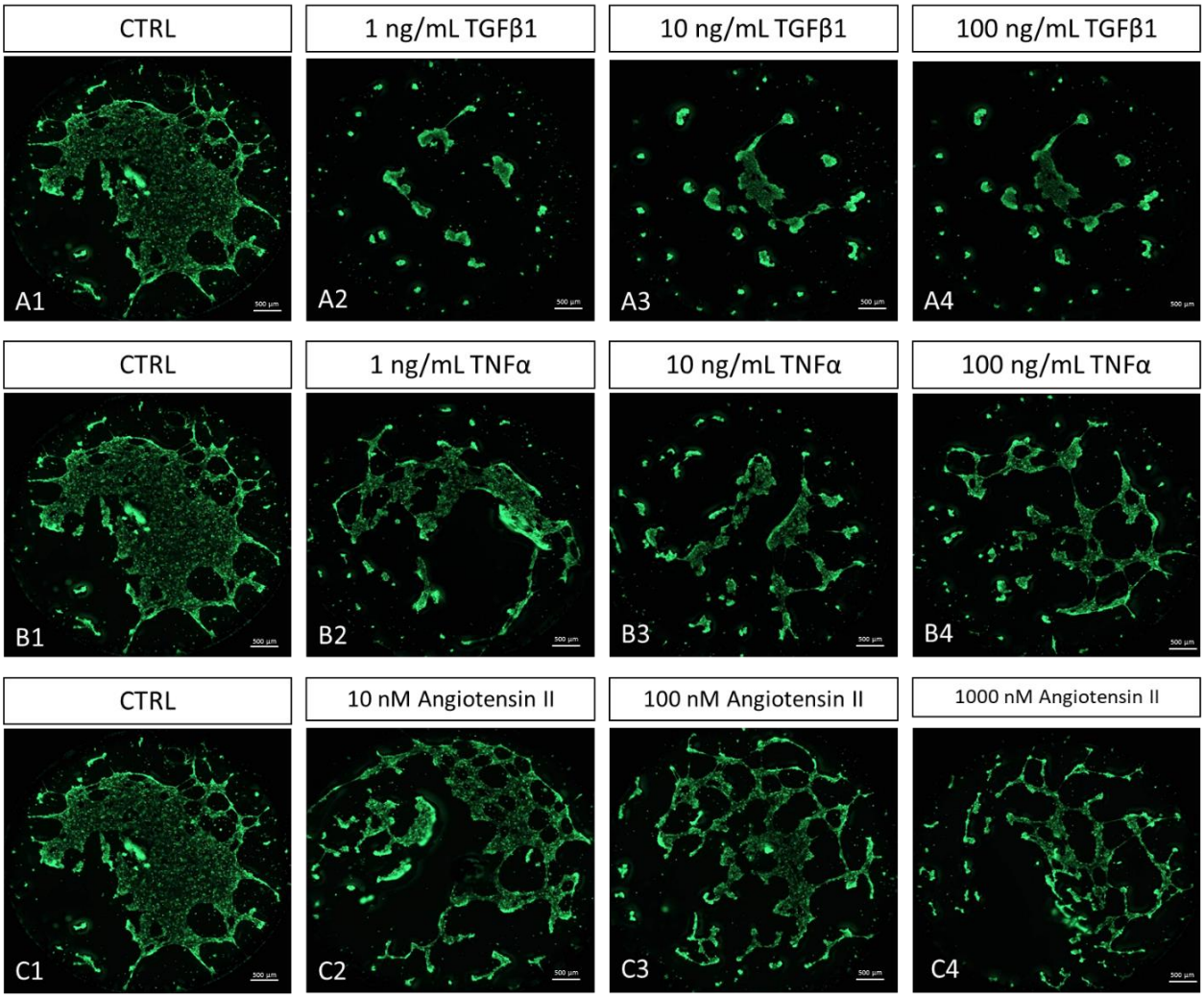

Figure 3.40. Endothelial tube formation assay performed after 18 hours of treatment with increasing concentrations of TGFβ1, TNFα, and Angiotensin II in HRPEC isolated via Percoll® density gradient centrifugation in combination with MACS CD31+. TGFβ1 inhibits endothelial tube formation as shown in [A2], [A3], [A4], TNFα in [B2], [B3], and [B4] and Angiotensin II in [C2], [C3, [C4] inhibit ETF to a lesser extent. Whole wells where imaged via ImageXpress Pico 4X Objective. Images were analysed via CXR. Datapoints represent the mean between two biological replicates and two technical replicates, while error bars represent SD. Statistical significance is depicted as '' ($p < 0.05$).*

Endothelial tube formation assay was performed as previously described with HRPEC isolated via the combined method treated with increasing concentrations of pro-fibrotic compounds to mimic the phenomenon of capillary rarefaction which accompanies renal fibrosis in chronic kidney disease (CKD). TGFβ1 and TNF-α seem to halt microvascular formation whereas angiotensin II seems to lead to formation of more capillaries *in vitro.*

3.8 Discussion

The proximal tubule interstitial interface is comprised by three main cellular components and a specific type of extracellular matrix, namely renal epithelial proximal tubule cells (hPTC), renal fibroblasts (HRF), renal peritubular endothelial cells (HRPEC), and the tubular basement membrane (TBM). These cellular and extracellular structures function as a whole to promote and support the main functions of the proximal tubule, which are reabsorption and secretion of endogenous and exogenous solutes from the blood to the urine and vice versa. For this structure to perform its physiological function properly, the cellular components have to exert specific phenotypical and functional characteristics. In the healthy human kidney, proximal tubule cells express tight junctions that allow for polarisation which results in expression of specific solute transporters on the apical or basolateral cell membrane, which in turn leads to the formation of a leak-tight epithelium that lines the TBM as a monolayer (Witzgall, 1999). Human renal fibroblasts are resident mesenchymal cells that provide trophic support to the epithelial and endothelial component of the interstitial interface via crosstalk and producing the TBM (Meran & Steadman, 2011). Peritubular endothelial cells are the endothelial counterpart of the proximal tubule cell: they express polarised diaphragmatic fenestrations that allow for the passage of solutes and immune complexes from the blood to the ultrafiltrate (Dumas et al., 2021b). When the renal parenchyma undergoes chronic and acute injury, these phenotypes change: proximal tubule cells lose their tight junctions which leads to loss of transporter and epithelial barrier function, some resident fibroblasts acquire contractile myofibroblast phenotype while others migrate from the bone marrow, and endothelial cells undergo partial dedifferentiation into non polarised cells or undergo apoptosis because of capillary rarefaction. Therefore, when purifying cell populations from the human kidney to build an *in vitro* model of proximal tubule interstitial interface which contains cells which are able to acquire maladaptive fibrotic phenotype, phenotyping of such components is of primary importance. This chapter focuses on demonstrating that the phenotype obtained from each cell type is that of the components of a healthy renal epithelial interstitial interface. Immunofluorescence staining, flow cytometry, and functional assays specific for hPTC, HRF, and HRPEC have been employed to validate the isolation protocols that have been optimised throughout this project to obtain these primary cell types from the human kidney cortex. The data presented in this chapter aims at taking the reader through the optimisation steps that each isolation protocol described in **Chapter 2** underwent in order to establish solid and reproducible protocols for the isolation of human proximal tubule cells (hPTC), human renal fibroblasts (HRF), and human renal peritubular endothelial cells (HRPEC) from the kidney cortex. Regarding the isolation of hPTC, we can infer that purification of Percoll® density gradient centrifugation isolated renal epithelial cells via positive selection of AQP1+ cells has shown to yield a more phenotypically pure population of proximal tubule cells as compared to cells isolated via Percoll® density gradient centrifugation only. Differences in gene expression of transporters (**Figure 3.4**) demonstrate that the epithelial monolayers obtained by culturing the purer cell population (MACS AQP1+) could represent an immature version of the proximal tubule, virtually lacking expression of key transporters such as OAT1, OAT3, cubilin, and URAT1. Conversely, upregulation of OCT2 expression in the purer population is backed by greater transporter functionality as suggested by the

radiolabelled creatinine flux assay performed on both cell populations (**Figure 3.5**). The Percoll® density gradient centrifugation followed by MACS AQP1+ purification method could be employed in case a cell population with higher transporter expression of selected protein was needed, but the simpler isolation method was taken forward to perform all other experiments that involve hPTC in this project because of its relative technical simplicity, inexpensiveness and overall reliability. One of the limitations of the flow cytometry assay panel used to phenotype putative renal epithelial cells obtained from the human kidney cortex is that it only includes markers for renal epithelial cells, namely aquaporin 1 (AQP1), aquaporin 2 (AQP2), and uromodulin (UMOD), without taking into account the potential presence of other cell types which are abundant in the renal parenchyma such as renal fibroblasts, podocytes, and endothelial cells (Balzer et al., 2022). Ideally, the flow cytometry panel would have included markers for all the cell types listed.

Our data demonstrates that hPTC successfully form the epithelial barrier *in vitro,* showing positive expression of proximal tubule markers (**Figures 3.7 and 3.8**), primary cilium presence (**Figures 3.9 and 3.10**), and polarised solute transporter expression (**Figures 3.11 and 3.12**). Moreover, we were able to pinpoint the timepoint of culture at which primary hPTC *in vitro* retain key transporter expression at the mRNA level (**Figure 3.14**) while having formed tight junctions by expressing relevant protein complexes (**Figures 3.15 to 3.17**) and having avoided activation of pathways that lead to spontaneous epithelial-to-mesenchymal transition (**Figure 3.18**). In conclusion, hPTC isolated from the human kidney cortex via Percoll® density gradient centrifugation should be used for further experiments between day 7 and 8 of culture. Referring to the isolation of HRF described in **3.4**, the data displayed in this section confirms that we have successfully isolated human renal fibroblasts from the kidney cortex via a novel protocol which allows to simultaneously isolate human proximal tubule cells and renal fibroblasts, which is fundamental to proceed to co-culturing these two cell types from one biological replicate, namely, from the same patient. The isolated human renal fibroblasts are characterised displaying retention of mesenchymal phenotype via phase contrast images (**Figure 3.20**), immunofluorescence staining (**Figure 3.22**), and flow cytometry (**Figure 3.23**). The culture conditions for human renal fibroblasts in monoculture were optimised by choosing the appropriate cell culture media. Furthermore, addition of L-ascorbate to the cultures suggests an amelioration of cell health and viability (**Figures 3.24 and 3.25**). The established isolation protocol and culture condition are applied for all subsequent experiments carried out throughout the project. Regarding the isolation of HRPEC, our findings indicate that we were able to optimise a robust and relatively fast isolation method to obtain human renal peritubular endothelial cells (HRPEC) from the human kidney cortex that does not require the use of a fluorescence-activated cell sorter (FACS). Thanks to the mass depletion of epithelial cells via Percoll® density gradient centrifugation previously optimised in our research group, subsequent expansion of cells under high concentrations of VEGF-A, and final purification via magnetic-activated cell sorter (MACS) of CD31 positive cells, we are able to obtain sufficient cells to allow for polarisation and microvasculature formation *in vitro.* As opposed to the evidence provided by Ligresti *et al.* (Ligresti et al., 2016), capillary network formation in the endothelial tube formation assay displayed in **Figures 3.37 to 3.40** is not dependent on the dose of VEGF-A present in the cell culture medium. Furthermore, our

initial findings relative to the effects of pro-fibrotic compounds on capillary rarefaction where HRPEC are stimulated by TGFβ1, TNFα, and angiotensin II in the context of the endothelial tube formation assay (**Figure 3.40**), indicate that the obtained HRPEC respond to pro-fibrotic stimuli and could be used as a high throughput *in vitro* capillary rarefaction for drug development to halt CKD and related disorders.

The results described in this chapter indicate that the cell populations obtained from each established method are likely to correspond to the phenotype we initially set out to obtain, however, phenotyping of each cell type should have been ideally compared to cell lines relevant to each isolated cell population. This was carried out in a rudimentary fashion when neonatal foreskin fibroblasts were compared to renal fibroblasts. Primary hPTC could have been compared to widely used cell lines such as RPTEC/TERT1 in terms of drug transporter genotypic and phenotypic profile (Simon-Friedt et al., 2015), TEER and tight junction formation assay. As for HRPEC, other renal endothelial cells should have been used as a comparison to confirm that the phenotype demonstrated by the cells is legitimate, such as glomerular endothelial cells which have several phenotypical features in common with HRPEC (Dylewski et al., 2020).

The limitations of magnetic-activated cell sorting (MACS) are many, in particular the possibility of only being able to select or deplete based on one marker. FACS could have been used, and the flow cytometry assays that had been developed to phenotype the three cell types could have been used to select a very pure population. In particular, within all cell types, we could have excluded cells expressing αSMA in order to avoid cells in partial EMT that could respond to the pro-fibrotic stimuli only after treatment.

An ideal experiment to compare the isolated cell types to cell lines would have involved both single-cell RNA sequencing and flow cytometry, to see how mRNA fingerprint would differ between immortalised epithelial cells and PTC. Single-cell RNA sequencing is an extremely powerful tool that has revolutionised ideas around cellular phenotype and, therefore, cellular identity. The transcriptomic signature of single cells in the human kidney gives rise to clusters of cellular populations that show variable transcriptional programs for example between male and female sexes. If enough samples of each cell type isolated from different donors could have been compared with RNA-seq, this could have given valuable information about the transcriptional signature of each cell type which could have been compared to the Human Gene and Protein Atlas. This concept could have been extended to samples obtained from CKD patients (McEvoy et al., 2022).

Chapter 4. Characterisation of 3D *in vitro* proximal tubule model.

4.1 Introduction

The previous chapters have discussed in detail isolation methods, culture conditions, and characterisation of all the "building blocks" needed to generate a 3D *in vitro* proximal tubule model. Literature on 3D proximal tubule models (Fransen et al., 2021), (Homan et al., 2016), (Lin et al., 2019) demonstrates that co-culture of proximal tubule cells with other components of the interstitial interface, namely endothelial cells, fibroblasts, and the tubular basement membrane leads to improvement of many key features of the proximal tubule cells such as transporter expression, transporter function, epithelial barrier function, and overall cell viability and survival. The extracellular matrix supporting the proximal tubule interstitial interface constitutes an integral part of the structure of this segment of the nephron. This semipermeable membrane provides structural and trophic support to the epithelial cell monolayer that covers this surface, and the physical features and mechanics of this structure seem to influence renal tubular cell health and behaviour. Variations in its stiffness has been linked to the pathophysiology of a number of conditions – not only in the kidney, but also in the heart and in the lung. Cell-matrix interactions are a focal point of interest particularly in the development of renal fibrosis, therefore experiments carried out during the course of this project have taken into account the importance of such interactions. The main constituents of the tubular basement membrane (TBM) are collagen IV and laminin, and thickening of this ECM is an hallmark of disease for conditions linked to CKD such as diabetic nephropathy (D. Wang et al., 2022). When it comes to differentiation, it has been demonstrated that the renal tubular epithelium loses some of its in vivo characteristics when translated to an *in vitro* platform, such as tight junction formation and key drug transporter expression (Love et al., 2019). These characteristics seem to be retained if an ECM with appropriate stiffness and elasticity is used to culture the cells. Having considered these findings, and having demonstrated in Chapter 3 that the human primary proximal tubule cells isolated from the renal cortex do retain tight junction formation and drug transporter function, within the following chapter the hypothesis that an exogenous ECM can drive the differentiation of hPTC *in vitro* will be explored.

This chapter focuses on comparing these key features between all the 3D models that were generated during the course of this project. A number of techniques were implemented to select the most appropriate 3D *in vitro* model to be taken forward as a high throughput platform for induction of renal fibrosis. First and foremost, it was fundamental to demonstrate that the co-culture models retained epithelial barrier formation, which was measured by trans epithelial electrical resistance (TEER) assay, Lucifer Yellow leakage assay, and presence of tight junction protein zonula occludens 1 (ZO1). Ideally, the co-culture models would exert higher levels of drug transporter expression, both at the mRNA and protein level, as compared to the monoculture hPTC model. These hypotheses were assessed via Real Time quantitative PCR (RT-qPCR) for the genes encoding for a panel of transporter proteins and immunofluorescence staining. Furthermore, higher transporter expression would be expected to result in higher transporter function in the co-culture models, which

was assessed via radiolabelled creatinine and para-aminohippuric acid (PAH) transport and uptake assay, and fluorescent-labelled albumin uptake assay.

Aims

The aim of the work presented in this chapter is to select, characterise, and optimise culture conditions for a 3D *in vitro* co-culture model of the proximal tubule interstitial interface suitable for induction of molecular events that recapitulate the process of renal fibrosis for high throughput screening purposes. The reader will be taken through the different co-culture techniques implemented to derive autologous 3D models from the human kidney cortex. Mainly, the chapter focuses on contact co-culture models, where different cell types are cultured within the same compartment of Transwell® or ThinCert™ inserts, spatially separated co-culture, where one or more cell types are cultured on the underside of the inserts' permeable membrane being separated from the cell type cultured on the apical side of the membrane, and non-contact co-culture, where cells are cultured on the insert membrane and on the bottom of the well of a Transwell® or ThinCert™ system.

4.2 Assembly and characterisation of 3D in vitro co-culture models

4.2.1 Assembly of 3D co-culture models with physical separation of component cells

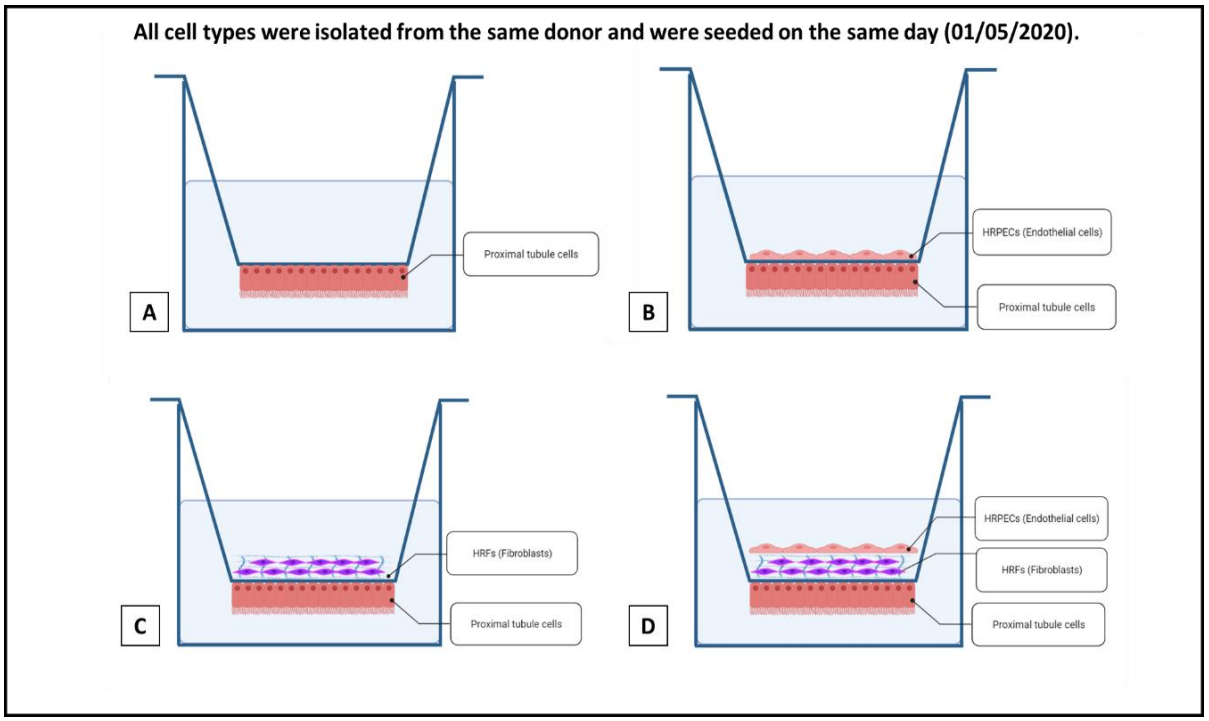

Figure 4.1. Graphical representation of 3D models cultured on Transwell® inserts [A] hPTC cultured on the underside of the insert (Control) [B] HRPEC on the apical side, hPTC on the underside of the insert [C] HRF on the apical side, hPTC on the underside of the insert [D] HRPEC and HRF co-cultured on the apical side, hPTC on the underside of the insert.

The first trialled way of co-culturing different cell types isolated from the same renal cortex was to use a co-culture system where hPTC were physically separated from the other two cell types by the Transwell® insert semipermeable membrane. This entailed to first isolate endothelial cells (HRPEC) and fibroblasts (HRF) (in the graphs these are referred to as "HE" and "HF" to shorten axis labels), to culture them onto the apical side of Transwell® inserts, incubate the inserts in the incubator for 4 hours at 37°C to let the cells attach and subsequently flip the inserts upside down to allow seeding of proximal tubule cells. The inserts were left for 4 hours more in the incubator to promote cell adhesion and then flipped back into the upright position inside a 24-well plate (**Figure 4.1**). This is a lengthy process that required same-day isolation of three cell types with at least two different isolation methods plus 8 hours of incubation, which has proven to be technically challenging. Leak-tightness of the co-culture models was compared via measurement of Lucifer Yellow leakage between the apical and basolateral compartment of the Transwell® chamber (**Figure 4.2**). After 1 hour of incubation, leakage from the apical to the basolateral compartment of the inserts was significantly lower for hPTC in co-culture with HRF as compared to the control condition, hPTC in monoculture. After 2 hours of incubation with Lucifer Yellow, leakage was significantly lower for hPTC cultured with HRPEC. When gene expression of key drug transporters in hPTC was assessed and compared to the expression of the same genes in hPTC monolayers, mRNA expression seemed to be upregulated when hPTC were cultured with HRPEC (**Figure 4.3**).

These results seemed promising, especially regarding the 3D model where hPTC were co-cultured with HRPEC, but the technical complexity and labour intensity required to produce these models using cells from the same renal cortex deemed this process unsuitable for a high throughput platform.

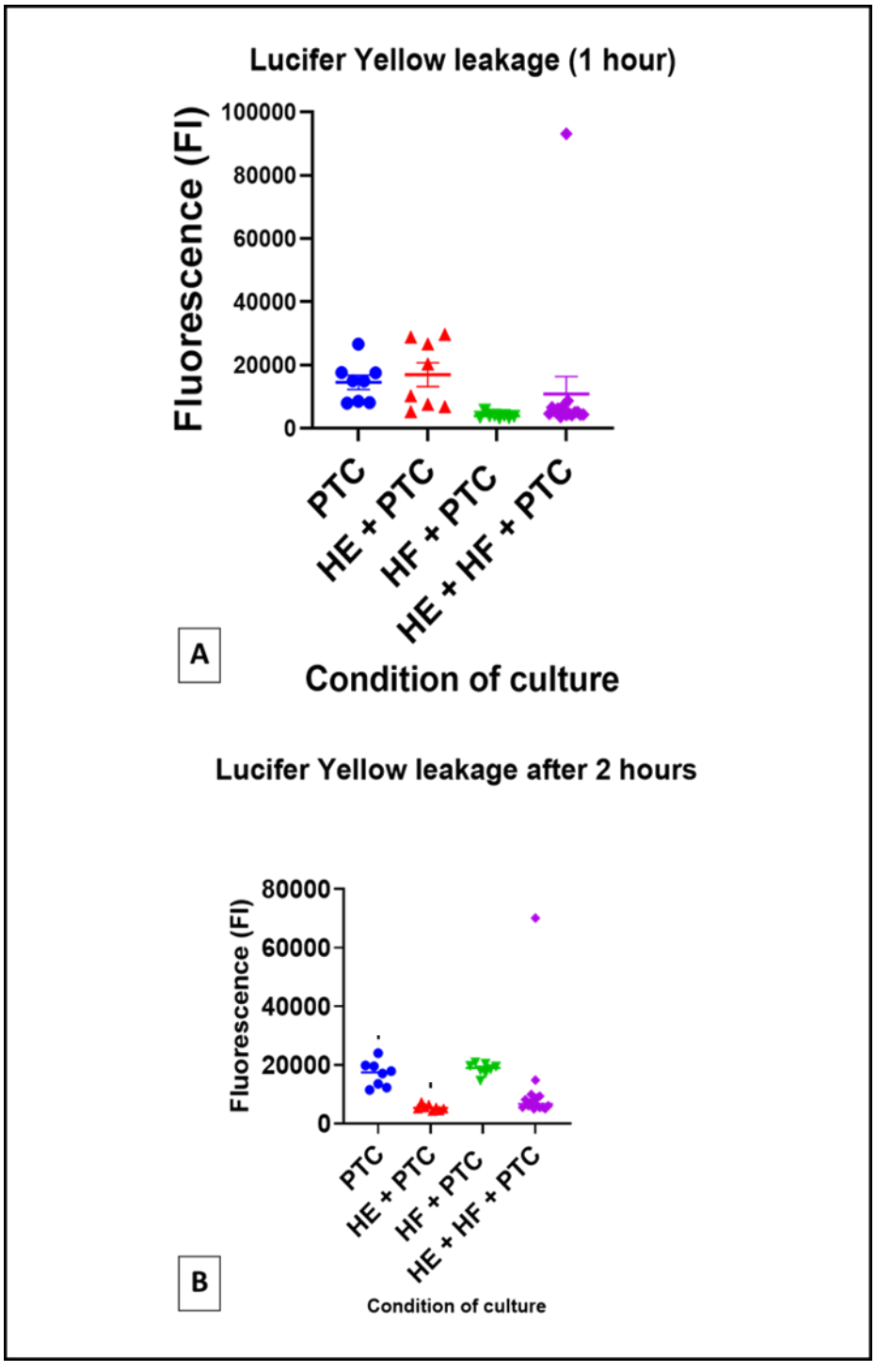

Figure 4.2. [A] Lucifer Yellow leakage after 1 hour from apical to basolateral compartment compared between 3D models. [B] Lucifer Yellow leakage after 2 hours. Contact co-culture between epithelial cells (PTC), endothelial cells (HE), and fibroblasts (HF) leads to leakier co-culture models as compared to monoculture models. Experiment performed on one biological replicate (n=1) and eight technical replicates per condition; error bars represent SD.

Drug transporters in hPTC in co-culture with HRF and HRPEC

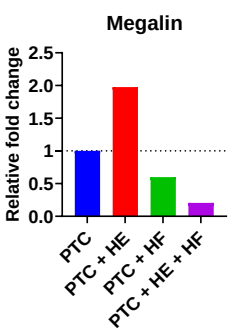

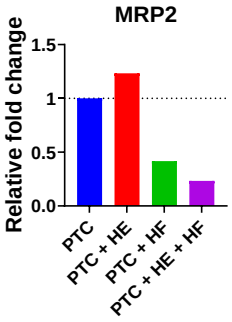

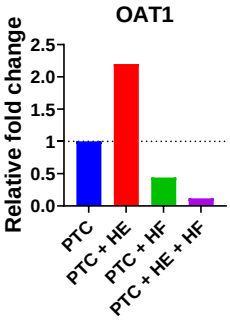

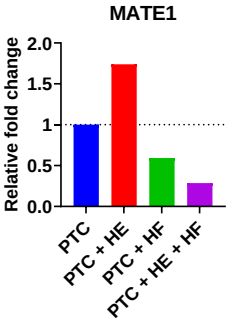

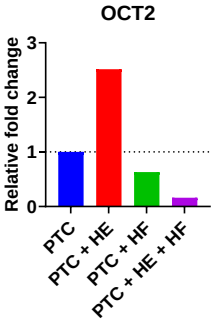

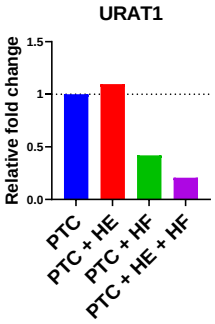

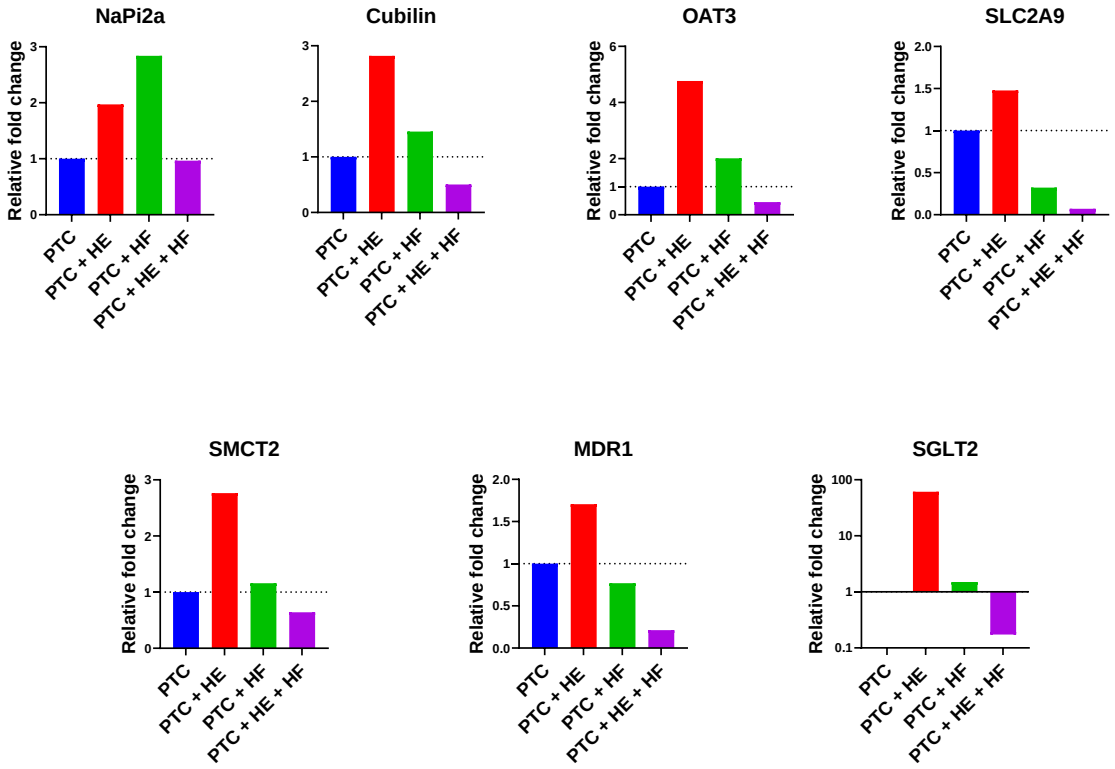

Figure 4.3. Effects of co-culture on relative fold change mRNA expression of drug transporters megalin, MRP2, OAT1, OCT2, URAT1, MATE1, NaPi2a, cubilin, OAT3, SLC2A9, SMCT2, MDR1, SGLT2. All genes encoding for key transporters are upregulated when proximal tubule cells are in co-culture with endothelial cells (PTC+HE) as compared to PTC in monoculture. NaPi2a, Cubilin, OAT3, and SMCT2 are upregulated in PTC+HF. mRNA was isolated from hPTC within 3D models cultured on Transwell® inserts from one biological replicate (n=1).

4.2.2 Assembly of 3D co-culture models using collagen support and multiple cell donors

To overcome the technical and time management issues faced with the previous method, the different cellular components of the model were isolated from two different donors. Firstly, HRPEC and HRF were isolated from the first donor; the cells were cultured on the apical side of the required number of inserts and grown to confluency. When a second kidney was donated to our research group, hPTC were isolated and seeded on the underside of the inserts as previously described. In addition to the models previously tested, two novel potential models were trialled: HRF were embedded in rat tail Collagen I with hPTC cultured onto the underside on the insert (**Figure 4.4 [D]**), and HFR + HRPEC were embedded in rat tail Collagen I with hPTC cultured on the underside (**Figure 4.4 [E]**). The ideal extracellular matrix employed in a fully human *in vitro* assay platform of the renal tubules should be either human derived or synthetic, following the first principle of the 3Rs. However, due to availability of reagents within our research group, we decided to employ an animal-derived ECM for preliminary experiments around the culture of primary kidney cells, therefore collagen I from rat tail was used. As shown in **Figure 4.5**, HRF retained mesenchymal phenotype (FSP1+) and formed 3D structures when embedded in rat tail Collagen I. As opposed to the previous experiment, gene expression of key transporters was not upregulated when hPTC were cultured with HRPEC, but megalin, MRP2, OAT1 and URAT1 were upregulated when hPTC were in culture with HRF (**Figure 4.6**).

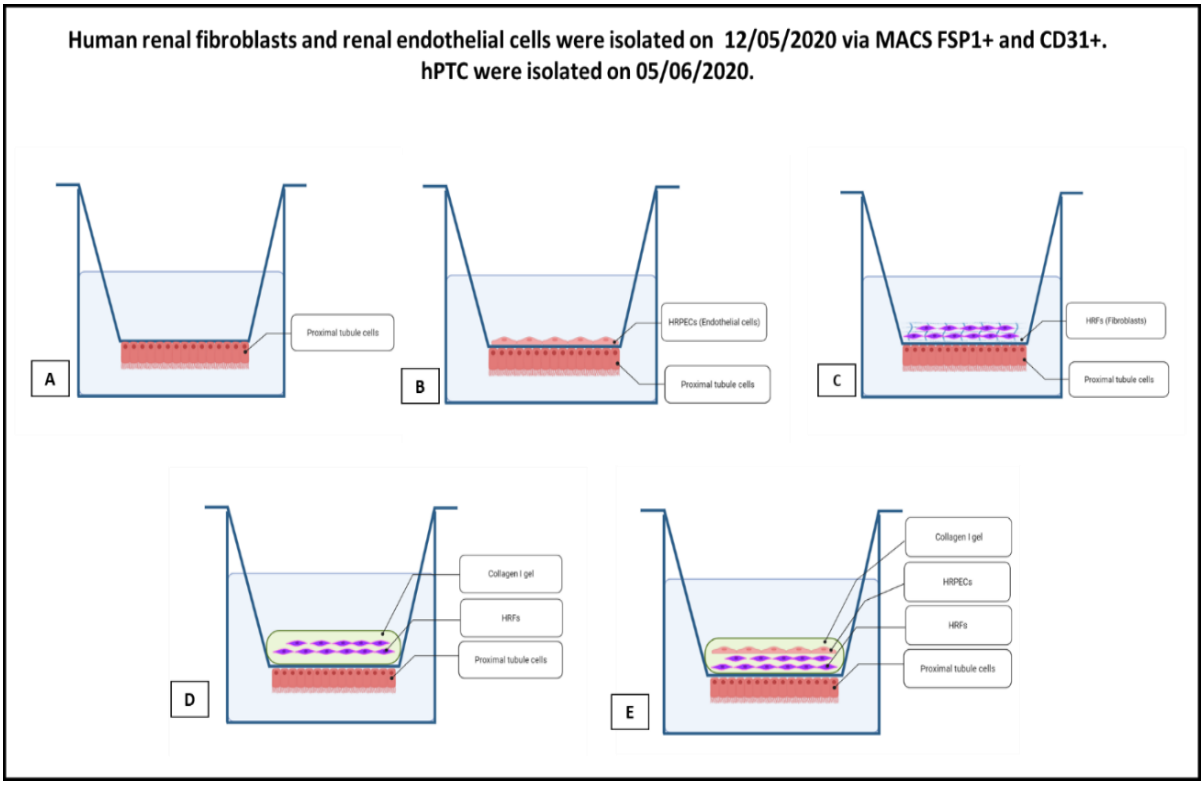

Figure 4.4. Graphical representation of 3D models cultured on Transwell® inserts [A] hPTC seeded on the underside of the insert (Control) [B] HRPEC on the apical side, hPTC on the underside of the insert [C] HRF on the apical side, hPTC on the underside of the insert [D] HRFs

embedded in Collagen I on the apical side, hPTC on the underside of the insert, [E] HRF and HRPEC embedded in Collagen I on the apical side, hPTC on the underside of the insert.

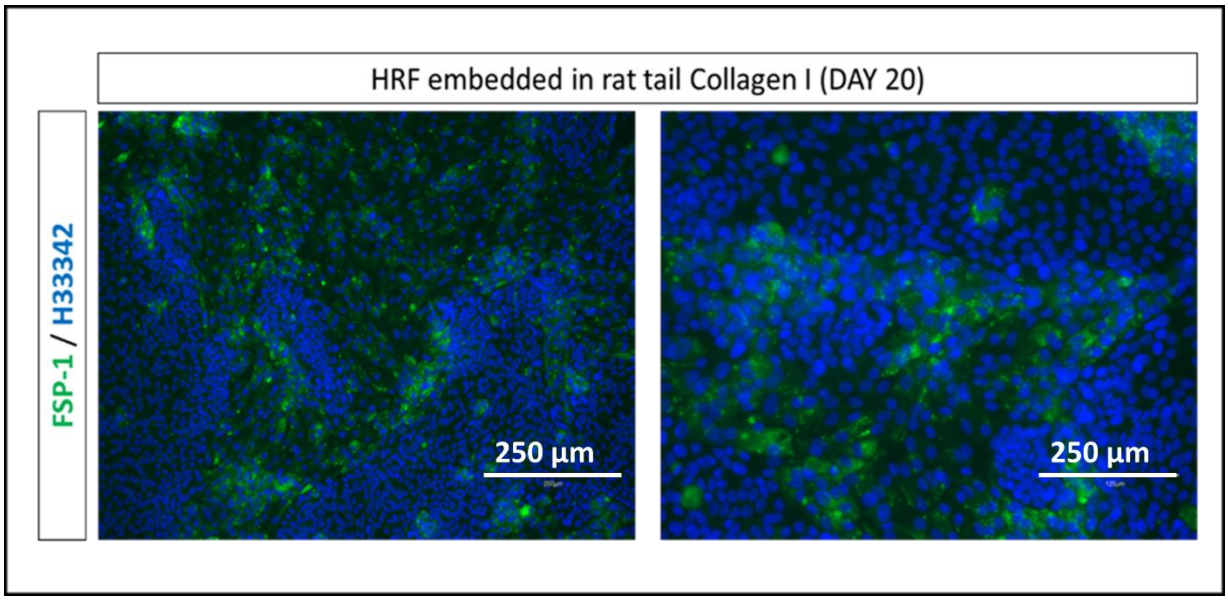

Figure 4.5. Fluorescence images of human renal fibroblasts embedded in rat tail Collagen I staining positively for FSP1 (fibroblast specific protein 1) and forming 3D structures (scale bars=250µm).

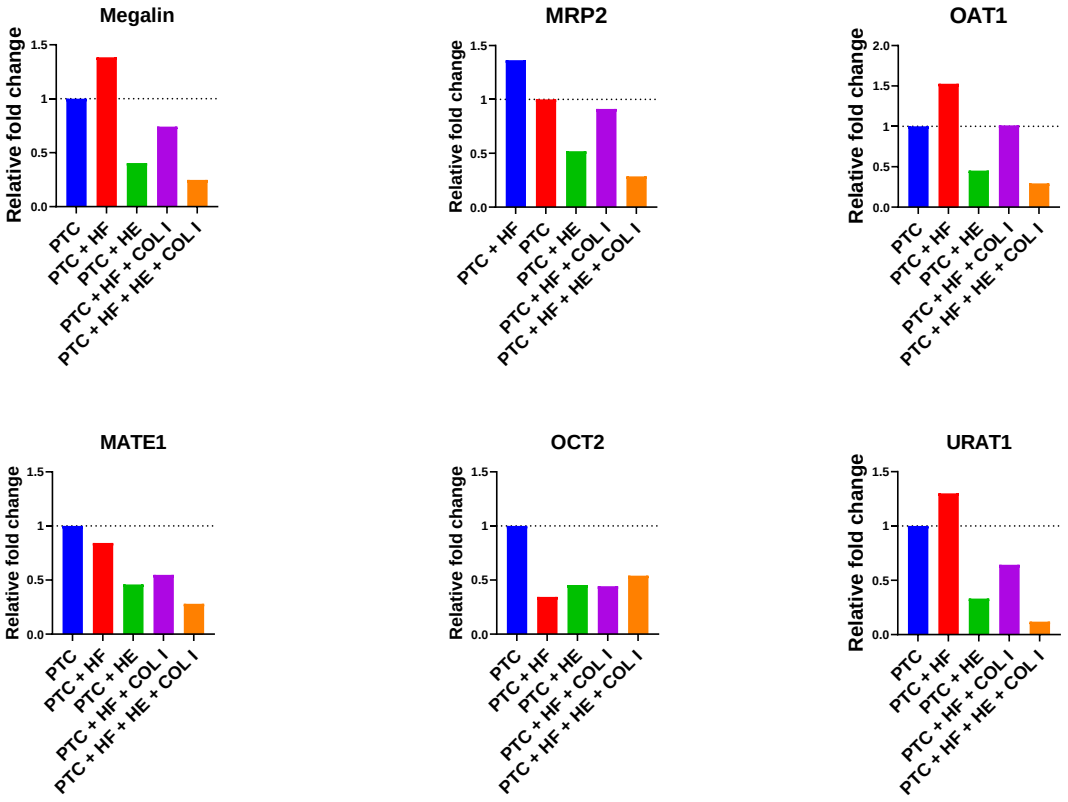

Figure 4.6. Effects of co-culture on relative fold change of gene expression of drug transporters Megalin, MRP2, OAT1, OCT2, URAT1, MATE1. Proximal tubule cells and fibroblasts in co-culture (PTC+HF) show Megalin, MRP2, OAT1, URAT1 upregulation as compared to PTC in mono-culture, while all other co-culture models show downregulation of all target genes.

4.2.3 Assembly of 3D co-culture models with hPTC and HRF in contact

Since contact co-culture of hPTC with HRF had led to upregulation of genes encoding for key transporters (**Figure 4.6**), the effects of contact co-culture of hPTC with HRF were assessed in greater detail by comparing hPTC in monoculture to the co-culture model (**Figure 4.7**). The phase-contrast image of hPTC in **Figure 4.8** displays the formation of an epithelial monolayer, whereas in the co-culture condition hPTC + HRF form complex 3D structures that no longer resemble an epithelial monolayer. When gene expression was assessed via RT-qPCR, upregulation from 10 to 1000- fold was detected in the hPTC + HRF contact co-culture model (**Figure 9**). These promising results lead to focusing the following experiments on contact co-culture 3D models and widening the characterization of models via functional assays to probe transporter function.

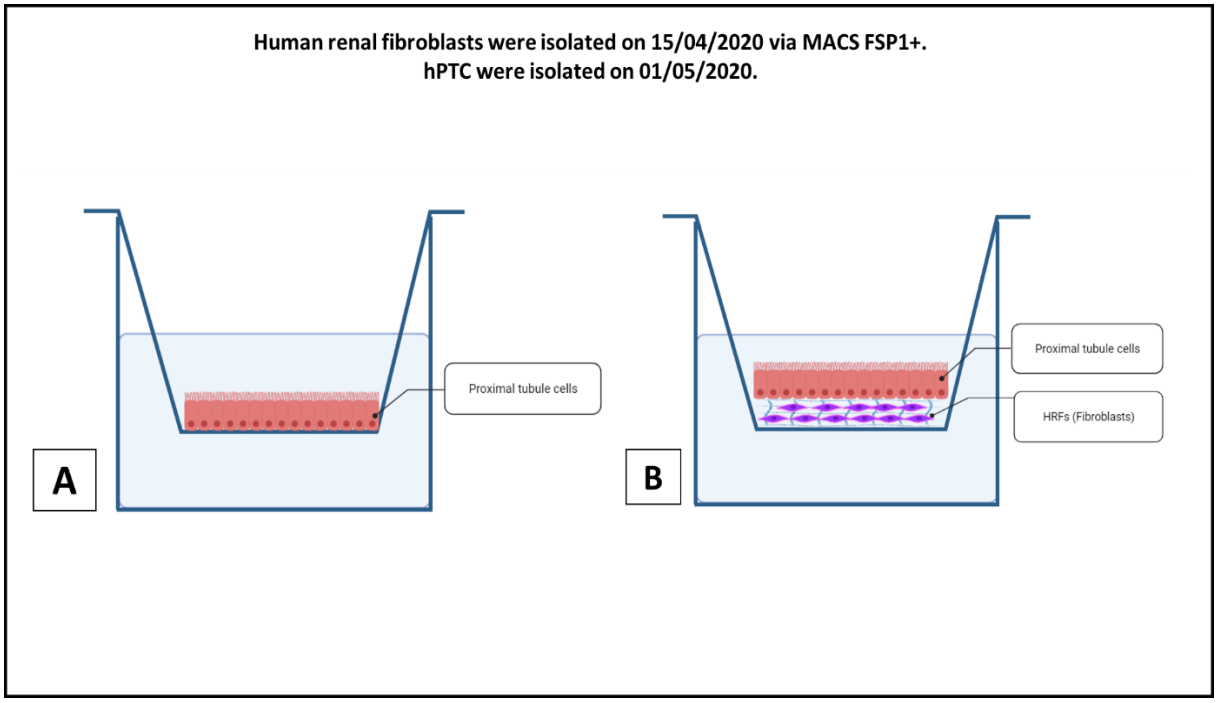

Figure 4.7. Graphical representation of 3D models cultured on Transwell® inserts [A] hPTC seeded on the apical side of the insert (Control) [B] HRF and hPTC in contact co-culture on the apical side of the insert.

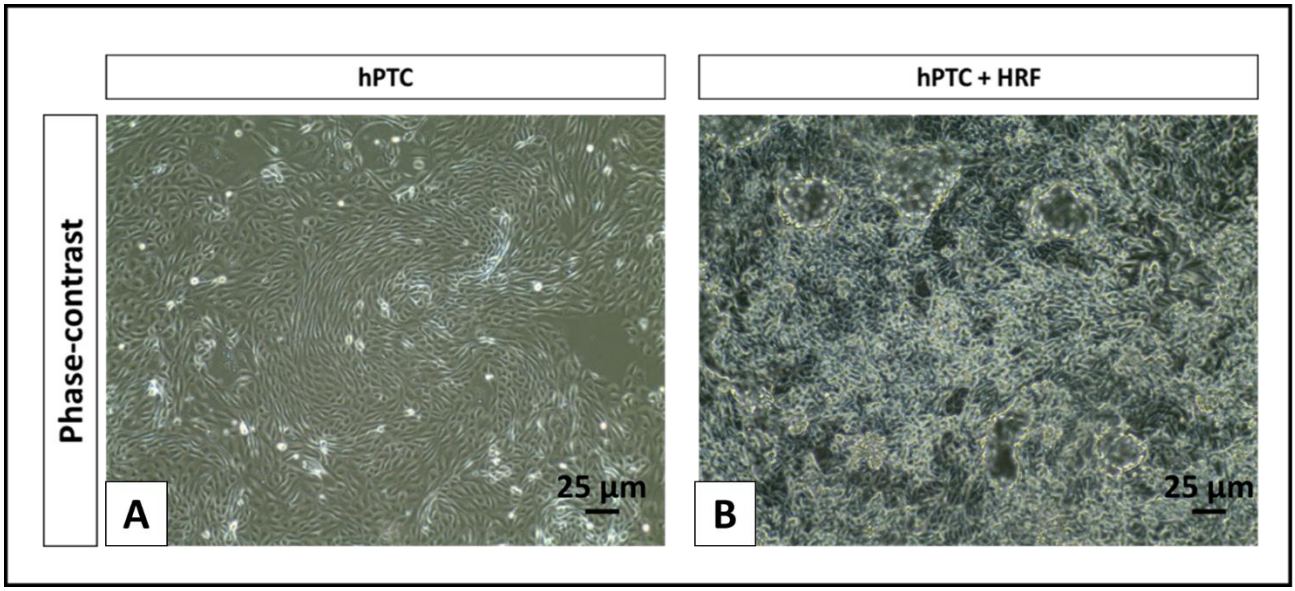

Figure 4.8. Phase-contrast images of primary proximal tubule cells (hPTC) [A] in monoculture showing characteristic cobblestone morphology and tight junction formation and [B] in contact co-culture with human renal fibroblasts (HRF) showing formation of nodes and multicellular structures (scale bars=25µm).

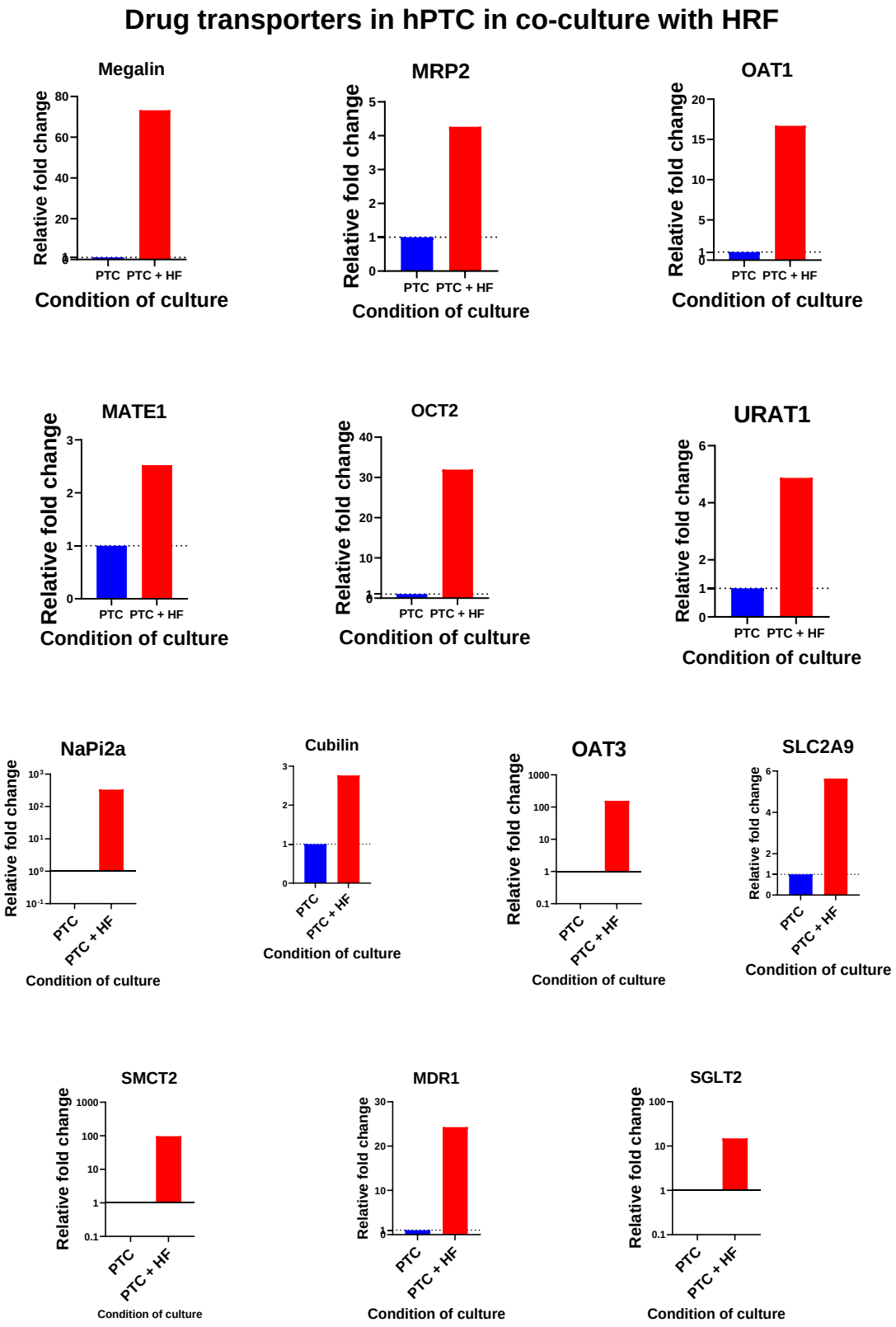

Figure 4.9. Effects of co-culture of proximal tubule cells (PTC) with fibroblasts (HF) on relative fold change mRNA expression of drug transporters megalin, MRP2, OAT1, OCT2, URAT1, MATE1, NaPi2a, cubilin, OAT3, SLC2A9, SMCT2, MDR1, SGLT2. The genes encoding for these key transporters are upregulated in the PTC+HF co-culture model as compared to PTC in

monoculture. mRNA was isolated from hPTC within 3D models cultured on Transwell® inserts from one biological replicate (n=1).

4.2.4 Assembly of 3D co-culture models with hPTC, HRF and HRPEC in contact

The aim of the experiments performed on the models represented in **Figure 4.10** was to assess whether contact co-culture with HRF and HRPEC had a beneficial impact on growth and function of proximal tubule cells. To assess epithelial barrier integrity, trans epithelial electrical resistance (TEER) was measured over culture time (**Figure 4.11**). These curves highlight that only the contact co-culture model comprising epithelial and endothelial cells (hPTC + HRPEC) reached the threshold TEER value of 60 $\Omega*cm^2$ which is linked to a functional, leak-tight epithelial/endothelial barrier, while HRF in co-culture with hPTC appears to disrupt the epithelial monolayer as the TEER value plummets below 50 $\Omega*cm^2$ for hPTC + HRF. In fact, at the mRNA level most transporters are upregulated, although not significantly, in the hPTC + HRF contact co-culture model (**Figure 4.12**). For this reason, we chose to perform functional quantification of creatine and p-aminohippurate flux using this model. The functional data displayed in **Figures 4.13 and 4.14** shows that flux of radiolabelled creatinine and para-aminohippuric acid (PAH) across this model is disrupted. Creatinine flux across the hPTCs monolayer (**Figure 4.13 [A] "PTC"**) is moving in the expected direction since the secretory flux (J_{B-A}) is greater than the absorptive flux (J_{A-B}), while across the hPTC + HRF contact co-culture model creatinine is moving in the opposite direction (J_{A-B} is greater than J_{B-A}). The same pattern can be recognized when comparing the flux of PAH across hPTC versus hPTC + HRF (**Figure 4.14**).

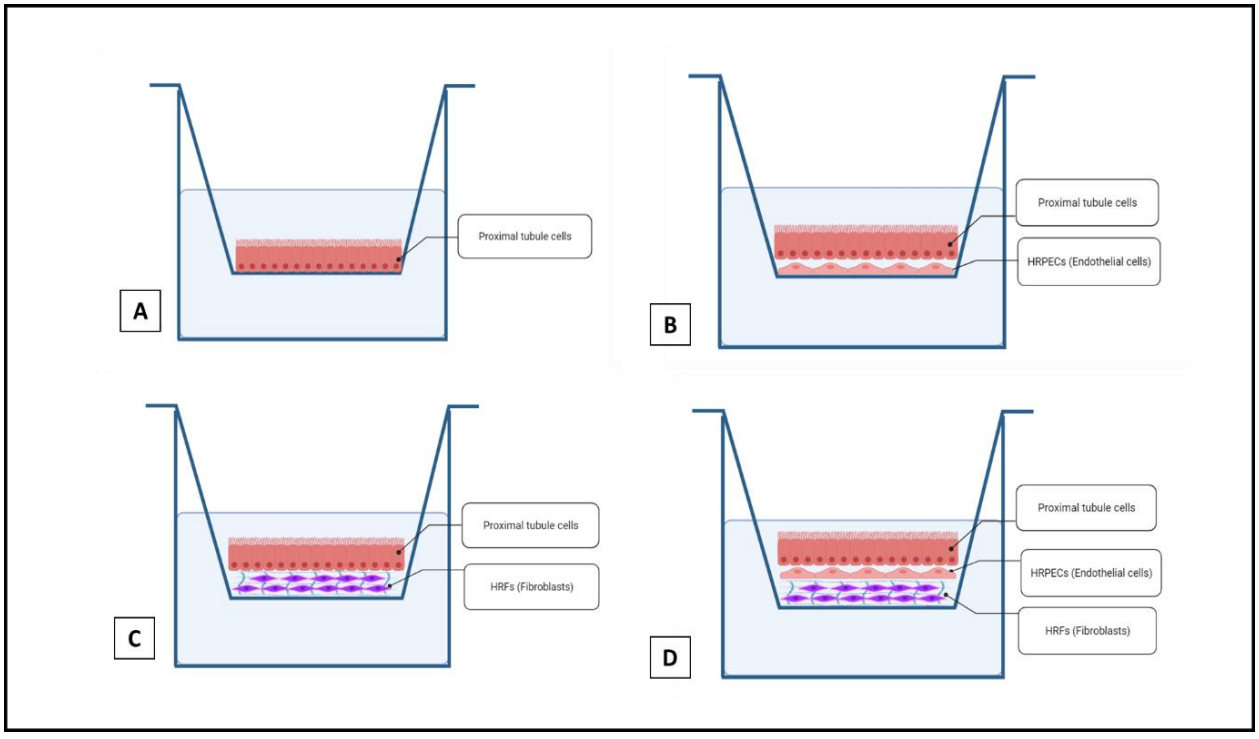

Figure 4.10. Graphical representation of 3D models cultured on Transwell inserts (A) hPTC seeded on the apical side of the insert (Control) (B) HRPEC and hPTC in contact co-culture on the apical side of the insert (C) HRF and hPTC in contact coculture on the apical side of the insert (D) HRF, HRPEC, hPTC in contact co-culture on the apical side of the insert.

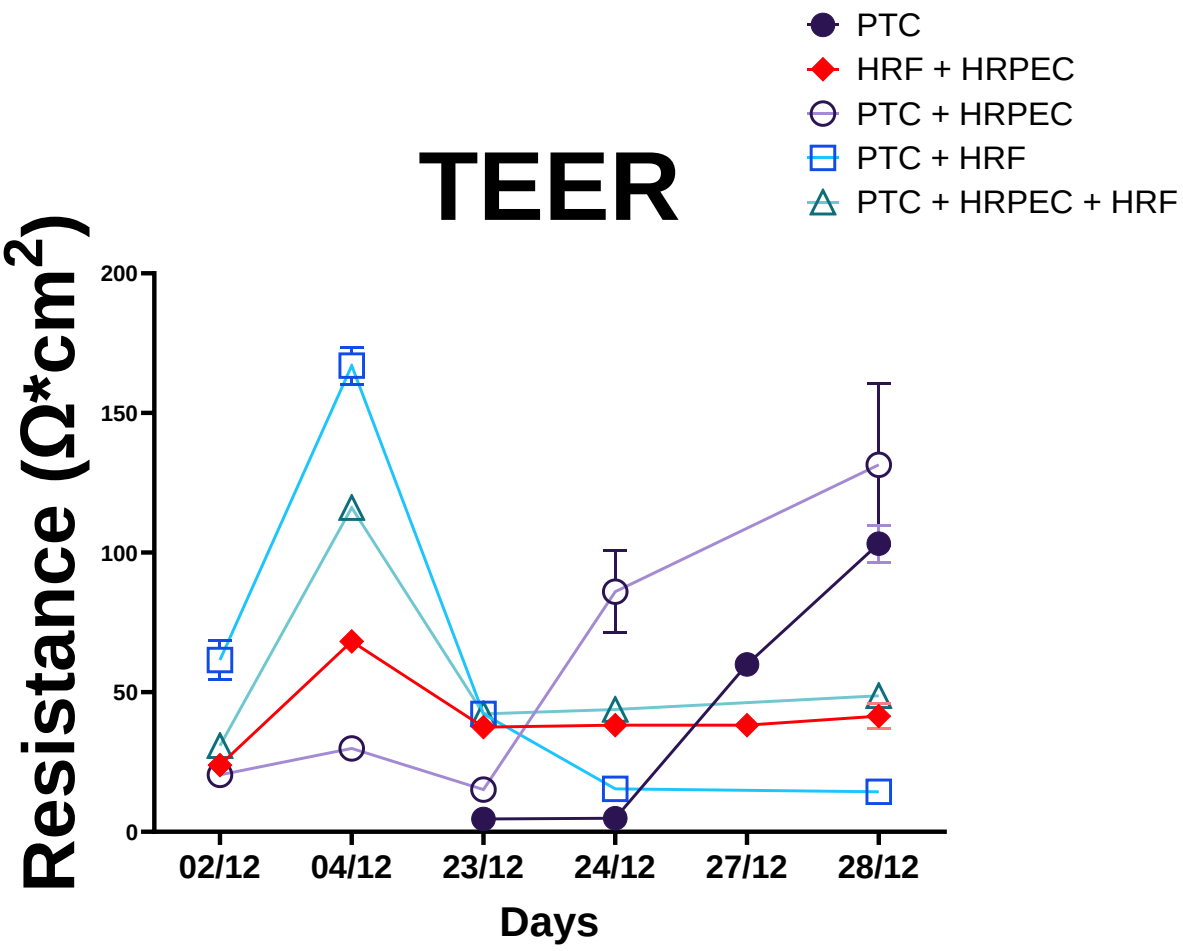

*Figure 4.11. TEER measurements of 3D co-culture models comprising of human renal fibroblasts (HRF), human renal peritubular endothelial cells (HRPEC), and proximal tubule cells (hPTC) compared to hPTC monolayers over time in culture. PTC in monoculture and PTC+HRPEC reach the TEER threshold of 60 Ω*cm², while HRF+HRPEC, PTC+HRF, PTC+HRPEC+HRF do not reach it.*

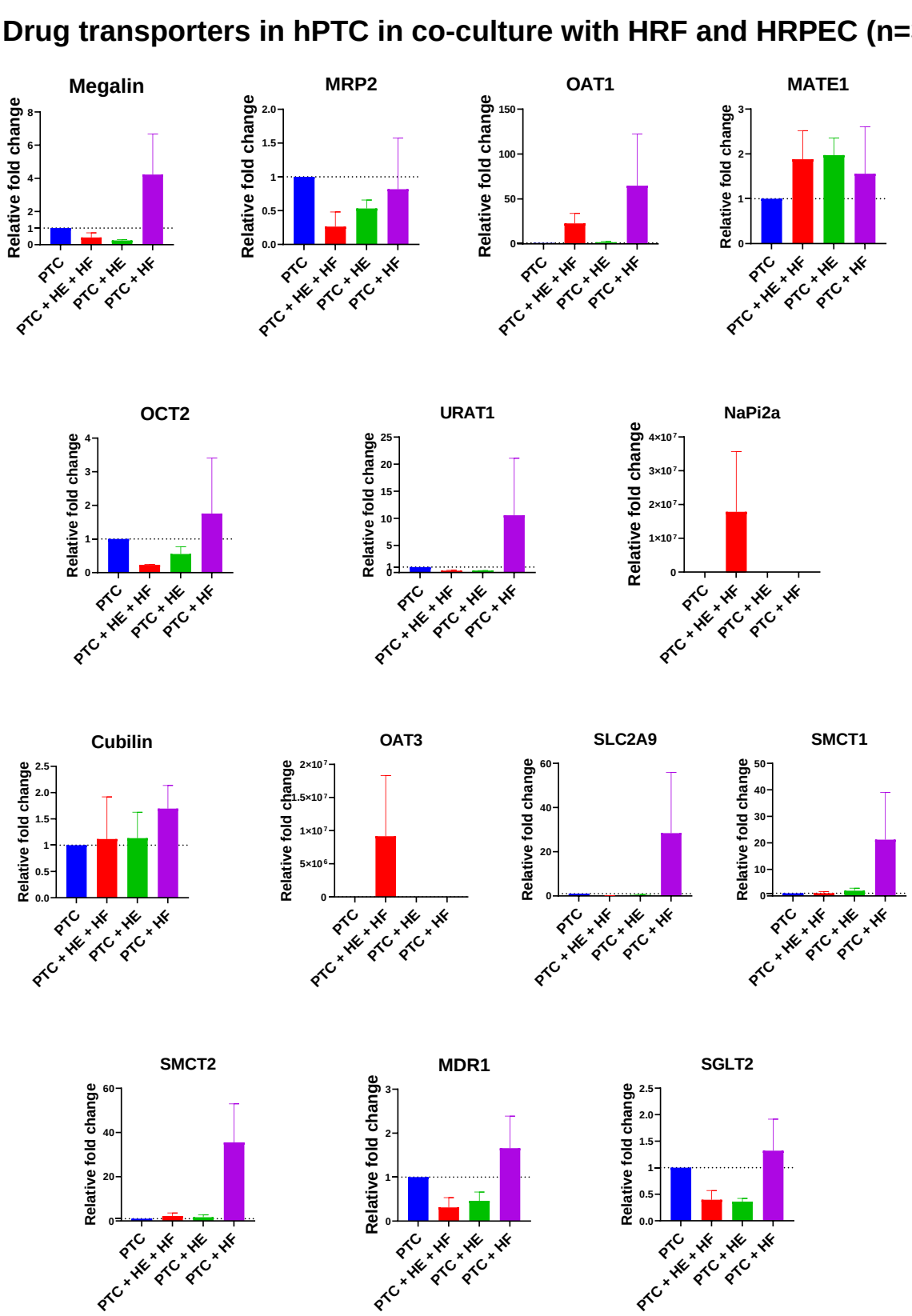

Figure 4.12. Effects of co-culture on relative fold change mRNA expression of drug transporters megalin, MRP2, OAT1, OCT2, URAT1, MATE1, NaPi2a, cubilin, OAT3, SLC2A9, SMCT2, MDR1, SGLT2. Relative to proximal tubule cells in monoculture (PTC), gene expression of megalin, OAT1, MATE1, OCT2, URAT1, cubilin, SLC2A9, SMCT1, SMCT2, MDR1, and SGLT2 is

upregulated in PTC in co-culture with fibroblasts (HF); OAT1, NaPi2a, cubilin, and OAT3 are upregulated in PTC in co-culture with fibroblasts and endothelial cells (PTC+HE+HF); MATE1 and cubilin are upregulated in PTC in co-culture with endothelial cells (PTC+HE). mRNA was isolated from hPTC within 3D models cultured on Transwell® inserts from three biological replicates (n=3).

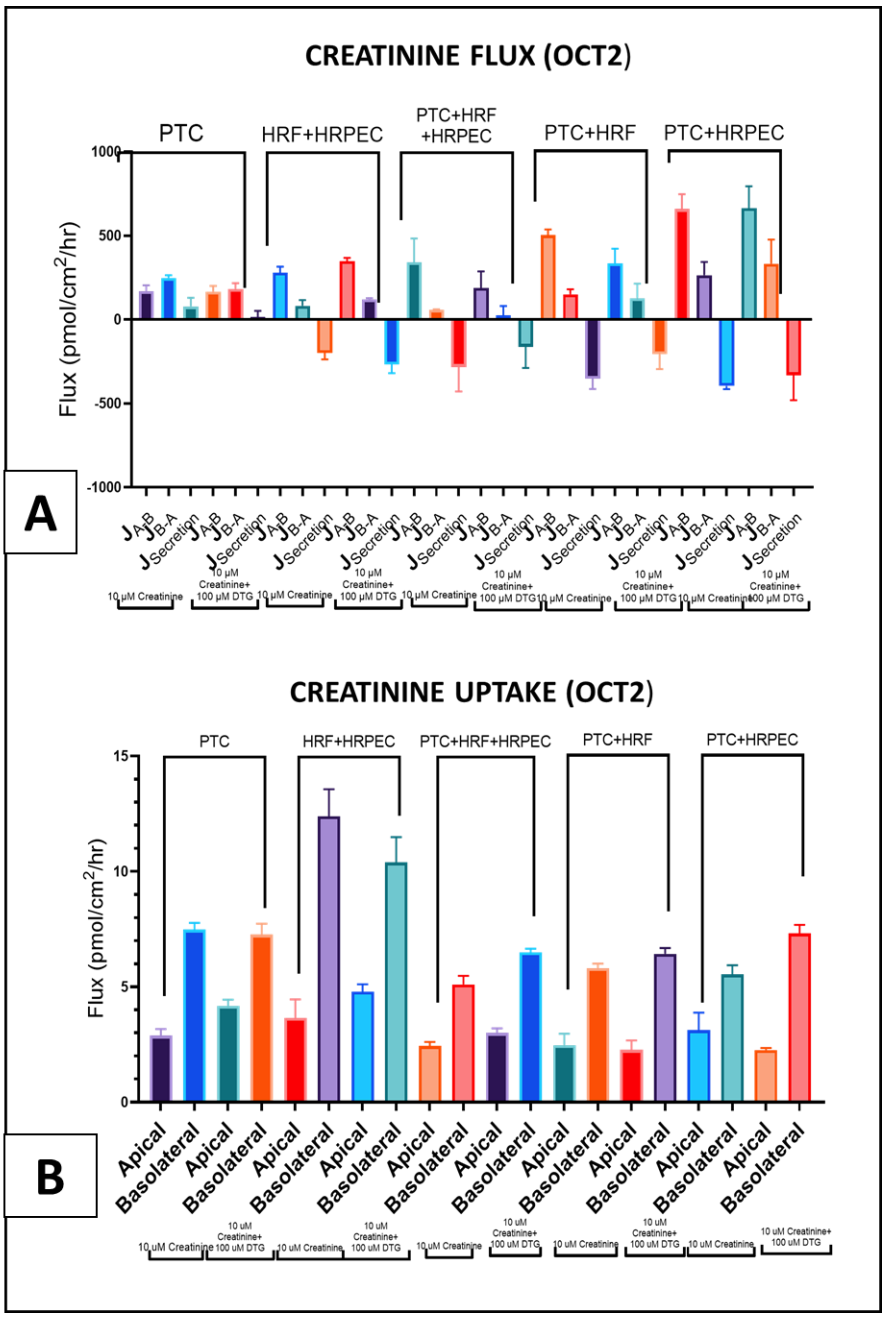

Figure 4.13. [A] Creatinine flux across 3D models compared to hPTC monolayers with and without OCT2 inhibitor (dolutegravir) after 60 minutes corrected for paracellular flux with mannitol (n=1). Only PTC in monoculture show creatinine flux typical of a renal epithelium where basolateral to apical transport is higher than apical to basolateral transport, as compared to the 3D co-cultures HRF+HRPEC, PTC+HRF+HRPEC, PTC+HRF, PTC+HRPEC which show dysregulated creatinine flux. [B] Creatinine uptake from 3D models compared to hPTC monolayers with or without OCT2 inhibitor after 60 minutes. As compared to PTC in

monoculture, HRF+HRPEC display higher creatinine uptake, while all other 3D constructs (PTC+HRF+HRPEC, PTC+HRF, PTC+HRPEC) display lower creatinine uptake. Experiment performed on one biological repeat (n=1), data is presented as mean ± SEM between three technical repeats per condition (n=1).

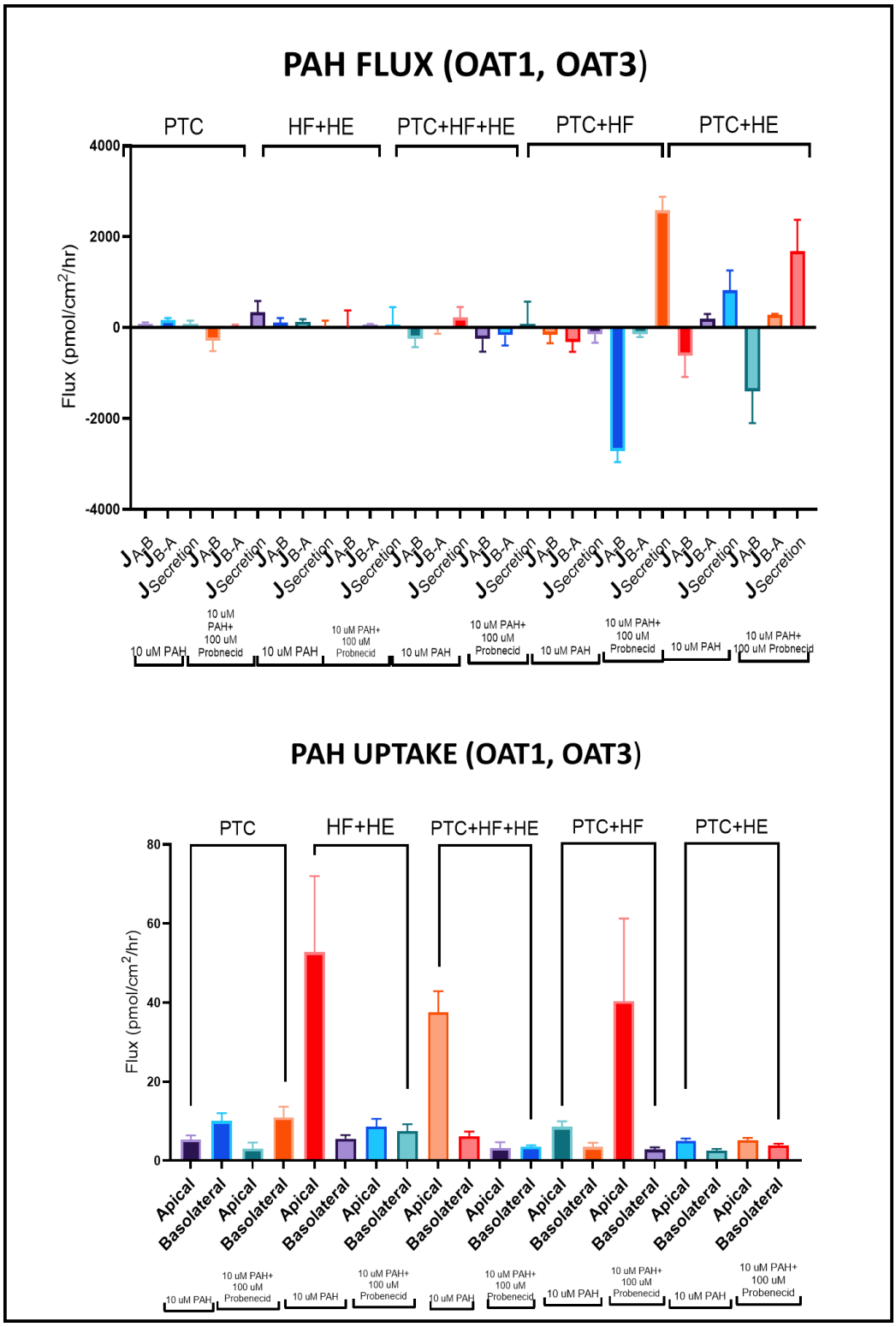

Figure 4.14. [A] PAH flux across 3D models compared to PTCs monolayers with and without OAT1, OAT3 inhibitor (probenecid) after 60 minutes corrected for paracellular flux with

mannitol (n=1). [B] Creatinine uptake from 3D models compared to PTCs monolayers with or without OAT1, OAT3 inhibitor after 60 minutes. Experiment performed on one biological repeat (n=1), data is presented as mean ± SEM between three technical repeats per condition (n=1).

4.2.5 Alternative 3D model format with hPTC on basolateral face of the Transwell® insert.

Spatially separated co-culture models where hPTC and the other two cellular components were isolated from two different donors (as previously described) were explored in an experiment involving the models represented in **Figure 4.15**, where epithelial cells are physically separated from other cell types by the insert's permeable membrane, which draws a parallel with the first co-culture experiment shown in this chapter (**Figure 4.1**). Since the results from the contact co-culture experiment had led to theorize that other cell types in culture with epithelial cells disrupt appropriate epithelial barrier function, the aim was to assess transporter function of the non-contact co-culture 3D models. TEER measurements over culture time represented in **Figure 4.16 [A]** show that all assessed models reached the 60 Ω*cm^2 TEER threshold value, therefore using a permeable membrane to spatially separate different cellular components allowed hPTC to exhibit optimal epithelial barrier function. Furthermore, hPTC + HRF demonstrated to reach a significantly higher TEER value as compared to hPTC in monoculture. CellTiter-Glo ATP assay was performed on the models to assess cell viability, showing significantly reduced cell viability of hPTC in culture with both other cell types (**Figure 4.16 [B]**). Regarding the functional characterization, this experiment also investigated whether HRF and HRPEC can transport creatinine and PAH. Both cell types show some degree of OCT2, OAT1, OAT3 function. Conversely, both hPTC + HRF and hPTC + HRPEC model do not show creatinine nor PAH flux in the correct direction (**Figures 4.17 and 4.18).**

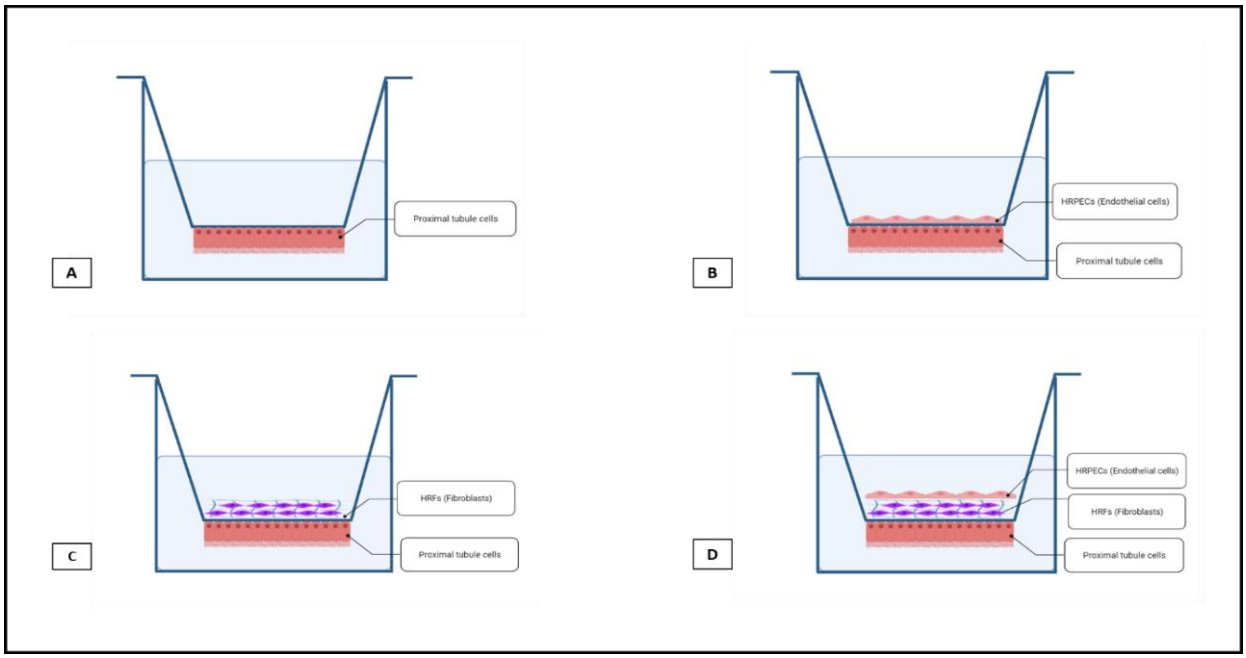

Figure 4.15. Graphical representation of 3D models cultured on Transwell® inserts [A] hPTCs seeded on the underside of the insert [Control] [B] HRPEC on the apical side, hPTC on the underside of the insert [C] HRF on the apical side, hPTC on the underside of the insert [D] HRPEC and HRF co-cultured on the apical side, hPTC on the underside of the insert.

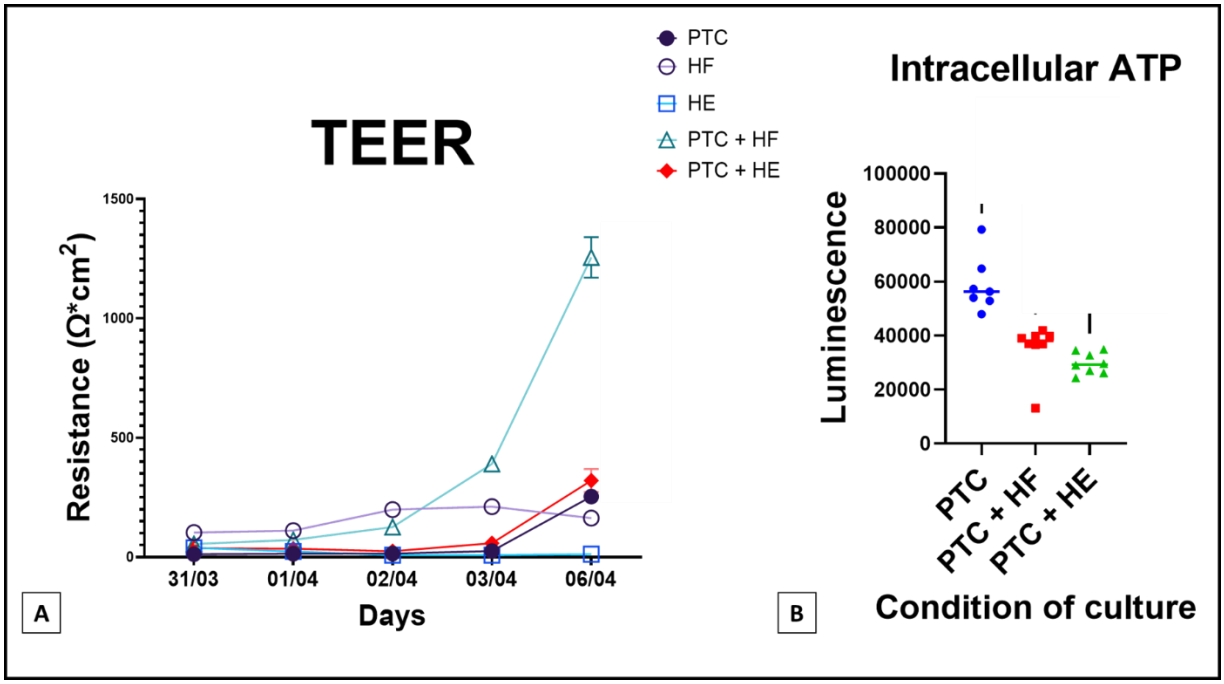

Figure 4.16. [A] TEER measurements of 3D models compared to hPTC monolayers over time in culture. When PTC are cultured on the basolateral side of the insert and fibroblasts on the apical side, TEER measured after 7 days of culture is higher than in PTC in monoculture. [B] Cell viability assay measuring intracellular ATP of hPTC in co-culture with HRF and HRPEC showing that PTC+HF and PTC+HE are leakier than PTC in monoculture.

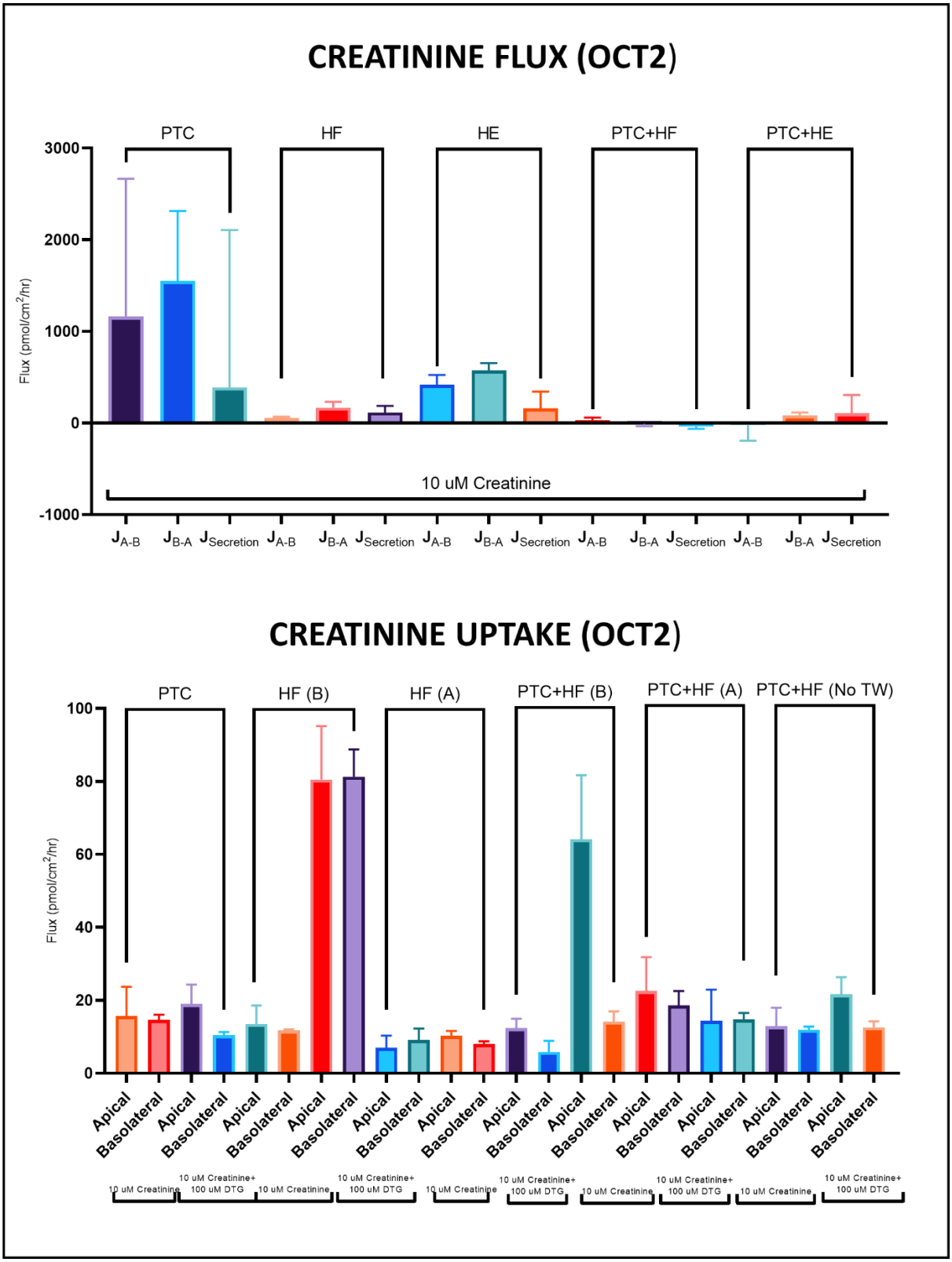

Figure 4.17. [A] Creatinine flux across 3D models compared to hPTC monolayers with and without OCT2 inhibitor (dolutegravir) after 60 minutes corrected for paracellular flux with mannitol (n=1). [B] Creatinine uptake from 3D models compared to PTCs monolayers with or without OCT2 inhibitor after 60 minutes. Experiment performed on one biological repeat (n=1), data is presented as mean ± SEM between three technical repeats per condition (n=1).

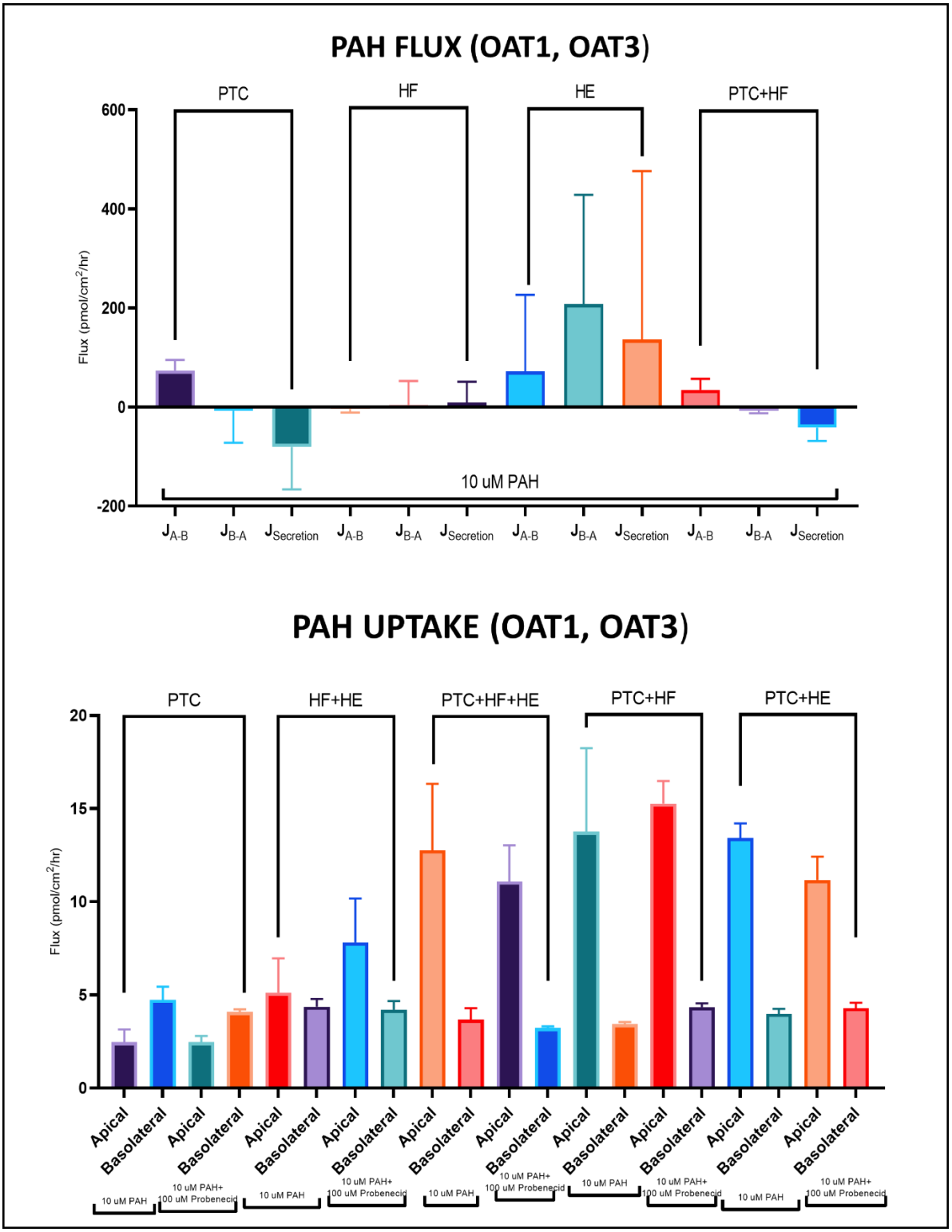

Figure 4.18. [A] PAH flux across 3D models compared to hPTC monolayers with and without OAT1, OAT3 inhibitor (probenecid) after 60 minutes corrected for paracellular flux with mannitol (n=1). [B] Creatinine uptake from 3D models compared to hPTC monolayers with or without OAT1, OAT3 inhibitor after 60 minutes (n=1). Data are presented as Mean ± SEM.

4.2.6 Preventing the ability of HRFs to disrupt epithelial integrity

Contact co-culture of proximal tubule cells with human renal fibroblasts had given the best results so far in terms of gene expression of key solute transporters, but 3D construct formation had proven to disrupt the epithelium making measuring a potential increase in transporter function unfeasible. Therefore, we decided to focus on exploring the relationship between fibroblasts and proximal tubule cells to build a model that could exploit the trophic support given by the fibroblasts to the epithelial cells without disrupting their barrier function. **Figure 4.20** represent all the hPTC/HRF co-culture combinations explored in a series of experiments. Model [B] was formed by hPTC and HRF in contact co-culture on the apical side of the insert [PTC + HF (A)], model (C) was formed by hPTC and HRFs not cultured in contact but seeded on opposite sides of the insert [PTC + HF (B)], and model (D) was generated by PTCs cultured on the apical side of the insert while HRF were cultured on the bottom of well [PTC + HF (No TW)]. TEER measurements in **Figure 4.21** demonstrate that model C [PTC + HF (B)] and D [PTC + HF (No TW)], where epithelial cells are not in direct physical contact with fibroblasts, reach the threshold TEER value of 60 $\Omega*cm^2$, hence these two models allow for epithelial barrier formation. Conversely, model B [PTC + HF (A)] does not reach said value. Gene expression of key transporters is upregulated mainly for the contact co-culture model B [PTC + HF (A)], while megalin, cubilin, and OAT1 are slightly upregulated for model C [PTC + HF (B)] (**Figure 4.22**). When transporter function of the three different models is characterized, model C [PTC + HF (B)] shows greater net secretion of creatinine from the basolateral to the apical side of the insert as compared to the hPTC monolayer (**Figure 4.23**).

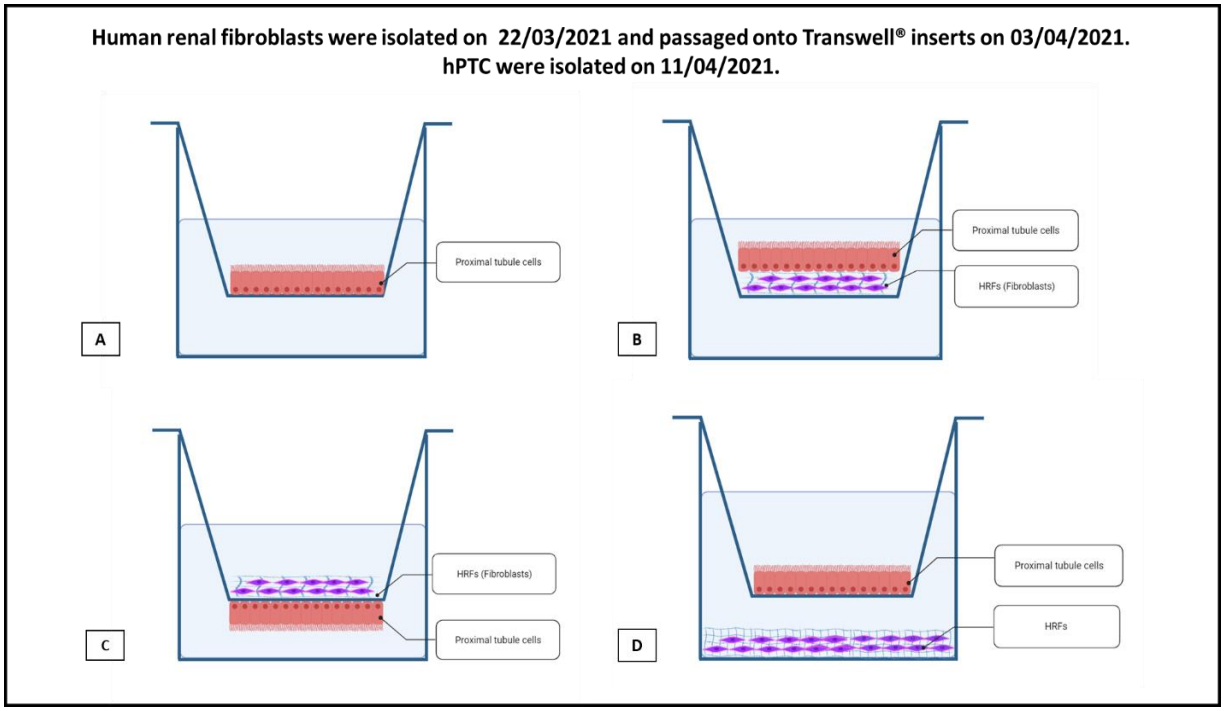

Figure 4.19. Graphical representation of 3D models cultured on Transwell® inserts [A] hPTC seeded on the apical side of the insert (Control) [B] HRF and hPTC in contact co-culture on the apical side of the insert [C] HRF on the apical side, hPTC on the underside of the insert [D] hPTC on the apical side of the insert, HRF on the bottom of the well.

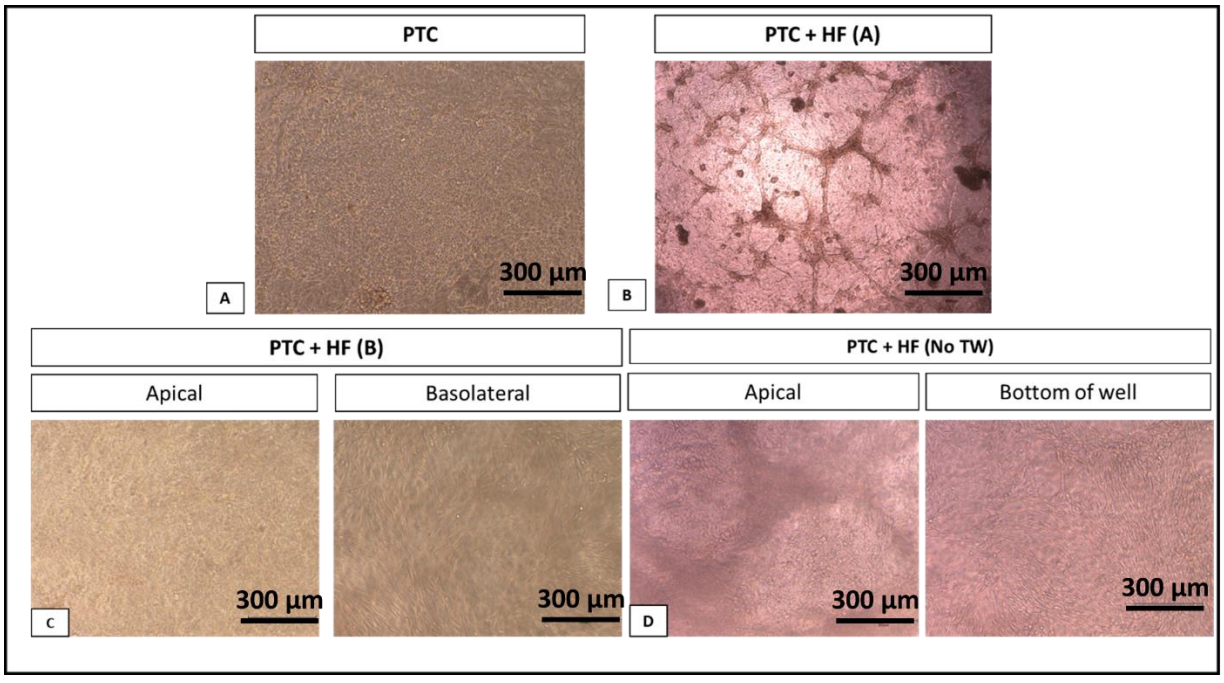

Figure 4.20. Phase-contrast images of monolayers and 3D models [A] hPTC on the apical side of the insert showing characteristic epithelial morphology [B] hPTC and HRF in contact co-culture on the apical side of the insert showing 3D structure formation [C] hPTC on the apical side of the inserts, HRF on the underside [D] hPTC on the apical side on the insert, HRF on the bottom of the well (scale bars=300µm).

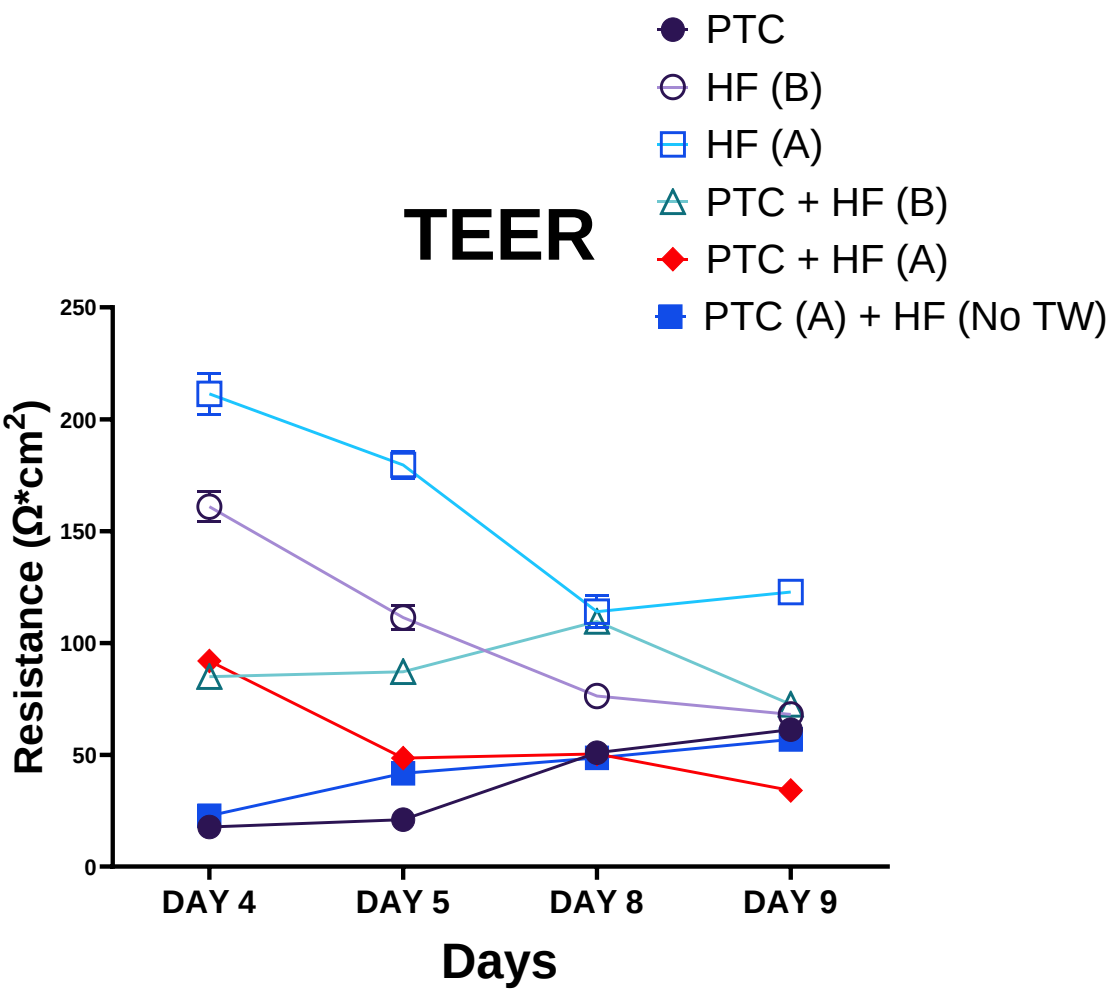

*Figure 4.21. TEER measurements of 3D models compared to hPTC monolayers over time in culture. PTC in monoculture are compared to fibroblasts in monoculture on the basolateral side of the insert (HF B), on the apical side of the insert (HF A), and to fibroblasts in co-culture PTC+HF(B) and PTC+HF(A), and fibroblasts in non-contact co-culture with PTC (PTC A + HF No TW). All the 3D models, apart from PTC + HF (A) in contact co-culture, reach threshold TEER of 60 Ω*cm^2.*

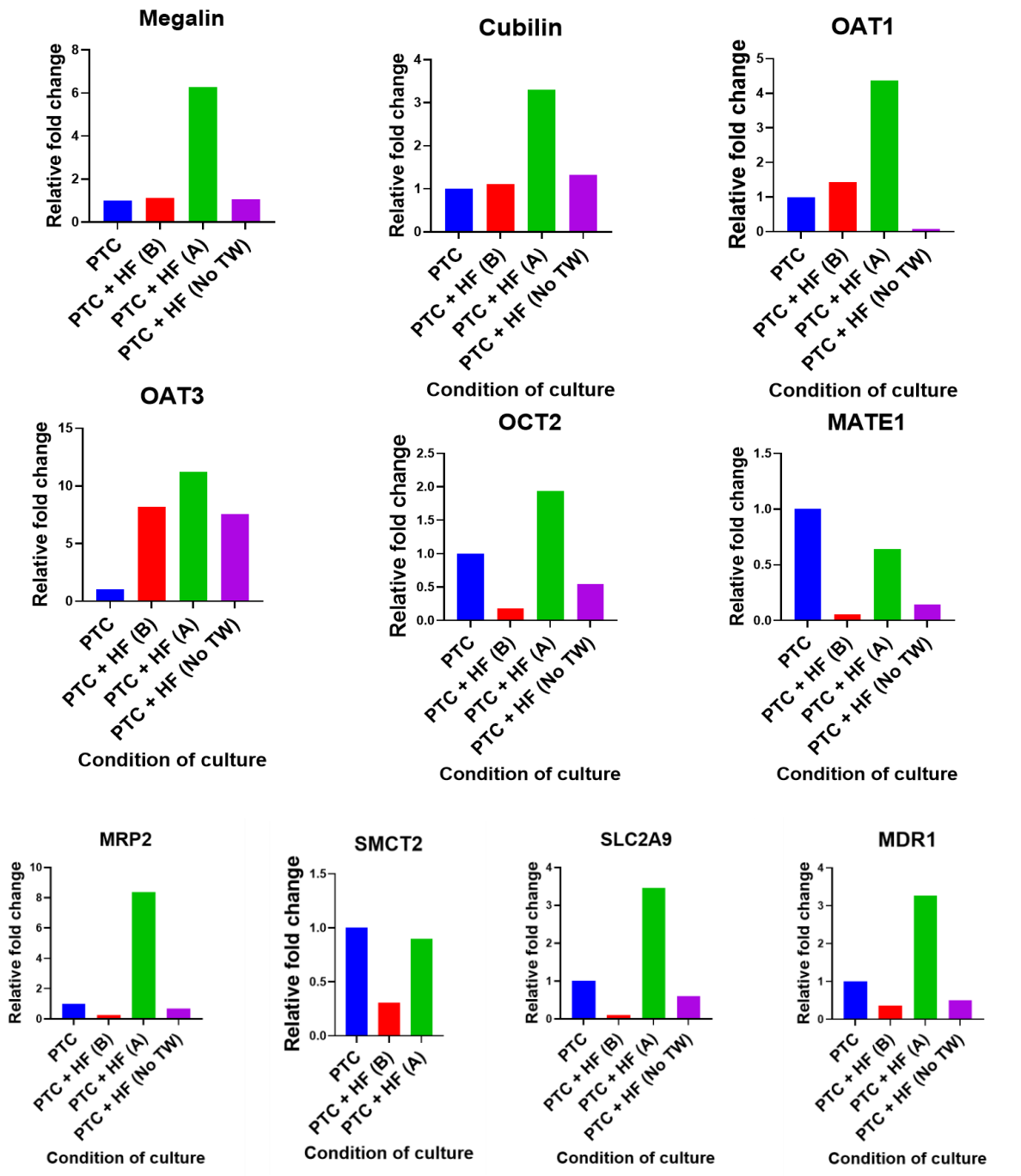

Figure 4.22. Effects of co-culture on relative fold change of gene expression of drug transporters Megalin, Cubilin, OAT1, OAT3, OCT2, MATE1, MRP2, SMCT2, SLC2A9, MDR1 (n=1) highlighting upregulation of gene expression in proximal tubule cells in co-culture with PTC [PTC + HF (A)] as compared to PTC in monoculture.

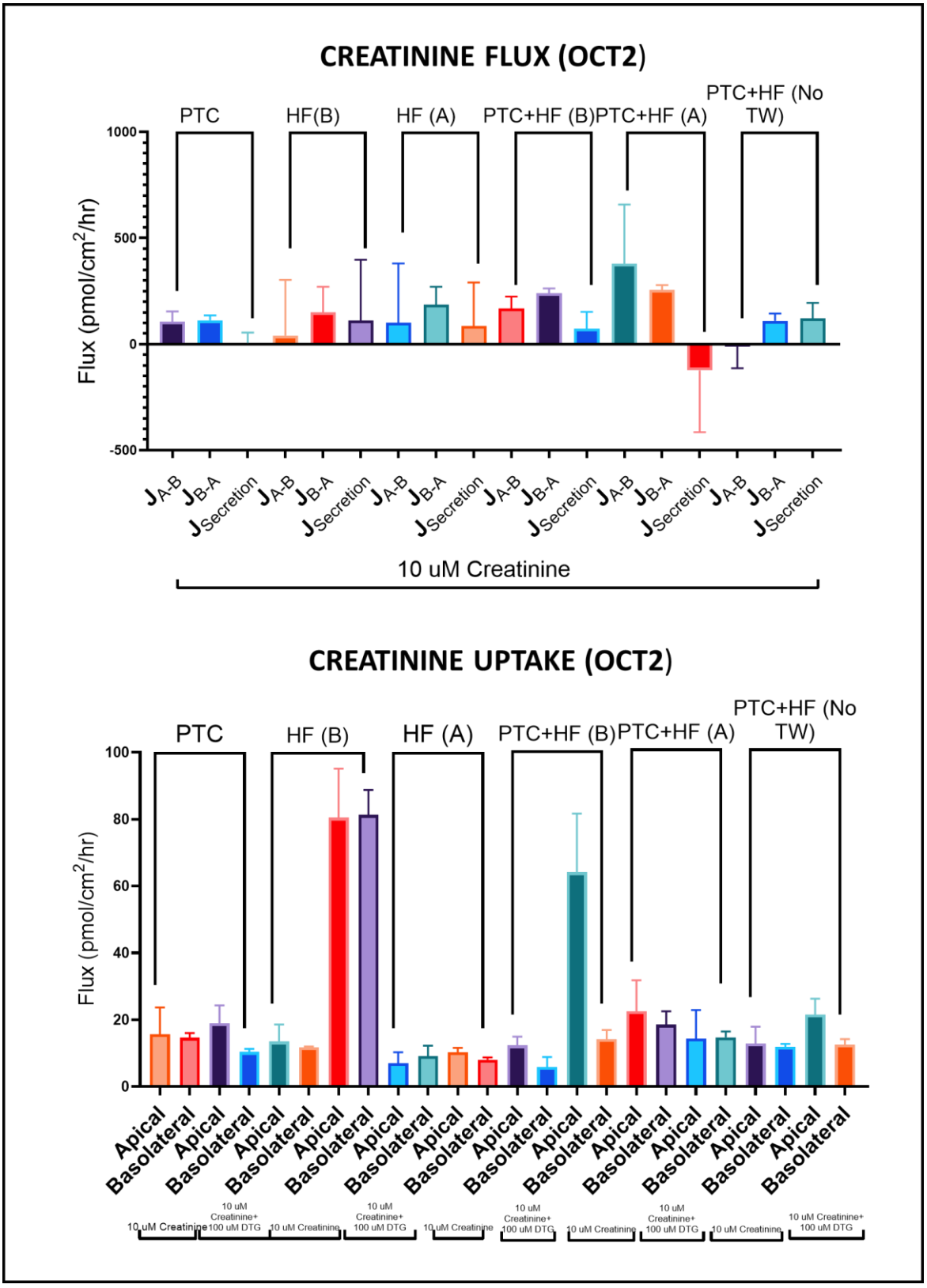

Figure 4.23. [A] Creatinine flux across 3D models compared to hPTC monolayers with and without OCT2 inhibitor (dolutegravir) after 60 minutes corrected for paracellular flux with mannitol. Proximal tubule cells in co-culture with fibroblasts cultured on the basolateral side of the insert [PTC + HF (B)] show greater secretion than PTC in monoculture. [B] Creatinine uptake from 3D models compared to PTCs monolayers with or without OCT2 inhibitor after 60

minutes. Experiment performed on one biological repeat (n=1), data is presented as mean ± SEM between three technical repeats per condition (n=1).

4.2.7 Halting HRF migration into the epithelial monolayer: irradiation, mitomycin C treatment, and gel embedment in contact co-culture.

Now that the relationship between hPTC and HRF has been explored, the experiments shown below will focus on maintaining the trophic support that HRF exert on hPTC while preventing them from disrupting the epithelial barrier. Three ways of cease fibroblast migration have been tested: irradiation, mitomycin C treatment, and gel embedment.

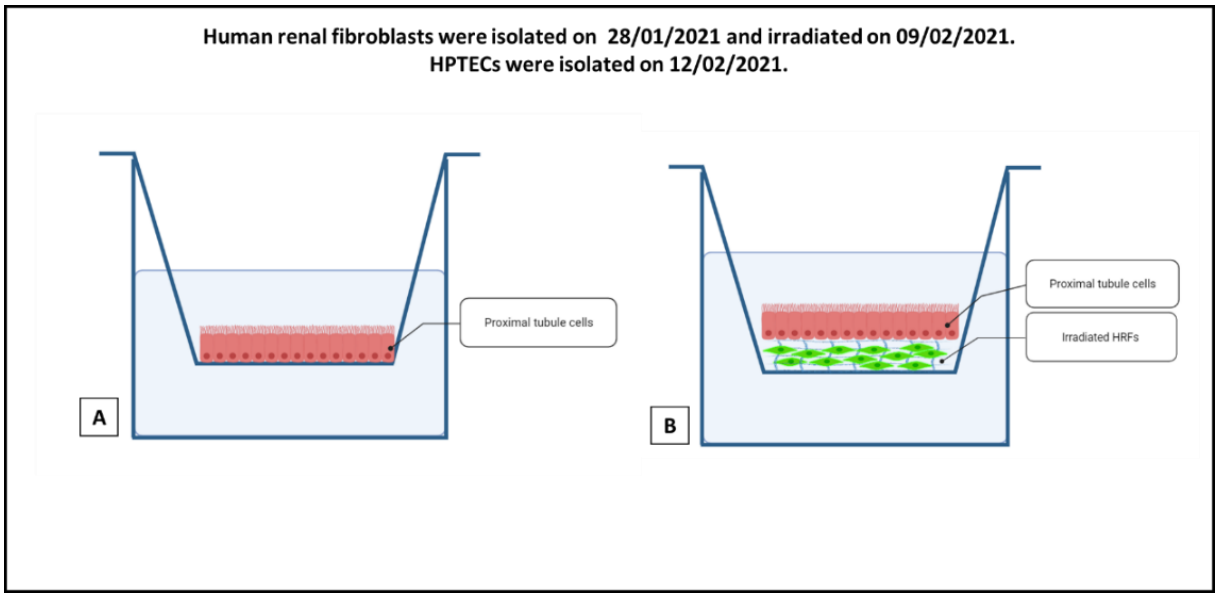

Figure 4.24. Graphical representation of 3D models cultured on Transwell® inserts [A] hPTC seeded on the apical side of the insert (control) [B] Irradiated HRF and hPTC in contact co-culture on the apical side of the insert.

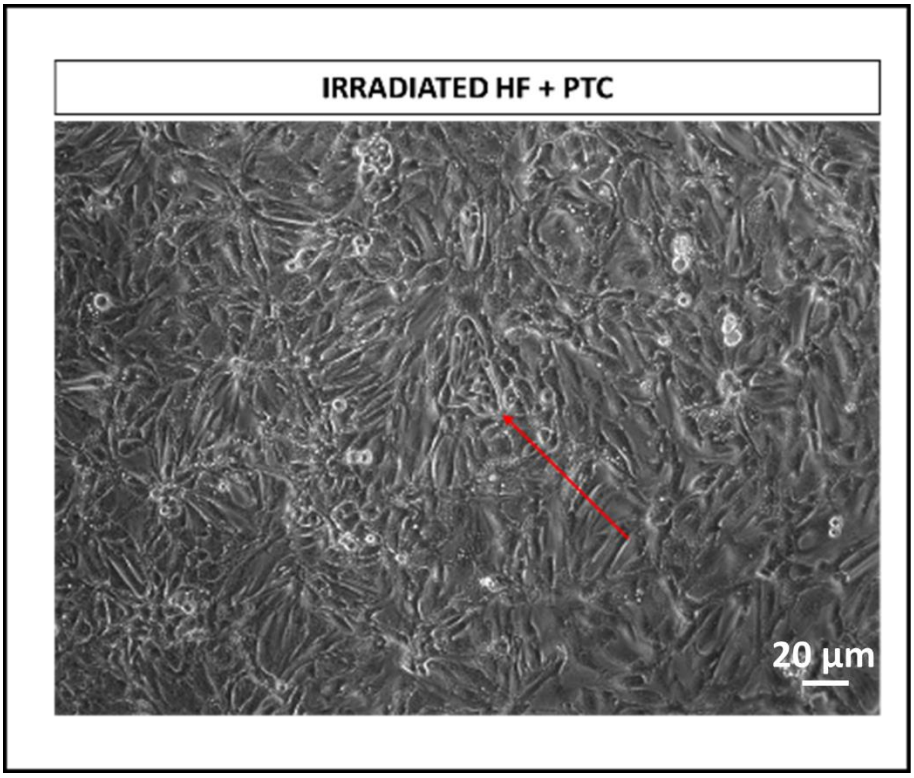

Figure 4.25. Phase-contrast image of epithelial cells colony on confluent irradiated HRF (scale bar=20µm).

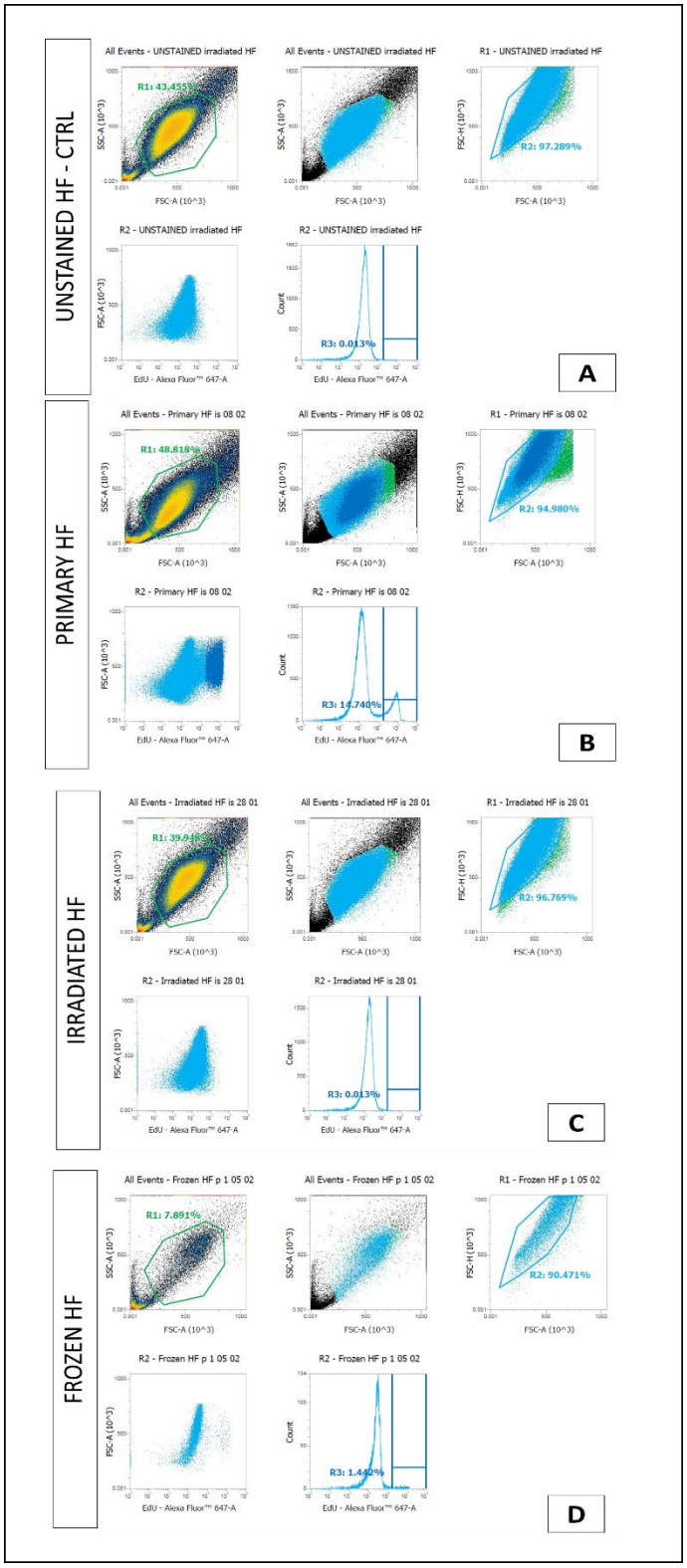

Figure 4.26. Flow cytometry histograms and dot plots representing the percentages of proliferating cells after irradiation and freeze/thaw cycle via Click-iT® Plus EdU Alexa Fluor® 647 cell proliferation assay [A] unstained cells show 0.013% positivity to EdU Alexa Fluor® 647, [B] primary fibroblasts show 14.74% positivity [C] irradiated fibroblasts show 0.013% positivity [D] frozen/thawed fibroblasts show 1.442% positivity to the proliferation marker.

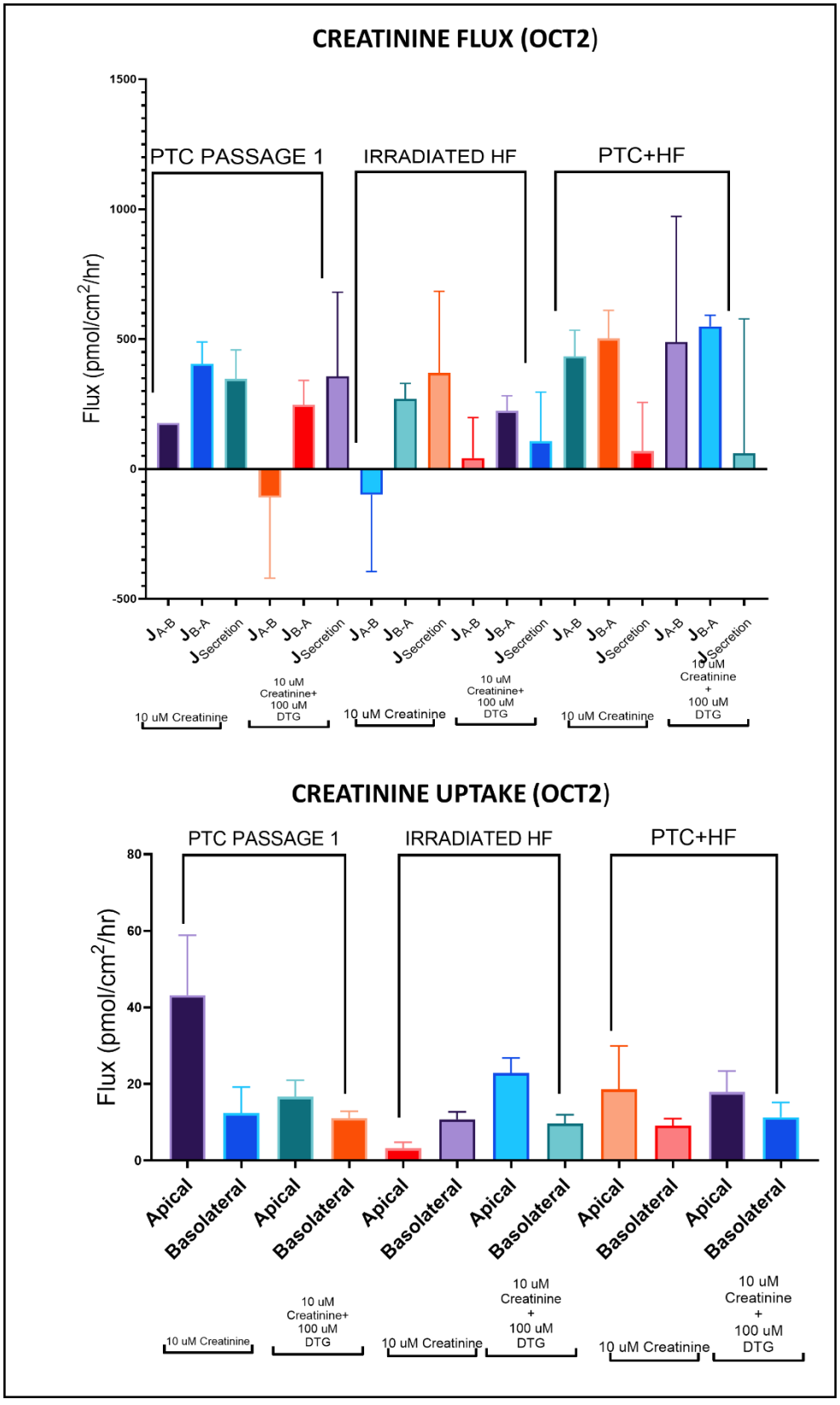

Figure 4.27. [A] Creatinine flux across 3D models compared to hPTC monolayers with and without OCT2 inhibitor (dolutegravir) after 60 minutes corrected for paracellular flux with mannitol. Only PTC in monoculture display characteristic direction of creatinine flux as compared to 3D constructs and irradiated fibroblasts [B] Creatinine uptake from 3D models compared to hPTC monolayers with or without OCT2 inhibitor after 60 minutes. Experiment

performed on one biological repeat (n=1), data is presented as mean ± SEM between three technical repeats per condition (n=1).

Human renal fibroblasts were irradiated to cease cell proliferation and migration so that these cells could be used as "feeder layer" for the epithelial cells cultured in direct contact with them (**Figure 4.24**). It is important to highlight that irradiation induces senescence, which could mimic a maladaptive state which is undesirable in a healthy model of epithelium. Proximal tubule cells colonies successfully formed on top of irradiated HRF (**Figure 4.25**). The irradiation method optimized among Prof. Armstrong's research group proved to be successful for this cell type as no treated cells are positive for the Click-iT® Plus EdU Alexa Fluor® 647 cell proliferation assay (**Figure 4.26**)**.** Furthermore, hPTC seeded onto irradiated HRF not only seemed to retain correct creatinine handling across the model but also to secrete creatinine greatly as compared to hPTC only **(Figure 4.27).**

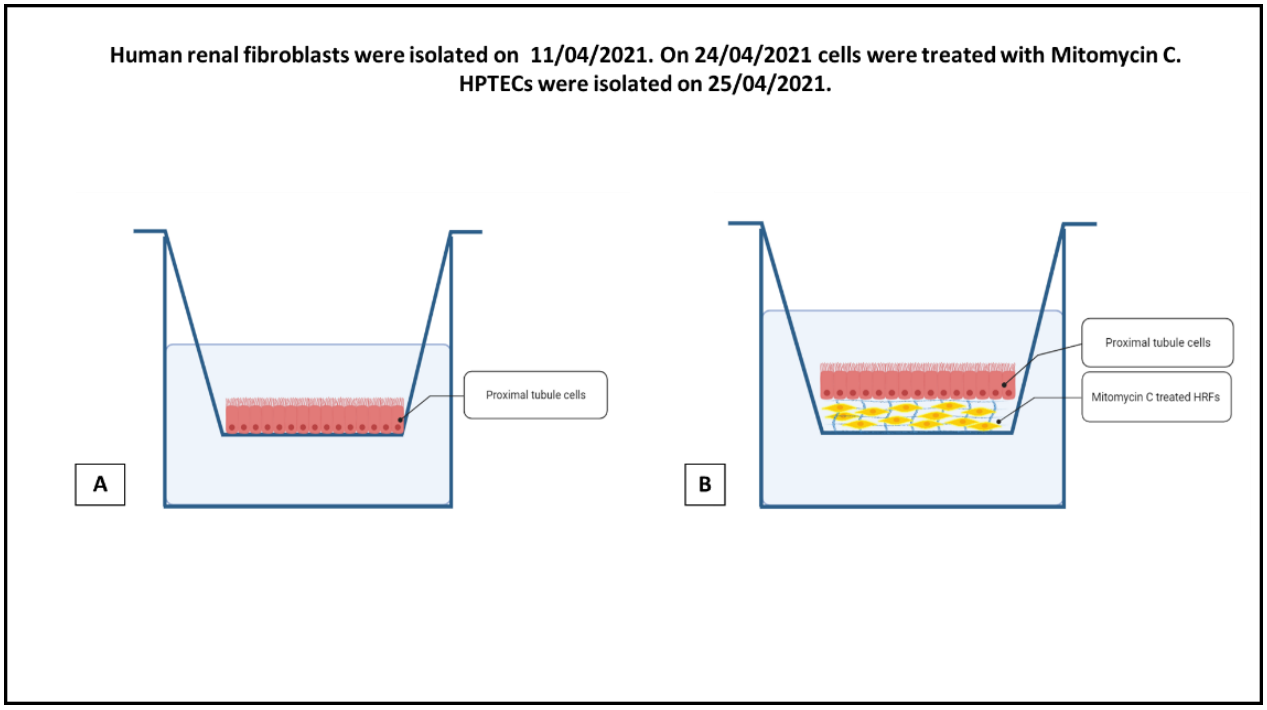

Figure 4.28. Graphical representation of 3D models cultured on Transwell® inserts [A] hPTC seeded on the apical side of the insert (Control) [B] Mitomycin C treated HRF and hPTC in contact co-culture on the apical side of the insert.

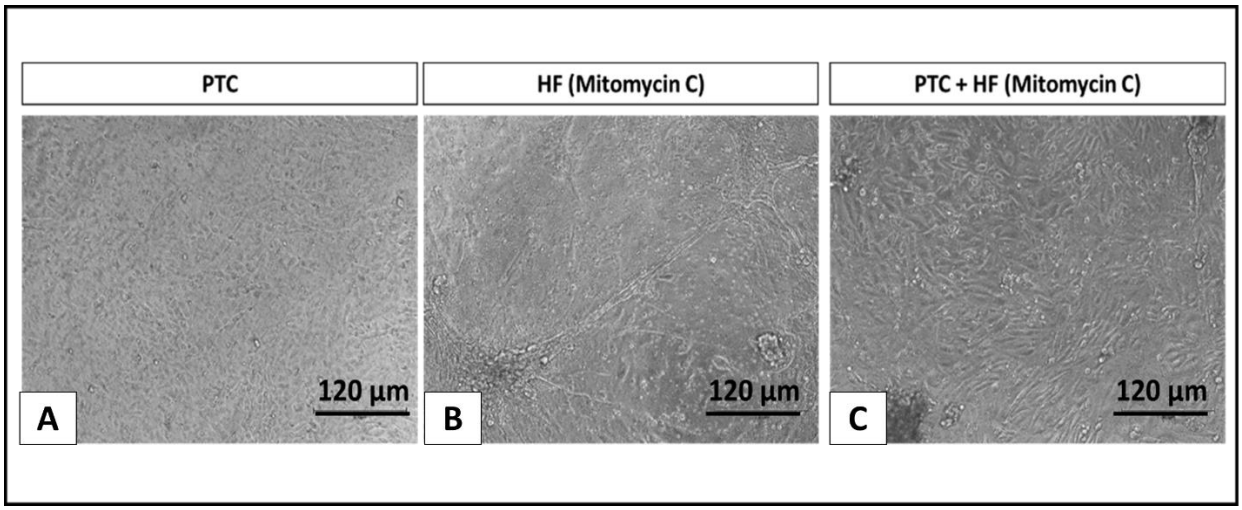

Figure 4.29. Phase-contrast images of monolayers and 3D models [A] hPTC on the apical side of the insert [B] Mitomycin C treated HRF on the apical side of the insert [C] hPTC and Mitomycin C treated HRF on the apical side of the insert (scale bars=120µm).

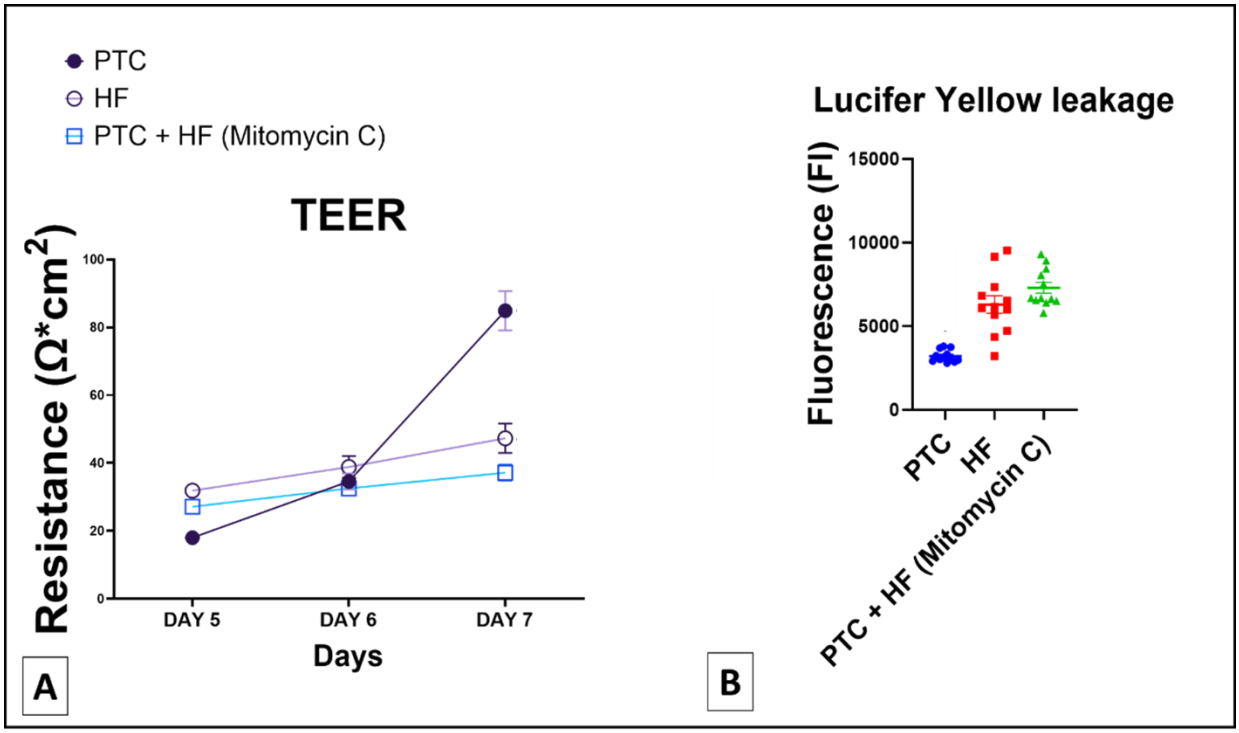

*Figure 4.30. [A] TEER measurements of 3D models compared to hPTC monolayers over time in culture showing that fibroblasts (HF) nor PTC in co-culture with senescent fibroblasts reach threshold TEER of 60 Ω*cm^2 [B] Lucifer Yellow leakage from apical to basolateral compartment across hPTC (Control) and 3D models shows that fibroblasts and PTC in co-culture with senescent fibroblasts form significantly leakier models than PTC in monoculture.*

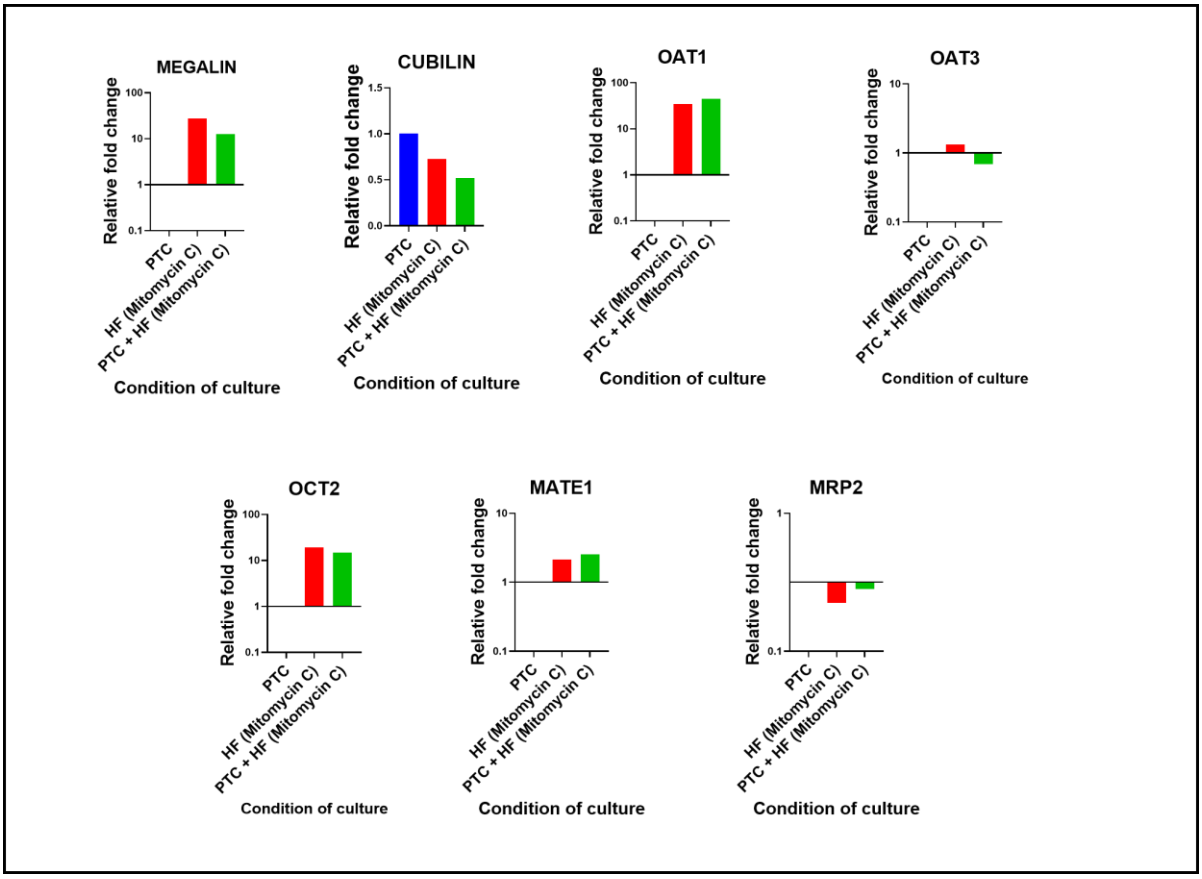

Figure 4.31. Effects of co-culture on relative fold change of gene expression of drug transporters megalin, cubilin, OAT1, OAT3, OCT2, MATE1, MRP2. Gene expression for megalin, OAT1, OCT2, MATE1 is upregulated in senescent fibroblasts and in proximal tubule cells in co-culture with senescent fibroblasts [PTC + HF (Mitomycin C)] as compared to proximal tubule cells in monoculture.

Human renal fibroblasts were treated with the potent DNA crosslinker mitomycin C, a chemotherapeutic agent, that is known to halt cellular proliferation (Cheng et al., 2016). Concentrations and duration of treatment to ensure complete ceasing of cell proliferation were optimized among Newcells Biotech's laboratories. Proximal tubule cells were cultured on top of the "feeder layer". **Figure 4.29** shows that hPTC in direct contact with treated HRF did not form a consistent epithelial monolayer. TEER values **(Figure 4.30 [A])** for this model and lucifer yellow leakage after 1 hour of incubation **(Figure 4.30 [B])** confirm lack of epithelial barrier function. Data on gene expression of key transporter show that upregulation of megalin, cubilin, OAT1, OCT2, and MATE1 is maintained, hence mitomycin C treated HRF provide trophic support to epithelial cells but they do not allow tight cell-cell junction to form.

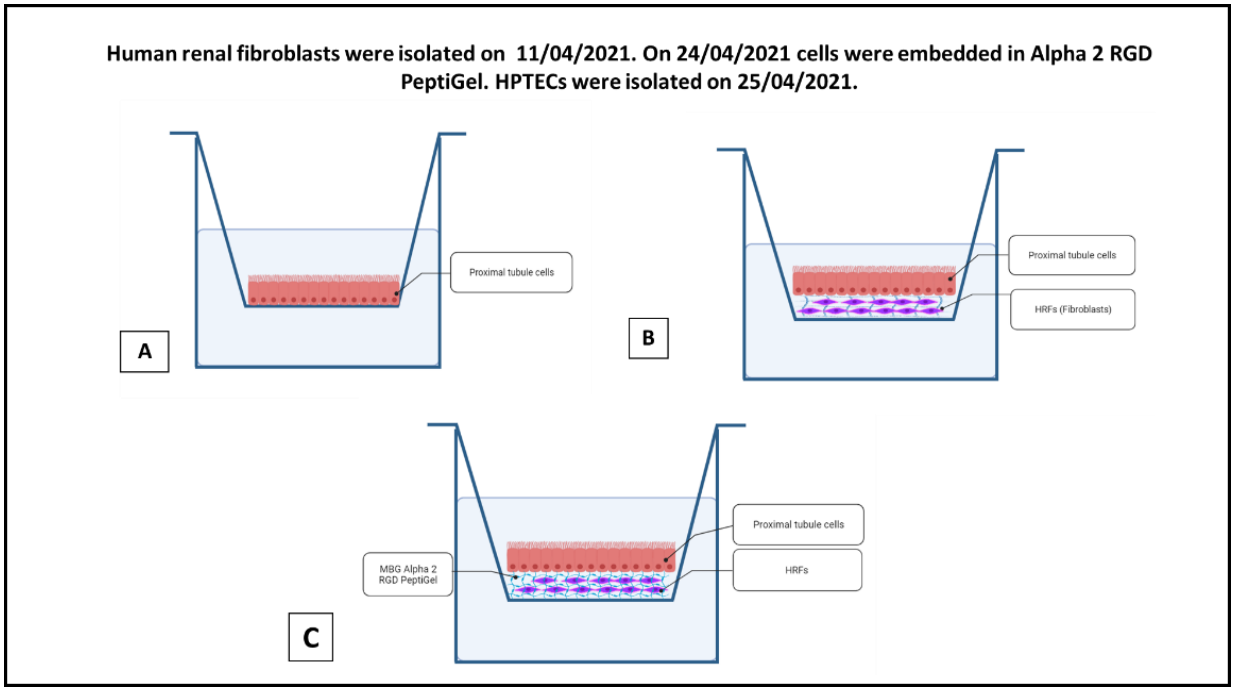

Figure 4.32. Graphical representation of 3D models cultured on Transwell® inserts [A] hPTC seeded on the apical side of the insert (Control) [B] HRF and hPTC co-cultured on the apical side of the insert [C] HRF are embedded in Alpha 2 RGD PeptiGel® and hPTC are cultured on top of the gel on the apical side of the insert.

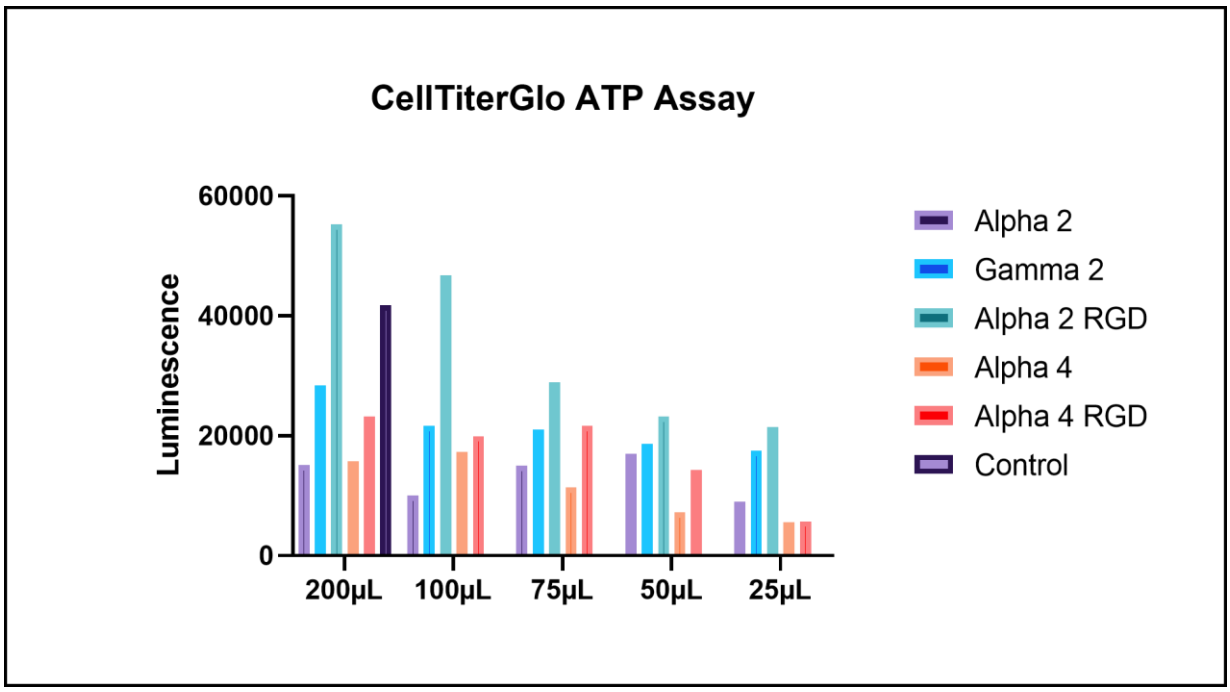

Figure 4.33. CellTiter-Glo® Intracellular ATP assay was performed on HRF embedded in a range of volumes of different types of PeptiGels® produced by Manchester BIOGELS to compare cell viability and choose the most suitable hydrogel. PeptiGel Alpha 2 RGD induces the highest increase in intracellular ATP as compared to control fibroblasts not embedded in gel. Experiment performed on one biological replicate. Experiment and data analysis performed by Donovan O'Brien.

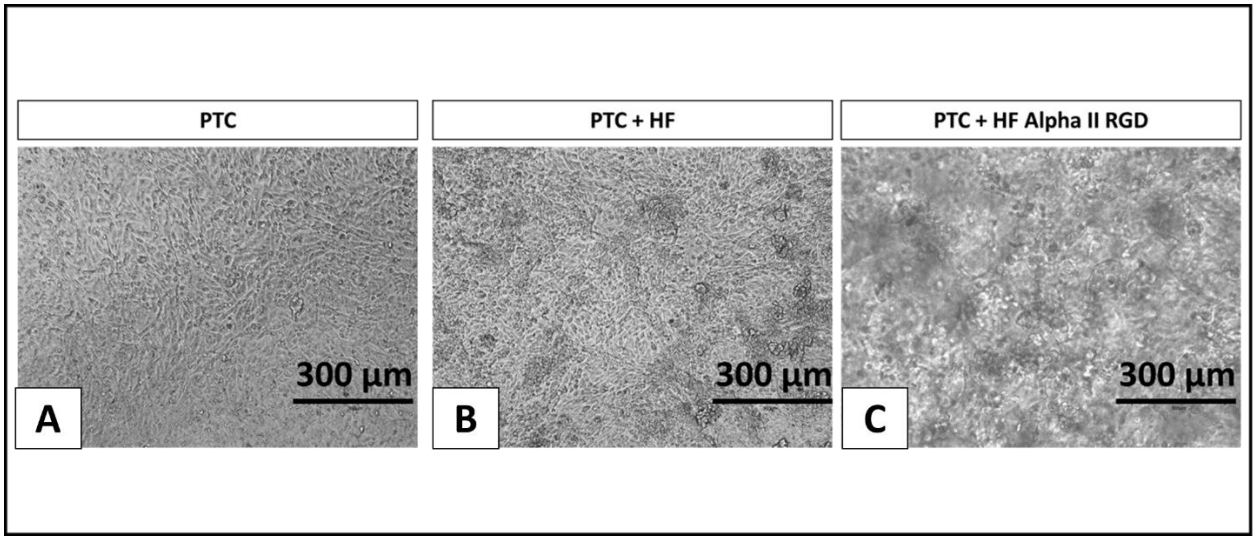

Figure 4.34. Phase-contrast images of monolayers and 3D models [A] hPTC on the apical side of the insert with characteristic cobblestone morphology [B] hPTC and HRF in contact co-culture on the apical side of the insert showing nodule formation [C] HRF are embedded in Alpha 2 RGD PeptiGel® and hPTC are cultured on top of the gel on the apical side allowing for epithelial colony attachment (scale bars=300µm).

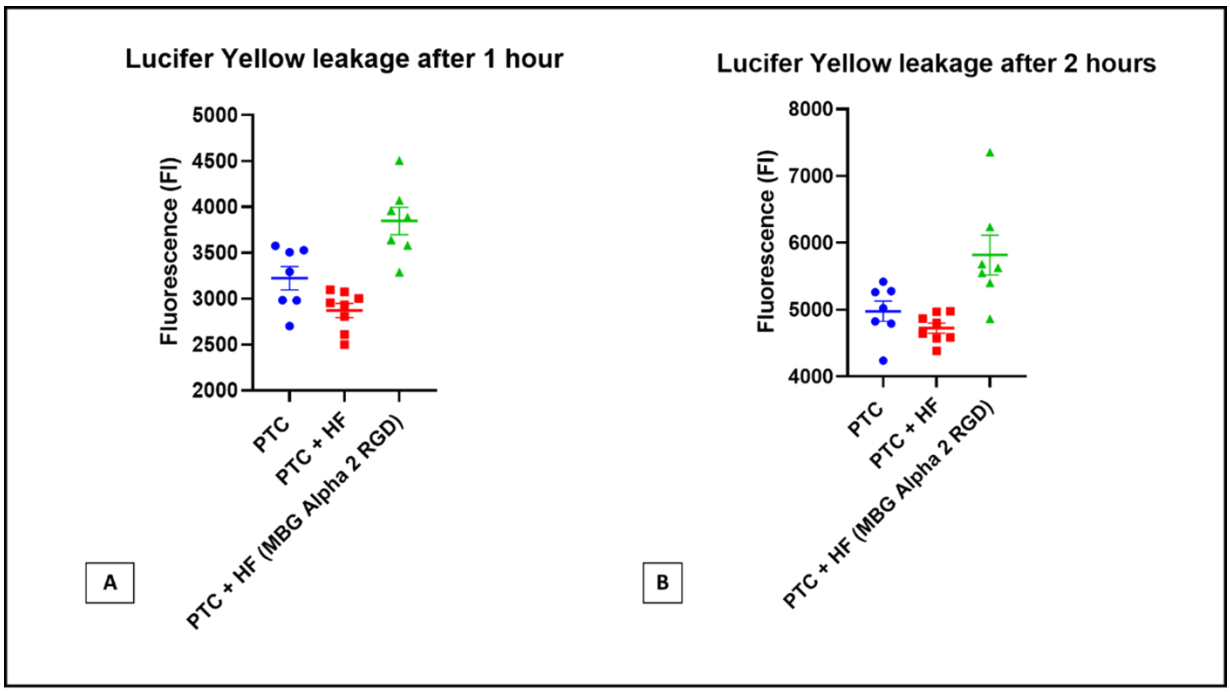

Figure 4.35. Lucifer Yellow leakage from apical to basolateral compartment across hPTC (Control) and 3D models after 1 and 2 hours. Proximal tubule cells cultured onto fibroblasts embedded in PeptiGel Alpha 2 RGD form a leakier epithelium [A] as compared to PTC in monoculture. Experiment performed on one biological replicate (n=1) and seven technical replicates, data presented as mean ± SD.

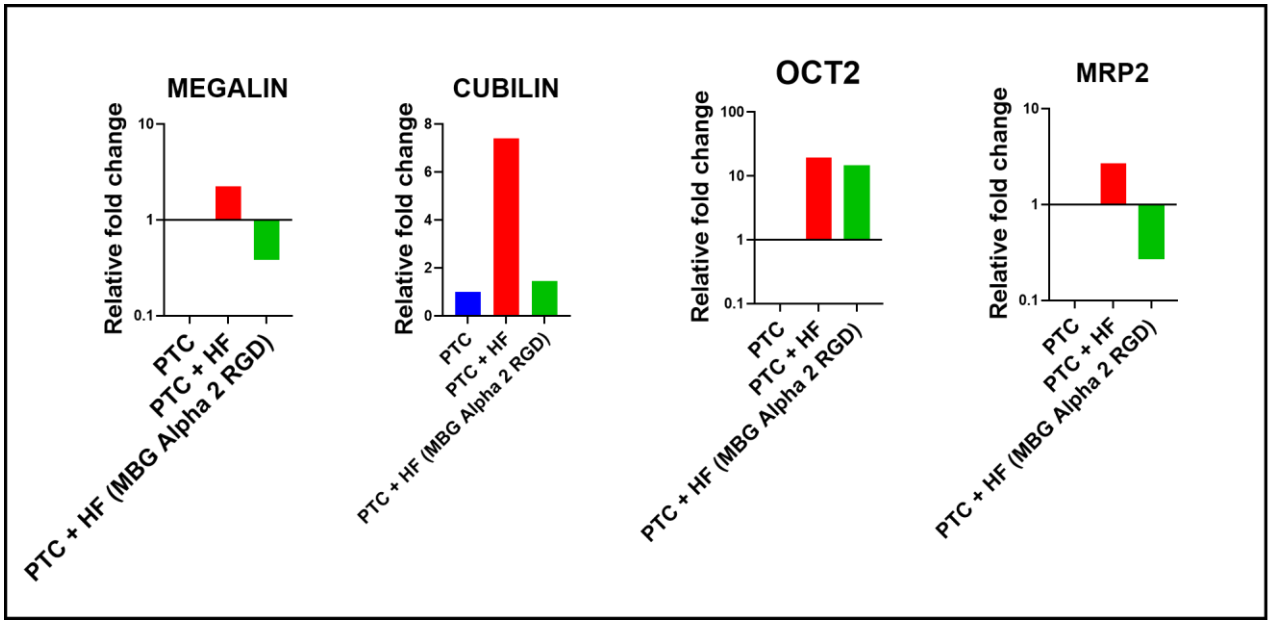

Figure 4.36. Effects of co-culture on relative fold change of gene expression of drug transporters megalin, cubilin, OCT2, MATE1, MRP2. Transporter gene expression of megalin, cubilin, OCT2, and MRP2 is upregulated in PTC in co-culture with fibroblasts (PTC + HF) relative to PTC in monoculture, while cubilin and OCT2 are upregulated in PTC on PeptiGel Alpha 2 RGD embedded fibroblasts, and megalin and MRP2 are downregulated in this model.

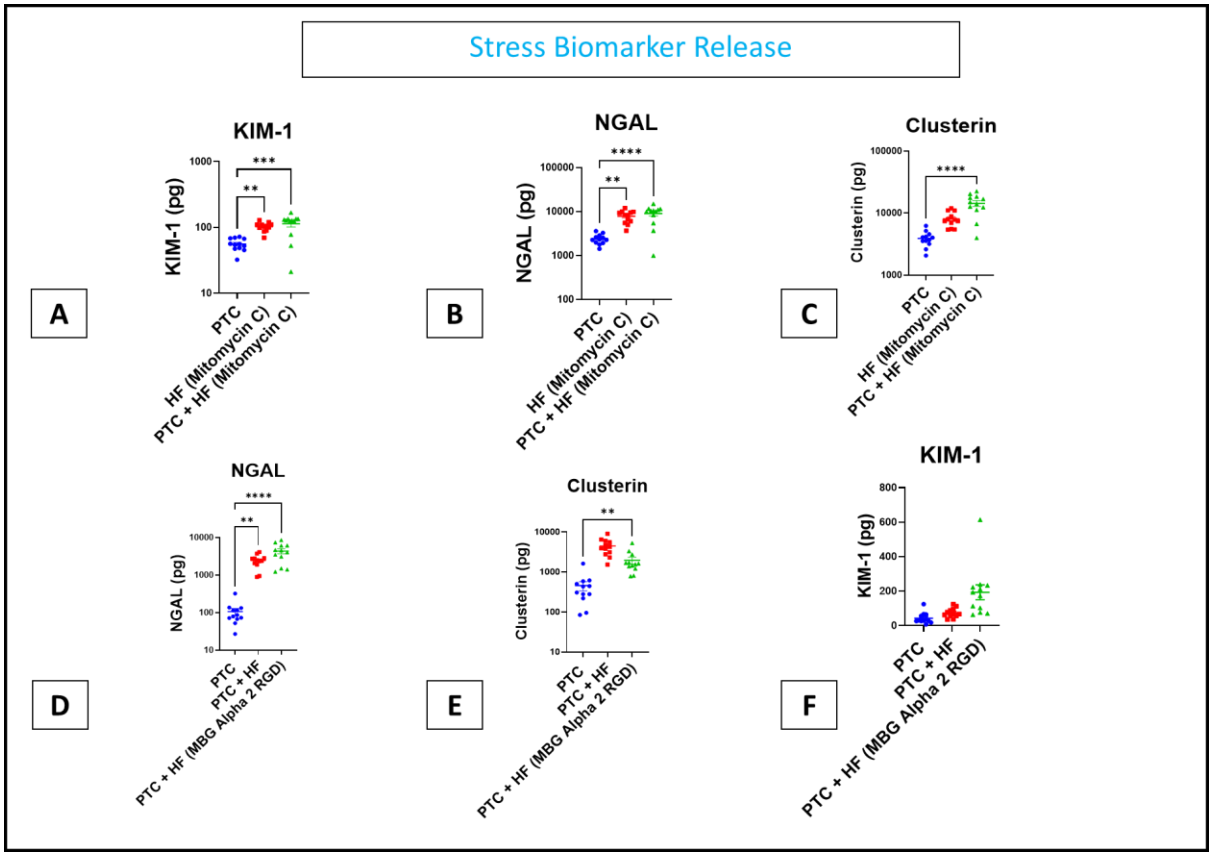

*Figure 4.37. Stress biomarker release from hPTC and HRF monolayers compared to 3D models. The graphs show that renal specific stress biomarkers KIM-1, NGAL, and clusterin are significantly increased for all the 3D constructs as compared to PTC in monoculture. Experiment performed on one biological replicate (n=1) and twelve technical replicates, data presented as mean ± SD. Statistical significance is depicted as '**' $p < 0.01$, '***' $p < 0.001$, '****' $p < 0.0001$.*

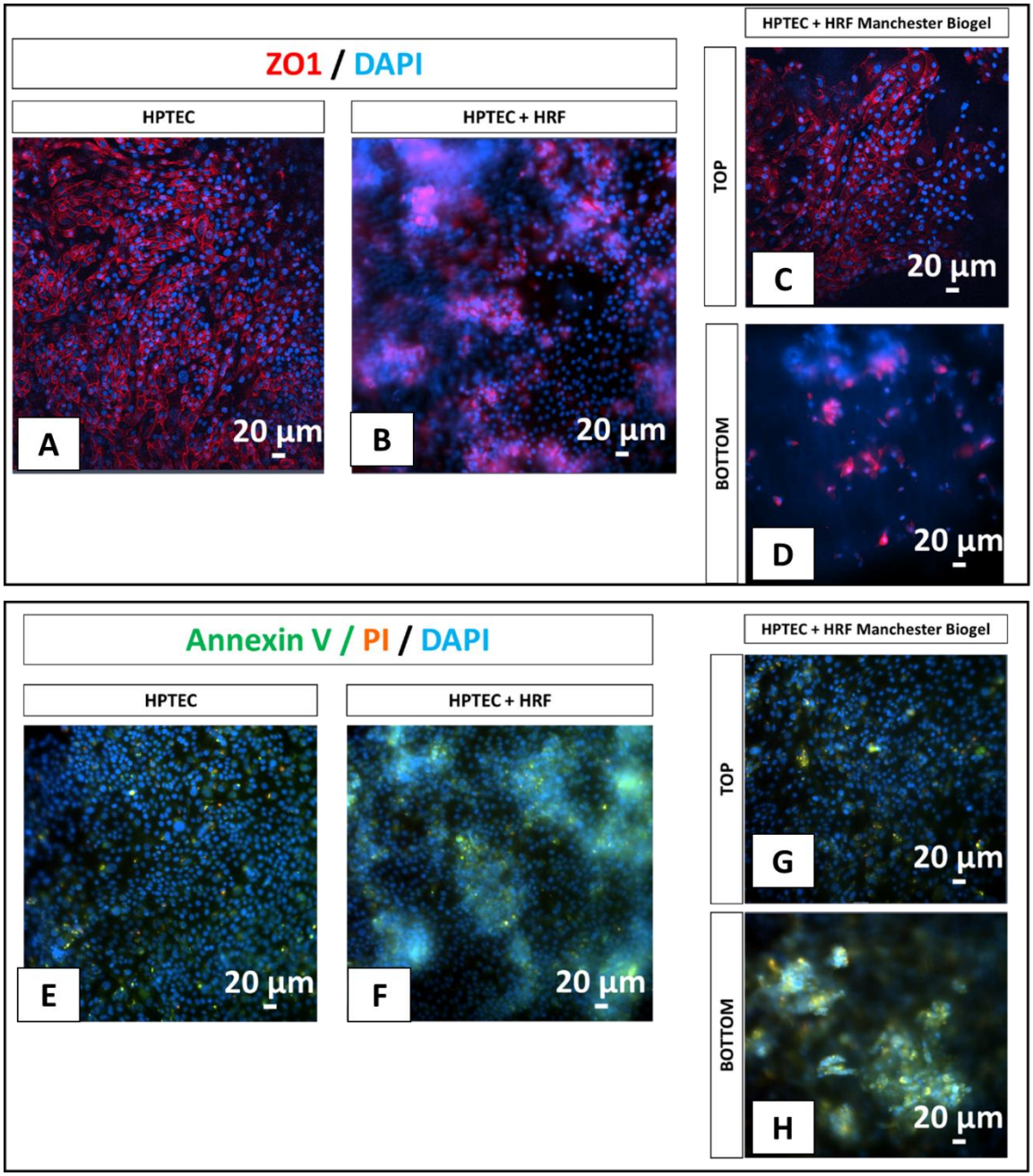

Figure 4.38. Fluorescence images of [A] hPTC, [B] hPTC + HRF in contact co-culture, and [C], [D] HRF embedded in PeptiGel® Alpha 2 RGD with hPTC on the apical side of ThinCert™ insert showing effective tight junction formation staining positive for ZO-1 (in red). Fluorescence images depicting apoptotic cells (in green), necrotic cells (in orange) in [E] hPTC, [F] hPTC and HRF in contact co-culture, and [G], [H] HRF embedded in PeptiGel® Alpha 2 RGD with hPTC on the apical side of ThinCert™ insert staining (scale bars=20µm).

Finally, the contact co-culture hPTC + HRF model was compared to hPTC cultured on top of HRF embedded in a commercially available, synthetic extra-cellular matrix (ECM), as represented in **Figure 4.32**. Different types of synthetic ECMs were purchased from Manchester BIOGEL and their ability of embedding human renal fibroblasts was assessed via CellTiter-Glo® intracellular ATP assay. The graph shown in **Figure 4.33** demonstrates that HRF are most viable when embedded in 200 µL of Alpha 2 RGD. This type of PeptiGel® was selected to run our co-culture experiments.

Phase-contrast images of the HRF-embedded co-culture model in **Figure 4.34** show epithelial colony attachment on the gel surface, but due to the PeptiGel® ultrastructure it is challenging to assess whether a full epithelial monolayer has formed. Comparison of lucifer yellow leakage after 1 and 2 hours across 3D models shows that hPTC and hPTC + HRF are more leak-tight in absence of the PeptiGel® (**Figure 4.35**). Assessment of gene expression of transporters shows that the trophic support exerted by HRF is somewhat retained in presence of the gel since cubilin and OCT2 expression is upregulated (**Figure 4.36**). Stress biomarkers released in the cell culture medium were measured for hPTC, hPTC + HRF, hPTC cultured on mitomycin C-treated HRF, and hPTC cultured on HRF embedded in Alpha 2 RGD PeptiGel. Release of KIM-1, NGAL and clusterin in the medium is increased in presence of the PeptiGel (**Figure 4.37**). The three biomarkers detected are specifically released during renal injury, in fact kidney injury molecule (KIM-1) is a protein which has been pinpointed as being an injury marker predictive of renal proximal tubule injury which is shed into the urine after nephrotoxic events (Han et al., 2002). Immunofluorescence staining for tight junction marker ZO-1 was performed to compare epithelial monolayer formation between hPTC + HRF with or without Alpha 2 RGD. **Figure 4.38 [C]** shows successful tight junction formation between proximal tubule cells grown on top of the gel. **Figure 4.38 [F]** displays Annexin-V+ apoptotic nodule formation in absence of Alpha 2 RGD while PTCs grown on top of the gel (**Figure 4.38 [G])** exhibit a comparable degree of apoptotic cells to the control.

4.3 Non-contact co-culture of hPTC with HRF enhances epithelial barrier formation.

KIM-1, NGAL, and clusterin are three Food & Drugs Administration (FDA) qualified urinary biomarkers of kidney injury. *In vitro,* they are used to measure proximal tubule cell stress levels and they are associated to nephrotoxicity. Proximal tubule cells in culture release a basal amount of these biomarkers, simply because they are *in vitro* and not in a whole functioning organ in the human body (Bajaj et al., 2020). Therefore, we expected biomarkers release to decrease when hPTC were in culture with HRF, since the latter mimic more closely the *in vivo* milieu. Interestingly, **Figure 4.39** shows that also HRF monolayers release these biomarkers. Furthermore, hPTC grown in model **D** [PTC + HF (No TW)] from **Figure 4.19** release a significantly lower amounts of KIM-1 and clusterin, while model **B** [PTC + HF (A)] and **C** [PTC + HF (B)] release significantly lower amounts of NGAL.

To further investigate the differences between proximal tubule cells in contact co-culture and non-contact co-culture with human renal fibroblasts, we looked at the structure of the microtissues formed by the cells cultured on transparent ThinCert™ inserts via high content

imaging. Four conditions were considered: hPTC on the apical side of the insert cultured with REGM™ Renal Epithelial Growth Medium (control), hPTC on the apical side of the insert and HRF on the bottom of the well both cultured with REGM™, hPTC on the apical side of the insert cultured with REGM™ and HRF on the bottom of the well cultured with FGM-2™ Fibroblast Growth Medium, and hPTC and HRF on the apical side of the inserts cultured with REGM™ on the apical compartment and FGM-2™ on the basolateral compartment.

Images displayed in **Figures 4.40** show proximal tubule cells in the above-mentioned culture conditions staining positively for the tight junction marker ZO-1 **(in red)**. hPTC in monoculture form an intact monolayer **(Figure 4.40 [A]),** which is disrupted in the co-culture with HRF on the bottom of the well when using REGM™ on both sides of the insert **(Figure 4.40 [B])**. Conversely, intensity of staining and monolayer integrity seems greater than the control in **Figure 4.40 [A]**. Finally, **Figure 4.40 [D]** shows hPTC and HRF cultured on the same surface forming nodules or 3D structures and disrupting monolayer integrity.

Images displayed from **Figure 4.41** show proximal tubule cells in the same culture conditions staining positively for the apoptosis marker Annexin V-FITC **(in green).** The second culture condition shows a slight increase in number of apoptotic cells **(Figure 4.41 [B])**, while the contact co-culture condition **(Figure 4.41 [D])** shows that the nodules formed on the insert are apoptotic.

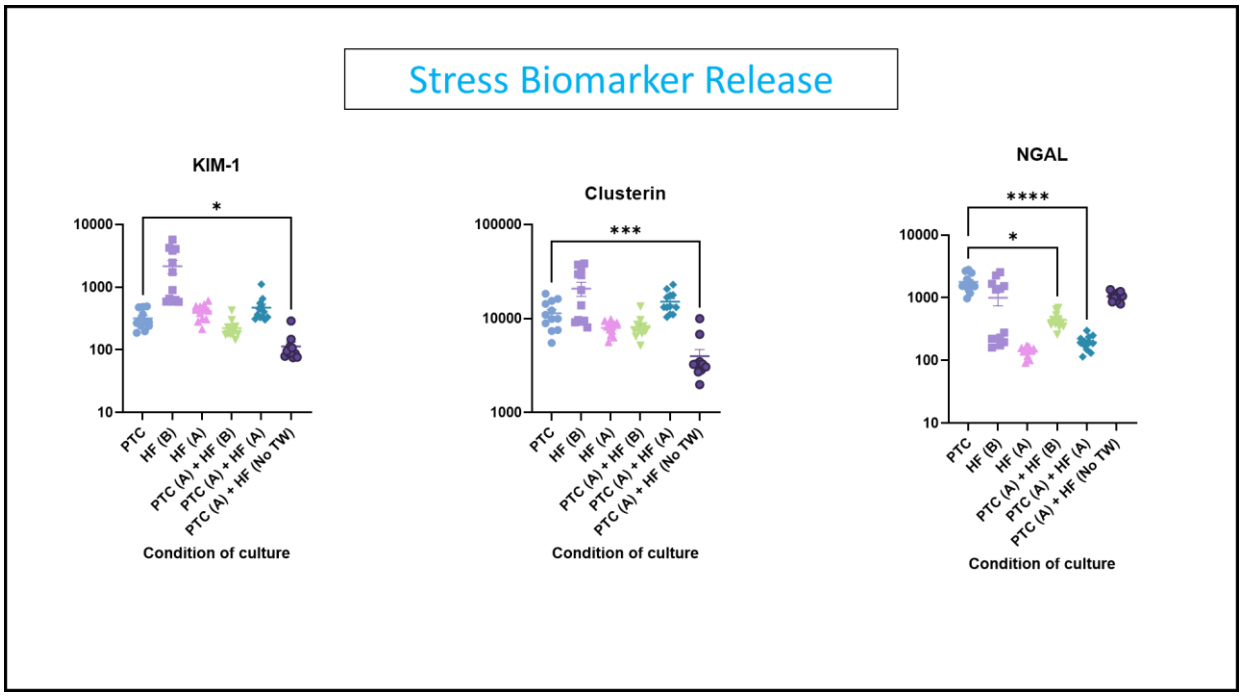

Figure 4.39. Stress biomarker release from hPTC and HRF monolayers compared to 3D models constituted by fibroblasts cultured on the apical [A] and basolateral [B] side on the insert in contact and non-contact co-culture with PTC. Non-contact co-culture model PTC [A] + HF [No TW] shows significantly reduced KIM-1 and clusterin release as compared to hPTC in monoculture. Data are presented as Mean ± SD (n=1). Statistical significance is depicted as '' $p < 0.05$, '**' $p < 0.01$, '***' $p < 0.001$, '****' $p < 0.0001$*

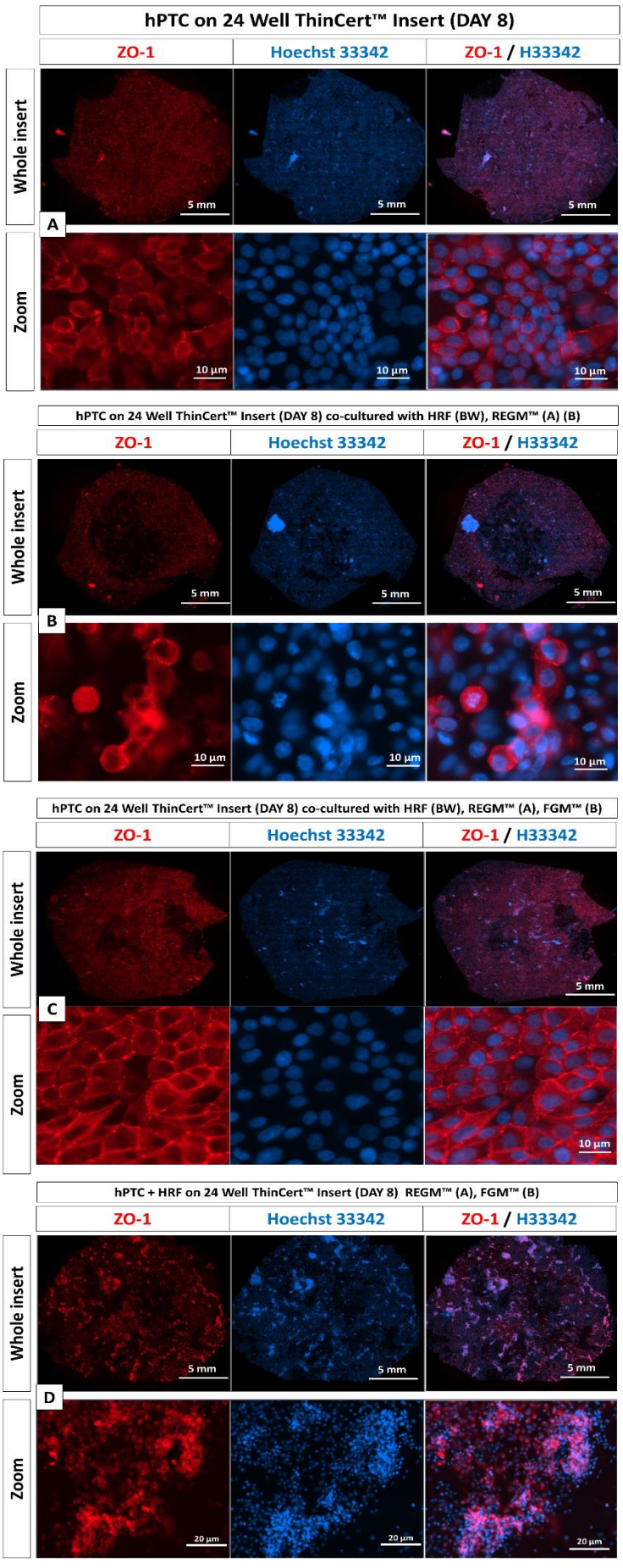
hPTC on 24 Well ThinCert™ Insert (DAY 8)
ZO-1
Hoechst 33342
ZO-1 / H33342
Whole insert
Zoom
A
5 mm
10 µm
hPTC on 24 Well ThinCert™ Insert (DAY 8) co-cultured with HRF (BW), REGM™ (A) (B)
B
hPTC on 24 Well ThinCert™ Insert (DAY 8) co-cultured with HRF (BW), REGM™ (A), FGM™ (B)
C
hPTC + HRF on 24 Well ThinCert™ Insert (DAY 8) REGM™ (A), FGM™ (B)
D
20 µm

Figure 4.40. Fluorescence image of hPTC on ThinCert® insert in mono- and co-culture [A] staining positive for ZO-1in monoculture [B] hPTC staining positive for ZO-1, HRFs were cultured on the bottom of the well and are not visible in the picture, both cell types are cultured in REGM [C] hPTC staining positive for ZO-1, with HRF cultured on the bottom of the well, cultured in FGM-2 and REGM. [D] hPTC and HRF co-cultured on ThinCert™ insert staining positive for ZO-1 and forming nodules (scale bars=5 mm, 10µm, 20µm).

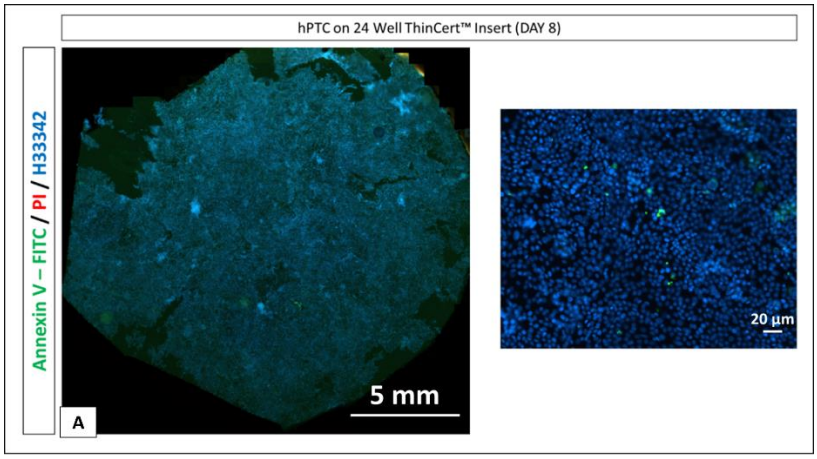
hPTC on 24 Well ThinCert™ Insert (DAY 8)
Annexin V – FITC / PI / H33342
5 mm
A
20 µm

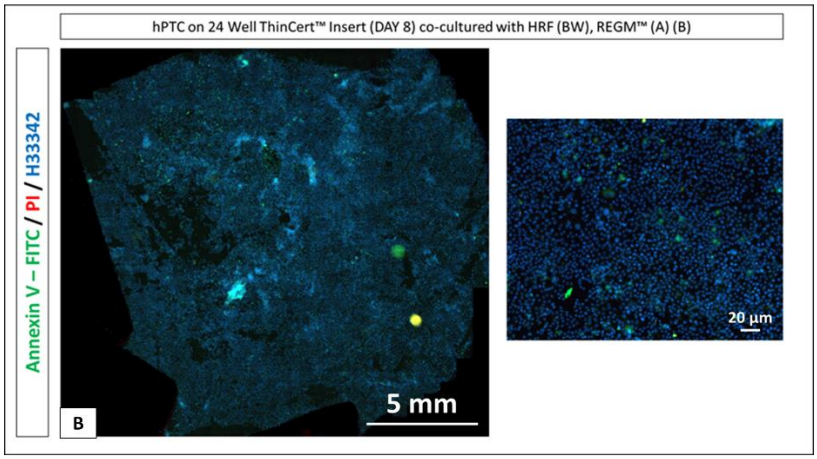
hPTC on 24 Well ThinCert™ Insert (DAY 8) co-cultured with HRF (BW), REGM™ (A) (B)
Annexin V – FITC / PI / H33342
5 mm
B
20 µm

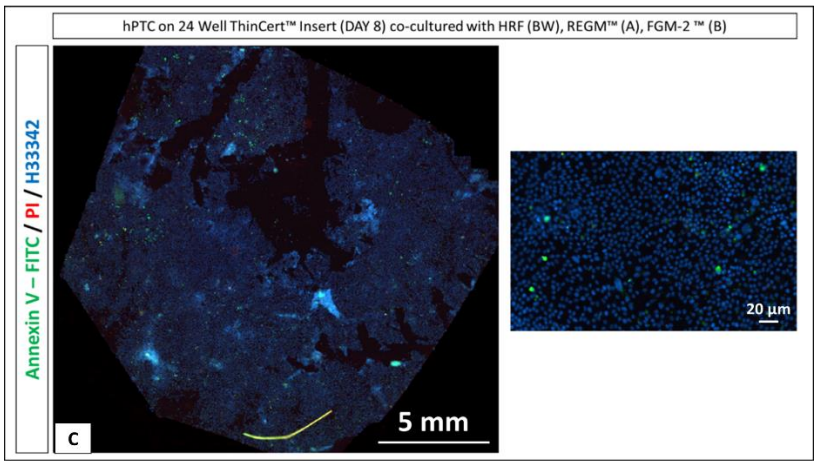
hPTC on 24 Well ThinCert™ Insert (DAY 8) co-cultured with HRF (BW), REGM™ (A), FGM-2 ™ (B)
Annexin V – FITC / PI / H33342
5 mm
C
20 µm

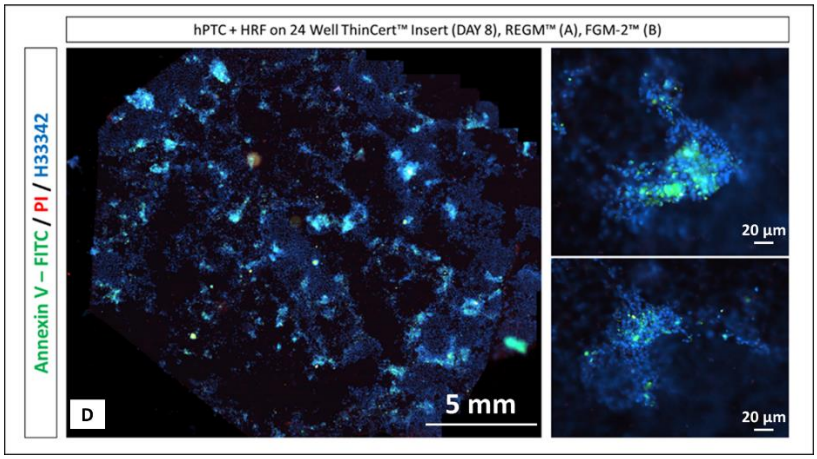
hPTC + HRF on 24 Well ThinCert™ Insert (DAY 8), REGM™ (A), FGM-2™ (B)
Annexin V – FITC / PI / H33342
5 mm
D
20 µm
20 µm

Figure 4.41. Fluorescence image of hPTC on ThinCert® insert in mono- and co-culture showing apoptotic cells (in green) and necrotic cells (in orange) [A] PTC in monoculture showing a low number of apoptotic cells, as for non-contact co-culture models with HRF shown in [B], [C]. [D] contact co-culture model with PTC and HRF showing apoptotic nodule formation (scale bars=5 mm, 20µm)

Since we have demonstrated that fibroblasts in direct contact with proximal tubule cells not only migrate into nodules and disrupt epithelial barrier function but also increase the chances of apoptosis, we wanted to explore whether mimicking the presence of fibroblasts in the co-culture model by adding compounds that would simulate co-culture conditions could increase epithelial cell viability. Therefore, hPTC were treated with medium that was in contact with serum-starved HRF for 24 hours (conditioned medium), with exogenous insulin-like growth factor 1 (IGF-1) which has shown to promote hPTC growth and is released by HRF (Johnson et al., 1997), and VEGF-A to mimicry the presence of vasculature. Exogenous IGF-1 and VEGF-A treatment increased proximal tubule cell viability (**Figure 4.42**)**.** Using media conditioned by the presence of fibroblasts to stimulate proximal tubule growth could be a way to simplify the 3D model, especially because this method would be more representative of the epithelial-fibroblast crosstalk found *in vivo*, since the ratio between tubular epithelial cells and fibroblasts increases only after injury.

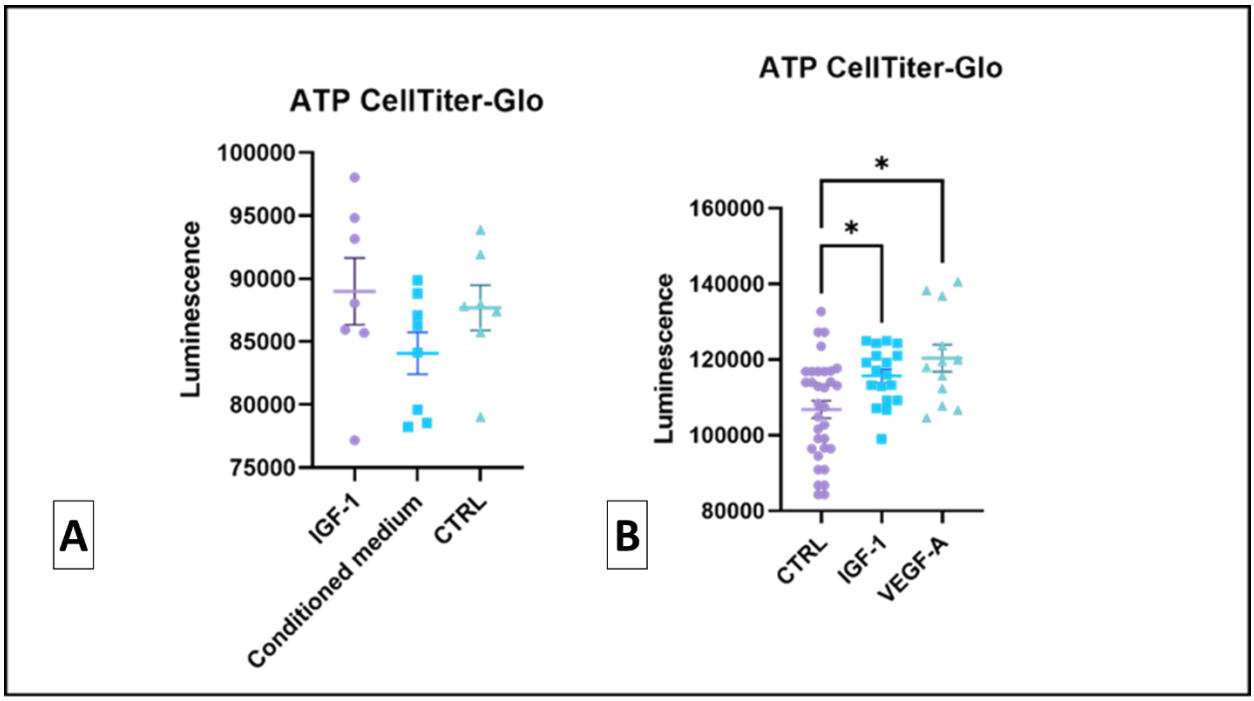

Figure 4.42. Cell viability assay measuring intracellular ATP of hPTC (untreated control) to hPTC treated with IGF-1, fibroblasts-condition medium and VEGF-A. Experiment performed on two separate biological repeats (n=2). Error bars represent SD between technical repeats. Statistical significance is depicted as '' ($p < 0.05$).*

The data displayed above demonstrates that although some of the methods used to halt fibroblast migration into the epithelial monolayer lead to a moderate degree of success, such as embedding HRF in gel, the amount of optimisation required to obtain a 3D *in vitro* model suitable for renal fibrosis treatment seemed to be far too large and challenging for the length of this project. Therefore, we selected the *in vitro* model that suited our purpose best. This model is generated by isolating human renal fibroblasts from the human kidney cortex as

described in **2.2.2,** whereby fibroblasts are first expanded via Percoll® density gradient isolation, cultured to confluency onto T-75 flasks in FGM™-2 medium, purified via MACS based on positivity to FSP-1, and finally cultured onto the bottom of the well of a 96-Transwell® plate coated with Biogel-X hydrogel. In parallel, proximal tubule cells are isolated from the same human kidney cortex via Percoll® density gradient isolation as described in **2.2.1** and seeded directly onto the inserts of a 96-Transwell® plate in REGM™ medium. Both cell types are left to grow to near-confluency for 3 to 4 days, to then be assembled in co-culture until complete epithelial barrier formation is achieved, as highlighted by optimal TEER threshold achievement. REGM™ medium is maintained for the apical (epithelial) compartment and FGM™-2 is maintained for the basolateral (fibroblast) compartment. Aside from retaining proximal tubule cell transporter expression and function, the model allowed human renal fibroblasts to exert their trophic support to the epithelial monolayer. Furthermore, the proposed model allowed us to isolate both cell types from an autologous tissue rendering the model patient-specific. The platform is composed by proximal tubule cells cultured on the apical side of a transparent insert and human renal fibroblasts cultured on the optically clear bottom of the well. The model is developed on a 96-Transwell® plate to allow for high throughput multiplex experiments focusing on the use of high content imaging, high throughput flow cytometry, and further assays. The images in **Figure 4.43** demonstrate that the automated confocal microscope Zeiss® LSM800 Airyscan was able to focus and image both apical and basolateral cell culture surfaces of a transparent Transwell® insert. Proximal tubule cells demonstrate positive expression of tight junction marker ZO-1 (zonula occludens 1) while human renal fibroblasts express FSP-1 (fibroblast specific protein 1).

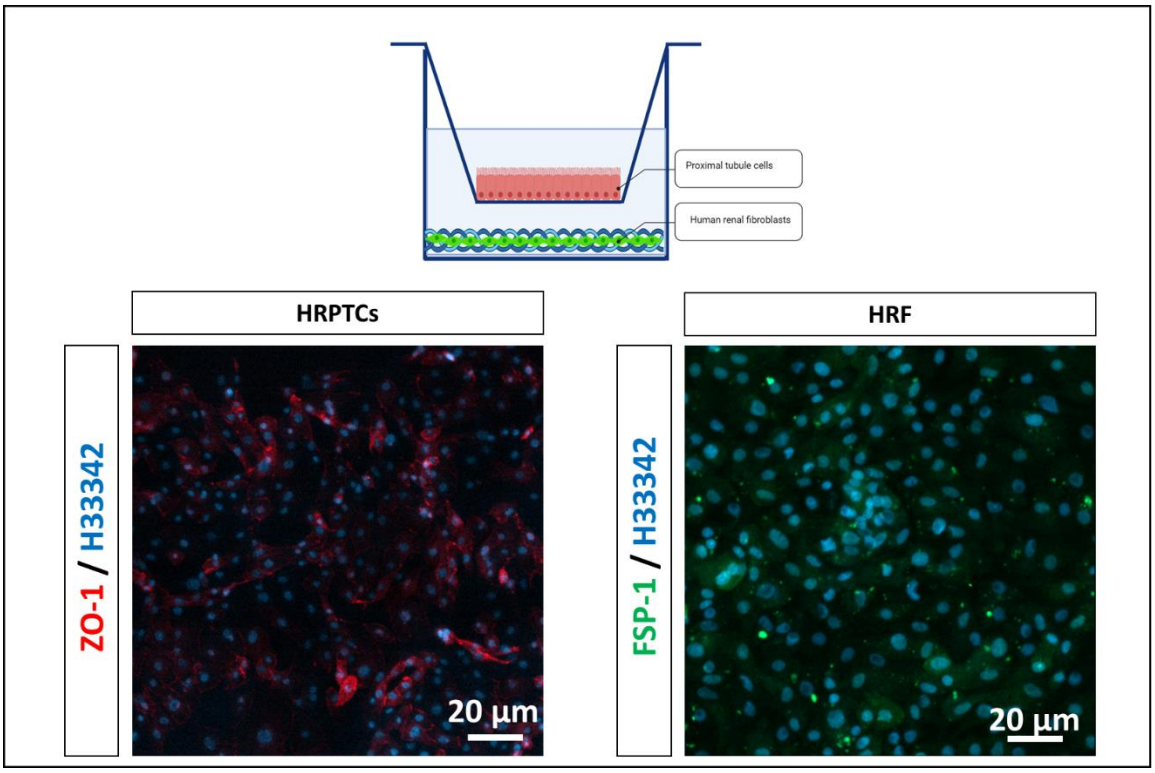

Figure 4.43. Graphical representation and correspondent confocal images of hPTC on the apical side of Transwell® inserts staining positive for ZO-1 (zonula occludens 1) and HRF on the bottom of the well staining positive for FSP-1 (fibroblast specific protein 1) (scale bars=20 µm).

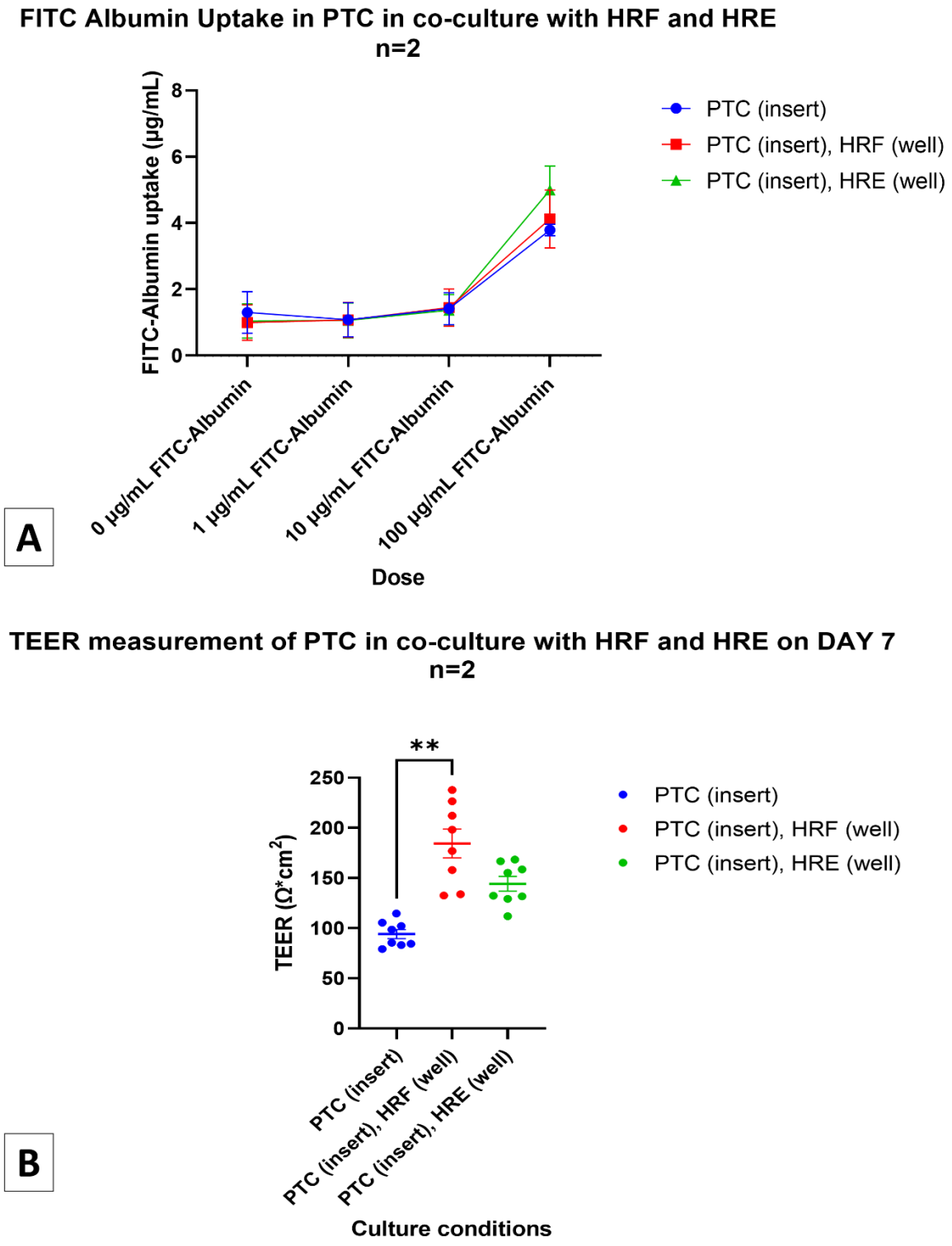

*Figure 4.44. [A] FITC Albumin uptake in hPTC in monoculture and non-contact co-culture with HRF and HRPEC when cells are exposed to increasing concentrations of FITC-Albumin (µg/mL) [B] Trans-epithelial electrical resistance (TEER) measurements comparing hPTC in monoculture and non-contact co-culture with HRF and HRPEC. Experiment performed on two biological replicates (n=2) and four technical replicates, data presented as mean ± SD. Statistical significance is depicted as '**' $p < 0.01$.*

The graphs displayed in **Figure 4.44** refer to experiments which aimed at comparing hPTC in monoculture to hPTC in non-contact co-culture with HRF and HRPEC in terms of ability to uptake the plasma protein albumin conjugated to the fluorophore FITC (**Figure 4.44 [A]**) and in terms of epithelial barrier formation measured via TEER (**Figure 4.44 [B]**). The data collected from two biological replicates demonstrates that the presence of HRF or HRPEC in culture does not disrupt albumin uptake, and that the presence of HRF in culture seems to cause a tightening in the epithelial barrier mirrored by a significant increase in TEER measurement for the [PTC (insert), HRF (well)] condition as compared to [PTC (insert)] in monoculture.

The fluorescence images shown in **Figure 4.45** focus on highlighting the differences in expression of key solute transporters in the proximal tubule OAT1, OAT3, and megalin in hPTC in monoculture as compared to the non-contact co-culture models containing HRF and HRPEC. Although this is a qualitative estimation of transporter expression based on observation of single example images, the images shown below suggest that OAT1, OAT3, and megalin are expressed by hPTC in monoculture, and there seems to be an increase in expression of OAT1 in the [hPTC + HRF] co-culture condition represented by a marked increase in cells positive to the antibody against the transporter. Therefore, the data relative to the non-contact co-culture models suggests that HRF in co-culture with hPTC are able to exert trophic support to the formation of the epithelial monolayer which is mirrored by increased TEER and expression of drug transporters as compared to the monoculture model without disruption of solute uptake.

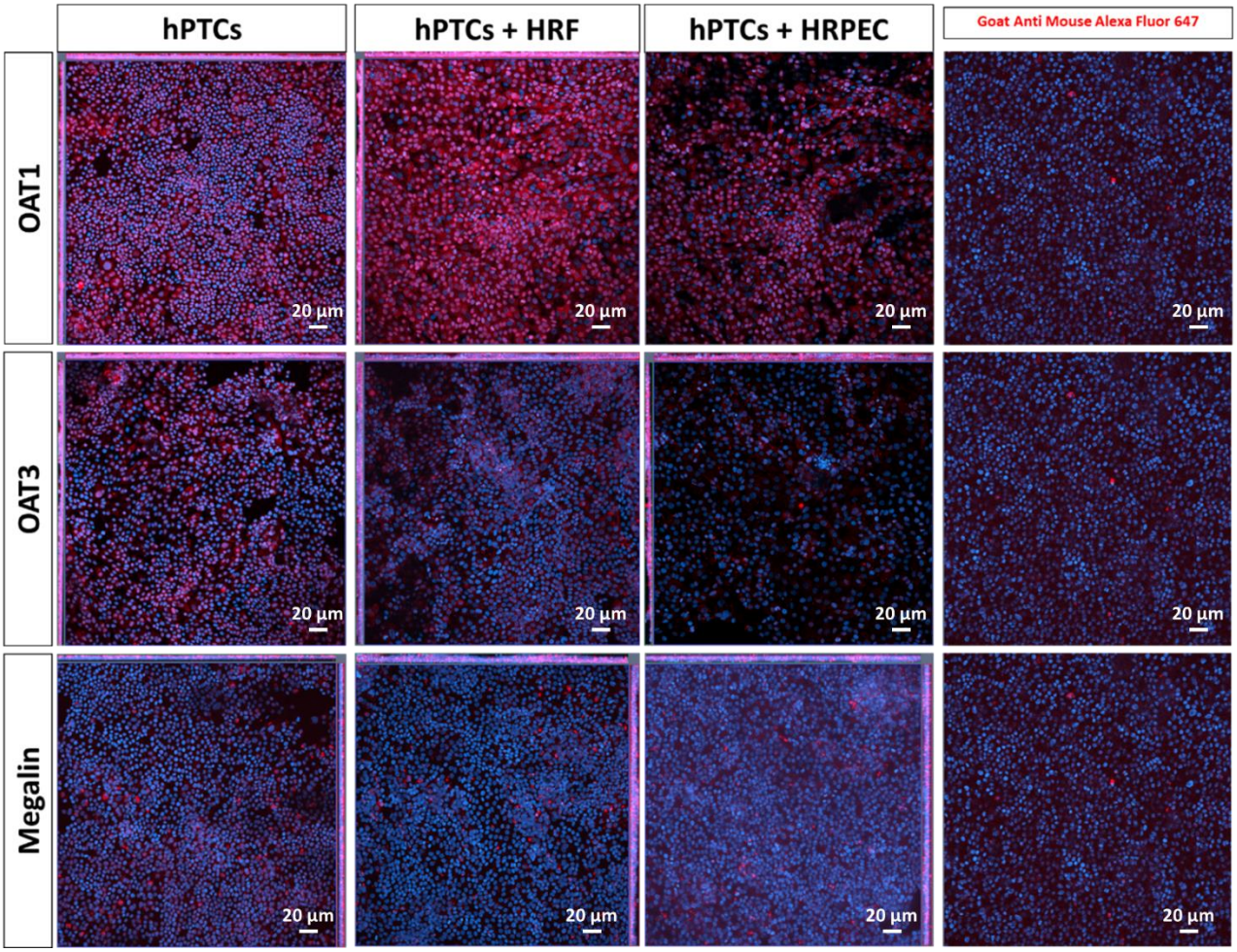

Figure 4.45. Fluorescence images of hPTC monolayers comparing OAT1, OAT3, and megalin transporter expression across non-contact co-culture conditions. OAT1 expression increases when PTC are in co-culture with HRF and HRPEC as compared to PTC in monoculture (scale bars=20 µm).

4.4 Discussion

Several complex models of 3D proximal tubules have been developed in the past 20 years due to the shift towards replacing experimental animal models with physiologically relevant *in vitro* models. Aceves, J.O. et al. describe a method to overcome the difficulty in obtaining primary kidney tissue by deriving renal epithelial tubular cells from kidney organoids. These cells are then cultured onto perfused cylindrical channels embedded in ECM. The cell-containing cylinders are placed next to one another in order to stimulate drug transporter expression and simulate solute uptake and transport in the proximal tubule (Aceves et al., 2022). Carracedo, M. et al. take the cell-lined cylinder concept a step further by culturing two distinct cylindrical structures lined by proximal tubule cells and endothelial cells, respectively, and perfused by a closed-loop system to connect them. Upon culturing this 3D model onto a microfluidic chip, the phenotype of the cells contained by the organ-on-a-chip was determined by single-cell RNA sequencing, whereby these culture conditions were compared to a 2D Transwell® model. Both the epithelial and endothelial components displayed transcriptome signature closer to native proximal tubule interstitial interface when cultured in 3D and under simulated flow rather than in static 2D condition (Carracedo et al., 2023). Immortalised cell lines are an extremely valuable tool in *in vitro* modelling, but they often display loss of key features of their tissue of origin, which in the case of the proximal tubule are polarisation, and epithelial barrier formation. Mizuguchi K., et al. developed a spheroid 3D culture method to induce these features in immortalised cell line human kidney-2 (HK-2) with the use of an extracellular matrix, which brought to enhanced transporter expression as compared to the 2D model (Mizuguchi et al., 2021). The use of another key immortalised human proximal tubule-derived cell line in the development of 3D models has been investigated by Vidal Yucha, SE et al. whereby RPTEC-TERT1 cells have been used to culture tubule organoids called ‘tubuloids’. The tubuloids were compared to 2D culture of the same cells type, where the 3D structures demonstrated to be more sensitive to nephrotoxic treatments and to more closely recapitulate hPTC phenotype (Vidal Yucha et al., 2022). Similarly, Nieskens, TTG et al. explored the use of dual-channel Nortis™ chip to culture primary human proximal tubule cells as compared to 2D culture demonstrating polarization, primary cilia expression, transporter function, and appropriate nephrotoxic response to specific compounds (Nieskens et al., 2020).

The data presented in this chapter demonstrates that we successfully developed a protocol for the co-culture of proximal tubule cells and human renal fibroblasts, whereby tubular epithelial functions are retained, epithelial barrier function is enhanced as compared to the monoculture condition, and one of the components of the proximal tubule interstitial interface is incorporated in the model, making it three-dimensional and suitable for the induction of a multifaceted condition such as renal fibrosis. We trialled several ways of co-culturing proximal tubule cells with the other two selected components of the proximal tubule interstitial interface, namely renal fibroblasts, and renal peritubular endothelial cells. Initially, different cell types were being isolated from two different kidney donors, thus this was posing technical limitations to the construction of the model due to the unpredictability of tissue availability that could leave the cell type cultured first waiting for the following layer of cells indefinitely. This would have impacted the reproducibility of such model deeming this

co-culture technique unsuitable for the creation of an assay platform that requires a level of standardization. The transcriptomics data collected from these initial experiments indicated that the combination between proximal tubule cells and renal fibroblasts was leading to the most promising increase in expression of key solute transporters, suggesting the presence of fibroblasts in culture could offer trophic support to the epithelial cells, thus mimicking the *in vivo* conditions by means of cellular crosstalk. For these reasons, we decided to concentrate our efforts in finding a way to isolate epithelial cells and fibroblasts from the same donor kidney and co-culture them. The trialled contact co-culture models lead to a great increase in gene expression of key transporters but the presence of fibroblasts in culture seemed to disrupt epithelial monolayer formation, which subsequently impacted transporter function. Hence, the focus of our experiments was shifted onto maintaining the trophic support that fibroblasts seemed to be exerting onto the epithelial cells while making sure that the mesenchymal cells would not disrupt correct proximal tubule cell function. The trialled methods to impede fibroblast migration into the epithelial monolayer were fibroblast irradiation, mitomycin C treatment, where both methods intended to halt fibroblast proliferation without inducing cell death, and embedment of fibroblasts in hydrogel. The latter method led to a moderate degree of success in halting fibroblast movement while keeping the cells alive, since we managed to culture an epithelial monolayer which formed ZO1+ tight junctions on top of fibroblasts embedded in hydrogel, but this co-culture method would have required a significant amount of optimisation, especially regarding transporter function measurement which would have been complicated by the presence of the hydrogel. Therefore, we opted for a solution whereby the fibroblasts could not possibly migrate into the epithelial monolayer since they were physically separated from their epithelial counterparts by being cultured at the bottom of the well of a Transwell® plate whilst proximal tubule cells were cultured on the apical side of the Transwell® insert. Thanks to this non-contact co-culture technique, epithelial barrier function was maintained together with functional solute transport and fibroblasts' trophic support, making this 3D *in vitro* model of the proximal tubule interstitial interface suitable for induction of renal fibrosis and measurement of relevant endpoints via high content imaging and high throughput flow cytometry.

The limitations around the proposed 3D model of proximal tubule interstitial interface stem mainly from the spatial separation between the two cellular components incorporated within the model, proximal tubule cells and renal fibroblasts. The decision to pursue a non-contact co-culture model derived from the challenges encountered with the maintenance of epithelial barrier function of hPTC in co-culture with fibroblasts, which migrated into the epithelial monolayer formed by such cells disrupting their healthy physiological function. Within the timeframe and budget available, the non-contact co-culture seemed to be the best one to preserve epithelial barrier and transporter function while retaining the presence of fibroblasts for trophic support. Since the cell types are ultimately cultured and treated separately, one other feasible option would have been to expose hPTC and HRF separately to respective condition media. The secretome released by HRF in monoculture could have enhanced the cell viability and key phenotypical features of hPTC. As shown in Figure 4.40, pursuing contact co-culture would have been possible if the migration of HRF into the epithelium could have

been halted. The employment of a hydrogel with the appropriate stiffness, which would have allowed the fibroblasts to proliferate and secrete growth factors useful to support epithelial growth as well as stifling their migration, could have solved the challenges posed by the contact co-culture model. Furthermore, the encapsulation of the fibroblasts would have provided with two faces of gels that could have been layered with epithelial cells on one side and peritubular endothelial cells on the other side. These improvements to the 3D model could have been implemented on Transwell inserts, but a number of microfluidic chips are available on the market which would have provided an excellent platform for the co-culture of a complex structure like the proximal tubule interstitial interface. The ideas herein described could point towards the direction of the future work around a healthy *in vitro* 3D model of proximal tubule, whereby different synthetic ECM/hydrogels could be tested to embed renal fibroblasts at the same time as co-culturing hPTC and HRPEC, and subsequently transfer the culture conditions of such constructs to a microfluidic platform such as the Mimetas OrganoPlate (Vormann et al., 2018).

Despite the challenges encountered when developing the 3D co-culture model, more complex platforms could have been used to allow the growth of fully differentiated renal epithelial cells. Microfluidic platforms have been in use for a number of years and have proven to be suitable for the assembly of 3D models of various tissues. An elegant solution to the migration of fibroblasts into the epithelial layer could have been to expose the proximal tubule cells to media conditioned by fibroblasts and endothelial cells, and vice versa, which could have led to the exploration of interesting pathways in terms of cross-talk between cell types.

Chapter 5. Development of a 3D *in vitro* model of renal fibrosis in the proximal tubule.

5.1 Introduction

In renal fibrosis, the human renal fibroblast is activated into a contractile cell called myofibroblast which expresses the protein α smooth muscle actin (α-SMA). A plethora of pro-fibrotic cytokines has been shown to activate renal fibroblasts to myofibroblasts *in vitro*, with large amounts of evidence supporting the theory that transforming growth factor β1 (TGFβ1) is the main driver of the maladaptive cellular process. Epithelial cells undergoing epithelial-to-mesenchymal transition (EMT) in all tissues display disintegration of tight junctions (zonula occludens 1, ZO1), downregulation of epithelial markers (E-Cadherin), and upregulation of mesenchymal markers (Vimentin). Cell cycle dysregulation and defective mesenchymal-epithelial crosstalk are two of the mechanisms thought to be involved in partial epithelial-to-mesenchymal transition (pEMT), whereby epithelial cells partially lose tight junction and adhesion protein expression while gaining *de novo* migratory and contractile phenotype, with involvement of cell signalling pathways that promote proliferation (Sheng & Zhuang, 2020b). The epidemiological correlation between acute kidney injury (AKI) and chronic kidney disease (CKD) seen *in vivo* is linked to progressive renal fibrosis.

Therefore, the *in vitro* model of renal fibrosis that will be presented in this chapter has been designed to take into consideration both aetiologies by stimulating renal cells with endogenous and exogenous pro-fibrotic compounds. The endpoints measured by the assays developed specifically to measure phenotypic changes related to fibrosis have been selected to investigate the key events that occur in renal fibrosis, such as EMT/pEMT (epithelial-to-mesenchymal transition, partial) in proximal tubular epithelial cells, ECM (extracellular matrix) deposition in renal fibroblasts, metabolic changes, cell health, cell cycle dysregulation, stress biomarker and chemokine release. To address the involvement of mesenchymal-epithelial crosstalk, experiments are carried out in proximal tubule cells and renal fibroblasts both in mono- and co-culture for all endpoints. For the monoculture models, primary human proximal tubule cells (hPTC) and human renal fibroblasts (HRF) are cultured onto 96-well black walled plates. For the co-culture experiments, hPTC are cultured onto the apical membrane of 96-Transwell inserts while renal fibroblasts are cultured on the well bottom, which is referred to as 'non-contact co-culture'. As discussed in **Chapter 4** culture conditions for the model are established and characterised as healthy phenotype. The models are then treated with a cocktail of known pro-fibrotic cytokines, namely TGFβ1, TNFα, and Angiotensin II, and the nephrotoxic compound polymyxin B. The compounds used to induce fibrosis in epithelial cells and fibroblasts in the context of this *in vitro* model act on specific cell signalling pathways that are activated upon binding of TGFβ1, TNFα, and angiotensin II. Canonical TGFβ1 signalling is mediated by Smad. MAPK is an effector of the pathway and could be a good marker to show that the pathway is being activated in the epithelium (Wrana & Attisano, 2000). NF-kB is an inducible transcription factor, induced by TNFα binding to specific receptors. It causes proliferation in renal fibroblasts, mediates inflammation in the renal parenchyma and is linked to hypertension in the kidney since it enhances the effects of angiotensin II on the renin-angiotensin-aldosterone system (RAAS). NF-kB is therefore a marker of TNFα-mediated

pathways activation (Zhang & Sun, 2015). Angiotensin II seem to induce apoptosis and autophagy in the proximal tubule in rodent models. These effects are mediated via the induction of TGFβ1 and ROS production. However, a specific mediator of angiotensin II action on the RAAS could be myeloid differentiation protein-2 (MD2) which seems to be a significant contributor to the hypertension-induced renal injury (Z. Xu et al., 2017). It is essential to acknowledge that the doses of pro-fibrotic compounds used to treat both hPTC and HRF in mono- and co-culture are supraphysiological as to obtain a measurable dose-response relationship between the insult and the biological effects measured in the *in vitro* models, and that the proposed assays to do include positive controls that highlight activation of said cell signalling pathways.

To investigate the fundamental maladaptive process of cell cycle dysregulation in renal fibrosis, cell proliferation is monitored both in hPTC and HRF via EdU (5-ethynyl-2'-deoxyuridine) incorporation assay. The percentage of cells incorporating EdU in the DNA, hence in S-phase of the cell cycle, is measured via flow cytometry after treatment with pro-fibrotic compounds. Concomitantly with proliferation and cell cycle dysregulation, apoptosis and necrosis occur when cells of the renal milieu undergo cytokine stimulation (Thomas et al., 1998); therefore, these two processes are monitored via Annexin V-FITC / Propidium Iodide (PI) flow cytometry assay, where Annexin V-FITC is binding to phosphatidylserine residues translocated to the cell surface at early apoptotic stages and PI is staining necrotic cells. Cellular energy metabolism regulation is key for maintaining overall normal renal function; thus, this is highly controlled especially in cells with high metabolic needs such as renal tubular epithelial cells. Specifically, healthy proximal tubule cells contain many mitochondria and utilise most of the adenosine triphosphate (ATP) produced in the kidney. Perturbation of metabolic pathways due to cytokine- and drug-induced renal injury leads to a phenomenon known as metabolic reprogramming, whereby proximal tubule cells shift from mitochondrial oxidative phosphorylation to aerobic glycolysis. Strong evidence supports the theory that alterations in metabolic pathways in both renal epithelial cells and fibroblasts lead to renal fibrosis (Zhu et al., 2021); therefore, the proposed *in vitro* model of renal fibrosis is assayed to assess cell viability after pro-fibrotic treatment via intracellular ATP measurement. As a measurement of epithelial barrier function disruption, trans epithelial electrical resistance (TEER) is measured in hPTC in co-culture with HRF after treatment with pro-fibrotic compounds alone and in combination. Finally, the model is characterised from a histological standpoint for each cell type, where three biomarkers relative to renal fibrosis are considered, namely tight junction markers ZO-1 and E-Cadherin, and mesenchymal marker vimentin for hPTC; extracellular matrix markers collagen I and fibronectin, and myofibroblast marker α smooth muscle actin (αSMA) for HRF.

Aims

The non-contact co-culture 3D in vitro model of the proximal tubule interstitial interface comprising renal fibroblasts and proximal tubule cells has been chosen and characterised as explained in **Chapter 4** to establish an *in vitro* model of renal fibrosis for high throughput screening (**Figure 5.1**). To our knowledge, studies regarding multicellular 3D models of the

proximal tubule interstitial interface suitable for these scopes have not been published yet. Thus, the objectives of this chapter are:

- To establish conditions of culture for hPTC and HRF in mono- and co-culture which allow for treatment with pro-fibrotic compound
- To induce phenotypical changes in hPTC and HRF that resemble the hallmarks of progressive renal fibrosis *in vivo* via TGFβ1, TNFα, angiotensin II, and polymyxin B treatment
- To develop high throughput assays to measure the induced phenotypical changes in terms of cell health, cell cycle, EMT/pEMT markers, ECM deposition, and soluble biomarkers release
- To establish dose-response curves that display the relationship between the measured endpoints and the dose of pro-fibrotic treatments

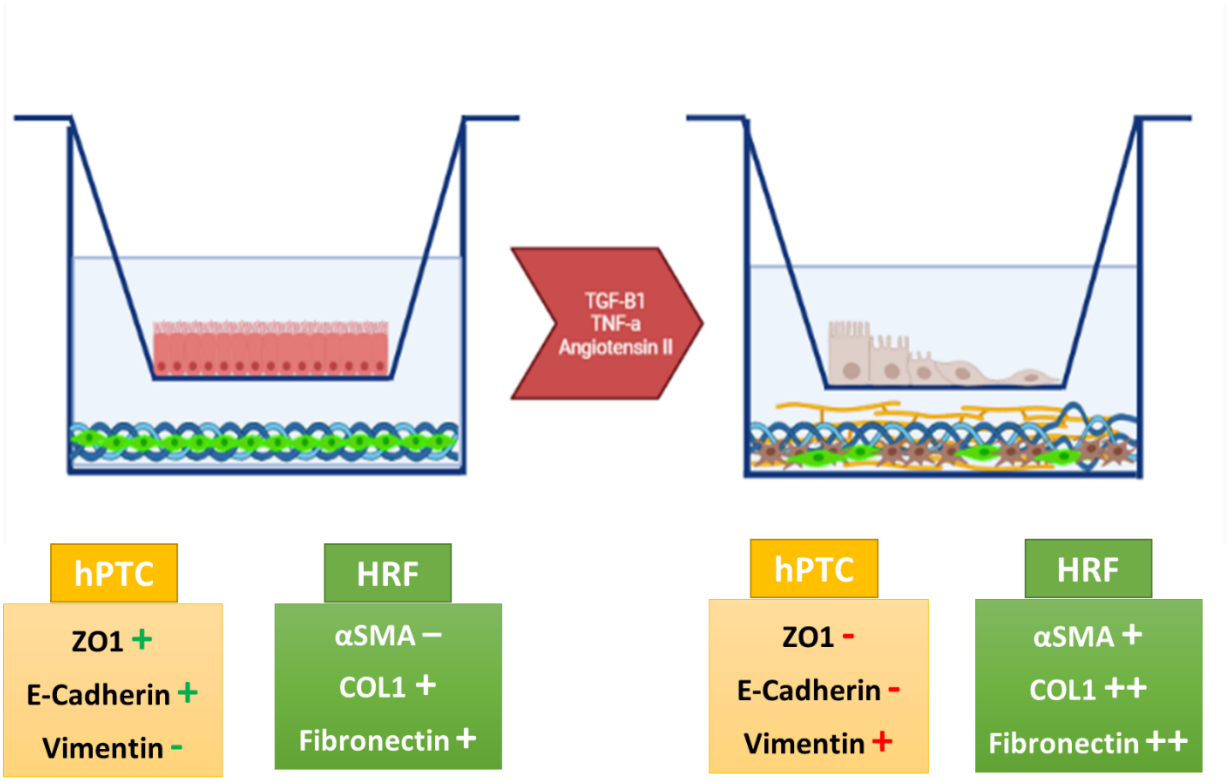

Figure 5.1. Graphical depiction of renal fibrosis assay platform development of multi-well inserts.

5.2 Synthetic extracellular matrix BiogelX™ RGD halts fibroblast-to-myofibroblast activation and ECM deposition in human renal fibroblasts.

A large body of clinical evidence indicates that renal fibrosis can be pinpointed as a histological phenomenon which involves *de novo* extracellular matrix deposition in the renal parenchyma. In the histopathology field, the word *sclerosis* is used to define a hardening of a biological tissue, which in the case of renal tubule-interstitial fibrosis is associated to wound healing and subsequent scarring (Bülow & Boor, 2019). The main drivers of extracellular matrix deposition in this maladaptive process are renal fibroblasts that under pro-fibrotic stimuli have transdifferentiated into contractile myofibroblasts. Fibroblast-to-myofibroblast activation is not only driven by immune-mediated stimuli involving pro-fibrotic cytokines, as recent investigations suggest that mechanical stimuli are a key factor in promoting the process. In synthesis, the microenvironment that the cells are embedded in influences cell fate as physical cues related to mechanical stress can be sensed by fibroblasts. Therefore, the renal parenchyma's *sclerosis* can be sensed by renal fibroblasts, which in the *in vitro* field can be translated into extracellular matrix stiffness (D'Urso & Kurniawan, 2020). *In vitro* studies carried out on breast tissue fibroblasts and cardiac fibroblasts have shown that stiffer synthetic ECMs that mimic pathological conditions of relevant organs lead to fibroblast-to-myofibroblast activation reflected in an increase in αSMA cellular content and larger cellular area, thus supporting the theory that the mechanical properties of ECM *in vivo* have an influence on fibroblast phenotype maintenance (Schwager et al., 2019).

In the context of developing a renal fibrosis *in vitro* assay platform which entails inducing the disease phenotype via pro-fibrotic cytokine treatment, it is essential to avoid accidental fibroblast-to-myofibroblast activation prior treatment. Therefore, primary human renal fibroblasts are cultured onto an array of commercially available synthetic hydrogels that resemble the mechanical properties of *in vivo* extracellular matrix. The trialled hydrogels are representative of a range of stiffnesses from 1 to 10 kPa and three of them include functionalised moieties to resemble the nanostructure of the *in vivo* ECM, namely RGD functionalisation (fibronectin) and GFOGER (collagen I). To reduce the stiffness of such hydrogels in order to obtain a rather soft matrix that would mimic the healthy tubule-interstitial microenvironment, the synthetic ECMs are diluted in deionised water at 0.1%, 0.01%, 0.001% v/v and the wells of a clear bottom black walled 96-well plate are coated with Manchester Biogels' PeptiGels® Alpha II, Alpha IV, Gamma II, Alpha IV RGD, BiogelX™ RGD, rat tail Collagen I. Subsequently, human renal fibroblasts are cultured to confluency on the array plate and αSMA expression, fibronectin and collagen I deposition are qualitatively and quantitatively compared between control condition (HRF on uncoated wells) and coated wells. Furthermore, the presence of the hydrogel must allow for immunofluorescence staining and imaging, in particular unspecific binding of primary and secondary antibodies and trapping of such compounds in the synthetic ECM has to be avoided by selecting the appropriate dilution factor as initial experiments have shown that the thickness and viscosity of the coating can lead to artefacts when imaging the cells.

Array plates are imaged with high content imaging microscope Zeiss® CellDiscoverer7. Relevant protein expression on fluorescent stained HRF is quantified via a custom image

analysis workflow which is established via the image analysis software Zeiss® ZEN Pro using segmentation of cell nuclei based on Hoechst 33342 staining (object 1 – hierarchical) and segmentation of cell body based on αSMA, fibronectin, and collagen I expression (objects 2, 3, 4 – non-hierarchical). Mean intensity fluorescence per cell body – or protein content per cell – is quantified and plotted in relationship to the type of hydrogel coating and dilution factor (**Figure 5.2**). Quantification of the images highlighted that there is a degree of activation of the HRF population in the uncoated control condition, thus rendering the selection of a coating hydrogel to reduce culture vessel stiffness essential. Although from the quantitative analysis none of the hydrogels considered seem to significantly reduce ECM deposition and *de novo* α-SMA expression (**Figure 5.3**), qualitative observation of the images indicates that the presence of BiogelX™ RGD at dilution 0.001% v/v seems to halt fibroblast activation in terms of *de novo* expression of αSMA and ECM deposition in terms of fibronectin and collagen I as compared to the uncoated control, as displayed in **Figures 5.4 to 5.6**. Primary and secondary antibody specificity towards examined markers is verified by "secondary antibody only" negative control images in **Figure 5.7.** Therefore, these data suggest that primary human renal fibroblasts transdifferentiate to contractile myofibroblasts when cultured on uncoated cell culture vessels, thus requiring a synthetic extracellular matrix coating to maintain healthy non-fibrotic phenotype until intentional pro-fibrotic cytokine treatment is applied to the cell population. Hence, synthetic ECM BiogelX™ RGD at dilution 0.001% v/v is used to coat wells for HRF culture for all subsequent experiments in the context of the development of the renal fibrosis *in vitro* assay platform.

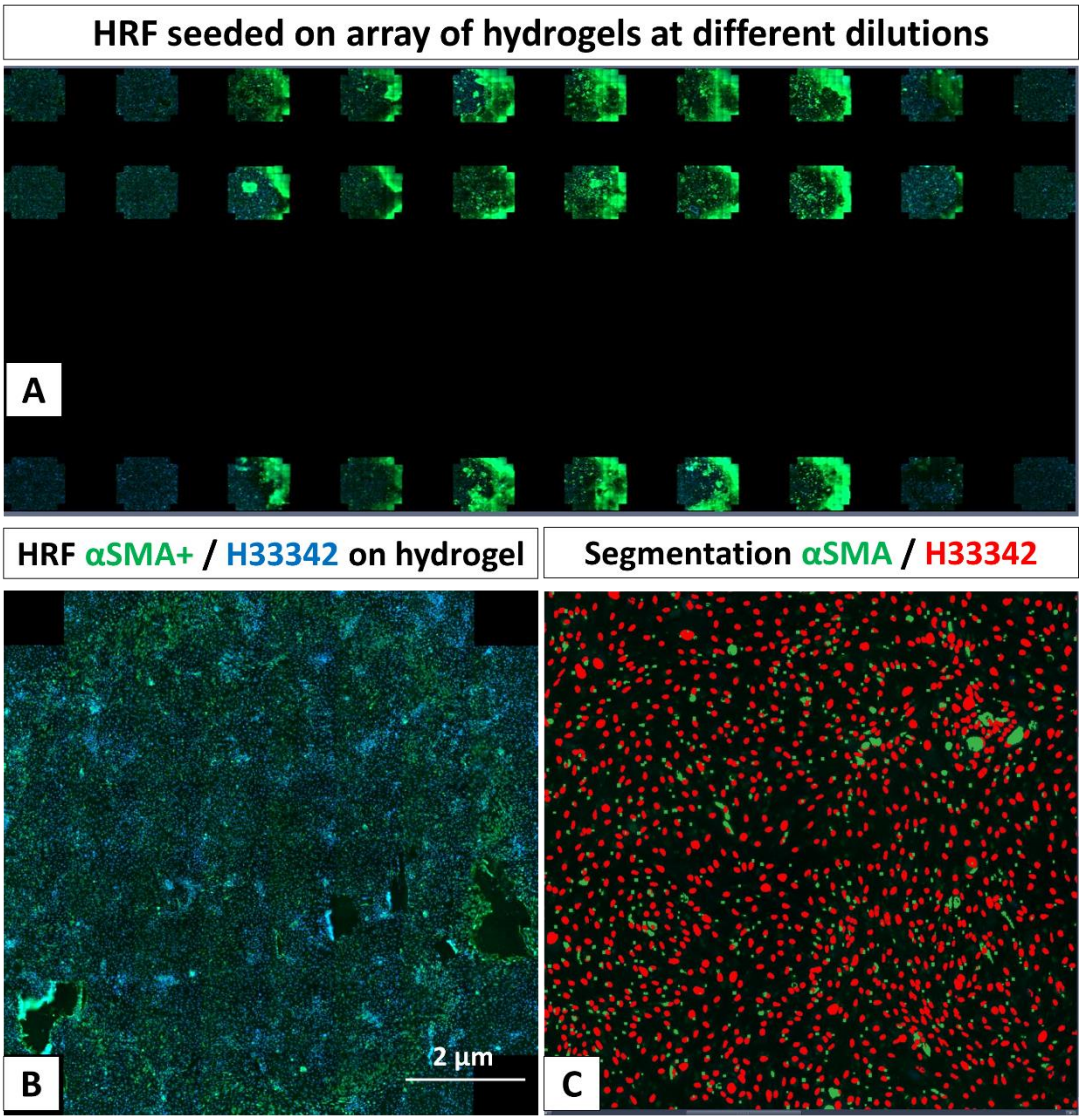

Figure 5.2. Example figures representing workflow followed to select appropriate hydrogel coating to halt fibroblast-to-myofibroblast activation of HRF. [A] Cells are seeded onto a clear bottom 96-well black walled plate coated with an array of synthetic ECM, and [B] their positivity to αSMA, collagen I, and fibronectin is[C] quantified as mean intensity fluorescence per cell via segmentation (scale bar=2 µm).

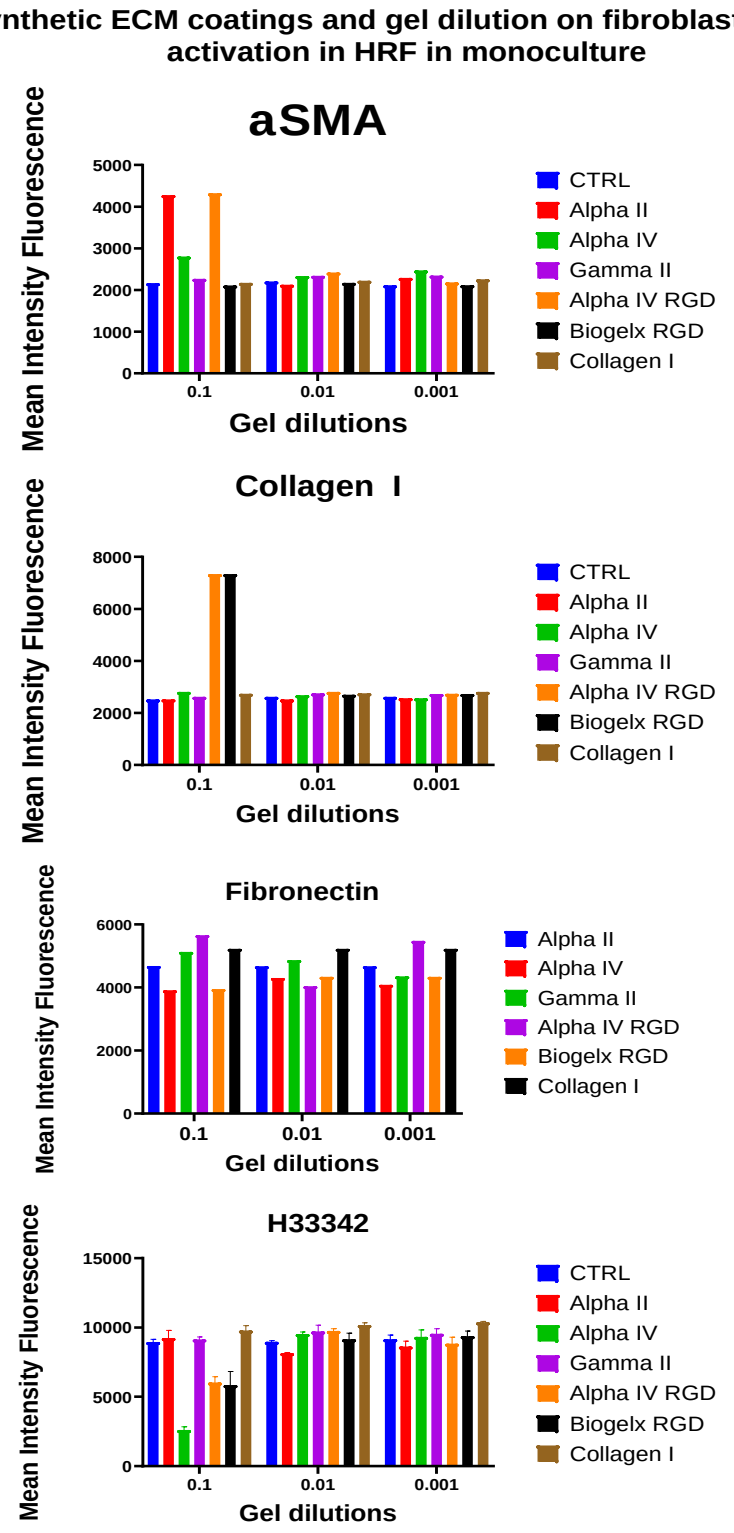

Figure 3. Quantification of mean intensity fluorescence of immunofluorescence staining of biomarkers associated with fibroblast-to-myofibroblast transition performed on HRF cultured to confluency on 96-well black walled plates on synthetic ECMs at increasing concentrations. (A) nuclear stain Hoechst 33342, (B) α smooth muscle actin (αSMA), (C) Collagen I, (D) Fibronectin. Experiment performed on one biological replicate (n=1); error bars in graph [A] represent SD among technical repeats.

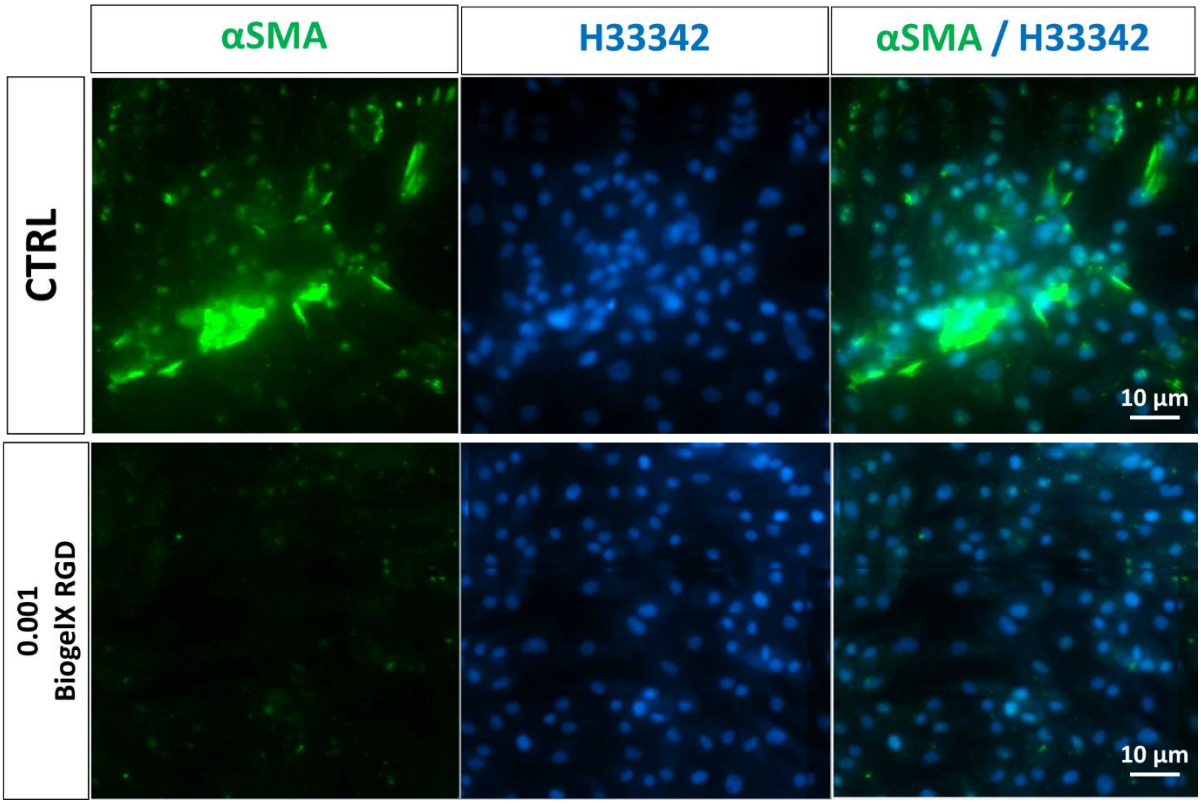

Figure 5.4. Fluorescence images representing HRF cultured onto cell culture treated plastic (clear bottom 96-well black walled plate) and onto wells coated with 0.001% BiogelX RGD showing positivity to myofibroblast marker αSMA (scale bars=10 µm)..

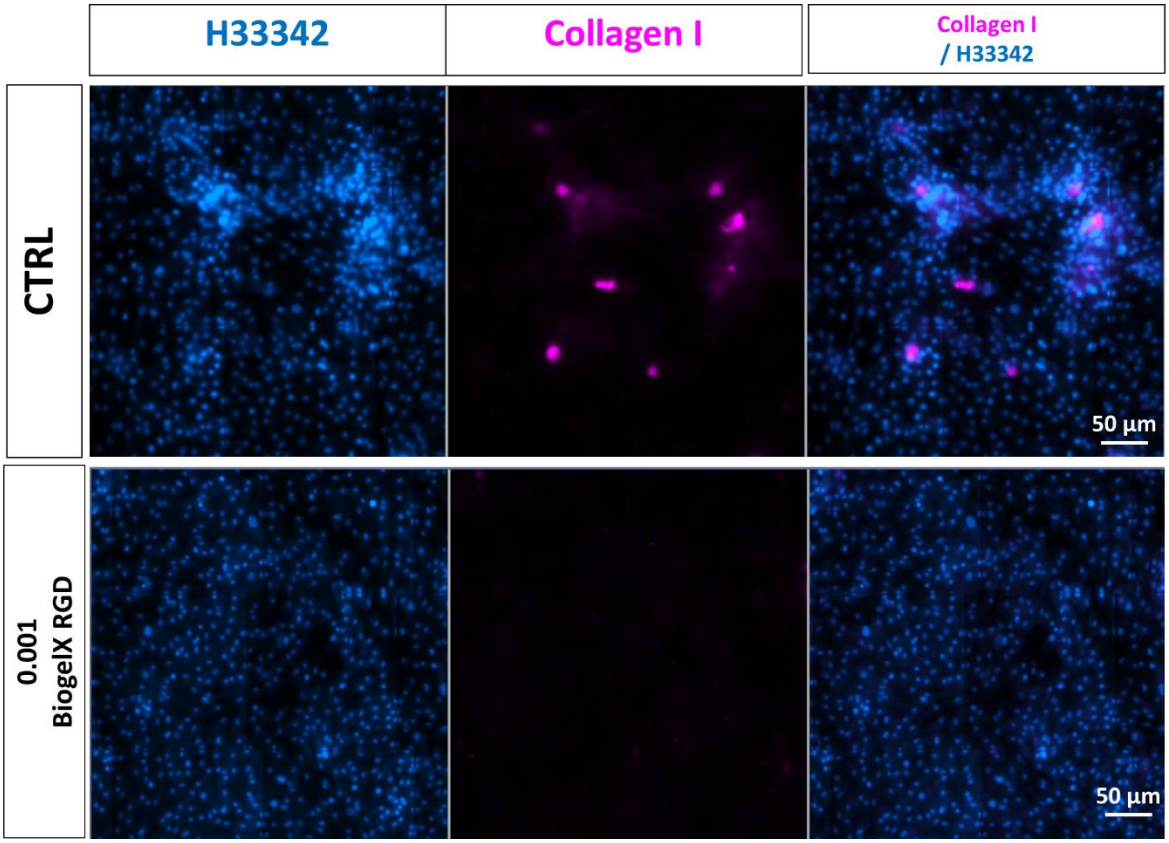

Figure 5.5. Fluorescence images representing HRF cultured onto cell culture treated plastic (clear bottom 96-well black walled plate) and onto wells coated with 0.001% BiogelX RGD showing positivity to ECM marker collagen I (scale bars=50 µm).

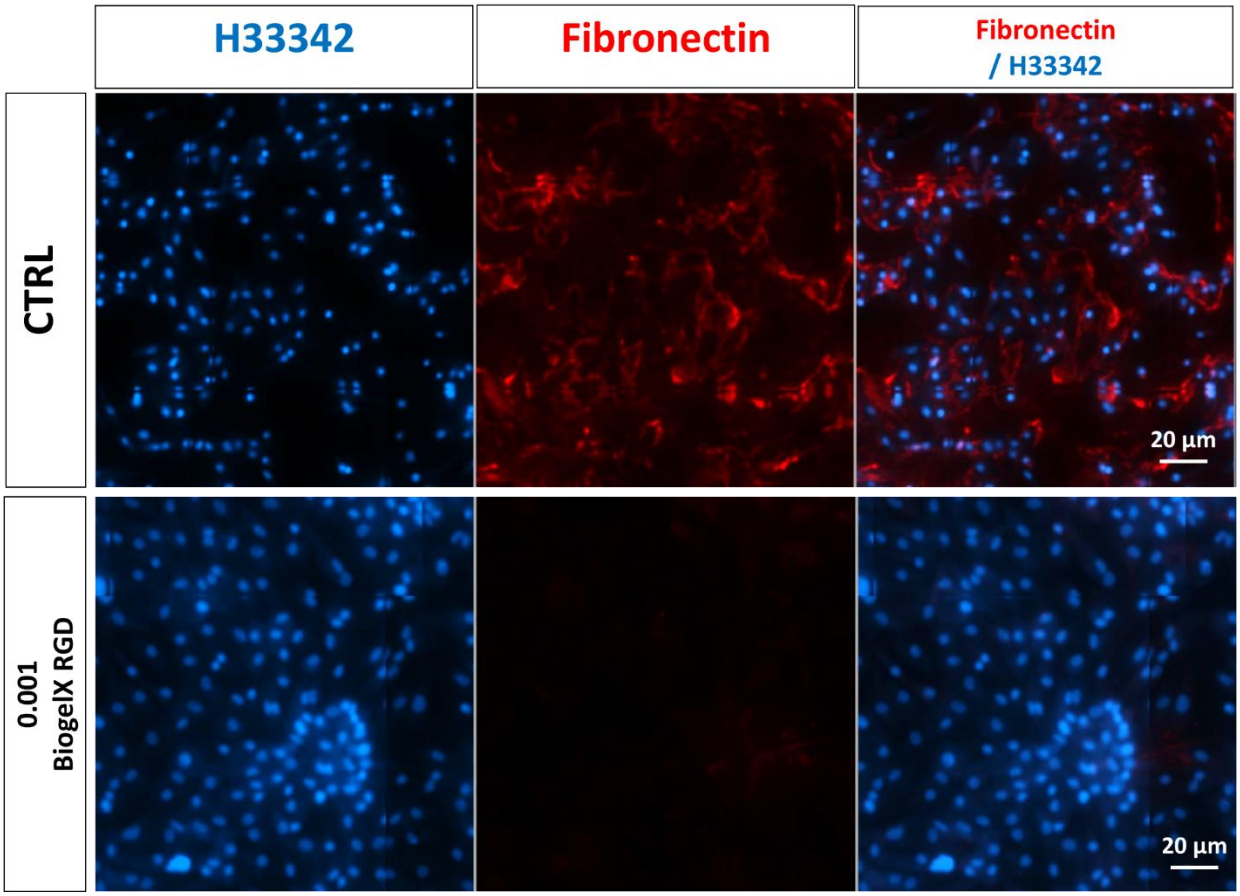

Figure 5.6. Fluorescence images representing HRF cultured onto cell culture treated plastic (clear bottom 96-well black walled plate) and onto wells coated with 0.001% BiogelX RGD showing positivity to ECM marker fibronectin (scale bars=20 µm).

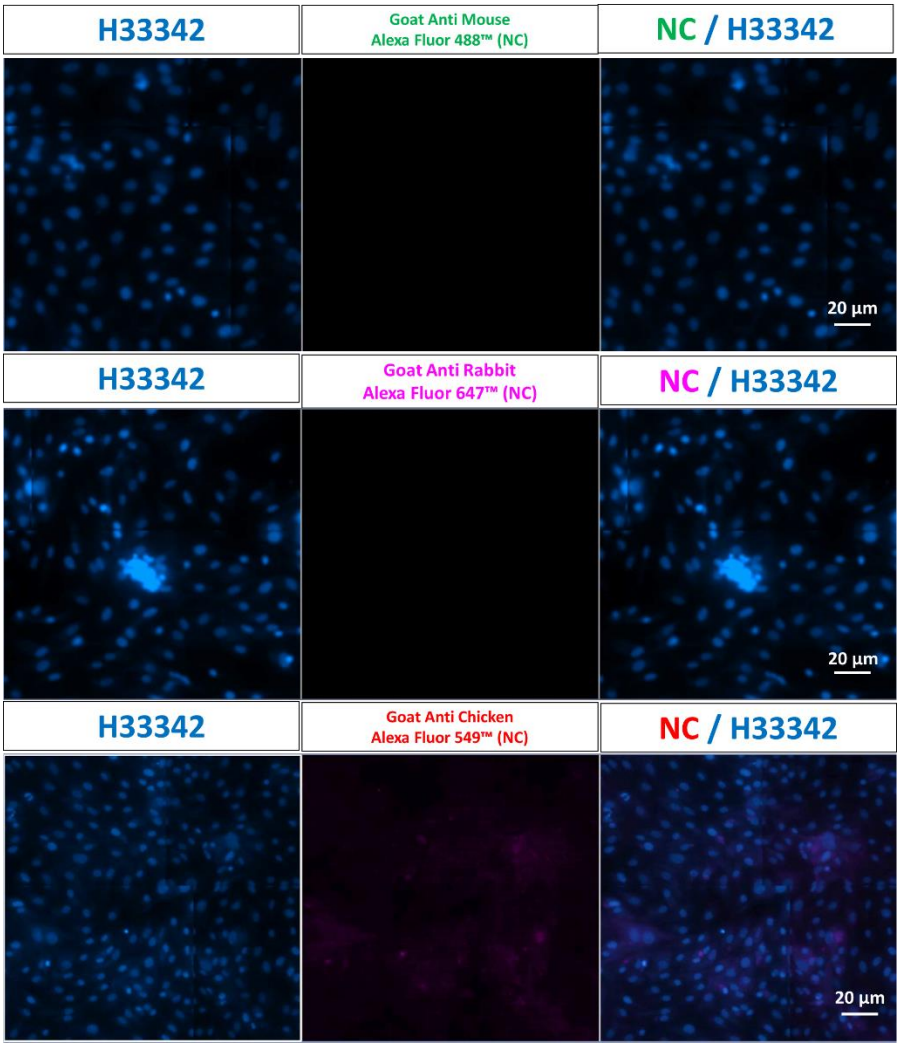

Figure 5.7. Fluorescence images representing HRF "secondary antibody only" negative controls, showing negativity to unspecific binding of Goat Anti Mouse Alexa Fluor 488™, Goat Anti Rabbit Alexa Fluor 647™, Goat Anti Chicken Alexa Fluor 594™ (scale bars=20 µm).

5.3 hPTC and HRF survival time in culture.

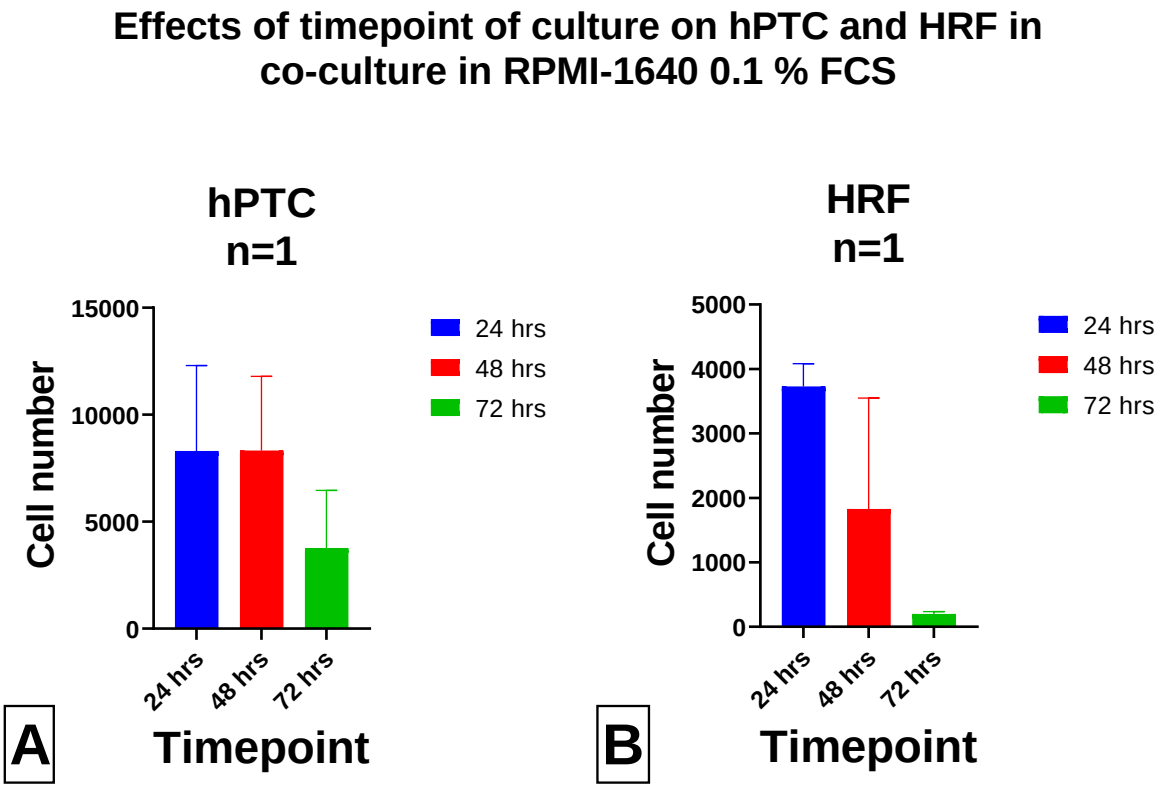

Figure 5.8. Quantification of cell number per well based on cell segmentation in hPTC and HRF in co-culture cultured in RPMI-1640 0.1% FCS on 96-Transwell plates cultured for 24, 48 and 72 hours. Experiment performed on one biological replicate and two technical replicates per condition; error bars represent SD.

To determine at which timepoint measurements of endpoints relevant to the development of the renal fibrosis *in vitro* assay platform would be possible, survival time in co-culture of hPTC and HRF is established by quantifying cell number per well via segmentation as described in **2.7.9.** Once both hPTC and HRF monolayers have reached confluency, media is changed from REGM™ / FGM™ to RPMI-1640 0.1% FCS for 72 hours in total and two wells per timepoint are fixed and immunofluorescence stained at 24, 48, and 74 hours. Two cell culture media as vehicle treatment were compared in order to select the one which would interfere the least with the pro-fibrotic treatments, therefore cell viability assay measuring changes in intracellular ATP was used to detect whether using RPMI-1640 0.1% FCS or REGM™ (Renal Epithelial Growth Medium) would yield to different treatment effects in the presence of pro-fibrotic compounds. Treatments carried by RPMI-1640 0.1% FCS induced a lower variability between datapoints, therefore this type of cell culture media was used to carry out all the following experiments.

The data displayed in **Figure 5.8** refer to an experiment performed on one biological replicate, and it suggests that cell number per well decreases over days of culture when both hPTC and HRF are exposed to RPMI-1640 0.1% FCS. Especially for HRF (**Figure 5.8, [B]**), cell number per well drops below ~2000 cells/well after 48 hours, and to 1000 cells/well after 72 hours of

exposure to RPMI-1640 0.1% FCS. Therefore, since hPTC and HRF seem to survive after 24 hours in vehicle treatment medium RPMI-1640 0.1% FCS, but to die at longer timepoints probably due to the low concentration of serum in the medium, this timepoint was selected to measure all endpoints investigated via assays developed on the renal fibrosis *in vitro* model.

5.4 hPTC in monoculture migrate into nodules after pro-fibrotic treatment

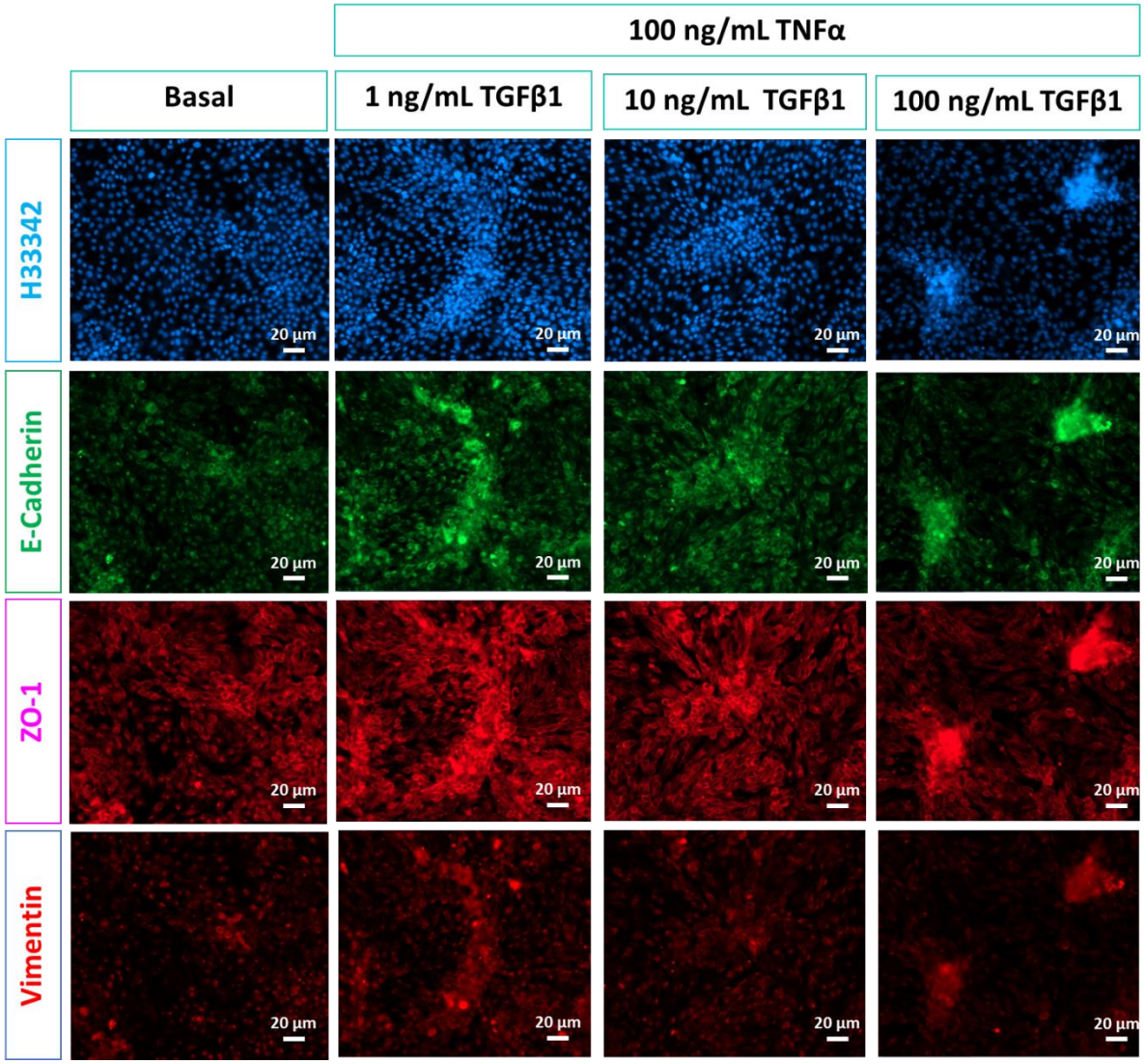

Figure 5.9. Fluorescence images of hPTC monolayers in monoculture cultured on black walled 96-well plates treated with a fixed concentrarion of TNFα (100 ng/mL TNFα) and increasing concentrations of TGFβ1 for 24 hours. Cells were fixed and immunofluoresce-stained with nuclear stain Hoechst 33342, and antibodies against tight junction markers ZO-1 and E-Cadherin, and mesenchymal marker vimentin. Exposure times and focus were kept constant across the plate. Images were acquired at 20X magnification on Zeiss CellDiscoverer7 (scale bars=20 µm).

Now that the conditions and timepoints of treatment for both hPTC and HRF are established, the aim is to perform a preliminary experiment to investigate whether epithelial cells effectively respond to treatment with pro-fibrotic compounds from a qualitative standpoint.

The first experiments on hPTC were run on monolayers cultured on black walled 96-well plates which were imaged with the high content microscope Zeiss CellDiscoverer7. For structural reasons, this microscope has a limited focal range for the 10X and 20X objectives therefore it has not been initially possible to image cells in co-culture on 96-Transwell plates and, since the ImageXpress Pico with wider focal range has become available for use later in the course of this project, preliminary qualitative experiments were run on cells in monoculture.

Confluent hPTC monolayers are treated with combinations of pro-fibrotic compounds TGFβ1, TNFα, and angiotensin II at increasing concentrations, as described in **2.7.1.** After 24 hours of treatment, they were fixed and immunofluorescence stained with antibodies against tight junction markers E-Cadherin and ZO-1, and the mesenchymal marker vimentin, while the cell nuclei are counterstained with Hoechst 33342. After pro-fibrotic treatment, we expected to detect epithelial barrier disruption denoted by loss of tight junction markers and *de novo* acquisition of vimentin, which would indicate epithelial-to-mesenchymal transition. **Figure 5.9** displays hPTC treated with a fixed concentration of TNFα (100 ng/mL) and increasing concentrations of TGFβ1 (1, 10, 100 ng/mL) for 24 hours, as this appeared to be the compound combination that lead to the most striking change observed between treated wells and control wells. Whilst the basal untreated cells show epithelial monolayer formation with tight junction expression and limited expression of vimentin, the main feature of these images is the noticeable migration of treated epithelial cells into aggregates or clumps, which from now on will be referred to as *nodules.* The expression of E-Cadherin and ZO-1 seems to be upregulated within the boundaries of the nodules whereas it is downregulated in the remaining monolayer beyond the nodular periphery. This effect seems to be more noticeable as the treatment concentration increases. Furthermore, the nodules express vimentin too. Specificity of the primary antibodies in use is confirmed by 'secondary antibody only' negative controls shown in **Figure 5.10**.

These nodules not only seem to be produced by the migration of epithelial cells into clumps, but also the cell nuclei images suggest that there is an increase in the number of cells that end up forming these aggregates as compared to the basal image. These observations beg the questions of whether cell numbers might increase after pro-fibrotic treatment and whether there is a dose-response correlation between the concentration of compounds to which the cells are exposed to and the increase in cell number, and whether this effect is embedded in the apparent epithelial nodule formation herby highlighted. The next sections will be aiming at answering these questions through the development of novel assays to uncover the underlying mechanisms that lead to the observed effects.

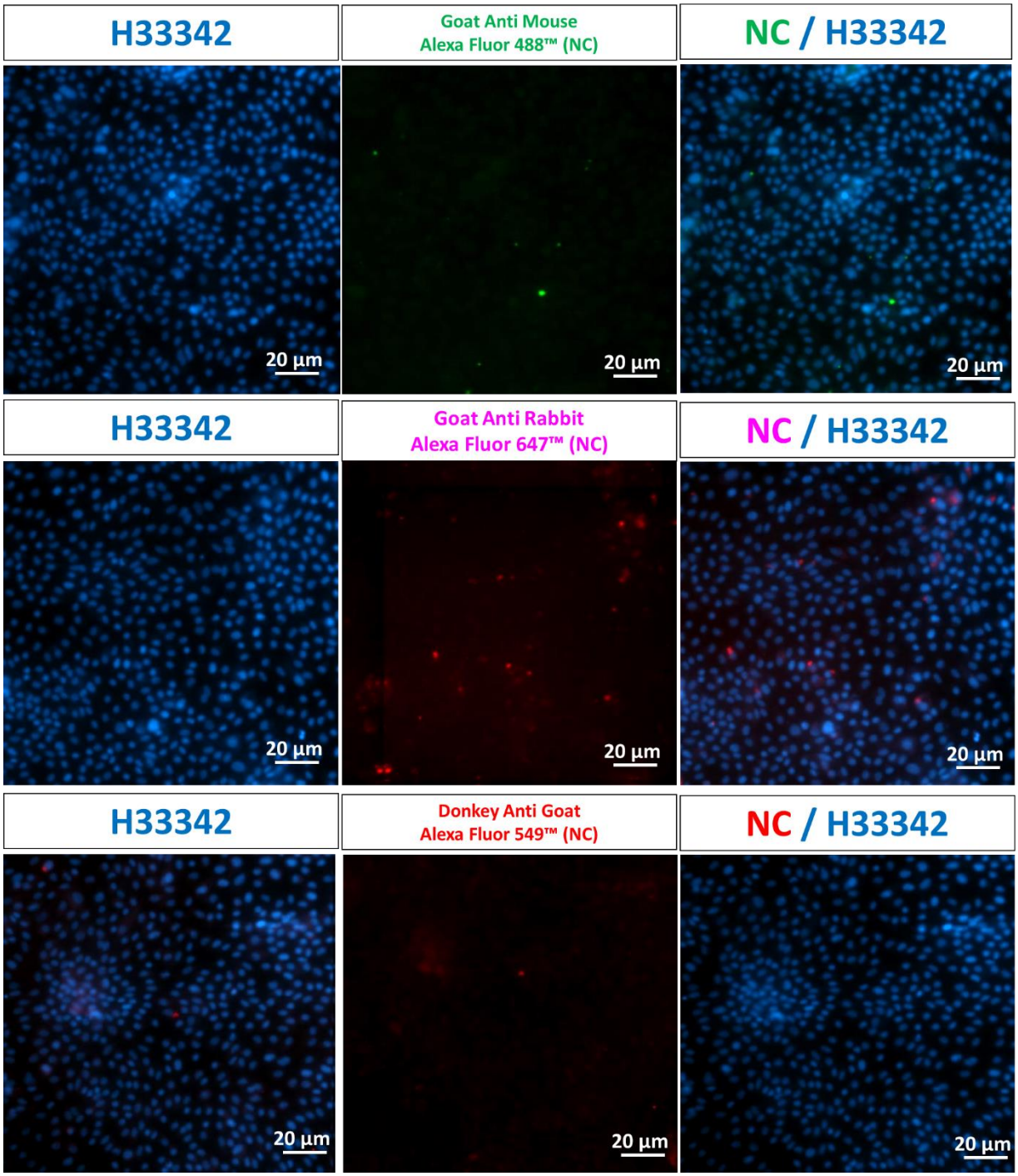

Figure 5.10. Fluorescence images representing hPTC "secondary antibody only" negative controls, showing negativity to unspecific binding of Goat Anti Mouse Alexa Fluor 488™, Goat Anti Rabbit Alexa Fluor 647™, Donkey Anti Goat Alexa Fluor 594™ (scale bars=20 µm)..

5.5 Pro-fibrotic treatment leads to changes in hPTC and HRF cell number, cell viability, and TEER in monoculture and co-culture

To assess changes in cell number in both hPTC and HRF after pro-fibrotic treatment, an assay is developed as described in **2.7.8** via high content imaging, using the microscope ImageXpress Pico and the image analysis software CellReporterXpress. The aim of these experiments is not only to investigate the correlation between concentration of pro-fibrotic compound treatments and cell number in hPTC and HRF, but also to evaluate whether conditions of culture of both cell types, in terms of monoculture and co-culture, influence the response of the cell population to the pro-fibrotic stimuli. Experiments in mono- and co-culture are performed on three biological replicates per condition.

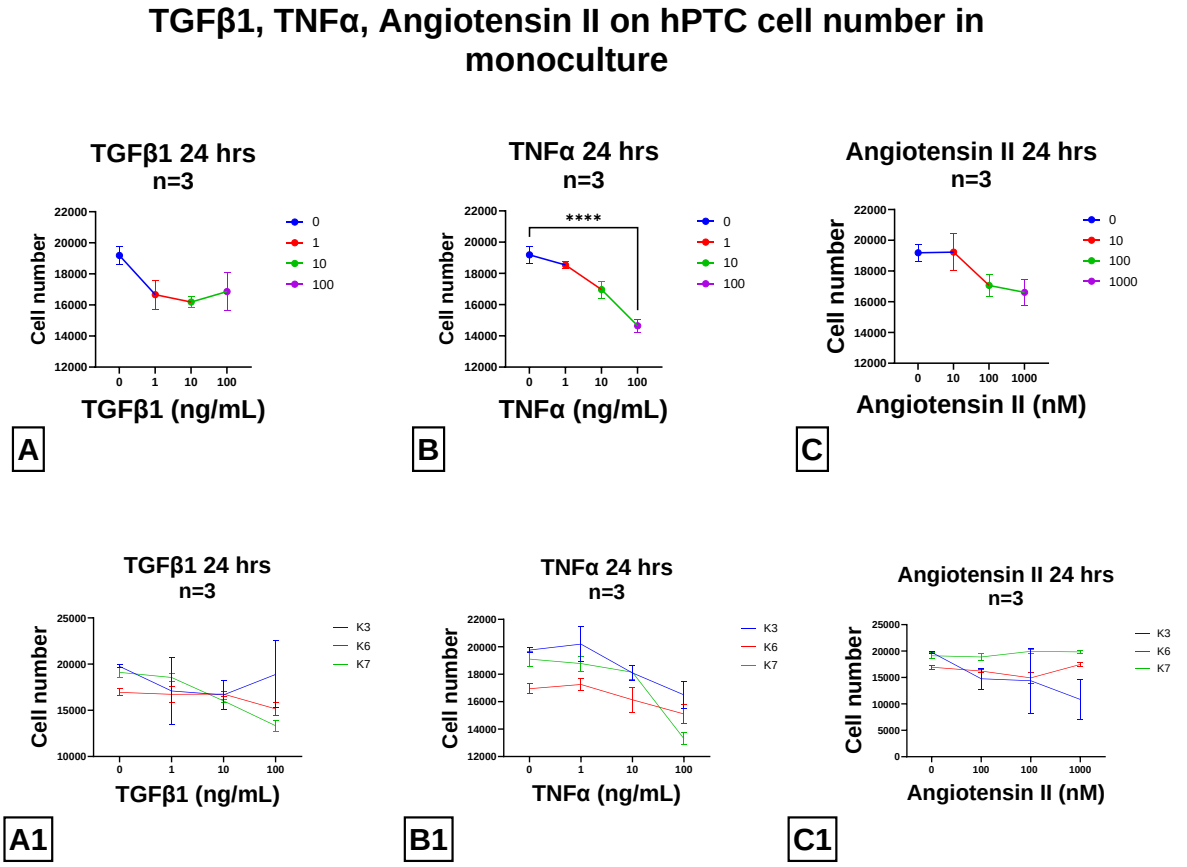

*Figure 5.11. Effects of [A] TGFβ1, [B] TNFα, [C] Angiotensin II 24 hours treatment on cell number in hPTC monolayers cultured on black walled 96-well plates. Each data point is the mean of three biological (K3, K6, K7) plotted individually in [A1], [B1], [C1]. TNFα in [B] induces a significant dose-dependent decrease in hPTC cell number. Error bars represent S.E.M. Statistical significance depicted as '****' signifies p < 0.0001.*

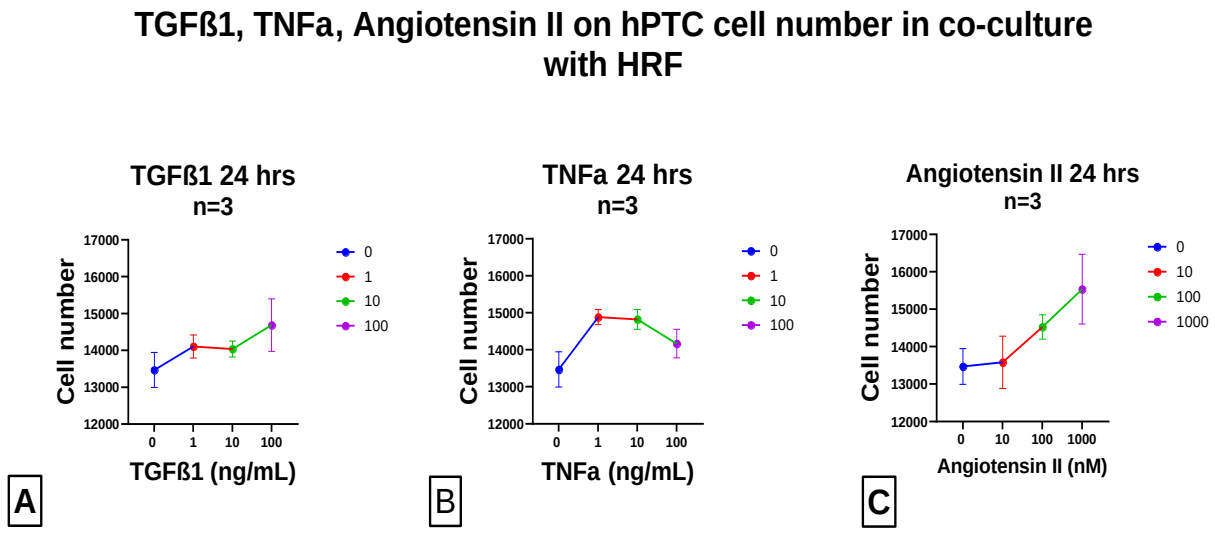

Figure 5.12. Effects of [A] TGFβ1, [B] TNFα, [C] Angiotensin II 24 hours treatment on cell number in hPTC monolayers cultured on 96-Transwell inserts. Each data point is the mean of three biological (K8, K9, K10) and two technical replicates. Error bars represent S.E.M.

Considering the dose-response curves displayed in **Figures 5.11 and 5.12**, it is observable that treatment with the same compound in hPTC in different culture conditions leads to strikingly different trends in terms of the relationship between dose and response (cell number / well). TGFβ1 treatment leads to a decrease in cell number per well in hPTC in monoculture, whereas in co-culture it leads to cell number increase, although not significantly [**Figure 5.11 [A], Figure 5.12 [A]**). TNFα treatment induces a significant decrease in cell number in hPTC in monoculture (**Figure 5.11 [B]**) and leads to non-significant cell number decrease in co-culture (**Figure 5.12 [B]**); while angiotensin II treatment leads to a descending trend in cell number per well in monoculture (**Figure 5.11 [C]**), whereas in co-culture it leads to an ascending trend (**Figure 5.12 [C]**). In summary, these dose-response curves show that pro-fibrotic treatment of hPTC in monoculture leads to a general decrease in cell number per well, while the same treatments in hPTC in co-culture lead to an increasing trend in cell number per well.

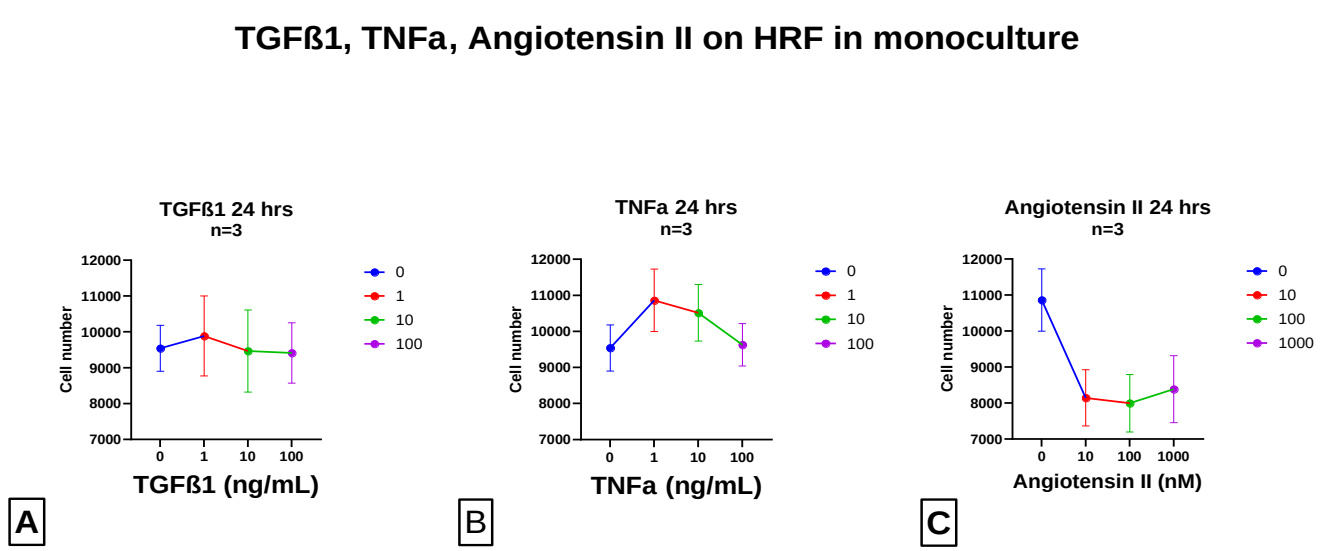

Figure 5.13. Effects of [A] TGFβ1, [B] TNFα, [C] Angiotensin II 24 hours treatment on cell number in HRF monolayers cultured on black walled 96-well plates. Each data point is the mean of three biological (K3, K6, K7) and two technical replicates. Error bars represent S.E.M.

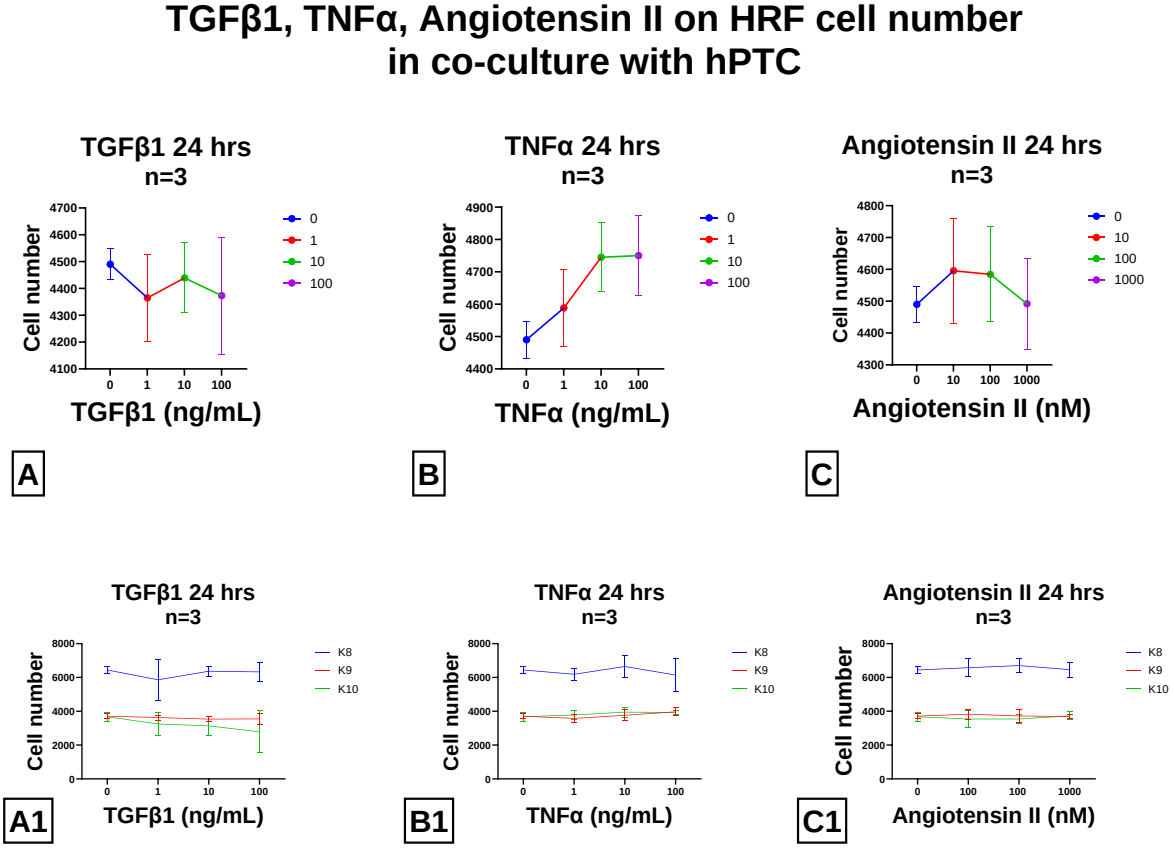

Figure 5.14. Effects of [A] TGFβ1, [B] TNFα, [C] Angiotensin II 24 hours treatment on nodule number in HRF monolayers cultured on 96-Transwell well bottoms. Each data point is the mean of three biological (K8, K9, K10) plotted individually in [A1], [B1], [C1]. Error bars represent S.E.M.

To investigate whether the variations in cell numbers seen in epithelial cells after pro-fibrotic treatment occur also in human renal fibroblasts, the same dose-response curves are plotted for HRF in mono- and co-culture and they are shown in **Figure 5.13 and 5.14**. None of the curves show statistically significant differences between untreated control and increasing concentrations of treatments since the biological variability between the three biological replicates is too great to measure any changes in cell number per well as the concentration of compounds increase. Therefore, other assays are developed and used to monitor changes in the HRF cell population in the renal fibrosis *in vitro* model, as it will be described in the next sections.

CellTiter-Glo® Luminescent Cell Viability Assay is another method used to monitor cell number and viability of a cell population which employs the measurement of intracellular ATP read and plotted as luminescence. To investigate the effects of pro-fibrotic treatments on cell viability of hPTC and HRF in mono- and co-culture, dose-response curves are plotted for each of the compounds used in all of the culture conditions. When the assay is performed on two biological replicates of hPTC in monoculture (**Figure 5.15 [A], [B], [C]**), no statistically significant changes between doses can be observed because of the strikingly different response to treatments displayed by the two biological replicates (**Figure 5.15 [A1]/[A2], [B1]/[B2], [C1]/[C2]).**

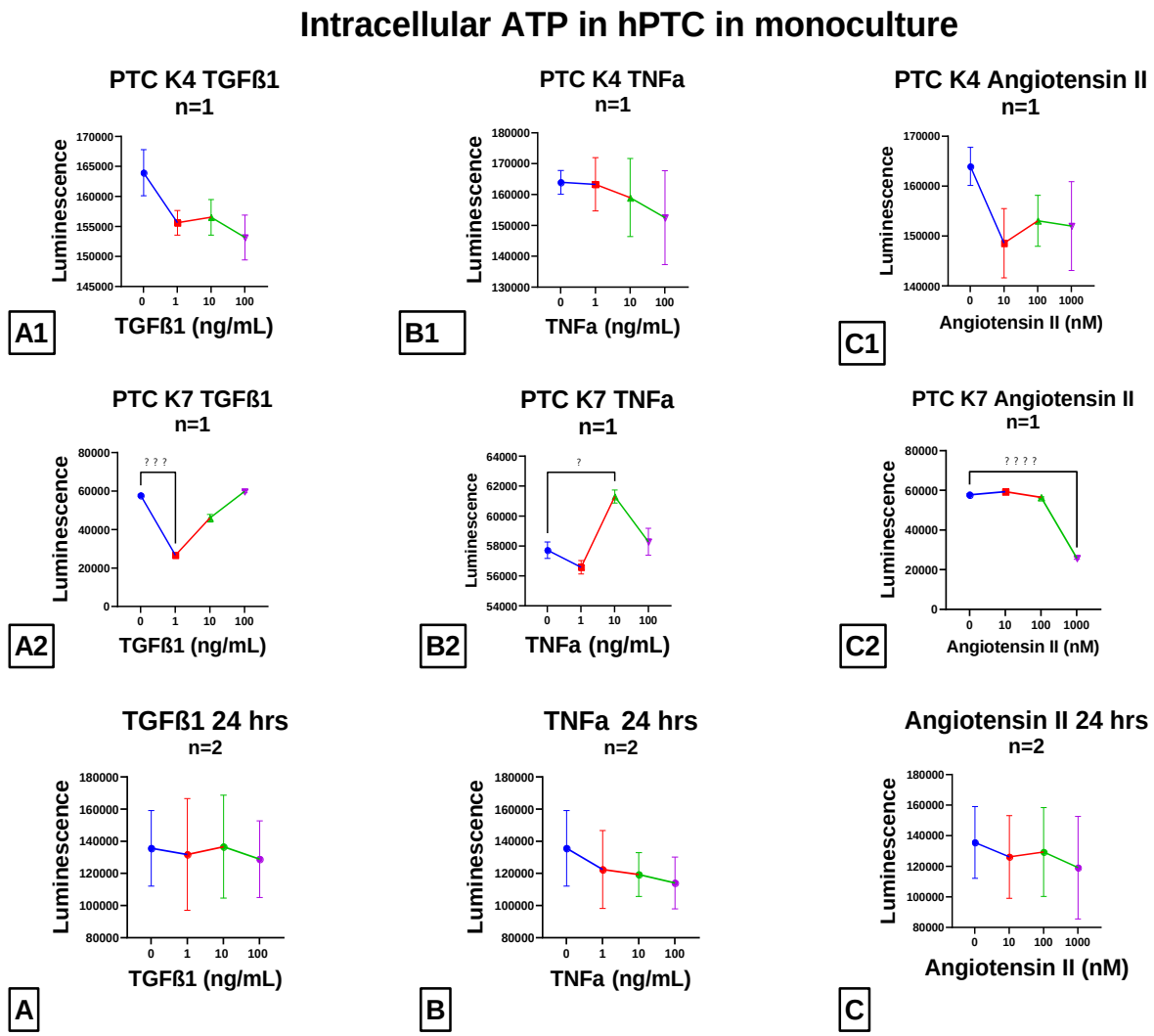

*Figure 5.15. Cell viability assay CellTiter-Glo measuring intracellular ATP via luminescent signal performed after 24 hours of treatment with increasing concentrations of TGFß1, TNFα, and Angiotensin II in hPTC in monoculture [K4, K7] on 96-well black walled plates. Patient-patient variability can be appreciated by the different responses to pro-fibrotic drugs shown in A1, A2, B1, B2, C1, C2. Datapoints represent the mean between three technical repeats (A1, A2, B1, B2, C1, C2) and two biological repeats (A, B, C) while error bars represent SD (n=2). Statistical significance depicted as '****' signifies p < 0.0001, '***' p < 0.001, '*' p < 0.05.*

Conversely, when the cell viability assay is performed on three biological replicates of hPTC in co-culture (**Figure 5.16**), the dose-response curves are able to take into account the biological variability between replicates, which is shown by the ability of the assay to detect statistically significant changes between the luminescence signals recorded after stimulation with different concentrations of compounds. Cells are treated with the three pro-fibrotic compounds of choice, plus polymyxin B which induces oxidative stress, cell injury, and apoptosis in tubular epithelial cells, and IGF-1 (insulin-like growth factor 1) which inhibits apoptosis and stimulates proliferation in tubular epithelial cells *in vitro* and *in vivo*. These two compounds are used in assays performed in the renal fibrosis co-culture model as 'positive' and 'negative' controls during assay development – their role will be determined by the

endpoint measured by the assay. Notably, TNFα (**Figure 5.16 [B]**) and the exogenous pro-fibrotic compound polymyxin B (**Figure 5.16 [E]**) are able to induce a significant decrease in cell viability in hPTC in co-culture.

Intracellular ATP in hPTC in co-culture

A

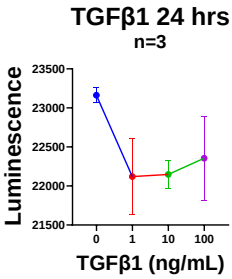

A1

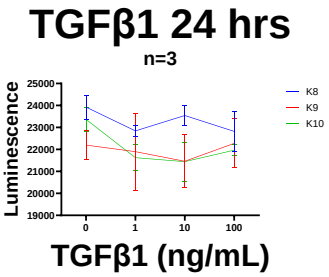

B

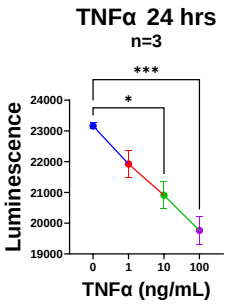

B1

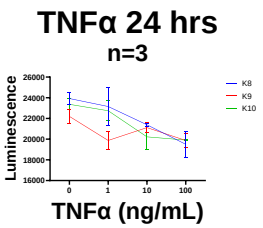

C

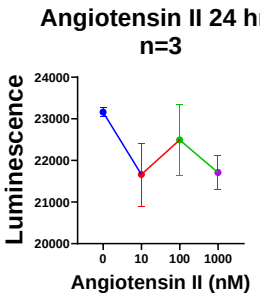

C1

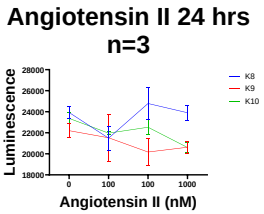

D

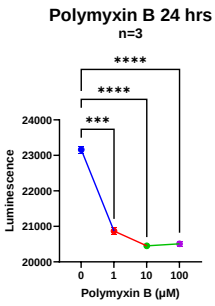

D1

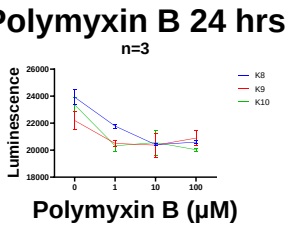

E

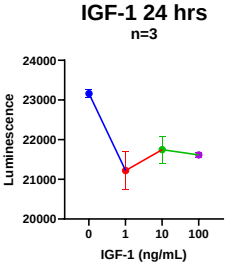

E1

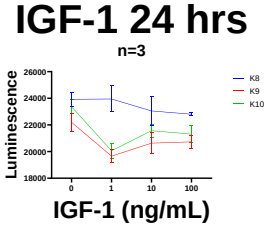

*Figure 5.16. Cell viability assay CellTiter-Glo measuring intracellular ATP via luminescent signal performed after 24 hours of treatment with increasing concentrations of TGFβ1, TNFα, Angiotensin II, IGF-1 and polymyxin B in hPTC in co-culture [K8, K9, K10] on 96-Transwell plates' well insert. Datapoints represent the mean between three biological repeats (A, B, C, D, E) while error bars represent SEM (n=3). TNFα and polymyxin B cause a significant dose-dependent decrease of intracellular ATP in hPTC in co-culture. Statistical significance depicted as '****' signifies p < 0.0001, '***' p < 0.001, '*' p < 0.05.*

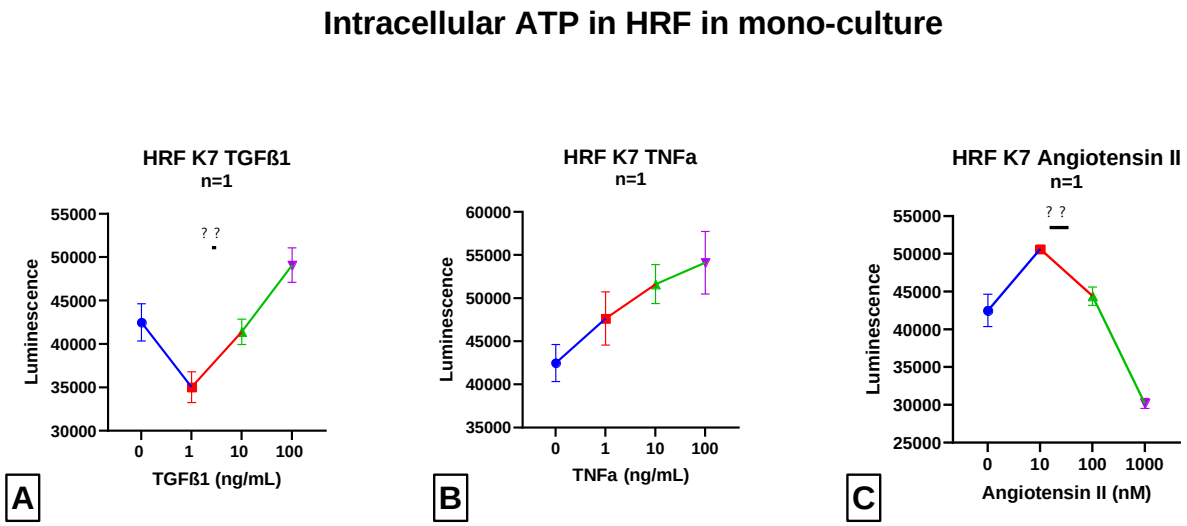

*Figure 5.17. Cell viability assay CellTiter-Glo measuring intracellular ATP via luminescent signal performed after 24 hours of treatment with increasing concentrations of TGFβ1, TNFα, and Angiotensin II in HRF in monoculture [K7] on 96-well black walled plates. Datapoints represent the mean between three technical repeats (A, B, C) while error bars represent SD (n=1). Statistical significance depicted as '**' signifies p < 0.01.*

Intracellular ATP in HRF in co-culture with hPTC

A

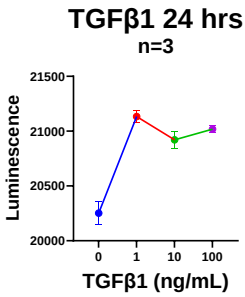

A1

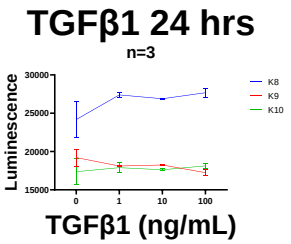

B

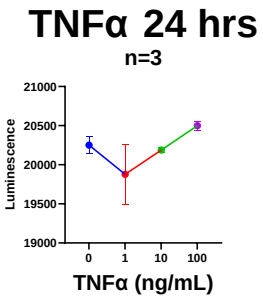

B1

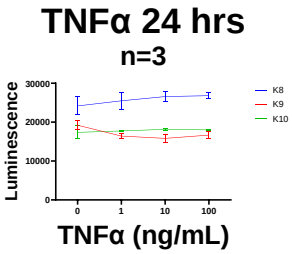

C

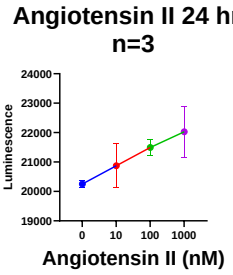

C1

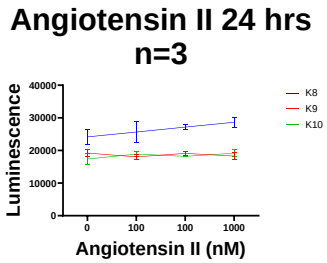

D

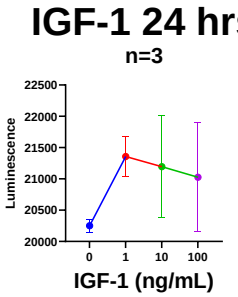

D1

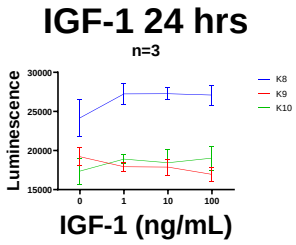

E

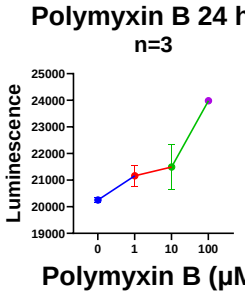

E1

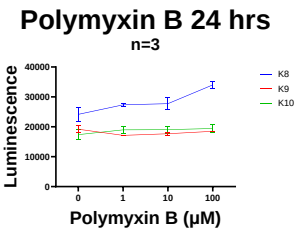

Figure 5.18. Cell viability assay CellTiter-Glo measuring intracellular ATP via luminescent signal performed after 24 hours of treatment with increasing concentrations of TGFβ1, TNFα, Angiotensin II, IGF-1 and polymyxin B in HRF in co-culture [K8, K9, K10] on 96-Transwell plates' well bottom. Datapoints represent the mean between three biological repeats (A, B, C, D, E) while error bars represent SEM (n=3).

The cell viability assay is also performed on HRF in mono- and co-culture. For technical reasons, the experiment is performed only on one biological replicate for the monoculture condition (**Figure 5.17**), so relevant statistical tests are performed among technical replicates within one biological replicate. The dose-response curves displayed in this figure suggest that TGFβ1 and angiotensin II induce measurable changes in cell viability in HRF, whereas in three biological replicates of HRF in co-culture, although no statistically significant changes are detected, endogenous pro-fibrotic compounds treatment (**Figure 5.18 [A], [B], [C]**) seem to induce an increase in cell viability which is displayed as an increasing trend in the dose-response curves.

Trans epithelial electrical resistance (TEER) measurement is an assay that can be used to detect changes in the state of the epithelial barrier after treatments in hPTC co-cultured on 96-Transwell inserts with HRF. In this case, the assay is used to establish a correlation between the dose of pro-fibrotic compound used and the TEER measurement in $\Omega*cm^2$. An increase in TEER can be interpreted both as an effective increase of the number of cells per insert present after 24 hours of treatment, and/or a tightening of the tight junctions that seal the epithelial barrier, whereas a decrease in TEER can be explained as a decrease in cell number per insert and/or downregulation of tight junction protein expression. In both cases, a discrepancy from the untreated control hPTC monolayer can be interpreted as a disruption of the epithelial barrier caused by pro-fibrotic treatment, which is the expected response from epithelial monolayers undergoing epithelial-to-mesenchymal transition.

TEER measurement of hPTC in co-culture

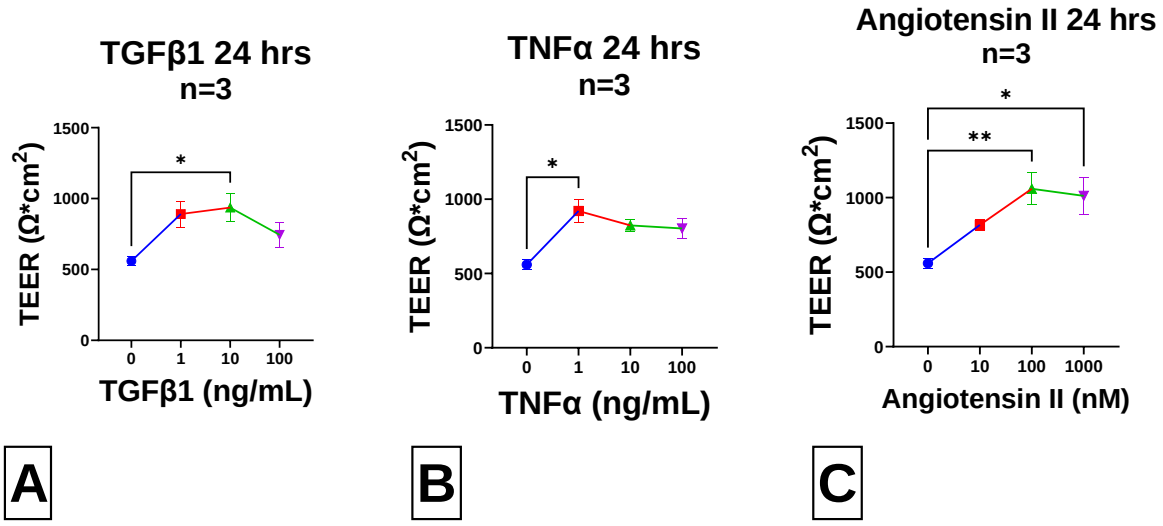

*Figure 5.19. Trans Epithelial Electrical Resistance (TEER) measured on day 8 of culture and after 24 hours of treatment with increasing concentrations of TGFβ1 (A), TNFα (B), and angiotensin II in hPTC in co-culture with HRFs [K8, K9, K10] on 96-Transwell plates' well insert. TEER is expressed in Ω*cm^2 , concentrations are expressed in nM and ng/mL. Each datapoint represents the mean between three biological repeats while error bars represent SEM. Statistical significance is depicted as '*' $p < 0.05$, '**' $p < 0.01$.*

TEER is measured in treated and untreated hPTC monolayers on inserts after 24 hours of pro-fibrotic treatment. The dose-response curves displayed **Figure 5.19** aim at investigating the relationship between concentration of pro-fibrotic treatments and TEER measurement in Ω*cm^2 . **Figure 5.19 [A]** shows that 10 ng/mL TGFβ1 treatment produces a statistically significant increase in TEER in hPTC, **[B]** highlights that 1 ng/mL TNFα treatment produces a significant increase in TEER as compared to untreated control, and **[C]** shows that with 100 nM and 1000 nM angiotensin II TEER measurements increase significantly. This figure represents the effects of a single compound on TEER while the graphs data not shown in this thesis represent the effects of a fixed concentration of one compound mixed with an increasing dose of another compound. For example, the addition of increasing doses of TNFα to TGFβ1 produces an initial increase in TEER at lower doses, although not statistically significant, followed by a return to baseline at higher concentrations. None of the compound combinations lead to a significant variation in TEER measurements as compared to untreated control. **Figure 5.20** displays the effects of polymyxin B and IGF-1 on TEER. Both compounds do not lead to significant changes in TEER of hPTC monolayers.

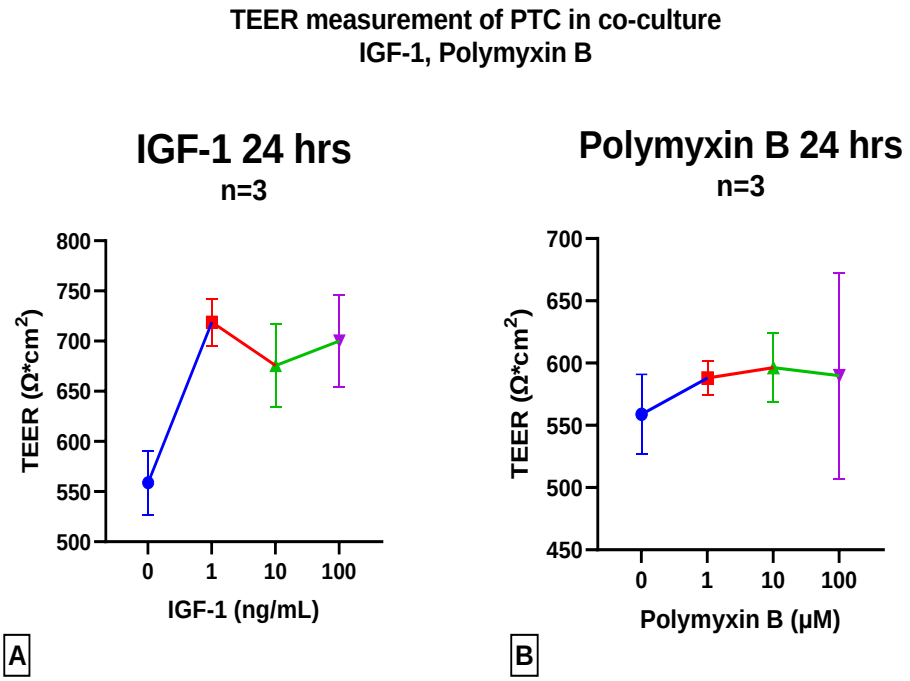

*Figure 5.20. Trans Epithelial Electrical Resistance (TEER) measured on day 8 of culture and after 24 hours of treatment with increasing concentrations of IGF-1 (A) and polymyxin B (B) in hPTC in co-culture with HRFs [K8, K9, K10] on 96-Transwell plates' well insert. TEER is expressed in Ω*cm² , concentrations are expressed in nM and ng/mL. Each datapoint represents the mean between three biological repeats while error bars represent SEM.*

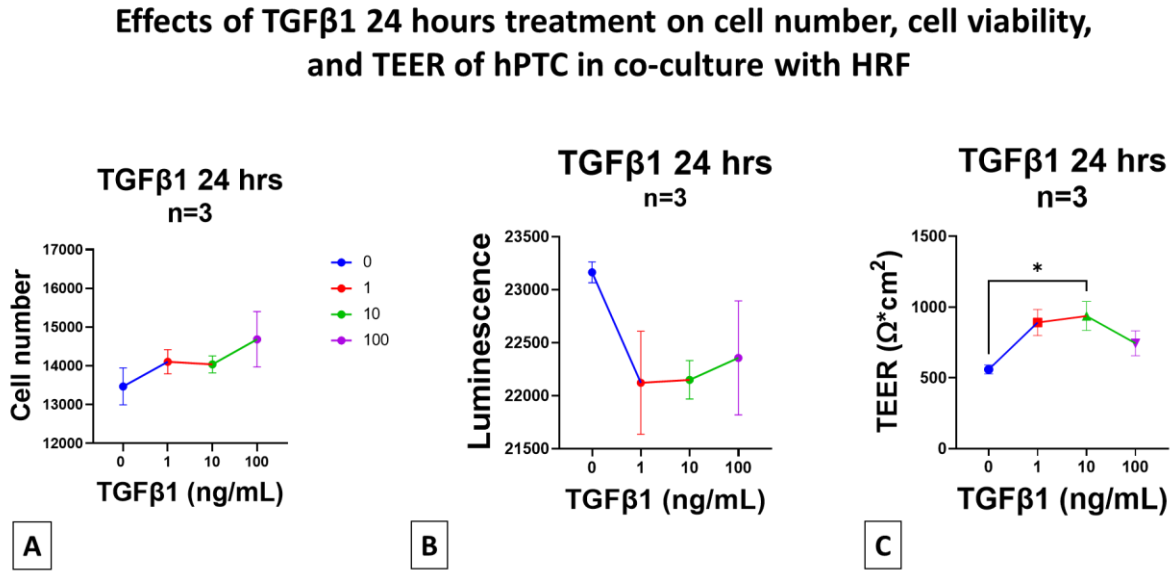

Figure 5.21. Dose-response curves displaying the effects of TGFβ1 on cell number, cell viability, and TEER in hPTC in co-culture with HRF [K8, K9, K10] on 96-Transwell plates' well insert Each datapoint represents the mean between three biological repeats while error bars represent SEM. Statistical significance is depicted as '' $p < 0.05$.*

In summary, the data displayed so far suggest that endogenous pro-fibrotic compounds TGFβ1, TNFα, and angiotensin II have different effects on hPTC in monoculture and co-culture,

and that changes in cell health and number can be measured with a number of assays developed over the course of this project. While the cell number assay seems to be able to detect significant changes in treated hPTC in monoculture, CellTiter-Glo® Luminescent Cell Viability Assay and TEER measurement assay seem to be better suited to investigating the relationship between pro-fibrotic compounds dose and biological effect in hPTC in co-culture. These assays are not able to detect significant changes in cell health of treated HRF, therefore other assays will be developed and employed for the study of these cells in the context of renal fibrosis. **Figure 5.21** summarises the effects of an increasing dose TGFβ1 on hPTC in co-culture, highlighting that the increasing trend in cell number per well [A] as the dose increases could be reflected by a significant increase in TEER **[C].** Interestingly, TNFα seems to induce the same increasing trend in cell number and TEER (**Figure 5.22 [A], [C]**) in response to the increasing dose, while cell viability significantly decreases **[B]** as the dose increases. Regarding angiotensin II (**Figure 5.23**), the same increasing trend is displayed for cell number (not significant) and TEER (significant).

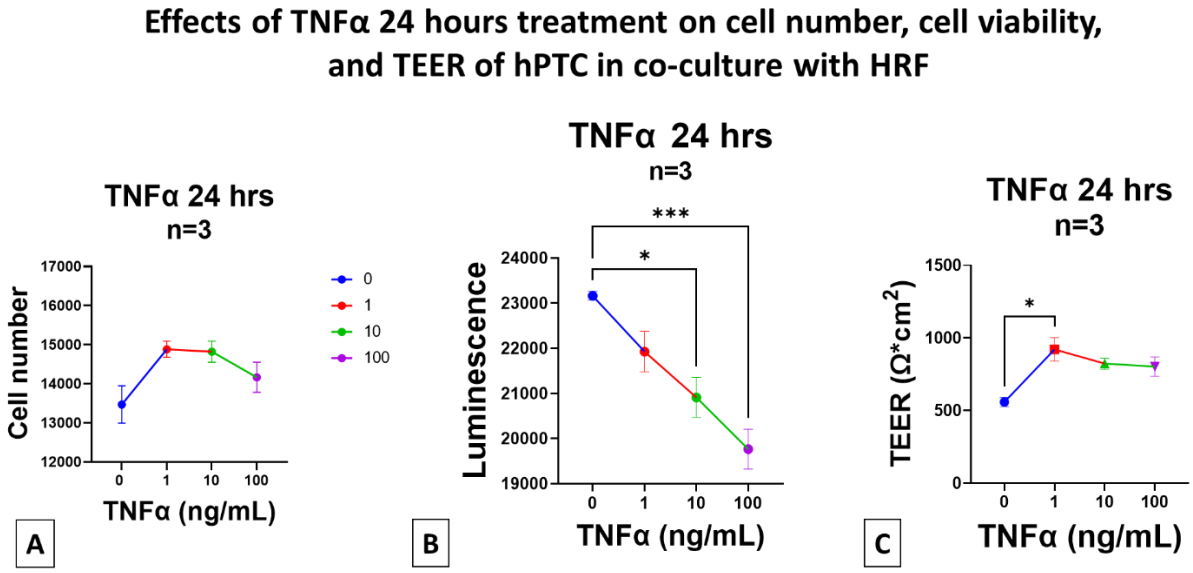

Figure 5.22. Dose-response curves displaying the effects of TNFα on cell number, cell viability, and TEER in hPTC in co-culture with HRF [K8, K9, K10] on 96-Transwell plates' well insert Each datapoint represents the mean between three biological repeats while error bars represent SEM. Statistical significance is depicted as '' $p < 0.05$, '***' $p < 0.001$.*

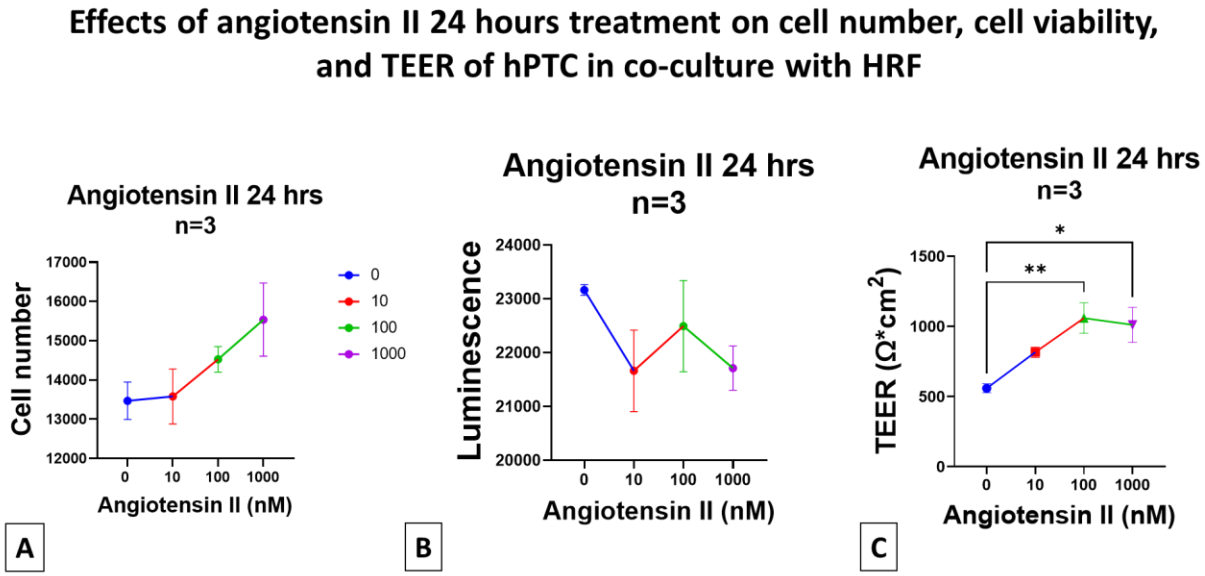

Figure 5.23. Dose-response curves displaying the effects of angiotensin II on cell number, cell viability, and TEER in hPTC in co-culture with HRF [K8, K9, K10] on 96-Transwell plates' well insert Each datapoint represents the mean between three biological repeats while error bars represent SEM. Statistical significance is depicted as '' $p < 0.05$, '**' $p < 0.01$.*

5.6 TNFα treatment increases hPTC proliferation in co-culture, angiotensin II treatment decreases HRF proliferation in co-culture

The data illustrated so far hint at various processes happening simultaneously among the hPTC and HRF microtissues after pro-fibrotic stimuli which lead to changes in the state of the epithelial barrier. As discussed in **1.3.6**, cell cycle dysregulation, apoptosis, and necrosis related pathways are triggered during the progression of renal fibrosis and in pathways involved in EMT. Therefore, to further investigate the cellular mechanisms underlying renal fibrosis in our *in vitro* model, we developed assays to measure apoptosis, necrosis, and cell proliferation in relationship to the dose of pro-fibrotic compound treatment in hPTC and HRF in mono- and co-culture via high throughput flow cytometry.

To assess the effects of pro-fibrotic treatments on apoptosis and necrosis, Annexin-V/PI apoptosis / necrosis assay is performed. **Figures 5.24 and 5.25** depict the gating strategy employed to extrapolate the percentage of apoptotic and necrotic cells among a hPTC and HRF cell populations selected by size and granularity (FSC-A / SSC-A), followed by singlets (FSC-A / FSC -H), and finally apoptotic (Annexin V – FITC-A) and necrotic (PI-A) cells. When hPTC in monoculture are treated with endogenous pro-fibrotic compounds (**Figure 5.26 and 5.27),** dose-response curves obtained from these experiments show the biological variability between the two biological replicates considered (**Figures 5.26 and 5.27 [A1], [B1], [C1]**) is too large to draw any conclusions since cells isolated from K5 seem to be more sensitive to the treatment as compared to cells isolated from K6. As per hPTC in co-culture (**Figures 5.28 and 5.29**), no significant differences are found after pro-fibrotic treatment as compared to the control with all compounds via apoptosis and necrosis assays. For technical reasons, the apoptosis and necrosis assays are performed on only one biological replicate for the HRF in monoculture condition (**Figures 5.30 and 5.31**). Similar conclusions to those discussed around hPTC can be drawn from apoptosis, and necrosis assays performed on HRF in co-culture, since the biological variability between the three biological replicates K8, K9, and K10 is too great to detect any significant changes between cell populations treated with different doses of compounds, as demonstrated by **Figures 5.32 and 5.33 [A1], [B1], [C1], [D1], [E1].** Effectively, apoptosis and necrosis assays cannot be used in the context of our *in vitro* assay platform to investigate the effects of pro-fibrotic compounds on hPTC and HRF as they are not able to detect any changes in percentages of apoptotic and necrotic cells as the concentration of treatments increases.

To monitor the effects of pro-fibrotic treatments on proliferation, Click-iT® Plus EdU Alexa Fluor® 647 proliferation assay was used via high throughput flow cytometry on single-cell suspensions of hPTC and HRF in mono- and co-culture. The same gating strategy previously described is used to extrapolate the percentage of proliferating cells among cell populations treated at increasing concentrations of pro-fibrotic compounds (**Figure 5.34 and 5.35**), where the histogram gate is set to include singlets which have incorporated nucleotide analog EdU conjugated to Alexa Fluor® 647 which are in fact cells in S-phase of the cell cycle, thus proliferating. hPTC in monoculture are treated and percentages of proliferating hPTC are shown in **Figure 5.36 [A1], [B1], [C1]**. Based on the error bars depicting standard deviation, although the assay used has worked successfully, the variability between the considered

biological replicates is too large hence it is not possible to conclude whether TGFβ1, TNFα, and Angiotensin II cause proliferation in hPTC in monoculture via this assay. Conversely, the data shown in **Figure 5.37 [B2]** suggests that TNFα induces proliferation in hPTC in co-culture after 24 hours of treatment. Regarding HRF in monoculture, the data collected from two biological replicates is plotted in **Figure 5.38** which shows that TGFβ1 and TNFα seem to induce an increasing trend in percentage of proliferating cells but this is not statistically significant. When HRF are treated in co-culture, angiotensin II and polymyxin B show to inhibit cell proliferation significantly, as displayed in **Figure 5.39 [C2], [D2].**

From the data presented in this section, we can conclude that TNFα causes a significant increase in proliferation in hPTC in co-culture, while angiotensin II and polymyxin B cause a significant decrease in proliferation of HRF in co-culture. Having examined the effects induced on TEER and cell number in hPTC in co-culture by TGFβ1, angiotensin II, and IGF-1 we expected to detect a significant increase in proliferation also for epithelial cells treated with such compounds, especially for IGF-1. We hypothesised that the reason why we could not detect an increase in proliferation with a flow cytometry-based assay is because epithelial cells migrate into nodules after treatment, and nodules are excluded from the cell population under investigation by the gating strategy which is designed to include singlets only. Therefore, doublets which have incorporated EdU Alexa Fluor® 647 have been plotted against the increasing doses of compounds, showing that IGF-1 induces a significant increase in this parameter, suggesting that hPTC might be acquiring migratory and proliferative phenotype after treatment. Epithelial cells with this phenotype do not seem to be found in the singlet population, which points towards developing assays to better define the phenotype of the cells that constitute the epithelial nodules.

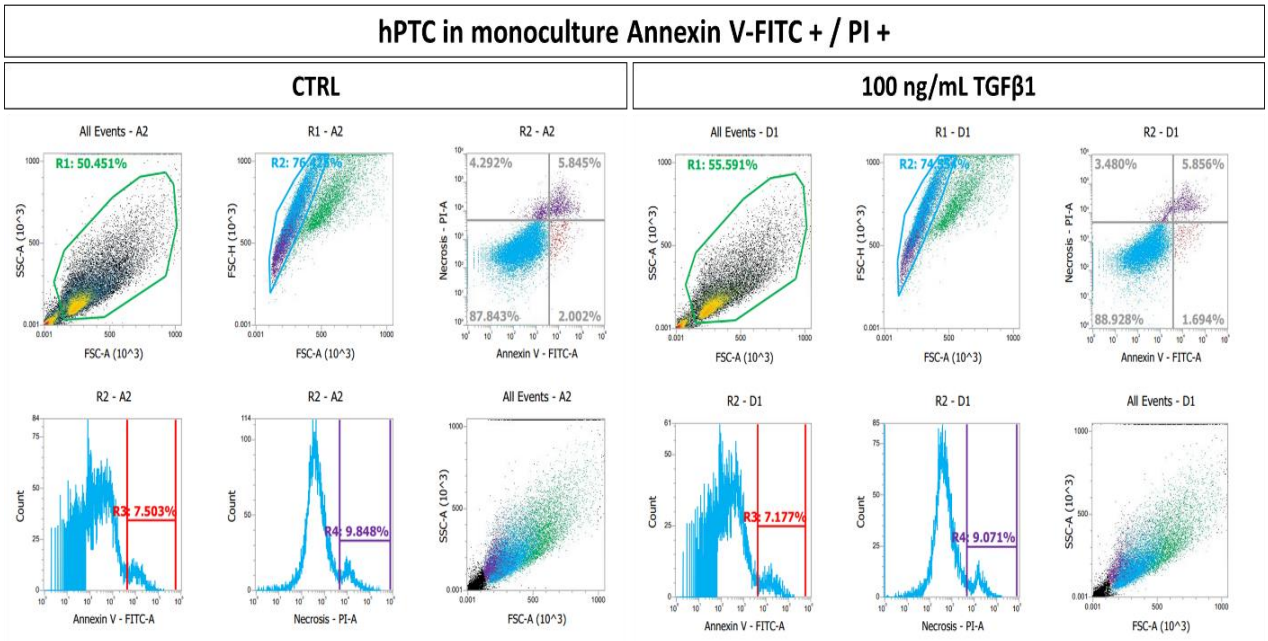

Figure 5.24. Flow cytometry dot plots and histograms representing gating process used to extrapolate percentages of apoptotic (Annexin V – FITC +) and necrotic (PI +) cells among the single cell populations of untreated and 100 ng/mL TGFβ1 treated hPTC in monoculture.

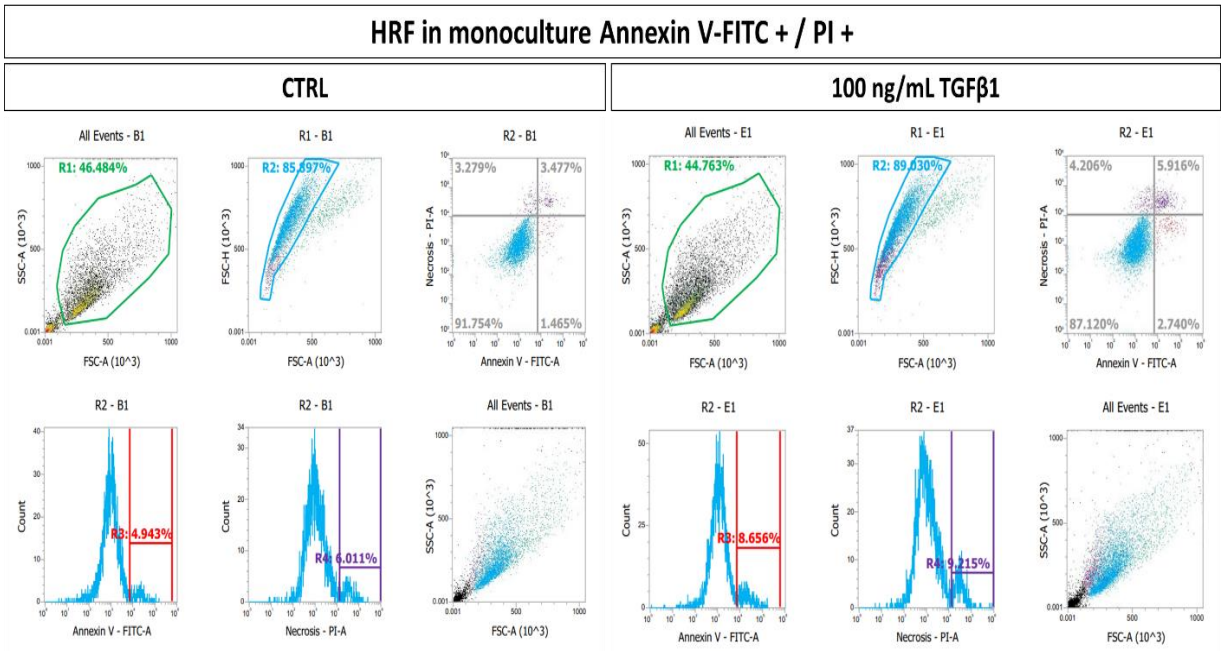

Figure 5.25. Flow cytometry dot plots and histograms representing gating process used to extrapolate percentages of apoptotic (Annexin V – FITC +) and necrotic (PI +) cells among the single cell populations of untreated and 100 ng/mL TGFβ1 treated HRF in monoculture.

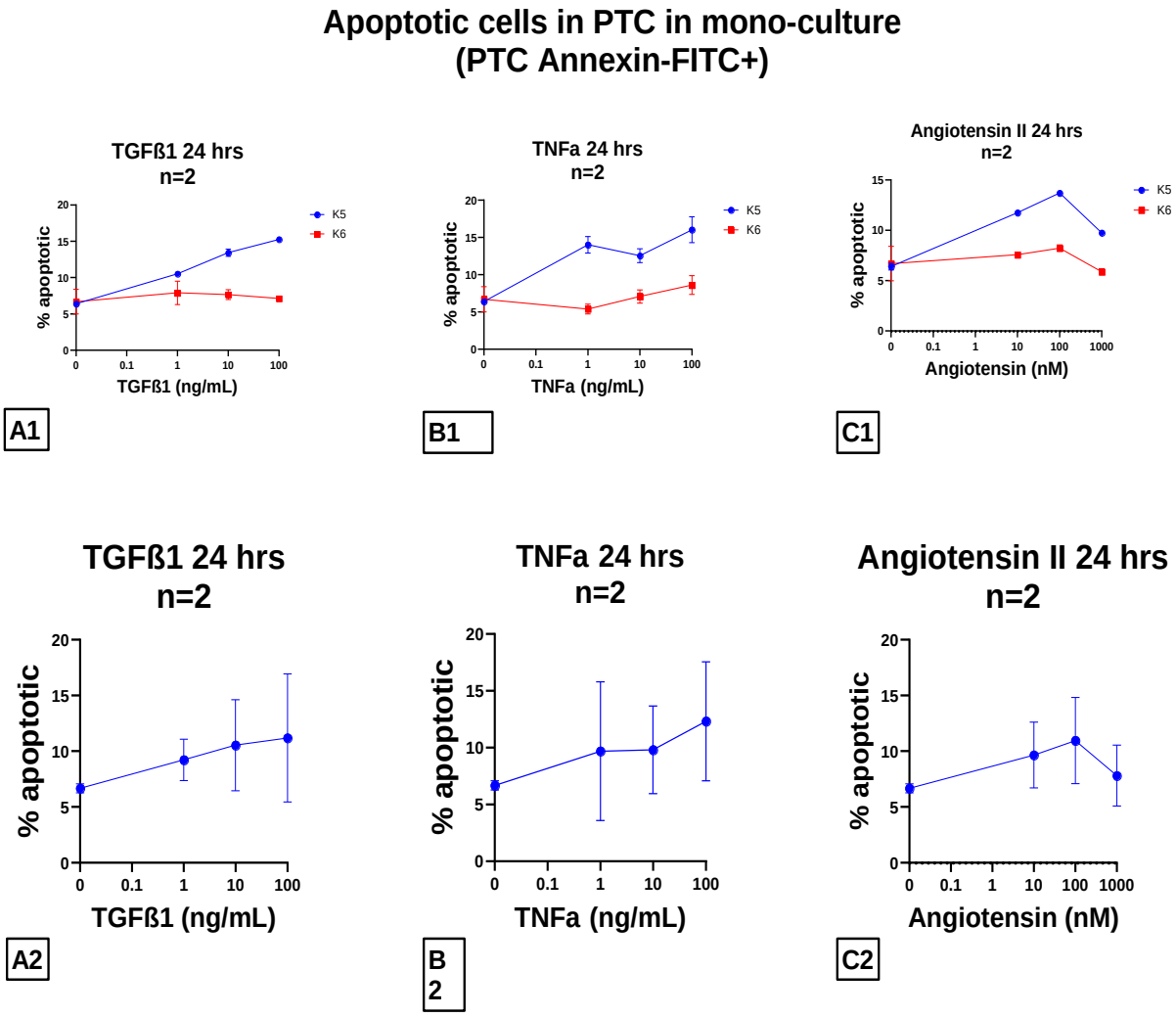

Figure 5.26. Flow cytometry apoptosis assay measuring the percentage of doublets positive to Annexin V among the cell population performed after 24 hours of treatment with increasing concentrations of TGFβ1, TNFα, and Angiotensin II in hPTC in monoculture [K5, K6] on 96-well black walled plates. Datapoints represent the mean between three technical repeats (A1, B1, C1) and two biological repeats (A2, B2, C2) while error bars represent SD (n=2).

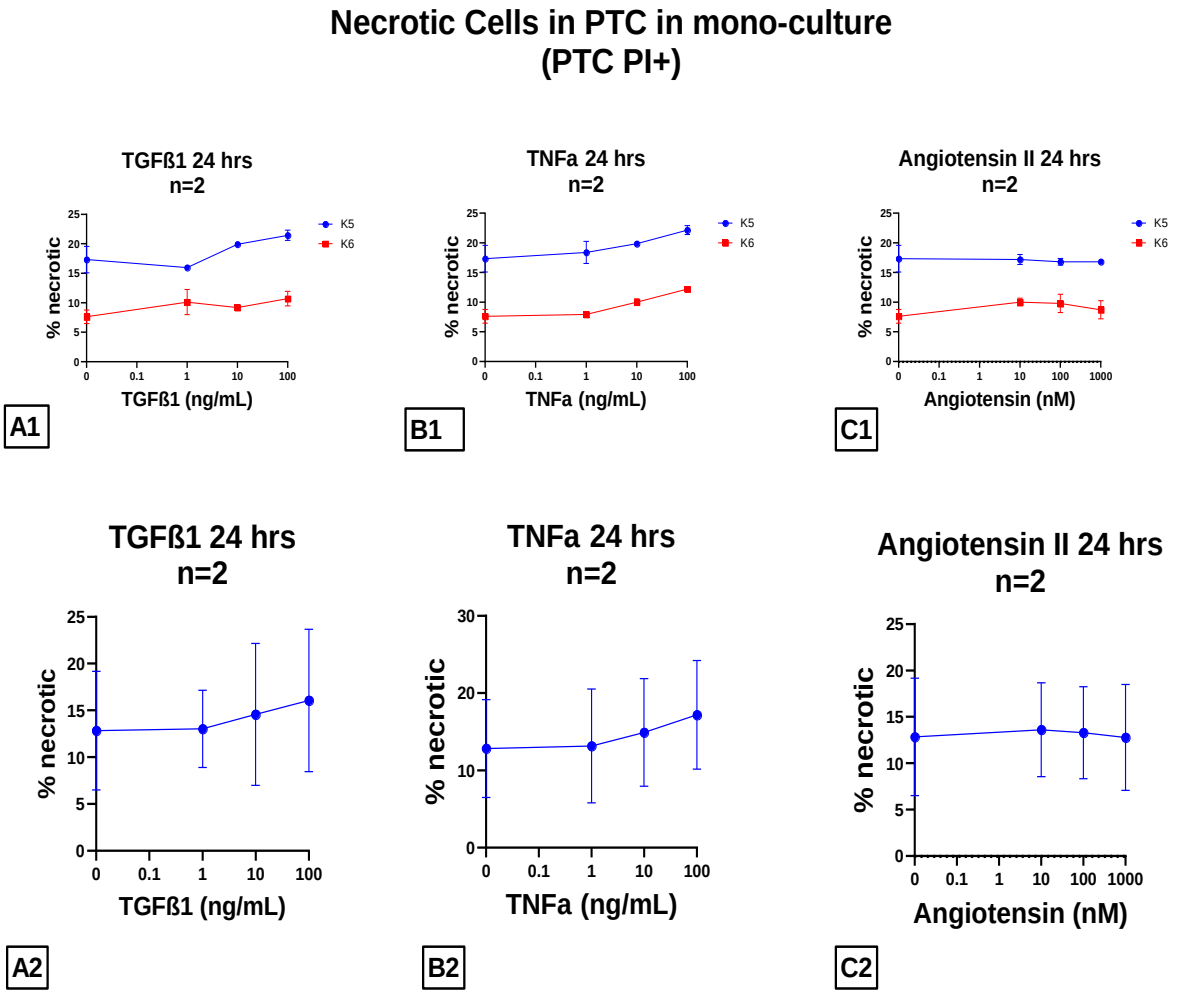

Figure 5.27. Flow cytometry necrosis assay PI staining measuring the percentage of cells positive to PI among the cell population performed after 24 hours of treatment with increasing concentrations of TGFβ1, TNFα, and Angiotensin II in hPTC in monoculture [K5, K6] on 96-well black walled plates. Datapoints represent the mean between three technical repeats (A1, B1, C1) and two biological repeats (A2, B2, C2) while error bars represent SD (n=2).

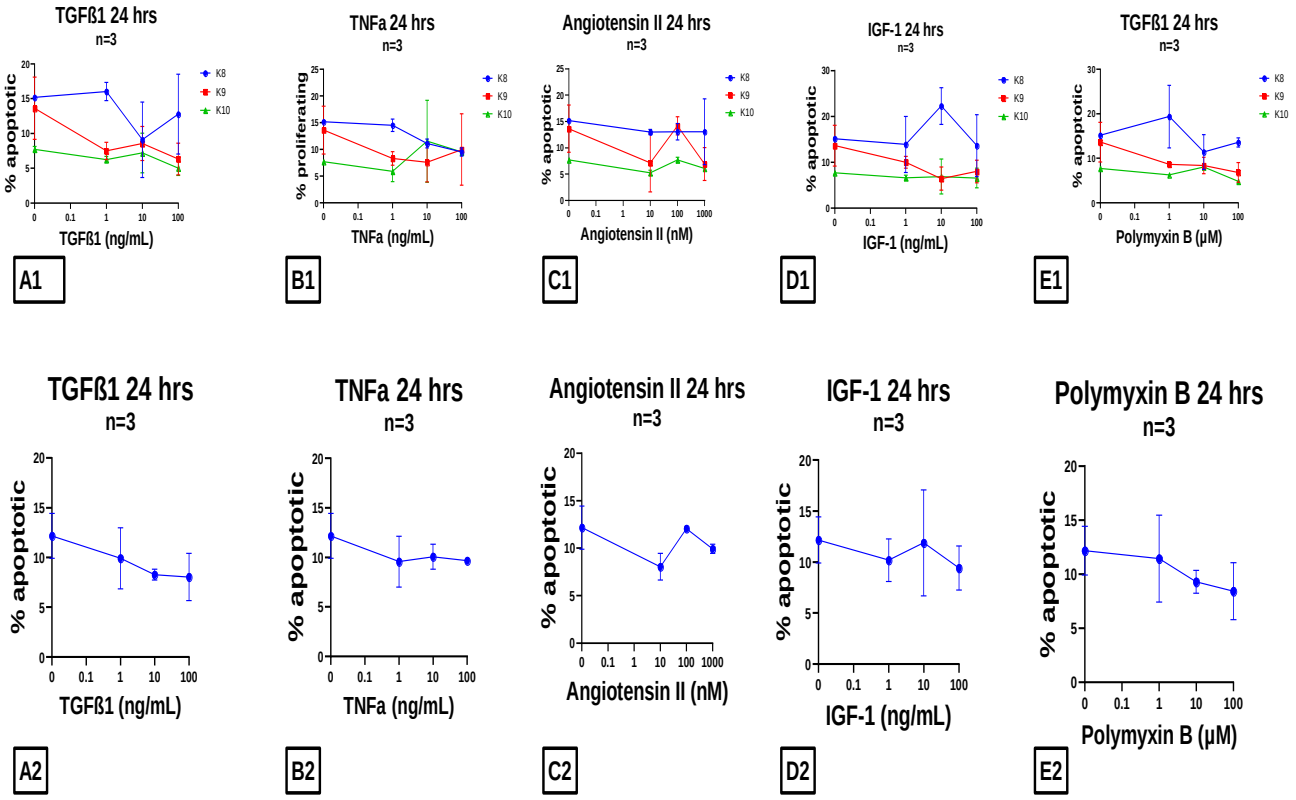

Figure 5.28. Flow cytometry apoptosis assay staining measuring the percentage of cells positive to Annexin V-FITC among the cell population performed after 24 hours of treatment with increasing concentrations of TGFβ1, TNFα, and Angiotensin II in hPTC in co-culture [K8, K9, K10] on 96-Transwell plates' inserts. Datapoints represent the mean between three technical repeats (A1, B1, C1, D1, E1) and three biological repeats (A2, B2, C2, D2, E2) while error bars represent SEM (n=3).

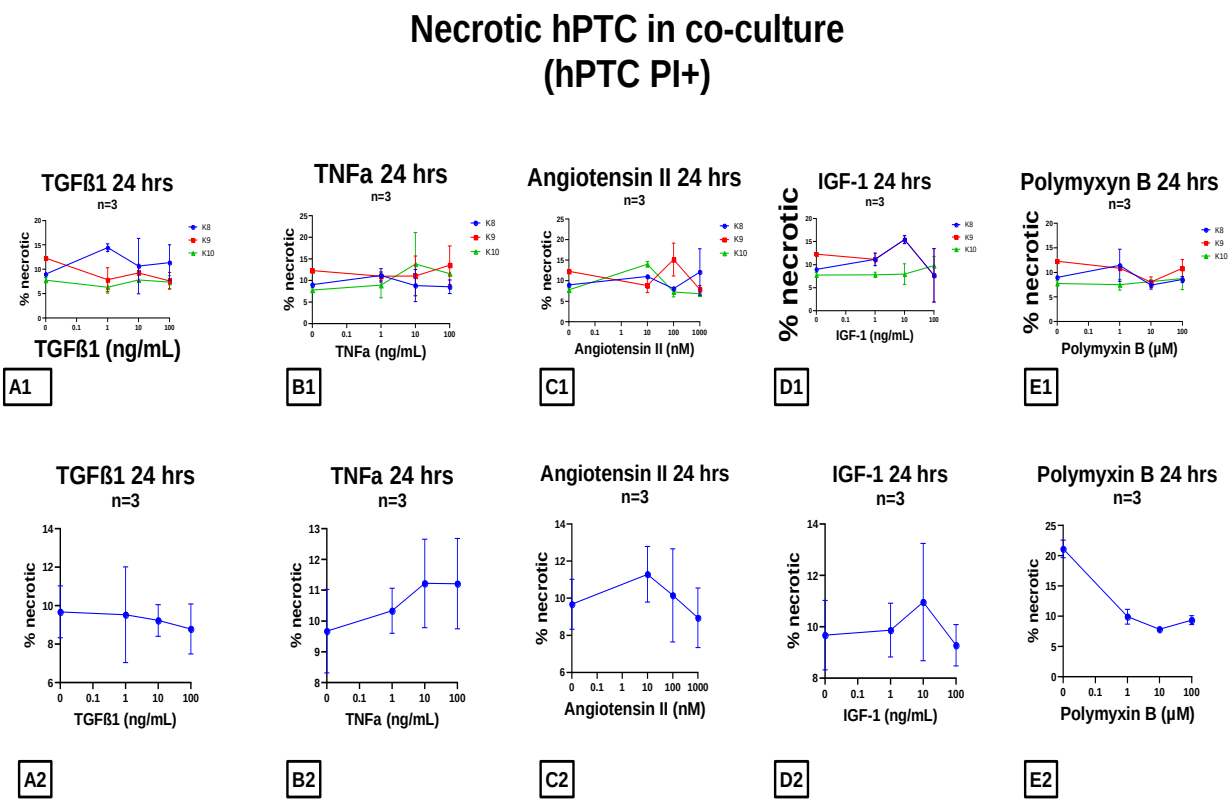

Figure 5.29. Flow cytometry necrosis assay PI staining measuring the percentage of cells positive to PI among the cell population performed after 24 hours of treatment with increasing concentrations of TGFβ1, TNFα, and Angiotensin II in hPTC in co-culture [K8, K9, K10] on 96-Transwell plates' inserts. Datapoints represent the mean between three technical repeats (A1, B1, C1, D1, E1) and three biological repeats (A2, B2, C2, D2, E2) while error bars represent SEM (n=3).

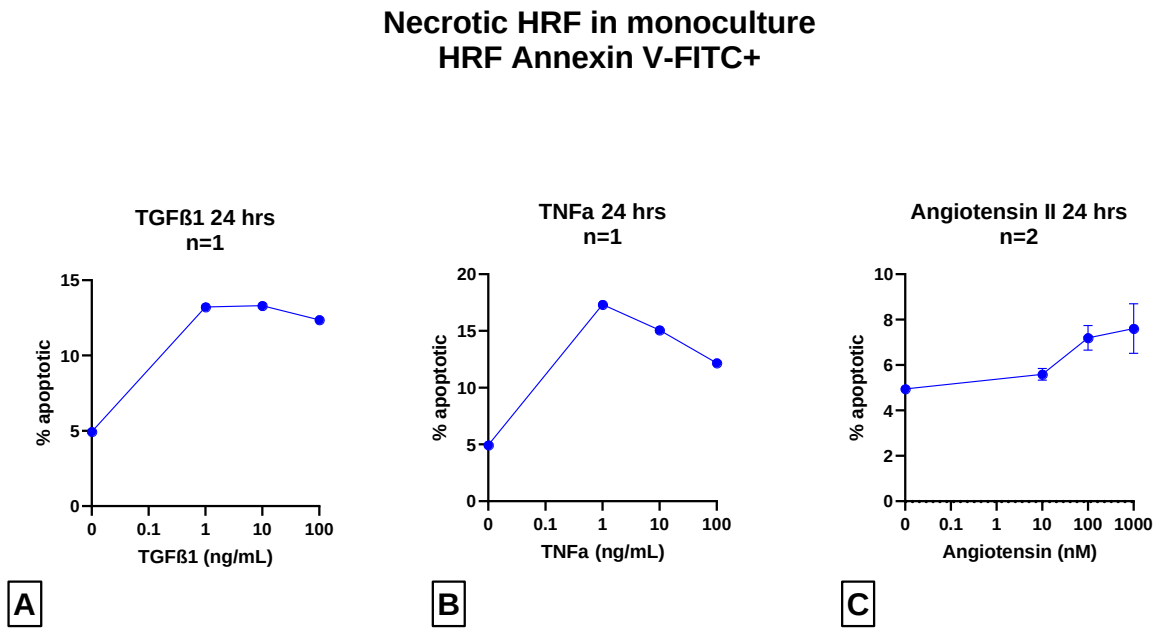

Figure 5.30. Flow cytometry apoptosis assay staining measuring the percentage of cells positive to Annexin V-FITC among the cell population performed after 24 hours of treatment with increasing concentrations of TGFβ1, TNFα, and Angiotensin II in HRF in monoculture [K5, K6] on 96-well black walled plates. Datapoints represent one biological repeat (A) and the mean between two biological repeats (B, C) while error bars represent SD (n=2).

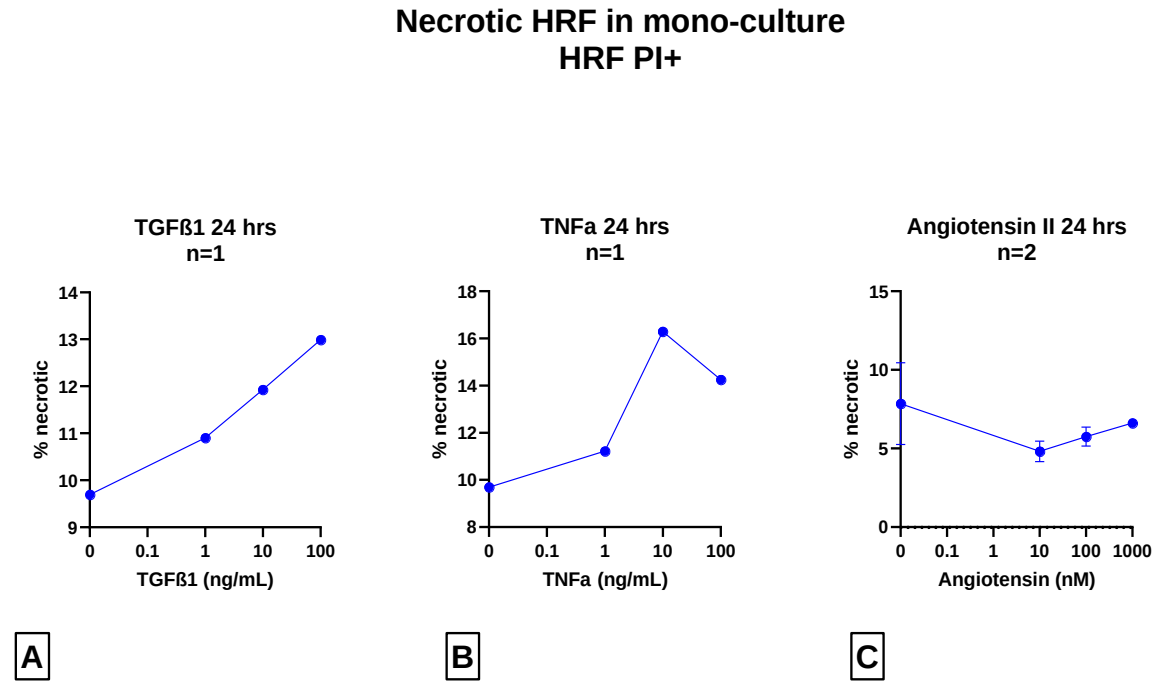

Figure 5.31. Flow cytometry necrosis assay PI staining measuring the percentage of cells positive to PI among the cell population performed after 24 hours of treatment with increasing concentrations of TGFβ1, TNFα, and Angiotensin II in hPTC in monoculture [K5, K6] on 96-well black walled plates. Datapoints represent one biological repeat (A) and the mean between two biological repeats (B, C) while error bars represent SD (n=2).

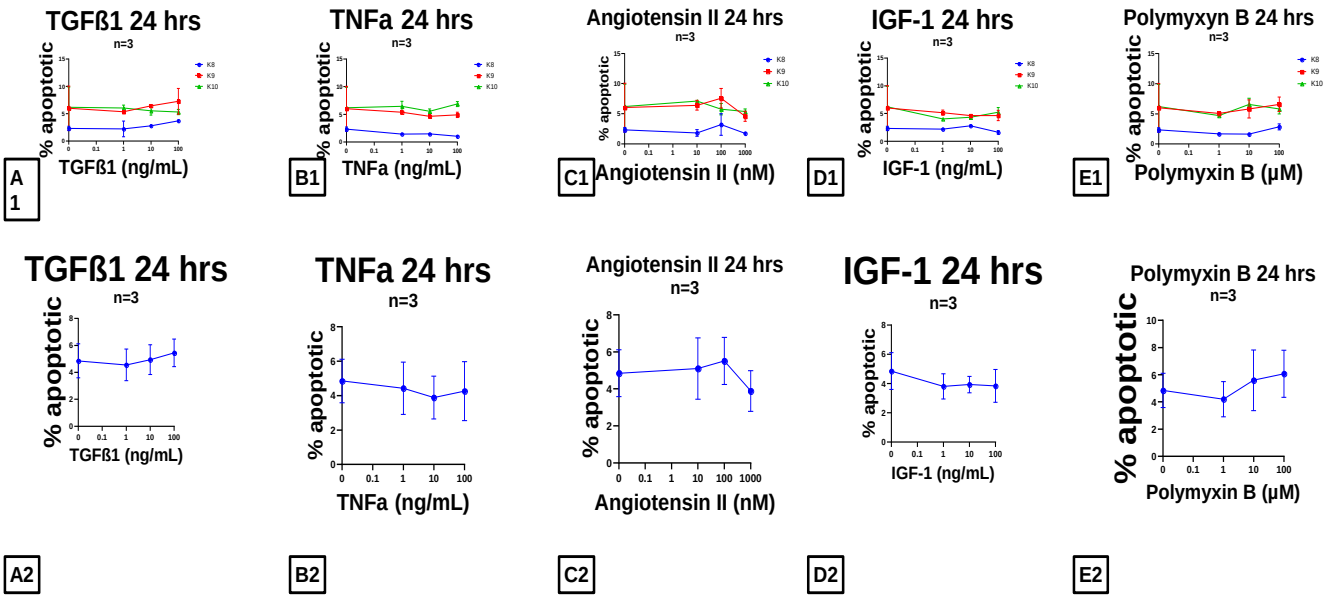

Figure 5.32. Flow cytometry apoptosis assay staining measuring the percentage of cells positive to Annexin V-FITC among the cell population performed after 24 hours of treatment with increasing concentrations of TGFβ1, TNFα, and Angiotensin II in HRF in co-culture [K8, K9, K10] on 96-Transwell plates' well bottom. Datapoints represent the mean between three technical repeats (A1, B1, C1, D1, E1) and three biological repeats (A2, B2, C2, D2, E2) while error bars represent SEM (n=3).

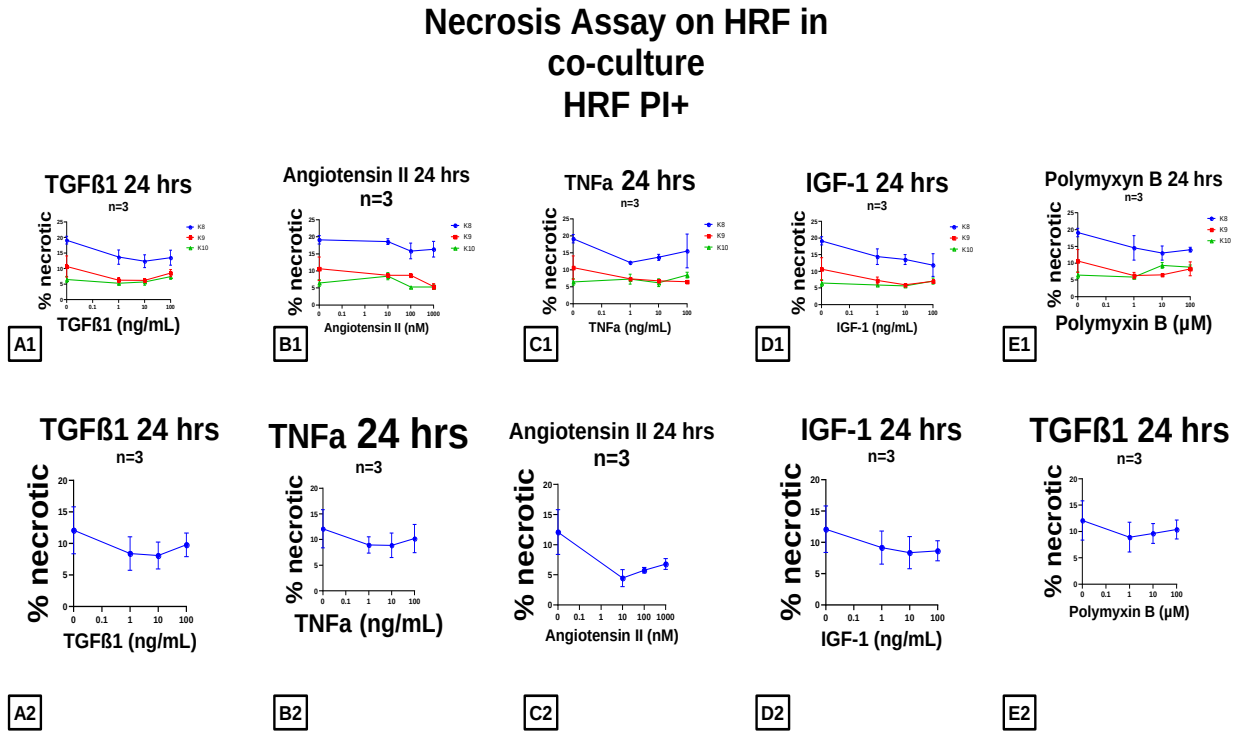

Figure 5.33. Flow cytometry necrosis assay PI staining measuring the percentage of cells positive to PI among the cell population performed after 24 hours of treatment with increasing concentrations of TGFß1, TNFα, and Angiotensin II in HRF in co-culture [K8, K9, K10] on 96-Transwell plates' well bottom. Datapoints represent the mean between three technical repeats (A1, B1, C1, D1, E1) and three biological repeats (A2, B2, C2, D2, E2) while error bars represent SEM (n=3).

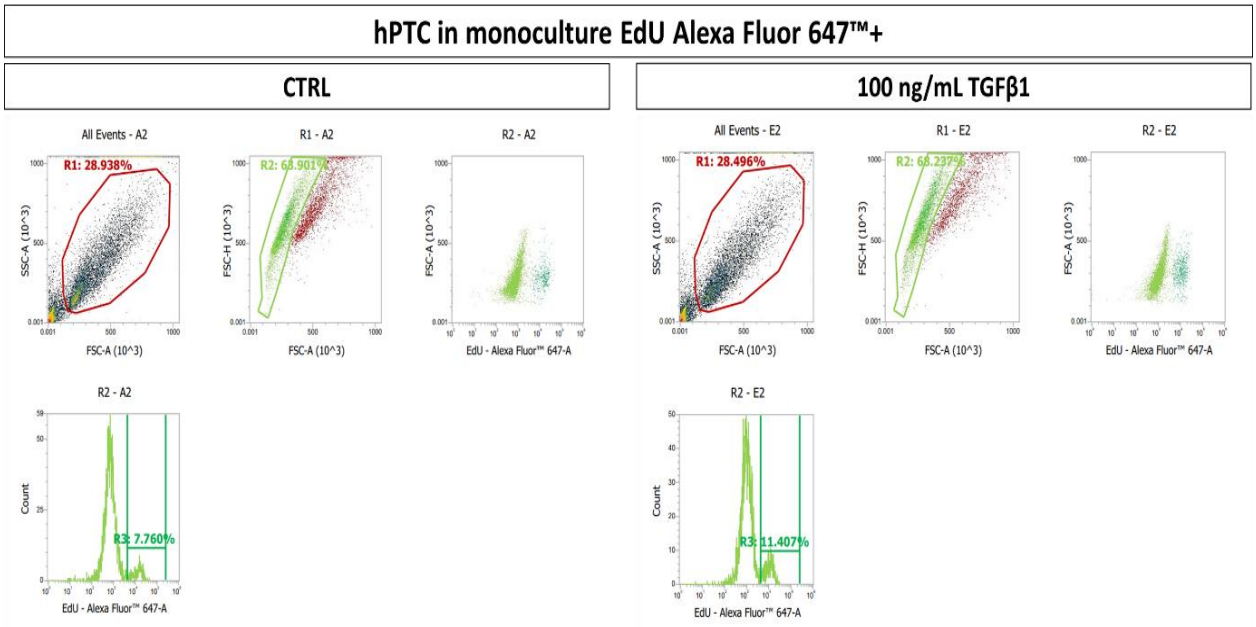

Figure 5.34. Flow cytometry dot plots and histograms representing gating process used to extrapolate percentages of proliferating cells (EdU Alexa Fluor 647™ +) among the single cell populations of untreated and 100 ng/mL TGFß1 treated hPTC in monoculture.

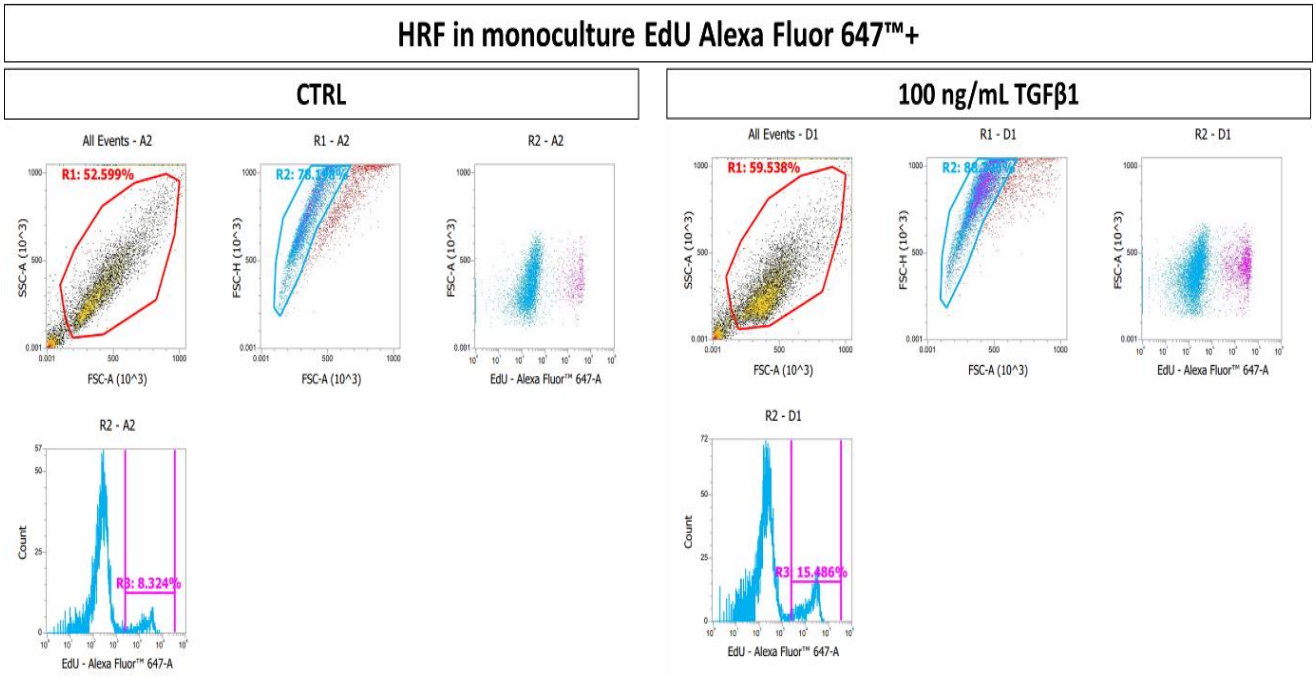

Figure 5.35. Flow cytometry dot plots and histograms representing gating process used to extrapolate percentages of proliferating cells (EdU Alexa Fluor 647™ +) among the single cell populations of untreated and 100 ng/mL TGFβ1 treated HRF in monoculture.

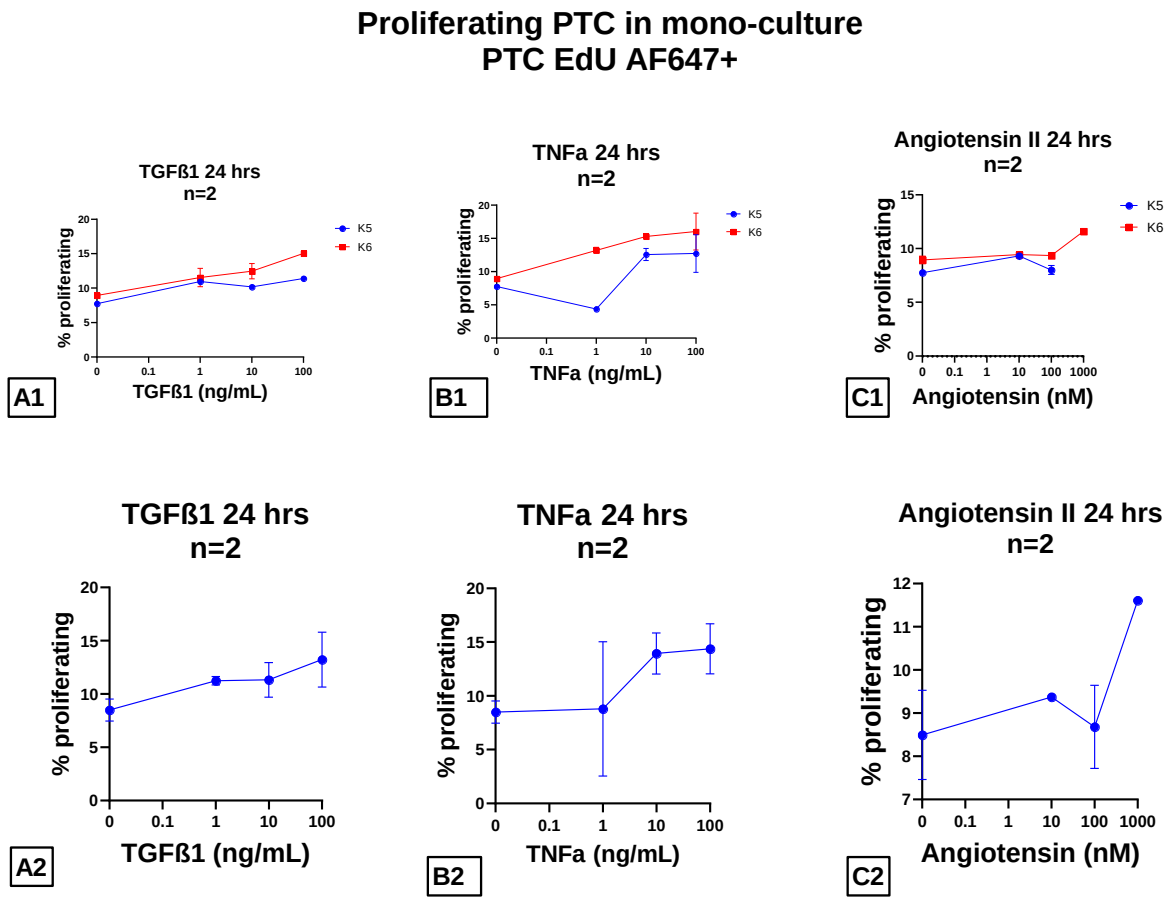

Figure 5.36. Flow cytometry cell proliferation assay Click-iT® Plus EdU Alexa Fluor® 647 measuring the percentage of proliferating hPTC (based on positivity to Alexa Fluor® 647) performed after 24 hours of treatment with increasing concentrations of TGFβ1, TNFα, and Angiotensin II in hPTC in monoculture [K5, K6] on 96-well black walled plates. Datapoints represent the mean between three technical repeats (A1, B1, C1) and two biological repeats (A2, B2, C2) while error bars represent SD (n=2).

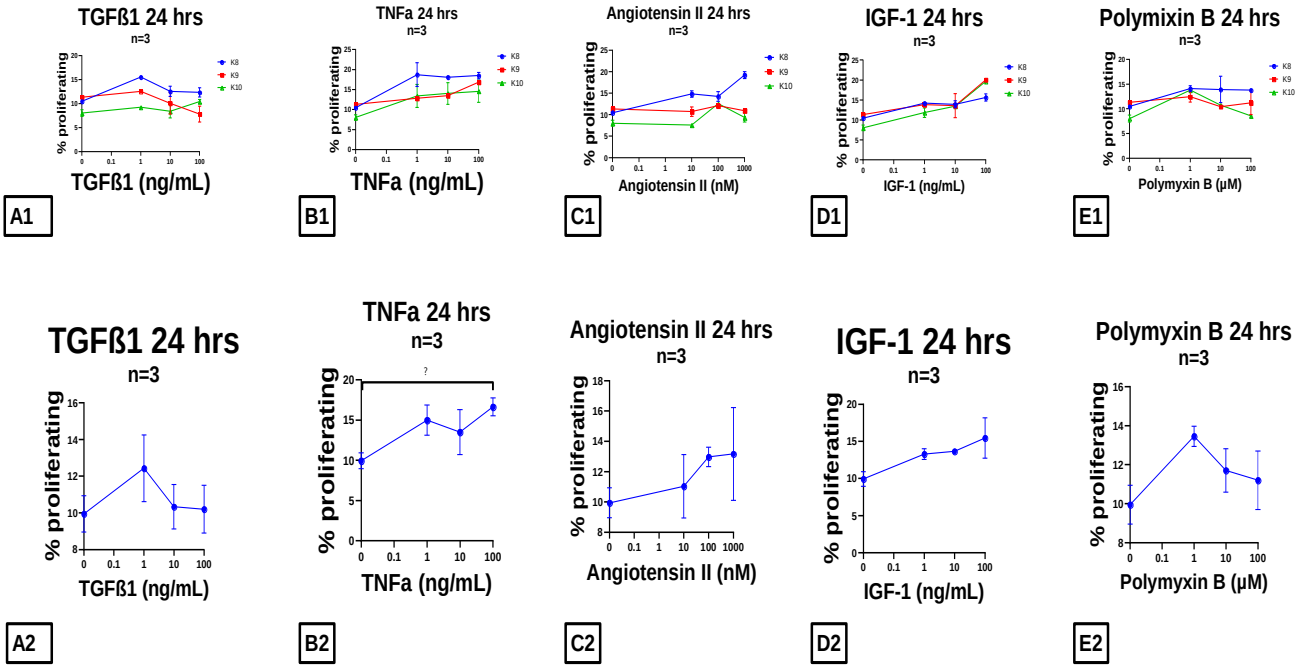

Figure 5.37. Flow cytometry cell proliferation assay Click-iT® Plus EdU Alexa Fluor® 647 measuring the percentage of proliferating hPTC (based on positivity to Alexa Fluor® 647) performed after 24 hours of treatment with increasing concentrations of TGFß1, TNFα, and Angiotensin II in hPTC in co-culture [K8, K9, K10] on 96-Transwell plates' inserts. Datapoints represent the mean between three technical repeats (A1, B1, C1, D1, E1) and three biological repeats (A2, B2, C2, D2, E2) while error bars represent SEM (n=3).

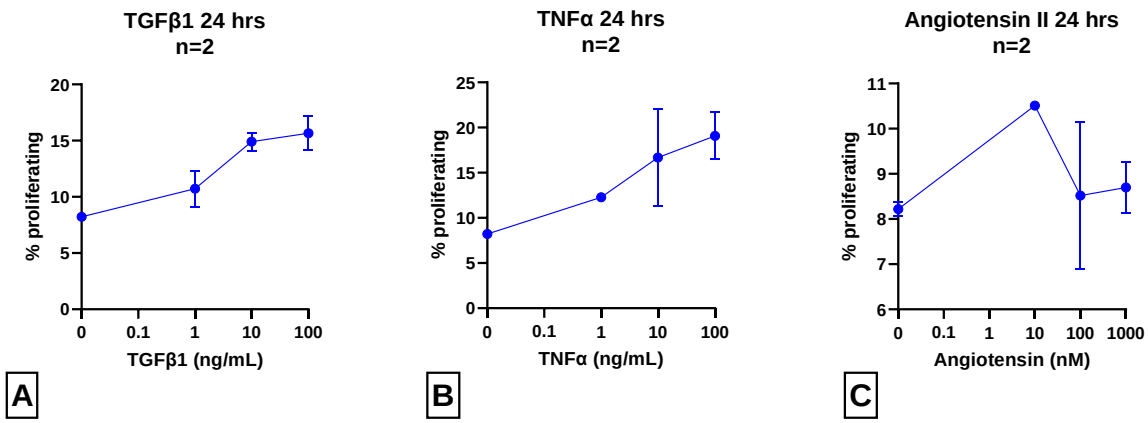

Figure 5.38. Flow cytometry cell proliferation assay Click-iT® Plus EdU Alexa Fluor® 647 measuring the percentage of doublets positive to Alexa Fluor® 647 among the cell population performed after 24 hours of treatment with increasing concentrations of TGFβ1, TNFα, and Angiotensin II in HRF in monoculture [K5, K6] on 96-well black walled plates. Datapoints represent the mean between two biological repeats (A, B, C) while error bars represent SD (n=2).

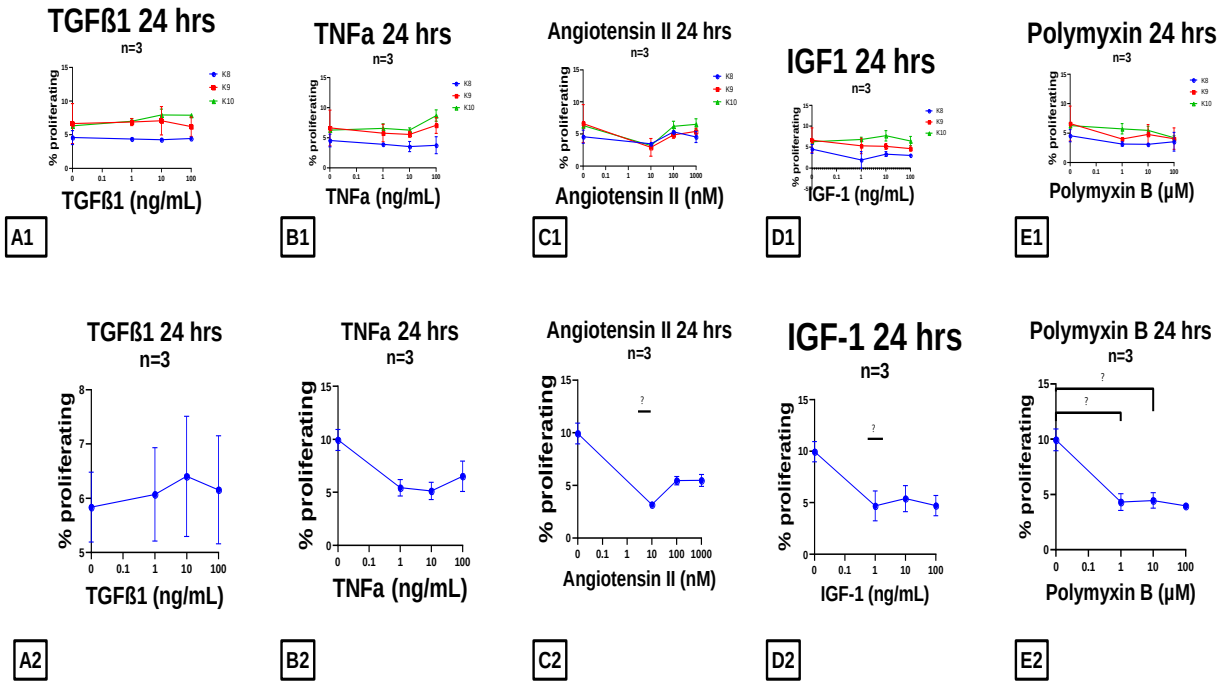

Figure 5.39. Flow cytometry cell proliferation assay Click-iT® Plus EdU Alexa Fluor® 647 measuring the percentage of proliferating HRF (based on positivity to Alexa Fluor® 647) performed after 24 hours of treatment with increasing concentrations of TGFß1, TNFα, and Angiotensin II in HRF in co-culture [K8, K9, K10] on 96-Transwell plates' well bottom. Datapoints represent the mean between three technical repeats (A1, B1, C1, D1, E1) and three biological repeats (A2, B2, C2, D2, E2) while error bars represent SEM (n=3). Statistical significance is depicted as '' $p < 0.05$, '**' $p < 0.01$.*

5.7 Pro-fibrotic treatment induces αSMA+ epithelial nodule formation which disrupts the epithelial barrier

To better investigate the phenomenon of nodule formation after pro-fibrotic treatment of tubular epithelial cells, nodule number is measured and plotted against the increasing dose of treatments via a high content imaging assay developed with the ImageXpress Pico and CellReporterXpress software, as described in **2.7.9.** The dose-response curves displayed in **Figures 5.40 and 5.41** show that, although nodules are definitely forming and they can be detected both in mono- and co-culture on epithelial monolayers, there is no significant difference between untreated and treated hPTC in both culture conditions. Since this assay does not yield to any conclusion on whether it is possible to establish a correlation between the nodules' characteristics and the dose of pro-fibrotic compound used, we decided to develop assays to investigate the single cell populations that constitute the epithelial monolayer, and consequently the nodules, and their phenotypes in terms of expression of tight junction markers and mesenchymal markers.

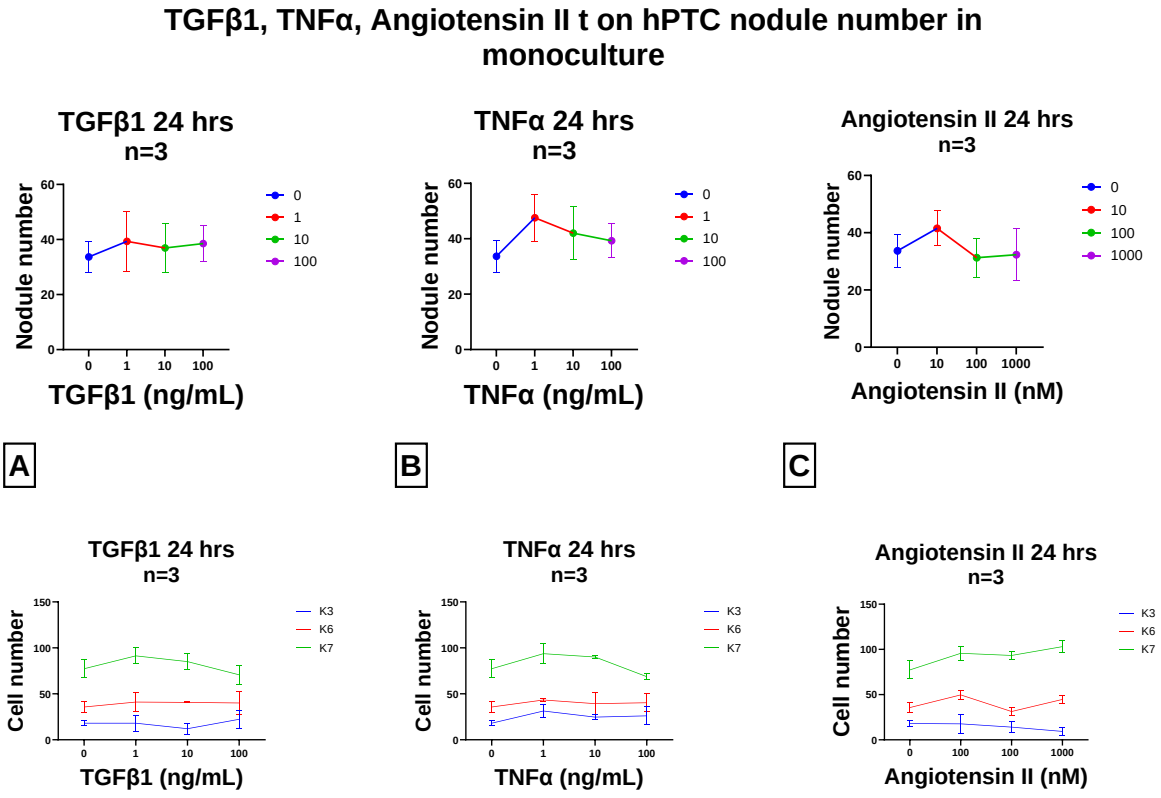

Figure 5.40. Effects of [A] TGFβ1, [B] TNFα, [C] Angiotensin II 24 hours treatment on nodule number in hPTC monolayers cultured on black walled 96-well plates. Each data point is the mean of three biological (K3, K6, K7) and two technical replicates. Error bars represent S.E.M.

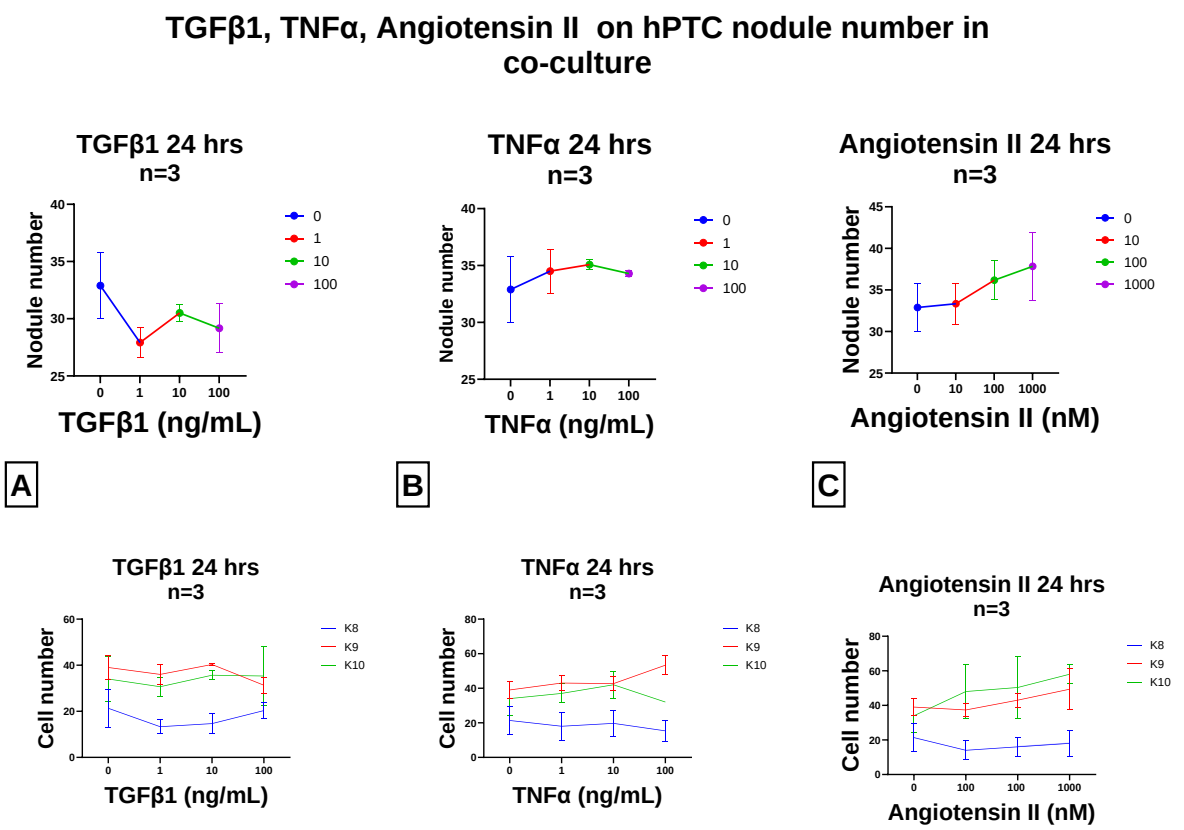

Figure 5.41. Effects of [A] TGFβ1, [B] TNFα, [C] Angiotensin II 24 hours treatment on nodule number in hPTC monolayers cultured on 96-Transwell inserts. Each data point is the mean of three biological (K8, K9, K10) and two technical replicates. Error bars represent S.E.M.

A high content imaging assay to quantify the expression of tight junction markers ZO-1 and E-Cadherin and the mesenchymal marker vimentin is developed in hPTC in mono- and co-culture. Cells are cultured to confluency, treated with increasing concentrations of TGFβ1, TNFα, and angiotensin II for 24 hours, after which they are fixed and immunofluorescence stained as described in **2.7.3.** Plates are imaged with high content imager ImageXpress Pico and two algorithms to quantify the average cell and nodule fluorescence intensity of secondary antibodies against primary antibodies against ZO-1, E-Cadherin, and vimentin within the cells and nodules boundaries are established via image analysis software CellReporterXpress, as described in **2.7.9**. Furthermore, average nuclear Hoechst 44423 intensity and average nuclear area are also quantified via the algorithm. These endpoints are measured in three biological replicates per culture condition, and they are plotted in dose-response curves where the average cell and nodule fluorescence intensity of expressed protein is the response (Y axis) and the concentration of pro-fibrotic treatment is the dose (X axis). Measurements from single cells are plotted as frequency of distribution curves, where each curve represents the distribution of a cell population treated with a specific concentration of pro-fibrotic compound. The frequency of distribution graphs aims at evaluating and highlighting the heterogeneity of tight junction and mesenchymal markers expression in cells within the same cell population, where one cell population is constituted by the single cell endpoints measured in three wells treated with the same concentration of

pro-fibrotic compound in three biological replicates. In other words, frequencies of distribution curves are used in this context to *profile* the intensity-based features of a particular cell population and to visually aggregate the single-cell data in a way that will underline the effects of the increasing dose of pro-fibrotic treatment on a specific feature of the cell population. Therefore, a shift in shape or 'bin centre' of these curves as compared to the curve representing the untreated cell population will mark a potential correlation between the pro-fibrotic treatment and the measured variation in any intensity-based cell feature. Frequency of distribution curves are thus used to compare the effects of pro-fibrotic compounds on epithelial cells, and they are a suitable tool to highlight differences in cell population profiles; however, they cannot be used to display the statistical variation between the means of the measured endpoints for each concentration of compound. Hence, to investigate the statistical significance of these measurements, the next step would have been firstly to assess whether the dataset is normally distributed via normality tests of D'Agostino, Anderson-Darling, Shapiro-Wilk, and Kolmogorov-Smirnov, and secondly to perform two-way ANOVA with multiple comparisons (Dunnett's test), or non-parametric Kruskal-Wallis test with Dunn's multiple comparisons test, where the means of the treated groups would have been compared to the untreated control cell population (H. J. Motulsky, GraphPad Statistics Guide). For technical reasons associated to the computing power of the computers available to use over the course of this project, we could not perform these statistical tests on the collected measurements as the samples considered were too large.

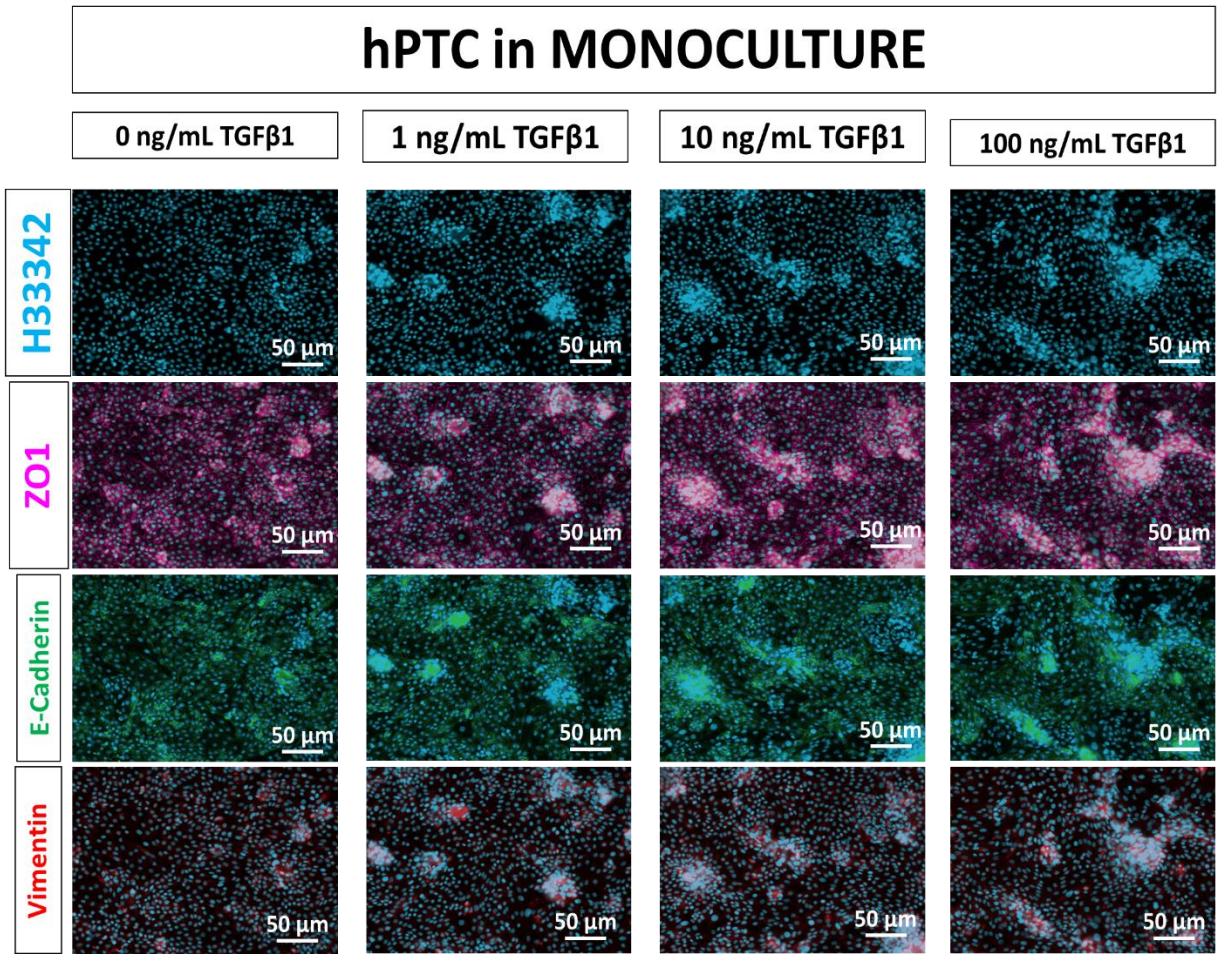

Figure 5.42. Fluorescence images of hPTC monolayers in monoculture cultured on black walled 96-well plates treated with increasing concentrations of TGFβ1 for 24 hours. Cells were fixed and immunofluoresce-stained with nuclear stain Hoechst 33342, and antibodies against tight junction markers ZO1 and E-Cadherin, and mesenchymal marker Vimentin. Exposure times and focus were kept constant across the plate. Images were acquired at 10X magnification (scale bars=50µm)

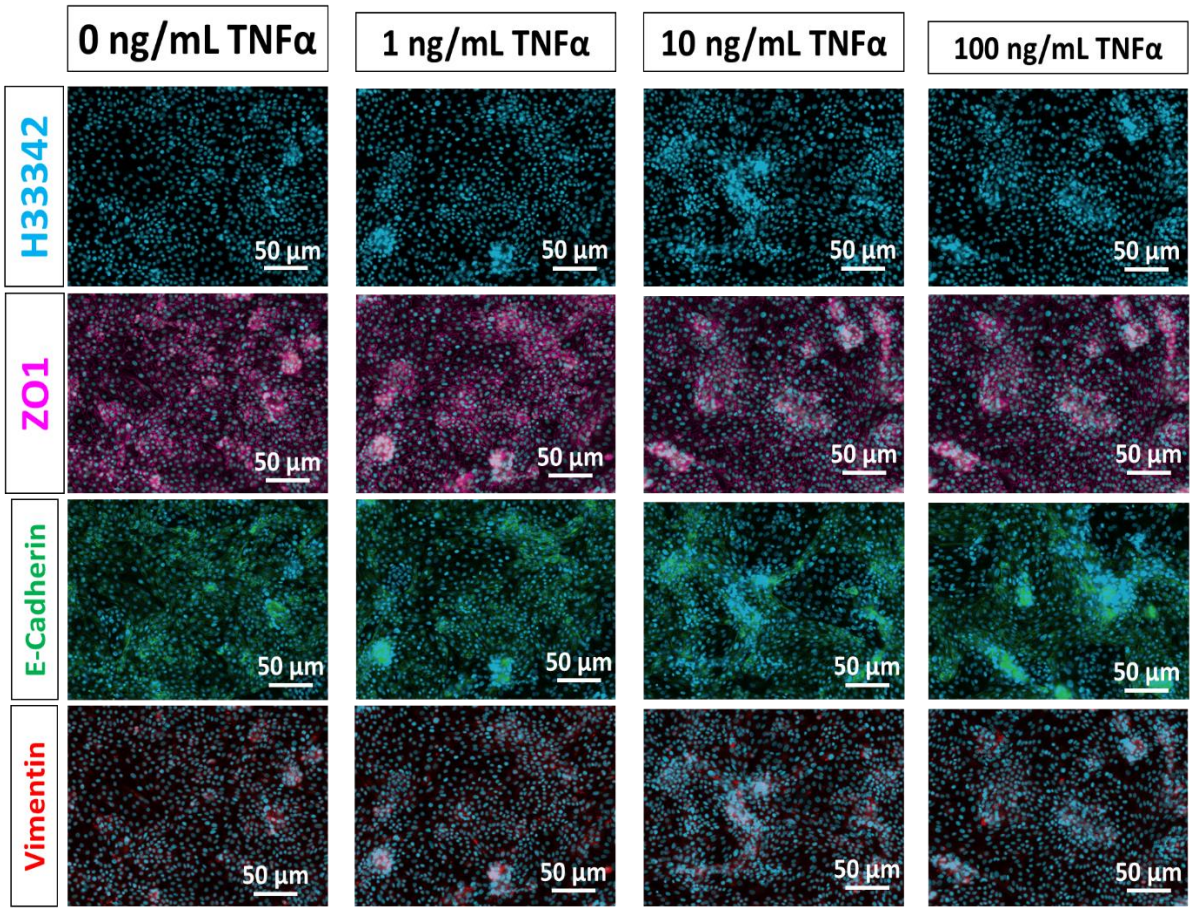

Figure 5.43. Fluorescence images of hPTC monolayers in monoculture cultured on black walled 96-well plates treated with increasing concentrations of TNFα for 24 hours. Cells were fixed and immunofluoresce-stained with nuclear stain Hoechst 33342, and antibodies against tight junction markers ZO1 and E-Cadherin, and mesenchymal marker Vimentin. Exposure times and focus were kept constant across the plate. Images were acquired at 10X magnification (scale bars=50µm).

Figures 5.42 to 5.45 represent fields of view taken from imaged wells of hPTC in monoculture expressing ZO-1, E-Cadherin and vimentin exemplifying the changes observed in epithelial monolayer integrity after treatment with endogenous pro-fibrotic compounds TGFβ1, TNFα, angiotensin II and the xenobiotic polymyxin B. The main feature portrayed by Figures 42 to 44 is the apparent migration of hPTC into nodules, which seem to have a higher intensity of fluorescence relative to fluorophores associated to nuclear stain Hoechst 33342, ZO-1, E-Cadherin, and vimentin as compared to the surrounding cells forming the monolayer. **Figure 5.45** shows hPTC monolayers treated with polymyxin B: nodules are visible at lower concentrations of treatment whereas the highest dose of compound used (100 µM), cell nuclei appear to be sparser as compared to lower doses of treatment and the untreated control, which indicates a level of nephrotoxicity which is to be expected due to the mechanism of action of the compound of interest.

An example of image quantification of cell intensity-based features via the previously described algorithms is shown in **Figure 5.46**. The endpoints of nuclear area, average nuclear intensity of Hoechst 33342, average cell intensity of E-Cadherin (Alexa Fluor 488™), average cell intensity of vimentin (Alexa Fluor 594™), and average cell intensity fluorescence of ZO-1

(Alexa Fluor 647™) are plotted against the increasing dose of TGFβ1 treatment in dose-response curves (**Figure 5.46 [A], [B], [C], [D]**) with the corresponding frequency of distribution curve (**Figure 5.46 [A1], [B1], [C1], [D1]**), whereby the **blue curve** represents the distribution of one intensity-based feature for the untreated cell population, the **red curve** represents the cell population treated with 1 ng/mL TGFβ1, the **green curve** is associated to the cell population exposed to 10 ng/mL TGFβ1, and the **purple curve** to 100 ng/mL TGFβ1. Although it is possible to appreciate differences in shapes in the frequency of distribution curves associated with treated cell populations as compared to the untreated control curve, the curves' bin centres do not shift as the dose of treatment changes, meaning that the most frequent values measured among each cell population do not vary in relationship to TGFβ1 concentration. As previously stated, it is not possible to indicate whether the differences in endpoints measured among different cell population are significant; however, the frequency of distribution curves suggest that hPTC in monoculture treated with an increasing concentration of TGFβ1 exert similar phenotype to the untreated cells in terms of nuclear area and intensity of staining, and expression of tight junction and mesenchymal markers. Therefore, the same intensity-based features are plotted as dose-response curves and frequency of distribution curves for the epithelial nodules formed after TGFβ1 treatment of hPTC in monoculture (**Figure 5.47**). In the nodules' case, the analysed population is constituted by a lower number of objects as compared to the correspondent cell population which does not follow the Gaussian distribution of residuals, so it has been possible to perform a non-parametric Kruskal-Wallis one-way with Dunn's post hoc test to determine the statistical significance of the differences between nodules' features in relationship to the dose of treatment. Thus, it is possible to conclude that the average intensity of Hoechst 33342 nuclear staining significantly increases within the boundaries of the nodules as the concentration of TGFβ1 increases (**Figure 5.47 [B])**, and that the average expression of E-Cadherin within the nodules significantly increases at 10 ng/mL TGFβ1 as compared to the untreated control (**Figure 5.47 [C])**, whereas nodule area, and average expression of vimentin and ZO-1 do not change after pro-fibrotic treatment (**Figure 5.47 [A], [D], [E]**).

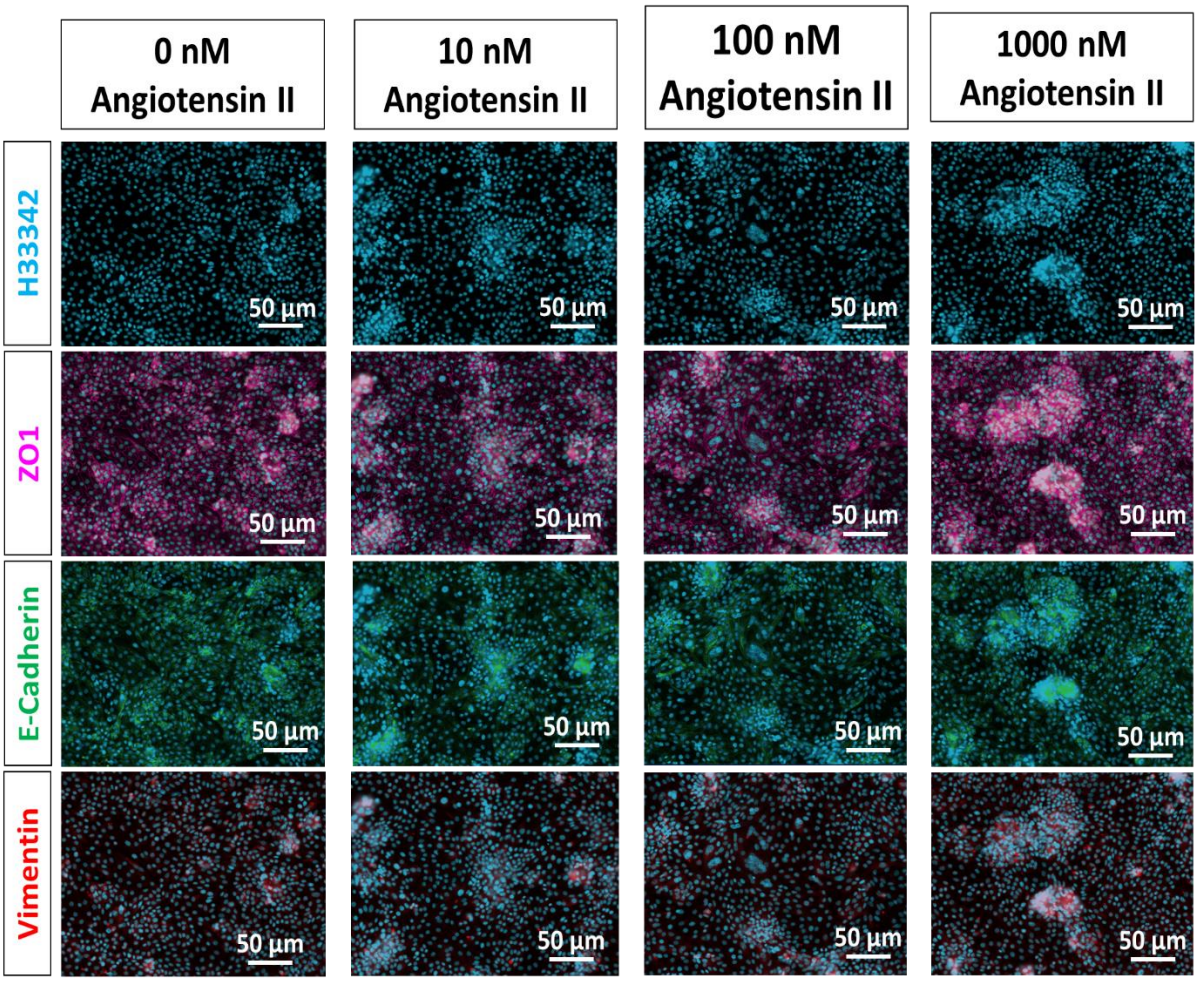

Figure 5.44. Fluorescence images of hPTC monolayers in monoculture cultured on black walled 96-well plates treated with increasing concentrations of Angiotensin II for 24 hours. Cells were fixed and immunofluoresce-stained with nuclear stain Hoechst 33342, and antibodies against tight junction markers ZO1 and E-Cadherin, and mesenchymal marker Vimentin. Exposure times and focus were kept constant across the plate. Images were acquired at 10X magnification (scale bars=50µm).

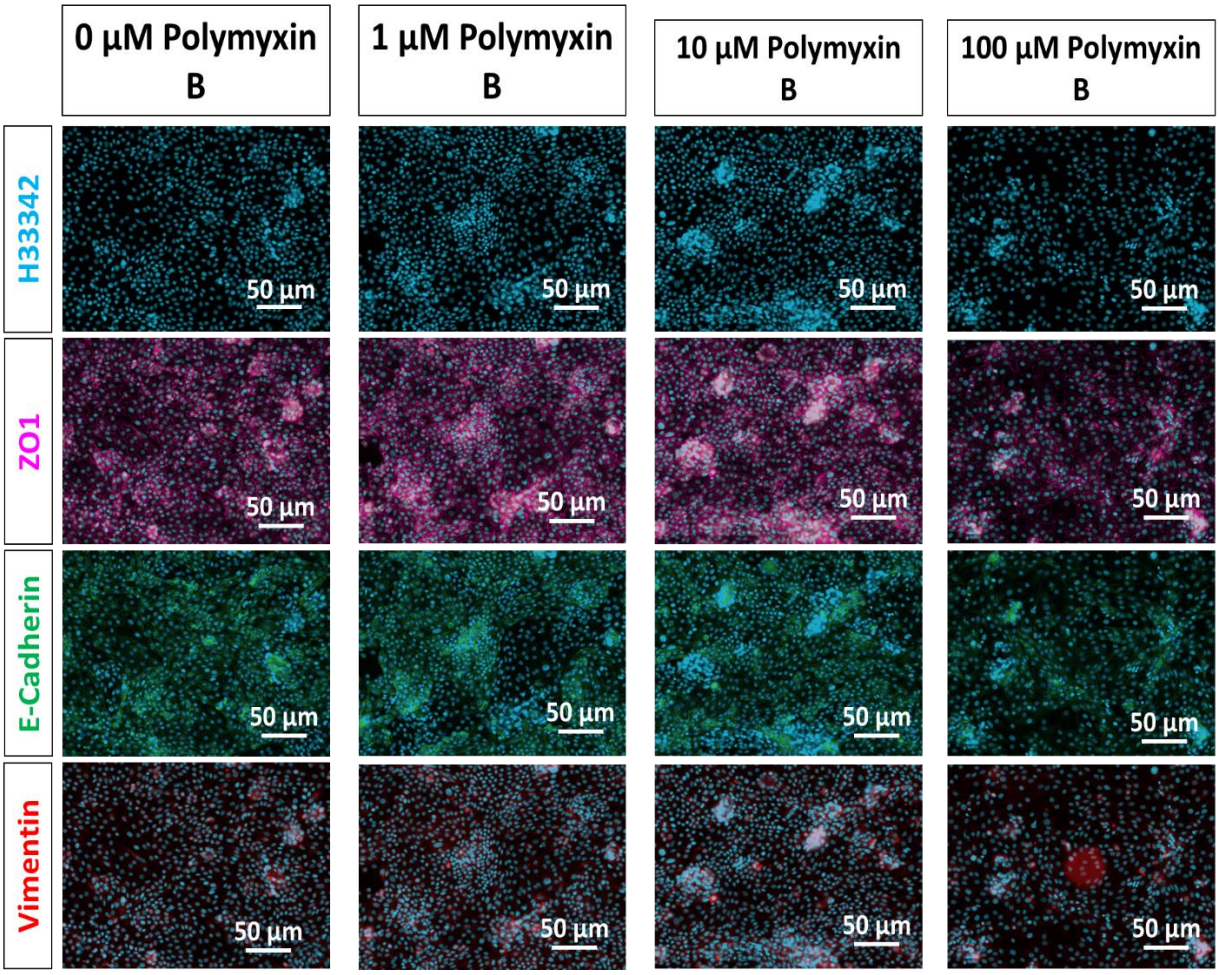

Figure 5.45. Fluorescence images of hPTC monolayers in monoculture cultured on black walled 96-well plates treated with increasing concentrations of polymyxin B for 24 hours. Cells were fixed and immunofluoresce-stained with nuclear stain Hoechst 33342, and antibodies against tight junction markers ZO1 and E-Cadherin, and mesenchymal marker Vimentin. Exposure times and focus were kept constant across the plate. Images were acquired at 10X magnification (scale bars=50µm).

hPTC in monoculture on 96-well black walled plates
TGFβ1, cell measurements

A

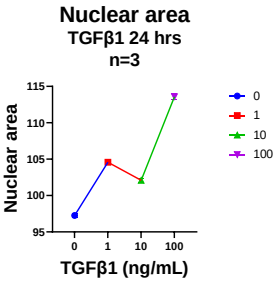

A1

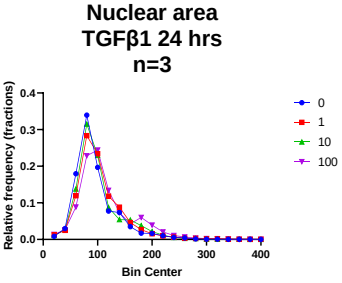

B

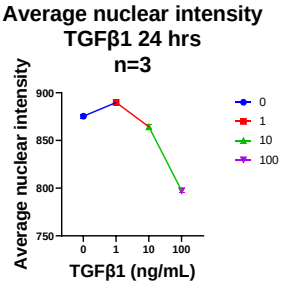

B1

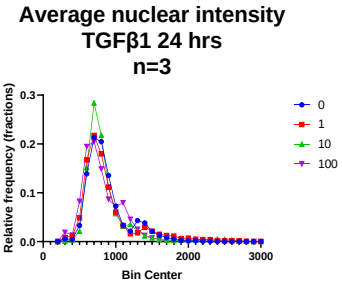

C

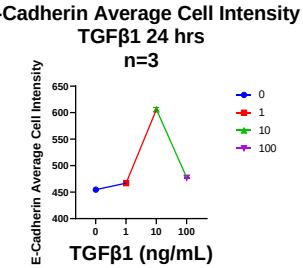

C1

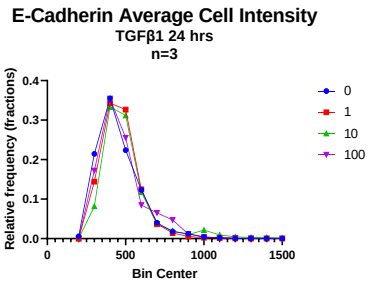

D

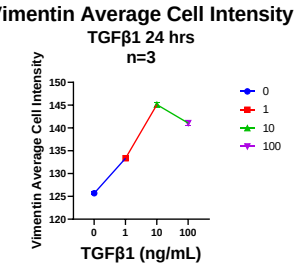

D1

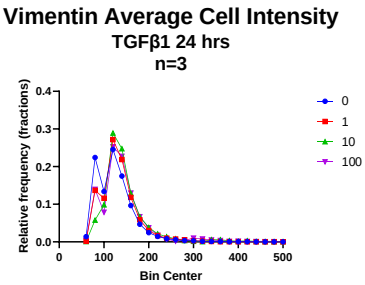

E

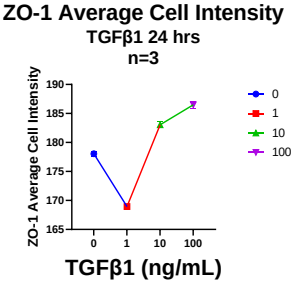

E1

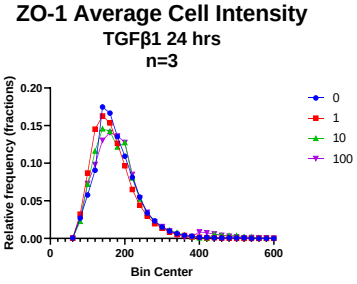

Figure 5.46. Effects of TGFβ1 24 hours treatment in hPTC monolayers in monoculture on nuclear area, average H33342 nuclear intensity, E-Cadherin average cell intensity, Vimentin average cell intensity, and ZO-1 average cell intensity depicted as dose-response curves and frequency of distribution graphs. Each data point is the mean of three biological (K3, K6, K7) and two technical replicates. Error bars represent S.E.M.

hPTC in monoculture on 96-well black walled plates
TGFβ1, nodule measurements

A

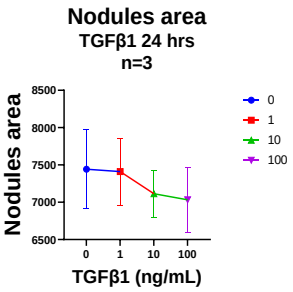

A1

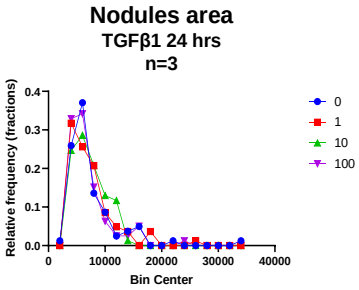

B

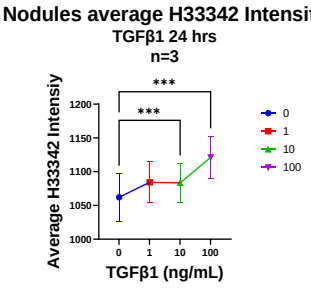

B1

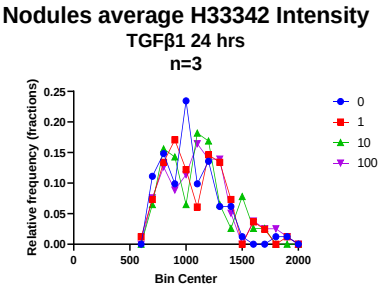

C

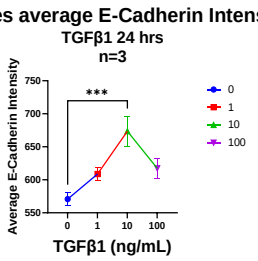

C1

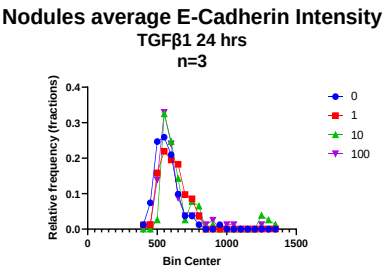

D

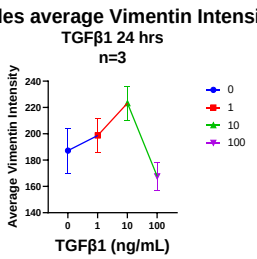

D1

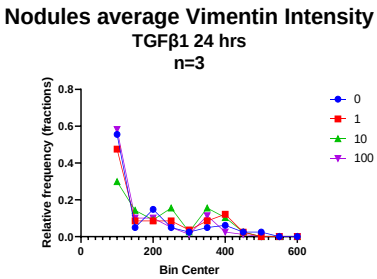

E

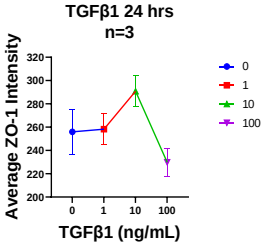

E1

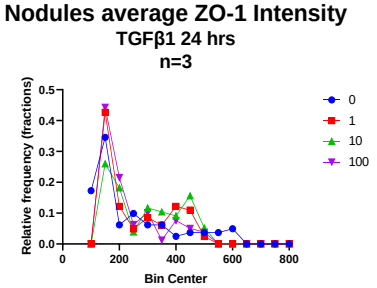

Figure 5.47. Effects of TGFβ1 24 hours treatment in hPTC nodules in monoculture on nodule area, average H33342 nodule intensity, E-Cadherin average nodule intensity, Vimentin average nodule intensity, and ZO-1 average nodule intensity depicted as dose-response curves and frequency of distribution graphs. Each data point is the mean of three biological (K3, K6, K7) and two technical replicates. Error bars represent S.E.M.

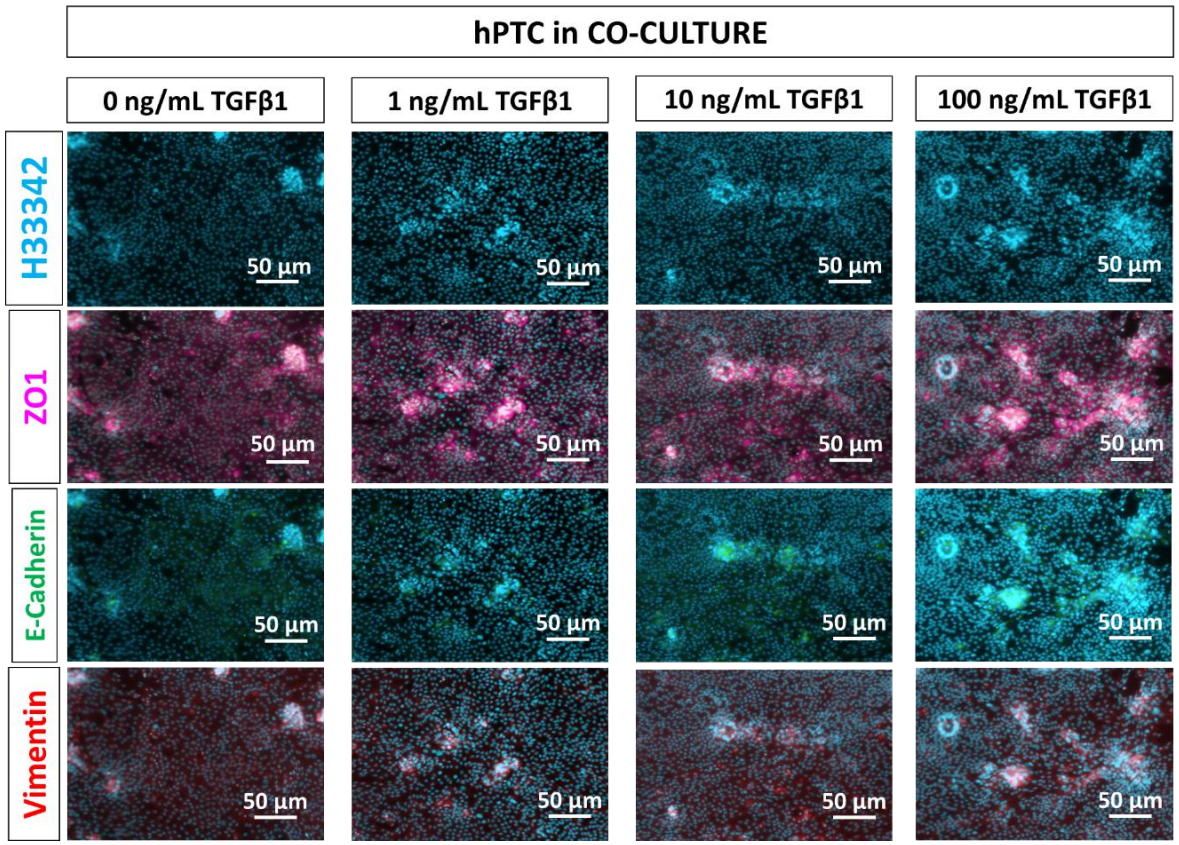

Figure 5.48. Fluorescence images of hPTC monolayers in co-culture cultured on 96-Transwell inserts treated with increasing concentrations of TGFβ1 for 24 hours. Cells were fixed and immunofluoresce-stained with nuclear stain Hoechst 33342, and antibodies against tight junction markers ZO1 and E-Cadherin, and mesenchymal marker Vimentin. Exposure times and focus were kept constant across the plate. Images were acquired at 10X magnification (scale bars=50µm).

The algorithms used to investigate variations in tight junction and mesenchymal marker expression in the context of renal fibrosis are used on hPTC in co-culture, too. **Figures 5.48 to 5.50** display hPTC monolayers on 96-Transwell inserts treated with increasing concentrations of TGFβ1, TNFα, and angiotensin II expressing ZO-1, E-Cadherin, and vimentin. Regarding the single-cell data, nuclear area, average nuclear intensity of Hoechst 33342 staining, and average cell expression of the markers are plotted as dose-response curves and frequency of distribution curves as previously described. As for the monoculture condition, the most striking feature noticeable in these images is the presence of epithelial nodules appearing among the monolayers as the concentration of treatment increases. **Figure 5.52** focuses on describing the effects of TGFβ1 on intensity-based features of hPTC in co-culture. The frequency of distribution curves show that there is a variation in the frequency of distribution of the cell populations as compared to the untreated control curve when nuclear area,

average nuclear intensity of Hoechst 33342 staining, and average cell expression of ZO-1 are measured as the bin centre of curves associated with treatment shifts. The shift of between the untreated and treated frequency of distribution curves is more pronounced after TNFα treatment (**Figure 5.53**) for average nuclear intensity of Hoechst 33342 staining, average cell expression of E-Cadherin, average cell expression of vimentin, and average cell expression of ZO-1. Regarding the effects of angiotensin II on hPTC in co-culture (**Figure 5.54**), the widest shift between frequency of distribution curves representing treated and untreated cell population is displayed by endpoints measuring average cell expression of vimentin and ZO-1, and for both features the most striking change in phenotype seem to take place at the highest dose of 1000 nM angiotensin II.

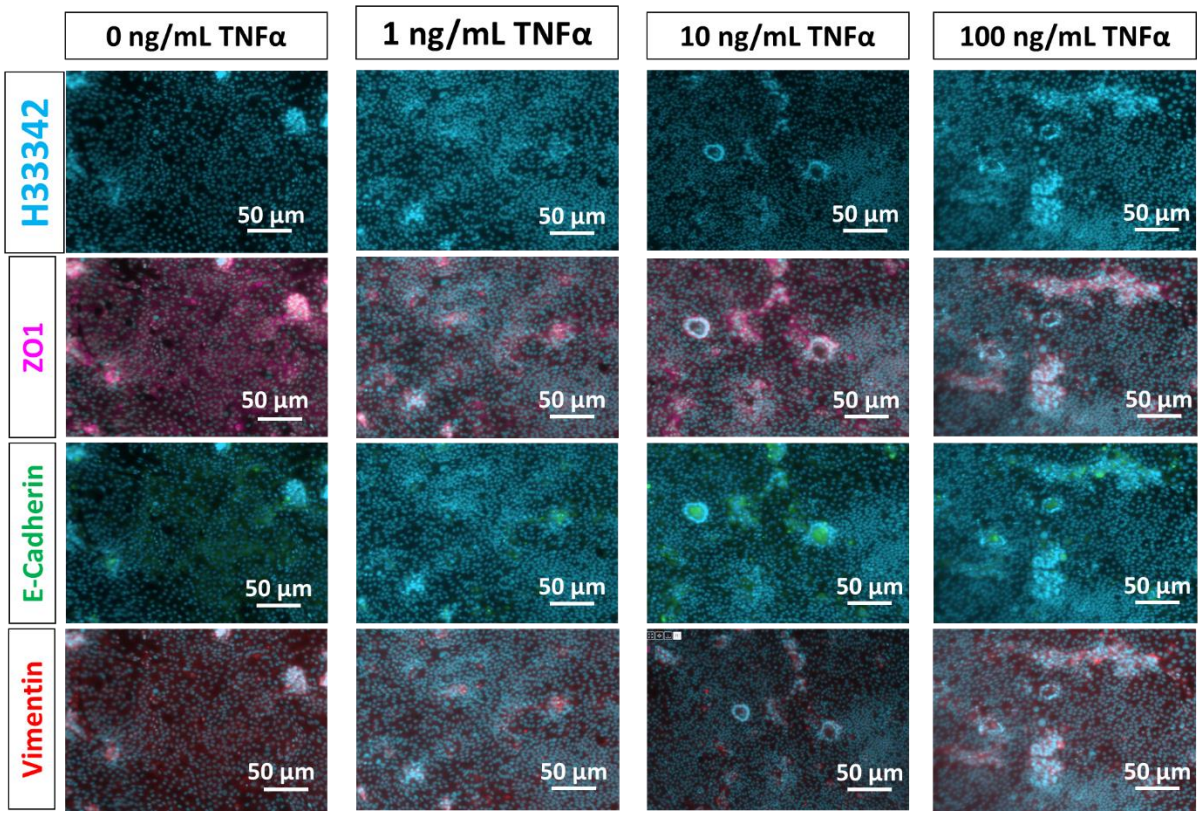

Figure 5.49. Fluorescence images of hPTC monolayers in co-culture cultured on 96-Transwell inserts treated with increasing concentrations of TNFα for 24 hours. Cells were fixed and immunofluoresce-stained with nuclear stain Hoechst 33342, and antibodies against tight junction markers ZO1 and E-Cadherin, and mesenchymal marker Vimentin. Exposure times and focus were kept constant across the plate. Images were acquired at 10X magnification (scale bars=50µm).

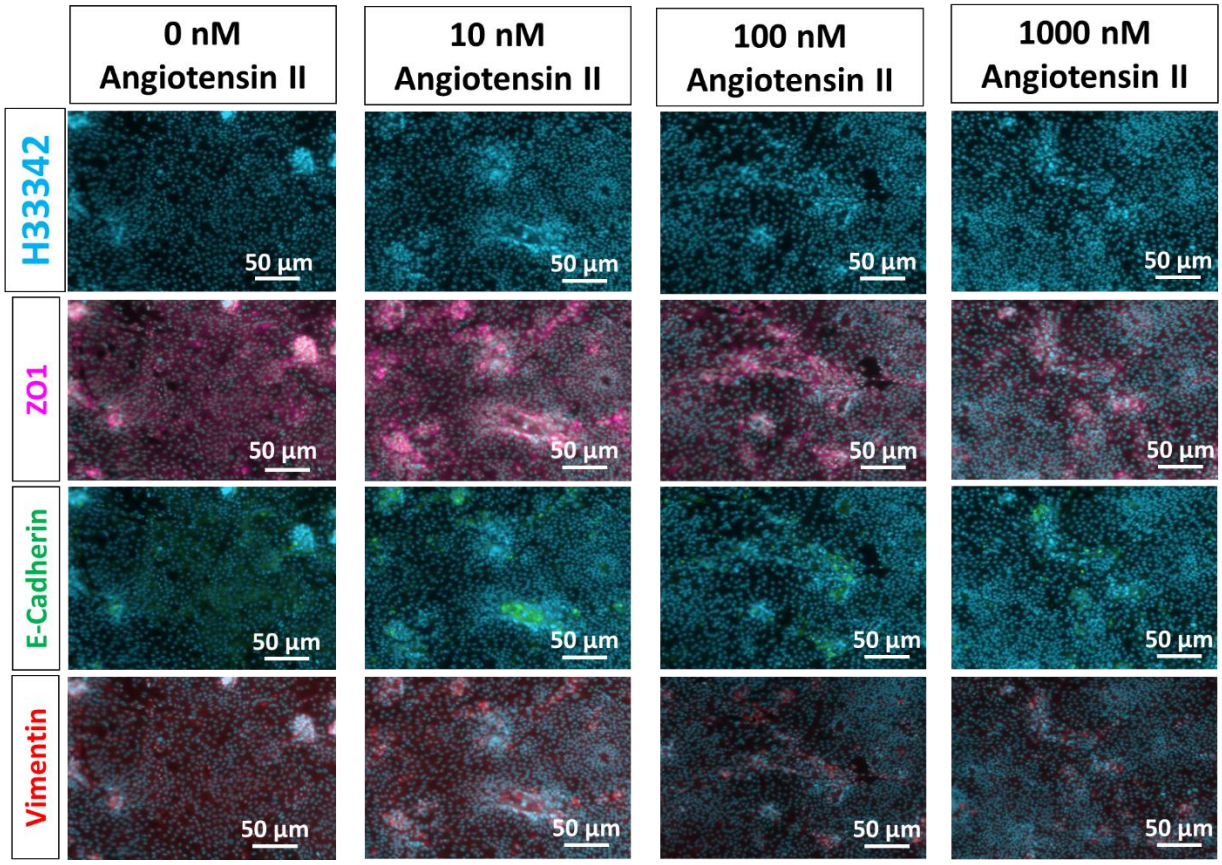

Figure 5.50. Fluorescence images of hPTC monolayers in co-culture cultured on 96-Transwell inserts treated with increasing concentrations of angiotensin II for 24 hours. Cells were fixed and immunofluoresce-stained with nuclear stain Hoechst 33342, and antibodies against tight junction markers ZO1 and E-Cadherin, and mesenchymal marker Vimentin. Exposure times and focus were kept constant across the plate. Images were acquired at 10X magnification (scale bars=50µm).

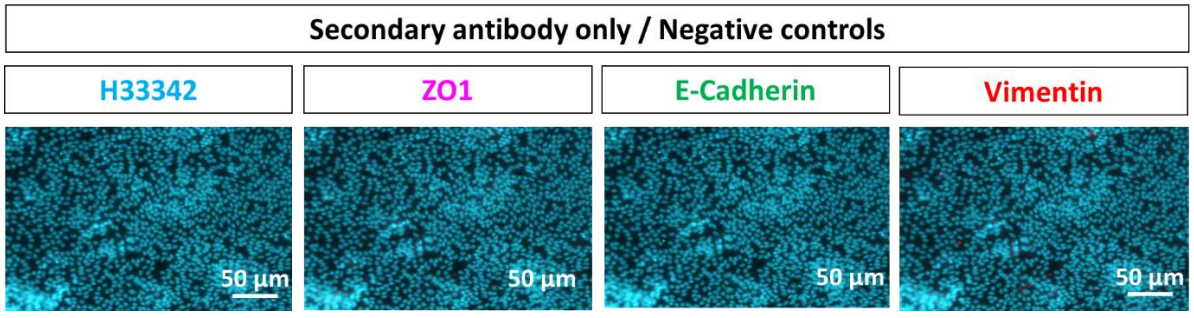

Figure 5.51. Fluorescence images of hPTC monolayers in monoculture cultured on 96-Transwell inserts. Cells were fixed and immunofluoresce-stained with nuclear stain Hoechst 33342, and secondary antibodies used in previous experiments namely, goat anti rabbit Alexa Fluor 647 (ZO1), goat anti mouse Alexa Fluor 488 (E-Cadherin), and donkey anti goat Alexa Fluor 594 (Vimentin). Exposure times and focus were kept constant across the plate. Images were acquired at 10X magnification (scale bars=50µm).

TGFβ1 does not induces significant changes in the endpoints measured in the nodule formation assays (**Figure 5.55**). TNFα induces a significant decrease in expression of vimentin within the epithelial nodules. Angiotensin II induces a significant increase in nodule area as the dose increases **(Figure 5.56**). Treatment of hPTC in co-culture with 1000 nM angiotensin II also induces a significant decrease in E-Cadherin, vimentin, and ZO-1 expression within the nodules (**Figure 5.57**).

hPTCs in co-culture on 96-Transwell plate, well insert
TGFß1, cell measurements

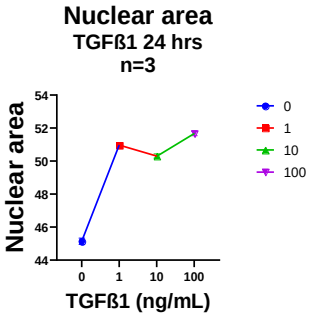

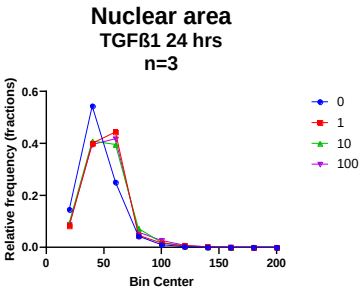

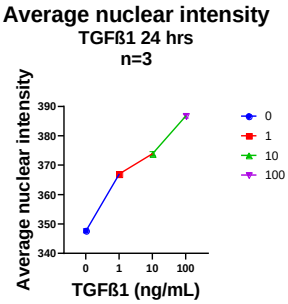

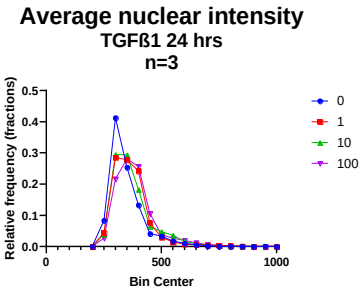

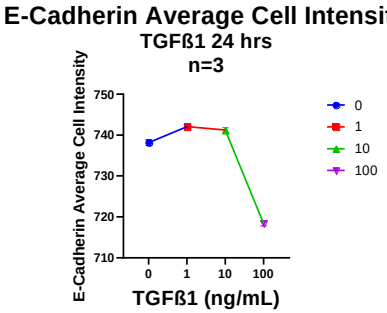

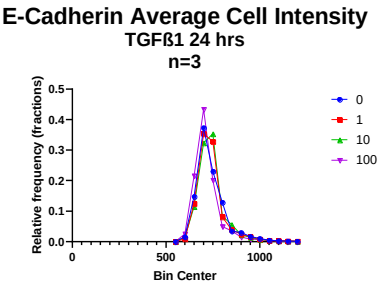

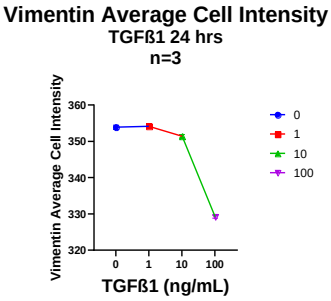

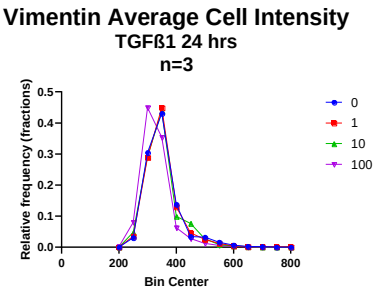

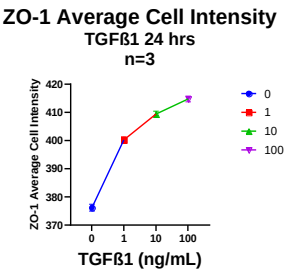

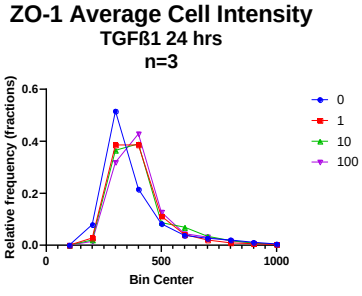

Figure 5.52. Effects of TGFβ1 24 hours treatment in hPTC monolayers in co-culture on nuclear area, average H33342 nuclear intensity, E-Cadherin average cell intensity, Vimentin average cell intensity, and ZO-1 average cell intensity depicted as dose-response curves and frequency of distribution graphs. Each data point is the mean of three biological (K8, K9, K10) and two technical replicates. Error bars represent S.E.M.

hPTCs in co-culture on 96-Transwell plate, well insert
TNFα, cell measurements

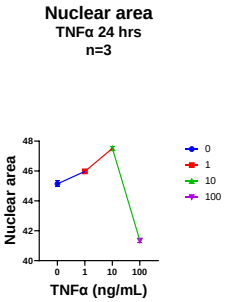

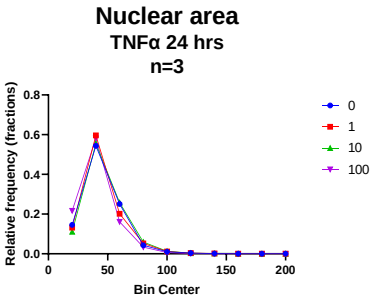

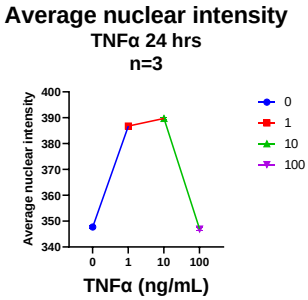

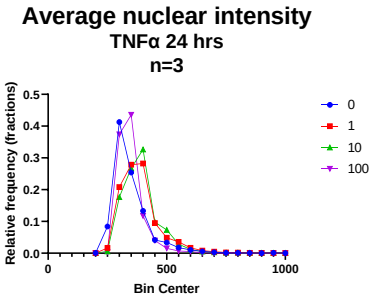

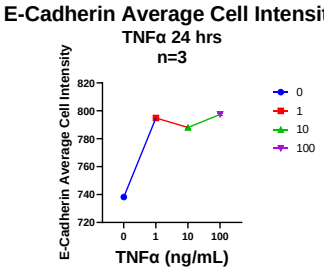

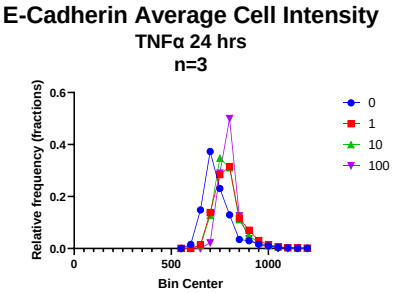

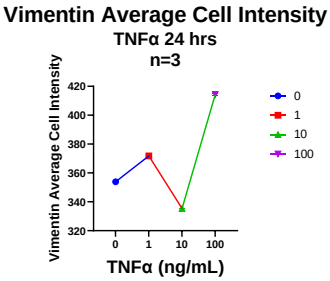

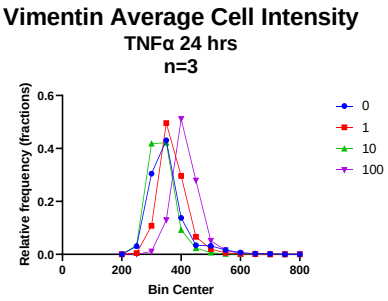

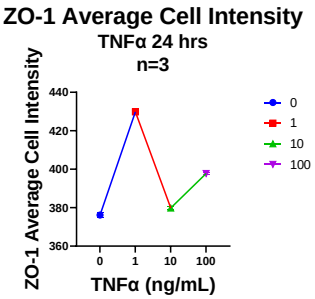

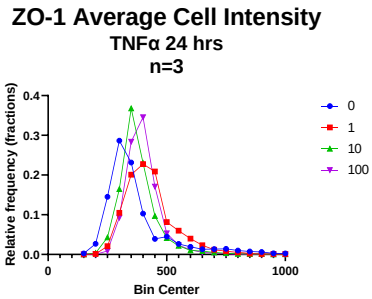

Figure 5.53. Effects of TNFα 24 hours treatment in hPTC monolayers in co-culture on nuclear area, average H33342 nuclear intensity, E-Cadherin average cell intensity, Vimentin average cell intensity, and ZO-1 average cell intensity depicted as dose-response curves and frequency of distribution graphs. Each data point is the mean of three biological (K8, K9, K10) and two technical replicates. Error bars represent S.E.M.

hPTCs in co-culture on 96-Transwell plate, well insert
Angiotensin II, cell measurements

Nuclear area
Angiotensin II 24 hrs
n=3

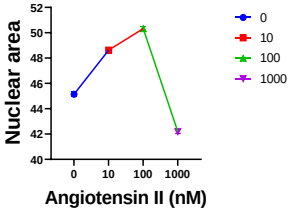

Nuclear area
Angiotensin II 24 hrs
n=3

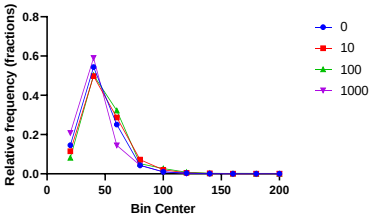

Average nuclear intensity
Angiotensin II 24 hrs
n=3

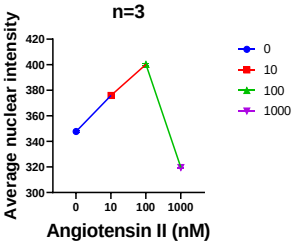

Average nuclear intensity
Angiotensin II 24 hrs
n=3

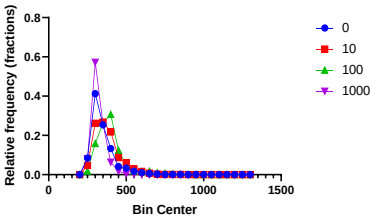

E-Cadherin Average Cell Intensity
Angiotensin II 24 hrs
n=3

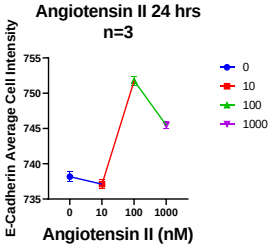

E-Cadherin Average Cell Intensity
Angiotensin II 24 hrs
n=3

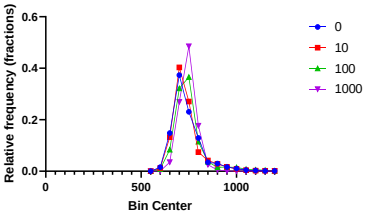

Vimentin Average Cell Intensity
Angiotensin II 24 hrs
n=3

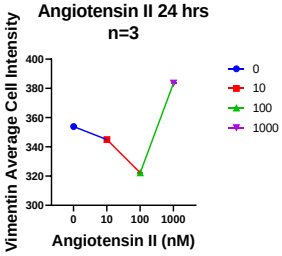

Vimentin Average Cell Intensity
Angiotensin II 24 hrs
n=3

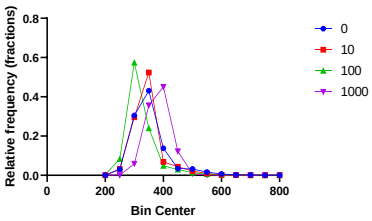

ZO-1 Average Cell Intensity
Angiotensin II 24 hrs
n=3

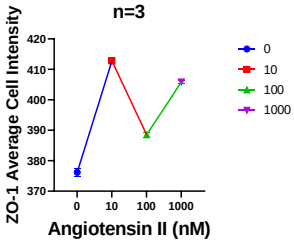

ZO-1 Average Cell Intensity
Angiotensin II 24 hrs
n=3

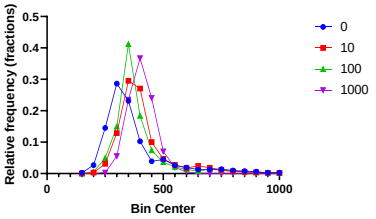

Figure 5.54. Effects of Angiotensin II 24 hours treatment in hPTC monolayers in co-culture on nuclear area, average H33342 nuclear intensity, E-Cadherin average cell intensity, Vimentin average cell intensity, and ZO-1 average cell intensity depicted as dose-response curves and frequency of distribution graphs. Each data point is the mean of three biological (K8, K9, K10) and two technical replicates. Error bars represent S.E.M.

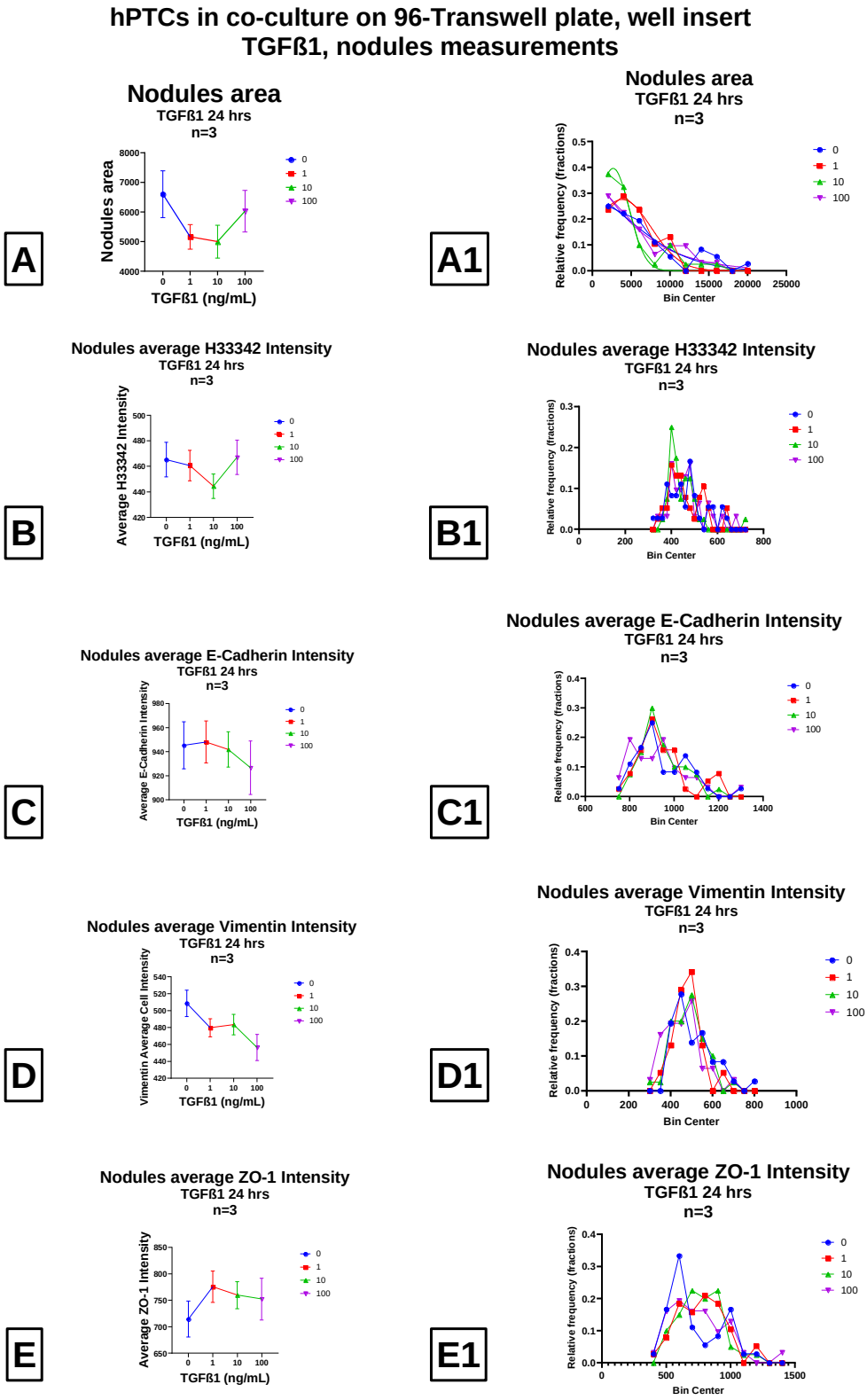

Figure 5.55. Effects of TGFß1 24 hours treatment in hPTC nodules in co-culture on nuclear area, average H33342 nuclear intensity, E-Cadherin average cell intensity, Vimentin average cell intensity, and ZO-1 average cell intensity depicted as dose-response curves and frequency of distribution graphs. Each data point is the mean of three biological (K8, K9, K10) and two technical replicates. Error bars represent S.E.M.

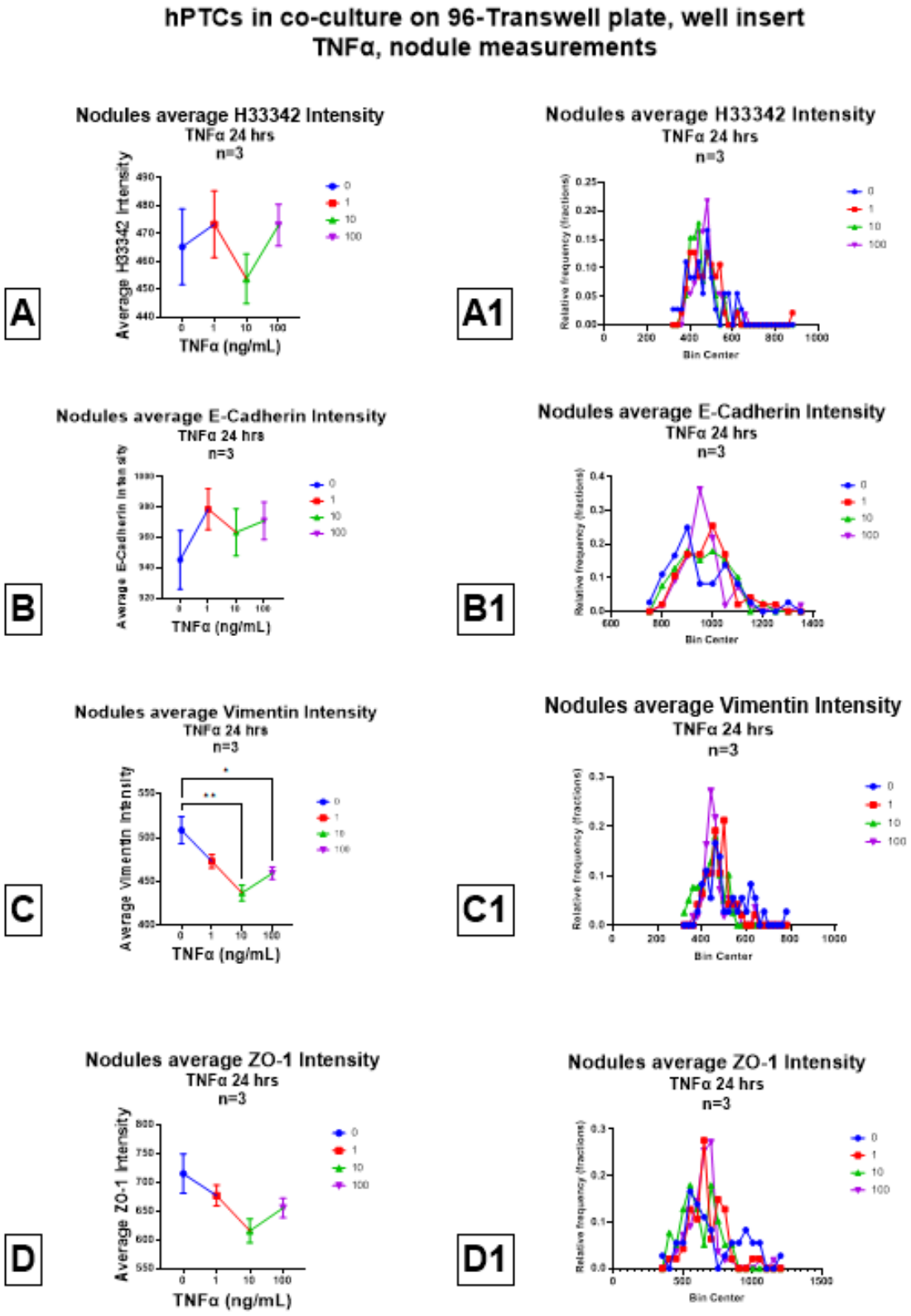

Figure 5.56. Effects of TNFα 24 hours treatment in hPTC nodules in co-culture on nuclear area, average H33342 nuclear intensity, E-Cadherin average cell intensity, Vimentin average cell intensity, and ZO-1 average cell intensity depicted as dose-response curves and frequency of distribution graphs. Each data point is the mean of three biological (K8, K9, K10) and two

technical replicates. Error bars represent S.E.M. Statistical significance is depicted as '' p<0.05, '**' p<0.01.*

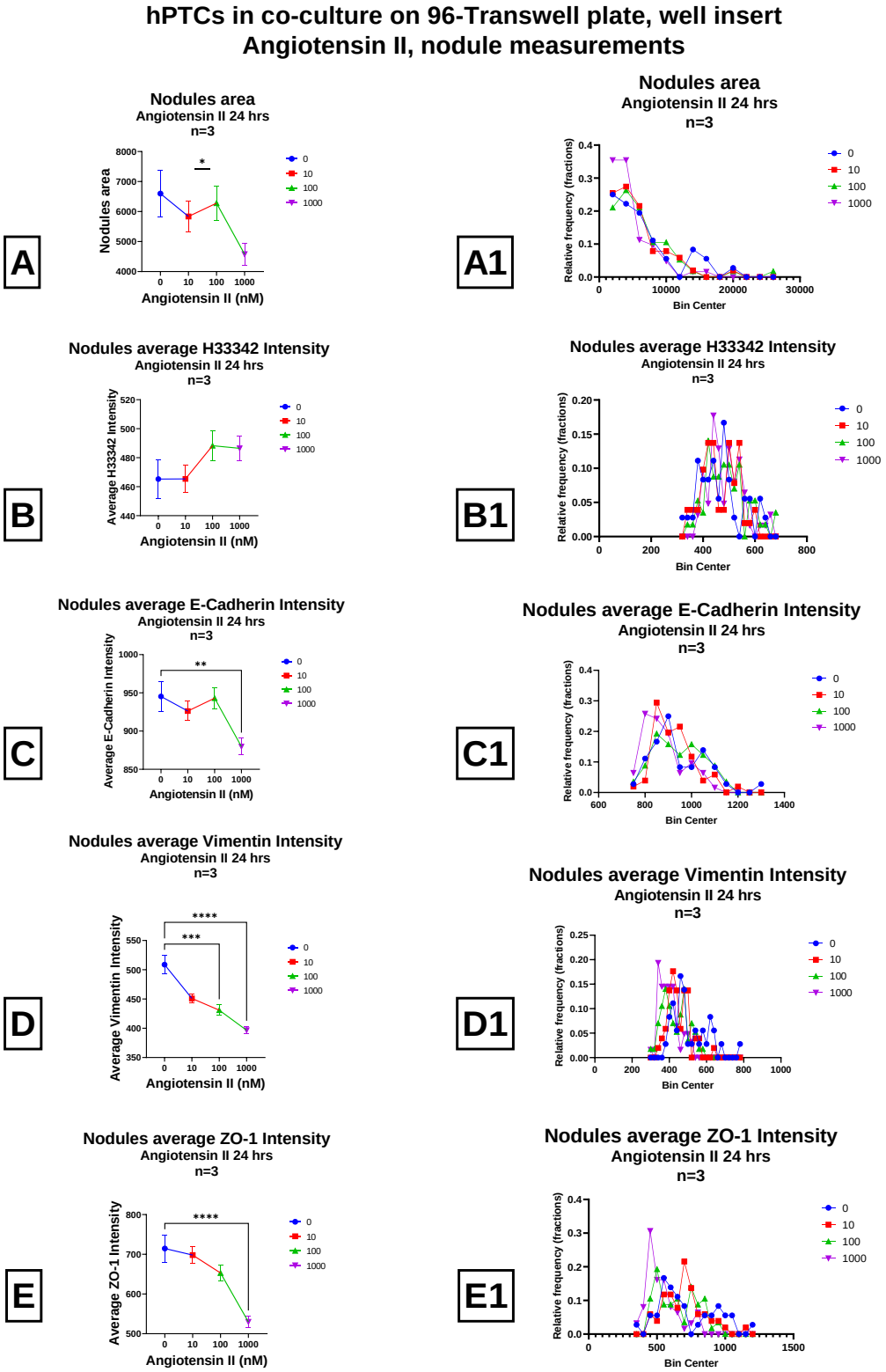

Figure 5.57. Effects of Angiotensin II 24 hours treatment in hPTC nodules in co-culture on nuclear area, average H33342 nuclear intensity, E-Cadherin average cell intensity, Vimentin average cell intensity, and ZO-1 average cell intensity depicted as dose-response curves and

frequency of distribution graphs. Each data point is the mean of three biological (K8, K9, K10) and two technical replicates. Error bars represent S.E.M. Statistical significance is depicted as '' p<0.05, '**' p<0.01.*

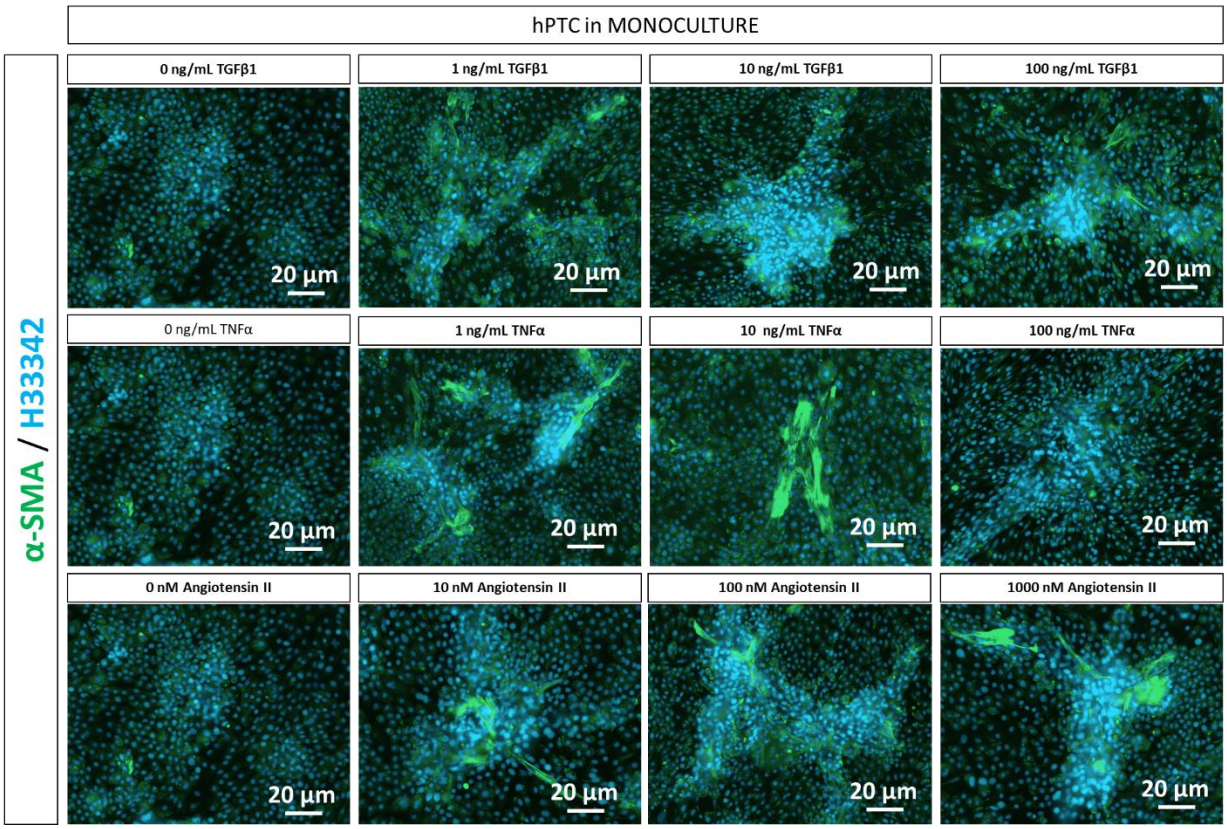

Figure 5.58. Fluorescence images of hPTC monolayers in monoculture cultured on black walled 96-well plates treated with increasing concentrations of polymyxin B for 24 hours. Cells were fixed and immunofluoresce-stained with nuclear stain Hoechst 33342, and antibodies against tight junction markers ZO1 and E-Cadherin, and mesenchymal marker Vimentin. Exposure times and focus were kept constant across the plate. Images were acquired at 10X magnification (scale bars=50µm)..

The data showcased so far highlight that the assays developed via high content imaging are able to profile the phenotypical changes associated with treatment of hPTC in mono- and co-culture by comparing the intensity-based endpoints measured from cell populations treated with increasing doses of pro-fibrotic compounds to the ones of the untreated cell population. Furthermore, image analysis of nodules formed by epithelial cells after pro-fibrotic treatment indicates that these objects' features change depending on type and concentration of treatment to which the cells are exposed. We hypothesise that the formation of the epithelial nodules is associated with epithelial barrier disruption which is underlined by the significant changes in TEER measurements post-treatment displayed in **Figure 5.19.** As explored in Chapter 4, when trialling different co-culture methods of tubular epithelial cells and renal fibroblasts we discovered that when culturing both cell types in the same compartment (contact co-culture model), cells would assemble and form 3D structures that would disrupt the epithelial barrier function rendering the *in vitro* model of the proximal tubule interstitial interface leaky and unable to actively transport compounds from lumen to the interstitium

and vice versa. Furthermore, we proved that the presence of renal fibroblasts in culture disrupted tight junction formation and maintenance in the epithelial monolayer by immunofluorescence staining for ZO-1. The agglomerates – or *nodules* – were positive for apoptosis marker Annexin V, suggesting the cells that formed these structures were somewhat resembling fibrotic phenotype. After these observations, we decided to investigate further the phenotype of the cells making up the nodules formed after pro-fibrotic treatment. hPTC monolayers are treated with increasing concentrations of TGFβ1, TNFα, and angiotensin II, and they undergo immunofluorescence staining with a primary antibody against mesenchymal marker αSMA and a secondary antibody conjugated to Alexa Fluor 488™. The images obtained from this experiment are shown in **Figure 5.58.** The untreated control hPTC shown in the first column displays some basal nodule formation, but these structures do not seem to express the marker, whereas the nodules formed after treatment with increasing concentrations of all the pro-fibrotic compounds show clear presence of contractile fibres typical of myofibroblasts. Hence, these images suggest that the nodules formed by epithelial cells in response to pro-fibrotic stimuli *in vitro* are formed by proximal tubule cells that acquire a migratory and contractile phenotype by undergoing partial epithelial-to-mesenchymal transition, since they acquire *de novo* αSMA but still express tight junction markers ZO-1 and E-Cadherin within the boundaries of the nodules, thus disrupting epithelial barrier maintenance.

5.8 Pro-fibrotic treatment induces extracellular matrix deposition in HRF in monoculture and co-culture

The assays developed and described so far were aimed mostly at the epithelial component of the renal fibrosis *in vitro* model. Most of the assays developed for the quantification of post-treatment phenotypical changes in hPTC were applied to the human renal fibroblast monolayers too but were largely unable to monitor changes in the cellular molecular events stimulated by pro-fibrotic compounds. Therefore, *ad hoc* high content imaging assays were developed to quantify extracellular matrix deposition onto the synthetic hydrogel coating and fibroblast-to-myofibroblast activation by αSMA expression. Experiments were performed on three biological replicates per culture condition. Human renal fibroblasts were treated with increasing concentrations of pro-fibrotic compounds for 24 hours, where HRF in monoculture were exposed directly to the vehicle of treatment containing the pro-fibrotic compound, whereas HRF in co-culture were exposed indirectly to the treatment (via leakage from the apical compartment and cross-talk with hPTC monolayer); they were fixed and analysed using immunofluorescence staining with antibodies against components of the extracellular matrix (ECM) collagen I and fibronectin, and myofibroblast marker αSMA, with respective secondary antibodies conjugated to fluorophores. Plates are imaged with the high content imager ImageXpress Pico and analysed with an appropriate algorithm via CellReporterXpress, as described in **2.7.9. Figures 5.59 to 5.62** display the images obtained from treating HRF in monoculture with TGFβ1, TNFα, angiotensin II, and polymyxin B: the untreated control images in the first columns show some basal deposition of ECM and some cytoplasmic, but not cytoskeletal, expression of αSMA, while the first two compounds seem to be inducing visible deposition of collagen I and fibronectin (**Figures 5.59 and 5.60**), and co-localization of such ECM fibres with αSMA+ contractile sheaths. The phenotypical changes seem to be most prominent after TNFα treatment, while the presence of myofibroblast-associated fibres is visible at higher concentrations of treatment for both angiotensin II and polymyxin B. An example of image analysis quantification of the monoculture experiments via cell segmentation on CellReporterXpress is shown in **Figure 5.63.** The effects of TGFβ1 treatment on HRF are represented in frequency of distribution graphs relative to endpoints nuclear area, average nuclear intensity of Hoechst 33342, and αSMA (**Figure 5.63 [A1], [B1], [C1]**) which show an overlap between the curves representing the untreated and treated cell populations, suggesting that these intensity-based features do not change as the concentration of compound increases. Conversely, a definite shift is noticeable between the untreated curve (**in blue**) and the treated ones for average cell intensity of fibronectin and collagen I (**Figure 5.63 [D1], [E1]**). To establish whether there is a correlation between the dose of pro-fibrotic compound to which HRF are exposed to and the deposition of extracellular matrix onto the synthetic hydrogel, the mean fluorescence intensity per well emitted by immunofluorescence stained HRF monolayers on black walled 96-well plates excited at the appropriate wavelength is read on the CLARIOstar™ Plate Reader; the hypothesis being that the fluorescence signal emitted by the secondary antibodies conjugated to different fluorophores which have reacted with the primary antibodies against ECM, myofibroblast markers, and nuclear stain will be proportional to the amount of contractile fibres produced by the renal fibroblasts. The results of this experiment are presented in **Figures 5.64 to 5.66,** where the mean intensity

fluorescence per well for each wavelength / marker is plotted against the increasing dose of TGFβ1, TNFα, and angiotensin II. Notably, TGFβ1 seem to induce a significant increase in collagen I deposition at 100 ng/mL as compared to the untreated control (**Figure 5.64 [D]**). TNFα at 10 ng/mL induces a significant increase in mean fluorescence relative to Hoechst 33342 (**Figure 5.65 [A]**), which can be interpreted as an increase in cell number or in DNA being produced in the context of proliferation, while 1 ng/mL TNFα produce a significant increase in fibronectin and collagen I deposition (**Figure 5.65 [C], [D]**) as compared to untreated HRF. Angiotensin II treatment does not seem to induce any significant changes in HRF phenotype (**Figure 5.66**). According to this assay, αSMA expression does not seem to vary significantly as the dose of pro-fibrotic treatments increases.

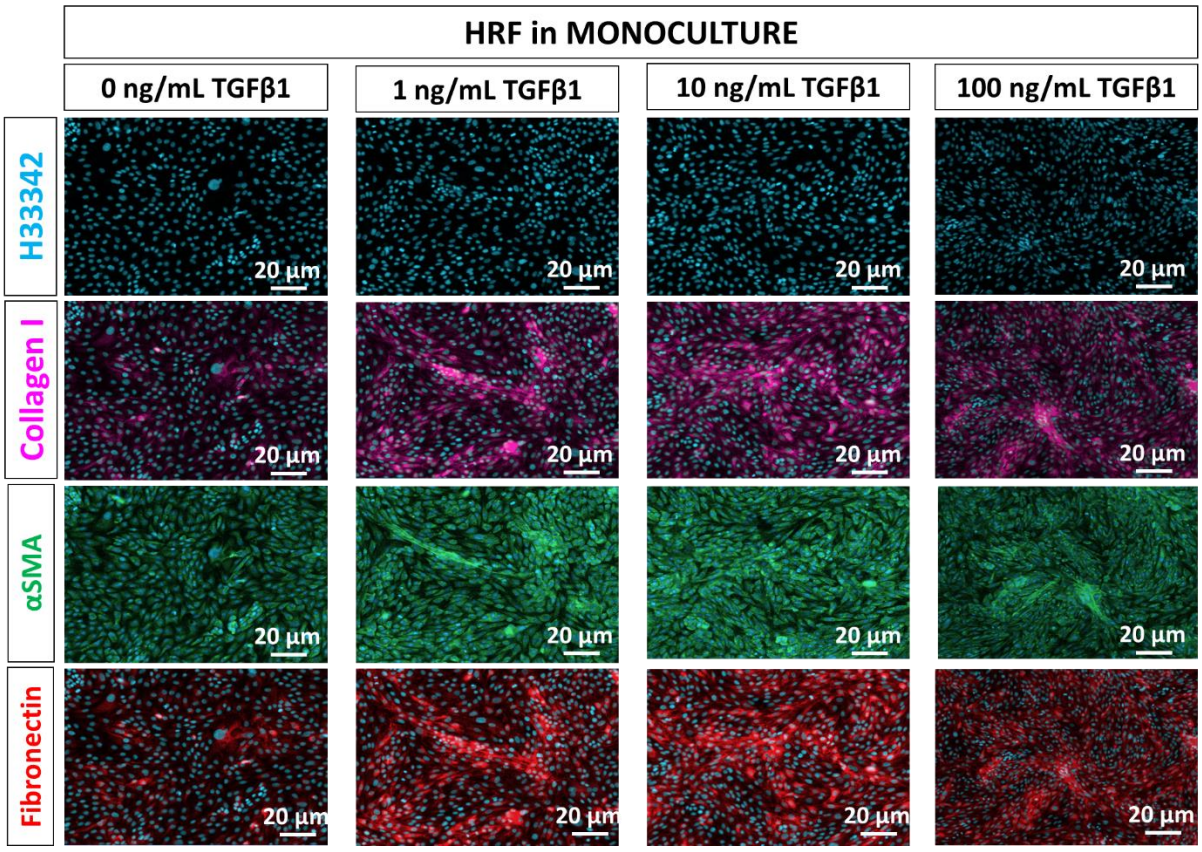

Figure 5.59. Fluorescence images of HRF monolayers in monoculture cultured on black walled 96-well plates treated with increasing concentrations of TGFβ1 for 24 hours. Cells were fixed and immunofluoresce-stained with nuclear stain Hoechst 33342, and antibodies against extra cellular matrix (ECM) components collagen I and fibronectin, and mesenchymal marker α-SMA. Exposure times and focus were kept constant across the plate. Images were acquired at 20X magnification (scale bars=20µm).

.

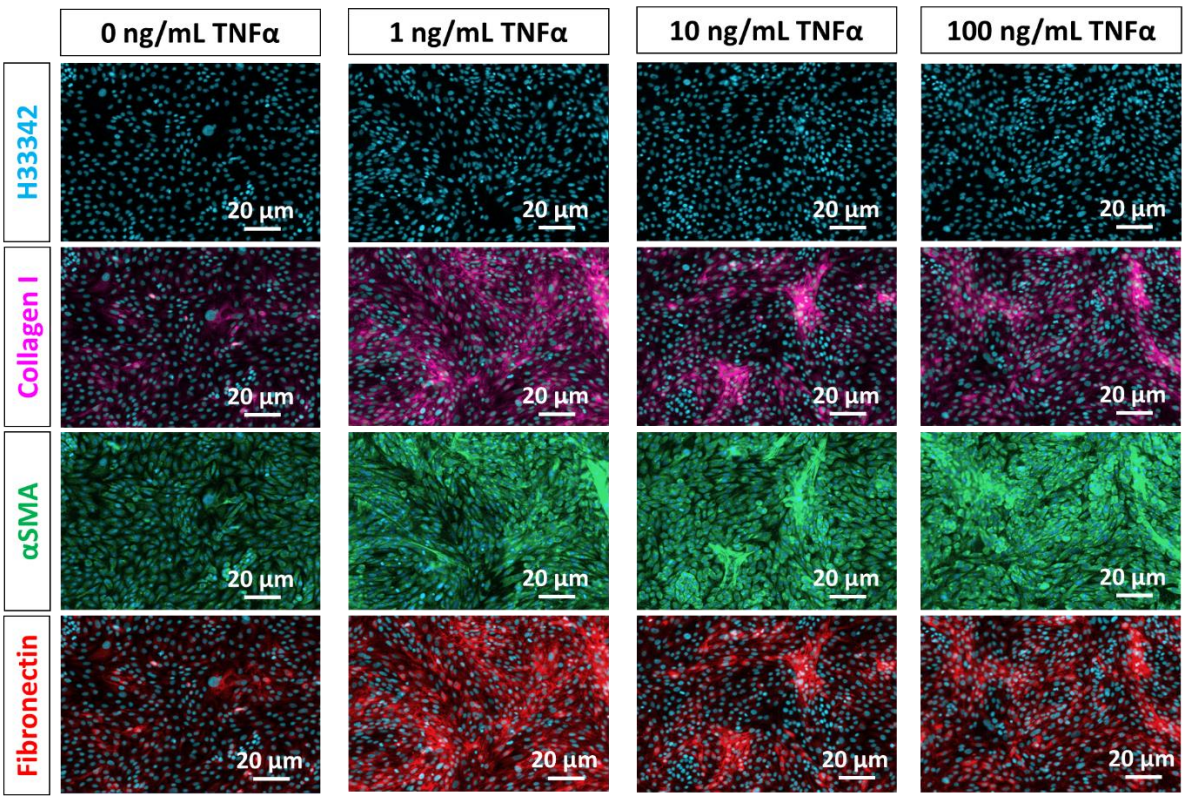

Figure 5.60. Fluorescence images of HRF monolayers in monoculture cultured on black walled 96-well plates treated with increasing concentrations of TNFα for 24 hours. Cells were fixed and immunofluoresce-stained with nuclear stain Hoechst 33342, and antibodies against extra cellular matrix (ECM) components collagen I and fibronectin, and mesenchymal marker α-SMA. Exposure times and focus were kept constant across the plate. Images were acquired at 20X magnification (scale bars=20µm)..

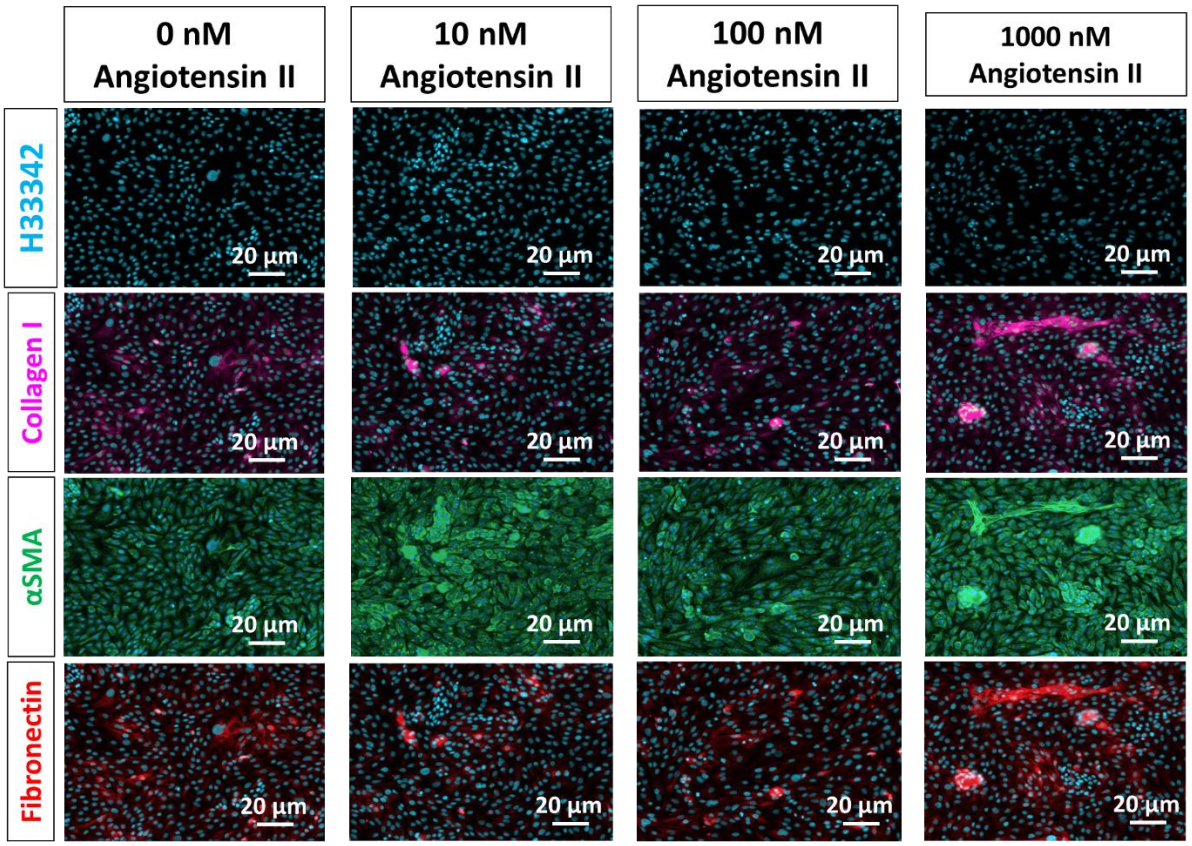

Figure 5.61. Fluorescence images of HRF monolayers in monoculture cultured on black walled 96-well plates treated with increasing concentrations of Angiotensin II for 24 hours. Cells were fixed and immunofluoresce-stained with nuclear stain Hoechst 33342, and antibodies against extra cellular matrix (ECM) components collagen I and fibronectin, and mesenchymal marker α-SMA. Exposure times and focus were kept constant across the plate. Images were acquired at 20X magnification (scale bars=20µm).

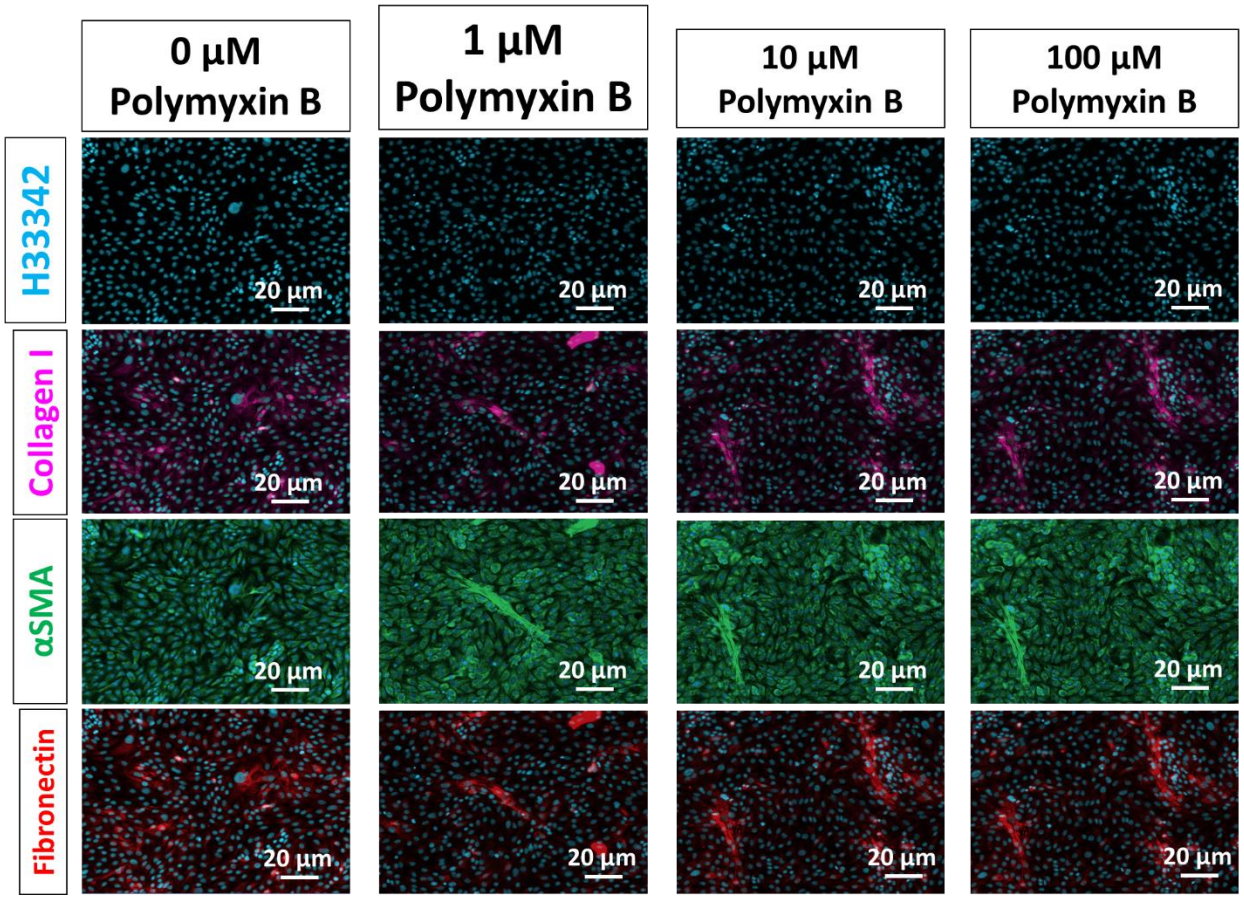

Figure 5.62. Fluorescence images of HRF monolayers in monoculture cultured on black walled 96-well plates treated with increasing concentrations of polymyxin B for 24 hours. Cells were fixed and immunofluoresce-stained with nuclear stain Hoechst 33342, and antibodies against extra cellular matrix (ECM) components collagen I and fibronectin, and mesenchymal marker α-SMA. Exposure times and focus were kept constant across the plate. Images were acquired at 20X magnification (scale bars=20µm).

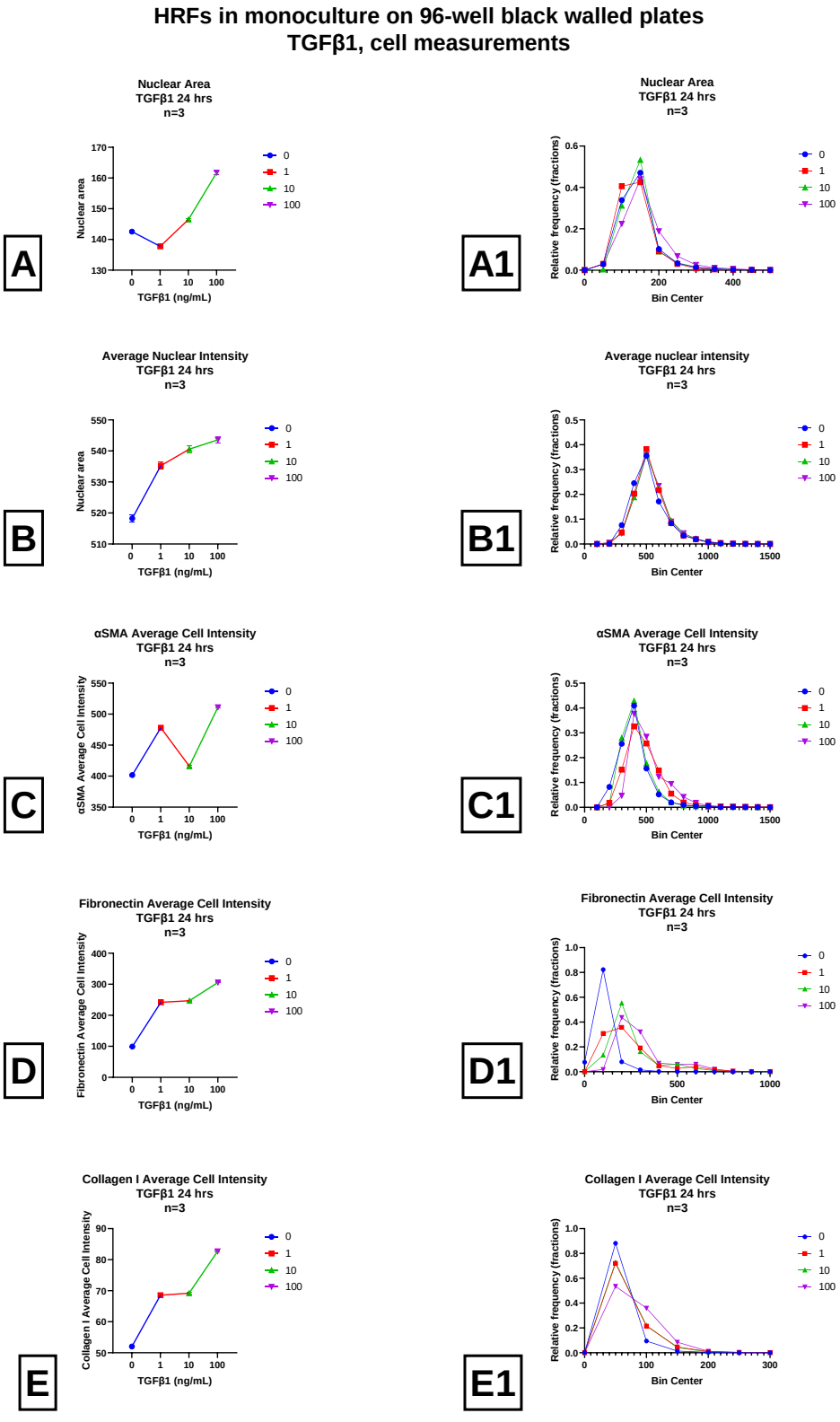

Figure 5.63. Effects of TGFβ1 24-hour treatment in HRF monolayers in monoculture on nuclear area, average H33342 nuclear intensity, αSMA average cell intensity, Fibronectin average cell intensity, and Collagen I average cell intensity depicted as dose-response curves and frequency of distribution graphs. Each data point is the mean of three biological (K3, K6, K7) and two technical replicates. Error bars represent S.E.M.

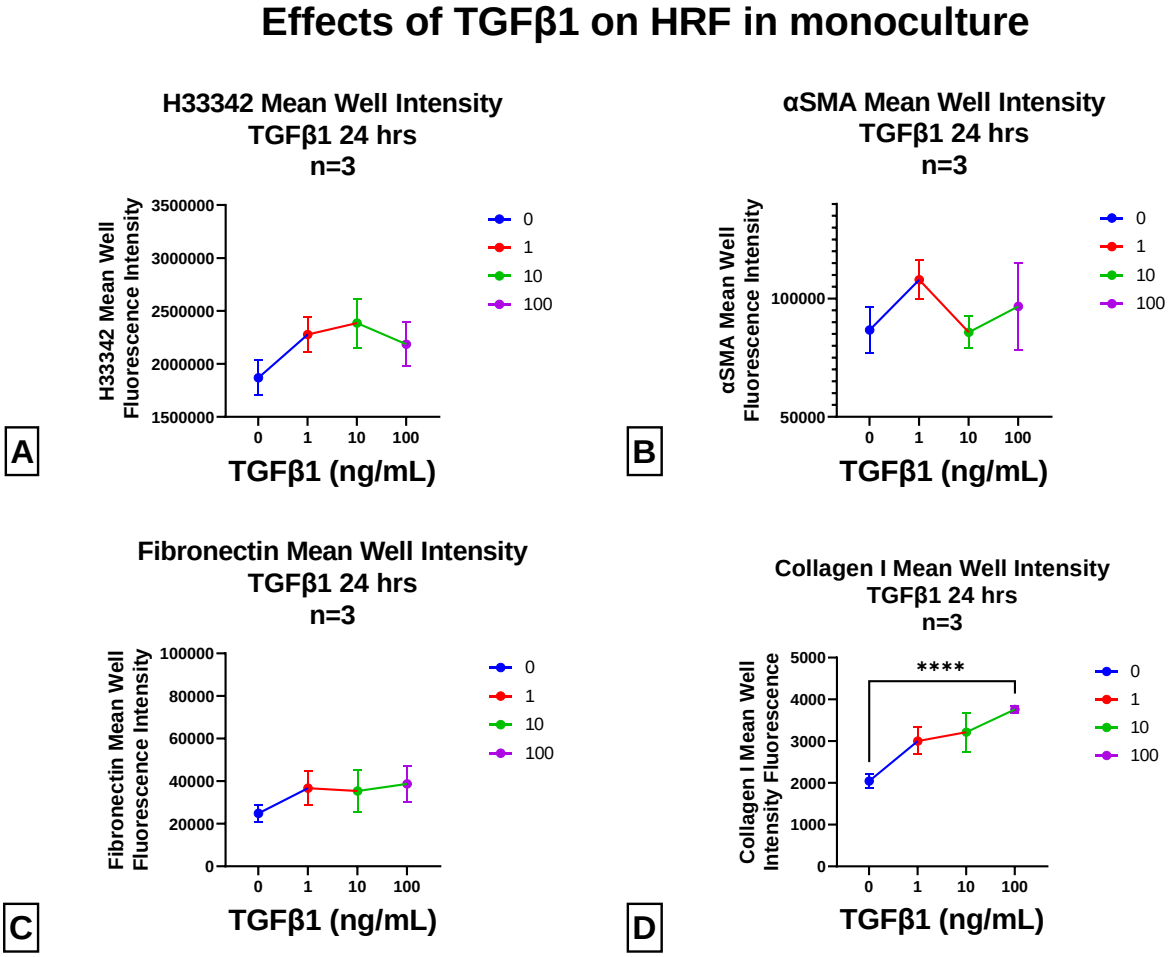

*Figure 5.64. Effects of TGFβ1 24 hours treatment in HRF monolayers in monoculture on mean fluorescence intensity well measurements of H33342 , αSMA, Fibronectin, and Collagen I depicted as dose-response curves. Each data point is the mean of three biological (K3, K6, K7) and two technical replicates. Error bars represent S.E.M. Statistical significance is depicted as '****' p<0.0001.*

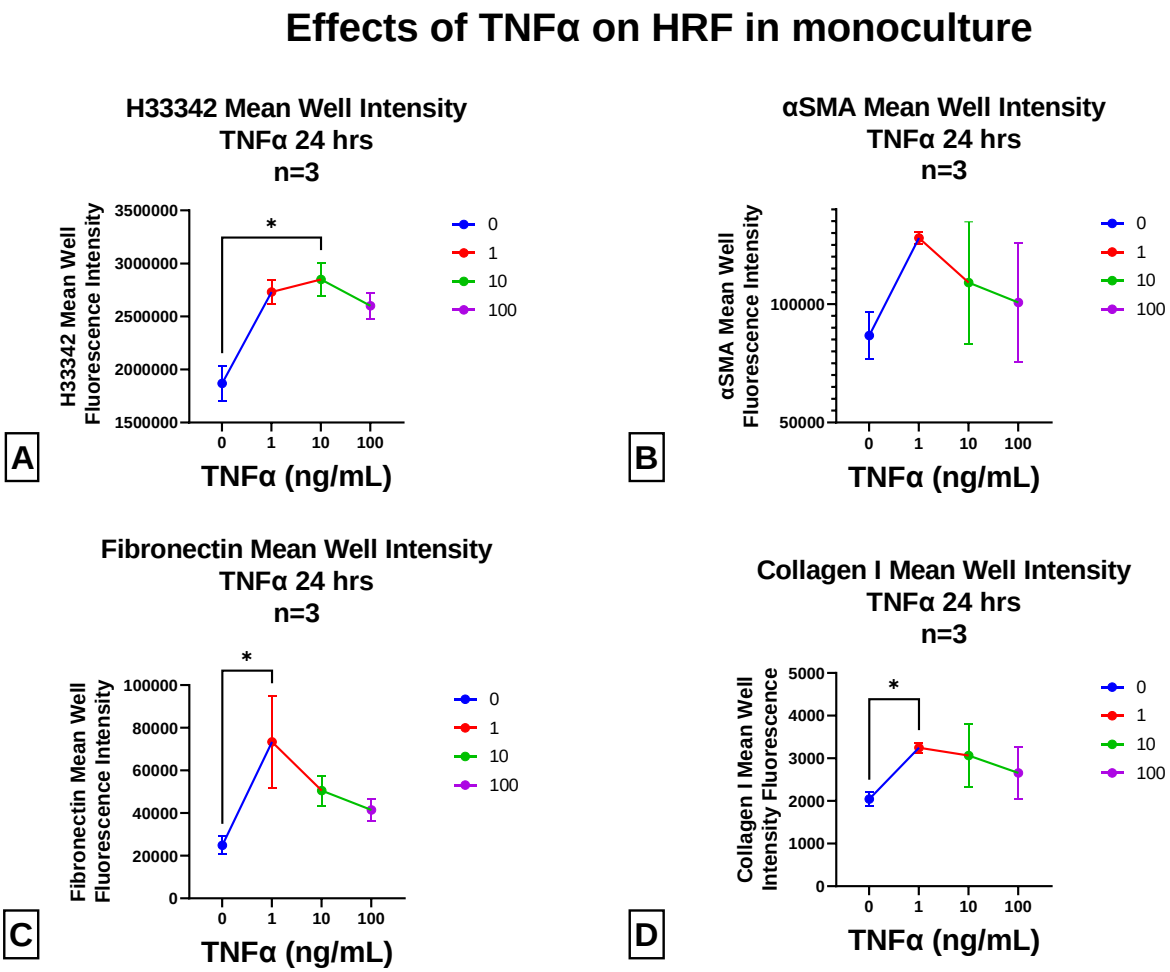

Figure 5.65. Effects of TNFα 24 hours treatment in HRF monolayers in monoculture on mean fluorescence intensity well measurements of H33342, αSMA, Fibronectin, and Collagen I depicted as dose-response curves. Each data point is the mean of three biological (K3, K6, K7) and two technical replicates. Error bars represent S.E.M. Statistical significance is depicted as '' p<0.05.*

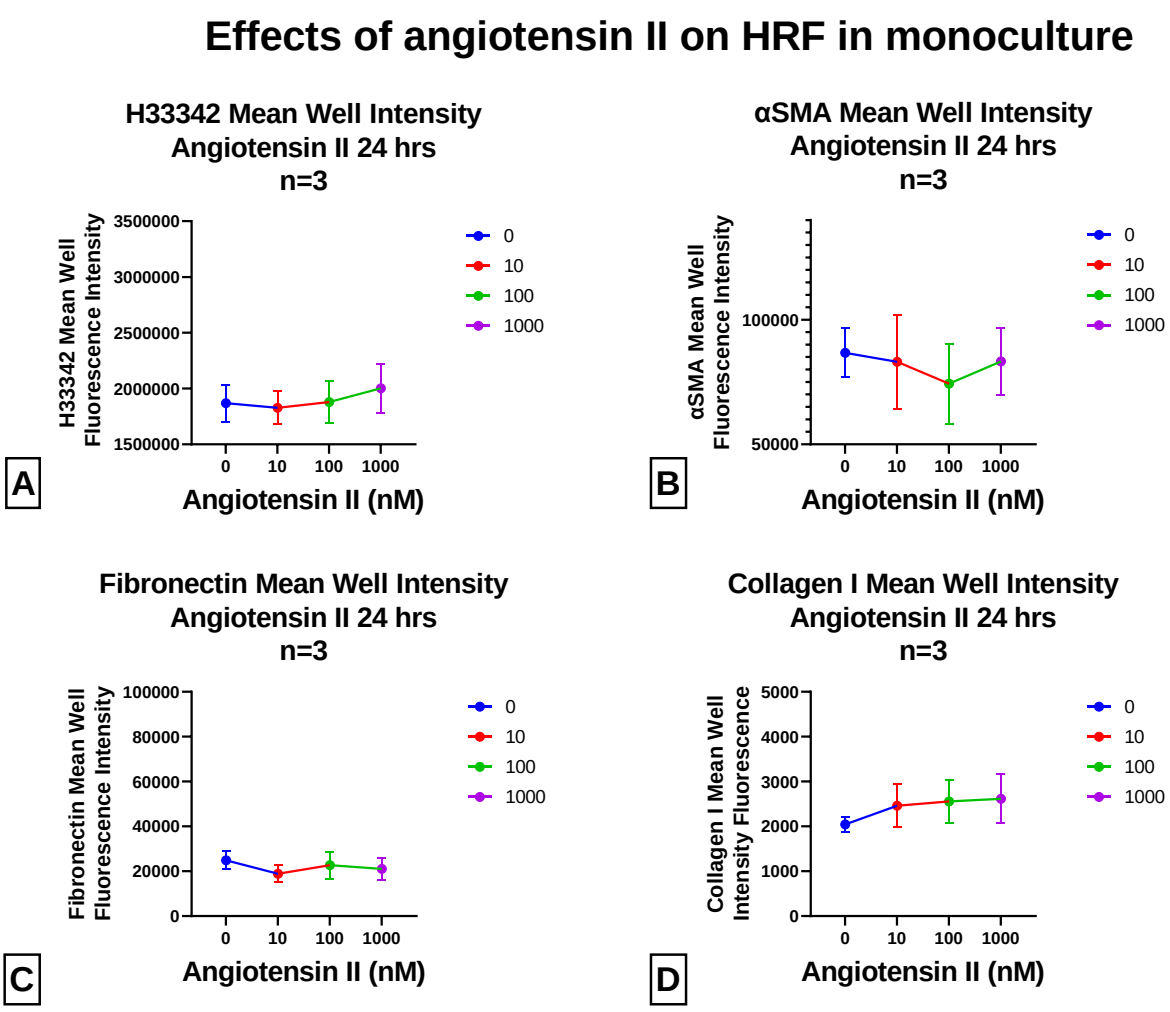

Figure 5.66. Effects of Angiotensin II 24 hours treatment in HRF monolayers in monoculture on mean fluorescence intensity well measurements of H33342, αSMA, Fibronectin, and Collagen I depicted as dose-response curves. Each data point is the mean of three biological (K3, K6, K7) and two technical replicates. Error bars represent S.E.M.

HRF monolayers in co-culture with hPTC grown on the well bottoms of hydrogel-coated 96-Transwell plates are subject to the same immunofluorescence staining, imaging and image analysis procedures previously described after indirect pro-fibrotic treatments. **Figures 5.67 to 5.69** display the images obtained from these experiments, where the first columns represent the untreated control. Overall, the visual difference between untreated control and treated cells in terms of expression of ECM deposition markers seems to be less prominent than in the monoculture images. From a qualitative standpoint, **Figure 5.68** suggests that TNFα might induce the most striking phenotypical change in HRF in co-culture as compared to the milder effects induced by TGFβ1 (**Figure 5.67**) and angiotensin II (**Figure 5.69**). The images are quantified via segmentation on CellReporterXpress as presented in **Figures 5.71 to 5.73**: TGFβ1 treatment produces a slight shift in average cell intensity of collagen I between curves relative to untreated and treated cell populations (**Figure 5.71**), while TNFα and angiotensin II induce a marked shift in the frequency of distribution curves relative to fibronectin and collagen I expression (**Figures 5.72 and 5.73**). In conclusion, pro-fibrotic treatments of HRF seem to induce more conspicuous variations in phenotype in monoculture

rather than in co-culture, in both cases effectively pushing renal fibroblasts towards the expected ECM-depositing, contractile fibrotic phenotype.

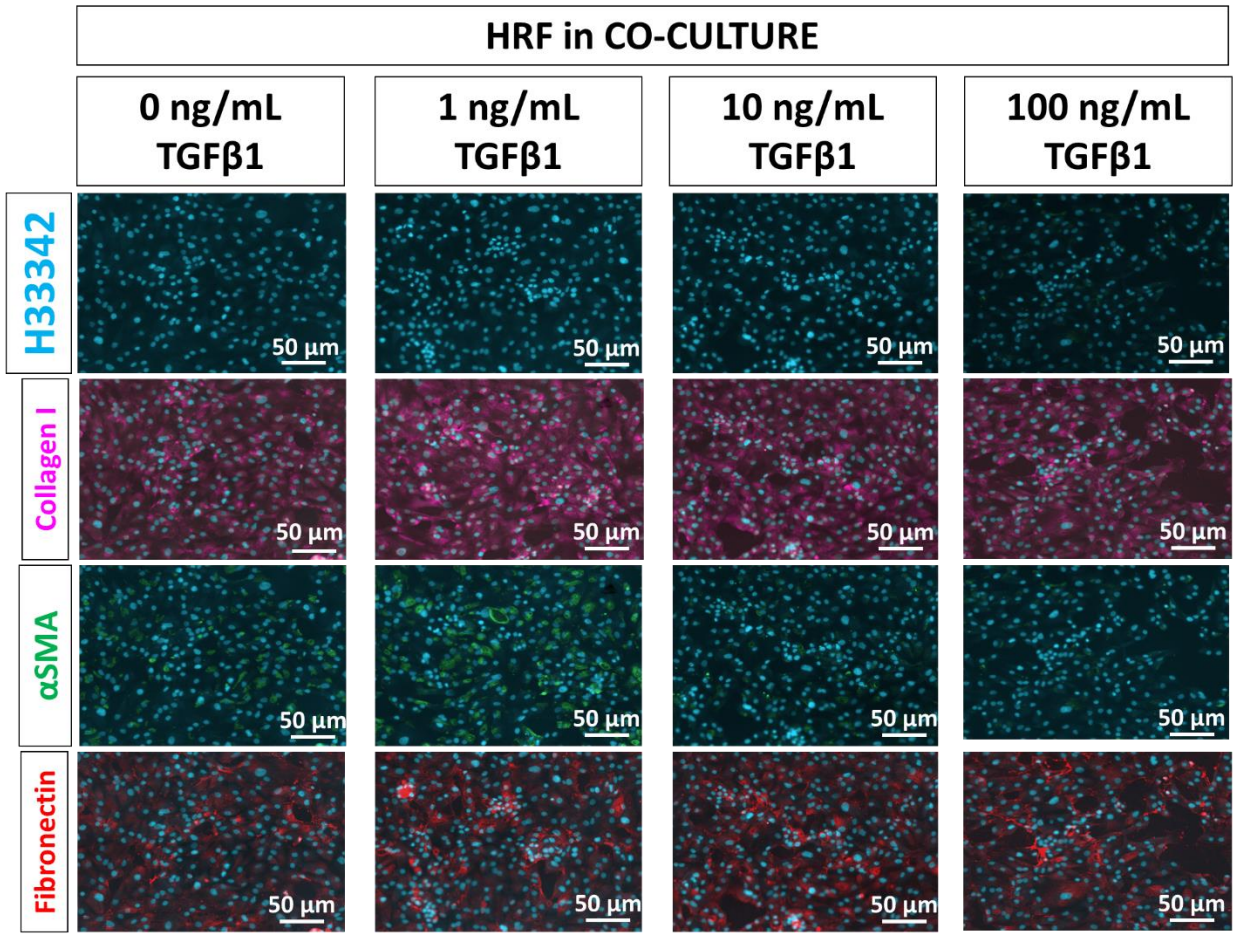

Figure 5.67. Fluorescence images of HRF monolayers in co-culture cultured on 96-Transwell well bottoms treated with increasing concentrations of TGFβ1 for 24 hours. Cells were fixed and immunofluoresce-stained with nuclear stain Hoechst 33342, and antibodies against extra cellular matrix (ECM) components collagen I and fibronectin, and mesenchymal marker α-SMA. Exposure times and focus were kept constant across the plate. Images were acquired at 20X magnification (scale bars=50µm).

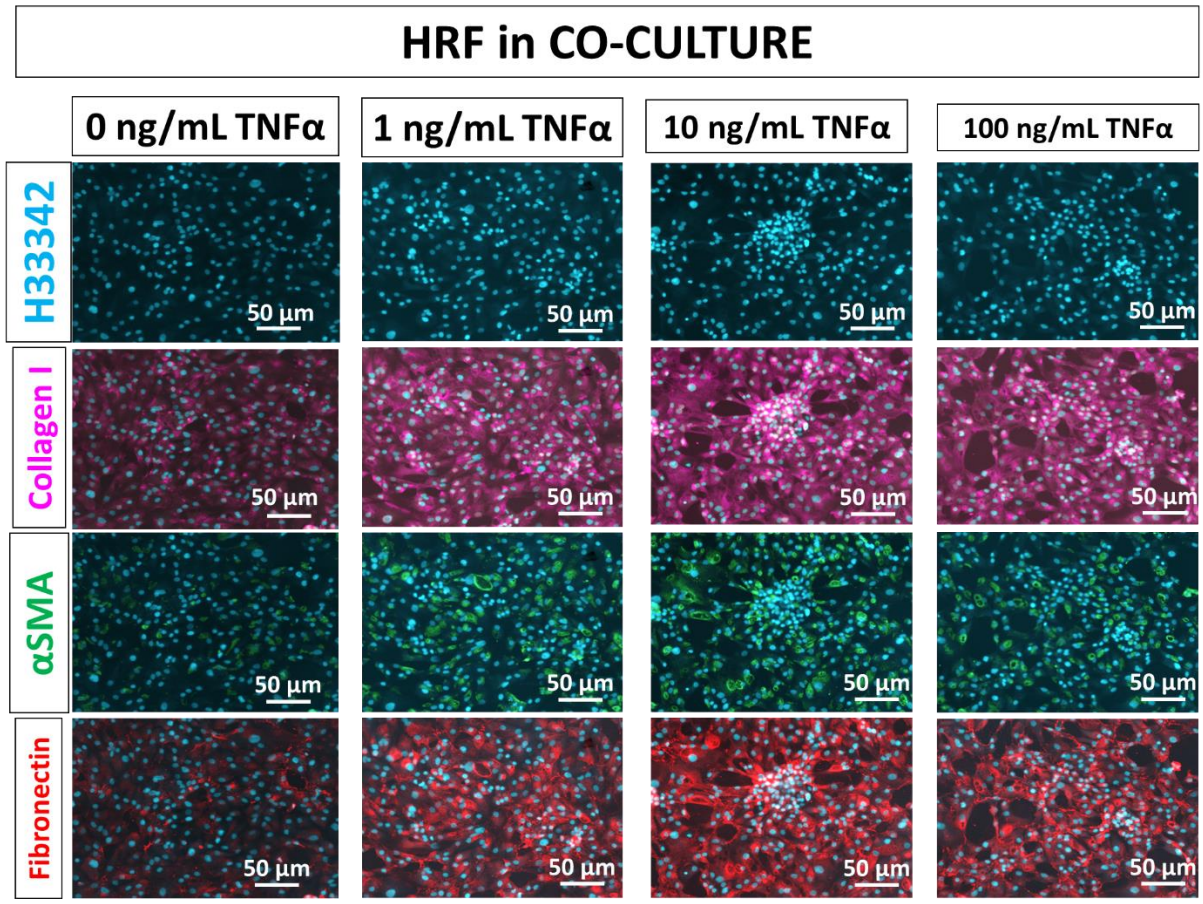

Figure 5.68. Fluorescence images of HRF monolayers in co-culture cultured on 96-Transwell well bottoms treated with increasing concentrations of TNFα for 24 hours. Cells were fixed and immunofluoresce-stained with nuclear stain Hoechst 33342, and antibodies against extra cellular matrix (ECM) components collagen I and fibronectin, and mesenchymal marker α-SMA. Exposure times and focus were kept constant across the plate. Images were acquired at 20X magnification (scale bars=20µm).

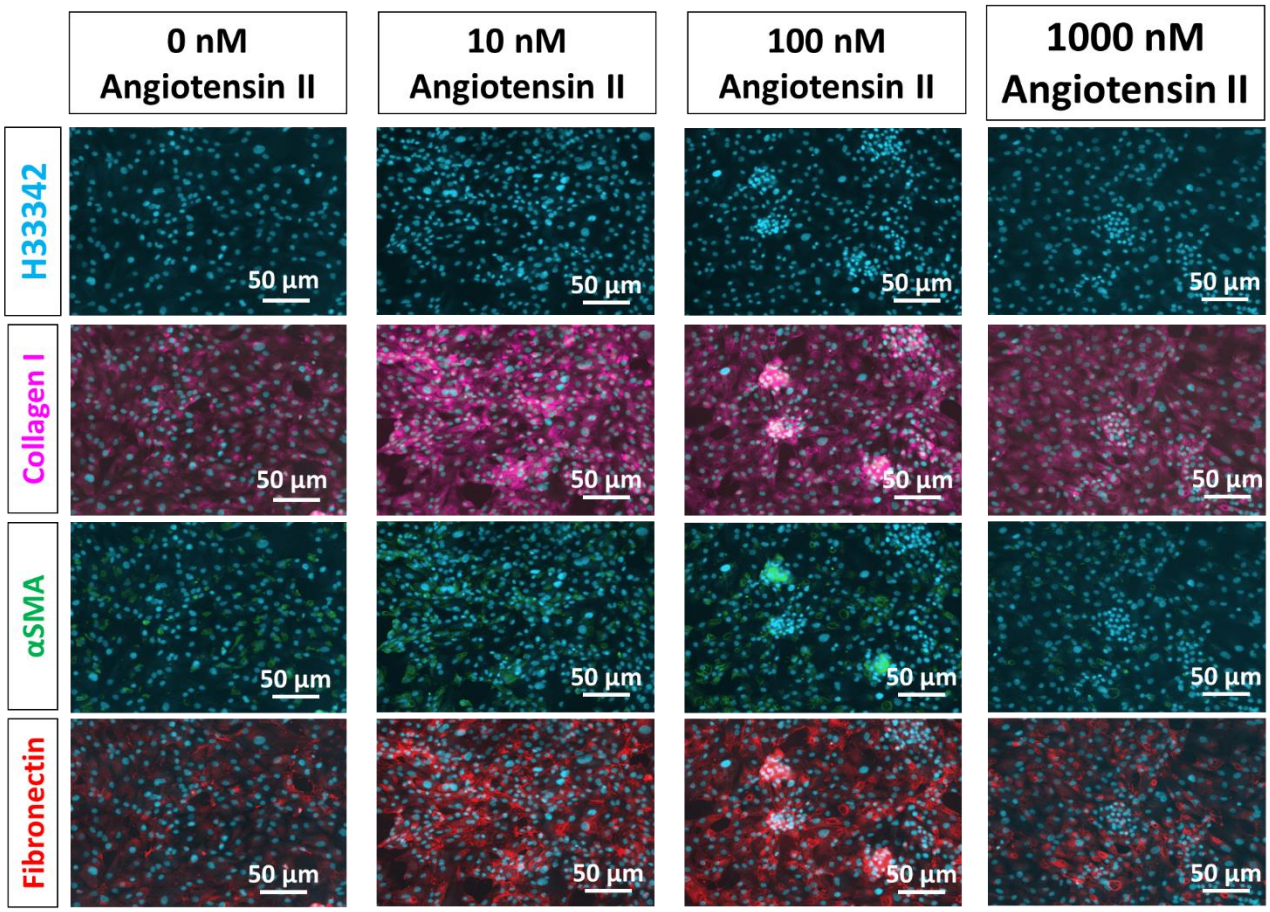

Figure 5.69. Fluorescence images of HRF monolayers in co-culture cultured on 96-Transwell well bottoms treated with increasing concentrations of angiotensin II for 24 hours. Cells were fixed and immunofluoresce-stained with nuclear stain Hoechst 33342, and antibodies against extra cellular matrix (ECM) components collagen I and fibronectin, and mesenchymal marker α-SMA. Exposure times and focus were kept constant across the plate. Images were acquired at 20X magnification (scale bars=50µm)..

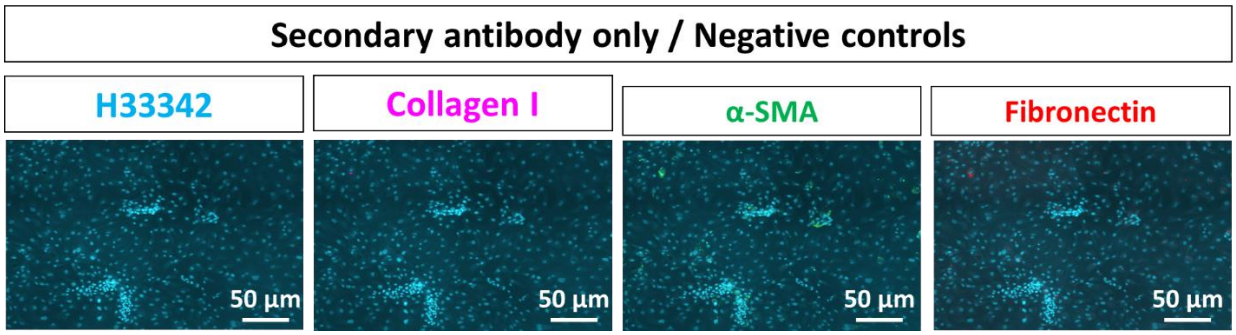

Figure 5.70. Fluorescence images of hPTC monolayers in monoculture cultured on 96-Transwell inserts. Cells were fixed and immunofluoresce-stained with nuclear stain Hoechst 33342, and secondary antibodies used in previous experiments namely, goat anti rabbit Alexa Fluor 647 (Collagen I), goat anti mouse Alexa Fluor 488 (α-SMA), and donkey anti goat Alexa Fluor 594 (Fibronectin). Exposure times and focus were kept constant across the plate. Images were acquired at 10X magnification (scale bars=50µm)..

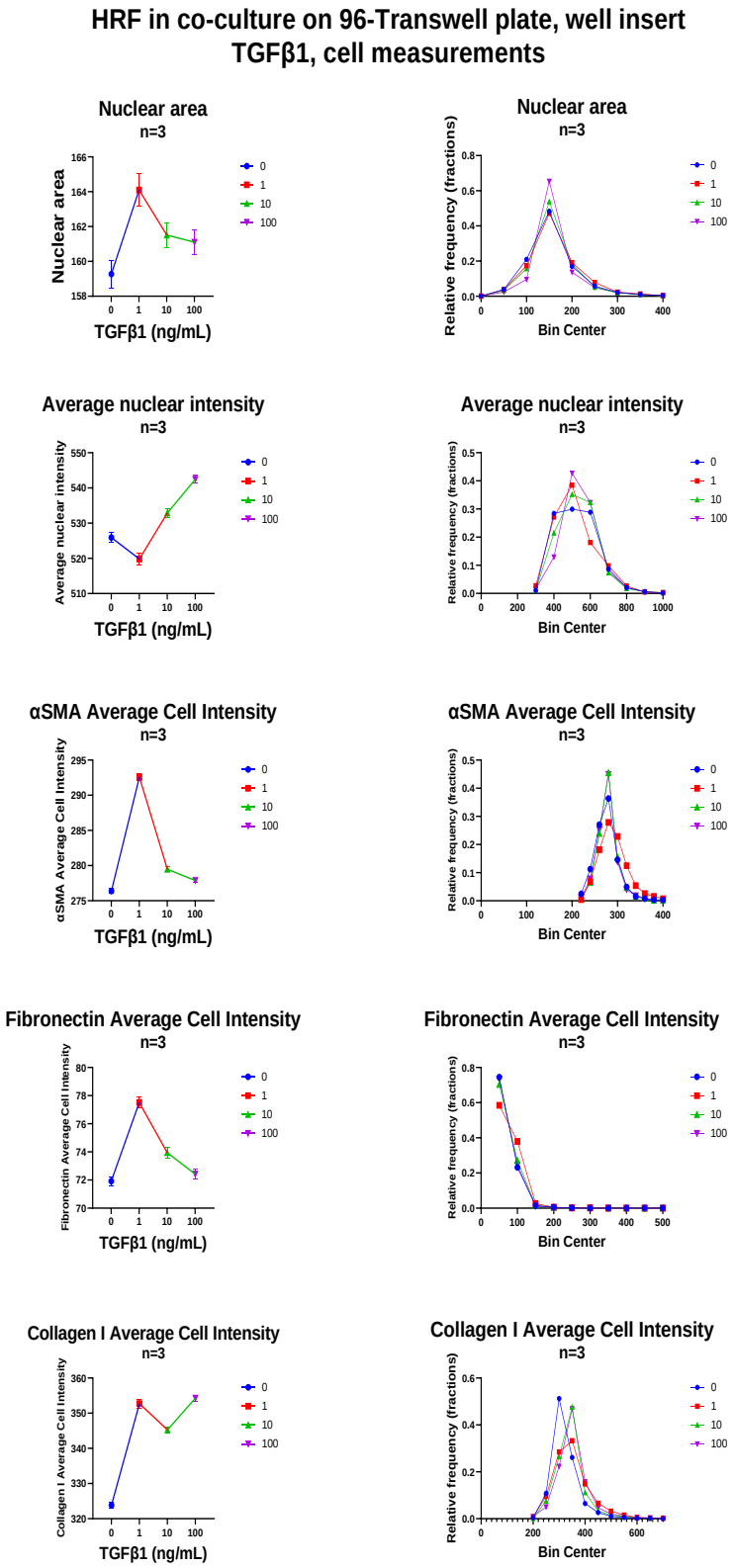

Figure 5.71. Effects of TGFβ1 24-hour treatment in HRF monolayers in co-culture on nuclear area, average H33342 nuclear intensity, αSMA average cell intensity, Fibronectin average cell intensity, and Collagen I average cell intensity depicted as dose-response curves and frequency of distribution graphs. Each data point is the mean of three biological (K8, K9, K10) and two technical replicates. Error bars represent S.E.M.

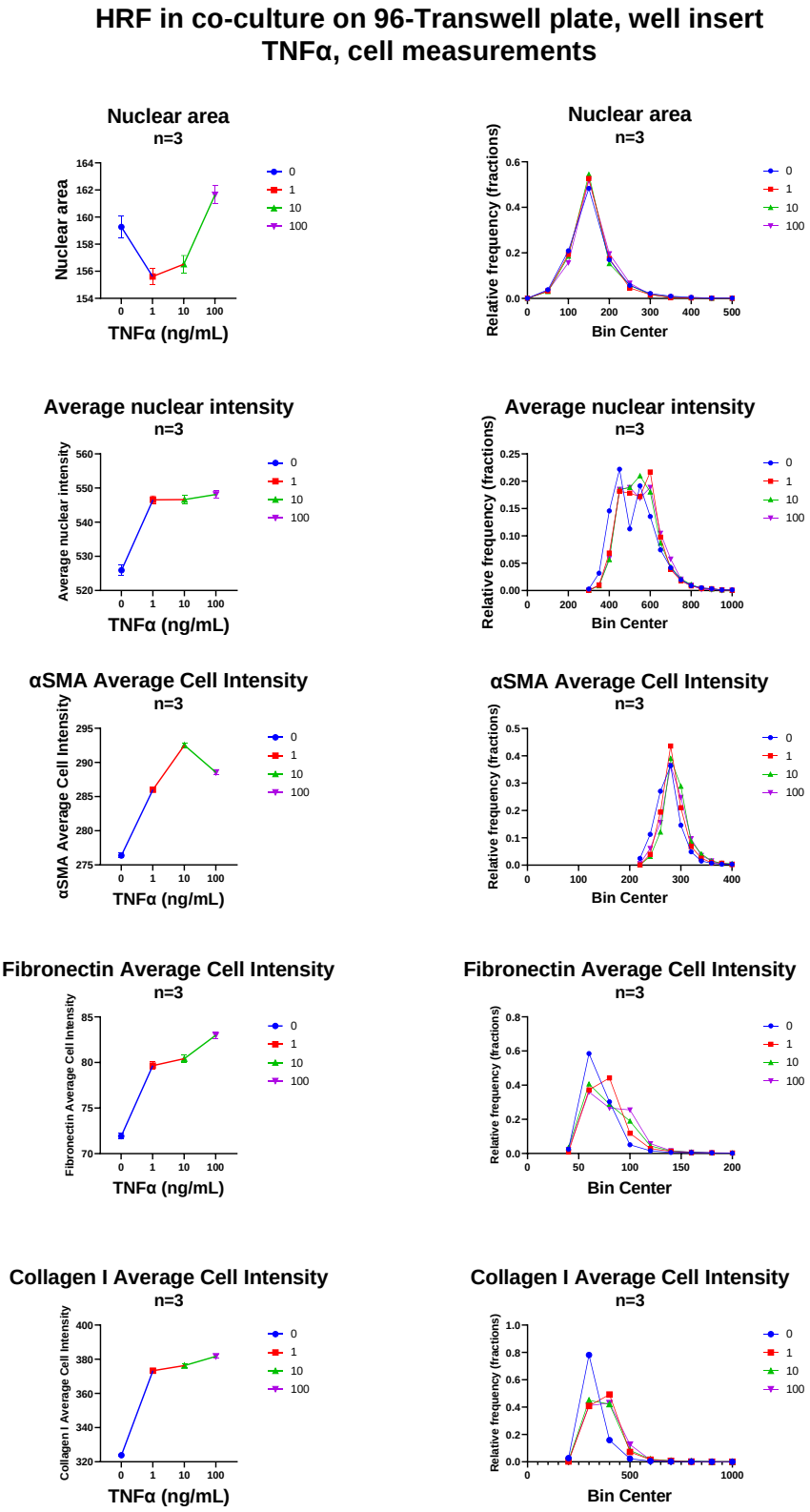

Figure 5.72. Effects of TNFα 24-hour treatment in HRF monolayers in co-culture on nuclear area, average H33342 nuclear intensity, αSMA average cell intensity, Fibronectin average cell intensity, and Collagen I average cell intensity depicted as dose-response curves and frequency of distribution graphs. Each data point is the mean of three biological (K8, K9, K10) and two technical replicates. Error bars represent S.E.M.

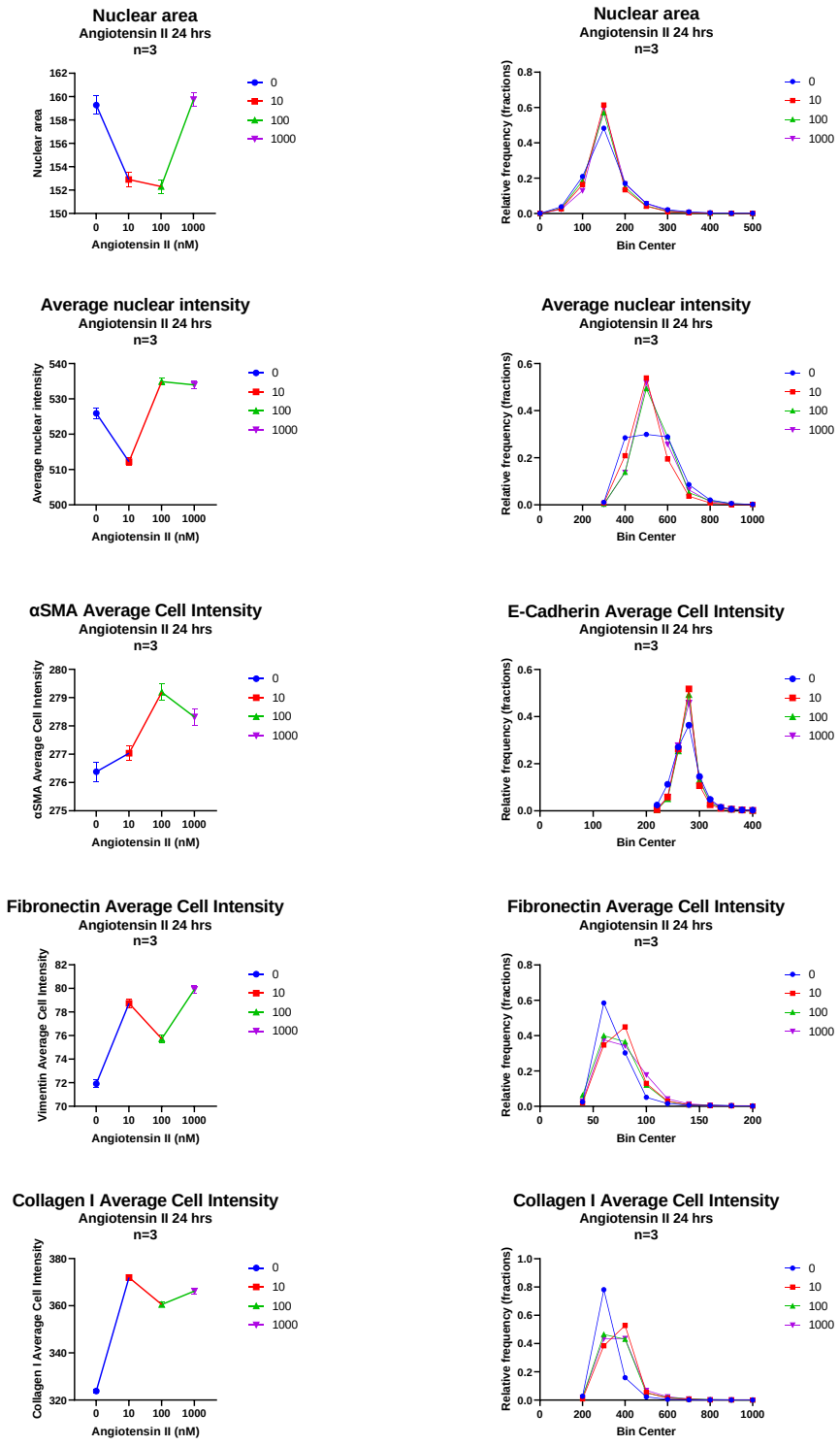

Figure 5.73. Effects of Angiotensin II 24 hour treatment in HRF monolayers in co-culture on nuclear area, average H33342 nuclear intensity, αSMA average cell intensity, Fibronectin average cell intensity, and Collagen I average cell intensity depicted as dose-response curves and frequency of distribution graphs. Each data point is the mean of three biological (K8, K9, K10) and two technical replicates. Error bars represent S.E.M.

5.9 Acute kidney injury biomarkers KIM-1, NGAL, and clusterin are not upregulated after pro-fibrotic treatment, but HRF-released chemokines are.

Now that the effects of pro-fibrotic compounds on the proximal tubule interstitial interface model mimicking the pathological *milieu* found *in vivo* during the progression of renal tubule-interstitial fibrosis have been investigated in depth in terms of phenotypical changes in both epithelial cells and fibroblasts, the aim is to explore the relationship between progressive renal fibrosis and acute kidney injury on our model. The main research question addressed by this section is whether the stress biomarkers upregulated in acute kidney injury mediated by nephrotoxic tubular damage, namely KIM-1, NGAL, and clusterin, can be considered as soluble predictors of progressive renal fibrosis, and subsequently CKD, in our *in vitro* model. As it has been previously demonstrated in our research group (Bajaj et al., 2018) , when hPTC monolayers are exposed to known nephrotoxic compounds, they release the soluble biomarkers which can be measured with a chemiluminescence ELISA assay (described in **2.7.6**) developed by other research group members prior to the start of this project.

Two biological replicates of hPTC in monoculture and three biological replicates of hPTC in co-culture are treated for 24 hours with increasing concentrations of pro-fibrotic compounds TGFβ1, TNFα, and angiotensin II. The supernatant media is sampled post-treatment, the actual amount of KIM-1, NGAL, and clusterin per well is quantified in picograms via the described assay, and the measurements are plotted against increasing concentrations of compounds. To account for the variation in cell number induced by the treatments, the actual amount of protein is divided by the corresponding intracellular ATP measurement in terms of luminescence and by cell number corresponding to the respective concentration of pro-fibrotic compound, thus generating dose-response curves displaying the amount of biomarkers (pg) released into the supernatant by each cell over 24 hours of treatment. The dose-response curves obtained by treatment of hPTC in monoculture are shown in **Figures 5.74 to 5.76**. The experiments were run on biological replicates K4 and K7, from which only the data regarding intracellular ATP was available, but not cell counts per well. When considering the raw amounts of biomarkers released after TGFβ1 treatment (**Figure 5.74 [A1], [B1], [C1]**), clusterin and KIM-1 release seems to significantly decrease as compared to the untreated control as TGFβ1 concentration increases, while these changes are not reflected by curves referring to the proteins' raw amount averaged by intracellular ATP proportional to luminescent signal (**Figure 5.74 [A2], [B2], [C2]**). No significant changes in stress biomarkers release are induced by TNFα and angiotensin II treatment (**Figures 5.75 and 5.76**) in hPTC in monoculture. In regard to the experiments performed on hPTC in co-culture with HRF on 96-Transwell inserts, dose-response curves generated after pro-fibrotic treatment are presented in **Figures 5.77 to 5.79**: the only instance in which a significant variation in KIM-1 release can be detected is mediated by TNFα treatment (**Figure 5.78 [B2]**), where the actual amount of KIM-1 (pg) is averaged by the luminescence signal proportional to intracellular ATP corresponding to the condition of treatment. TNFα does not seem to influence the release of NGAL and clusterin. Likewise, TGFβ1 (**Figure 5.77**) and angiotensin II (**Figure 5.79**) do not induce significant variations in stress biomarker release after 24 hours of treatment. Therefore, we can conclude that in the context of our *in vitro* model of renal fibrosis, TGFβ1,

TNFα, and angiotensin II do not cause soluble biomarkers release during nephrotoxic injury of tubular epithelial cells to be released into the supernatant by hPTC in co-culture with HRF.

Since the assays measuring KIM-1, NGAL, and clusterin release did not yield to any detectable changes, we decided to search for measurable soluble biomarkers upregulated after pro-fibrotic treatment. As discussed in **1.3.6**, cells of the renal interstitium release chemokines under proinflammatory stimuli which are part of the cascades of cellular events that lead to progressive renal fibrosis. Hence, we expect primary human renal fibroblasts cultured *in vitro* to respond to TGFβ1 stimulation by releasing such compounds. If chemokine release is upregulated in the disease state, these molecules could be used as soluble biomarkers to predict progression of the molecular mechanisms underlying renal fibrosis. Human renal fibroblasts isolated from a single donor are grown in mono- and co-culture, and they are treated with 100 ng/mL TGFβ1 for 24 hours. HRF in monoculture are directly exposed to the treatment whereas cells in co-culture are indirectly exposed to the compound as it is applied to the apical compartment of the Transwell® system, the supernatant from untreated control and treated cells is collected and microarray spotted membranes provided in the Human Chemokine Antibody Array are exposed to the media in order to screen between thirty-eight potential targets. Results from this experiment are displayed in **Figure 5.80**: 100 ng/mL TGFβ1 treatment induces a significant increase in the release of IL-8 and GRO-α in HRF in monoculture as compared to the untreated control (**Figure 5.80 [A]**), while the same treatment applied indirectly to HRF in co-culture leads to a significant decrease in GRO release as compared to untreated cells (**Figure 5.80 [A]**). Furthermore, MCP-1 seem to be highly expressed in the supernatant in both culture and treatment conditions, although no significant differences are found between treated and untreated cells. Ergo, soluble biomarkers IL-8, GRO-α, GRO, and MCP-1 could be considered to predict progression or halting of chronic kidney disease modelled in the context of a renal fibrosis *in vitro* assay platform.

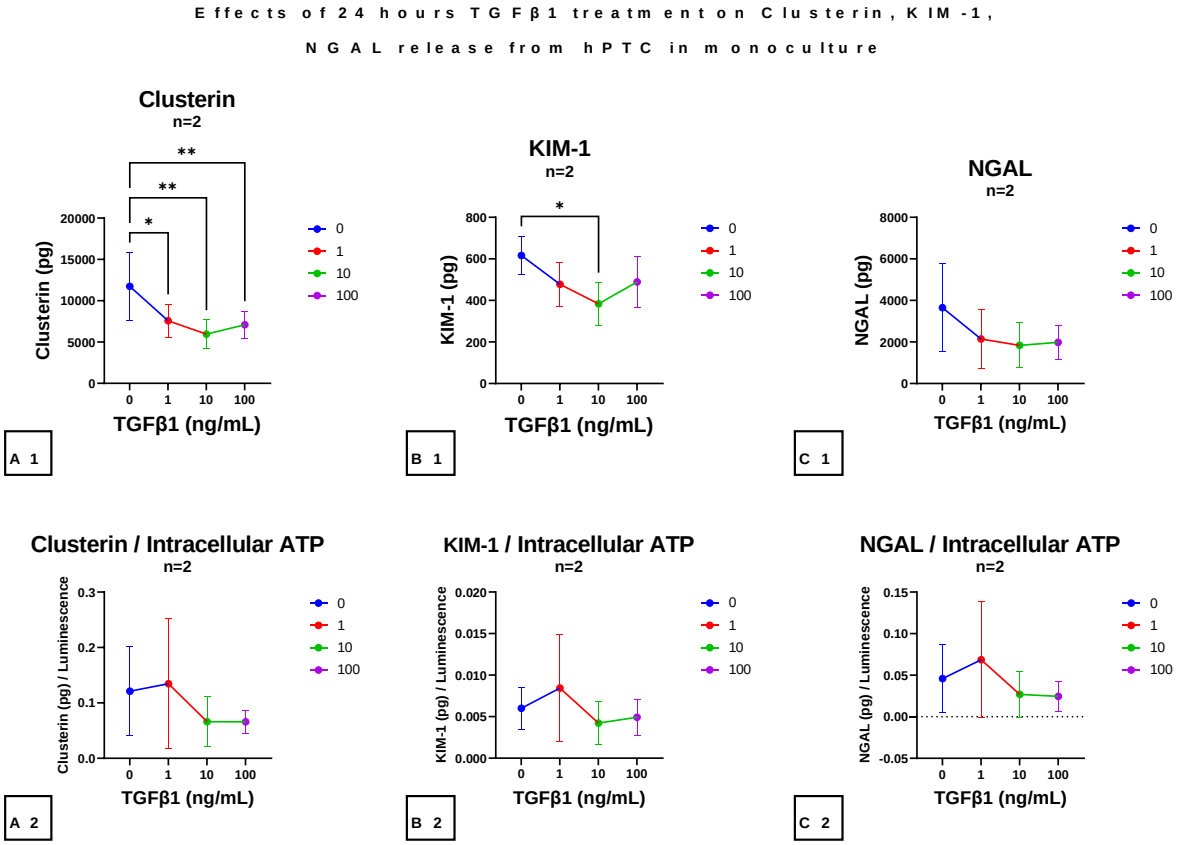

Figure 5.74. Stress biomarker secretion from hPTC monolayers treated with increasing concentrations of TGFβ1 (ng/mL) for 24 hours, presented as actual amount of protein (pg) (A1, B1, C1) and amount of protein (pg) relative to intracellular ATP (luminescence) (A2, B2, C2). Each data point is the mean of two biological (K4, K7) and three technical replicates. Error bars represent S.D. Statistical significance is depicted as '' p<0.05, '**' p<0.01,*

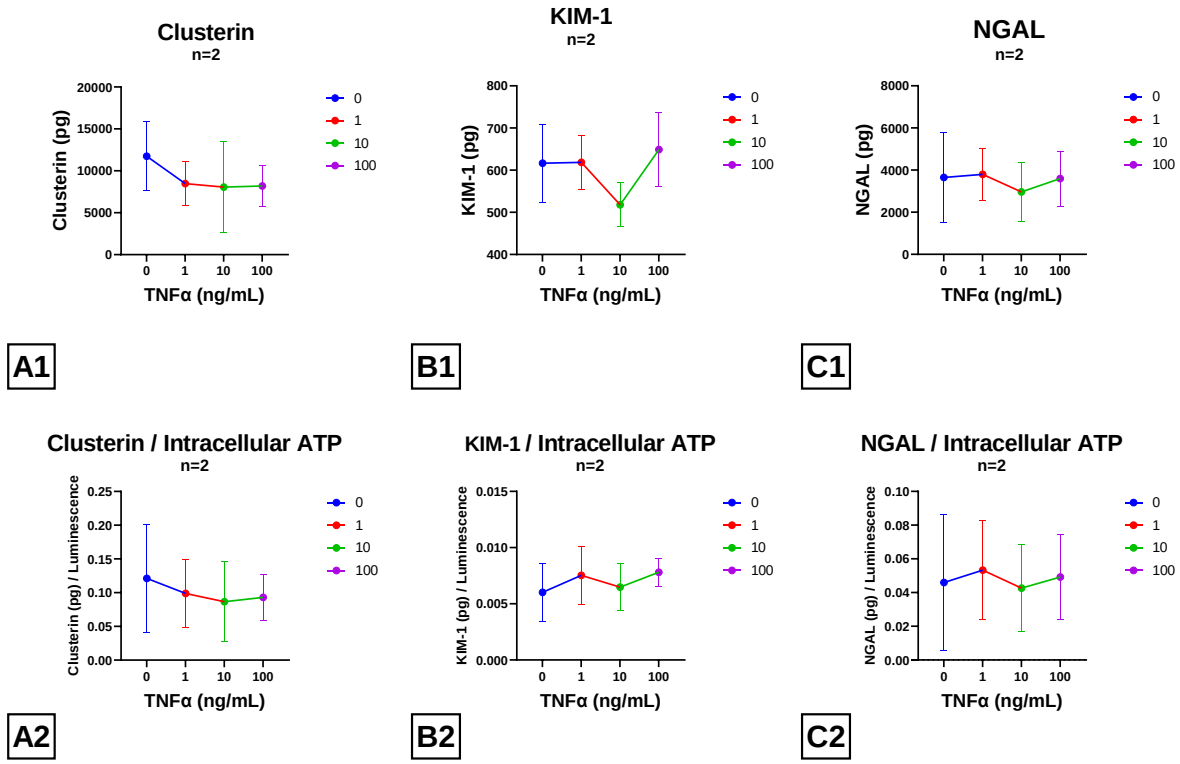

Figure 5.75. Stress biomarker secretion from hPTC monolayers treated with increasing concentrations of TNFα (ng/mL) for 24 hours, presented as actual amount of protein (pg) (A1, B1, C1) and amount of protein (pg) relative to intracellular ATP (luminescence) (A2, B2, C2). Each data point is the mean of two biological (K4, K7) and three technical replicates. Error bars represent S.D.

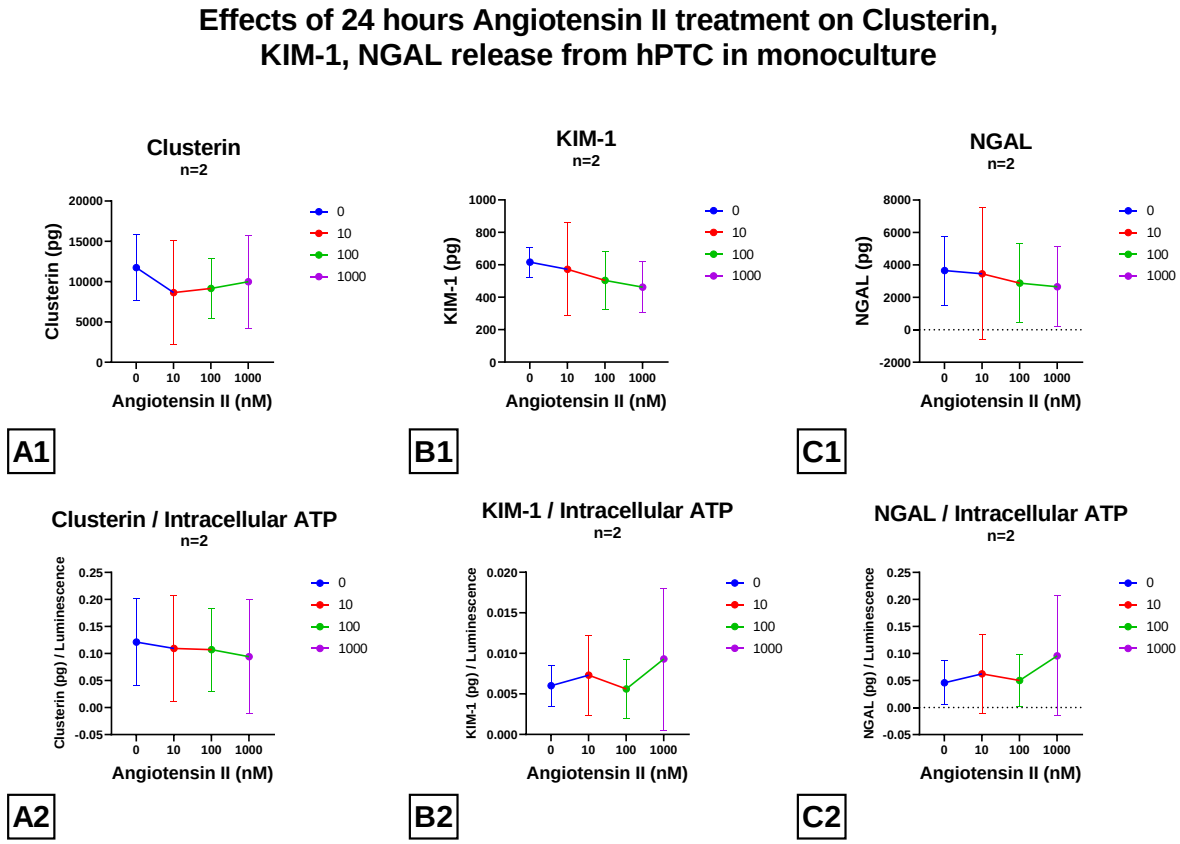

Figure 5.76. Stress biomarker secretion from hPTC monolayers treated with increasing concentrations of Angiotensin II (nM) for 24 hours, presented as actual amount of protein (pg) (A1, B1, C1) and amount of protein (pg) relative to intracellular ATP (luminescence) (A2, B2, C2). Each data point is the mean of two biological (K4, K7) and three technical replicates. Error bars represent S.D.

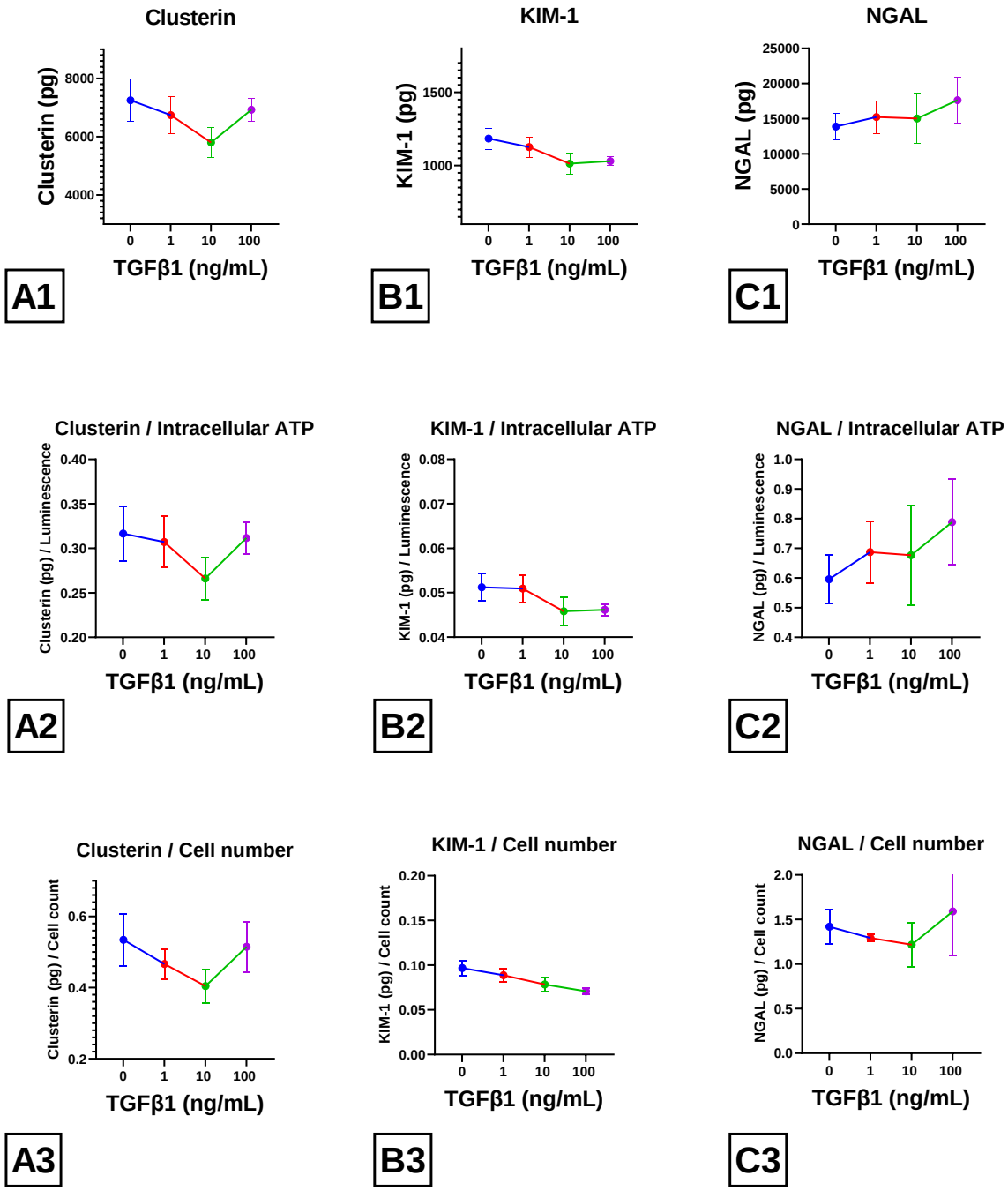

Figure 5.77. Stress biomarker secretion from hPTC monolayers treated with increasing concentrations of TGFβ1 for 24 hours, presented as actual amount of protein (pg) (A1, B1, C1), amount of protein (pg) relative to intracellular ATP (luminescence) (A2, B2, C2), and amount of protein (pg) relative to cell count (A3, B3, C3). Each data point is the mean of three biological (K8, K9, K10) and two technical replicates. Error bars represent S.E.M.

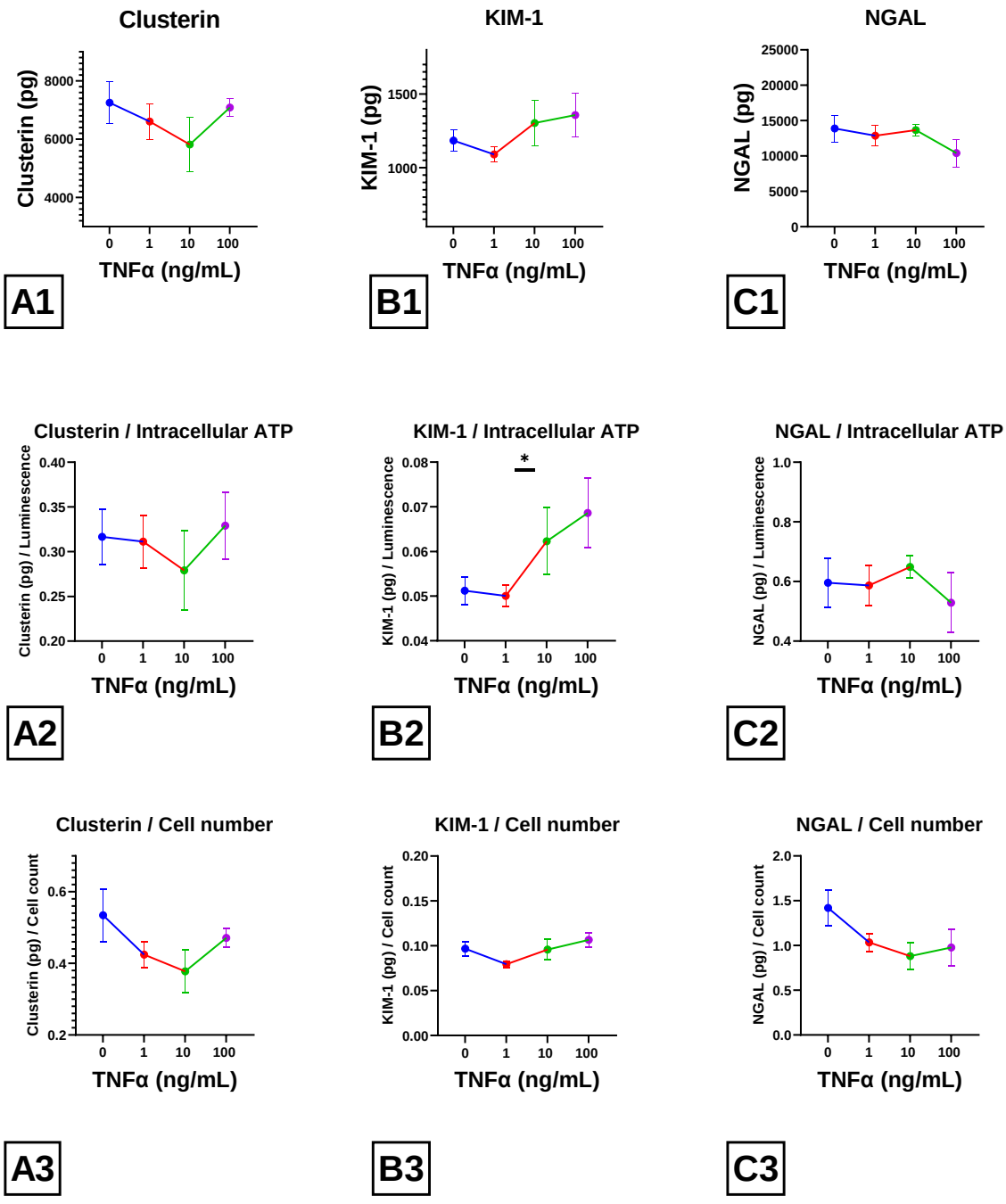

Figure 5.78. Stress biomarker secretion from hPTC monolayers treated with increasing concentrations of TNFα for 24 hours, presented as actual amount of protein (pg) (A1, B1, C1), amount of protein (pg) relative to intracellular ATP (luminescence) (A2, B2, C2), and amount of protein (pg) relative to cell count (A3, B3, C3). Each data point is the mean of three biological (K8, K9, K10) and two technical replicates. Error bars represent S.E.M.

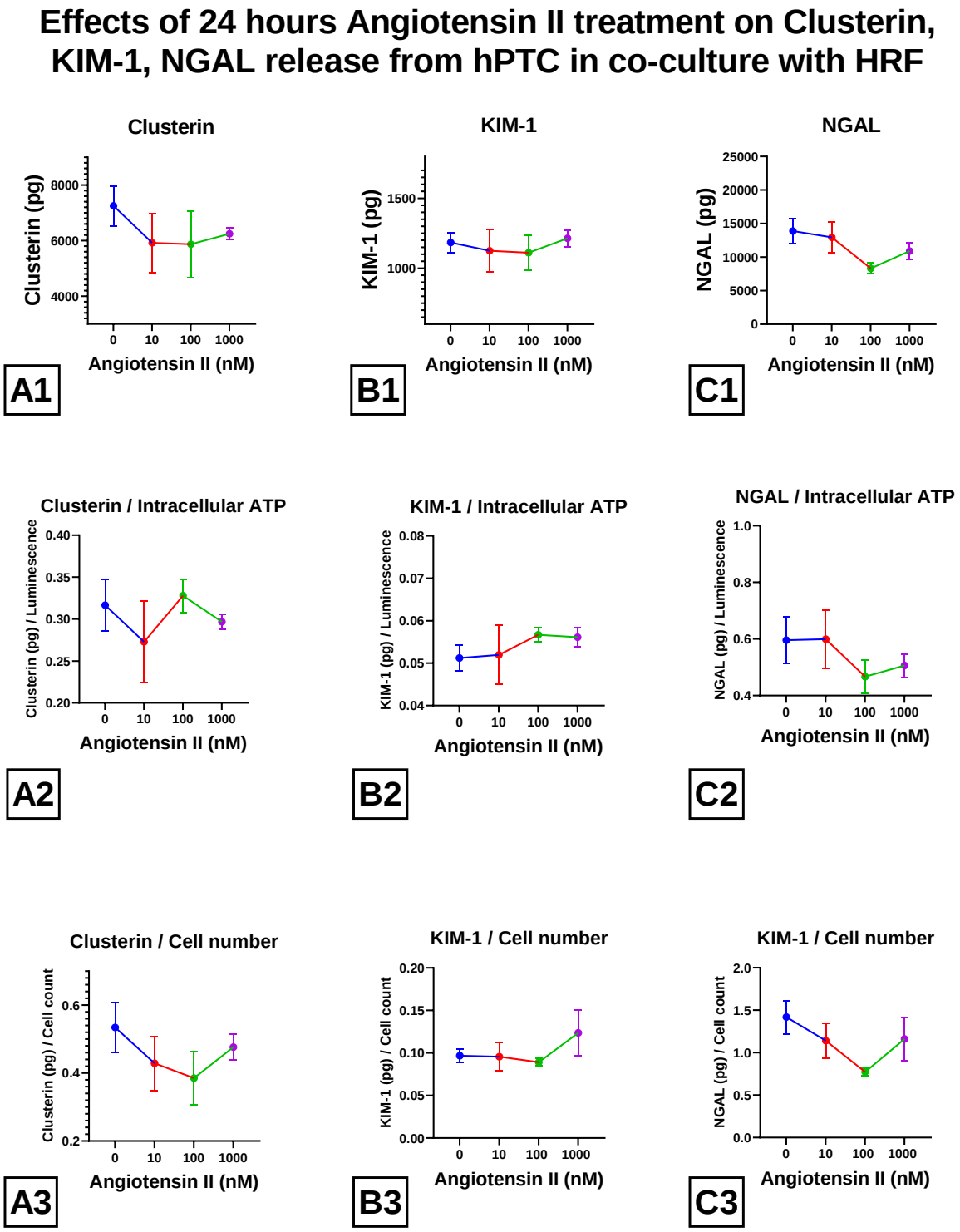

Figure 5.79. Stress biomarker secretion from hPTC monolayers treated with increasing concentrations of Angiotensin II for 24 hours, presented as actual amount of protein (pg) (A1, B1, C1), amount of protein (pg) relative to intracellular ATP (luminescence) (A2, B2, C2), and amount of protein (pg) relative to cell count (A3, B3, C3). Each data point is the mean of three biological (K8, K9, K10) and two technical replicates. Error bars represent S.E.M.

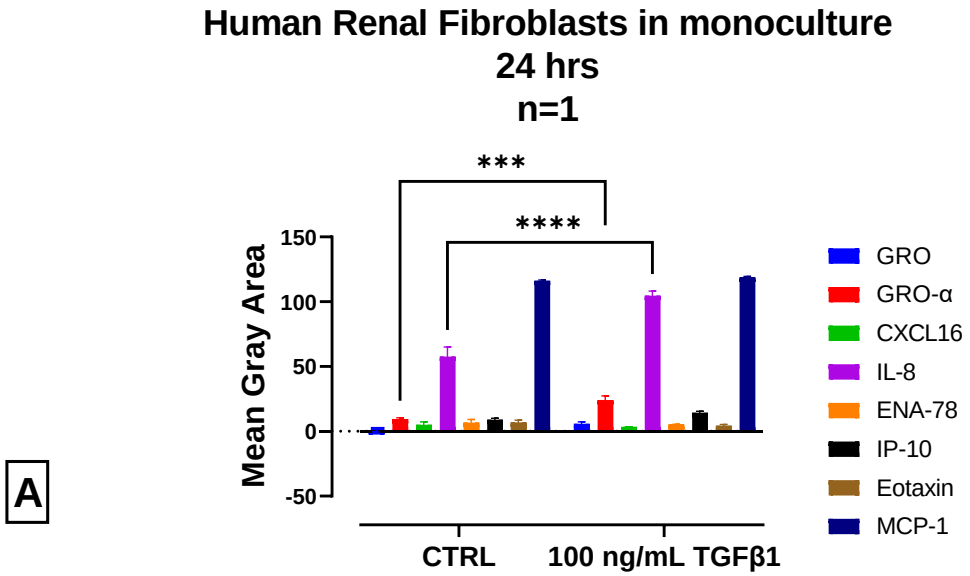

A

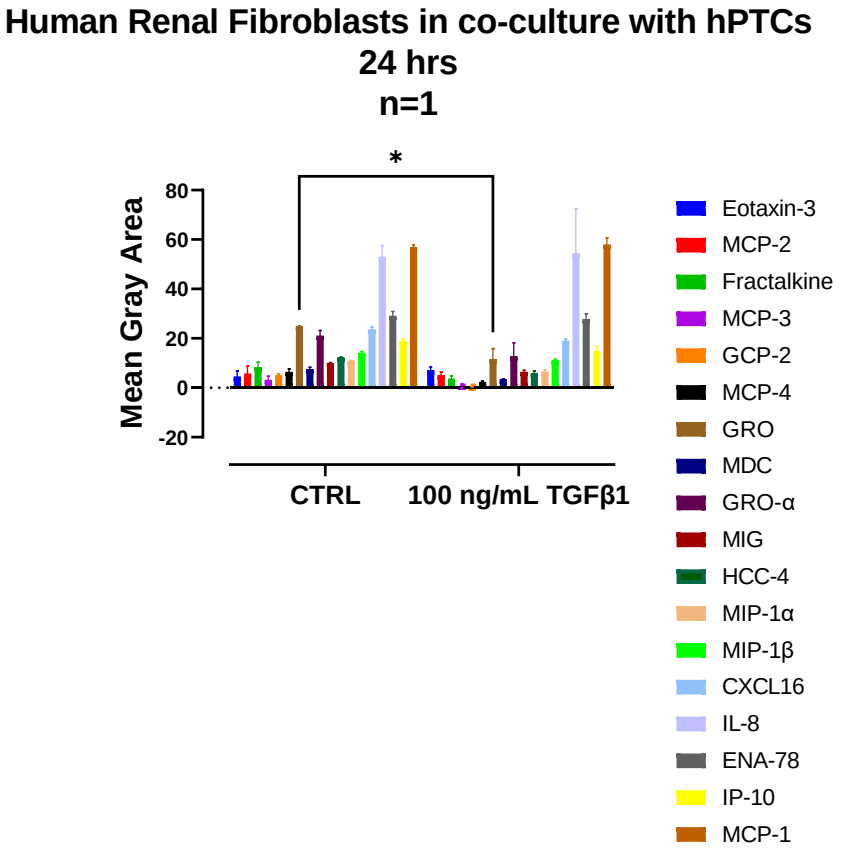

B

Figure 5.80. Chemokines secretion from HRF monolayers treated with 100 ng/mL TGFβ1 in [A] monoculture and [B] co-culture with hPTC expressed as mean gray area. The experiment was performed in one biological replicate. Each data point is the mean of two technical replicates.

Error bars represent S.D. Statistical significance is depicted as '' p<0.05, '***' p<0.001, p<0.0001.*

5.10 Discussion

This chapter delves into the findings and implications stemming from our exploration of renal fibrosis *in vitro* models, building upon the insights gained from other researchers' work. Our aim is to closely mimic the cellular and molecular events observed in human pathology, transitioning away from traditional animal models towards *in vitro* approaches utilizing human kidney cells. Many different approaches towards modelling the proximal tubule in the context of progressive renal fibrosis have been explored, including the use of human kidney cells, either immortalized, reprogrammed, or transfected, to mimic clinical presentations at histological and molecular levels. Notable studies include those by Kopp's group using TGFβ1-induced fibrosis models (Q. Xu et al., 2007) for the screening anti-fibrotic compounds, while other groups have established a microfluidic platform to study epithelial-to-mesenchymal transition (M. Zhou et al., 2014), and developed a hydrogel-based 3D model to monitor cross-talk between proximal tubule cells and fibroblasts during nephrotoxic insults (Nugraha et al., 2017). Despite advancements, current models have limitations, necessitating the development of more structurally complex 3D models using primary human kidney cells. Inspired by these pioneering studies, we advocate for the development of more sophisticated 3D models, utilizing primary human kidney cells to better recapitulate renal function and pathology, and to bridge the gap between experimental models and clinical reality. These studies have laid crucial groundwork, demonstrating the feasibility of using in vitro models to replicate histological and molecular intricacies of renal fibrosis. The use of High Content Imaging (HCI) is central to the investigation carried out in this chapter, as demonstrated by Palano et al. and Marwick et al., an innovative technique that promises to revolutionize compound screening by enabling comprehensive analysis of cellular changes (Palano et al., 2020), (Marwick et al., 2021). Drawing upon the transformative potential of HCI showcased in studies on cardiac and lung fibrosis by Sieber et al., we aim to identify promising anti-fibrotic compounds and elucidate their mechanisms of action (Sieber et al., 2018).

When looking at all the assays performed across all the *in vitro* models of the proximal tubule interstitial interface, namely hPTC and HRF in monoculture and co-culture, we can conclude that based on the endpoint considered there will be more or less variability between data gathered from the same biological replicate. For instance, output from assays used to investigate the effects of pro-fibrotic compounds on cell cycle and health such as cell proliferation, apoptosis, and necrosis assays (**5.6**) is expressed as percentage of cells positive for a specific marker over a population. The data suggest that the change in phenotype induced by pro-fibrotic treatments measured by these assays are not necessarily robust enough to take into account the biological variability among replicates. Conversely, the assays that use a single-cell approach to investigate the state of each cell in a population seem to be more sensitive and to yield statistically significant variations in dose-response curves when control and treated populations are compared. Therefore, the data gathered from high content imaging assays are the piece of information that has informed this discussion the most. The high content imaging data presented in this chapter in **5.7** and **5.8** suggests that we

were able to induce fibrosis in the form of partial epithelial-to-mesenchymal transition (pEMT) in hPTC and extra-cellular matrix deposition (ECM) in HRF. The frequency of distribution graphs plotted for each of the measurements obtained by high content imaging demonstrate that there is a dose-dependent shift in the distribution of the cell populations for all the EMT and ECM deposition markers considered, showing that both hPTC and HRF are responding to pro-fibrotic treatments. Proximal tubule cells seem to acquire a migratory phenotype when exposed to pro-fibrotic compounds as they aggregate into nodules which, depending on culture conditions, show up- or downregulation of tight junction markers, suggesting dysregulation of epithelial barrier function, which is reflected by significant variations in TEER measurements post pro-fibrotic treatment. **Figure 5.58** shows that the epithelial nodules formed after pro-fibrotic treatment are positive for myofibroblast mesenchymal marker α smooth muscle actin, demonstrating that stimulated epithelial cells are going towards the pEMT pathway. Similar aggregates of myofibroblasts and fibroblasts surrounded by epithelial cells are found in idiopathic pulmonary fibrosis, where these lesions are considered a hallmark of progressive fibrosis. In the context of pulmonary pathophysiology, these histological formations are called *fibroblastic foci*, and their number and morphological characteristics are correlated to patient mortality (Calabrese et al., 2022). The similarity of this phenomenon to the epithelial nodule formation observed in our *in vitro* model of renal fibrosis opens many potential research questions which can be answered via further investigation around the nodules' phenotype and mechanism of formation driven by pro-fibrotic stimuli. However, it is important to note that each pro-fibrotic compound used activates specific cell signalling pathways which are implicated in the progression of renal fibrosis (Wrana & Attisano, 2000), but the absence of positive controls highlighting activation of such pathways deems the obtained responses of difficult interpretation. This work could have been carried out in parallel on a human-derived commercially available cell line such as RPTEC/TERT1, to investigate whether the variation between data points collected via apoptosis/necrosis and cell proliferation assays could have been due to patient-to-patient biological variability rather than assay sensitivity or assay robustness issues. A response, especially in terms of apoptosis and necrosis, should have been expected in hPTC at much lower doses of TGFβ1 and TNFα (Misseri et al., 2005), since its proven *in vitro* effect, instead the flow cytometry data shown does not reflect this.

Thus, future experiments centred around further development and amelioration of the *in vitro* renal fibrosis assay platform shall focus firstly on extending the timepoint of treatment of hPTC and HRF to 48 and 72 hours, which would primarily require to modify the composition of the vehicle medium treatment since the data gathered during this project suggests that the lack of serum and growth factors in the medium could be leading to premature cell death. To achieve this objective, the "original" media composition of the co-culture model could be maintained and pro-fibrotic compounds could be delivered directly in REGM™ and FGM™. Moreover, since epithelial nodule formation seems to be the key phenomenon observed in stimulated hPTC, an assay measuring the expression of αSMA and extracellular matrix deposition within the boundaries of the nodules in relationship to the dose of pro-fibrotic treatments could be developed via high content imaging. Finally, since stress biomarkers KIM-1, NGAL, and clusterin do not seem to be released in the context of the modelled disease, a

chemokine release chemiluminescence assay could be developed to measure IL-8, GRO-α, and MCP-1 release in the supernatant of treated human renal fibroblasts.

The endogenous cytokines and hormones TGFβ1, TNFα, and angiotensin II have been identified to be key activators of cell signalling pathways involved in progressive renal fibrosis linked to chronic kidney disease (K. K. Kim et al., 2018), (Lavoz et al., 2012). Therefore, these compounds have been selected to mimic renal fibrosis in the *in vitro* model of proximal tubule interstitial interface herein presented. The model presented consists of only three of the multiple components of the renal interstitium, namely proximal tubule cells, renal fibroblasts, and the extracellular matrix, lacking the immune cellular component which is involved in the progression of renal fibrosis (Dong et al., 2023). From a theoretical standpoint, the assays utilised to investigate the induction of renal fibrosis in the developed model focus almost completely on the measuring epithelial-to-mesenchymal transition (EMT) in the epithelial monolayer and fibroblast-to-mesenchymal transition (FMT) in the fibroblast layer, even though many relevant publications in the field of renal fibrosis have questioned the centrality of EMT in the progression of renal fibrosis *in vivo* (Kriz et al., 2011), (Lovisa et al., 2016), (Sheng & Zhuang, 2020a). As presented in this chapter, the idea around the development of this *in vitro* renal fibrosis assay platform is that the pro-fibrotic compounds used for treatment can induce tight junction dissolution and epithelial barrier dysregulation in the proximal tubule monolayer, which are indeed hallmarks of progressive renal fibrosis *in vivo*, however only a small proportion of injured epithelial cells are likely to fully transdifferentiate into myofibroblasts capable of depositing extracellular matrix. The same applies to renal fibroblasts, since a large proportion of myofibroblasts migrates from the bone marrow upon renal injury and proliferates within the renal parenchyma (LeBleu et al., 2013). The proposed model should take into account the different theories around what drives renal fibrosis in vivo, avoiding artefacts which could only be induced *in vitro*.

In the future, these experiments should be repeated on primary proximal tubule cells alongside with a cell line, including the crucial positive control for each pro-fibrotic compound used i.e. Smad1 activation for TGFβ1, employing a validated apoptosis/necrosis and cell proliferation assay (P. Zhou et al., 2020).

Chapter 6: Discussion and concluding remarks

The aim of this project was to develop a fully human 3D in vitro model of the proximal tubule interstitial interface suitable for the induction of renal fibrosis for high throughput drug screening and development purposes. The two main research questions that this thesis addresses are 'whether primary proximal tubule cells derived from the human kidney cortex display a more physiologically relevant phenotype when co-cultured with other cellular components of the renal interstitium (namely renal fibroblast and human renal peritubular endothelial cells) as compared to a monoculture model' and 'whether treatment of the co-culture model with endogenous pro-fibrotic compounds can induce renal fibrosis (a hallmark of CKD) in a measurable dose-response fashion'.

Chronic kidney disease (CKD) is a disorder that can arise from several different aetiologies, and it is defined as a significant reduction in renal function reflected as glomerular filtration rate (GFR) lower than 60 mL/min per 1.73 m^2 for a duration of at least 3 months, independent of causation. Metabolic syndrome involving diabetes, obesity and hypertension seem to be the main underlying causes of CKD in the Western world, although the prevalence and aetiology of the disease varies globally according to the average income of a specific geographical area, which means social determinants and ethnicity come into play to determine susceptibility to the disease. Genetic and epigenetic background have shown to be influential on CKD progression; a prime example of inheritable genetic factors determining the establishment of the disease are mutations related to polycystic kidney disease (PKD) while environmental stressors to which a cohort could be exposed during development can lead to disease occurrence because of susceptibility to the metabolic syndrome. During the course of CKD, most patients are asymptomatic or have generic symptoms such as fatigue and weight loss, that is, until the largest extent of renal function has been lost due to disease progression resulting in organ damage. In the clinical setting, proteinuria and above average blood urea nitrogen are predictors of CKD and associated mortality, although definitive evidence of the presence of CKD is obtainable uniquely via histological examination of renal biopsies. Chronic kidney disease manifests itself onto the renal tissue as renal fibrosis, which is defined as maladaptive wound healing process which leads to functional renal parenchyma being substituted by scarred, nonfunctional tissue unable to carry out physiological kidney functions such as filtration, reabsorption, and secretion of solutes. Specifically, CKD and its histological presentation, renal fibrosis, exhibits in patients' renal biopsies as glomerular sclerosis, tubular atrophy, and tubule-interstitial scarring. Disorders associated with the metabolic syndrome lead to changes in plasma composition in terms of protein and glucose concentration, thus leading to a cascade of events involving modifications to systolic blood pressure, changes in hormonal release which affects the glomerular filtration rate (GFR) by leading to a state of hyperfiltration in each glomerulus. Furthermore, as previously mentioned, the ultrafiltrate composition to which the tubule-interstitium is exposed triggers an inflammatory response of the renal parenchyma, whereby mainly epithelial and endothelial cells release pro-inflammatory cytokine and recruit resident and circulating immune cells, which exacerbate

the cytokine and chemokine storm now present in the renal *milieu*. Alongside these phenomena, injury of the endothelium triggers microvascular damage (also known as capillary rarefaction) which leads to tubule-interstitial hypoxia and subsequent production of reactive oxygen species (ROS). As the inflammatory *milieu* becomes established in the renal parenchyma, pushing pro-fibrotic cytokine-releasing epithelial cells towards apoptosis, resident quiescent renal fibroblasts become increasingly involved in driving the disease to its known histological presentation. Renal fibroblasts, which normal function is to exert trophic and structural support to the other cellular components of the renal parenchyma, under pro-inflammatory and pro-fibrotic stimuli acquire activated migratory myofibroblast phenotype thus exerting contractile properties and depositing excessive extracellular matrix *in lieu* of the injured and apoptotic epithelium and endothelium, hence completing the maladaptive wound healing cascade typical of CKD (Webster et al., 2017). Essentially, the four cell types belonging to the renal parenchyma mentioned so far (the epithelial cells, endothelial cells, myofibroblasts, and immune cells) respond to the metabolic syndrome mediated injury by attempting to curb the damage and preserve organ function, ending up not only contributing to progressive injury but effectively driving scar tissue formation. In particular, myofibroblasts seem to be at the center of renal fibrosis progression, as renal fibroblasts, renal epithelial cells, and endothelial cells residing in the organ parenchyma can all transdifferentiate into such activated forms in a number of cellular processes that have been the focus of much investigation over the last two decades, namely fibroblast-to-myofibroblast transition (FMT), epithelial-to-mesenchymal transition (EMT), and endothelial-to-mesenchymal transition (EndoMT) (Lovisa et al., 2016). The cell signaling pathway involving TGFβ (transforming growth factor β) is the principal driver of such transitions: TGFβ superfamily members exert their biological effects by binding to transmembrane receptors that interact with intracellular mediators of the Smad family, which once phosphorylated form a complex with common mediator Co-Smads, which in turn regulate gene expression (Wrana & Attisano, 2000). TGFβ mediated and Smad signaling are at the center of the cascade of events that leads to epithelial-to-mesenchymal transition, alongside with other cell signaling pathways that have shown to be triggered during this process, namely Notch, Wnt/B-Catenin, and Hedgehog signaling pathways (Yuan et al., 2022). Besides TGFβ having been identified as one of the main mediators of renal fibrosis, the establishment and maintenance of the inflammatory *milieu* in the renal parenchyma is key in the progression of the disease, thus highlighting the importance of TNFα in this scenario. TNFα is a potent pro-inflammatory cytokine which is produced by both renal epithelial cells and immune cells, and it is known to activate inflammatory cell signaling pathways nuclear factor-κB (NF-κB), mitogen-activated protein kinase (MAPK), and caspase (Yuan et al., 2022). Furthermore, the renin-angiotensin-aldosterone system (RAAS) has shown to be highly implicated in the early stages of CKD, since it regulates fluid homeostasis by effecting handling of solutes in the kidney and blood pressure, thus being a prime target for pharmacological interventions such as RAAS inhibitors aimed at alleviating the strain of progressive renal fibrosis on the kidney function. In fact, angiotensin II is a hormone which can induce pro-fibrotic effects on the renal epithelial cells

independently from pathways activated by TGFβ (Lavoz et al., 2012). The activation and release of these effectors and cell signaling pathways lead to progressive scarring and loss of kidney function which eventually leads to end stage renal disease (ESRD), or premature death associated to cardiovascular events (Webster et al., 2017). The diagnostic criteria for CKD defined around renal biopsies involve histological characterization of patients' samples whereby the tissue is embedded in paraffin before undergoing periodic acid-Schiff (PAS) and Masson's trichrome staining which are utilized to visualize ECM deposition at the glomerular and tubule-interstitial level, while immunofluorescence staining with antibodies against immunoglobulins IgG, IgM, and IgA, complement pathway components, and kappa and lambda chains is performed on snap-frozen samples to investigate the degree of inflammation and immune response present in the renal parenchyma (Agarwal et al., 2013).

Current non-pharmacological treatments of CKD involve dialysis and kidney transplant, while the few available pharmacological treatments focus on slowing down disease progression by controlling blood pressure and plasma composition thus reducing hemodynamic injury rather than targeting the blockade of the aforementioned cell signaling pathways to ameliorate or ideally revert trans-differentiation of functional components of the renal parenchyma to activated myofibroblasts (Webster et al., 2017). Hence, there is currently a worldwide interest in developing new effective treatments for CKD, leading to a push from pharmaceutical companies and other stakeholders in the field of drug development and drug discovery to develop novel models of renal fibrosis which should closely recapitulate the fibrotic renal parenchyma from a molecular and histological standpoint – encompassing the presentation of renal fibrosis in terms of phenotypical changes and involvement of relevant cell signaling pathways. *In vivo* animal models of renal fibrosis have provided invaluable insight into the underlying molecular mechanisms of the disease, allowing researchers to induce injury targeted to the kidneys while gathering data from systemic and histological findings, but the nature of animal disease modelling does not allow for high throughput testing of new molecular entities in development as the next generation of anti-fibrotic compounds, because of ethical and financial constraints.

Therefore, *in vitro* models of renal fibrosis are highly sought after in the field, ideally mirroring the pathophysiology of the disease progression in all aspects, both at the intracellular level and in terms of hallmark phenotypical and structural changes. The ideal *in vitro* model of renal fibrosis should be nephron segment specific as the phenotype and functions of the cellular components of each segment of the nephron are highly specialized, it should be derived from human tissue to avoid posing ethical questions relative to animal tissue handling, and it should recapitulate the complexity of the microenvironment it is mimicking, therefore requiring more than one cellular component to be able to construct a faithful model of the disease. Furthermore, the phenotype and physiological function of each specific nephron segment should be retained by the cells used *in vitro*, as demonstrating measurable response to pro-fibrotic injury does not correlate with the ability of the model to filtrate, reabsorb, and secrete solutes. Moreover, the model should be suitable for assay development involving state-of-the-

art high throughput techniques such as high content imaging, flow cytometry, transcriptomics, and proteomics.

To answer the two main questions of this thesis as stated at the beginning of this discussion, firstly we established robust protocols to isolate and characterise the "building blocks" of the proximal tubule interstitial interface which lead to prove that proximal tubule cells (hPTC) can be isolated from the renal cortex via density gradient centrifugation, and that when cultured on permeable membranes they form polarised monolayers which express key solute transporters and exerting epithelial barrier function, recapitulating *in vitro* their *in vivo* phenotype. However, as trans-epithelial electrical resistance (TEER), a key measurement of epithelial barrier function, rose, transporter expression decreased over time. Renal fibroblasts (HRF) isolated via magnetic activated cell sorting (MACS) displayed characteristic mesenchymal phenotype, while human renal peritubular endothelial cells (HRPEC) isolated via density gradient centrifugation followed by MACS displayed expression of pan-endothelial markers and diaphragmatic fenestration in vitro. To assess whether co-culture could improve hPTC phenotype, epithelial cells were co-cultured with HRF and HRPEC via different iterations of contact and non-contact co-culture. When assembling the 3D models, we discovered that HRF would invade the epithelial monolayer if in contact with hPTC, disrupting the essential barrier function performed by the proximal tubule, thus pointing us in the direction of non-contact co-culture. This solution was implemented to answer our first research question, proving that the presence of renal fibroblasts in the 3D co-culture model enhances epithelial barrier formation. Secondly, we hypothesized that endogenous pro-fibrotic compounds could be used to induce renal fibrosis in vitro which would resemble the cellular events and histological presentation found in CKD patients. By employing a synthetic ECM, we demonstrated that renal fibroblasts can be maintained in culture without acquiring myofibroblast features, typical of the fibrotic interstitium. Furthermore, we show that the selected treatments alter epithelial barrier function in hPTC via αSMA+ nodule formation and cause ECM deposition in HRF, thus mimicking some of the key features that define renal fibrosis *in vivo*. Interestingly, we did not detect an increase in renal epithelial stress biomarker release (KIM-1, NGAL, and clusterin) after pro-fibrotic insult, while we measured upregulation of HRF-released chemokines.

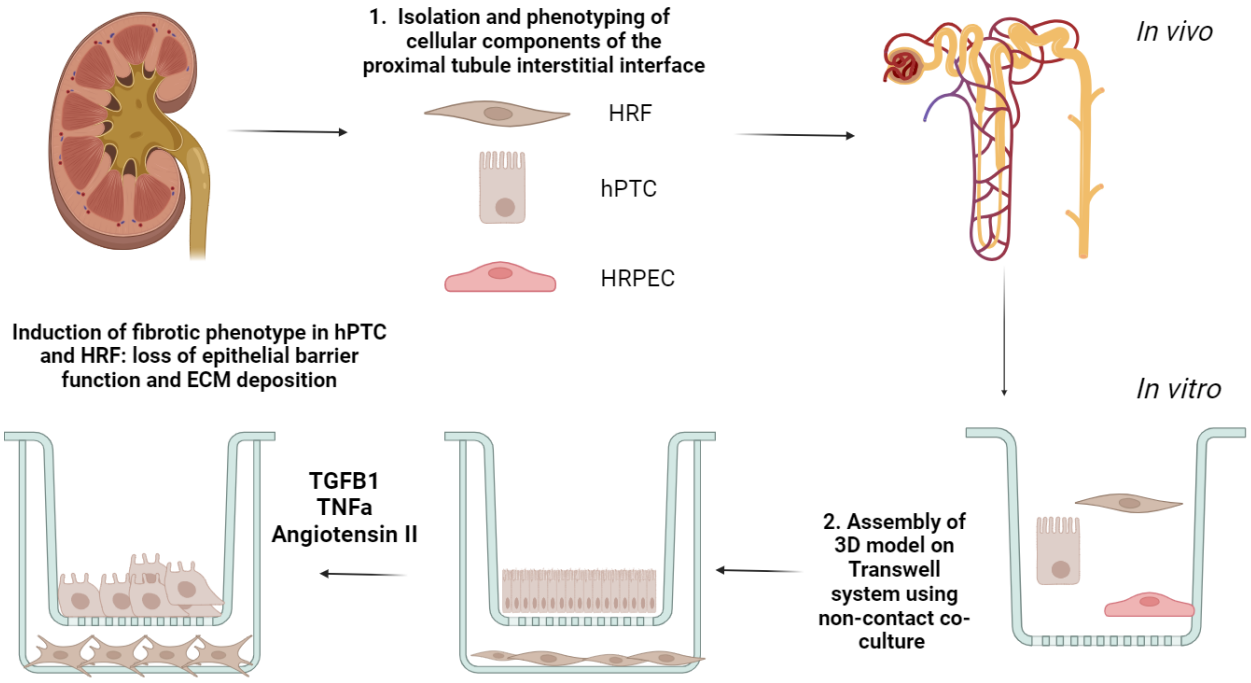

Figure 6.1. Graphical representation of the main findings of this thesis. Cells isolated from the human kidney cortex can be used to culture an autologous 3D model of the proximal tubule interstitial interface composed by human renal fibroblasts (HRF), human proximal tubule cells (hPTC), and human renal peritubular endothelial cells (HRPEC) on Transwell systems. Pro-fibrotic compounds treatment is then employed to induce renal fibrosis, one of the underlying mechanisms of chronic kidney disease, which induces measurable phenotypical changed in both epithelial cells and fibroblasts.

A graphical summary representing the key findings reported in this thesis is depicted in **Figure 6.1**. These findings indicate that it is possible to develop a 3D in vitro proximal tubule model completely derived from primary human cortex from kidneys rejected by the national transplant program which can be used to model renal fibrosis *in vitro,* which in the future might replace the use of animal models of disease in the field of chronic kidney disease, despite there being still many challenges and open research questions which have been highlighted by the experimental work conducted during this project. The results described in **Chapter 3** show that proximal tubule cells (hPTC) isolated via Percoll® density gradient centrifugation display the desired phenotype which encompasses cobblestone morphology (**Chapter 3, Figure 3.6**), proximal tubule markers expression (**Chapter 3, Figures 3.7** and **3.8**), apical cilia expression (**Chapter 3, Figures 3.9** and **3.10**), polarised solute transporters expression (**Chapter 3, Figures 3.12** and **3.13**), mRNA expression of genes encoding for key transporters (**Chapter 3, Figure 3.14**), evident epithelial barrier function formation measured via trans epithelial electrical resistance (TEER) assay (**Chapter 3, Figure 3.15**) allowed by expression of tight junction markers ZO-1 (**Chapter 3, Figure 3.16**) and E-Cadherin (**Chapter 3, Figure 3.17**), and absence of expression of mesenchymal marker vimentin prior pro-fibrotic stimulation (**Chapter 3, Figure 3.18**). The characterisation of this cell type confirms and

expands the findings published in our research group's seminal study regarding the isolation and characterisation of hPTC from the human kidney cortex (Brown, Sayer, Windass, Haslam, De Broe, et al., 2008). However, the loss of expression of drug transporters as culture time progresses limits the "shelf life" of this cell population, hinting at the fragility of this highly differentiated phenotype *in vitro*. This suggests that primary hPTC dedifferentiate *in vitro* (Lacueva-Aparicio et al., 2022), making primary renal epithelial cells not amenable to expansion via passaging, since dissolution of tight junctions via enzymatic trypsinisation would lead to further epithelial marker loss. On the other hand, currently commercially available human-derived immortalised cell lines such as RPTEC/TERT1 (Simon-Friedt et al., 2015), (Wieser et al., 2008) have only been partially characterised from a functional standpoint, since the published literature does not report of assays assessing OAT1, OAT3, OCT2, MATE1 transporters function in this cell line, possibly because of low expression of these proteins in the model. Transporter expression decreases as time in culture progresses, which warns us against passaging primary renal epithelial cells as they dedifferentiate rather quickly losing the capability to reabsorb and filtrate compounds. Our primary cells have in fact shown to respond to a range of nephrotoxic stimuli in a dose-dependent fashion (Bajaj et al., 2020). Moreover, immortalized cell lines of proximal tubule cells compared to fresh primary isolated tubular epithelial cells have shown that, despite the cell line retaining morphological characteristics of hPTC, the enzymatic and transporter activity of cell lines is far lower than in primary cells (Racusen et al., 1997), since the immortalization process extends their shelf life while leading cells to dedifferentiate.

A newly established isolation method has been implemented for the isolation of renal fibroblasts from the kidney cortex concomitantly with the isolation of proximal tubule cells from the same organ. Human renal fibroblasts were isolated via Percoll® density gradient centrifugation, where cells were expanded to confluency and subsequently purified via magnetic activated cell sorting (MACS) for cells expressing FSP-1. These human renal fibroblasts (HRF) have shown to express mesenchymal markers FSP-1, CD44, CD90, and CD105 in phenotyping experiments performed via immunofluorescence staining (**Chapter 3, Figure 3.22**), and flow cytometry (**Chapter 3, Figure 3.23**). HRF culture conditions were optimised following experiments performed prior the start of this project on fibroblast cell line NEO3, determining appropriate culture conditions comprise the presence of L-ascorbate in the cell growth media (**Chapter 3, Figure 3.24**). One of the main limitations of this isolation method is that the specificity of fibroblast specific protein 1 (FSP1) as a unique marker of renal fibroblasts has been debated by sources in the literature. As Nishitani et al. explains, fibroblasts positive for FSP-1 are found in severely fibrotic areas of tissue biopsies of patients with IgG nephropathy, posing the question of whether this marker could be indicative of cells undergoing epithelial-to-mesenchymal transition (Nishitani et al., 2005b). Furthermore, the human renal fibroblasts isolated via the established method were phenotyped based on mesenchymal markers CD44, CD90, and CD105, but did not investigate the potential positivity of the cell population to renal epithelial markers. In other words, the flow cytometry assay

employed to assess whether MACS purification had effectively enriched the isolated renal cell population did not consider the presence of epithelial cells within the unsorted population. The use of fluorescence-activated cell sorting (FACS) with a panel of antibodies designed to consider the multitude of cell types present in the renal cortex (i.e. tubular epithelial cells, podocytes, pericytes, endothelial cells) could have provided a more robust purification method to obtain *de facto* renal fibroblasts.

Finally, the optimisation steps that lead to the establishment of the isolation protocol for human renal peritubular endothelial cells (HRPEC) are described in **Chapter 3**. Although HRPEC did not end up being part of the proximal tubule interstitial interface model because of reasons relative to technical aspects and project timeline, it has been worthwhile covering this interesting part of the project since this cell type could be used in future experiments advancing the capabilities of the model generated over the course of these three years. The seminal study published by Ligresti *et al.* (Ligresti et al., 2016) proposing a protocol for the isolation of HRPEC from the kidney cortex highlighted the complexity and tediousness related not only to the isolation process but especially to the maintenance in culture of PV-1 expression which marks the diaphragmatic fenestration, one of the main phenotypical differences between the cellular constituents of glomerular and peritubular capillaries. The isolation protocol proposed in this thesis streamlines the one proposed in the aforementioned study by using Percoll® density gradient centrifugation to deplete epithelial cells from the kidney cortex digest – which are concomitantly used to culture tubular epithelial cells - followed by MACS CD31+ purification, thus avoiding the use of fluorescence activated cell sorting (FACS), a laborious and expensive isolation technique which is not scalable. Our isolation protocol allows produce large quantities of HRPEC which form polarised capillaries when cultured on a permeable membrane, expressing the diaphragmatic fenestration marker PV-1 (**Chapter 3, Figure 3.36**). Furthermore, in agreement with the cited study, HRPEC require high concentrations of VEGF-A during expansion and culture (**Chapter 3, Figure 3.33**), but seem to be able to form tubules independently of the concentration of VEGF-A present in culture (**Chapter 3, Figure 3.38**). Moreover, HRPEC isolated with the suggested method respond to pro-fibrotic stimuli (**Chapter 3, Figure 3.40**) in the context of the endothelial tube formation assay (ETFA) thus making this cell type suitable for incorporation in the *in vitro* renal fibrosis model, where endothelial cells treatment with pro-fibrotic compounds could mimic *in vitro* the phenomenon of capillary rarefaction seen in patients with CKD. The obtained renal peritubular endothelial cells expressed several of the putative markers of this cell type; however, the most widely accepted method of assessing the presence of the diaphragmatic fenestration is scanning electron microscopy (SEM) (Dumas et al., 2021b), which in this project has been used solely to highlight the presence of tight junctions between HRPEC. Further characterisation will be required in order to obtain a complete picture of the HRPEC phenotype.

Once the isolation protocols for all the cell types expected to be in the *in vitro* model of renal fibrosis had been optimised, the next challenge within this project was to establish a co-

culture model that would allow the maintenance of the phenotype of each cell type involved and that would exert the physiological functions carried out by the proximal tubule interstitial interface *in vivo.* The iterations of contact co-culture and non-contact co-culture models have been described and characterised in detail in **Chapter 4.** The experiments hereby displayed focused on comparing the co-culture models to the existing monoculture hPTC in vitro model described by Brown *et al.* (Brown, Sayer, Windass, Haslam, De Broe, et al., 2008), investigating whether the crosstalk with HRF and HRPEC allowed by the co-culture could have trophic effects on the epithelial layer, thus enhancing epithelial barrier formation, polarisation, cell health, key transporter expression, and function. Transcriptomic data collected from contact co-culture experiments (**Chapter 4, Figures 4.9 and 4.12**) demonstrated that gene expression of key transporters in hPTC in direct contact with HRF is upregulated as compared to hPTC in monoculture, hence the relationship between epithelial and mesenchymal cells was explored in further experiments. Several ways of co-culturing hPTC and HRF were trialled in a series of experiments, where it became apparent that HRF cultured in direct contact with hPTC were disrupting the epithelial barrier formation and, subsequently, appropriate solute handling (**Chapter 4, Figures 4.19 to 4.23**). Therefore, methods to halt fibroblasts migration into the epithelial monolayer to avoid disrupting proximal tubule functions were investigated, namely fibroblasts irradiation, treatment with mitomycin C, and embedment in a synthetic ECM. The last method lead to the most promising results since it allowed epithelial cells to form a monolayer expressing ZO-1 on top of viable HRF embedded in PeptiGel® Alpha 2 RGD (**Chapter 4, Figure 4.38**), so this model could ideally have been taken forward as a renal fibrosis assay platform but it would have required a great deal of optimisation before considering it a viable option, mainly due to the limitations imposed by the presence of the synthetic ECM to compounds flux and uptake assays. Hence, our efforts were focused on characterising and optimising culture conditions of the model that would render fibroblast migration into the epithelial monolayer impossible: a spatially separated co-culture model comprising hPTC and HRF. The selected model is constructed by a monolayer of hPTC cultured on the apical side of a 96-Transwell® transparent insert and a monolayer of HRF cultured on the bottom of the well coated with a synthetic ECM, and it shows epithelial barrier formation and effective fluorescent albumin uptake (**Chapter 4, Figure 4.44**) alongside with polarised expression of key solute transporters OAT1, OAT3, and megalin (**Chapter 4, Figure 4.45**). The proposed model is cultured on a high throughput platform which allows for applications such as high content imaging and flow cytometry, it is constituted by primary, autologous patient-derived epithelial and mesenchymal cells that have been characterised in terms of phenotype, genotype, and function. Despite having proven that the developed co-culture model is able to form and maintain epithelial barrier function, and that the presence of fibroblasts in culture enhances epithelial barrier function as compared to a monoculture epithelial model, the transporter function of the model did not improve significantly as we expected. Renal epithelial-to-fibroblast crosstalk seems to be implicated the reduction of the impacts of kidney injury (Schulz et al., 2022), hinting at a protective role of interstitial fibroblasts towards the epithelial parenchyma prior to their activation. Conversely, after acute kidney injury, tubular

epithelial cells seem to promote interstitial fibroblast activation which is essential in the cellular and molecular cascade of events that take place to control the damage to the renal parenchyma caused by the initial injury (D. Zhou et al., 2019). Using the developed model to further explore the relationship between epithelial cells and fibroblasts in health and disease states could lead to a better understanding of why the co-culture seem to improve certain aspects of the epithelial components but not others.

The designed non-contact co-culture model was utilised to model renal fibrosis in the proximal tubule interstitial interface. To explore the relationship between hPTC and HRF in the context of fibrosis, the cells were treated as mono- and co-cultures with increasing concentrations of endogenous pro-fibrotic compounds TGFβ1, TNFα, and angiotensin II, and exogenous nephrotoxic compound polymyxin B, and an array of assays were developed to investigate specific aspects of the cellular events and molecular mechanisms underlying the progression of renal fibrosis *in vivo*. **Chapter 5** describes the development of high content imaging assays designed to monitor epithelial-to-mesenchymal transition (EMT) in epithelial cells by measuring phenotypical changes in expression of tight junction markers ZO-1, E-Cadherin, and mesenchymal marker vimentin, and fibroblast-to-myofibroblast transition (FMT) and ECM deposition in HRF by measuring *de novo* expression of αSMA as marker of acquisition of migratory activated phenotype, fibronectin and collagen I as ECM markers. In the context of fibrosis, cell health was measured via cell viability assay, while proliferation, apoptosis, and necrosis were measured via high throughput flow cytometry, and TEER assay was used to monitor epithelial barrier disruption under pro-fibrotic stimuli. Finally, soluble stress biomarkers KIM-1, clusterin, and NGAL, which have been implicated as predictors of acute kidney injury (AKI), which is in turn associated with progression to CKD (Ferenbach & Bonventre, 2016), were measured after pro-fibrotic stimuli in epithelial cells, alongside with measurement of chemokine release in fibroblasts. Firstly, we demonstrated maintenance of non-activated phenotype by renal fibroblasts by culturing this cell type onto a soft synthetic ECM that would mimic healthy renal parenchyma, as opposed to stiffer cell culture plastic that would have induced FMT (**Chapter 5, Figures 5.4 to 5.6**). We stimulated hPTC in monoculture with high doses of TGFβ1, TNFα, and angiotensin II to assess qualitatively whether a change in phenotype would occur stimulated epithelial cells migrated into nodules while disrupting the adjacent monolayer in terms of loss of tight junctions expression (**Chapter 5, Figure 5.9**). These findings hinted that pro-fibrotic treatments were able to induce epithelial barrier disruption after 24 hours, which was confirmed by measurement of TEER values of stimulated hPTC in co-culture (**Chapter 5, Figure 5.19**). A single-cell approach was applied to data collected via high content imaging to investigate the effects of pro-fibrotic treatments on hPTC and HRF populations both in mono- and co-culture by plotting frequency of distribution graphs that would define a profile for the untreated populations versus the ones treated with increasing concentrations of treatments for each of the EMT and ECM deposition markers (**Chapter 5, Sections 6 and 7**). The shifts shown by the frequency of distribution profiles indicate that we were able to induce a change in expression of the selected markers via pro-

fibrotic treatment, thus confirming that both cell types considered are responding to the stimuli in a complex and concerted manner. Under pro-fibrotic stimuli and in both conditions of culture, proximal tubule cells migrate into nodules thus disrupting the epithelial monolayer and its tight junctions; furthermore, hPTC aggregated into nodules show acquisition of *de novo* expression of αSMA, thus confirming their transition towards contractile activated myofibroblast (EMT) initiated by pro-fibrotic stimuli (**Chapter 5, Figure 5.58**). Importantly, we demonstrated that stimulated HRF are able to deposit ECM and that this phenomenon takes place in a dose-dependent fashion for fibronectin and collagen I. Release of stress biomarkers normally assayed in the context of AKI did not seem to take place in hPTC treated with pro-fibrotic compounds (**Chapter 5, Section 5.8**); therefore chemokines released by renal fibroblasts exposed to TGFβ1 were measured via chemiluminescence microarray highlighting IL-8, GRO-α, and MCP-1 release after pro-fibrotic stimulus. These findings indicate that the primary cell populations isolated from the human kidney cortex respond to pro-fibrotic treatments; however, TNFα is a known inductor of apoptosis in proximal tubule cells (Lange-Sperandio et al., 2003), which we failed to demonstrate both in mono- and co-culture. This could be due to the patient-patient biological variability between donors used. In fact, as the single patient data shown in plots derived from human kidney donors K3, K6, K7, K8, K9, K10, despite the statistical analysis demonstrating narrow standard deviations (SD) within each individual biological replicate, the standard error of the mean (SEM) obtained by pooling the biological replicates into one plot becomes too large to make any dose-dependent responses measurable. Furthermore, despite renal cortex dissection being performed carefully to avoid necrotic or fibrotic tissue areas, by considering the medical history of the donor patients (displayed in **Chapter 2, Table 2.1**) which (K6, K7, K9: hypertension; K8: diabetes) one could infer that the lowered response to the pro-fibrotic compounds could be explained by pre-existing activation of cell signalling pathways associated with pEMT and renal fibrosis. Further characterisation with different apoptosis and necrosis assays e.g. using high content imaging instead of flow cytometry could elucidate the reasons behind the 3D-model-attenuated response to injury.

The *in vitro* assay platform of proximal tubule interstitial interface produced throughout the project have several limitations derived from time constraints, primary tissue availability, and technical resources within our group. Despite the presented model being relatively simple to co-culture and up-scalable for high throughput, it lacks some highly desirable features that could be incorporated in future versions of this model. As discussed in a review article from Lacueva-Aparicio, et al., the presence of a synthetic or human derived extra cellular matrix to mimic the tubular basement membrane in the model should have been considered (Lacueva-Aparicio et al., 2022). Since the primary cells used to build the model were isolated from human kidneys, the ECM could have been derived from the tissue itself as demonstrated by Kim JW, et al. whereby the renal parenchyma is decellularized, perfused, and the remaining structure is lyophilised and cross-linked into hydrogels at different stiffnesses (J. W. Kim et al., 2022). The isolated primary components of the 3D model are then cultured onto the

endogenous matrix, making this a completely autologous fully human model capable of retaining differentiated phenotype for all cell types, in particular hPTC and HRPEC for an extended period of time in culture. A number of microfluidics platforms are available on the market such as Mimetas OrganoPlate™, Nortis ParVivo™, and Emulate Chip-A1™ which have been widely used to develop valuable *in vitro* assay platforms which closely resemble in vivo conditions. The organ-on-a-chip technology could have been employed within this project to make the model of proximal tubule interstitial interface more physiologically relevant. It would be particularly useful for such platform to take into account the presence of the flow of urine within the tubules and blood within the peritubular capillaries, that is, in the form of shear stress, that can be mimicked *in vitro* via mechanical stimuli applied to microfluidic systems (Birdsall & Hammond, 2021). In the context of CKD, changes in shear stress are associated with changes in the phenotype of epithelial and endothelial components, therefore varying the degree of shear stress applied to a microfluid chip containing primary renal cells could eventually induce renal fibrosis.

In terms of the induction of renal fibrosis, if the cells had been cultured onto a microfluidic membrane, the disease state could have been induced by a collection of stimuli which occur in the human body, such as inflammatory and pro-fibrotic cytokine, modulating ECM stiffness and shear stress (Maggiorani et al., 2015). By modulating all these factors, different stages of progressive renal fibrosis could have been mimicked on the same platform. Furthermore, other aetiologies of the disease could have been explored, for example diabetic nephropathy by having a high glucose component within the media. In this microfluidic organ-on-a-chip renal fibrosis platform, phenotypical changes of all components could be monitored via high content imaging of immunofluorescence-stained cells. A similar panel to the one used within this thesis could have been used to determine the creation of a fibrotic milieu within the microtissue, with a focus on loss of tight junctions and epithelial barrier integrity for the epithelial monolayer, and a focus on modification to the diaphragmatic fenestration in the endothelial tubule. Due to the crosstalk between the different components of the model initiated by the pro-fibrotic stimuli, fibroblasts would have acquired myofibroblast phenotype depositing their own ECM within the autologous ECM in which they were themselves embedded. This could have been tracked by staining and quantification of Collagen IV, Collagen I, Fibronectin, and Laminin fibres.

One of the limitations to the proposed model arises from the lack of endothelial and immune components within the 3D structure, as capillary rarefaction and inflammatory cytokines release from resident and recruited immune cells in the renal parenchyma are key contributors to the progression of renal fibrosis *in vivo.* Therefore, future experiments should focus on incorporating renal peritubular endothelial cells (HRPEC) within the *in vitro* model of renal fibrosis since we have demonstrated that this cell population responds to pro-fibrotic stimuli. The diaphragmatic fenestration expressing PV-1 has been targeted for anti-fibrotic drug delivery in animal models of lung fibrosis (Marchetti et al., 2019), therefore the presence of this structure in our model could make it palatable for drug and target discovery in our field.

As stated repeatedly throughout this thesis, renal fibrosis is essentially defined as progressive scarring of the renal parenchyma which eventually leads to loss of kidney function. This definition stresses how fundamental histological changes to the organ structure are to the progression and subsequent diagnosis of CKD; thence, the ideal *in vitro* model of renal fibrosis in the proximal tubule interstitial interface should resemble as closely as possible a CKD patient's biopsy. This idea underlines one of the limitations of such a model, since the data hereby discussed focuses on changes in tight junction expression and *de novo* acquisition of mesenchymal markers in the epithelial monolayer, which represents the functional tubular parenchyma in the kidney, rather than focusing on what the definition of *scarring* entails. Therefore, future experiments should investigate whether hPTC migrating into nodules are depositing extracellular matrix in excess within the boundaries of these structures when undergoing pro-fibrotic stimuli. A novel high content imaging assay could be developed whereby the total and nodule-specific amount of ECM deposited by hPTC are plotted against the increasing concentration of pro-fibrotic compound, so to extrapolate dose-response curves that would describe the progression of scarring *in vitro.* The addition of the immune component and measurement of ECM deposition in the epithelial microtissue would render our patient-derived model closely comparable to a CKD renal biopsy, providing drug developers in the field with an invaluable tool to develop new treatments that could extend the life expectancy of millions of patients around the globe.

Currently available *in vitro* renal fibrosis models either lack complexity, or do not prove appropriate nephron segment function. Moein *et al.* proposes an *in vitro* renal fibrosis model induced via TGFβ1 treatment and hypoxia comparing it to the unilateral ureter obstruction (UUO) animal model. This *in vitro* model is made from unspecified and uncharacterized cells cultured from the kidney cortex which have not been purified or selected based on their phenotype in any way. The readouts provided in this study focus only on the transcriptome isolated from the cell population after pro-fibrotic injury, therefore making it challenging to pinpoint from which cellular component of the kidney cortex are the fibrosis-related mRNA redouts arising (Moein et al., 2020). A model proposed by Bon *et al.* exploits the spontaneous accumulation and acquisition of fibrotic phenotype arising from contact co-culture of epithelial cells and renal fibroblasts to obtain a model of disease. The data presented in **Chapter 4** demonstrates that this co-culture method does not allow epithelial cells to retain their absorptive and secretory functions. This study does not compare untreated – thus representing the healthy, functional kidney - versus fibrotic models, as it focuses on inhibiting ECM deposition which is not the only mechanism involved in fibrosis progression, and it does not provide any information about epithelial barrier integrity as it is not possible to do so without first proving expression of tight junctions (Bon et al., 2019). As the same research group presents in their previous study (Qureshi et al., 2017), primary passaged renal epithelial cells and fibroblasts are stimulated with TGFβ1 and ECM deposition is measured via high content imaging. Both cell types in monoculture demonstrate their ability to respond to the stimulus which induces a significant increase in deposition of ECM which gives a cue for future

experiments relative to our model, despite the conclusion to this study selecting the presented contact co-culture model as a viable option for proximal tubule interstitial interface modelling. Such a model is taken forward in their next study as it has been shown to spontaneously deposit large amounts of ECM, essentially disregarding the useful data that could have been obtained by using a specific stimulus to induce fibrosis such as investigating the dose-dependent relationship between concentration of pro-fibrotic treatment and ECM deposition. Furthermore, this study uses passaged primary cells which in fact do not respond to the nephrotoxic stimuli they are exposed to. Moll et al. proposes a model whereby epithelial and mesenchymal cells are used to culture a 3D model (Moll et al., 2013b), although the fibroblasts utilized in this context are dermal fibroblasts since the investigators could not overcome the issue of spontaneous fibroblast-to-myofibroblast activation by contact with stiff cell culture material surfaces which is commonly seen in renal fibroblasts. The very promising model proposed by Nugraha et al., where proximal tubule cells are allowed to form polarized spheroids in a 3D hydrogel before being overlayed with quiescent fibroblasts (Nugraha et al., 2017), is undermined by the use of cell line HKC-8 which exerts far less solute handling properties as compared to primary cells.

Our model of renal fibrosis in the proximal tubule interstitial interface proposes to address the limitations pointed out within these studies as it has been characterized in every component to assure that spontaneous FMT and EMT are absent and that cells acquire fibrotic phenotype only when prompted to do so – that is, when undergoing pro-fibrotic stimuli. In particular, the proposed model was selected specifically because it did not seem possible to retain epithelial barrier function, which is essential to allow for selective reabsorption and secretion of compounds, in a contact co-culture model as renal fibroblasts would disrupt epithelial barrier formation, thus most probably acquiring fibrotic phenotype before being stimulated, making it impossible to measure transporter function with our established radiolabeled compound flux assay and fluorescent albumin uptake and to develop assays that would describe the relationship between the increasing dose of pro-fibrotic compound used in the treatment and the measured biological response. Also, it would make it impossible to pose any research question relative to tight junction expression in epithelial cells as these would not form properly in contact co-culture. The *in vitro* model of renal fibrosis proposed in this thesis mimics the proximal tubule interstitial interface by incorporating in its 3D structure autologous primary tubular epithelial and mesenchymal cells. The presented model is designed to act as an assay platform for the development of high throughput assays, with a focus on high content imaging.

The renal fibrosis *in vitro* model developed throughout this project is novel and pushes the field of *in vitro* disease modeling forward because of its unique characteristics that make it amenable for therapeutic drug and target discovery. As opposed to microfluidic platforms which often rely on a steep learning curve in terms of tissue culture technique or on the employment of external pumps and plate rockers, this fully human, autologous model is simple to assemble and exploits the simplicity of the Transwell insert technology to co-culture

two distinct cell types within the same cell culture system. It is a high throughput platform that is up scalable for screening of compound libraries. Despite these considerations, the model could be greatly improved by future work which would result in a renal fibrosis platform that would closely mimic the disease in vivo. The readouts would have to include the hallmarks of disease already considered in this thesis, such as the deposition of extracellular matrix, subsequent scarring, and loss of epithelial barrier and transporter function, alongside accurate readings of cell health and proliferation. Considering the relevance of renal fibrosis in the context of chronic kidney disease, the model should take into account different aetiologies of disease, such as diabetic nephropathy, acute kidney injury, and immune-mediated chronic interstitial inflammation. Cell culture media would be used to vehiculate specific treatments to induce fibrosis via a different pathway or aetiology, in order to represent as many aetiologies of disease as possible. Known effectors of cell signaling pathways could be used as a positive control highlighting the effective targeting of each desired molecular route to renal fibrosis.

In conclusion, the *in vitro* 3D model of renal fibrosis in the proximal tubule interstitial interface explored in this thesis is comprised of primary renal epithelial and mesenchymal cells which show appropriate phenotype and function, thus rendering this platform a promising alternative to *in vivo* animal models of CKD. It successfully recapitulates the key processes that are known to be implicated in the progression of renal fibrosis *in vivo*, both from a cellular and molecular standpoint. The model is suitable for high throughput applications in drug development and discovery.

Supplementary material

Abstract accepted and presented as poster presentation at CKD World Summit 2022, 1-3 March, Boston MA.

aProximate™ Fibrosis Model: a novel *in vitro* 3D model of CKD in the proximal tubule for high throughput screening.

Elena Tasinato[1,2], Kathryn Garner[1], Lyle Armstrong[1,2], Colin DA Brown[1]

In chronic kidney disease (CKD), increased deposition of extracellular matrix (ECM) in the tubule interstitium combined with epithelial-to-mesenchymal transition (EMT) leads to a loss of renal function. We have developed a fully human, donor-derived renal fibrosis *in vitro* assay. We have isolated and characterized pure populations of proximal tubule cells (aProximate™ PTCs) and renal fibroblasts from human kidneys and cultured them in monolayers. Subsequently, we have assembled the Fibrosis model on Corning® HTS 96-Transwell® inserts and induced fibrosis via treatment with hormone and cytokine combinations. The changing state of the system is monitored via high content imaging.

1. Newcells Biotech Ltd, The Biosphere, Draymans Helix, South Street, Newcastle upon Tyne NE4 5BX 2. Institute of Genetic Medicine, Newcastle University, International Centre for Life, Central Parkway, Newcastle upon Tyne NE1 3BZ

References

Aceves, J. O., Heja, S., Kobayashi, K., Robinson, S. S., Miyoshi, T., Matsumoto, T., Schäffers, O. J. M., Morizane, R., & Lewis, J. A. (2022). 3D proximal tubule-on-chip model derived from kidney organoids with improved drug uptake. *Scientific Reports*, *12*(1), 14997. https://doi.org/10.1038/s41598-022-19293-3

Agarwal, S., Dinda, A., & Sethi, S. (2013). Basics of kidney biopsy: A nephrologist's perspective. *Indian Journal of Nephrology*, *23*(4), 243. https://doi.org/10.4103/0971-4065.114462

Allison, S. J. (2015). Targeting EMT to reverse renal fibrosis. *Nature Reviews Nephrology*, *11*(10), 565–565. https://doi.org/10.1038/nrneph.2015.133

Astashkina, A. I., Mann, B. K., Prestwich, G. D., & Grainger, D. W. (2012). A 3-D organoid kidney culture model engineered for high-throughput nephrotoxicity assays. *Biomaterials*, *33*(18), 4700–4711. https://doi.org/10.1016/j.biomaterials.2012.02.063

Atkinson, J., Boden, T., Mocho, J.-P., & Johnson, T. (2021). Refining the unilateral ureteral obstruction mouse model: No sham, no shame. *Laboratory Animals*, *55*(1), 21–29. https://doi.org/10.1177/0023677220909401

Bajaj, P., Chowdhury, S. K., Yucha, R., Kelly, E. J., & Xiao, G. (2018). Emerging Kidney Models to Investigate Metabolism, Transport, and Toxicity of Drugs and Xenobiotics. *Drug Metabolism and Disposition*, *46*(11), 1692–1702. https://doi.org/10.1124/dmd.118.082958

Bajaj, P., Chung, G., Pye, K., Yukawa, T., Imanishi, A., Takai, Y., Brown, C., & Wagoner, M. P. (2020). Freshly isolated primary human proximal tubule cells as an in vitro model for the detection of renal tubular toxicity. *Toxicology*, *442*, 152535. https://doi.org/10.1016/j.tox.2020.152535

Balzer, M. S., Rohacs, T., & Susztak, K. (2022). How Many Cell Types Are in the Kidney and What Do They Do? *Annual Review of Physiology*, *84*, 507–531. https://doi.org/10.1146/annurev-physiol-052521-121841

Barrett, K. E., Barman, S. M., Boitano, S., & Brooks, H. L. (2018). Renal Function & Micturition. In *Ganong's Review of Medical Physiology, 25e*. McGraw-Hill Education. accessmedicine.mhmedical.com/content.aspx?aid=1115832688

Barrett, K. E., Barman, S. M., Boitano, S., & Reckelhoff, J. F. (2017). Regulation of Extracellular Fluid Composition & Volume. In *Ganong's Medical Physiology Examination & Board Review*. McGraw-Hill Education. accessmedicine.mhmedical.com/content.aspx?aid=1142557219

Bäumner, S., & Weber, L. T. (2018). Nephropathic Cystinosis: Symptoms, Treatment, and Perspectives of a Systemic Disease. *Frontiers in Pediatrics*, *6*. https://doi.org/10.3389/fped.2018.00058

Belayev, L. Y., & Palevsky, P. M. (2014). The link between acute kidney injury and chronic kidney disease. In *Current Opinion in Nephrology and Hypertension* (Vol. 23, Issue 2, pp. 149–154). https://doi.org/10.1097/01.mnh.0000441051.36783.f3

Birdsall, H. H., & Hammond, T. G. (2021). Role of Shear Stress on Renal Proximal Tubular Cells for Nephrotoxicity Assays. *Journal of Toxicology*, *2021*, 6643324. https://doi.org/10.1155/2021/6643324

Bon, H., Hales, P., Lumb, S., Holdsworth, G., Johnson, T., Qureshi, O., & Twomey, B. M. (2019). Spontaneous Extracellular Matrix Accumulation in a Human in vitro Model of Renal Fibrosis Is Mediated by αV Integrins. *Nephron*, *142*(4), 328–350. https://doi.org/10.1159/000499506

Bonventre, J. v. (2008). Kidney injury molecule-1 (KIM-1): A specific and sensitive biomarker of kidney injury. *Scandinavian Journal of Clinical and Laboratory Investigation*, *68*(SUPPL. 241), 78–83. https://doi.org/10.1080/00365510802145059

Brown, C. D. A., Sayer, R., Windass, A. S., Haslam, I. S., de Broe, M. E., D'Haese, P. C., & Verhulst, A. (2008). Characterisation of human tubular cell monolayers as a model of proximal tubular xenobiotic handling. *Toxicology and Applied Pharmacology*, *233*(3), 428–438. https://doi.org/10.1016/j.taap.2008.09.018

Brown, C. D. A., Sayer, R., Windass, A. S., Haslam, I. S., De Broe, M. E., D'Haese, P. C., & Verhulst, A. (2008). Characterisation of human tubular cell monolayers as a model of proximal tubular xenobiotic handling. *Toxicology and Applied Pharmacology*, *233*(3), 428–438. https://doi.org/10.1016/j.taap.2008.09.018

Buchser, W., Collins, M., Garyantes, T., Guha, R., Haney, S., Lemmon, V., Li, Z., & Trask, O. J. (2004). *Assay Development Guidelines for Image-Based High Content Screening, High Content Analysis and High Content Imaging*.

Bui, T. M., Wiesolek, H. L., & Sumagin, R. (2020). ICAM-1: A master regulator of cellular responses in inflammation, injury resolution, and tumorigenesis. *Journal of Leukocyte Biology*, *108*(3), 787–799. https://doi.org/10.1002/JLB.2MR0220-549R

Bülow, R. D., & Boor, P. (2019). Extracellular Matrix in Kidney Fibrosis: More Than Just a Scaffold. *Journal of Histochemistry & Cytochemistry*, *67*(9), 643–661. https://doi.org/10.1369/0022155419849388

Caetano-Pinto, P., Janssen, M. J., Gijzen, L., Verscheijden, L., Wilmer, M. J. G., & Masereeuw, R. (2016). Fluorescence-Based Transport Assays Revisited in a Human Renal Proximal Tubule Cell Line. *Molecular Pharmaceutics*, *13*(3), 933–944. https://doi.org/10.1021/acs.molpharmaceut.5b00821

Calabrese, F., Lunardi, F., Tauro, V., Pezzuto, F., Fortarezza, F., Vedovelli, L., Faccioli, E., Balestro, E., Schiavon, M., Esposito, G., Vuljan, S. E., Giraudo, C., Gregori, D., Rea, F., & Spagnolo, P. (2022). RNA Sequencing of Epithelial Cell/Fibroblastic Foci Sandwich in Idiopathic Pulmonary Fibrosis: New Insights on the Signaling Pathway. *International Journal of Molecular Sciences*, *23*(6), 3323. https://doi.org/10.3390/ijms23063323

Carracedo, M., Robinson, S., Alaei, B., Clausen, M., Hicks, R., Belfield, G., Althage, M., Bak, A., Lewis, J. A., Hansen, P. B. L., & Williams, J. M. (2023). 3D vascularised proximal tubules-on-a-multiplexed chip model for enhanced cell phenotypes. *Lab on a Chip*, *23*(14), 3226–3237. https://doi.org/10.1039/d2lc00723a

Chandrasekaran, V., Carta, G., da Costa Pereira, D., Gupta, R., Murphy, C., Feifel, E., Kern, G., Lechner, J., Cavallo, A. L., Gupta, S., Caiment, F., Kleinjans, J. C. S., Gstraunthaler, G., Jennings, P., & Wilmes, A. (2021). Generation and characterization of iPSC-derived renal proximal tubule-

like cells with extended stability. *Scientific Reports*, *11*(1), 11575. https://doi.org/10.1038/s41598-021-89550-4

Chen, J., Chen, J.-K., & Harris, R. C. (2012). Angiotensin II Induces Epithelial-to-Mesenchymal Transition in Renal Epithelial Cells through Reactive Oxygen Species/Src/Caveolin-Mediated Activation of an Epidermal Growth Factor Receptor–Extracellular Signal-Regulated Kinase Signaling Pathway. *Molecular and Cellular Biology*, *32*(5), 981–991. https://doi.org/10.1128/mcb.06410-11

Cheng, S.-Y., Seo, J., Huang, B. T., Napolitano, T., & Champeil, E. (2016). Mitomycin C and decarbamoyl mitomycin C induce p53-independent p21WAF1/CIP1 activation. *International Journal of Oncology*, *49*(5), 1815–1824. https://doi.org/10.3892/ijo.2016.3703

Christensen, E. I., & Birn, H. (2002). Megalin and cubilin: multifunctional endocytic receptors. *Nature Reviews Molecular Cell Biology*, *3*(4), 258–267. https://doi.org/10.1038/nrm778

Chung, A. C. K., & Lan, H. Y. (2011). Chemokines in renal injury. In *Journal of the American Society of Nephrology* (Vol. 22, Issue 5, pp. 802–809). https://doi.org/10.1681/ASN.2010050510

Cristofori, P., Zanetti, E., Fregona, D., Piaia, A., & Trevisan, A. (2007). Renal Proximal Tubule Segment-Specific Nephrotoxicity: An Overview on Biomarkers and Histopathology. *Toxicologic Pathology*, *35*(2), 270–275. https://doi.org/10.1080/01926230601187430

de Fátima Fernandes Vattimo, M., Watanabe, M., da Fonseca, C. D., de Moura Neiva, L. B., Pessoa, E. A., & Borges, F. T. (2016). Polymyxin B Nephrotoxicity: From organ to cell damage. *PLoS ONE*, *11*(8). https://doi.org/10.1371/journal.pone.0161057

Denu, R. A., Nemcek, S., Bloom, D. D., Goodrich, A. D., Kim, J., Mosher, D. F., & Hematti, P. (2016). Fibroblasts and Mesenchymal Stromal/Stem Cells Are Phenotypically Indistinguishable. *Acta Haematologica*, *136*(2), 85–97. https://doi.org/10.1159/000445096

DesRochers, T. M., Palma, E., & Kaplan, D. L. (2014). Tissue-engineered kidney disease models. *Advanced Drug Delivery Reviews*, *69–70*, 67–80. https://doi.org/10.1016/j.addr.2013.12.002

Dong, Z., Chen, F., Peng, S., Liu, X., Liu, X., Guo, L., Wang, E., & Chen, X. (2023). Identification of the key immune-related genes and immune cell infiltration changes in renal interstitial fibrosis. *Frontiers in Endocrinology*, *14*, 1207444. https://doi.org/10.3389/fendo.2023.1207444

Dumas, S. J., Meta, E., Borri, M., Luo, Y., Li, X., Rabelink, T. J., & Carmeliet, P. (2021a). Phenotypic diversity and metabolic specialization of renal endothelial cells. *Nature Reviews Nephrology*, *17*(7), 441–464. https://doi.org/10.1038/s41581-021-00411-9

Dumas, S. J., Meta, E., Borri, M., Luo, Y., Li, X., Rabelink, T. J., & Carmeliet, P. (2021b). Phenotypic diversity and metabolic specialization of renal endothelial cells. *Nature Reviews. Nephrology*, *17*(7), 441–464. https://doi.org/10.1038/s41581-021-00411-9

D'Urso, M., & Kurniawan, N. A. (2020). Mechanical and Physical Regulation of Fibroblast–Myofibroblast Transition: From Cellular Mechanoresponse to Tissue Pathology. *Frontiers in Bioengineering and Biotechnology*, *8*. https://doi.org/10.3389/fbioe.2020.609653

Dylewski, J. F., Wilson, N., Lu, S., Jat, P., Weiser-evans, M., Panzer, S. E., & Blaine, J. (2020). Isolation, purification, and conditional immortalization of murine glomerular endothelial cells of microvascular phenotype. *MethodsX*, *7*, 101048. https://doi.org/10.1016/j.mex.2020.101048

Eaton, D. C., & Pooler, J. P. (2018). Renal Functions, Basic Processes, and Anatomy. In *Vander's Renal Physiology, 9e*. McGraw-Hill Education. accessmedicine.mhmedical.com/content.aspx?aid=1160609600

Eymael, J., Willemsen, B., Xu, J., Mooren, F., Steenbergen, E., Wetzels, J. F., Dijkman, H., Jansen, J., van der Vlag, J., & Smeets, B. (2022). Motile Cilia on Kidney Proximal Tubular Epithelial Cells Are Associated With Tubular Injury and Interstitial Fibrosis. *Frontiers in Cell and Developmental Biology*, *10*. https://doi.org/10.3389/fcell.2022.765887

Ferenbach, D. A., & Bonventre, J. V. (2016). Acute kidney injury and chronic kidney disease: From the laboratory to the clinic. *Néphrologie & Thérapeutique*, *12*, S41–S48. https://doi.org/10.1016/j.nephro.2016.02.005

Ferrell, N., Desai, R. R., Fleischman, A. J., Roy, S., Humes, H. D., & Fissell, W. H. (2010). A microfluidic bioreactor with integrated transepithelial electrical resistance (TEER) measurement electrodes for evaluation of renal epithelial cells. *Biotechnology and Bioengineering*, *107*(4), 707–716. https://doi.org/10.1002/bit.22835

Finnigan, N. A., & Leslie, S. W. (2022). *Polycystic Kidney Disease In Adults*.

Fransen, M. F. J., Addario, G., Bouten, C. V. C., Halary, F., Moroni, L., & Mota, C. (2021). Bioprinting of kidney *in vitro* models: cells, biomaterials, and manufacturing techniques. *Essays in Biochemistry*, *65*(3), 587–602. https://doi.org/10.1042/EBC20200158

Gewin, L., & Zent, R. (2012). How Does TGF-β Mediate Tubulointerstitial Fibrosis? *Seminars in Nephrology*, *32*(3), 228–235. https://doi.org/10.1016/j.semnephrol.2012.04.001

Grande, M. T., Sánchez-Laorden, B., López-Blau, C., De Frutos, C. A., Boutet, A., Arévalo, M., Rowe, R. G., Weiss, S. J., López-Novoa, J. M., & Nieto, M. A. (2015). Snail1-induced partial epithelial-to-mesenchymal transition drives renal fibrosis in mice and can be targeted to reverse established disease. *Nature Medicine*, *21*(9), 989–997. https://doi.org/10.1038/nm.3901

Grande, M. T., Sánchez-Laorden, B., López-Blau, C., de Frutos, C. A., Boutet, A., Arévalo, M., Rowe, R. G., Weiss, S. J., López-Novoa, J. M., & Nieto, M. A. (2015). Snail1-induced partial epithelial-to-mesenchymal transition drives renal fibrosis in mice and can be targeted to reverse established disease. *Nature Medicine*, *21*(9), 989–997. https://doi.org/10.1038/nm.3901

Griffin, B. R., Faubel, S., & Edelstein, C. L. (2019). Biomarkers of drug-induced kidney toxicity. In *Therapeutic Drug Monitoring* (Vol. 41, Issue 2, pp. 213–226). Lippincott Williams and Wilkins. https://doi.org/10.1097/FTD.0000000000000589

Grimwood, L., & Masterson, R. (2009). *Propagation and Culture of Renal Fibroblasts* (pp. 25–37). https://doi.org/10.1007/978-1-59745-352-3_3

Guo, J., Guan, Q., Liu, X., Wang, H., Gleave, M. E., Nguan, C. Y. C., & Du, C. (2016). Relationship of clusterin with renal inflammation and fibrosis after the recovery phase of ischemia-reperfusion injury. *BMC Nephrology*, *17*(1). https://doi.org/10.1186/s12882-016-0348-x

Guzzi, F., Cirillo, L., Roperto, R. M., Romagnani, P., & Lazzeri, E. (2019). Molecular Mechanisms of the Acute Kidney Injury to Chronic Kidney Disease Transition: An Updated View. *International Journal of Molecular Sciences*, *20*(19), 4941. https://doi.org/10.3390/ijms20194941

Han, W. K., Bailly, V., Abichandani, R., Thadhani, R., & Bonventre, J. V. (2002). Kidney Injury Molecule-1 (KIM-1): a novel biomarker for human renal proximal tubule injury. *Kidney International*, *62*(1), 237–244. https://doi.org/10.1046/j.1523-1755.2002.00433.x

Hewitson, T. D. (2012). Fibrosis in the kidney: Is a problem shared a problem halved? *Fibrogenesis and Tissue Repair*, *5*(SUPPL.1). https://doi.org/10.1186/1755-1536-5-S1-S14

Homan, K. A., Kolesky, D. B., Skylar-Scott, M. A., Herrmann, J., Obuobi, H., Moisan, A., & Lewis, J. A. (2016). Bioprinting of 3D Convoluted Renal Proximal Tubules on Perfusable Chips. *Scientific Reports*, *6*(1), 34845. https://doi.org/10.1038/srep34845

Hon, Y. Y. (2016). Dose Adjustment in Renal and Hepatic Disease. In L. Shargel & A. B. C. Yu (Eds.), *Applied Biopharmaceutics & Pharmacokinetics, 7e*. McGraw-Hill Education. accesspharmacy.mhmedical.com/content.aspx?aid=1117902762

Humes, H. D., Mackay, S. M., Funke, A. J., & Buffington, D. A. (1999). Tissue engineering of a bioartificial renal tubule assist device: In vitro transport and metabolic characteristics. *Kidney International*, *55*(6), 2502–2514. https://doi.org/10.1046/j.1523-1755.1999.00486.x

Humphreys, B. D., Lin, S.-L., Kobayashi, A., Hudson, T. E., Nowlin, B. T., Bonventre, J. V, Valerius, M. T., McMahon, A. P., & Duffield, J. S. (2010). Fate tracing reveals the pericyte and not epithelial origin of myofibroblasts in kidney fibrosis. *The American Journal of Pathology*, *176*(1), 85–97. https://doi.org/10.2353/ajpath.2010.090517

Jalanko, H. (2009). Congenital nephrotic syndrome. *Pediatric Nephrology*, *24*(11), 2121–2128. https://doi.org/10.1007/s00467-007-0633-9

Jansen, J., Fedecostante, M., Wilmer, M. J., Peters, J. G., Kreuser, U. M., van den Broek, P. H., Mensink, R. A., Boltje, T. J., Stamatialis, D., Wetzels, J. F., van den Heuvel, L. P., Hoenderop, J. G., & Masereeuw, R. (2016). Bioengineered kidney tubules efficiently excrete uremic toxins. *Scientific Reports*, *6*(1), 26715. https://doi.org/10.1038/srep26715

Johnson, D. W., Saunders, H. J., Brew, B. K., Ganesan, A., Baxter, R. C., Poronnik, P., Cook, D. I., György, A. Z., Field, M. J., & Pollock, C. A. (1997). Human renal fibroblasts modulate proximal tubule cell growth and transport via the IGF-I axis. *Kidney International*, *52*(6), 1486–1496. https://doi.org/10.1038/ki.1997.479

Jun, D. Y., Kim, S. Y., Na, J. C., Lee, H. H., Kim, J., Yoon, Y. E., Hong, S. J., & Han, W. K. (2018). Tubular organotypic culture model of human kidney. *PLoS ONE*, *13*(10). https://doi.org/10.1371/journal.pone.0206447

Kandasamy, K., Chuah, J. K. C., Su, R., Huang, P., Eng, K. G., Xiong, S., Li, Y., Chia, C. S., Loo, L.-H., & Zink, D. (2015). Prediction of drug-induced nephrotoxicity and injury mechanisms with human induced pluripotent stem cell-derived cells and machine learning methods. *Scientific Reports*, *5*(1), 12337. https://doi.org/10.1038/srep12337

Kashoor, I., & Batlle, D. (2019). Proximal renal tubular acidosis with and without Fanconi syndrome. *Kidney Research and Clinical Practice*, *38*(3), 267–281. https://doi.org/10.23876/j.krcp.19.056

Kida, Y. (2020). Peritubular Capillary Rarefaction: An Underappreciated Regulator of CKD Progression. *International Journal of Molecular Sciences*, *21*(21), 8255. https://doi.org/10.3390/ijms21218255

Kim, J. W., Nam, S. A., Yi, J., Kim, J. Y., Lee, J. Y., Park, S.-Y., Sen, T., Choi, Y.-M., Lee, J. Y., Kim, H. L., Kim, H. W., Park, J., Cho, D.-W., & Kim, Y. K. (2022). Kidney Decellularized Extracellular Matrix Enhanced the Vascularization and Maturation of Human Kidney Organoids. *Advanced Science (Weinheim, Baden-Wurttemberg, Germany)*, *9*(15), e2103526. https://doi.org/10.1002/advs.202103526

Kim, K. K., Sheppard, D., & Chapman, H. A. (2018). TGF-β1 Signaling and Tissue Fibrosis. *Cold Spring Harbor Perspectives in Biology*, *10*(4). https://doi.org/10.1101/cshperspect.a022293

King, S. M., Higgins, J. W., Nino, C. R., Smith, T. R., Paffenroth, E. H., Fairbairn, C. E., Docuyanan, A., Shah, V. D., Chen, A. E., Presnell, S. C., & Nguyen, D. G. (2017). 3D Proximal Tubule Tissues Recapitulate Key Aspects of Renal Physiology to Enable Nephrotoxicity Testing. *Frontiers in Physiology*, *8*. https://doi.org/10.3389/fphys.2017.00123

Kriz, W., Kaissling, B., & Le Hir, M. (2011). Epithelial-mesenchymal transition (EMT) in kidney fibrosis: fact or fantasy? *The Journal of Clinical Investigation*, *121*(2), 468–474. https://doi.org/10.1172/jci44595

Kurtzeborn, K., Cebrian, C., & Kuure, S. (2018). Regulation of Renal Differentiation by Trophic Factors. *Frontiers in Physiology*, *9*. https://doi.org/10.3389/fphys.2018.01588

Lacueva-Aparicio, A., Lindoso, R. S., Mihăilă, S. M., & Giménez, I. (2022). Role of extracellular matrix components and structure in new renal models in vitro. *Frontiers in Physiology*, *13*, 1048738. https://doi.org/10.3389/fphys.2022.1048738

Lamouille, S., Xu, J., & Derynck, R. (2014). Molecular mechanisms of epithelial-mesenchymal transition. In *Nature Reviews Molecular Cell Biology* (Vol. 15, Issue 3, pp. 178–196). https://doi.org/10.1038/nrm3758

Lange-Sperandio, B., Fulda, S., Vandewalle, A., & Chevalier, R. L. (2003). Macrophages induce apoptosis in proximal tubule cells. *Pediatric Nephrology (Berlin, Germany)*, *18*(4), 335–341. https://doi.org/10.1007/s00467-003-1116-2

Lavoz, C., Rodrigues-Diez, R., Benito-Martin, A., Rayego-Mateos, S., Rodrigues-Diez, R. R., Alique, M., Ortiz, A., Mezzano, S., Egido, J., & Ruiz-Ortega, M. (2012). Angiotensin II Contributes to Renal Fibrosis Independently of Notch Pathway Activation. *PLoS ONE*, *7*(7), e40490. https://doi.org/10.1371/journal.pone.0040490

le Hir, M., Hegyi, I., Cueni-Loffing, D., Loffing, J., & Kaissling, B. (2005). Characterization of renal interstitial fibroblast-specific protein 1/S100A4-positive cells in healthy and inflamed rodent kidneys. *Histochemistry and Cell Biology*, *123*(4–5), 335–346. https://doi.org/10.1007/s00418-005-0788-z

LeBleu, V. S., Taduri, G., O'Connell, J., Teng, Y., Cooke, V. G., Woda, C., Sugimoto, H., & Kalluri, R. (2013). Origin and function of myofibroblasts in kidney fibrosis. *Nature Medicine*, *19*(8), 1047–1053. https://doi.org/10.1038/nm.3218

Lemley, K. v., & Kriz, W. (1991). Anatomy of the renal interstitium. *Kidney International*, *39*(3), 370–381. https://doi.org/10.1038/ki.1991.49

Ligresti, G., Nagao, R. J., Xue, J., Choi, Y. J., Xu, J., Ren, S., Aburatani, T., Anderson, S. K., MacDonald, J. W., Bammler, T. K., Schwartz, S. M., Muczynski, K. A., Duffield, J. S., Himmelfarb, J., & Zheng,

Y. (2016). A Novel Three–Dimensional Human Peritubular Microvascular System. *Journal of the American Society of Nephrology*, *27*(8), 2370–2381. https://doi.org/10.1681/ASN.2015070747

Lin, N. Y. C., Homan, K. A., Robinson, S. S., Kolesky, D. B., Duarte, N., Moisan, A., & Lewis, J. A. (2019a). Renal reabsorption in 3D vascularized proximal tubule models. *Proceedings of the National Academy of Sciences*, *116*(12), 5399–5404. https://doi.org/10.1073/pnas.1815208116

Lin, N. Y. C., Homan, K. A., Robinson, S. S., Kolesky, D. B., Duarte, N., Moisan, A., & Lewis, J. A. (2019b). Renal reabsorption in 3D vascularized proximal tubule models. *Proceedings of the National Academy of Sciences*, *116*(12), 5399–5404. https://doi.org/10.1073/pnas.1815208116

Little, M. (2016). Generating kidney tissue from pluripotent stem cells. *Cell Death Discovery*, *2*(1), 16053. https://doi.org/10.1038/cddiscovery.2016.53

Llames, S., García-Pérez, E., Meana, Á., Larcher, F., & del Río, M. (2015). Feeder Layer Cell Actions and Applications. *Tissue Engineering Part B: Reviews*, *21*(4), 345–353. https://doi.org/10.1089/ten.teb.2014.0547

Love, H. D., Ao, M., Jorgensen, S., Swearingen, L., Ferrell, N., Evans, R., Gewin, L., Harris, R. C., Zent, R., Roy, S., & Fissell, W. H. (2019). Substrate Elasticity Governs Differentiation of Renal Tubule Cells in Prolonged Culture. *Tissue Engineering. Part A*, *25*(13–14), 1013–1022. https://doi.org/10.1089/ten.TEA.2018.0182

Lovisa, S., LeBleu, V. S., Tampe, B., Sugimoto, H., Vadnagara, K., Carstens, J. L., Wu, C.-C., Hagos, Y., Burckhardt, B. C., Pentcheva-Hoang, T., Nischal, H., Allison, J. P., Zeisberg, M., & Kalluri, R. (2015). Epithelial-to-mesenchymal transition induces cell cycle arrest and parenchymal damage in renal fibrosis. *Nature Medicine*, *21*(9), 998–1009. https://doi.org/10.1038/nm.3902

Lovisa, S., Zeisberg, M., & Kalluri, R. (2016). Partial Epithelial-to-Mesenchymal Transition and Other New Mechanisms of Kidney Fibrosis. *Trends in Endocrinology & Metabolism*, *27*(10), 681–695. https://doi.org/10.1016/j.tem.2016.06.004

Maggiorani, D., Dissard, R., Belloy, M., Saulnier-Blache, J. S., Casemayou, A., Ducasse, L., Grès, S., Bellière, J., Caubet, C., Bascands, J. L., Schanstra, J. P., & Buffin-Meyer, B. (2015). Shear stress-induced alteration of epithelial organization in human renal tubular cells. *PLoS ONE*, *10*(7). https://doi.org/10.1371/journal.pone.0131416

Makris, K., & Spanou, L. (2016). Acute Kidney Injury: Definition, Pathophysiology and Clinical Phenotypes. *The Clinical Biochemist. Reviews*, *37*(2), 85–98.

Maleki, M., Ghanbarvand, F., Behvarz, M. R., Ejtemaei, M., & Ghadirkhomi, E. (2014). Comparison of Mesenchymal Stem Cell Markers in Multiple Human Adult Stem Cells. *International Journal of Stem Cells*, *7*(2), 118–126. https://doi.org/10.15283/ijsc.2014.7.2.118

Marchetti, G. M., Burwell, T. J., Peterson, N. C., Cann, J. A., Hanna, R. N., Li, Q., Ongstad, E. L., Boyd, J. T., Kennedy, M. A., Zhao, W., Rickert, K. W., Grimsby, J. S., Dall'Acqua, W. F., Wu, H., Tsui, P., Borrok, M. J., & Gupta, R. (2019). Targeted drug delivery via caveolae-associated protein PV1 improves lung fibrosis. *Communications Biology*, *2*(1), 92. https://doi.org/10.1038/s42003-019-0337-2

Maric, C., & Hall, J. E. (2011). *Obesity, Metabolic Syndrome and Diabetic Nephropathy* (pp. 28–35). https://doi.org/10.1159/000324941

Martínez-Klimova, E., Aparicio-Trejo, O. E., Tapia, E., & Pedraza-Chaverri, J. (2019a). Unilateral Ureteral Obstruction as a Model to Investigate Fibrosis-Attenuating Treatments. *Biomolecules*, *9*(4). https://doi.org/10.3390/biom9040141

Martínez-Klimova, E., Aparicio-Trejo, O. E., Tapia, E., & Pedraza-Chaverri, J. (2019b). Unilateral Ureteral Obstruction as a Model to Investigate Fibrosis-Attenuating Treatments. *Biomolecules*, *9*(4), 141. https://doi.org/10.3390/biom9040141

Marwick, J. A., Elliott, R. J. R., Longden, J., Makda, A., Hirani, N., Dhaliwal, K., Dawson, J. C., & Carragher, N. O. (2021). Application of a High-Content Screening Assay Utilizing Primary Human Lung Fibroblasts to Identify Antifibrotic Drugs for Rapid Repurposing in COVID-19 Patients. *SLAS Discovery*, *26*(9), 1091–1106. https://doi.org/10.1177/24725552211019405

Mathialagan, S., Rodrigues, A. D., & Feng, B. (2017). Evaluation of Renal Transporter Inhibition Using Creatinine as a Substrate In Vitro to Assess the Clinical Risk of Elevated Serum Creatinine. *Journal of Pharmaceutical Sciences*, *106*(9), 2535–2541. https://doi.org/10.1016/j.xphs.2017.04.009

Maunsbach, A. B., Marples, D., Chin, E., Ning, G., Bondy, C., & Agre, P. (1997). *Aquaporin-1 Water Channel Expression in Human Kidney*.

McEvoy, C. M., Murphy, J. M., Zhang, L., Clotet-Freixas, S., Mathews, J. A., An, J., Karimzadeh, M., Pouyabahar, D., Su, S., Zaslaver, O., Röst, H., Arambewela, R., Liu, L. Y., Zhang, S., Lawson, K. A., Finelli, A., Wang, B., MacParland, S. A., Bader, G. D., … Crome, S. Q. (2022). Single-cell profiling of healthy human kidney reveals features of sex-based transcriptional programs and tissue-specific immunity. *Nature Communications*, *13*(1), 7634. https://doi.org/10.1038/s41467-022-35297-z

Meran, S., & Steadman, R. (2011). Fibroblasts and myofibroblasts in renal fibrosis. *International Journal of Experimental Pathology*, *92*(3), 158–167. https://doi.org/10.1111/j.1365-2613.2011.00764.x

Mescher, A. L. (2018). The Urinary System. In *Junqueira's Basic Histology: Text and Atlas, 15e*. McGraw-Hill Education. accessmedicine.mhmedical.com/content.aspx?aid=1160663250

Miners, J., Yang, X., Knights, K., & Zhang, L. (2017). The Role of the Kidney in Drug Elimination: Transport, Metabolism, and the Impact of Kidney Disease on Drug Clearance. *Clinical Pharmacology & Therapeutics*, *102*(3), 436–449. https://doi.org/10.1002/cpt.757

Misseri, R., Meldrum, D. R., Dinarello, C. A., Dagher, P., Hile, K. L., Rink, R. C., & Meldrum, K. K. (2005). TNF-alpha mediates obstruction-induced renal tubular cell apoptosis and proapoptotic signaling. *American Journal of Physiology. Renal Physiology*, *288*(2), F406-11. https://doi.org/10.1152/ajprenal.00099.2004

Mizuguchi, K., Aoki, H., Aoyama, M., Kawaguchi, Y., Waguri-Nagaya, Y., Ohte, N., & Asai, K. (2021). Three-dimensional spheroid culture induces apical-basal polarity and the original characteristics of immortalized human renal proximal tubule epithelial cells. *Experimental Cell Research*, *404*(1), 112630. https://doi.org/10.1016/j.yexcr.2021.112630

Moein, S., Moradzadeh, K., Javanmard, S., Nasiri, S., & Gheisari, Y. (2020). *In vitro* versus *in vivo* models of kidney fibrosis: Time-course experimental design is crucial to avoid misinterpretations of gene expression data. *Journal of Research in Medical Sciences*, *25*(1), 84. https://doi.org/10.4103/jrms.JRMS_906_19

Moll, S., Ebeling, M., Weibel, F., Farina, A., Araujo Del Rosario, A., Hoflack, J. C., Pomposiello, S., & Prunotto, M. (2013a). Epithelial cells as active player in fibrosis: findings from an in vitro model. *PloS One*, *8*(2), e56575. https://doi.org/10.1371/journal.pone.0056575

Moll, S., Ebeling, M., Weibel, F., Farina, A., Araujo Del Rosario, A., Hoflack, J. C., Pomposiello, S., & Prunotto, M. (2013b). Epithelial Cells as Active Player In Fibrosis: Findings from an In Vitro Model. *PLoS ONE*, *8*(2), e56575. https://doi.org/10.1371/journal.pone.0056575

Mühlhans, J., Brandstätter, J. H., & Gießl, A. (2011). The centrosomal protein pericentrin identified at the basal body complex of the connecting cilium in mouse photoreceptors. *PLoS ONE*, *6*(10). https://doi.org/10.1371/journal.pone.0026496

Nakai, T., Iwamura, Y., & Suzuki, N. (2021). Efficient isolation of interstitial fibroblasts directly from mouse kidneys or indirectly after ex vivo expansion. *STAR Protocols*, *2*(4), 100826. https://doi.org/10.1016/j.xpro.2021.100826

Nieskens, T. T. G., Persson, M., Kelly, E. J., & Sjögren, A.-K. (2020). A Multicompartment Human Kidney Proximal Tubule-on-a-Chip Replicates Cell Polarization-Dependent Cisplatin Toxicity. *Drug Metabolism and Disposition: The Biological Fate of Chemicals*, *48*(12), 1303–1311. https://doi.org/10.1124/dmd.120.000098

Nieskens, T. T. G., Peters, J. G. P., Schreurs, M. J., Smits, N., Woestenenk, R., Jansen, K., van der Made, T. K., Röring, M., Hilgendorf, C., Wilmer, M. J., & Masereeuw, R. (2016). A Human Renal Proximal Tubule Cell Line with Stable Organic Anion Transporter 1 and 3 Expression Predictive for Antiviral-Induced Toxicity. *The AAPS Journal*, *18*(2), 465–475. https://doi.org/10.1208/s12248-016-9871-8

Nishitani, Y., Iwano, M., Yamaguchi, Y., Harada, K., Nakatani, K., Akai, Y., Nishino, T., Shiiki, H., Kanauchi, M., Saito, Y., & Neilson, E. G. (2005a). Fibroblast-specific protein 1 is a specific prognostic marker for renal survival in patients with IgAN. *Kidney International*, *68*(3), 1078–1085. https://doi.org/10.1111/j.1523-1755.2005.00500.x

Nishitani, Y., Iwano, M., Yamaguchi, Y., Harada, K., Nakatani, K., Akai, Y., Nishino, T., Shiiki, H., Kanauchi, M., Saito, Y., & Neilson, E. G. (2005b). Fibroblast-specific protein 1 is a specific prognostic marker for renal survival in patients with IgAN. *Kidney International*, *68*(3), 1078–1085. https://doi.org/10.1111/j.1523-1755.2005.00500.x

Novikov, A., Fu, Y., Huang, W., Freeman, B., Patel, R., van Ginkel, C., Koepsell, H., Busslinger, M., Onishi, A., Nespoux, J., Vallon, V., & Ginkel, van C. (2019). SGLT2 inhibition and renal urate excretion: role of luminal glucose, GLUT9, and URAT1. *Am J Physiol Renal Physiol*, *316*, 173–185. https://doi.org/10.1152/ajprenal.00462.2018.-In

Nugraha, B., Mohr, M. A., Ponti, A., Emmert, M. Y., Weibel, F., Hoerstrup, S. P., Moll, S., Certa, U., Prunotto, M., & Pantazis, P. (2017). Monitoring and manipulating cellular crosstalk during kidney fibrosis inside a 3D in vitro co-culture. *Scientific Reports*, *7*(1), 14490. https://doi.org/10.1038/s41598-017-12683-y

Obrador Vera, G. T. (2017). Chronic Renal Failure and the Uremic Syndrome. In E. v Lerma, M. H. Rosner, & M. A. Perazella (Eds.), *CURRENT Diagnosis & Treatment: Nephrology & Hypertension, 2e*. McGraw-Hill Education. accessmedicine.mhmedical.com/content.aspx?aid=1149112956

Ogobuiro, I., & Tuma, F. (2024). *Physiology, Renal*.

Palano, G., Jansson, M., Backmark, A., Martinsson, S., Sabirsh, A., Hultenby, K., Åkerblad, P., Granberg, K. L., Jennbacken, K., Müllers, E., & Hansson, E. M. (2020). A high-content, in vitro cardiac fibrosis assay for high-throughput, phenotypic identification of compounds with anti-fibrotic activity. *Journal of Molecular and Cellular Cardiology*, *142*, 105–117. https://doi.org/10.1016/j.yjmcc.2020.04.002

Pannu, N., & Nadim, M. K. (2008). An overview of drug-induced acute kidney injury. *Critical Care Medicine*, *36*(Suppl), S216–S223. https://doi.org/10.1097/CCM.0b013e318168e375

Park, J.-G., Na, M., Kim, M.-G., Park, S. H., Lee, H. J., Kim, D. K., Kwak, C., Kim, Y. S., Chang, S., Moon, K. C., Lee, D.-S., & Han, S. S. (2020). Immune cell composition in normal human kidneys. *Scientific Reports*, *10*(1), 15678. https://doi.org/10.1038/s41598-020-72821-x

Perazella, M. A. (2018). Pharmacology behind Common Drug Nephrotoxicities. *Clinical Journal of the American Society of Nephrology*, *13*(12), 1897–1908. https://doi.org/10.2215/CJN.00150118

Perazella, M. A. (2019). Drug-induced acute kidney injury. *Current Opinion in Critical Care*, *25*(6), 550–557. https://doi.org/10.1097/MCC.0000000000000653

Perlman, R. L., & Heung, M. (2019). Renal Disease. In G. D. Hammer & S. J. McPhee (Eds.), *Pathophysiology of Disease: An Introduction to Clinical Medicine, 8e*. McGraw-Hill Education. accessmedicine.mhmedical.com/content.aspx?aid=1156659143

Perlman, R. L., Heung, M., & Ix, J. H. (2013). Renal Disease. In G. D. Hammer & S. J. McPhee (Eds.), *Pathophysiology of Disease: An Introduction to Clinical Medicine, 7e*. McGraw-Hill Education. accessmedicine.mhmedical.com/content.aspx?aid=1100861860

Pozzi, A., & Zent, R. (2010). ZO-1 and ZONAB Interact to Regulate Proximal Tubular Cell Differentiation. *Journal of the American Society of Nephrology*, *21*(3), 388–390. https://doi.org/10.1681/ASN.2010010061

Prunotto, M., Budd, D. C., Gabbiani, G., Meier, M., Formentini, I., Hartmann, G., Pomposiello, S., & Moll, S. (2012). Epithelial-mesenchymal crosstalk alteration in kidney fibrosis. *The Journal of Pathology*, *228*(2), 131–147. https://doi.org/10.1002/path.4049

Qureshi, O. S., Bon, H., Twomey, B., Holdsworth, G., Ford, K., Bergin, M., Huang, L., Muzylak, M., Healy, L. J., Hurdowar, V., & Johnson, T. S. (2017). An immunofluorescence assay for extracellular matrix components highlights the role of epithelial cells in producing a stable, fibrillar extracellular matrix. *Biology Open*, *6*(10), 1423–1433. https://doi.org/10.1242/bio.025866

Racusen, L. C., Monteil, C., Sgrignoli, A., Lucskay, M., Marouillat, S., Rhim, J. G. S., & Morin, J. (1997). Cell lines with extended in vitro growth potential from human renal proximal tubule: Characterization, response to inducers, and comparison with established cell lines. *Journal of Laboratory and Clinical Medicine*, *129*(3), 318–329. https://doi.org/10.1016/S0022-2143(97)90180-3

Ramesh, G., & Reeves, W. B. (2004). Inflammatory cytokines in acute renal failure. *Kidney International*, *66*, S56–S61. https://doi.org/10.1111/j.1523-1755.2004.09109.x

Ramseyer, V. D., & Garvin, J. L. (2013). Tumor necrosis factor-: regulation of renal function and blood pressure. *Am J Physiol Renal Physiol*, *304*, 1231–1242. https://doi.org/10.1152/ajprenal.00557.2012.-Tumor

Rauch, C., Feifel, E., Kern, G., Murphy, C., Meier, F., Parson, W., Beilmann, M., Jennings, P., Gstraunthaler, G., & Wilmes, A. (2018). Differentiation of human iPSCs into functional podocytes. *PLOS ONE*, *13*(9), e0203869. https://doi.org/10.1371/journal.pone.0203869

Sánchez-Romero, N., Schophuizen, C. M. S., Giménez, I., & Masereeuw, R. (2016). In vitro systems to study nephropharmacology: 2D versus 3D models. *European Journal of Pharmacology*, *790*, 36–45. https://doi.org/10.1016/j.ejphar.2016.07.010

Schulz, M.-C., Voß, L., Schwerdt, G., & Gekle, M. (2022). Epithelial-Fibroblast Crosstalk Protects against Acidosis-Induced Inflammatory and Fibrotic Alterations. *Biomedicines*, *10*(3). https://doi.org/10.3390/biomedicines10030681

Schwager, S. C., Bordeleau, F., Zhang, J., Antonyak, M. A., Cerione, R. A., & Reinhart-King, C. A. (2019a). Matrix stiffness regulates microvesicle-induced fibroblast activation. *American Journal of Physiology-Cell Physiology*, *317*(1), C82–C92. https://doi.org/10.1152/ajpcell.00418.2018

Schwager, S. C., Bordeleau, F., Zhang, J., Antonyak, M. A., Cerione, R. A., & Reinhart-King, C. A. (2019b). Matrix stiffness regulates microvesicle-induced fibroblast activation. *American Journal of Physiology-Cell Physiology*, *317*(1), C82–C92. https://doi.org/10.1152/ajpcell.00418.2018

Sheng, L., & Zhuang, S. (2020a). New Insights Into the Role and Mechanism of Partial Epithelial-Mesenchymal Transition in Kidney Fibrosis. *Frontiers in Physiology*, *11*, 569322. https://doi.org/10.3389/fphys.2020.569322

Sheng, L., & Zhuang, S. (2020b). New Insights Into the Role and Mechanism of Partial Epithelial-Mesenchymal Transition in Kidney Fibrosis. In *Frontiers in Physiology* (Vol. 11). Frontiers Media S.A. https://doi.org/10.3389/fphys.2020.569322

Sieber, P., Schäfer, A., Lieberherr, R., Le Goff, F., Stritt, M., Welford, R. W. D., Gatfield, J., Peter, O., Nayler, O., & Lüthi, U. (2018). Novel high–throughput myofibroblast assays identify agonists with therapeutic potential in pulmonary fibrosis that act via EP2 and EP4 receptors. *PLOS ONE*, *13*(11), e0207872. https://doi.org/10.1371/journal.pone.0207872

Simon-Friedt, B. R., Wilson, M. J., Blake, D. A., Yu, H., Eriksson, Y., & Wickliffe, J. K. (2015). The RPTEC/TERT1 Cell Line as an Improved Tool for In Vitro Nephrotoxicity Assessments. *Biological Trace Element Research*, *166*(1), 66–71. https://doi.org/10.1007/s12011-015-0339-y

Song, J., Yu, J., Prayogo, G. W., Cao, W., Wu, Y., Jia, Z., & Zhang, A. (2019). Understanding kidney injury molecule 1: a novel immune factor in kidney pathophysiology. In *Am J Transl Res* (Vol. 11, Issue 3). www.ajtr.org/ISSN:1943-8141/AJTR0088409

Soni, S. S., Cruz, D., Bobek, I., Chionh, C. Y., Nalesso, F., Lentini, P., de Cal, M., Corradi, V., Virzi, G., & Ronco, C. (2010). NGAL: A biomarker of acute kidney injury and other systemic conditions. In *International Urology and Nephrology* (Vol. 42, Issue 1, pp. 141–150). https://doi.org/10.1007/s11255-009-9608-z

Sorrell, J. M., Baber, M. A., & Caplan, A. I. (2007). A Self-Assembled Fibroblast-Endothelial Cell Co-Culture System That Supports in vitro Vasculogenesis by both Human Umbilical Vein Endothelial Cells and Human Dermal Microvascular Endothelial Cells. *Cells Tissues Organs*, *186*(3), 157–168. https://doi.org/10.1159/000106670

Stan, R. v., Tkachenko, E., & Niesman, I. R. (2004). PV1 Is a Key Structural Component for the Formation of the Stomatal and Fenestral Diaphragms. *Molecular Biology of the Cell*, *15*(8), 3615–3630. https://doi.org/10.1091/mbc.e03-08-0593

Stewart, B. J., Ferdinand, J. R., Young, M. D., Mitchell, T. J., Loudon, K. W., Riding, A. M., Richoz, N., Frazer, G. L., Staniforth, J. U. L., Vieira Braga, F. A., Botting, R. A., Popescu, D.-M., Vento-Tormo, R., Stephenson, E., Cagan, A., Farndon, S. J., Polanski, K., Efremova, M., Green, K., … Clatworthy, M. R. (2019). Spatiotemporal immune zonation of the human kidney. *Science (New York, N.Y.)*, *365*(6460), 1461–1466. https://doi.org/10.1126/science.aat5031

Stolz, D. B., & Sims-Lucas, S. (2015). Unwrapping the origins and roles of the renal endothelium. *Pediatric Nephrology*, *30*(6), 865–872. https://doi.org/10.1007/s00467-014-2798-3

Strutz, F., & Zeisberg, M. (2006). Renal Fibroblasts and Myofibroblasts in Chronic Kidney Disease. *Journal of the American Society of Nephrology*, *17*(11), 2992–2998. https://doi.org/10.1681/ASN.2006050420

Takata, K., Matsuzaki, T., Tajika, Y., Ablimit, A., & Hasegawa, T. (2008). Localization and trafficking of aquaporin 2 in the kidney. In *Histochemistry and Cell Biology* (Vol. 130, Issue 2, pp. 197–209). https://doi.org/10.1007/s00418-008-0457-0

Tan, R. J., Zhou, D., & Liu, Y. (2016a). Signaling Crosstalk between Tubular Epithelial Cells and Interstitial Fibroblasts after Kidney Injury. *Kidney Diseases*, *2*(3), 136–144. https://doi.org/10.1159/000446336

Tan, R. J., Zhou, D., & Liu, Y. (2016b). Signaling Crosstalk between Tubular Epithelial Cells and Interstitial Fibroblasts after Kidney Injury. *Kidney Diseases*, *2*(3), 136–144. https://doi.org/10.1159/000446336

Tasnim, F., & Zink, D. (2012). Cross talk between primary human renal tubular cells and endothelial cells in cocultures. *American Journal of Physiology-Renal Physiology*, *302*(8), F1055–F1062. https://doi.org/10.1152/ajprenal.00621.2011

Thomas, G. L., Yang, B., Wagner1, B. E., Savill2, J., Meguid, A., & Nahas, E. (1998). Nephrology Dialysis Transplantation Cellular apoptosis and proliferation in experimental renal fibrosis. In *Nephrol Dial Transplant* (Vol. 13).

Tokonami, N., Takata, T., Beyeler, J., Ehrbar, I., Yoshifuji, A., Christensen, E. I., Loffing, J., Devuyst, O., & Olinger, E. G. (2018). Uromodulin is expressed in the distal convoluted tubule, where it is critical for regulation of the sodium chloride cotransporter NCC. *Kidney International*, *94*(4), 701–715. https://doi.org/10.1016/j.kint.2018.04.021

Tummalapalli, L., Nadkarni, G. N., & Coca, S. G. (2016). Biomarkers for predicting outcomes in chronic kidney disease. In *Current Opinion in Nephrology and Hypertension* (Vol. 25, Issue 6, pp. 480–486). Lippincott Williams and Wilkins. https://doi.org/10.1097/MNH.0000000000000275

Turner, J. M., Bauer, C., Abramowitz, M. K., Melamed, M. L., & Hostetter, T. H. (2012). Treatment of chronic kidney disease. *Kidney International*, *81*(4), 351–362. https://doi.org/10.1038/ki.2011.380

Vallon, V. (2011). The proximal tubule in the pathophysiology of the diabetic kidney. *American Journal of Physiology-Regulatory, Integrative and Comparative Physiology*, *300*(5), R1009–R1022. https://doi.org/10.1152/ajpregu.00809.2010

Vidal Yucha, S. E., Quackenbush, D., Chu, T., Lo, F., Sutherland, J. J., Kuzu, G., Roberts, C., Luna, F., Barnes, S. W., Walker, J., & Kuss, P. (2022). "3D, human renal proximal tubule (RPTEC-TERT1) organoids 'tubuloids' for translatable evaluation of nephrotoxins in high-throughput". *PloS One*, *17*(11), e0277937. https://doi.org/10.1371/journal.pone.0277937

Vormann, M. K., Gijzen, L., Hutter, S., Boot, L., Nicolas, A., van den Heuvel, A., Vriend, J., Ng, C. P., Nieskens, T. T. G., van Duinen, V., de Wagenaar, B., Masereeuw, R., Suter-Dick, L., Trietsch, S. J., Wilmer, M., Joore, J., Vulto, P., & Lanz, H. L. (2018). Nephrotoxicity and Kidney Transport Assessment on 3D Perfused Proximal Tubules. *The AAPS Journal*, *20*(5), 90. https://doi.org/10.1208/s12248-018-0248-z

Vriend, J., Nieskens, T. T. G., Vormann, M. K., van den Berge, B. T., van den Heuvel, A., Russel, F. G. M., Suter-Dick, L., Lanz, H. L., Vulto, P., Masereeuw, R., & Wilmer, M. J. (2018). Screening of Drug-Transporter Interactions in a 3D Microfluidic Renal Proximal Tubule on a Chip. *The AAPS Journal*, *20*(5), 87. https://doi.org/10.1208/s12248-018-0247-0

Vriend, J., Pye, K. R., & Brown, C. (2021). In vitro models for accurate prediction of renal tubular xenobiotic transport in vivo. *Current Opinion in Toxicology*, *25*, 15–22. https://doi.org/10.1016/j.cotox.2020.12.001

Wan, J., Zhou, X., Cui, J., Zou, Z., Xu, Y., & You, D. (2013). Role of complement 3 in TNF-α-induced mesenchymal transition of renal tubular epithelial cells in vitro. *Molecular Biotechnology*, *54*(1), 92–100. https://doi.org/10.1007/s12033-012-9547-2

Wang, D., Sant, S., Lawless, C., & Ferrell, N. (2022). A kidney proximal tubule model to evaluate effects of basement membrane stiffening on renal tubular epithelial cells. *Integrative Biology : Quantitative Biosciences from Nano to Macro*, *14*(8–12), 171–183. https://doi.org/10.1093/intbio/zyac016

Wang, X., Sun, X., Li, C., Liu, Y., Zhang, L., Li, Y., Wu, Q., Li, S., & Li, Y. (2018). Establishing a Cell-Based High-Content Screening Assay for TCM Compounds with Anti-Renal Fibrosis Effects. *Evidence-Based Complementary and Alternative Medicine*, *2018*, 1–10. https://doi.org/10.1155/2018/7942614

Watanabe, N. , S. K. , S. Y. , S. K. , O. K. , K. R. , S. C. , W. J. , & M. H. (2011). (2011). *Involvement of MAPKs in ICAM-1 Expression in Glomerular Endothelial Cells in Diabetic Nephropathy*.

Webster, A. C., Nagler, E. V, Morton, R. L., & Masson, P. (2017). Chronic Kidney Disease. *The Lancet*, *389*(10075), 1238–1252. https://doi.org/10.1016/S0140-6736(16)32064-5

Wieser, M., Stadler, G., Jennings, P., Streubel, B., Pfaller, W., Ambros, P., Riedl, C., Katinger, H., Grillari, J., & Grillari-Voglauer, R. (2008). hTERT alone immortalizes epithelial cells of renal proximal tubules without changing their functional characteristics. *American Journal of Physiology. Renal Physiology*, *295*(5), F1365-75. https://doi.org/10.1152/ajprenal.90405.2008

Winfree, S., Al Hasan, M., & El-Achkar, T. M. (2022). Profiling Immune Cells in the Kidney Using Tissue Cytometry and Machine Learning. *Kidney360*, *3*(5), 968–978. https://doi.org/10.34067/KID.0006802020

Witzgall, R. (1999). The proximal tubule phenotype and its disruption in acute renal failure and polycystic kidney disease. *Experimental Nephrology*, *7*(1), 15–19. https://doi.org/10.1159/000020579

Wrana, J. L., & Attisano, L. (2000). The Smad pathway. *Cytokine & Growth Factor Reviews*, *11*(1–2), 5–13. https://doi.org/10.1016/S1359-6101(99)00024-6

Wu, H., & Humphreys, B. D. (2020). Single cell sequencing and kidney organoids generated from pluripotent stem cells. *Clinical Journal of the American Society of Nephrology*, *15*(4), 550–556. https://doi.org/10.2215/CJN.07470619

Wu, Y. S., Liang, S., Li, D. Y., Wen, J. H., Tang, J. X., & Liu, H. F. (2021). Cell Cycle Dysregulation and Renal Fibrosis. In *Frontiers in Cell and Developmental Biology* (Vol. 9). Frontiers Media S.A. https://doi.org/10.3389/fcell.2021.714320

Xu, Q., Norman, J. T., Shrivastav, S., Lucio-Cazana, J., & Kopp, J. B. (2007). In vitro models of TGF-β-induced fibrosis suitable for high-throughput screening of antifibrotic agents. *American Journal of Physiology-Renal Physiology*, *293*(2), F631–F640. https://doi.org/10.1152/ajprenal.00379.2006

Xu, Z., Li, W., Han, J., Zou, C., Huang, W., Yu, W., Shan, X., Lum, H., Li, X., & Liang, G. (2017). Angiotensin II induces kidney inflammatory injury and fibrosis through binding to myeloid differentiation protein-2 (MD2). *Scientific Reports*, *7*, 44911. https://doi.org/10.1038/srep44911

Yang, H.-C., Zuo, Y., & Fogo, A. B. (2010). Models of chronic kidney disease. *Drug Discovery Today: Disease Models*, *7*(1–2), 13–19. https://doi.org/10.1016/j.ddmod.2010.08.002

Yang, L., Besschetnova, T. Y., Brooks, C. R., Shah, J. v., & Bonventre, J. v. (2010). Epithelial cell cycle arrest in G2/M mediates kidney fibrosis after injury. *Nature Medicine*, *16*(5), 535–543. https://doi.org/10.1038/nm.2144

Yuan, Q., Tang, B., & Zhang, C. (2022). Signaling pathways of chronic kidney diseases, implications for therapeutics. *Signal Transduction and Targeted Therapy*, *7*(1), 182. https://doi.org/10.1038/s41392-022-01036-5

Zeiger, A. S., Loe, F. C., Li, R., Raghunath, M., & van Vliet, K. J. (2012). Macromolecular crowding directs extracellular matrix organization and mesenchymal stem cell behavior. *PLoS ONE*, *7*(5). https://doi.org/10.1371/journal.pone.0037904

Zeisberg, M., & Kalluri, R. (2015). Physiology of the Renal Interstitium. *Clinical Journal of the American Society of Nephrology*, *10*(10), 1831–1840. https://doi.org/10.2215/CJN.00640114

Zhang, H., & Sun, S.-C. (2015). NF-κB in inflammation and renal diseases. *Cell & Bioscience*, *5*(1), 63. https://doi.org/10.1186/s13578-015-0056-4

Zhou, D., Fu, H., Liu, S., Zhang, L., Xiao, L., Bastacky, S. I., & Liu, Y. (2019). Early activation of fibroblasts is required for kidney repair and regeneration after injury. *FASEB Journal : Official Publication of the Federation of American Societies for Experimental Biology*, *33*(11), 12576–12587. https://doi.org/10.1096/fj.201900651RR

Zhou, M., Ma, H., Lin, H., & Qin, J. (2014). Induction of epithelial-to-mesenchymal transition in proximal tubular epithelial cells on microfluidic devices. *Biomaterials*, *35*(5), 1390–1401. https://doi.org/10.1016/j.biomaterials.2013.10.070

Zhou, P., Wan, X., Zou, Y., Chen, Z., & Zhong, A. (2020). Transforming growth factor beta (TGF-β) is activated by the CtBP2-p300-AP1 transcriptional complex in chronic renal failure. *International Journal of Biological Sciences*, *16*(2), 204–215. https://doi.org/10.7150/ijbs.38841

Zhu, X., Jiang, L., Long, M., Wei, X., Hou, Y., & Du, Y. (2021). Metabolic Reprogramming and Renal Fibrosis. In *Frontiers in Medicine* (Vol. 8). Frontiers Media S.A. https://doi.org/10.3389/fmed.2021.746920

Zimmerman, K. A., Bentley, M. R., Lever, J. M., Li, Z., Crossman, D. K., Song, C. J., Liu, S., Crowley, M. R., George, J. F., Mrug, M., & Yoder, B. K. (2019). Single-Cell RNA Sequencing Identifies Candidate Renal Resident Macrophage Gene Expression Signatures across Species. *Journal of the American Society of Nephrology : JASN*, *30*(5), 767–781. https://doi.org/10.1681/ASN.2018090931

Acknowledgments

"Xe pezo el tacon del sbrego" is a Venetian proverb that could be translated into "The patch is worse than the tear" – which is a humorous way to summarize the main topic treated by this thesis, since renal fibrosis is a fascinating phenomenon where the kidney desperately tries to "patch itself up" in a cascade of unfortunate molecular events, ultimately losing its physiological functions and causing great havoc to all other organs in the human body.

The journey that lead me to consider the inner workings of chronic kidney disease and its underlying causes started with my Master's thesis, when my first PI, Dr Elisavet Vasilopoulou, granted me unlimited access to a lab where I could explore the relationship between chronic kidney disease and subclinical hypothyroidism using a murine model of nephrotoxic nephritis. Among the sunny forests and white shores of Kent, I spent hours and hours in a dark room looking at mouse kidney sections under the fluorescent lights of a rather old microscope, discovering the beauty and potential of immunofluorescence staining and imaging for the first time. Eager to follow the chronic kidney disease trail, a few months after my post in Kent I landed in Dr David Long's lab in bustling Holborn, where I had the chance to expand my knowledge in disease modeling by working on *in vivo* animal models of diabetic nephropathy. Among several other techniques, I had the chance to use state-of-the-art microscopes, approaching high content imaging and image analysis for the first time. My time in London was incredibly stimulating and productive, but the prospect of working on animal models for the foreseeable future did not sit right with me. By this point, my non-scientists friends at the pub would ask me more and more challenging questions about my position on the ethics and the future of my work on animals to which I could rarely give a coherent answer (not because of the pints, I promise), so it became clear that I needed to look further afield: if I was going to pursue a PhD in renal disease modelling, it was not going to be using animal models. Quite a few months of internet browsing later, one advert on findaphd.com caught my eye: it talked about iPSC and human-derived *in vitro* kidney models, and it mentioned pharmacology. "That's me!" – I thought as soon as I read the project description. My first time in Newcastle was also the day I met Lyle Armstrong and Colin Brown for the first time, and I must have made quite an impression because the same afternoon while on my train back to London I received an email that stated I was going to be offered the position for a 3-year PhD project. That was it. I moved to Newcastle about a month later, excited to work on the best model one could ever wish for: an actual human kidney. Many, many kidneys later, many nights spent in the lab chopping such kidneys later, here I am completing the PhD project on human *in vitro* renal models of CKD.

I would like to thank immensely my supervisors Colin Brown and Lyle Armstrong who took a chance on me, guided me through this incredible scientific journey and allowed me to express my creativity and passion for the subject while helping me grow into an actual scientist. I would like to thank Colin for having shown me resilience in spite of adversity, and that world pandemics and just life in general aren't enough to stop passion and discipline in pursuit of science and knowledge. I would like to thank Lyle for supporting my foolishness and sparking my creativity, and for reminding me that a good joke can make light of any catastrophically

failed experiment. This project would have not been possible without the existence of Newcells Biotech and its ever changing and ever-growing staff – in particular, I would like to thank Dr Git Chung, Dr Jelle Vriend and Keith Pye for their input and support during the first year of the project and for being great lab companions throughout the pandemic. Furthermore, I would like to thank Dr Kathryn Garner for her invaluable contributions during the final year of this project and thesis write up time. Dr Garner has shown me how to be a creative powerhouse in the lab with her infectious curiosity (especially when the going gets tough i.e., at the end of a PhD) and true passion for science and scientific research. I would like to thank all the other current and past members of Newcells Biotech's Kidney Team, especially my dear friends Lucy, Francesca, and Donovan for lighting up even the rainiest winter lab days with their laughter and friendship.

Besides being here in Newcastle for my research, I ended up making my home in the North East thanks to all the amazing friends I met over the past three years. Thanks for bearing with me and my constant complaints about fibroblasts migrating into the epithelial monolayer, kidneys coming late at night, TEER not reaching the threshold before the weekend started, microscopes not working properly, this thesis being too long and "impossible to finish". Despite all the experiments gone wrong, COVID-19, and all the heartache we still managed to go raving, camping, drinking, hiking, and exploring our minds between dazzling dancefloors and wind-battered landscapes, therefore I would like to thank my dearest friends Anastassia, Avril, Roy, Maddy, David, Ivo, Pete, and Mattia. In particular, I would like to thank Steven and Taya who have been very emotionally supportive throughout the thesis write up, especially by always being up for a pint or a glass of red wine. Finally, I would like to immensely thank my parents Dario and Marinella and my sister Valentina for having supported me from afar throughout this journey and for having believed in me since 1994. Being away from sunny Padova has not been easy at times, but I can confidently say it has been worth it.

Post scriptum. I would like to acknowledge the help that my ever-inspiring friend and partner Jack has given me over the last 6 months, holding my hand all the way while reviewing this thesis.